Strål säkerhets myndigheten
Swedish Radiation Safety Authority

Report

SSM's external experts' review of SKB's safety evaluation SE-SFL

2021:13

Date: May 2021
Report number: 2021:13
ISSN: 2000-0456
Available at www.ssm.se

SSM perspective

Background

In Sweden long-lived low- and intermediate level radioactive waste is planned to be disposed in a repository (SFL) in the Swedish crystalline rock at a depth around 500 m. The waste contains mainly the long-lived wastes from the operation and decommissioning of the Swedish nuclear reactor plants, as well as the long-lived wastes from early research in the Swedish nuclear program (legacy wastes), from medicine, industry and research including the European Spallation Source (ESS) research facility. The disposal concept for the SFL repository has been developed by SKB since the 1980th. A pre-study of the concept has been carried out (SKB TR-95-03) and a preliminary safety analysis (SKB TR-99-28) was previously published. The recently published safety evaluation of the SFL repository (SE-SFL, SKB TR-19-01) is a continuation of this conceptual development with the purpose of providing input to consecutive steps in the development of the repository.

The present report compiles the results from SSM's external experts' review of different focus areas of special interest to SSM in the authority's review of the safety evaluation SE-SFL. The areas of interest are hydrogeology, concrete degradation, radionuclide transport in the near-field and biosphere dose assessment. The general objective of these reviews has been to give support to SSM's assessment of the evaluation and to the authority's feedback to SKB on the continued development of the SFL repository concept and on SKB's development in general regarding assessment-level modelling.

Project information

Contact person at SSM: Jinsong Liu

Table of contents

This report concerns a study that has been conducted on the behalf of the Swedish Radiation Safety Authority, SSM. The conclusions and viewpoints presented in the report are those of the author(s) and do not necessarily coincide with those of SSM.

Strål
säkerhets
myndigheten
Swedish Radiation Safety Authority

Author: Joel Geier
Clearwater Hardrock Consulting, Corvallis, Oregon, U.S.A.

2021:13

1) Review of SE-SFL – Hydrogeology

Date: May 2021
Report number: 2021:13 **ISSN:** 2000-0456
Available at www.stralsakerhetsmyndigheten.se

Authors:Joel Geier[1)]
[1)] Clearwater Hardrock Consulting, Corvallis, Oregon, U.S.A.

1) Review of SE-SFL – Hydrogeology

Activity number: 3034111-01
Registration number: SSSM2020-3832
Contact person at SSM: Maria Bergström

Content

1. Introduction

The Swedish Nuclear Fuel and Waste Management Co. (SKB) has recently presented a safety evaluation of a conceptual design for a geological repository for long-lived radioactive waste, referred to as the SFL.

The safety evaluation, SE-SFL, is presented in SKB (2019; SKB TR-19-01) and a series of background reports. No site has yet been selected for the SFL, but the safety evaluation uses site-specific data from the Laxemar research site in eastern Småland, in order to assess the likelihood that a conceptual design proposed by Elfwing et al. (2013) could succeed in meeting the Swedish regulatory requirements (in terms of risk for the most-exposed group of future humans living at or near the site) for a realistic situation.

This document presents findings from a review of hydrogeological aspects of SE-SFL, commissioned by the Swedish Radiation Safety Authority (SSM). The review is based mainly on the top-level presentation in SKB (2019) and two supporting reports that describe hydrogeological modeling, Joyce et al. (2019) and Abarca et al. (2019), with reference to other background reports where necessary.

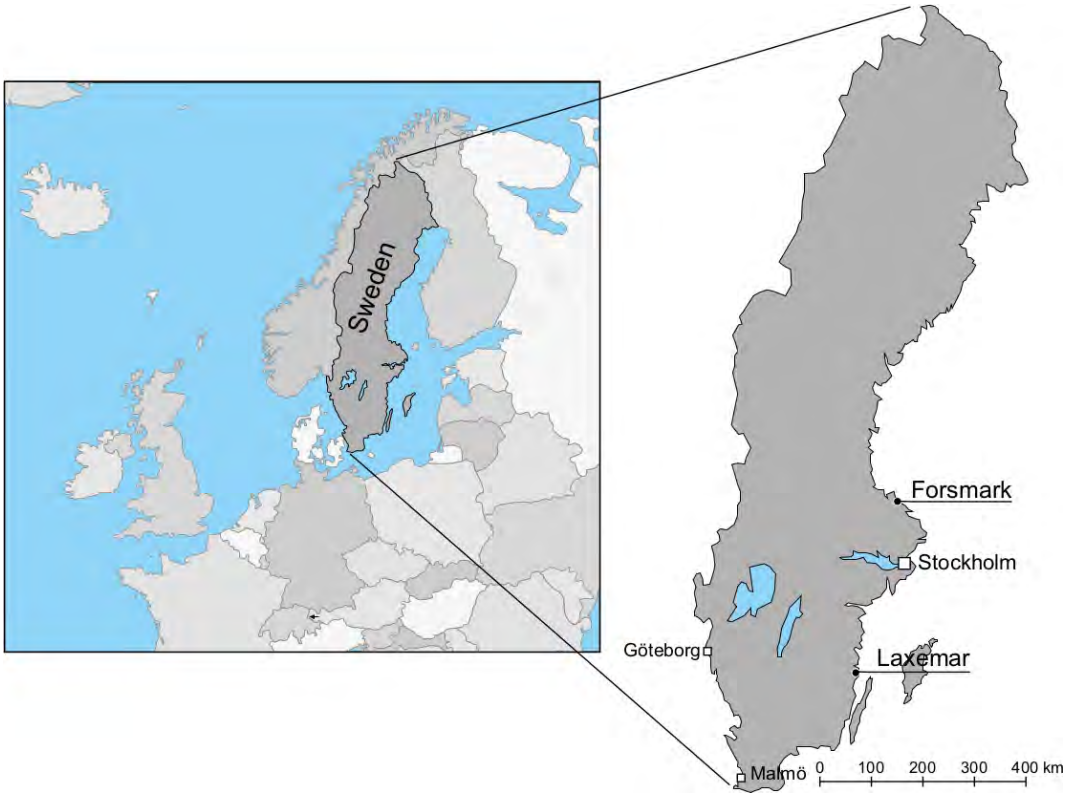

Figure 1. Location of the Laxemar and Forsmark sites in Sweden (from SKB TR-19-01).

1.1 Background

The SFL is one of three planned repositories in the Swedish system (Figure 2):

- A spent nuclear fuel (SNF) repository (currently in the licensing process for construction at Forsmark in northern Uppland) to handle reactor fuel rods which are the highest-level type of waste in terms of radioactivity;
- The SFR for short-lived, low- and intermediate-activity waste (currently in operation at Forsmark) to handle waste from reactor operations, such as protective clothing, certain reactor system components, and filters from cleaning reactor water, as well as certain types of medical and research waste.
- The SFL (an acronym of the Swedish name "Slutförvar för långlivat avfall") for long-lived, low- and intermediate-activity waste (still in the conceptual stage).

The SFL is intended to serve as a permanent disposal facility for long-lived low- and intermediate-level radioactive waste.

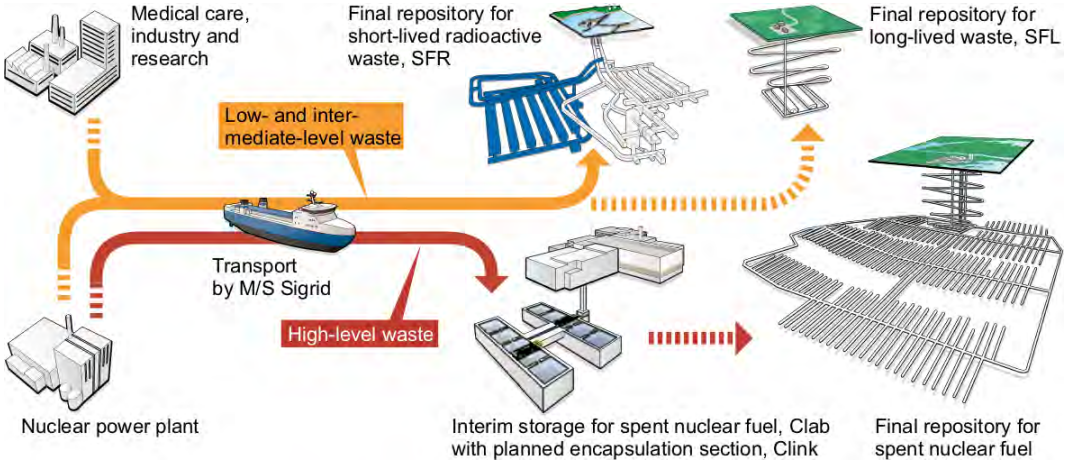

Figure 2. The planned system for radioactive waste disposal in Sweden (from SKB TR-19-01).

The concept presented by SKB (2019, SKB TR-19-01) is based on a repository located approximately 500 m underground in granitic rock, with two different disposal vaults:

- The BHK vault, with concrete encasing waste which consists of irradiated metallic components from nuclear power plants
- The BHA vault, with bentonite encasing waste which is of low activity but somewhat unknown material inventory, from a variety of sources including past medical, industrial and research programs.

Both vaults are planned as rectangular caverns with a nominal cross-section of 20 m × 20 m, with a length of 135 m for BHK and 170 m for BHA. The repository will also include a spiral access ramp for transport from the surface, and a vertical shaft for ventilation and personnel access. The access ramp and shaft will be closed off at the end of operation of the SFL around 2075 AD, using a combination of concrete plugs and bentonite to isolate the waste vaults, crushed rock in the middle section of the access ramp, and a combination of concrete seals and boulders at the top to deter future human intrusion.

The safety evaluation SE-SFL has been performed by SKB as a first evaluation of post-closure safety of this repository concept. This evaluation is not part of a license application, so technical review comments will serve in an advisory rather than formal regulatory context. As no location has been chosen for the repository, a former candidate site for the Swedish SNF repository, Laxemar, is used to demonstrate the concept.

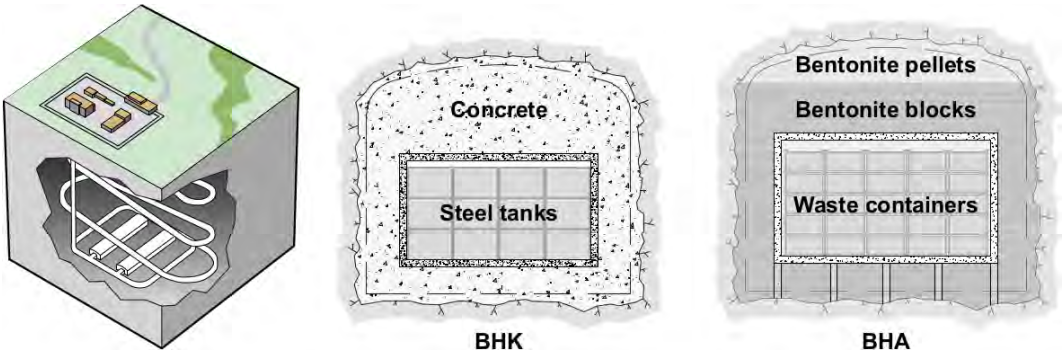

Figure 3. Schematic view of the SFL repository design (left) and cross sections of the BHK and BHA vaults (from SKB TR-19-01).

1.2 Scope of review

This review focuses on hydrogeological aspects of the SE-SFL safety evaluation, with emphasis on the **soundness of the conceptual models** and the **reasonableness of the modeling results** in light of the associated uncertainties. The key reports considered in this review are the main SE-SFL report (SKB TR-19-01 Chapters 4, 6, 7, and 8), the catchment- and facility-scale hydrogeological modeling report for temperate conditions (SKB R-19-02), and the near-field hydrogeological modeling for temperate conditions (SKB R-19-03).

The review assignment emphasizes review of hydrogeological modeling in the SE-SFL safety evaluation, specifically the choice of models and data for the evaluation, the suitability of SKB's arguments on the basis of assumptions made and supporting data, and handling of uncertainties. Hydrogeochemical aspects of the models presented in SKB R-19-02 are outside the required scope of the review. The methodology for the safety case as a whole (as presented in Chapters 2, 3, and 5 of the main SE-SFL report) and SKB's overall conclusions regarding the potential of the repository concept to fulfill regulatory requirements (as presented in Chapters 9 and 10 of the main SE-SFL report) are outside the mandate for this review. However, these aspects have been considered as context for judging which if any deficiencies in the hydrogeological modeling are most likely to be significant for the overall safety evaluation.

2. SKB’s presentation

This chapter summarizes the parts of SKB’s presentation that are relevant to the setup, application, and interpretation of results from the hydrogeological models. Section 2.1 summarizes the repository design concept in terms of specifications for the initial state of the repository components and descriptions of the surrounding geological and surface environment, which are considered as the starting point for analysis of the hydrogeological evolution. Section 2.2 summarizes the factors driving hydrogeological evolution, including external climate and sea level changes, as well as the long-term degradation of repository components, and outlines the main scenarios related to hydrogeology that SKB has considered. Section 2.3 summarizes the main hydrogeology-related scenarios considered in SKB’s evaluation of post-closure safety for the SFL concept. Finally, Section 2.4 describes the different hydrogeological models that have been used in support of SE-SFL.

2.1 Initial state

The initial state of the repository, defined as the expected state of the repository and its environs at the time of closure, is summarized in Chapter 4 of the Main Report (SKB 2019a) with further details presented in the Initial State Report (SKB 2019b). The brief summary here focuses on the main aspects that are relevant for hydrogeological evaluation.

2.1.1 BHK vault

In BHK the waste is initially enclosed in gasketed rectangular steel tanks (nominally 3.3 m by 1.3 m by 2.3 m high) with walls 5 to 20 cm thick (Figure 4), which will be effectively impermeable until breached by corrosion. The total volume of the waste packages is expected to be 6774 m^3 including an estimated 3100 m^3 void volume, of which 1200 m^3 is voids enclosed within the waste while the remaining 1900 m^3 is air space within the tanks.

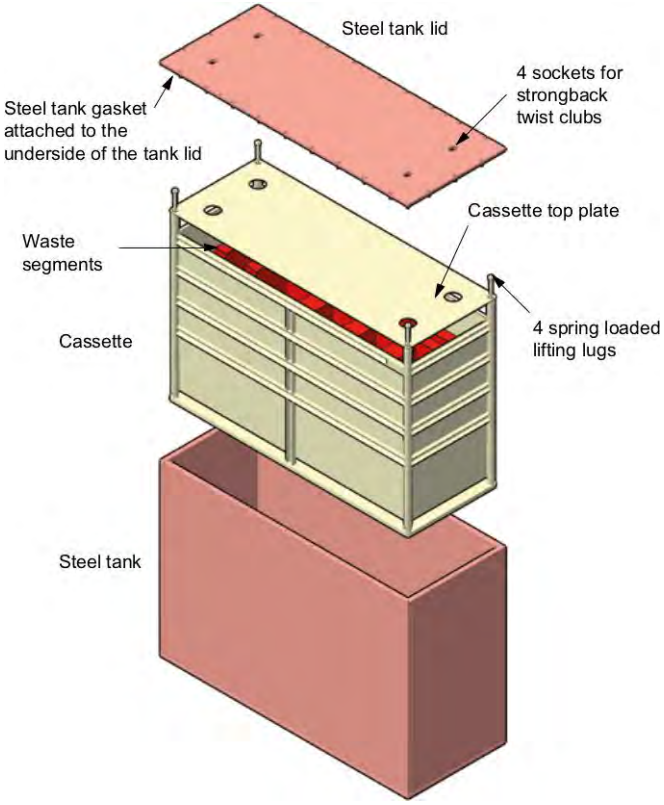

Figure 4. Schematic illustration of the steel tank used to package neutron-activated reactor components for storage in the BHK vault. From SKB TR-19-01.

These tanks are to be stacked inside a series of six precast concrete caissons in the BHK vault. The caissons have 0.5 m thick walls which will provide radiation shielding for on-going disposal operations in the vault. Each caisson is nominally 16 m long by 15 m wide by 8.4 m high, to allow stacking the tanks three high (see Figure 5).

Once a caisson has been stacked full of tanks, the void space between the tanks will be filled with cementitious grout, primarily to stabilize the stacked tanks and reduce void (also to provide mechanical support to resist external loads after closure, and to maintain alkaline chemistry to passivate the steel components to reduce corrosion rates). Then that section of the vault will be filled with concrete backfill to enclose the caisson as in Figure 5.

In simplified hydrogeological terms, the BHK vault at the time of closure will in effect be a large concrete-filled tunnel, with minor heterogeneity resulting from different types of concrete, and with nominally impermeable inclusions (the steel tanks). Although not explicitly stated in SKB TR-19-01 (nor shown in Figure 5), as a practical matter presumably the concrete floor below the caissons will need to be poured prior to placing and filling the caissons, so there will be a seam between this and the later concrete backfill. The possibility of void space at the concrete/bedrock interface, resulting either from imperfect backfilling or shrinkage of the concrete as it cures, is not discussed in either the main report (SKB, 2019a) or the related sections of the Initial State Report (SKB 2019b).

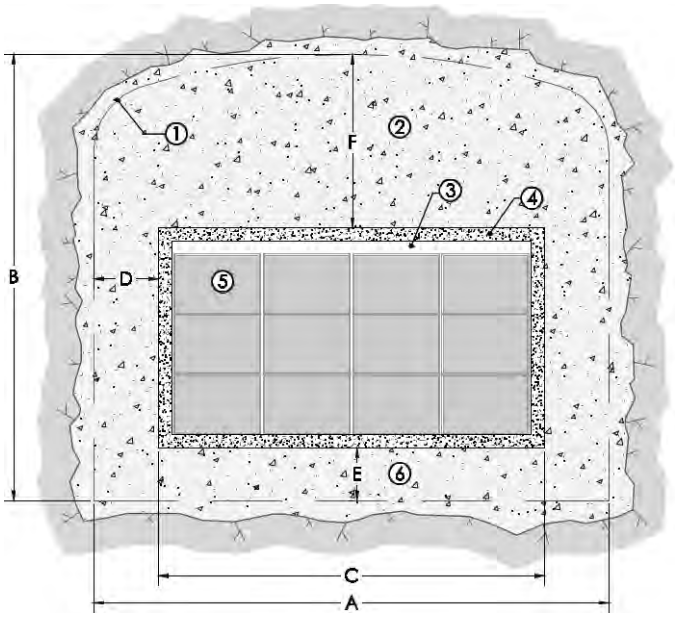

Figure 5. Schematic cross-section through a caisson in the BHK vault according to Elfwing et al. (2013). Numbers indicate (1) tunnel contour, (2) concrete backfill, (3) grouted void space inside caisson, (4) concrete caisson wall (0.5 m thick), (5) steel tanks, and (6) concrete below caisson. Nominal dimensions according to the design are A = 20.6 m, B – 19.6 m, C = 15 m, D = 2.8 m, E = 2.4 m, and F = 8.8 m.

2.1.2 BHA vault

In the BHA vault, waste is enclosed either in steel drums or steel/concrete molds which are placed in larger, open-top rectangular steel containers, with cementitious grout filling the interstices between drums/molds, and covering their tops (Figure 6). As for the BHK vault, the grout helps to stabilize the waste containers, fill the void space, provide mechanical strength to resist external forces during backfill and re-saturation of the repository, and contribute to high alkalinity in the vault and thus to the passivation of steel components to reduce the corrosion rate.

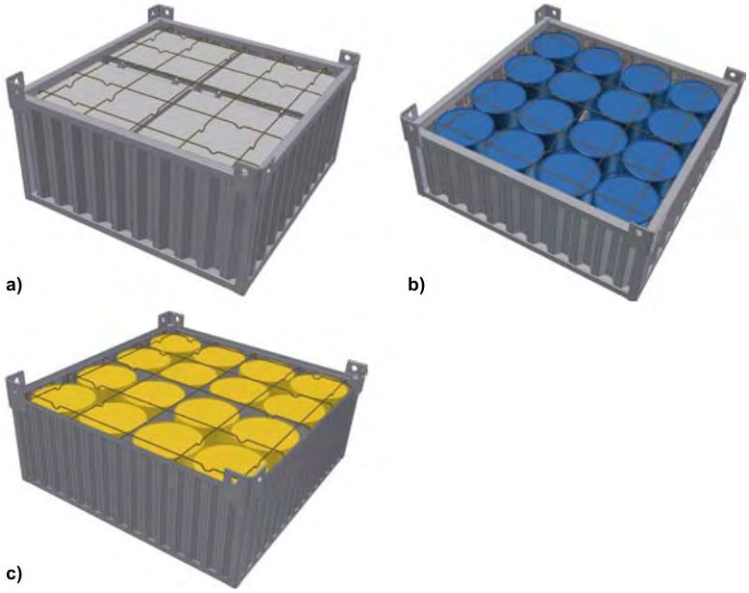

Figure 6. Schematic view of packing method for waste in the BHA vault, with welded steel containers enclosing (a) waste in standard molds, (b) waste in standard 200 L drums, and (c) waste in 280 L protection drums. The grid of lines over the top of the waste in each case represents steel reinforcement bars to stabilize cementitious grout that will be poured over the top of the waste molds or drums, up to the top of the outer container.

The BHA is backfilled with dry compacted swelling clay such as bentonite, rather than concrete (alternative materials with similar properties such as MX-80 clay may be considered). A single long concrete caisson, 16 m wide by 140 m long and 8.4 m high, is planned to provide radiation shielding during operation as well as an alkaline environment to further deter corrosion of steel components. This structure is constructed atop granite pillars which stand on the floor of the vault (Figure 7). After emplacement of the waste, empty voids between waste packages are grouted and a concrete lid is placed atop the structure.

At the time of closure, compacted bentonite blocks are placed beneath the base slab as well as on the sides and on top of the concrete structure. The top part of the vault is filled with bentonite pellets. The dry density of the bentonite upon emplacement is to be controlled to achieve a target hydraulic conductivity $K = 1\times10^{-13}$ m/s after saturation. This target value of K is expected to be sufficiently low that transport of radionuclides through the clay will be mainly by diffusion with negligible transport by advection.

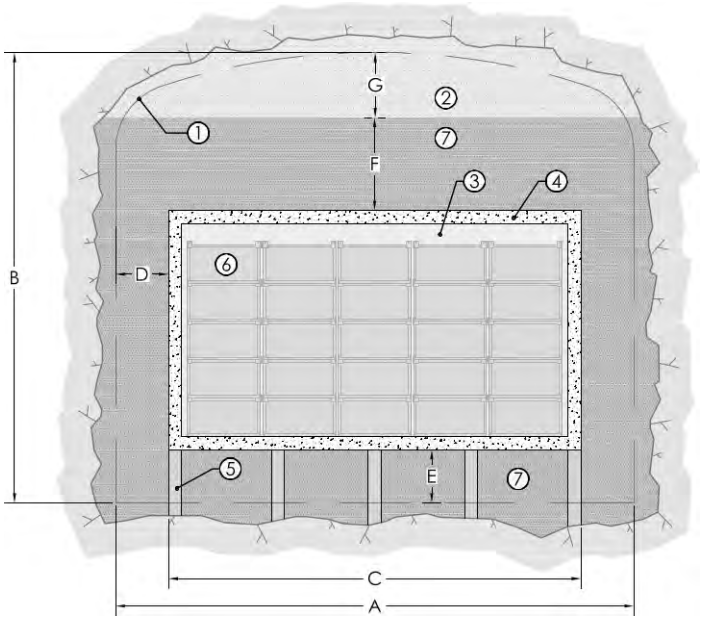

Figure 7. Schematic cross section through the BHA vault according to Elfwing et al. (2013). Numbers indicate (1) tunnel contour, (2) bentonite pellets placed as backfill in crowns space, (3) grouted void space inside caisson, (4) concrete caisson wall (0.5 m thick), (5) granite pillars, (6) waste packages, and (7) bentonite blocks. Nominal dimensions according to the design are A = 20.6 m, B – 18.5 m, C = 16 m, D = 2.3 m, E = 2.4 m, F = 4 m, and G = 3.7 m.

2.1.3 Closure components

The term "closure" in SKB's presentation refers to the methods for sealing the shaft and tunnels that are needed for construction and operation of the disposal facility. The closure components are intended to reduce water flow and potential transport via the tunnel components, to provide mechanical support to the rock to prevent tunnel collapse (which could open pathways for flow adjacent to the tunnels) and to deter future human intrusion.

The closure design for SFL is noted by SKB to be in a preliminary stage. It is described only briefly in two pages of text and figures in the Initial State Report (SKB 21019b) which are repeated verbatim in the Main Report (SKB 2019a).

The tunnel sections adjacent to the waste vaults (shaded blue in Figure 8) will be filled with bentonite of the same type used in the BHA vault, with mechanical plugs placed to confine the bentonite. Other tunnels at the repository level will be filled with crushed rock or similar material, with an assumed hydraulic conductivity of 10^{-5} m/s, porosity of 0.3, and effective diffusivity 6.0×10^{-10} m^2/s.

The spiral access tunnel will also be filled with crushed rock, except the uppermost 50 m section of access tunnel will be backfilled with boulders and a concrete plug to deter intrusion. A plug section with a hydraulically tight section of bentonite confined by cast

concrete is also planned somewhere along the access ramp; SKB (2019a,b) give a schematic cross section of the plug design but do not specify the position of the plug along the access tunnel.

The vertical shaft is planned to be sealed at the connections to the tunnels, using sections of bentonite confined by concrete plugs above and below each section. SKB (2019a,b) do not state what material will be used to backfill the remainder of the shaft. The blue shaded sections in Figure 8 suggest that the entire shaft will be sealed, but this seems to be contradicted by the text stating that only the connections to tunnels will be sealed.

SKB (2019a) note that any investigation boreholes would also need to be sealed, but these are not considered in the flow and transport modeling for SE-SFL.

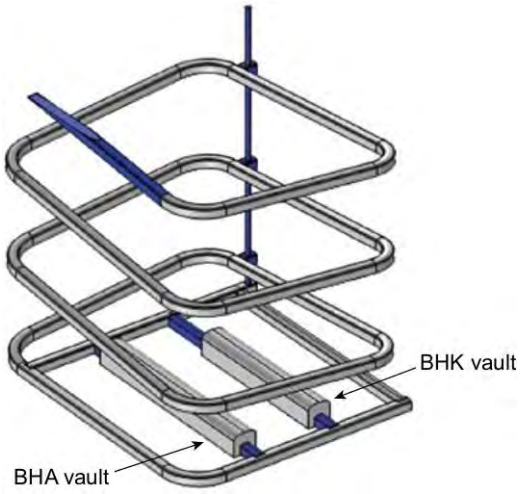

Figure 8. Locations of sealing sections (shaded in blue) to be installed at closure in the tunnel sections connecting between the vaults and the access tunnels, the vertical shaft and in the upper part of the access ramp.

2.1.4 Surface environment

For the main calculation case in SE-SFL, the surface climate at the time of closure in 2075 AD is assumed to be the same as the present-day climate at Laxemar, with a mean annual air temperature of +6.4 °C and annual precipitation of 553 mm. This is acknowledged by SKB (2019a) to be different from the most likely conditions, considering climate projections by the Intergovernmental Panel on Climate Change (IPCC) which take into account climate forcing by anthropogenic greenhouse gas emissions. The IPCC projections indicate an increase of about 3 to 4 °C in mean annual air temperature and a 20 to 30 % increase in annual precipitation by 2100 AD. Consequent changes in seasonality of precipitation and snow melt are not discussed but presumably would also be affected. Likewise the Baltic shoreline is assumed to be in its present-day position, neglecting eustatic sea level rise due to climate change, as well as the counteracting effect of post-glacial isostatic land rise (less than 2 cm over the past 20 years in the Laxemar area).

SKB (2019a) regard the use of present-day climate and shoreline position as having minor impact considering the preliminary nature of SE-SFL, but note that this complicates

comparisons with an alternative calculation case, the *increased greenhouse effect climate case* for the early post-closure period.

Brief descriptions of surface topography, regolith, limnic ecosystems, and near-surface hydrology are included based on the site-descriptive model from the prior investigations of Laxemar as a candidate site for a spent-fuel repository (SKB, 2009). Relief is limited with a maximum elevation about 50 m above the current Baltic sea level. The surface hydrologic system includes one lake (Frisksjön) with an area of 13 ha, three year-round streams and several ephemeral streams, most of which have been influenced by human agricultural activities.

The regolith is discontinuous with extensive bedrock exposures on the higher topography. Deposits in valleys are mainly of glacial origin, overlain by sand/gravel, clays, and gyttja (an organic-rich mud formed by decay of peat) and peats. Groundwater levels in the regolith are typically within 1 m of the ground surface, with a subdued correlation to topography (i.e. depths to the water table are typically greater in topographic highs) implying that near-surface patterns of groundwater recharge and discharge are strongly influenced by local topography.

2.1.5 Bedrock influences on hydrogeology

The bedrock geology at Laxemar is summarized in Section 4.6 of SKB (2019a), as part of the description of the initial state, with reference to the site descriptive model (SKB 2009) and the background description of bedrock geology (Wahlgren et al., 2008).

Lithology

The bedrock at Laxemar is dominated by crystalline rock of dioritic to granitic composition, formed as a series of igneous intrusions along an active continental margin during the Svecokarelian orogeny margin around 1.8 Ga ago (Wahlgren et al., 2008). A subsequent igneous intrusive episode around 1.45 Ga ago formed plutons within 15 km of Laxemar (the Götemar granite northwest of Laxemar and the Uthammar granite to the south); these younger granites are not found within the Laxemar site but localized fine-grained granite dikes at Laxemar may be related to the same magma source. The youngest magmatic rocks in the region are scattered dolerite (diabase) dykes, considered to be related to a regional system of N-S trending, ca. 1.0 – 0.9 Ga old dolerites that are found from Blekinge in southeastern Sweden to Dalarna in central Sweden.

Within the Laxemar site, the near-surface bedrock is dominated by granite and quartz monzodiorite (Figure 9). For SE-SFL, the position of the repository is chosen to lie mainly in the rock type referred to as Ävrö granite, but the southwestern part is within Ävrö quartz monzodiorite with significant content of diorite and gabbro.

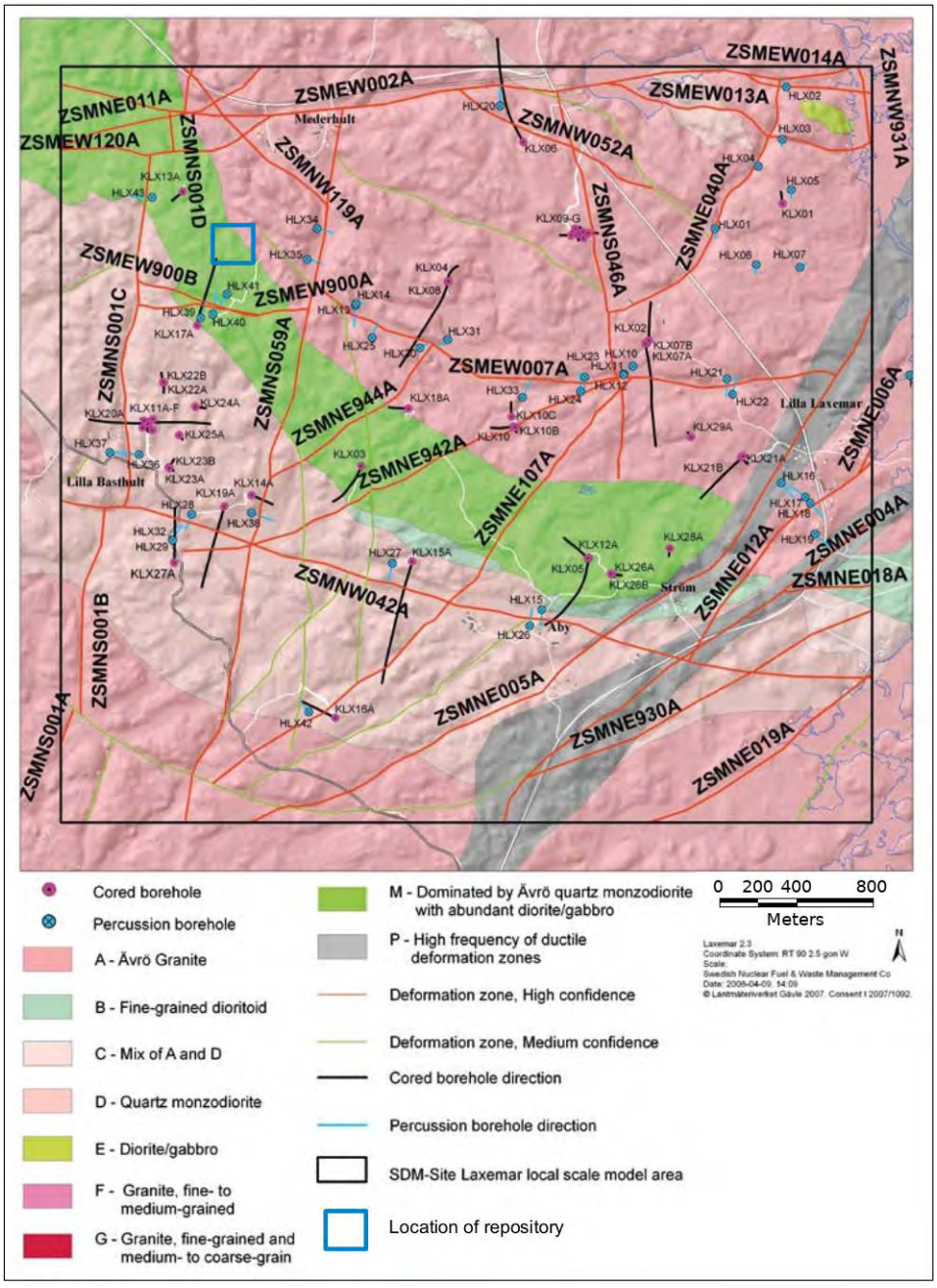

Figure 9. Overview of the lithology, deformation zones, and rock domains modeled deterministically in the Laxemar local model area (Wahlgren et al., 2008). The position chosen for the repository in SE-SFL is shown as a blue square. Note that the lithological boundaries shown at the surface may incline with depth.

Deformation zones

Since emplacement these rocks have been subjected to a complex series of tectonic regimes. Early on, when the rocks now found near surface were still deep in the crust, deformation tended to be as ductile strain, including regional-scale belts of high ductile

strain. Faulting during later deformations, after uplift and erosion left these rocks at shallower depths, was often by brittle reactivation of the ductile precursors (Wahlgren et al., 2008). The resulting system of brittle fault zones, referred to as deformation zones in SKB's local nomenclature, is characterized by a regional-scale pattern of anastomosing deformation zones with less-deformed blocks, referred to as "tectonic lenses," in between.

The Laxemar site is considered to lie within the northwestern part of such a tectonic lens, bordered to the north by the regional deformation zone labeled ZSMEW002A in Figure 9. The position chosen for the hypothetical repository in SE-SFL is also within the interior of a block bounded by local-scale deformation zones (shown as red lines in the figure). According to the site descriptive model (SKB, 2009), deformation zones with length scales of 1 km or larger are considered to be deterministically characterized by the site investigation program.

Hydraulic properties (hydraulic conductivity and thicknesses) of these deformation zones were assigned based on depth-dependent trends that were fitted to borehole estimates for each class of deformation zones with similar orientation (Figure 10). Details of this analysis and supporting data are presented by Rhén and Hartley (2009).

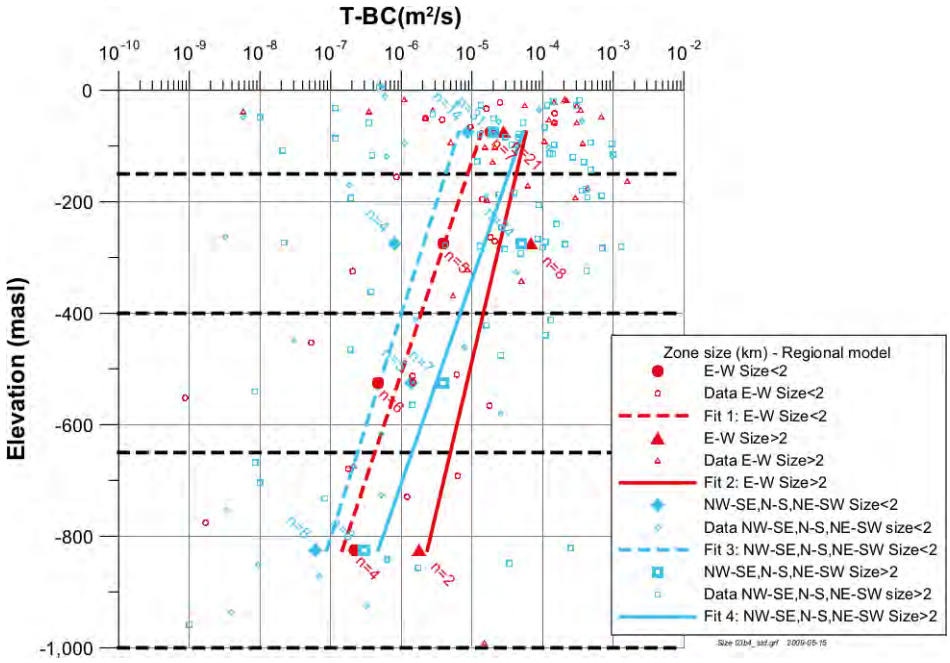

Figure 10. Deformation zone transmissivity (*T*) related to deformation zone orientation (strike direction) and size, versus elevation. The plotted values of transmissivities are interpreted as the best choice (T-BC) of the transmissivities evaluated from the available transient hydraulic test data. The larger symbols show geometric mean values of *T*. Fitted regression lines are labeled with the number of observations (*n*) for each class (based on Figure 5-3 of Rhén and Hartley, 2009).

Statistical description of rock mass fractures

The portion of the bedrock outside of the deterministic deformation zones is referred to as the *rock mass*, in SKB's nomenclature. Brittle faults and joints within the rock mass, on

length scales smaller than 1 km, are described in statistical terms as a discrete-fracture network (DFN) model.

The main basis for hydrogeological modeling of this rock mass, in SE-SFL, is a hydrogeological DFN model developed by Rhén and Hartley (2009) and elaborated by Joyce et al. (2010). The model is interpreted as representing only fractures that are at least partly open for flow (i.e. not including fractures that are sealed by fracture minerals and hence effectively impermeable).

The model is defined in terms of four *rock mass domains* as shown in Figure 11. Each of these domains is further divided into four *depth zones*:

DZ1: z = −150 to 0 m.a.s.l.
DZ2: z = −400 to −150 m.a.s.l.
DZ3: z = −650 to −450 m.a.s.l.
DZ4: z = −1000 to −6500 m.a.s.l.

where *z* is the elevation in meters above sea level (m.a.s.l.). This means that the model consists of a total of 16 subdomains, each for a different depth zone and rock mass domain.

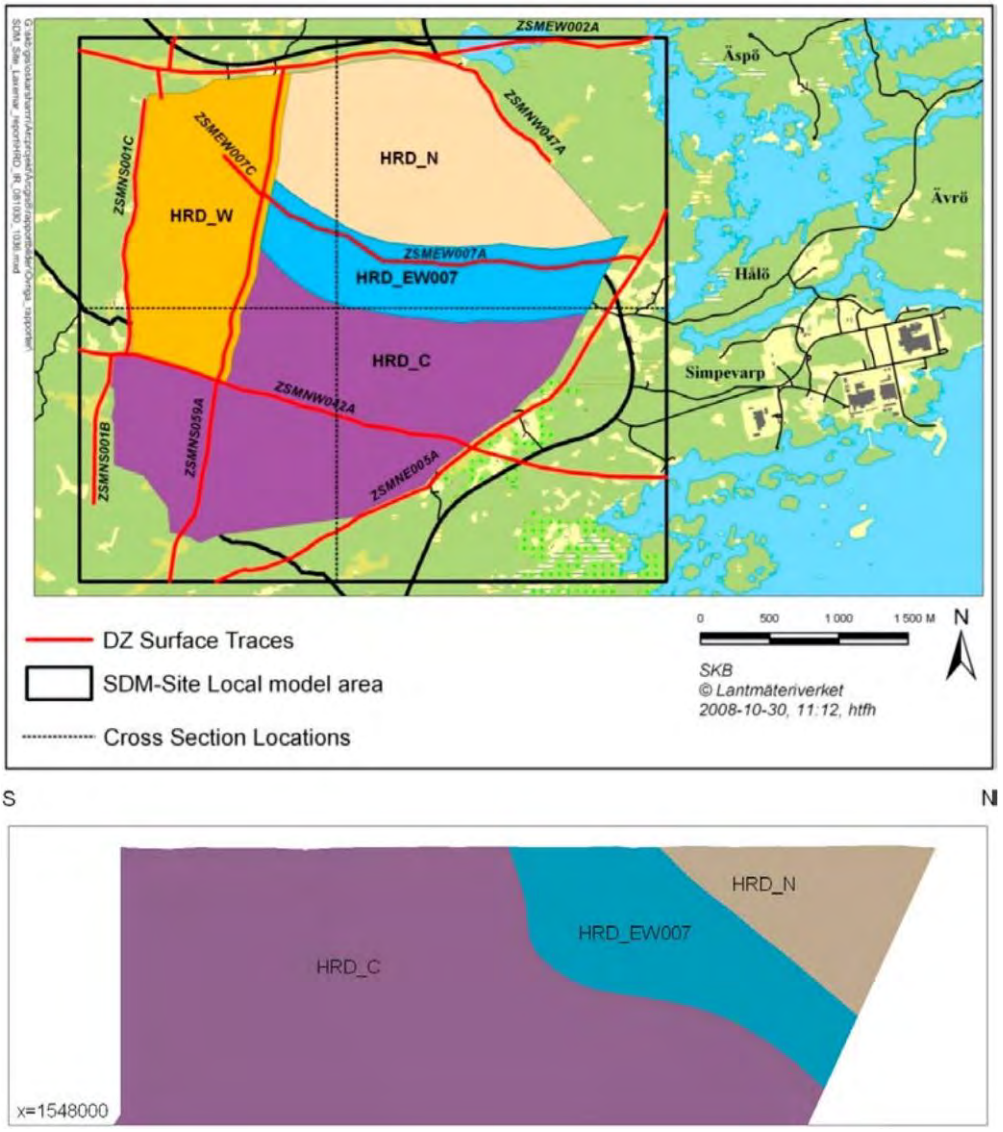

Figure 11. Rock mass domain model for Laxemar as defined by Rhén and Hartley (2009; Figures 3-4 and 3-5). Top: Plan view. Bottom: Vertical cross section from south (left) to north (right) at Easting X = 154 800 m. The area labeled as "SDM-Site Local model area" is the same as the "facility-focused model area" for SE-SFL as modeled by Joyce et al., (2019).

Within each of these subdomains, the DFN model is described in terms of multiple fracture sets, each of which is parameterized in terms of the following properties:

- fracture intensity P_{32} (total area of open fractures per unit volume of the domain),
- fracture orientation, treated as a probability distribution for fracture poles or normal vectors $\boldsymbol{n}$, assumed to be of spherical von Mises-Fisher form: $f(n) = \kappa exp\,(\bar{n}^T n)/(4\pi sinh\kappa)$
  where κ is the Fisher concentration parameter and $\bar{n}$ is the mean fracture pole (usually expressed in geological terms as trend and plunge);

- fracture radius r (assuming disc-shaped fractures), treated as a probability distribution of power-law (Pareto) form: $f(r) = k_r r_0^{k_r} / r^{k_r+1}$ where r_0 and k_r are fitted parameters;
- fracture transmissivity T, considered to be related to the fracture radius by a log-linear correlation with a random term: $log(T) = log(ar^b) + \sigma_{logT} N[0,1]$ where a and b are the offset and slope of the fitted correlation line in log space, $\sigma_{log\ T}$ is the standard deviation of log T about this line, and $N[0,1]$ is a random variate drawn from the unit normal distribution; and
- fracture transport aperture e_t (the mobile-water volume per unit area of each fracture plane), which effectively determines the ratio between groundwater flux and advective velocity in a given fracture.

The log-linear correlation model for T as a function of r is referred to as a "semi-correlated" model in SKB's nomenclature, to distinguish from an alternative, perfectly correlated model (with no random noise term).

Values of P_{32}, the mean pole (expressed as trend and plunge) and the other parameters κ, r_0, k_r, a, b, and $\sigma_{log\ T}$, for each fracture set in each subdomain, are listed in Tables 3-2 through 3-5 of Joyce et al. (2019).

The statistical model for fracture transport aperture e_t is not specified by Joyce et al. (2019). Based on the previous presentation of the Laxemar DFN model by Joyce et al. (2010), this is presumably treated as a log-linear function of T such that $e_t \propto T^{1/c}$, either according to the theoretical cubic law for Poiseuille flow between parallel plates, which implies $c = 3$, or an empirical relationship with $2 \leq c \leq 3$. This gap in SKB's documentation could not be resolved either from the SE-SFL reports or from background reports. In the independent calculations described in Section 4.2 of this review, several alternative models listed by Rhén et al. (2008) were tested to check the effects on flow-related performance parameters.

For the purposes of SE-SFL, this statistical description of hydraulically conductive fractures in the rock mass, together with the hydrogeological description of the deterministic deformation zones, is used as the basis for deriving effective hydrogeologic properties for the bedrock for the hydrogeological modeling by Joyce et al. (2019) and Abarca et al. (2019).

Effects of excavation on the bedrock around vaults and tunnels

Effects of repository excavation on the bedrock are not discussed in the presentation of the initial state by SKB (2019a), but the likelihood of an excavation-damaged zone is acknowledged in later discussion of repository evolution for the climate base case (Section 6.2.4). The effects of excavation damage have not been studied in SE-SFL. SKB (2019a) note that this is likely to be highly dependent on the site-specific rock mechanical properties and state of stress, as well as the detailed excavation methods used.

2.1.6 Groundwater types and distribution

Details of hydrogeochemistry were outside the scope of this review, but the initial distribution of groundwater types, particularly with regard to contrasts in groundwater salinity and density, is relevant for considering potential effects of density-dependent flow in the hydrogeological modeling. Groundwater types present at Laxemar include at least four end-member waters:

- fresh water of recent meteoric origin, mainly at shallow depths of 200 m or less and,
- older dilute water thought to represent relict glacial meltwater, mainly in lower-permeability portions of the rock at depths of 300 m to 600 m.
- older, more saline waters thought to derive from the Littorina Sea, and
- highly saline brines with Cl^- concentrations up to 1100 mg/L, thought to be very old water affected by rock-water interactions, found at depths of 900 m or more.

Below low-lying areas that were only uplifted above sea level in recent millennia, relict waters of recent Baltic origin may also be present in the shallow bedrock. Compositions intermediate to these end members, in terms of conservative ions and isotope ratios, are also encountered due to mixing.

2.2 Evolution of the repository

Evolution of the repository and its environs over the analysis period of 1 Ma after closure has been analyzed based on consideration of three hypothetical, idealized climate situations which are introduced in Section 2.5.7 of the main SE-SFL report, and analyzed in Chapter 6:

- *Base variant*: climate conditions are assumed to be identical to present-day conditions over the entire 1 Ma period; ongoing shoreline regression continues for the first 40 ka.
- *Increased greenhouse effect variant*: the future climate is affected by anthropogenic activities resulting in warmer-than-present-day conditions for the first 23 ka after closure, followed by a reversion to present-day climate; the warming climate is accompanied by short-term sea-level rise which is eventually offset by land rise.
- *Simplified glacial cycle variant*: future climate follows a reconstruction of the last glacial cycle with periods of temperate climate, periglacial conditions with permafrost, ice-sheet development and corresponding variations in sea level.

SKB (2019a) acknowledges that the first two of these variants are stylized rather than realistic scenarios, as the climate is expected to vary with continued warming in the near future before reversion to periglacial and glacial conditions. The analysis of these idealized situations is aimed to build understanding of the key factors affecting long-term repository safety rather than to predict the most likely outcome.

2.2.1 Base variant of the reference evolution

The presentation of the reference evolution for the base variant by SKB (2019a) includes a detailed discussion of evolution of the waste, the waste containers, and the engineered barriers, including aspects affecting the release of radionuclides as well as transport and retention within the containers and engineered barriers. For the purpose of this review, focus is limited to aspects of the evolution that are likely to influence the hydrogeology and are hence relevant for review of the hydrogeological modeling.

Evolution of external conditions

Shoreline regression due to ongoing land rise during the first 40 ka of the base variant, in the absence of any effects due to climate change, leaves the Laxemar site approximately 30 m higher above sea level. Areas still under sheltered inlets of the present-day Baltic are expected to accumulate sediments and undergo succession first to wetland, then terrestrial vegetation.

The main SE-SFL report section on regional hydrogeological conditions for the base variant (SKB 2019a Section 6.2.5) includes very little conceptual discussion of the effects of

site evolution on the development of the groundwater flow system. Instead it gives a condensed summary of the set-up for catchment-scale and facility-scale numerical models by Joyce et al. (2019), which will be described in Section 2.4 of the present review. Those numerical models do represent land rise and shoreline regression as time-dependent boundary conditions, and thus implicitly account for the shift toward a more terrestrial hydrogeological system with increasing influence of meteoric infiltration, and potentially longer discharge paths to the receding shoreline.

Evolution of the excavations for the waste vaults

Thermal and mechanical evolution of the vaults are discussed only briefly in SKB (2019a, Sections 6.2.3 and 6.2.4, respectively). According to Section 6.2.8 which discusses evolution of the waste, some heat generation from radioactive decay in the waste is expected. However during the first 500 years the volume-averaged temperature increase due to this heat source is at most about 1 °C for the BHK waste and less in the concrete backfill, decreasing to less than 0.2 °C after the first 500 years. The increase in temperature in the bentonite backfill of BHA is expected to be less than 0.1 °C. These minor temperature changes are expected to have negligible effect on the surrounding bedrock.

The current preliminary design for the SFL concept does not discuss which if any types of rock reinforcement methods such as rock bolts or shotcrete could be used to stabilize the excavation during the operational period, or what the design life of those components would be. SKB comment that the rock mechanical properties are strongly site-dependent, so a more specific analysis of rock mechanical evolution is not judged meaningful until a specific site is chosen.

Evolution of the engineered barriers in the BHK vault

The main engineered barrier in the BHK vault, concrete, is a brittle material subject to fracturing under load, and also subject to chemical leaching which could increase its porosity and hydraulic conductivity.

Rock mechanics modeling indicates that the concrete backfill in the BHK would only receive significant mechanical load from the bedrock if the surrounding rock has unrealistically low stiffness (i.e. Young's modulus of 25 GPa or less). Thus the hydraulic properties of the BHK are not expected to be significantly affected by mechanical loading from the bedrock, according to the analysis as summarized in SKB (2019a). This modeling work has not been examined in the course of the present review, but from the description in the Main Report it appears to have been an elastic analysis, which would not have taken into account inelastic deformation such as rock block failures due to degradation of rock support systems after closure.

Degradation of the concrete by groundwater leaching has been treated by Idiart et al. (2019) as summarized in Section 6.2.10 of SKB (2019a). Groundwater infiltrating the BHK backfill is expected to have pH just above neutral, which is sufficient to dissolve portlandite and eventually decalcify other phases in the concrete. Model results indicate

that these leaching processes could lead to a doubling of the initial concrete porosity (from an initial value of 0.11 to 0.22), to a depth of 0.1 m after 100 ka and to a depth of 0.8 m after 500 ka. The leaching is expected to be most aggressive at the point of inflow where the water is at its lowest pH, and least aggressive on the outflow side.

Evolution of the engineered barriers in the BHA vault

The main engineered barrier in the BHA vault, the bentonite backfill, is initially unsaturated and will resaturate at a rate controlled by inflow of groundwater, until it eventually reaches its design state.

The role of the bedrock portion of the groundwater flow system in controlling this process has been modeled by Abarca et al. (2019), treating the bentonite as an unsaturated porous medium as summarized in 2.4.5 of this review. The calculated time for resaturation ranges from 1.6 ka to 15 ka, depending on an *ad hoc* conductance term that is used to describe the coupling between the saturated portion of the bedrock and the bentonite, via an unsaturated fringe in the fractured bedrock.

During the time before the bentonite is fully saturated, uneven local saturation could lead to inhomogeneous swelling, SKB (2019a, Section 6.2.9). Local piping and erosion of the bentonite could also occur where inflow from high-transmissivity fractures is sufficient to overcome the initially low shear strength of the bentonite as it forms a gel at the wetted interface, before it absorbs enough water to develop higher swelling pressure. Scoping calculations in Appendix 1 of SKB (2019a) indicate that the loss of bentonite from this process is unlikely to be greater than about 0.01% of the total backfill volume. On this basis, significant loss of eventual sealing properties by the bentonite by this mechanism is regarded as unlikely.

The bentonite could act as a source of colloids to be released into the groundwater, particularly if groundwater with very low salinity should reach the BHA vault, allowing release of colloid-sized smectite particles. This could be possible after a prolonged temperate period (as considered in the base case) or during future glaciations (as considered in the simplified glacial variant). No quantitative assessment of potential colloid release from the BHA backfill has been made for SE-SFL, nor has the associated risk of colloid-assisted radionuclide transport been evaluated. SKB (2019a) note that this topic should be addressed further in future safety assessments for this concept.

2.2.2 Increased greenhouse effect variant

The increased greenhouse effect variant considers a warmer and wetter climate due to the combined effects of anthropogenic greenhouse gases and natural climate variation. SKB's analysis considers a stylized situation in which the warmer, wetter climate predicted for the IPCC intermediate-emissions scenario RCP4.5 is in effect at the time of closure and persist for 23 ka, after which the climate reverts to present-day temperatures and precipitation. More pronounced changes in temperature and precipitation (including the possibil-

ity for either higher or lower annual precipitation) could result from higher-emissions scenarios such as the IPCC's scenario RCP8.5, which may be more realistic considering the limited progress to date on curbing global greenhouse emissions; however such cases have not been considered in SE-SFL.

The initial time period includes a rise in sea level concordant with the regional sea-level effects for the RCP4.5 scenario. This affects the local coastline and base level for groundwater discharge, but is not sufficient to submerge the area above the SFL. Ongoing land uplift continues for 40 ka, as for the base variant, eventually offsetting and surpassing the effect of this initial rise in sea level.

SKB (2019a, Section 6.3.1) note that this is not a realistic scenario as the effects of human greenhouse gas emissions on air temperatures are expected to peak around 3000 AD, and then decline. This variant may have a lower maximum temperature than a more realistic scenario, but it extends this warm period over a longer period of time, and with a longer continuing temperate period for continuing infiltration of meteoric water, compared with a more realistic scenario of resumed glaciation cycles.

The main impacts of this variant on hydrogeology are (1) the increased precipitation combined with possible changes in seasonality of infiltration, and (2) potential for increased demand on surface and groundwater resources for irrigation, in a future warmer climate, despite the increase in annual precipitation.

The potential increase in demand for water stems from several factors that are recognized in SKB's assessment. Warmer temperatures imply both a longer growing season and higher rates of evapotranspiration by crops that are currently grown in the area (shifts to new crops made possible by a longer growing season were not considered). A predicted shift in the balance of monthly precipitation from summer to winter season means that less runoff may be available during the growing season. Warmer winter temperatures also mean that less winter precipitation is retained as snow cover. These circumstances may increase the likelihood of scenarios involving groundwater extraction that could enhance transport of radionuclides from the repository to the surface, by increasing groundwater flow through the repository. In extreme cases where a future climate leads to high rates of groundwater extraction sufficient to depress the water table over a large area, the possibility for reactivation of faults in an altered stress field could also arise as a possibility for consideration in a full safety assessment.

2.2.3 Simplified glacial cycle variant

The simplified glacial cycle variant is evaluated to address the potential effect of future cold-climate conditions, including permafrost and advance of a continental ice sheet over the repository. This variant is based on a reference glacial cycle scenario that was developed for SR-Can, a preliminary safety analysis for a hypothetical spent-nuclear-fuel repository at Laxemar (SKB 2006a). In SE-SFL, the evolution for the 100 000 year period starting in 2000 AD is repeated ten times to represent the effects of repeated Late Quaternary glacial–interglacial cycles during a one million year period after closure.

The conditions assumed for this variant are depicted in Figures 12 and 13. In this variant, the area immediately above the repository remains submerged for about 3000 years following deglaciation. Biosphere object 206, which is predicted to receive most of the discharge from the repository, remains submerged for another 5000 years. The variations in annual mean air temperature over each 100 000 year cycle (Figure 13) are treated simplistically as a series of step changes.

Periglacial conditions with permafrost are assumed to develop during periods when the mean annual air temperature drops below 0 °C. One periglacial period occurs about 17 000 years into this cycle but is followed by a return to temperate climate before the onset of a second periglacial period at around 50 000 years, which is followed by glaciation.

The maximum permafrost depth, based on previous thermal modeling for SR-Can (SKB, 2006b) is about 160 m for Laxemar. This is well above the proposed repository depth of 500 m, so based on those previous modeling results, the waste vaults should not be affected by freezing of pore water, though evaluation of previous thermal modeling is outside the scope of this review. Backfill and seals in the shallower parts of the shaft and access ramp could be affected by permafrost development to the stated depth of 160 m.

Glaciation and deglaciation impact the state of stress around the repository, both due to the load imposed by ice sheets that could exceed 2 km in thickness over the repository, and flexure of the Earth's lithosphere as the ice sheet advances and retreats. Changes in the magnitudes and directions of principal stresses, along with glacially induced pore pressures, could lead to changes in fracture transmissivity, as well as possible extension of fractures by hydraulic jacking or reactivation as faults. These processes have not been studied directly in SE-SFL but are noted (SKB 2019a, p.122) as processes that will need quantitative analysis in future safety analyses.

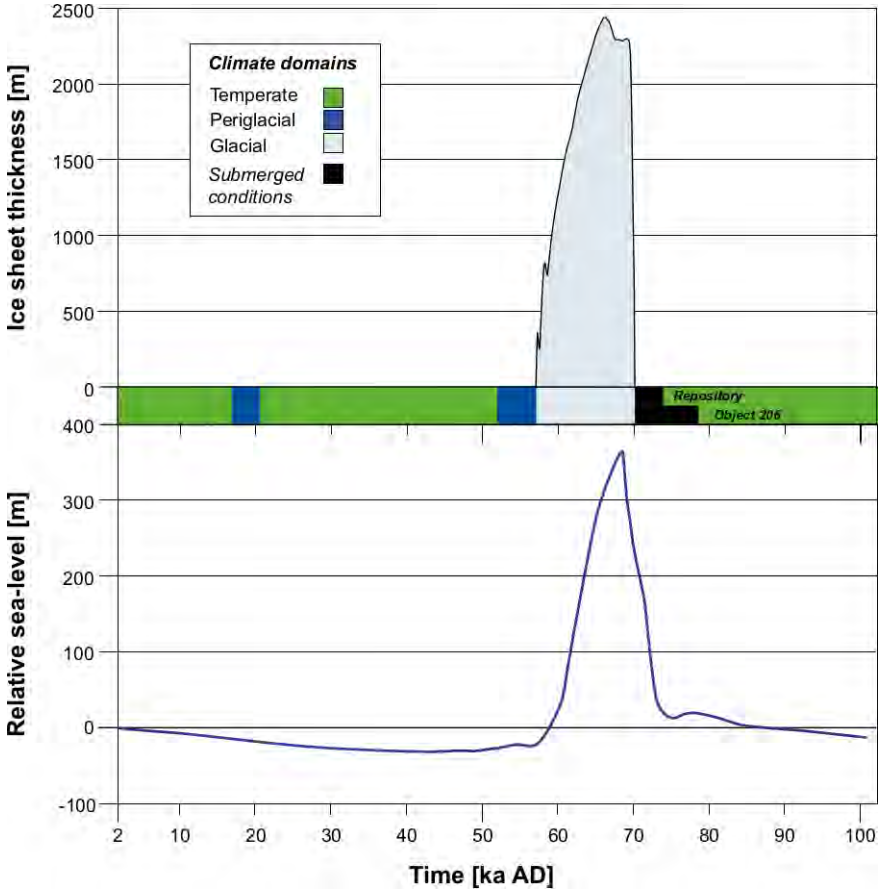

Figure 12. Evolution of climate and climate-related conditions for a simplified glacial-cycle climate case for Laxemar, extending 100 000 years into the future. The upper panel depicts the series of climate domains including two periglacial periods with permafrost development, and a glacial period with ice-sheet thickness increasing during glacial advance, then decreasing during glacial retreat. a glacial period following the second periglacial period. The lower panel shows the evolution of relative sea-level (with zero representing the present-day position). The periods of submergence, after glacial retreat, for the repository location and biosphere object 206 (which is indicated to receive most of the groundwater discharge from the repository), are shown as black bars in the upper panel. Reproduced from Figure 4-3 in the Climate report (SKB, 2019c). The width of the colored band in the upper panel (from 0 to −400 m) is purely for illustrative purposes and has no physical significance.

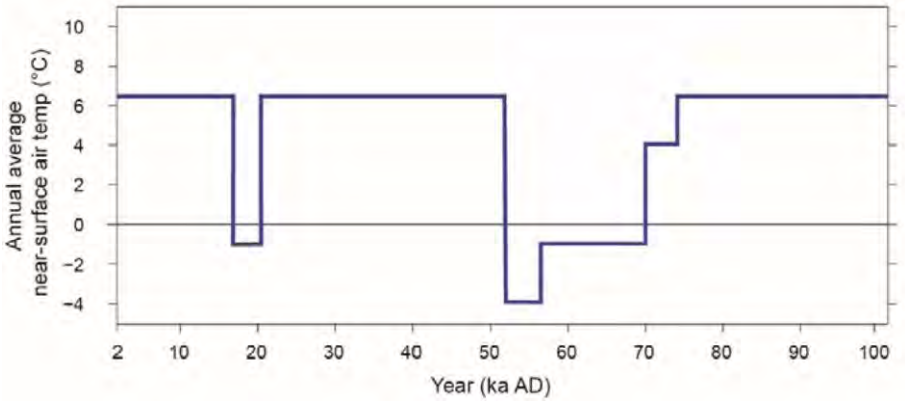

Figure 13 Evolution of annual average air temperature for the area above the hypothetical SFL at Laxemar for the simplified glacial-cycle climate case, extending 100 000 years into the future. Reproduced from Figure 4-4 in the Climate report (SKB, 2019c).

Earthquakes are acknowledged as a possibility, particularly in the early post-glacial period when the vertical compressive stress is reduced but horizontal stresses remain high, leading to potential for reverse (thrust) faulting. This possibility has not been quantitatively evaluated in SE-SFL due to the limited objectives for the current stage of evaluation for this repository concept, but an analysis should be expected as part of a full safety assessment in support of license application.

The hydrogeological evolution over a simplified glacial cycle is discussed in Sections 6.4.5 and 6.4.6 of SKB (2019a). For temperate periods, hydrogeological conditions are expected to be similar to those considered in the base variant, as modeled by Joyce et al. (2019) and discussed in Section 2.4 of this review. For periglacial, glacial and submerged conditions, no new hydrogeological analysis is presented; SKB (2019a) refer instead to the results of earlier modeling by Vidstrand et al. (2010) and related work.

During periglacial periods, permafrost is expected to strongly affect groundwater circulation by preventing recharge over most of the land surface, while focusing discharge into a few taliks (areas of unfrozen ground maintained by up welling groundwater from depth). SKB (2019a) note that taliks could be areas where humans are exposed to radionuclides during periglacial periods, due to the tendency for human settlement to occur along lakes and streams. However they note that radiation dose could be limited by the low food productivity in permafrost regions, requiring food to be gathered over large areas even for small communities. Permafrost growth may also lead to elevated salinity in liquid water inclusions in the permafrost and in water just below the base of the permafrost, due to salt freezing out from the pore water as it freezes (brine rejection). This process was found to be of only minor importance for conditions at the Forsmark site (Hartikainen et al., 2010), so it is judged also to be inconsequential for Laxemar.

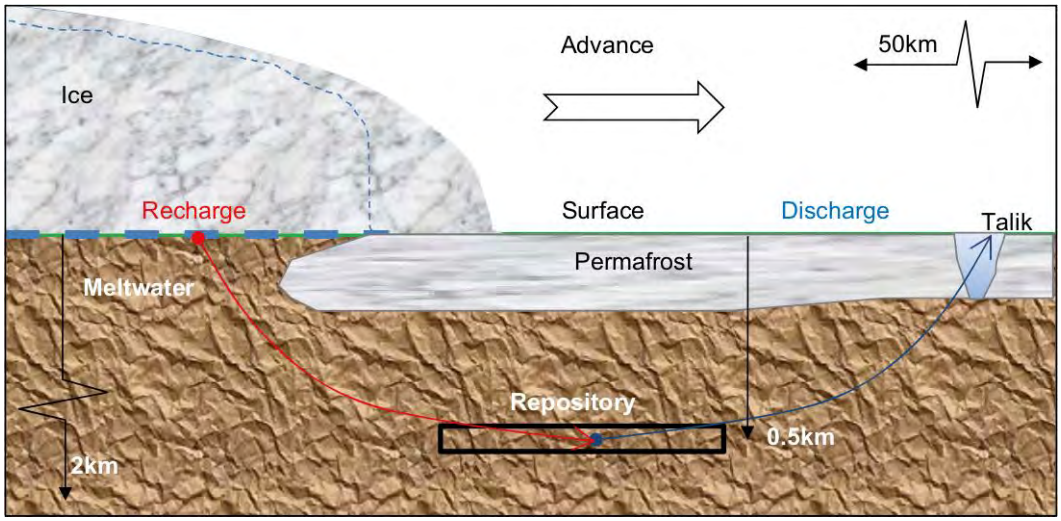

Figure 14 Conceptual illustration of the hydrogeology around a hypothetical repository ahead of an advancing ice sheet margin, with permafrost and taliks in the periglacial area ahead of the glacier. The elevation of the meltwater surface within the ice sheet is shown with a dashed blue line. Adapted from Figure 6-23 of SKB (2019a).

For the quantitative analyses in SE-SFL, the groundwater flow *pattern* derived from calculations by Joyce et al. (2019) for conditions in 2000 AD is assumed to persist for all stages of the simplified glacial cycle variant, but the flow magnitudes vary with shoreline displacement, bedrock freezing, and ice-sheet advance or retreat (SKB 2019a, p. 122). The maximum flow is assumed to occur when an advancing ice front is directly above the repository (as depicted in Figure 14).

The lengths of travel paths through the bedrock also vary with ice-sheet advance and retreat. Longer paths are stated to be assumed for an advancing ice sheet, due to the assumption that discharge is hindered by permafrost, and focused into taliks at some distance from the ice front. How this statement can be reconciled with the preceding statement, that a single flow pattern persists, is not clear from the brief presentation in Section 6.4.5 (SKB 2019a, p. 122). In the presentation of radionuclide transport calculations for this case in Section 8.6.2 (SKB 2019a, p. 180), a seemingly contradictory statement is given:

> *"The changes in the external conditions in this evaluation case are assumed to influence the rate of groundwater flow in the repository and the geosphere, but to have no effect on the pattern of the flow field and thus the length of the flow pathways."*

Glacial ice sheet advance and retreat are also expected to bring changes in salinity, due to upconing of deep groundwater ahead of the advancing or retreating ice front. Modeling of this effect by Gimeno et al. (2019) based on the results of Vidstrand et al. (2010) indicates that the periods of elevated salinity at repository depth are limited to relatively brief periods when the position of the ice front is very close to the repository. After the ice front passes, the salinity decreases due to the constant infiltration of dilute glacial melt waters. High salinity occurs again at the end of glaciation, as the ice front retreats back over the repository. A relatively fast turnover of groundwater is expected following glacial retreat, as glacial melt water is replaced by a succession of waters penetrating from

the surface, equivalent to the evolution of the saline Littorina Sea into the brackish Baltic Sea.

2.3 Evaluation of post-closure safety

A limited set of evaluation cases were selected for evaluation of post-closure safety. These consist of a *present-day evaluation case* plus fourteen additional evaluation cases as summarized in Figure 15. The key assumptions of these additional evaluation cases are summarized in Table 8-1 and described briefly in the remainder of Chapter 8 of SKB (2019a).

In this review, only evaluation cases that derive from changes in surface hydrology or bedrock hydrogeology are examined, leaving aside the cases that represent changes in radionuclide inventory, complexing or corrosion within the waste vaults, or alternative assumptions regarding biosphere conditions in the discharge area.

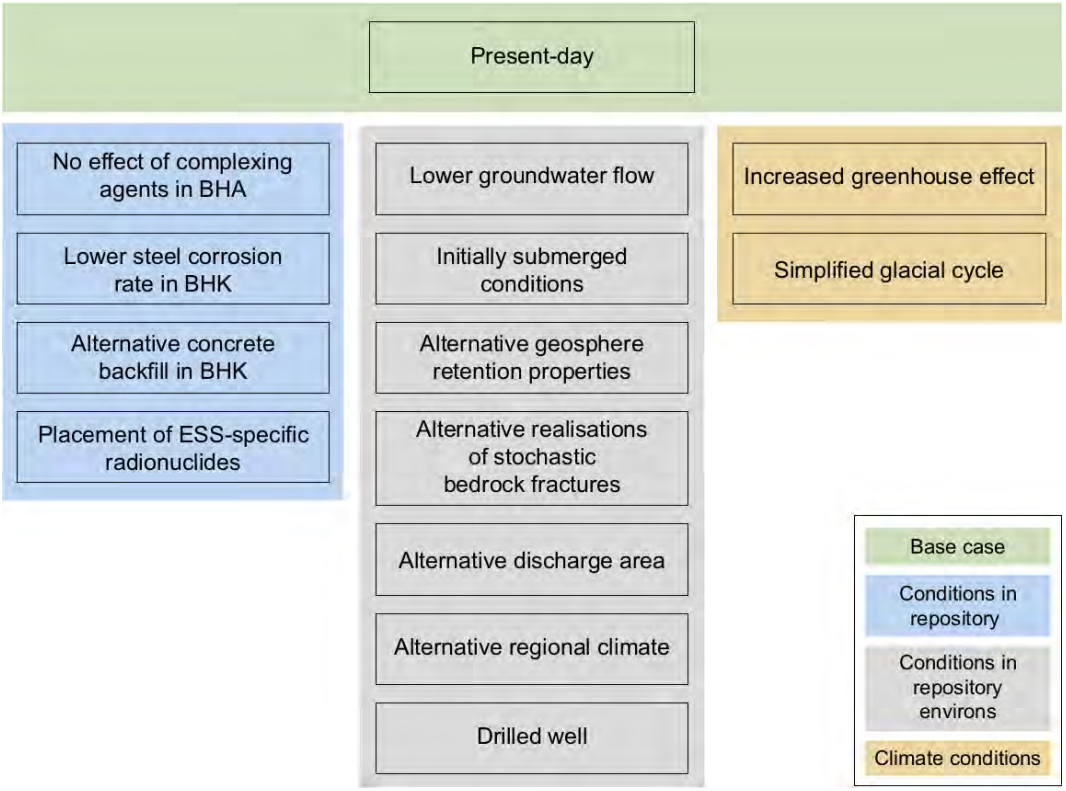

Figure 15 Evaluation cases included in the evaluation of the potential for the proposed repository concept, grouped and color-coded according to type of scenario driver (conditions in the repository, the repository environs or large-scale climate conditions). The acronym ESS stands for European Spallation Source, a neutron-source research facility under construction in Lund, Sweden. From Figure 8-1 of SKB (2019a).

The present-day evaluation case is treated as a base case for comparison with other evaluation cases. SKB (2019a) emphasize that, since SE-SFL is not part of a licensing application, the base case is not intended to establish a main scenario as defined by SSM's regulatory guidelines (SSM 2008). Likewise, the other evaluation cases are not considered to

be scenarios in the sense implied by the regulatory guidelines. In all evaluation cases, the repository is assumed to be constructed according to the proposed design concept.

2.3.1 Model chain and data flow

The radionuclide transport modeling methodology for SE-SFL uses a chain of models similar to what has been used in past evaluations of radionuclide transport for the proposed Swedish spent-nuclear fuel repository and for the SFR repository for short-lived radioactive waste. The general scheme is depicted in Figure 16.

The first main model in the chain is the near-field radionuclide transport model. In the context of SE-SFL, this represents dissolution of radionuclides from the waste and transport outward through the breached containers and engineered barriers (concrete caisson and bentonite backfill in the case of BHA, or concrete backfill in the case of BHK).

A multi-species compartment-model approach is used to calculate the transport of (radio)activity. Within each compartment, terms for each radionuclide species account for sorption and decay as well as in-growth by decay of parent radionuclides within the pore space of each compartment. Activity transfer terms account for advective and diffusive transport between compartments. The mathematical implementation and application are described in the SE-SFL radionuclide transport report (SKB 2019d) which was outside the scope of this review.

The near-field transport model uses data from the initial-state specification, plus results from models of engineered-barrier degradation, and results of the hydrogeological modeling. The key hydrogeological inputs to the near-field model are flowrates through the waste vaults; predicted groundwater chemistry is also used to calculate radionuclide release rates due to corrosion, and to determine sorption coefficients.

The far-field radionuclide transport model calculates transport along groundwater trajectories through the geosphere (bedrock and repository closure components) using the output of the near-field model as the source term. Along each trajectory, transport is modeled by a 1-D advection-dispersion equation with terms for radioactive decay and retardation due to matrix diffusion combined with linear, reversible sorption on matrix pore surfaces.

The key hydrogeological inputs to the far-field model are particle-tracking data from the hydrogeological modeling used to define the lengths of the trajectories, the advective travel times, and the transport resistance F (effectively, the incremental time that a unit volume of mobile water spends in contact with a unit fracture surface area across which diffusion into the rock matrix can occur, integrated along the length of the trajectory).

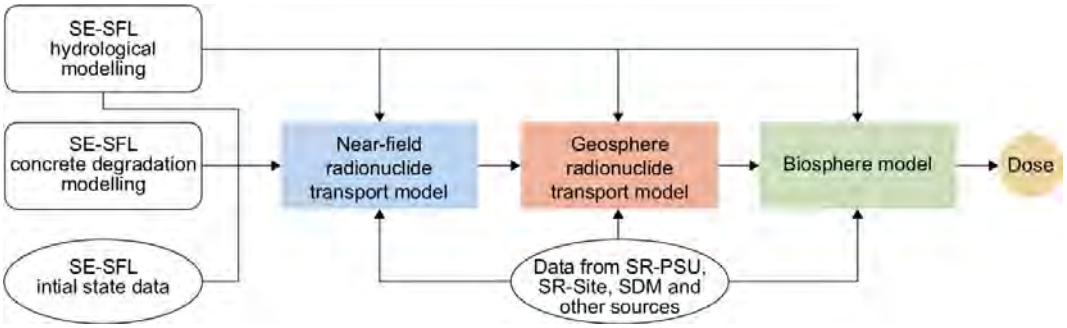

Figure 16 Schematic representation of the SE-SFL radionuclide transport model chain and main sources of input for the respective models. From Figure 7-2 of SKB (2019a).

The output from the far-field model is to a biosphere radionuclide transport model, which calculates transport between a network of compartments belonging to the *biosphere object* where a given group of groundwater trajectories have their discharge points. Compartments in the model for each biosphere object represent different layers of the regolith, surface water bodies, vegetation, and atmosphere.

The key input from the hydrogeological modeling to the biosphere model is the location of the discharge point for each trajectory, which determines which biosphere object the trajectory contributes to. Figure 17 shows the nine biosphere objects in the Laxemar area that are identified as receiving deep groundwater discharge from the vicinity of the repository. It can be noted that these objects, identified based on hydrogeological modeling of temperate conditions, may not be representative of future periglacial or glacial conditions.

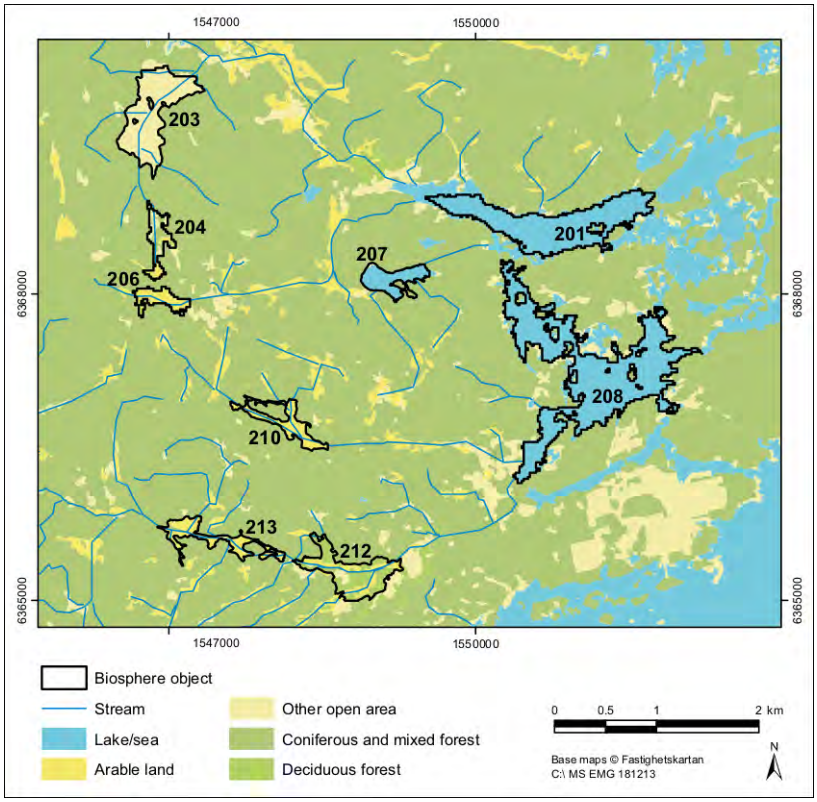

Figure 17 Outlines of the nine biosphere objects (201, 203, 204, 206, 207, 208, 210, 212, and 213) with reference to the present-day land use map at Laxemar. The objects 201 and 208 are future lake basins, smaller than the current sea basins. Adapted from Figure 4-149 of Joyce et al. (2019).

Finally, the outcome of biosphere modeling is used to calculate the radiation dose to future humans and animals making their home in that biosphere object (or growing or gathering food there), based on their potential exposure to the various media in which radionuclides accumulate. As indicated by Figure 16, there is no direct link between the hydrogeological modeling and dose calculations. However, water resource availability may affect the pathways for exposure, for example, if a warmer future climate leads to an increased need for irrigation of crops using water

2.3.2 Present-day evaluation case

The present-day evaluation case is described in Section 7.4 of SKB (2019a). External conditions in terms of climate and shoreline position remain constant based on conditions for 2000 AD. Internal conditions within the repository and surrounding bedrock evolve according to the base variant of the reference evolution.

Evolution of BHA flow and transport properties

The BHA is assumed to have constant flow and transport properties over the entire simulation period, corresponding to saturated, homogeneous conditions in the bentonite backfill. Potential effects of bentonite erosion, irregular homogenization, degradation, and chemical evolution are neglected in this evaluation case, though based on discussions given previously (in Section 6.2.9 of SKB 2019a and summarized earlier in this review), it is noted that further exploration is needed in future safety assessments.

For flow and near-field transport calculations, the hydraulic conductivity of the bentonite backfill is uniformly 1.0×10^{-13} m/s (according to SKB 2019a, p. 96, though this is stated to be 1.0×10^{-12} m/s on p. 97). The total flow rate through the vault calculated from the near-field hydrogeological modeling (by Abarca et al., 2019; see Section 2.4.4 of this review) is 2.2×10^{-2} m^3/y (22 L/y), of which 3.3×10^{-4} m^3/y (0.3 L/y) passes through the waste volume. As a simplification for the near-field transport model, water flow through the BHA is assumed to be along the length of the vault despite that the near-field hydrogeological model predicts that flow around and through the BHA vault would be vertical (downward).

For near-field transport calculations, porosity and effective diffusivity values in the BHA waste compartment and the bentonite backfill are assumed to be constant for the entire evaluation period, but the concrete structures surrounding the waste are assumed to degrade with time, with porosity increasing as for the BHK concrete (see below). This is stated to be a conservative assumption as the bentonite backfill will likely minimize leaching of the concrete. Effective diffusivities and diffusion-available porosity for anions

in the bentonite are assumed to be lower than for cations or neutral species, by factors of 0.08 and 0.4 respectively, due to anion exclusion.

Sorption coefficients for a few key radionuclides for both the BHA and BHK vault are listed in Table 7-1 of SKB (2019a). The selection of these values by Shahkarami (2019) is outside the scope of this review. However it may be noted that the effective sorption coefficient used for some radionuclides (most notably Tc-99) is reduced in BHA due to the presence of cellulose in some of the waste, which is a precursor to a complexing agent that can enhance solubility and thus reduce sorption effects.

Evolution of BHK flow and transport properties

For the BHK, the concrete backfill is assumed to degrade with time, mainly due to dissolution and leaching of cement hydrates. The degradation is considered to progress from the outside inward. For simplicity this is modeled as a stepwise process with three stages:

- *Intact concrete* (0 to 85 ka after closure): The concrete backfill is intact with uniform hydraulic conductivity of 8.3×10^{-10} m/s. This is referred to as "effective hydraulic conductivity" (SKB 2019a, p. 143) which could presumably include the contributions of fracturing to the net value, but this is not explicitly discussed. The period of 85 ka corresponds to the time after which portlandite is predicted to have been leached out of the outer quarter of the backfill. The flow through the BHK during this period is 1.1 m^3/y (1100 L/y), with 0.696 m^3/y (696 L/y) passing through the waste volume.
- *Degraded zone* (85 ka to 785 ka after closure): The outer half (by distance) of the concrete backfill is significantly more permeable than the inner, intact half, with a hydraulic conductivity of 1×10^{-7} m/s. According to SKB (2019a, p.143) this is assumed to prevail "until the calcium-silica-hydrate gel in the outer half of the backfill has leached out," but presumably this should refer to the inner half. During this stage, the total flow through the BHK vault increases relative to the preceding stage, but flow through the BHK waste *decreases* to just 0.020 m^3/y (20 L/y) as the higher-conductivity degraded zone effectively short-circuits the pressure gradient around the vault, decreasing the gradient (and hence flow) through the waste volume.
- *Degraded concrete* (785 ka to 1 Ma after closure): The full backfill volume is degraded with a hydraulic conductivity of 1×10^{-7} m/s. Both the total flow through the vault and the flow through the waste increase relative to the case of intact concrete (about 4 m^3/y through the vault and 0.4 m^3/y through the waste based on Figure 6-7 of SKB 2019a).

For the near-field radionuclide transport calculations by Shahkarami (2019), values of porosity and effective diffusivity in the concrete backfill are also assumed to increase with time, but linearly rather than as step changes, and at different rates depending on whether on the inflow or outflow side of the vault (Figure 18).

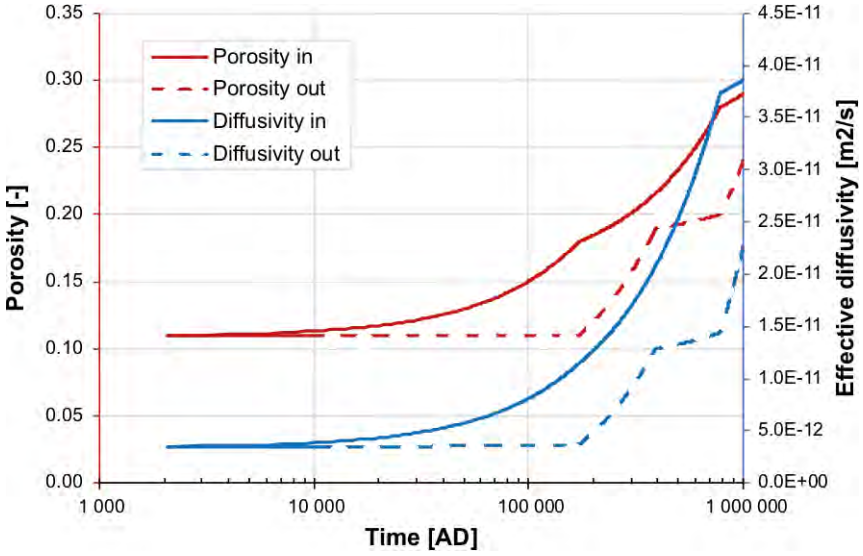

Figure 18 Development of porosity and effective diffusivity due to concrete degradation in the BHK backfill, in the inflow compartment (solid lines) and the outflow compartments (dashed lines). The data are linearly interpolated between time points at repository closure (2075 AD), and at 170, 390, 780, and 1 000 ka after closure. Adapted from Figure 7-10 of SKB (2019a).

Simplifications in the geosphere representation

Only a single realization of the DFN model representation of the sparsely fractured bedrock has been used to calculate effective hydraulic conductivity fields and the resulting flow fields for the catchment-focused model of Joyce et al. (2019) and the near-field hydrogeological model of Abarca et al., 2019 (reviewed in Section 2.4.3). This means that the stochastic variability of the DFN representation has not been addressed in these aspects of the hydrogeological modeling.

SKB (2019a, p. 151) note that different DFN realizations, among the five realizations tested in the facility-focused model of Joyce et al. (2019), led to different discharge locations at the surface, and thus potential release of radionuclides to different biosphere objects. In order to mitigate this issue, the analysis assumes that all radionuclides are released to a single biosphere object (206). This is asserted to be a conservative assumption relative to the alternatives of release being distributed over multiple biosphere objects, or concentrated to a different single biosphere object. However, this approach might not be conservative if another biosphere object could receive groundwater discharge with faster transport times.

SKB further notes that the particular DFN realization used for catchment-focused modeling had lower total dissolved solids (TDS) concentrations than the average over all five realizations. Thus the chosen realization may not be the most representative prediction of future groundwater chemistry.

Function of the repository design for the example location

The function of the repository is discussed based on the results of near-field, geosphere, and biosphere transport modeling in Section 7.5 of SKB (2019a). Radionuclide retention in the near-fields of both BHA and BHK is substantial, though with different mechanisms depending on the species. In the near-field, sorption onto cement and bentonite combined with short half-lives limits overall release of some radionuclides such as Ni-63. The slow rate of corrosion in BHK reduces the source term and hence the near-field activity releases for non-sorbing radionuclides such as C-14.

Retention in the geosphere is significant for radionuclides with high potential for sorption (such as Ag-108 and several Pu isotopes) as well as for radionuclides with short half lives in relation to travel times. For Tc-99 which has a longer half-life, geosphere retention is significant due to the combination of retardation in the rock matrix with decay. However for longer-lived and weakly sorbing radionuclides such as C-14 and Mo-93, the retention provided by the geosphere is minimal (Figure 19).

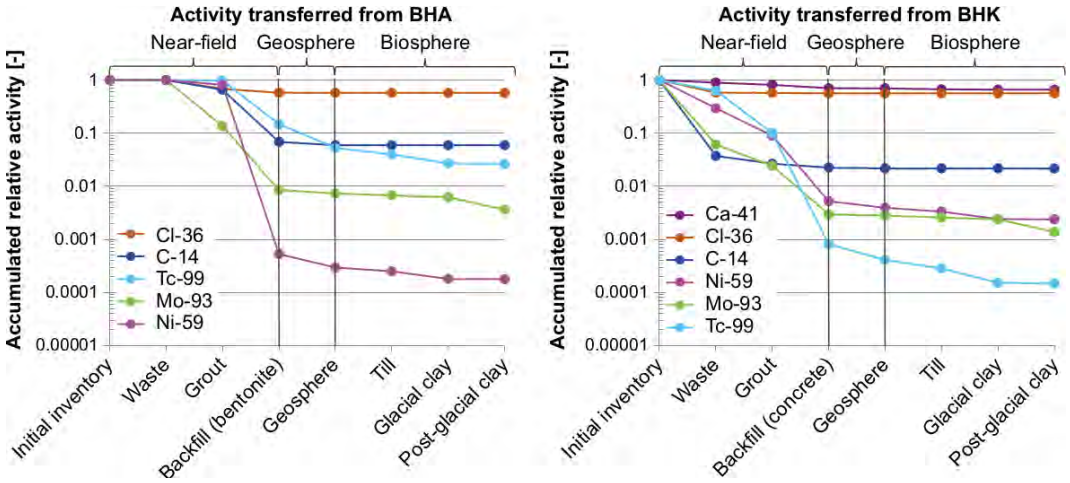

Figure 19 Relative activity transferred along the pathway from the initial inventory in BHA (left panel) and BHK (right panel) to the biosphere, accumulated over the entire analysis period of one million years. From Figure 7-12 of SKB (2019a).

For the base case, the peak total annual doses from BHA and BHK reach about 100 μSv and 50 μSv, respectively, which exceeds the dose corresponding to the regulatory limit (14 μSv). Thus for the assumptions of the base case, the repository design comes within less than an order of magnitude of meeting the regulatory requirement as expressed in terms of annual dose, but is not sufficient to meet the requirement.

2.3.3 Other evaluation cases

As the base case for the SFL design at this site comes close to meeting the regulatory threshold, the other evaluation cases considered explore the potential for the design to meet the requirement with alternative assumptions.

Alternative concrete backfill in BHK

The effect of using a higher-quality concrete backfill in BHK was checked by considering carrying out calculations for a case where the porosity and effective diffusivity of the concrete are reduced by half, and the advective flow scaled by factor 0.1 to reflect a corresponding decrease in permeability.

This evaluation case reduces the peak annual dose from BHK to less than 2 μSv, well below the value that corresponds to the regulatory limit in terms of risk. In this case, no credit is taken for reduction in the rate of concrete degradation which would be expected due to the reduced flow through the backfill, so even further reductions in late-time releases could be expected.

Lower groundwater flow

Lower groundwater flow could perhaps be achieved by locating the repository in a volume of rock with lower effective hydraulic conductivity than the example location in Laxemar. This possibility was scoped by considering three parametric variants of a case with reduced groundwater flow rates:

a) flow rates in the waste and backfill are scaled by a factor of 0.1, resulting in a factor of 10 increase in advective travel times and transport resistance F.

b) flow rates in the waste and backfill are scaled by a factor of 0.01, resulting in a factor of 100 increase in advective travel times and transport resistance F.

c) flow rates in the waste and backfill are scaled by a factor of 0.001, resulting in a factor of 1000 increase in advective travel times and transport resistance F.

For the BHK vault, all three of these cases were sufficient to reduce the peak annual dose to well below the regulatory limit. For the BHA vault, the case (a) with just a factor of 0.1 reduction in flow was not adequate to meet the regulatory limit (with Mo-93 and Cl-36 accounting for the peak annual dose in excess of the regulatory limit), but the other two cases were adequate.

Initially submerged conditions

If the SFL were located at a position that is currently below the seabed, reduced hydraulic gradients would be expected to limit groundwater flow for as long as the site remains submerged.

This possibility was explored by considering the following three cases in which the repository is initially subject to hydraulic gradients that are reduced by a factor of 100 relative to present-day gradients, then subjected to terrestrial effects starting:

a) immediately after closure,

b) 5000 years after closure, or

c) 10 000 years after closure.

In all cases, the biosphere object for releases starts as sea basin, which becomes a lake due to shoreline displacement, then with continuing land rise evolves to a mire which is eventually drained and cultivated. The onset of terrestrial influence on groundwater flow, assumed to begin when the average water depth decreases to 6 m, is simulated by a scaling factor applied to the flow magnitudes calculated for the base case (present-day conditions at the inland repository site).

These calculation cases produced delays in the release of radionuclides, corresponding to the period for which the repository remains submerged. However the subsequent behavior is more complicated than a simple delay, as seen in Figure 20. The annual dose for BHA is reduced by a greater factor than that for BHK during the initial submerged period. SKB (2019a, p. 170) state that this is due to the fact that releases from the BHA near-field are diffusion-controlled rather than advection-controlled as in BHK.

The onset of higher groundwater fluxes leads to an initial peak in annual dose, which results from advective flushing of radionuclides that accumulate in and around the vaults during the submerged period. In the case of BHK, for variant (a) this produces an initial peak dose higher than the dose curve for the base case. However in late time the results converge to the base case. Overall, the strategy of an initial submerged repository does not succeed in lowering the predicted peak annual dose to below the regulatory limit.

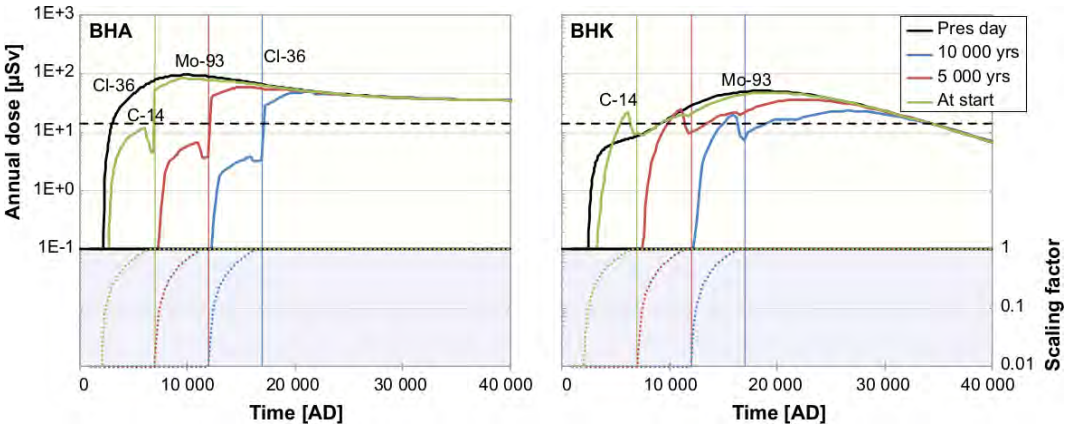

Figure 20 Annual dose from BHA (left) and BHK (right) in the three variants of the *initially submerged conditions* evaluation case. The terrestrial landscape starts to influence flow conditions in the waste vaults and the bedrock at the start of the simulation (green), after 5 000 years (red), or after 10 000 years (blue). The annual dose in the base case (for a repository located at the present-day inland site) is shown for reference (black). Dose-contributing radionuclides are indicated above the curves (early dose due to Cl-36 from BHA occurs in the base case only). The vertical green, red, and blue lines indicate when the biosphere

object for the corresponding variant is 1 m above sea level, allowing cultivation of the drained mire where radionuclides are assumed to discharge. Lower panels show the hydrological scaling factor for the near-field and the geosphere release. From Figure 8-10 of SKB (2019a).

Alternative geosphere retention properties

The importance of site-specific geosphere retention properties (sorption coefficients K_d and bedrock diffusivities D_e) was tested by substituting site-specific values from Olkiluoto, Finland or Forsmark, Sweden for more conservative values that were assumed in SE-SFL due to lack of site-specific data for Laxemar (and in some cases also Forsmark), in particular for Mo-93. Other aspects of the hydrogeology were assumed to be as in the base case.

The results as presented in Section 8.4.3 of SKB (2019a) show decrease of roughly a factor of two in the peak annual dose from BHA and BHK. In the case of BHA, the radionuclide principally responsible for the peak dose shifts from M-93 to Cl-36. However the effect is not sufficient to meet the dose level corresponding to the regulatory limit.

Alternative regional climate

This evaluation case considers how higher rates of shallow groundwater recharge and discharge, due to a wetter and/or cooler temperate climate, would affect biosphere transport and accumulation, and hence the effective dose. Changes in the deep groundwater flux affecting geosphere transport are not considered as part of this case. Effects on peak annual dose are found to be minor, with at most a reduction of 35%.

Alternative realizations of stochastic bedrock fractures

The effective hydraulic conductivity K governing groundwater flow through the bedrock was calculated using a stochastic discrete-fracture network (DFN) model by Joyce et al. (2019), as detailed in Section 2.4.1. Each stochastic realization of the DFN model results in a different heterogeneous K field, resulting in a different flow field. Also, four of the realizations (r2, r3, r4, and r5) evaluated by Joyce et al. (2019) included stochastic variation of hydraulic properties within the major deformation zones, in contrast to the first realization (r1) which assumed uniform properties within each deformation zone.

Consequently these different realizations yield values of the flow-related performance parameters that go into the near-field and geosphere radionuclide transport models:

- Fracture equivalent flow rate Q_{eq}, interpreted as the reciprocal of the diffusive resistance R_{eq} for the near-field model;
- Travel time t_w for a given flow path (i.e. geosphere transport trajectory);
- Wetted surface a_w for a given flow path

The last two parameters are related to the transport resistance F (which is proportional to t_w/a_w.

Distributions of Q_{eq} and t_w for each of the five realizations r1-r5 are shown in Figure 21. In realizations r1 and r3, the significantly higher Q_{eq} values and significantly lower t_w values are explained by large sub-vertical fractures that intersect the vaults. The realizations lacking such features, with lower Q_{eq} and higher t_w, would be expected to yield better retention and hence lower doses.

This was checked in this evaluation case by calculating geosphere release and consequent annual dose for each of the five realizations, and considering two different positions for the BHA vault in each case (i.e. switching the BHA vault to the BHK position and vice versa).

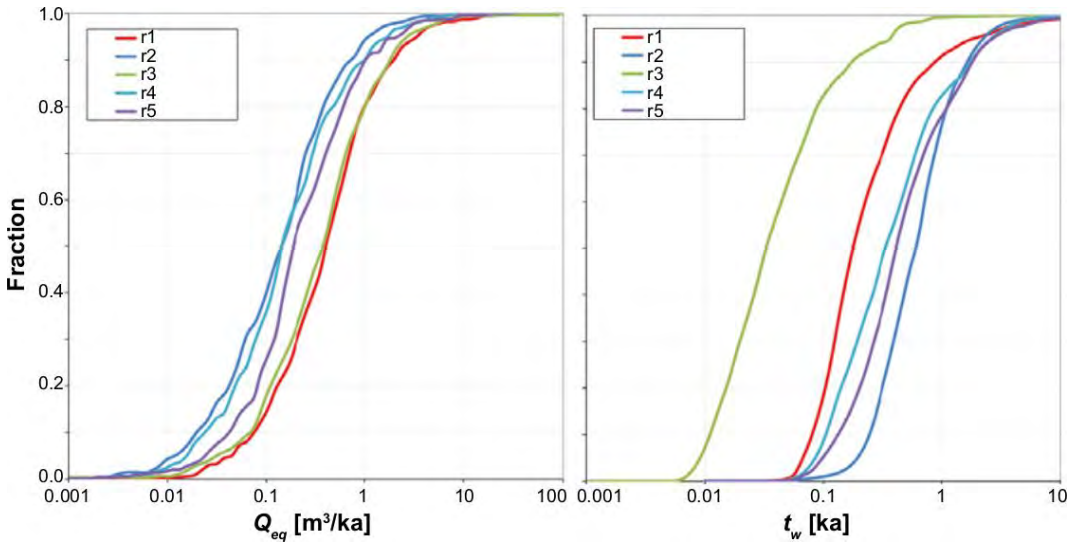

Figure 21 Cumulative distributions of equivalent flow Q_{eq} (left) and advective travel times t_w (right) for pathways originating from the BHA, for five different DFN realizations modeled by Joyce et al. (2019). Realization r1 (red curve) is the realization used in the base case. Figure adapted from Joyce et al. (2019).

The results of transport modeling and dose calculations for these five variants are summarized in Figure 22. The least peak annual dose results from realization r2 in combination with the BHA vault being located to the west of the BHK vault. Thus some improvement is seen from a realization lacking a large sub-vertical fracture connecting to BHA (such as found in r1 and r3), but this is still not sufficient to bring the peak dose down to a level consistent with the regulatory limit.

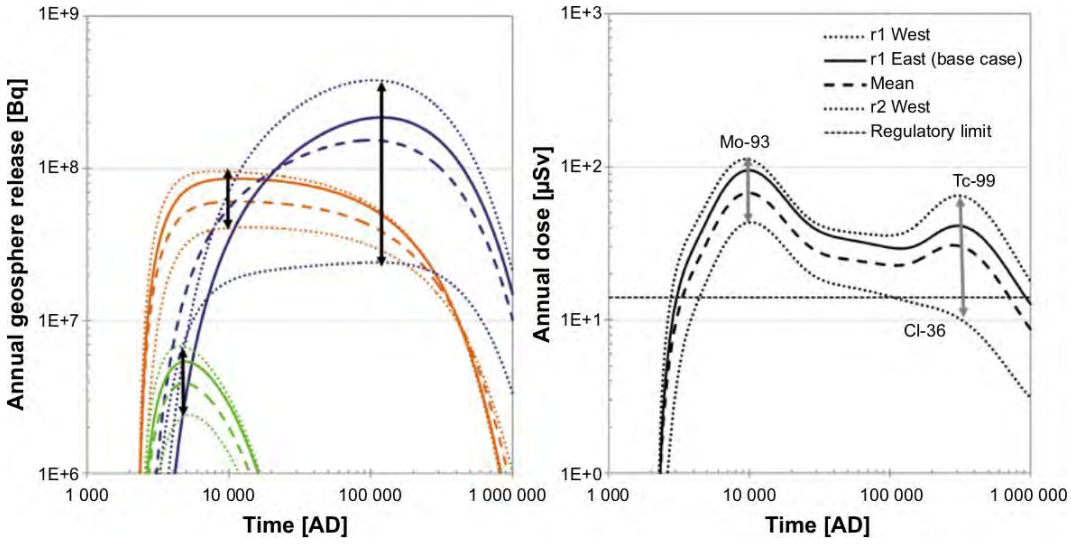

Figure 22 Annual geosphere releases and annual doses from BHA as calculated for five alternative realizations of stochastic bedrock fractures in combination with two different positions for BHA. The realizations with the largest and smallest values are indicated with dotted lines. The means over ten DFN variants are shown with a dashed line. The release and dose in the base case are shown with a solid line for comparison. Vertical arrows indicate the approximate range of maximum values. Left: Release of individual radionuclides; Cl-36 (brown), Mo-93 (green) and Tc-99 (dark blue). Right: Annual dose; dominant dose-contributing radionuclide indicated with text. From Figure 8-14 of SKB (2019a).

Drilled well

The *drilled well evaluation case* examines the potential dose resulting from household use of water from a domestic well drilled into the bedrock in the discharge area for the repository. The well is required to produce 700 L per day, with water used for drinking water and to irrigate vegetables in a garden plot relied upon as the sole source of vegetables and root crops, for a household of five individuals.

Details of the hydrogeological analysis for this case are presented by Joyce et al. (2019) and discussed further in Section 2.4.3 of this review. Of five feasible well locations in a discharge area 0.5 to 1 km north of the SFL (Figure 23), only one well (W3) is predicted to receive particles representing flow paths from the repository. This single well is used to assess the potential dose from this case.

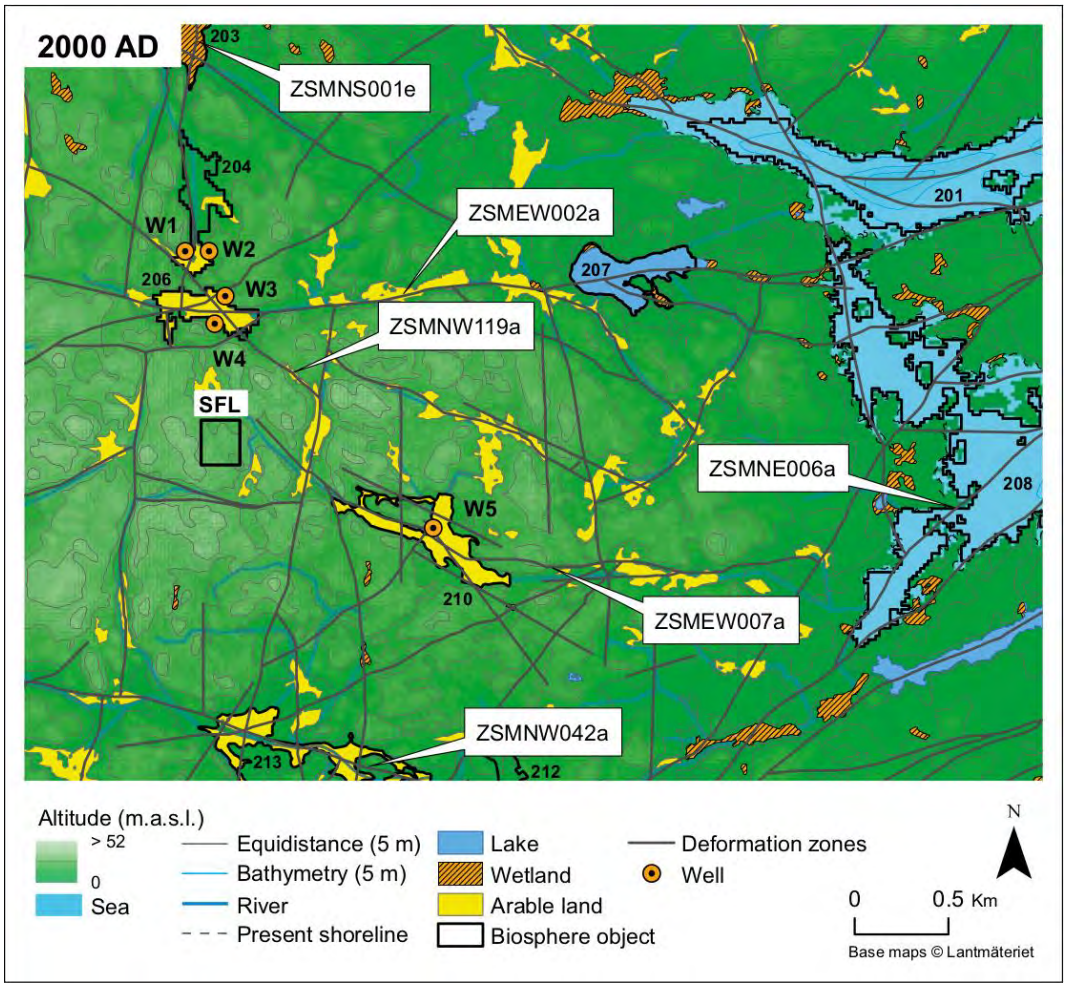

Figure 23 Well locations W1 through W5 evaluated in the *drilled well evaluation case*, shown in a map of the present Laxemar landscape. Biosphere objects are outlined in black and labeled with numbers (201, 203, …, 213). Key deformation zones in the Laxemar area are shown as traces in the horizontal plane 20 m below sea level and labeled (names starting with ZSM), The hypothetical location of the SFL repository (black square) is added for reference. From Figure 8-16 of SKB (2019a).

Pumping of the well at the prescribed rate is found to produce only minor perturbation to the hydrogeological performance measures for the repository. Therefore the release of radionuclides to the well is calculated simply as the base-case geosphere release times the fraction of particles captured by the well (3.1% for BHA and 2.1% for BHA). The concentration of radionuclides in the well water is calculated by dividing the geosphere release that reaches the well by the well extraction rate.

The small size of the exposed group for the case considered by SKB (5 individuals) justifies use of a more lenient annual risk criterion of 10^{-5} rather than 10^{-6}, according to regulatory guidance from SSM (2008). This corresponds to a maximum annual dose of 140 μSv for members of the exposed group. This argument may not be applicable for a case in which a larger population depends on water from multiple wells, or a well in which the capacity has been increased for example by hydraulic fracturing of the bedrock.

The predicted dose from the BHK stays nearly two orders of magnitude below this level throughout the 1 Ma assessment period (Figure 24). The predicted dose from BHA stays below this level for the first 300 ka, but then exceeds it and continues to rise through the end of the assessment period.

A shallower, dug well in the discharge area produces lower dose (according to results presented in Figure 7-16 of SKB 2019a) than a drilled well in bedrock. This is stated to be primarily because of reduction by radioactive decay along the transport pathway in till. The analysis of the case of a shallow, dug well is not presented in the documents reviewed here.

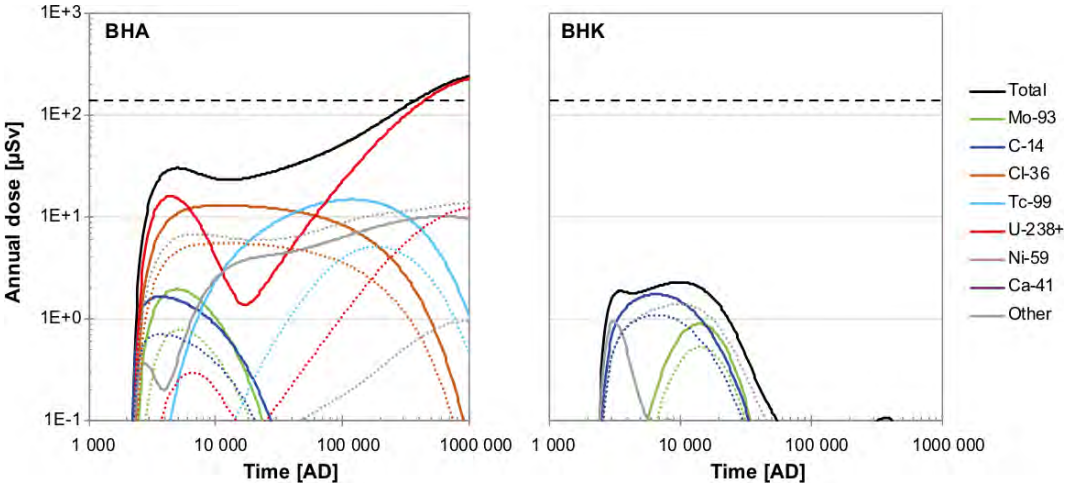

Figure 24 Predicted annual dose from BHA (left) and BHK (right) for a garden plot household in the *drilled well evaluation case*. Colors represent doses from individual radionuclides. Dotted lines represent the dose in the base case (for a garden plot household without exposure through fertilization with ash). The dose level of 140 µSv, corresponding to the regulatory risk limit of 10^{-5} for a small group, is shown with a black dashed line.

Increased greenhouse effect

The *increased greenhouse effect evaluation case* (Section 8.6.1 of SKB 2019a) considers effects of a future warmer climate caused by increased atmospheric CO_2, with decreased rate of groundwater discharge and surface runoff, and with an increased water deficit for crops.

This case is evaluated by adjusting certain biosphere model parameters for biosphere object 206 (increased atmospheric CO_2 and modified discharge rates for groundwater and surface water). This results in crop water deficits which are considered to be addressed in one of two ways (treated as variants of this evaluation case):

a) increased capillary rise of groundwater, or

b) irrigation with surface water.

In the first variant, the uptake of groundwater by crops leads to increased dose of some radionuclides, especially weakly sorbing radionuclides such as Cl-36. However C-14 is diluted by the higher atmospheric CO_2 concentration, and the assumed decrease in

groundwater discharge reduces dose from relatively short-lived radionuclides such as Mo-93 for which the dose is sensitive to the rate of decay versus the influx from groundwater. Hence the net increase in annual dose is generally minor (20% or less) for the capillary-rise variant. Use of surface water for irrigation has a minor effect in the opposite direction, decreasing the net dose.

The treatment of capillary rise in the biosphere model is not coupled to the groundwater flow model, so this analysis does not account for how increased transpiration could affect the shallow groundwater system (for example, causing increased shallow groundwater flow away from bedrock discharge areas).

The analysis presented in SKB (2019a) does not explore the alternative possibility, that groundwater pumped from wells could be used for irrigation instead of surface water, providing another path for exposure. The potential influence of irrigation was studied by Grolander and Jaeschke (2019), which is outside the scope of this review. A brief examination of that report has not clarified why irrigation using well water was not considered. The analysis by Grolander and Jaeschke (2019) does take into account the likelihood of longer-season crops with higher water demand (which was pointed out as a gap in a previous review related to extension of the SFR facility for SSM, by Geier, 2017), based on comparisons with present-day agriculture in regions with climates similar to the predicted future climate at Laxemar.

Simplified glacial cycle

The *simplified glacial cycle evaluation case* is aimed primarily to address the performance of the SFL repository concept for future colder climates, specifically periglacial, glacial, and post-glacial submerged conditions.

No hydrogeological modeling results specific to the SFL are presented. Rather, values of hydrogeological performance measures (Q_{eq}, t_w, a_w and F) for future cold periods are calculated by applying scaling factors to the corresponding performance measures that were calculated for temperate conditions by Joyce et al. (2019) and Abarca et al. (2019).

The derivation of the scaling factors is given in Appendix C of SKB (2019d). This appendix gives brief arguments for the choice of values based on previous modeling by Vidstrand et al. (2010, 2014), followed by a table which is reproduced here (Table 1). Scaling of the other performance parameters is not explained clearly in the documents examined for this review.

The presentation of results for this evaluation case in the SFL main report (SKB, 2019a) is very brief, with just two pages including figures. The main effects seen in terms of predicted annual dose (Figure 25) are a reduction of dose during periglacial and glacial periods, and an overall reduction in dose for the later temperate periods. The former effect is partly because of reduced potential for exposure during cold periods. The latter effect is attributable to the periodic interruptions in radionuclide accumulations in the soil layers that contribute to human exposure.

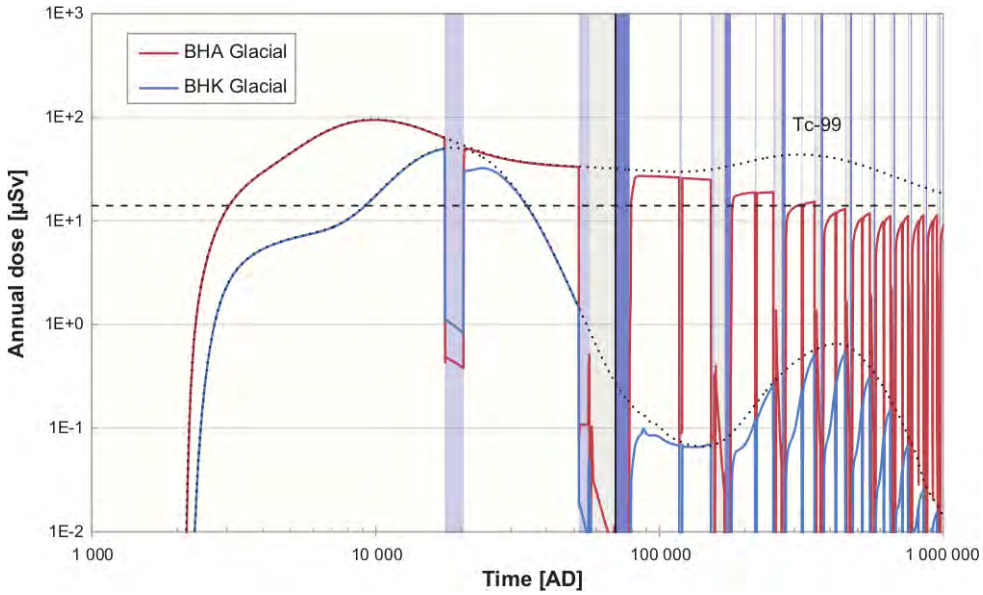

Figure 25 Annual dose for release from BHA (red line) and BHK (blue line) in the simplified glacial cycle evaluation case. Doses in the present-day evaluation case are shown for reference (black dotted lines), where exposure from Tc-99 dominates the dose from BHA during the second half of the simulation time. Background color represents climate domains (surface conditions) as in Figure 8-17. The vertical black line indicates the start of the second interglacial–glacial cycle. From Figure 8-21 of SKB (2019a) as corrected in SKB Errata 2020-02.

Table 1 Groundwater flow scaling factors and conditions for the first cycle of the simplified glacial cycle evaluation case. Submerged conditions refer to the duration of sea water-covered conditions for biosphere object 206. Groundwater flow rates are relative those in temperate terrestrial conditions. Note that the conditions are assumed to be unfrozen at repository depth throughout the analysis period. Reproduced from Table C-1 of SKB (2019d).

Time [AD]	Climate domain	State of discharge area	Conditions in bedrock above repository	Groundwater flow in repository and bedrock
2075 – 17 500	Temperate	Mire	Unfrozen	1
17 500 – 17 600	Periglacial	Mire freezes, start of discharge to lake talik	Frozen	1
17 600 – 20 400	Periglacial	Mire frozen. All release to lake talik	Frozen	1
20 400 – 20 500	Periglacial	Mire thaws, discharge in lake talik ends	Frozen	1
20 500 – 52 000	Temperate	Mire	Unfrozen	1
52 000 – 52 100	Periglacial	Mire freezes, start of discharge to lake talik	Frozen	1
52 100 – 56 200	Periglacial	Mire frozen. All release to lake talik	Frozen	1
56 200 – 57 000	Periglacial. Ice-sheet advancing towards Laxemar	Mire frozen. All release to lake talik	Frozen	Transition from 1 to 33
57 000 – 57 050	Glacial. Continued ice-sheet advance beyond Laxemar	Site ice-covered. All release to sea basin at ice margin	Frozen	Transition from 33 to 35
57 050 – 58 200	Glacial. Continued ice- sheet advance beyond Laxemar	Site ice-covered	Frozen during the first 50 years, then unfrozen	Transition 35 to 1
58 200 – 68 800	Glacial. Thawed bedrock conditions	Site ice-covered	Unfrozen	1
68 800 – 70 000	Glacial. Deglaciation of the Laxemar site	Site ice-covered	Unfrozen	Transition from 1 to 3
70 000 – 70 800	Submerged	Sea water depth above object ≥ 6 m	Unfrozen	Transition from 3 to 0.01
70 800 – 74 400	Submerged	Sea water depth above object ≥ 6 m	Unfrozen	0.01
74 400 – 78 700	Submerged	Transition from coastal sea to isolated lake	Unfrozen	Transition from 0.01 to 1
78 700 – 83 100	Temperate	Transition from lake to mire	Unfrozen	1
83 100 – 102 000	Temperate	Mire	Unfrozen	1

2.4 Hydrogeological modeling

The hydrogeological modeling in support of SE-SFL consists of three main, closely related numerical model setups which differ in the scales considered:

- Catchment-focused model (Joyce et al., 2019, Section 3.3), used to model the long-term evolution of groundwater composition during the ongoing temperate period, and to calculate groundwater density and pressure values at specific time slices which are then used in the facility-focused model.
- Facility-focused model (Joyce et al., 2019, Section 3.4), used to calculate flows around the waste vaults in the hypothetical SFL and to predicted transport trajectories and associated performance parameters used as input to the radionuclide transport models;
- Near-field model (Abarca et al., 2019), with a detailed representation of the waste vaults used to calculate flows through the vaults and waste;

In addition more specialized calculations are performed by Abarca et al. (2019, Chapter 8) to predict resaturation times for the BHA vault.

Each of these models uses different representations for different volumes of the model. The nominal dimensions of the different volumes and properties assumed for each are summarized in Table 2 and shown in Figure 26. Coupling between different volumes with different representations is automatic by "internal" boundary conditions (i.e. numerical constraints to guarantee conservation of mass and continuity of pressures and solute concentrations across the interfaces between volumes).

The boundaries of the catchment volume are adopted from a previous "regional-scale" model for SR-Site (Rhén et al., 2019). These are based on surface-water divides (inland) and the outermost position of the shoreline in the late temperate period (seaward).

The boundaries of the facility-scale volume are adopted from a previous "site-scale" model for SR-Site (Rhén et al., 2019). This boundary was originally adopted to contain a hypothetical spent-fuel repository that was evaluated in SR-Site. The facility considered in SE-SFL is near the NW corner of this volume (Figure 26) rather than centered within it. However this volume is only part of the facility-focused model, embedded within the larger catchment volume, so the effect of this uncentered location is just that lower-resolution portions of the surrounding volume are closer to the facility in the N and W directions than in other directions.

The near-field volume used by Abarca et al. (2019) is approximately centered on the SFL facility in the N-S and E-W directions. In the vertical direction it is bounded by surfaces at approximately half the depth to the vaults (so it contains the lower half of the spiral access tunnel) and 400 m below the vaults (in order to model flow paths that continue downward from the vaults for some distance before bending upward toward discharge areas.

All three of these models are based on the same underlying description of bedrock hydrogeological properties, which are upscaled in different ways as indicated in Table 2 and further summarized in Section 2.4.1.

Table 2: Dimensions and hydrogeological representation in the catchment-focused and facility-focused models of Joyce et al. (2019) and the near-field focused model of Abarca et al. (2019).

Property	Model focus	Catchment volume	Facility-scale volume	Near-field volume	Refined volume
E-W extent		21 km	4.2 km	1 km	0.6 km
N-S extent		13 km	4.2 km	1 km	0.6 km
Depth		Bedrock surface to 2.2 km deep	Bedrock surface to 1.3 km deep	z = −250 m to z = −900 m	60 m thick, containing vaults
Representation	catchment	ECPM	ECPM	--	ECPM
	facility	ECPM	DFN	--	DFN
	near-field			ECPM interpolated from catchment-scale	ECPM interpolated from catchment-scale
Resolution in bedrock	catchment	60 m cubes	30 m cubes	--	5 m cubes
	facility	60 m cubes	30 m cubes	--	5 m cubes
	near-field			Variable tetrahedra ($\lambda \approx 30$ m)	Variable tetrahedra ($\lambda \approx 5$ m)
DFN size range included (side lengths)	catchment	10 m to 1 km	10 m to 1 km	--	10 m to 1 km
	facility	10 m to 1 km	3 m to 1 km	--	0.7 m to 1 km in 280 m x 280 m x 83 m thick subvolume.
	near-field			Same as ...	Same as ...
Soil layer	catchment	60 m x 60 m × 1 m, saturated	30 m x 30 m × 1 m, saturated	--	N/A
	facility	60 m x 60 m × 1 m, variably saturated	30 m x 30 m × 1 m, variably saturated	--	N/A
	near-field			N/A	N/A
Dispersivity	catchment	α_L= 60 m α_T = 20 m	α_L= 30 m α_T = 10 m		Not stated
	facility	Not stated	Not stated	--	Not stated
Dispersivity	near-field			α_L= 15 m + 3λ α_T= 15 m + 1.5λ	α_L= 15 m + 3λ α_T= 15 m + 1.5λ
Repository	catchment				omitted
	facility				CPM
	near-field				CPM

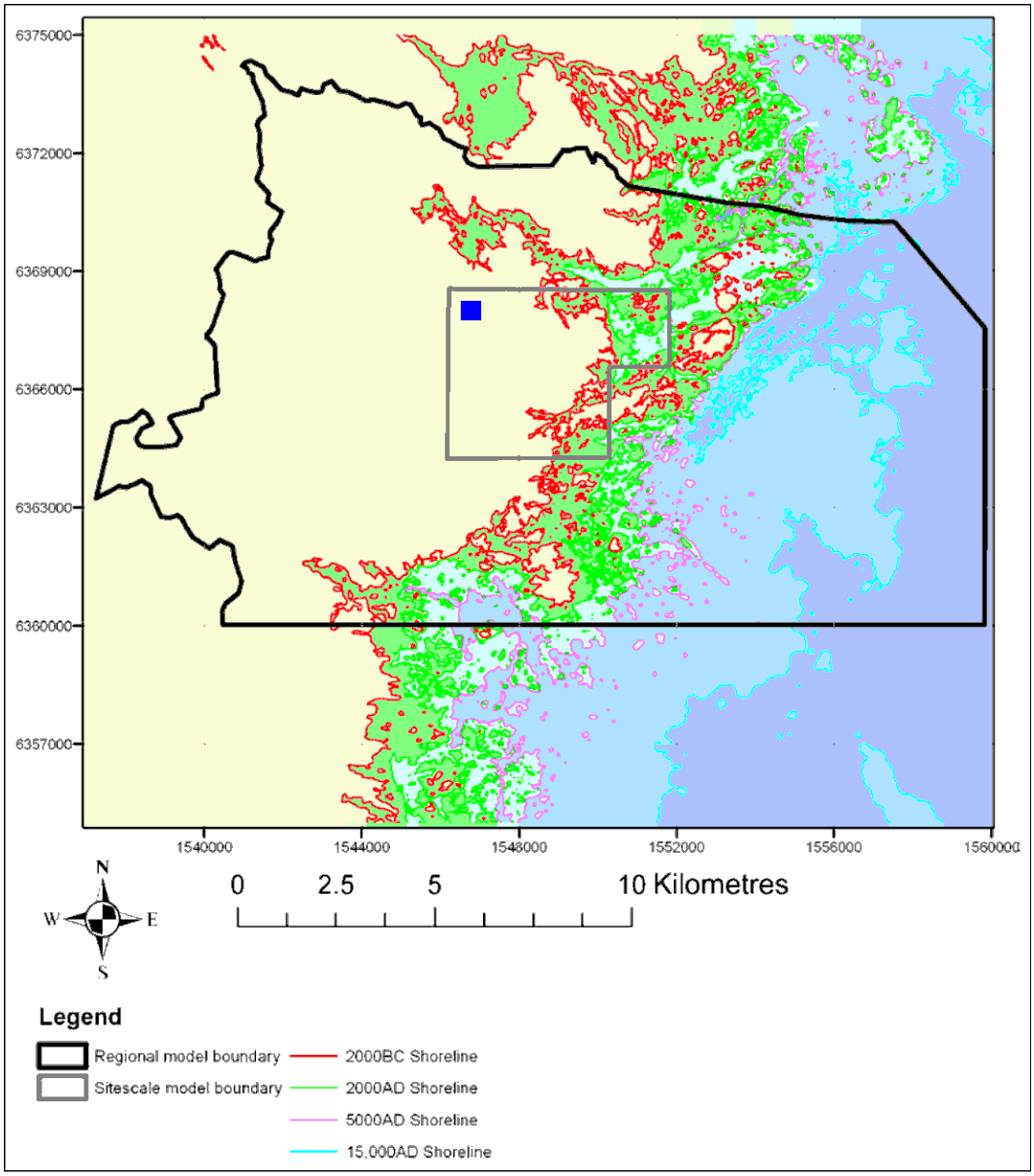

Figure 26 Boundaries of the catchment-scale model area (labeled as “regional-scale model boundary”) and facility-focused model area (labeled as “site-scale model boundary”) relative to shoreline locations at 2000 BC, 2000 AD, 5000 AD, and 15 000 AD (according to colors in legend). The position of the hypothetical SFL facility for SE-SFL is shown as a dark blue square. Modified from Figure 3-2 of Joyce et al. (2019).

2.4.1 Upscaling of hydrogeological properties

Bedrock hydrogeological properties for the models are based on a model adopted from Joyce et al. (2010), which was based in turn on a hydrogeological site descriptive model for Laxemar by Rhén et al. (2008). As described in Section 2.1.5, this model is based on separate descriptions of the hydraulically transmissive deformation zones (referred to as belonging to a *hydraulic conductor domain*, or HCD) and the remaining *rock mass* which is characterized in terms of a discrete-fracture network (DFN) model.

For the purposes of SE-SFL, this statistical description of hydraulically conductive fractures in the rock mass, together with the hydrogeological description of the deterministic deformation zones, is used as the basis for deriving effective hydrogeologic properties for the bedrock for the hydrogeological modeling by Joyce et al. (2019) and Abarca et al. (2019).

Hydraulic conductor domain (HCD)

Deformation zones treated as part of the hydraulic conductor domain (HCD) are represented as triangulated surfaces. For the main modeling case (combined with stochastic realization r1 of the DFN model) these are assigned transmissivities which are homogeneous in a given zone in the horizontal direction (i.e. along strike) but which decrease as a function of depth according to an exponential function, with empirical parameters fitted by Rhén et al. (2008) to data from borehole intercepts.

For four stochastic cases (combined with realizations r2, r3, r4, and r5 of the stochastic DFN), stochastic variation of transmissivity within the deformation zones is included, with a standard deviation in $\log_{10}(T)$ of 1.4. Conditional simulation is used so that these stochastic realizations match local measurements of transmissivity where boreholes intercept the deformation zones. The result of one of these stochastic realizations is illustrated in Figure 27.

Other hydraulic properties of the deformation zones (such as porosity, thickness, and specific storage) are not documented in Joyce et al. (2019) but are presumed here to be the same as used by Joyce et al., (2010).

The contribution of deformation zones to hydraulic conductivity on the scale of the calculation grid, for a given model volume, is calculated by an “implicit fracture zone” method (Hartley and Joyce, 2013) which adds the contribution to the effective hydraulic conductivity tensor for each voxel (model grid cell) intersected by any portion of the deformation zone, taking into account the volume of the cell that is intersected and the orientation of the zone.

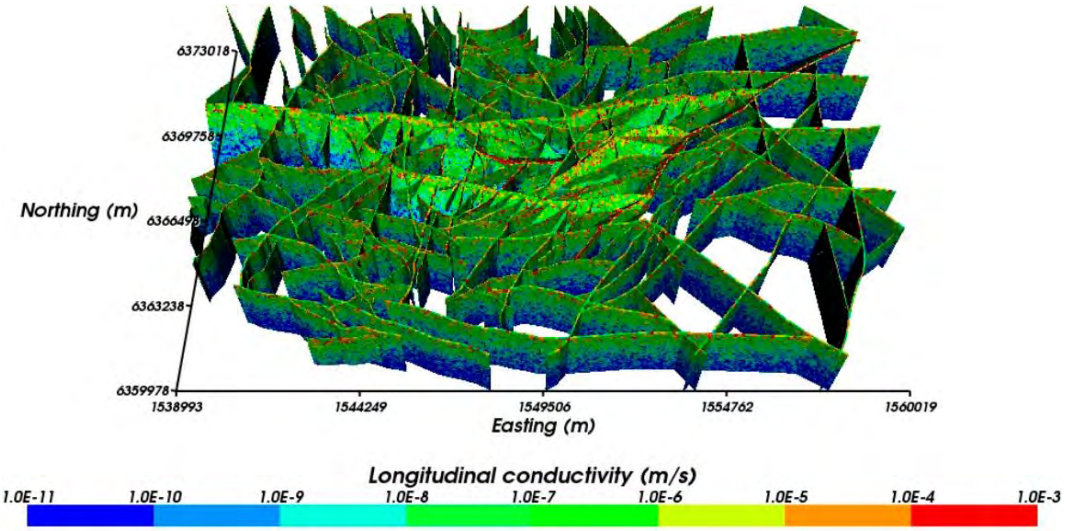

Figure 27. One realization of the modeled stochastic HCD colored according to hydraulic conductivity (Figure 3-1 of Joyce et al., 2019).

Upscaling of DFN representation

As summarized in Section 2.1.5 of this review, the *rock mass* (portion of the bedrock outside of deterministic deformation zones) is described in statistical terms as a discrete-fracture network (DFN) model, with different statistics for each of sixteen subdomains comprised of four rock mass domains divided into four depth zones. The values of the statistical parameters for each of these subdomains are taken from a DFN model previously developed for Laxemar by Joyce et al. (2010), and are listed in Tables 3-2 through 3-5 of Joyce et al. (2019).

This DFN representation was upscaled (converted) to an equivalent continuum porous medium (ECPM) representation using ConnectFlow version 11.2 (proprietary software of Amec Foster Wheeler, 2015). The upscaling method is described only briefly by Joyce et al. (2019).

From past analyses for SR-Site, the method is understood to be based on simulated permeameter approach (performing multiple block-scale flow simulations for each grid cell, with hydraulic gradients applied in different directions, and then fitting an equivalent hydraulic conductivity tensor $\boldsymbol{K}$ to the results). Isolated fractures which do not connect to any potential flow paths are deleted from the DFN realizations prior to calculating the equivalent $\boldsymbol{K}$.

The equivalent values of specific storage S_s and kinematic porosity ϕ are upscaled in an analogous way, by summing up the contributions of individual fractures within each grid cell. According to Rhén et al. (2008, p. 265), ϕ is calculated as the sum (over all fractures that are connected on the scale of the block) of fracture area within the block multiplied by the transport aperture e_t of the fracture. In Rhén et al. (2008) the following empirical relationship was used:

$$e_t = 0.705\ T^{0.404}$$

where e_t is in meters and T is in units of m^2/s, but several alternative relationships were also presented based on a compilation of tracer tests (Hjerne et al., 2010), and it is not clear which one has been used by Joyce et al. (2019).

Joyce et al. (2019) do not give a quantitative presentation of the upscaled values of hydraulic conductivity, apart from block diagrams of the model which use color to illustrate the variability of K along the edges of the model. Statistics for the block-scale properties from the same DFN model are presented in Appendix E of Joyce et al. (2010, Tables E-5 through E-10). These have been used for the basis of scoping calculations in Section 4.2 of this review.

Plots of the upscaled hydraulic conductivity (for example Figure 28) illustrate how narrow the region of detailed representation is around the vaults, before the transition to a more diffuse representation due to the ECPM upscaling to 30 m or 60 m blocks.

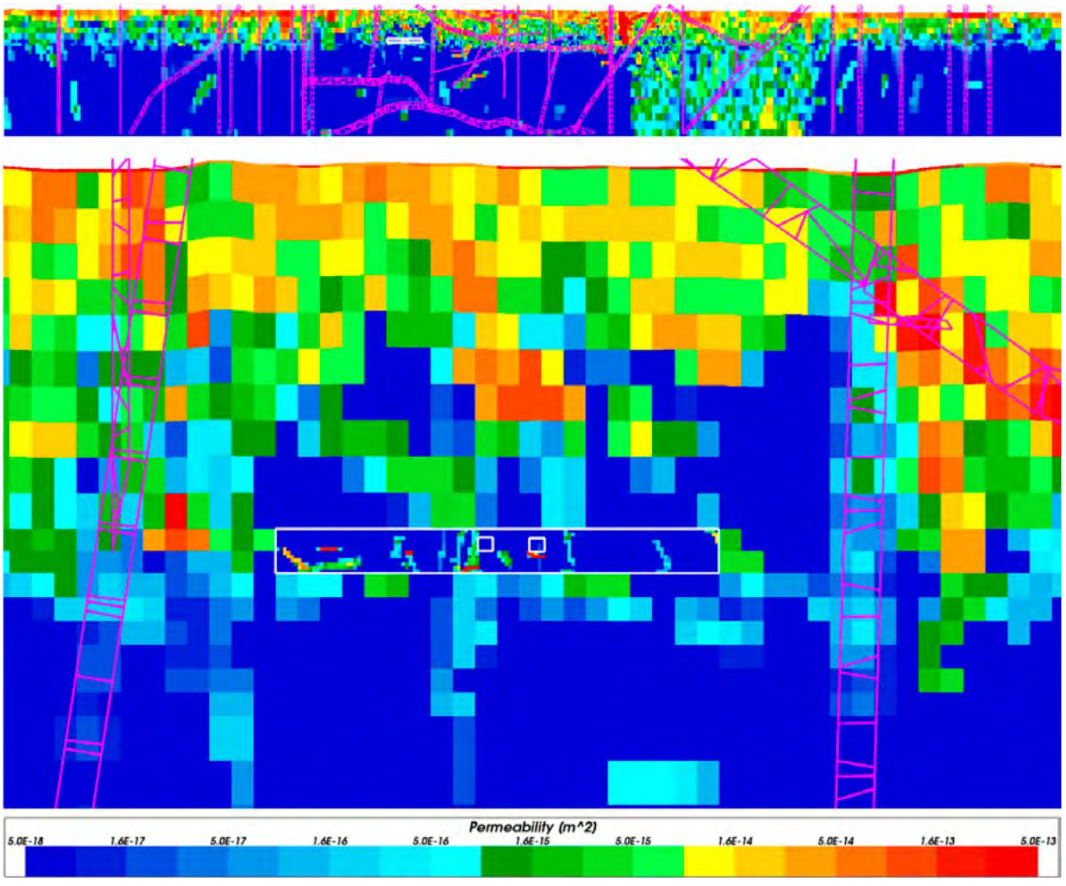

Figure 28. Vertical slices at different scales through the repository volume portion of the catchment-scaled DFN model, showing the permeability (k_{xx}) distribution for HRD realization r_1, according to the color scale at the bottom of the plot. The refined volume and repository vaults are outlined in white. Deformation zones are superimposed as purple lines. The top panel shows the full model down to an elevation of −2 075 m. The bottom panel shows a magnified view of the part of the model closest to the repository, down to an elevation of −850 m. No vertical exaggeration. Adapted from Figure 4-101 of Joyce et al. (2019).

Hydraulic soil domain (HSD)

The uppermost layer of the catchment-focused model represents soil layers as characterized by Bosson et al. (2009). These are represented with a finer vertical resolution than used for the bedrock, as four 1 m thick layers. The effective hydraulic conductivities of these layers are calculated as anisotropic, with a horizontal component based on the arithmetic mean of the corresponding soil layers, and a vertical component based on the harmonic mean.

An alternative, more detailed model was used to represent the HSD in the facility-focused model, using six layers that match the six layers defined by Bosson et al. (2009) with minor adjustments. This near-surface component of the model allows for variable saturation of the soil layers using a van Genuchten (1980) type model to relate relative permeability to saturation as a function of total pressure. The assigned values of soil permeability, specific storage coefficient, and porosity were calibrated to improve the match of modeled to observed pressure responses in shallow boreholes given data on spatial and temporal distribution of recharge from Bosson et al. (2009). This calibration is described in Section 4.1 of Joyce et al. (2019) as will be discussed further below.

2.4.2 Catchment-focused modeling

The catchment-focused model is used to model the long-term evolution of groundwater composition during the ongoing temperate period, calculate groundwater density and pressure values at specific time slices which are then used in the facility-focused model. This model does not include a representation of the repository, so the effective hydraulic conductivity of the portion of the model containing the repository may differ between this model and the more detailed-scale models which use this model for effective boundary conditions.

The boundary and initial conditions for groundwater flow are not stated by Joyce et al. (2019). In Section 3.3.4 (titled “Hydrogeochemical initial and boundary conditions”) they state that “initial conditions and boundary conditions used were the same as those in Joyce et al. (2010), except that reference water fractions were replaced by the equivalent mass fractions of the individual solutes.” On this basis, it is assumed here that the hydraulic boundary conditions and initial conditions were also the same as those in Joyce et al. (2010), namely “a recharge-discharge boundary condition on the top surface and no flow through the sides and bottom of the model.”

The initial hydrogeochemical conditions are specified with reference to the initial mass fractions of reference waters in the fractures, as shown in Figure 29. These are replaced in the present work with the component mass fractions for each of the reference waters as listed in Table 3. The hydrogeochemical boundary conditions used by Joyce et al. (2010) had a hydrochemical boundary condition at the base of the model, set to the initial values of the reference water fractions. The reference water fractions on the top boundary vary with time according to the elevation of shoreline with regard to the topography of the ground surface (and presumably the time-varying salinity of the Baltic for submerged portions, though this is not clearly stated).

The concentrations of solute affect groundwater density, which in turn affects groundwater flow, so groundwater flow and solute transport are coupled. In addition the groundwater is constrained to be at equilibrium with mineral phases in a thermodynamic database as used by Gimeno et al. (2010) supplemented by equilibrium constraints for quartz, calcite, FeS(ppt) and hematite, according to the following reactions with equilibrium constants (K, here only) as noted:

- Quartz: $SiO_2 + 2\ H_2O = Si(OH)_4$ $\log K = -3.746$
- Calcite: $CaCO_3 + H^+ = Ca_2^+ + HCO_3^-$ $\log K = 1.849$
- FeS(ppt): $FeS + H^+ = Fe^{2+} + HS^-$ $\log K = -3.00$
- Hematite: $Fe(OH)_3 + 3H^+ = Fe^{3+} + 3H_2O$ $\log K = -1.10$

The solute transport model takes into account advective-dispersive transport in fractures coupled with matrix diffusion. The dispersion tensor is calculated as the sum of a diffusive component (isotropic with molecular diffusion coefficient $D_e = 1.0 \times 10^{-9}$ m^2/s) plus dispersive components which depend on the advective velocity and longitudinal and transverse dispersion lengths, according to Equation 2-10 of Joyce et al. (2019).

Diffusion into and out of the rock matrix adjacent to the mobile water in fractures is modeled by a finite-volume method with five finite-volume matrix cells per finite element associated with a fracture. These have cell size increasing with distance into the matrix (Joyce et al., 2019, p. 33). Possible rate-dependence of the matrix pore volume accessible as a function of time is not considered. Matrix porosity is expressed in terms of a capacity factor $\sigma = 8 \times 10^{-3}$ (Joyce et al., 2019, p. 27). An intrinsic diffusion coefficient $D_i = 5.0 \times 10^{-14}$ m^2/s is used for diffusion in the matrix.

Calculations of coupled variable-density groundwater flow and solute transport were carried out by an iterative scheme in which the calculations for each time step include

- updating of groundwater density and viscosity based on solute concentrations,
- calculation of groundwater flow,
- calculation of component transport,
- calculation of water chemistry,
- update component mass fractions.

Within each time step, steps 1 through 3 may be iterated as needed improve accuracy. These calculations were carried out for a simulation period from 8000 BC to 60 000 AD using constant 20-year time steps. The water chemistry reaction calculations were performed using the IPhreeqc software library (Charlton and Parkhurst, 2011), only updating at locations where the mass fraction of any component had changed by 2% or more since the previous reactive-chemistry calculation at that location.

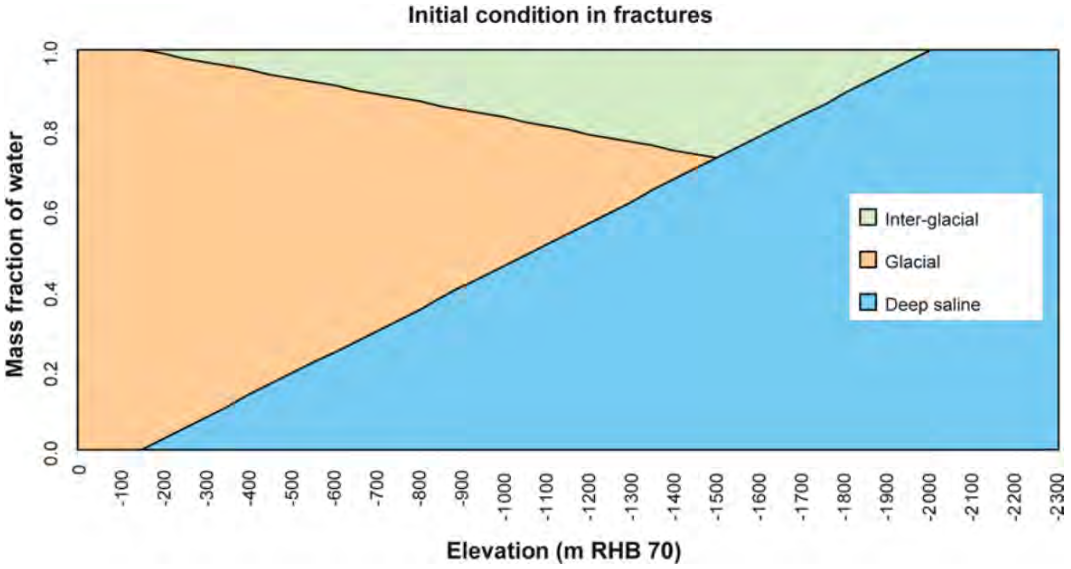

Figure 29 Initial conditions for mobile water in fractures in terms of mass fraction of reference waters, for the starting time of the catchment-focused model at 8000 BC. From Figure 3-8 of Joyce et al., (2020).

Table 3 Relation of reference water compositions to component mass fractions for the catchment-focused model at 8000 BC. From Table 3-7 of Joyce et al., (2019).

	Deep saline	Littorina	Altered Meteoric	Glacial	Interglacial
pH	8.000	7.952	7.842	9.300	7.909
pe	−4.448	−4.424	−1.046	−5.260	−3.160
Component mass fractions [kg/kgs]					
Al	1.847×10^{-10}	8.695×10^{-9}	5.477×10^{-9}	1.405×10^{-7}	7.753×10^{-9}
Br	3.080×10^{-4}	2.220×10^{-5}	0.000	0.000	3.430×10^{-5}
C	4.102×10^{-7}	1.931×10^{-5}	5.114×10^{-5}	1.023×10^{-6}	1.890×10^{-6}
Ca	1.836×10^{-2}	1.530×10^{-4}	7.150×10^{-6}	2.879×10^{-6}	1.585×10^{-3}
Cl	4.452×10^{-2}	6.641×10^{-3}	1.532×10^{-5}	7.963×10^{-7}	4.738×10^{-3}
F	1.523×10^{-6}	4.899×10^{-7}	3.850×10^{-6}	0.000	0.000
Fe	1.380×10^{-8}	7.861×10^{-7}	1.000×10^{-7}	4.469×10^{-8}	7.361×10^{-10}
K	2.980×10^{-5}	1.340×10^{-4}	2.970×10^{-6}	4.000×10^{-7}	4.001×10^{-6}
Li	4.417×10^{-6}	6.999×10^{-8}	1.100×10^{-8}	0.000	0.000
Mg	2.018×10^{-6}	4.479×10^{-4}	3.600×10^{-6}	1.000×10^{-7}	2.001×10^{-6}
Mn	1.333×10^{-7}	0.000	5.800×10^{-8}	0.000	0.000
Na	8.104×10^{-3}	3.673×10^{-3}	1.100×10^{-4}	1.700×10^{-7}	1.440×10^{-3}
S	2.879×10^{-4}	2.975×10^{-4}	1.195×10^{-5}	1.701×10^{-7}	1.252×10^{-4}
Si	2.298×10^{-6}	3.555×10^{-6}	3.801×10^{-6}	4.676×10^{-6}	3.620×10^{-6}
Sr	3.208×10^{-4}	2.680×10^{-6}	0.000	0.000	0.000

Three different calculation cases are simulated as detailed in Table 3-1 of Joyce et al. (2019):

1) No chemical reactions,
2) Equilibration of groundwater with calcite, quartz, and amorphous FeS,
3) Equilibration of groundwater with calcite, quartz, and iron (III) oxyhydroxide.

These are used to explore uncertainties associated with the hydrogeochemical interpretation of Laxemar.

The results from the catchment-focused model of groundwater evolution are presented in terms of reference water evolution (Section 4.2 of Joyce et al. 2019) and then in terms of the evolution of the spatial distributions of the individual components (Section 4.3). The presentation is mainly graphical as a series of color plots of vertical or horizontal cross-sections, with only brief discussion. The authors do not explain how the mixing fractions of reference waters are backed out of the mass fractions of individual components, e.g. using the method of Laaksoharju et al. (1999) as in previous work by SKB at this site. For reference-water evolution, Section 4.2.2 gives a single-paragraph narrative description of the model-predicted pattern of evolution for each of the reference waters, broadly consistent with the prior hydrogeochemical interpretation of Laxemar by Laaksoharju et al. (2009).

The presentation of component-wise evolution in Section 4.3 includes box-and-whisker plots to compare the results of the three calculation cases for total dissolved solids (TDS), chloride, magnesium, sodium, pH, calcium, inorganic carbon, redox potential (pE), sulfur and sulfide, and iron. Differences among these cases are generally negligible except for iron and sulfide which are influenced by the choice of redox pathway in Case 2 vs. Case 3, with a secondary effect on pE.

Numerical artifacts are noted for pE, pH and iron concentrations above the repository volume, assumed to result from insufficient resolution of the reaction front in the coarse grid used for this part of the model. Otherwise no discussion or sensitivity analysis is given of numerical stability of the model for the chosen iterative time-stepping scheme, or the degree to which any of the presented results could be influenced by numerical effects. This is surprising, considering that this appears to be the first practical application of the CONNECTFLOW software with coupling to the IPhreeqc library.

Sensitivities of the flow and transport results to the specific realization of the DFN model for the rock mass are evaluated in Section 4.4 of Joyce et al. (2019), by comparing results for the five realizations r1 through r5 (note that r2 through r5 also include stochastic heterogeneity within the HCD features). Variations in concentrations of chemical components within the repository volume are found to vary slightly depending on stochastic occurrence of large fractures, though the effect on mean concentrations is generally less than a factor of three between realizations.

Comparisons of model predictions to hydrogeological measurements are presented in Section 4.5 of Joyce et al. (2019), as a series of ten figures which show, for each of the two rock domains, the predicted profiles salinity and concentrations of chloride, calcium,

magnesium and sodium. The authors note that the results show very little difference between the three calculation cases for this study, and only minor differences with results from a previous implementation of the model by Joyce et al., (2010).

Some discrepancies between measurements and model predictions are apparent in these plots. For example, the model appears to predict a fairly uniform, nearly linear transition in salinity from freshwater at around 400 m depth, to concentrations of approaching 45 g/L at 1200 m depth (Figure 30), but the site data suggest that salinities remain relatively low until around 1000 m depth where there is a more abrupt transition. The authors give no discussion of this discrepancy for salinity, or of the other noticeable discrepancies for the cases of chloride, calcium, and magnesium. Possible consequences of these discrepancies are discussed briefly in Section 3.1 of this report.

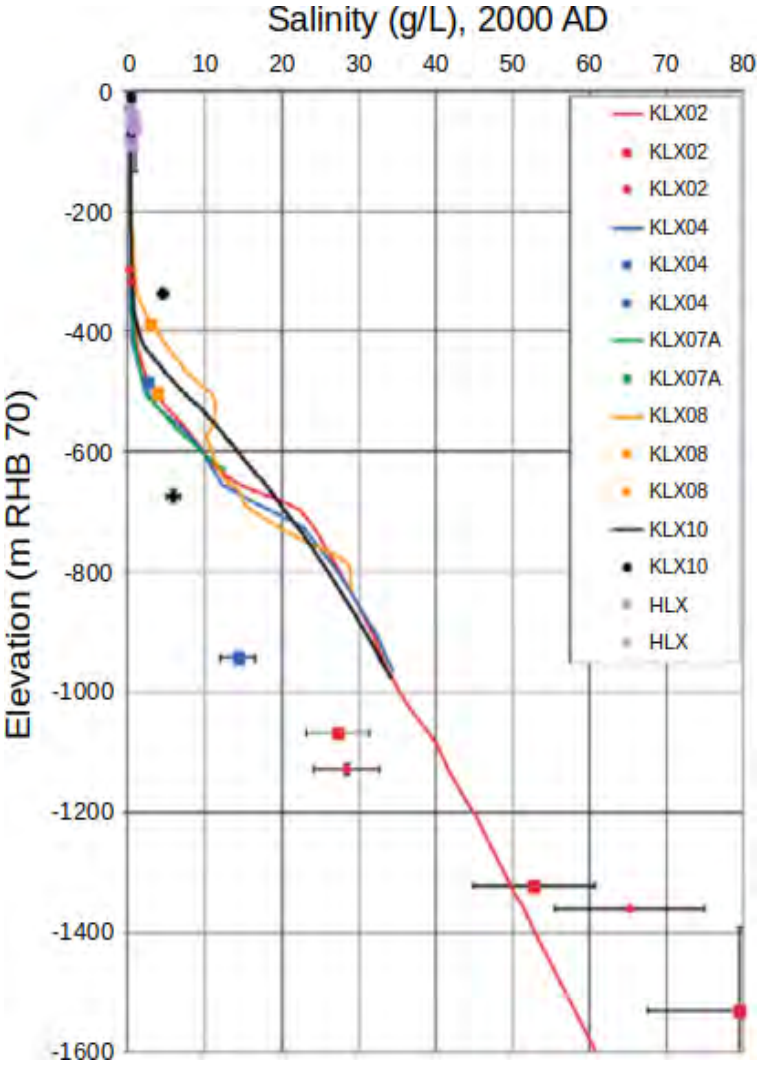

Figure 30. Comparison of the modeled and measured salinity distributions in the fracture system for boreholes in HRD_EW007 for Case 1 of the catchment-scale model. Square symbols are used for data rated as having higher quality (category 1–3 in the evaluation of Laaksoharju et al., 20009), and filled circles are used for category 4 data. The error bars on the data indicate the laboratory analytical error. Adapted from Figure 4-114 of Joyce et al. (2020) which includes similar results from Cases 2 and 3.

The sensitivity of the model to stochastic variability of the DFN model for the HRD is considered in Section 4.5.1 of Joyce et al. (2019). Comparison of the results with measurements are given for five realizations, for only for two boreholes, KLX03 and KLX08. Those two boreholes yielded only two measurements at or below the depth of the hypothetical SFL. Both of these salinity measurements at depth are outside of the observed range of variation among stochastic realizations, by a margin greater than can be explained by laboratory analytical errors (Figure 31). Significant discrepancies between model and measurements are also seen for chloride, calcium, and magnesium concentrations. The authors attribute these discrepancies to the fact that "there has been no attempt made to calibrate the current model (Joyce et al., 2019, p. 163) and also suggest that there is considerable uncertainty in the true values of these concentrations at depth due to limited data. They give no discussion, either in this section or in the summary and conclusions, as to what these results imply about the reliability of their predictions of hydrogeochemical evolution for application in SE-SFL.

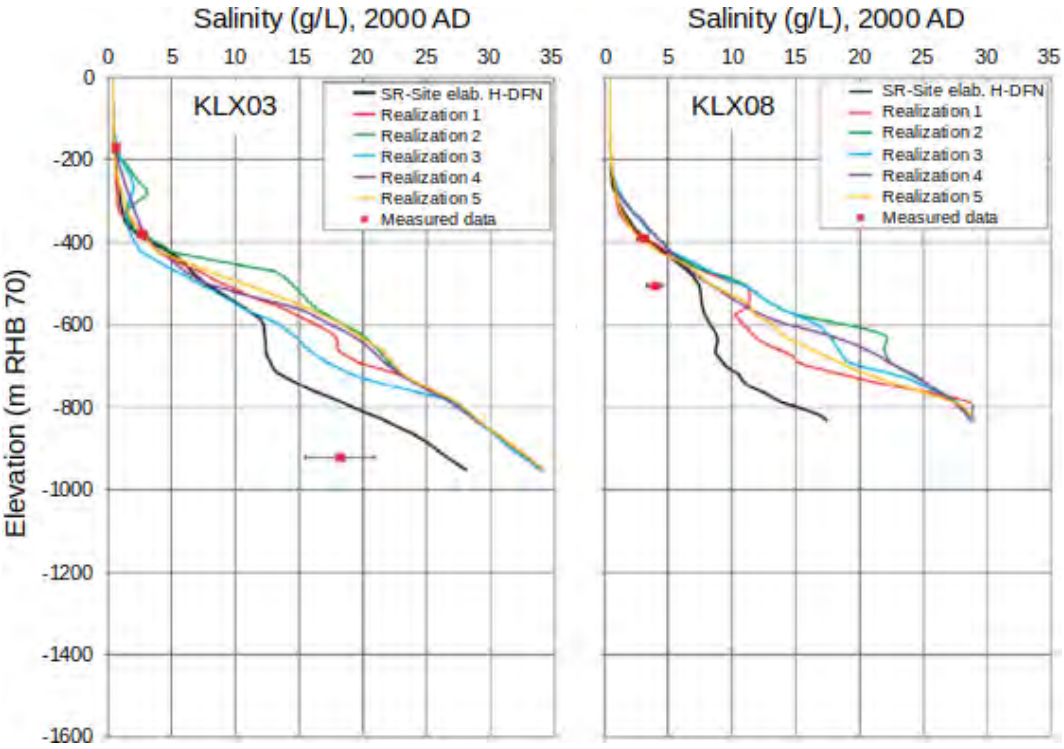

Figure 31. Comparison of the modeled salinity distributions in the fracture system for boreholes KLX03 (left) and KLX08 (right) for the SR-Site elaborated Hydro-DFN case (black line) and the five realizations of Case 1. The measured salinities are shown as square symbols (category 1–3 data). The error bars on the data indicate the laboratory analytical error. Adapted from Figure 4-123 of Joyce et al. (2019).

2.4.3 Facility-focused modeling

The facility-focused model covers the same spatial domain as the catchment-focused model, but differs in its representation of the volume around the vaults. The facility-focused model is used mainly to predict discharge locations for flow paths that pass through the vaults, and certain hydrogeological performance measures associated with these flow

paths (as detailed below). These predictions are carried out for a series of "time slices" which were considered to be of interest for the safety evaluation:

- 7980 BC (when the repository location is below the sea);
- 4000 BC, 2000 BC, and 0 AD (as the repository location rises progressively higher above the sea due to post-glacial isostatic rebound);
- 2000 AD (representing assumed conditions at time of repository closure); and 5000 AD, 20 000 AD and 60 000 AD (representing continuing land uplift at later stages of a temperate period).

Note that times in the past are considered, for the purposes of SE-SFL, to be representative of future conditions at similar stages of temperate climate evolution following future glaciations.

Representation of repository vaults and tunnels

The facility-focused differs in its representation of the repository facility and the surrounding rock in the following ways:

- using a DFN rather than ECPM representation for the facility-scale volume,
- including smaller scale fractures in a refined volume,
- representing the vaults and repository structures at the disposal depth by continuum elements, and
- representing other repository structures (spiral ramp and shaft) by planar conductive features.

More specifics regarding the sizes of these domains and their representation have been summarized in Table 2.

Selection of properties for regolith portion of model

Calibration of regolith layers is confusingly presented in the section (Section 3.3.3) on the catchment-focused model, while it seems to pertain to the facility-focused model. A set of variational cases were simulated and compared in terms of their match to head and pressure data from shallow boreholes. The set of regolith parameters that were judged to give the best results are summarized in Table 3-8 of Joyce et al. (2019). The comparison was subjective rather than systematic, without use of any method for iterative optimization.

Initial and boundary conditions

For each "time slice," water density values and water pressures as calculated by the catchment-focused model are transferred to the facility-focused model. The pressures are applied as an upper boundary condition. The water density values are assigned to points on fractures or in ECPM grid cells throughout the model domain.

These are stated to be used as "initial" and boundary conditions, but their application is for calculation of steady-state pressure solutions (Joyce et al., 2019, p. 35-36) so the term

"initial conditions" is confusing. Apparently what is meant is that the assigned water density values are used to define a spatial distribution of density which is assumed to remain constant for the given time slice.

Flow solution and particle tracking

For each time slice, a steady-state, density-dependent pressure solution, assuming fully saturated conditions, is then calculated consistent with the pressures imposed at the upper boundary, assuming no-flow conditions at the base of the model and on the sides of the catchment-scale domain. The choice of no-flow condition on the sides of the model is supported by the use of catchment boundaries (surface-water divides) as the boundary of the domain. The groundwater flow field within the model is calculated based on the local pressure gradients along with the local hydraulic properties.

Advective transport paths (streamlines) within the model are then traced by advective particle tracking, using forward tracking from fractures intersecting the vaults to determine discharge paths. At fracture intersections, flux-weighted probabilistic routing is used to determine which out-flowing branch receives the particle. Reverse tracking is also used to determine the corresponding recharge paths by which groundwater reaches the vaults.

Ten particles were released per fracture/vault intersection, regardless of the magnitude of the groundwater flux through a given fracture. The reason for using a fixed number of particles per fracture, rather than a number proportional to the flux, is not explained. The potential consequences of this choice for the calculated distributions of performance parameters is investigated by independent calculations in Chapter 4 of this review.

The ratio of advective velocity to groundwater flux through a fracture is controlled by the ratio of transmissivity to effective transport aperture, e_t. As noted above (Section 2.4.1), the relationship used by Joyce et al. (2019) is not clearly specified. There is analogous ambiguity for the deformation zones. According to Joyce et al. (2010) the effective transport aperture in deformation zones was calculated as:

$$e_t = \varphi\, b$$

where φ is the porosity and b is the thickness of the deformation zone at that point, but the deformation zone thicknesses are not stated in Joyce et al. (2019).

Joyce et al. (2019) note that some of the particles released into the model become "stuck" without reaching a discharge point. They attribute this to numerical imprecision, for example in dead-end branches of the fracture network which do not carry flow in steady-state conditions, but which particles could enter according to the particle-tracking algorithm if small numerical errors in the finite-element pressure solution indicate a non-zero component of water flux into such a dead-end branch. From the results presented in Chapter 4 of Joyce et al. (2019), typically fewer than half of the released particles arrive at the model boundaries.

Calculation of performance measures

The following performance measures are calculated directly from the flow solution for fractures intersecting the waste vaults:

- equivalent flow rate Q_{eq} [m^3/y] at the release point from the vault into a single fracture; and
- equivalent flux U [m^2/y] at the release point from the vault into a single fracture.

Here Q_{eq} is not an actual water flux but rather a representation of diffusive solute transfer from a nominally immobile volume (e.g. pore water in the bentonite or concrete backfill in a vault) into mobile water flowing along the vault/fracture interface, such that if the concentration of solute in the backfill at the interface is c_o, then the rate of diffusive solute transfer into the fracture is $Q_{eq}c_o$. A formula for Q_{eq} is derived (Joyce et al., 2019, Appendix B) based on simplified geometry following similar derivations developed by SKB for flow around a deposition hole in a spent-fuel repository (Neretnieks, 1980).

The equivalent flux U is calculated as a weighted average of flow rate per unit fracture width over all fractures f intersecting the vault:

$$U = \sum_f q_f L_f \Big/ \sum_f L_f$$

where L_f is the length of the intersection between the vault and a given fracture.

The remaining performance measures (path length L, travel time t, and transport resistance F) for each trajectory are calculated effectively as summations of the corresponding measures for a given segment of the trajectory (incremental length δL, incremental time $\delta t = e_t \delta L / q_f$, and incremental transport resistance $\delta F = 2\delta t / e_t$), over all steps in the trajectory.

Evolution of performance measures with time after closure

For the main calculation case (based on the single realization r1 of the DFN model without variability in the HCD transmissivities), results are presented as a series of plots showing the recharge and discharge locations for streamlines passing through the repository vaults, for each of the modeled time slices (Figures 4-126 through 4-133 of Joyce et al., 2019), as well as summary statistics and plots of the cumulative distribution functions (CDFs) of the performance measures Q_{eq}, U, t, L, and F (Table 4-4 and Figures 4-137 through 4-141).

Effects of stochastic variation in the DFN and HCD components of the model were also explored for the four additional realizations r2 through r5, and compared with the main calculation case for 2000 AD in Figures 4-142 through 4-149 and Table 4-5.

The results indicate that discharge locations in this model are strongly influenced by the deformation zones, especially for temperate situations where the repository site is fully

above sea level. Stochastic variability between realizations of the DFN and HCD transmissivity patterns may affect where discharge paths emerge along these structures, but not which structures serve as the key foci of discharge (Figure 32), particularly the zones ZSMNS001e and ZSMEW007a as labeled in the figure.

The main exception to this pattern is for the earliest time slice modeled, 7980 BC, when the site is still submerged, and the pattern of discharge is more diffuse. In that case additional deformation zones play a role, along with smaller-scale fractures represented in the stochastic DFN model.

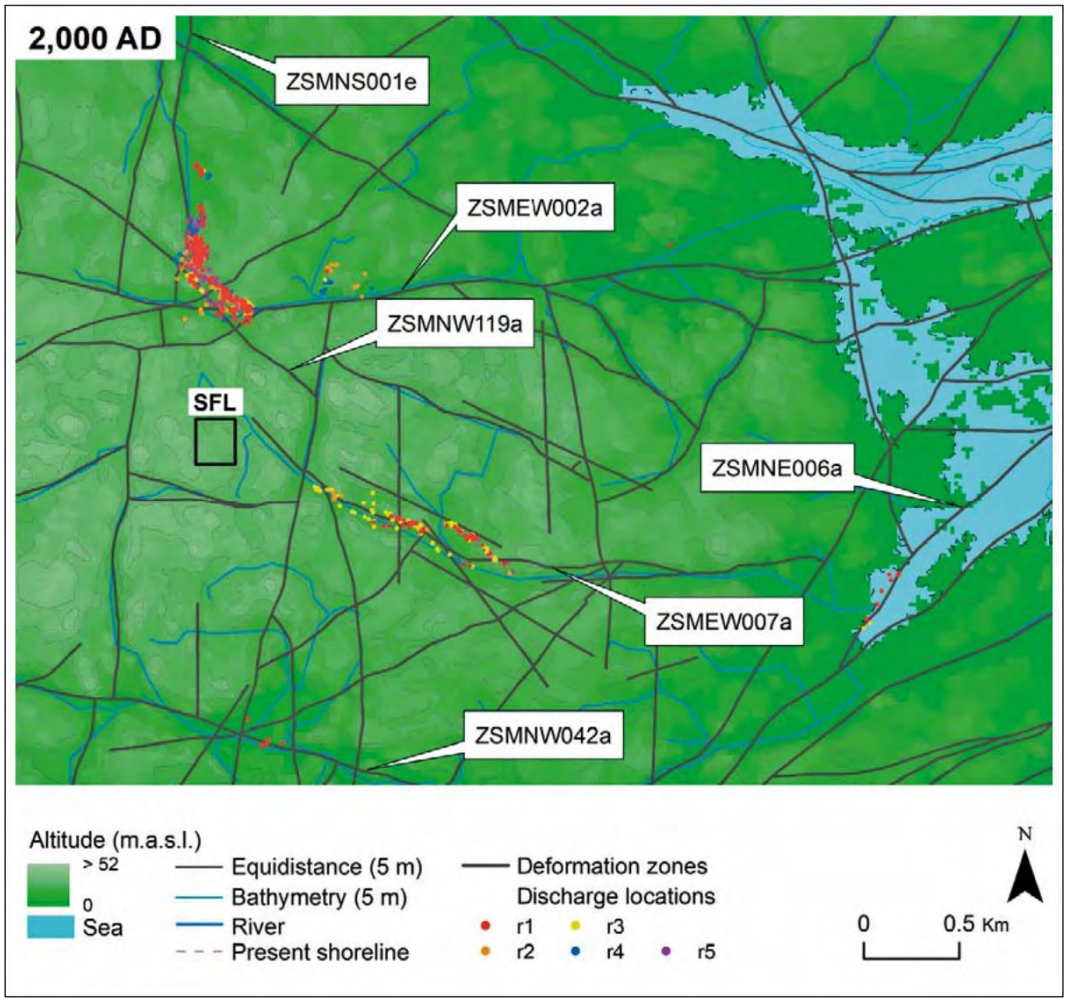

Figure 32 Particle discharge locations at the ground surface for each realization of Case 1 of the facility-focused model at 2000 AD, according to the color of the dots (r1=red, r2=orange, r3=yellow, r4=dark blue, r5=purple). The model surface is colored by elevation (land in green, sea in pale blue). Rivers (blue), present shoreline (dashed gray), deformation zones at −20 m elevation (dark gray) and the SFL repository location (black) are added for context. From Figure 4-149 of Joyce et al. (2019).

The distributions of performance parameters similarly show that, once the site emerges from the sea, continuing land rise through the temperate period has comparatively little effect on the cumulative distributions of transport resistance *F* (Figure 33) or other performance parameters.

Variation among realizations has a stronger effect, with one of the five realizations, r3, showing significantly faster transport times and lower transport resistance than the main calculation case (Figure 34). This indicates that connections formed by discrete fractures in the stochastic part of the model, together with variability in the deformation zones, could significantly affect retention in the geologic barrier.

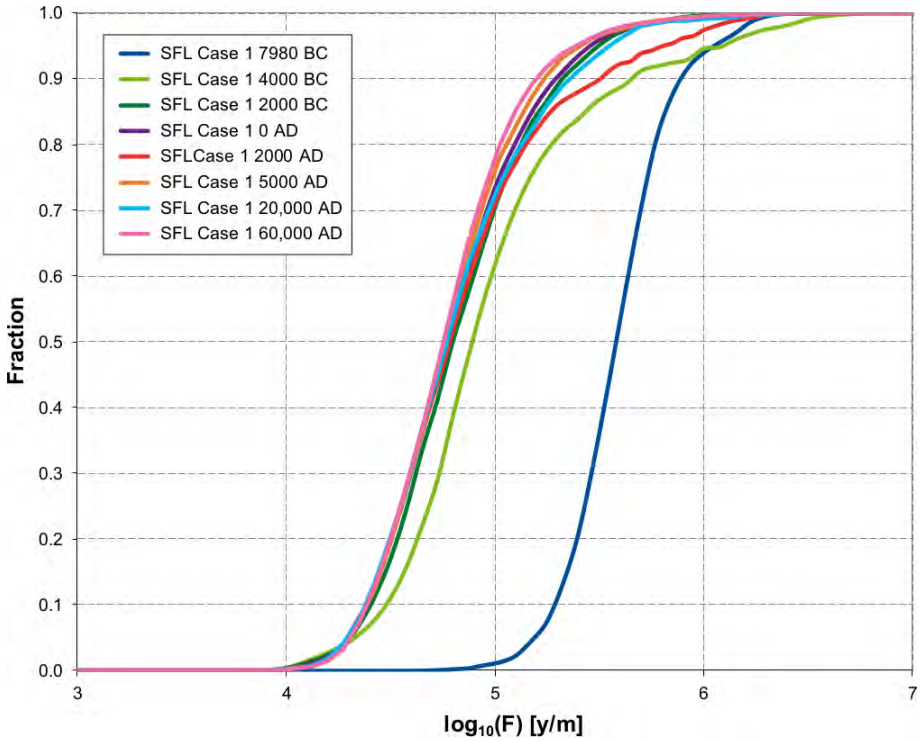

Figure 33 Cumulative distribution of flow-related transport resistance (F) for realization r1, Case 1 of the facility-focused model for particles released at different times (according to the legend), normalized for fraction of particles successfully reaching the model top boundary (34–47 %), From Figure 4-139 of Joyce et al. (2019).

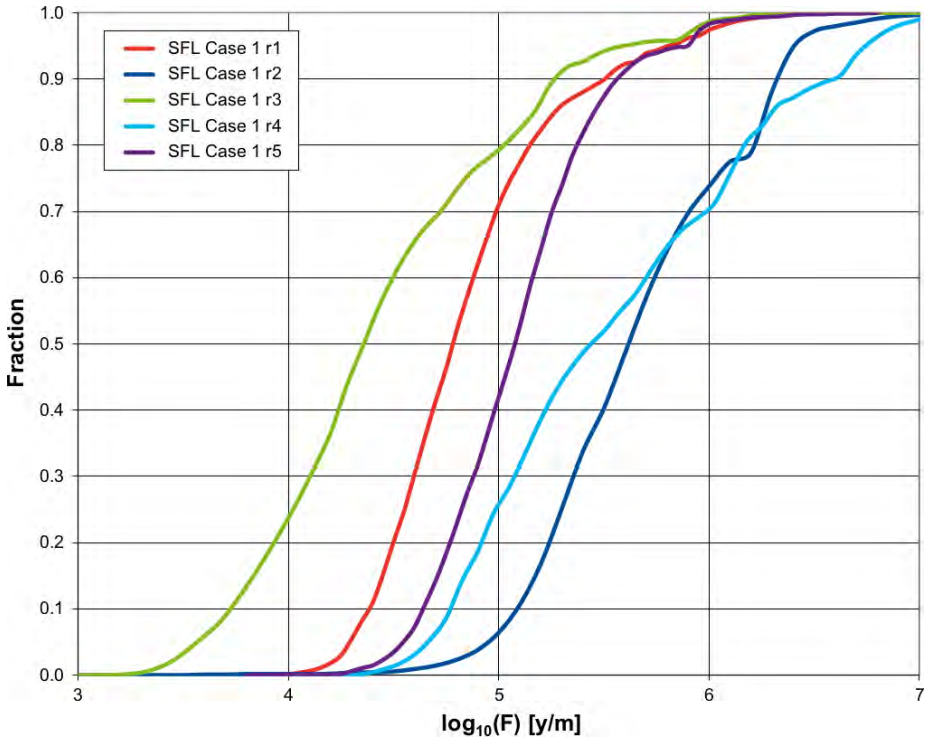

Figure 34 Cumulative distribution of flow-related transport resistance (F) for five realizations of Case 1 of the facility focused model, normalized for fraction of particles successfully reaching the model top boundary (26–46 %), released at 2000 AD. From Figure 4-144 of Joyce et al. (2019).

Effect of chemical reactions affecting groundwater density

The three chemical calculation cases considered (1: no chemical reactions, 2: equilibration of groundwater with calcite, quartz, and amorphous FeS, and 3: equilibration of groundwater with calcite, quartz, and iron oxyhydroxide) produce only minor effects on the flow-related performance parameters, as summarized in Table 4-6 and Figures 4-150 through 4-154 of Joyce et al. (2019). This low sensitivity is attributed to the low impact on groundwater densities. Results for Cases 1 and 3 are nearly identical. Case 2 produces slightly fewer high-*F* paths, but the frequency of low-*F* paths (which have a more critical impact on safety) is virtually unchanged.

Effect of concrete degradation

A case with degraded concrete in the BHK vault (represented by increasing the hydraulic conductivity from 8.3×10^{-10} m/s to 1.0×10^{-7} m/s) is also included in the Table 4-6 and Figures 4-150 through 4-154 of Joyce et al. (2019). The main effect is for more flow to pass through the vaults which (counter-intuitively) leads to lower values of Q_{eq} and U. This is explained by the fact that these measures depend on flow rates around the vaults which are reduced because the concrete in the BHK vault does not force as much flow to be diverted around the vault. This variant also produces more high-*F* paths relative to the base case, but the frequency of low-*F* paths is virtually unchanged.

Effect of water-supply wells

The effect of a water-supply well located in a discharge area for water passing through the repository was explored by considering five additional calculation cases, each with a 60 m deep well in a different location, pumped at a rate of 700 L/d. According to Joyce et al. (2019, Section 4.7) each of the five wells was confirmed to intersect at least one flowing fracture. Otherwise the rationale for choice of well locations is not explained.

Only one well location resulted in tracked particles reaching the well. In this case, of 4660 particles that leave the vaults, 116 (2.5%) reach the vaults. The number of "stuck" particles for this well case is not noted, but for other cases typically fewer than half of the particles reached the surface, so presumably this represents about 5% of the paths from the repository that reach the surface environment.

Effects of the wells perturbing nearby discharge paths (even paths that do not lead directly to the well) were evaluated in terms of impacts on flow-related performance parameters. Impacts were mostly minor but for two well locations, there was a decrease in the high-end tail of the distribution of *F* values.

2.4.4 Near-field hydrogeological modeling

The near-field model (Abarca et al., 2019) is used to calculate flows through the vaults and waste, as well as to model degradation of the concrete backfill in the BHK vault.

The commercial software COMSOL Multiphysics (COMSOL, 2015) is used to solve equations for density-dependent, saturated groundwater flow with coupled advective-dispersive transport of chloride (representing salinity). The equations solved account for quasi-steady Darcy flow (i.e. no storage effects due to changing pressures):

$$\nabla \cdot (\rho u) = 0$$

$$u = \frac{-k}{\mu}(\nabla p + \rho g \nabla z)$$

where ρ is the density, μ the dynamic viscosity, $\boldsymbol{u}$ the Darcy velocity, k the permeability of the porous medium, p the absolute water pressure, g the acceleration of gravity (9.81 m/s^2), and z is elevation.

Flow is coupled to steady-state transport of chloride as a function of water velocity and concentration gradients in the mobile pore water (i.e. no matrix diffusion):

$$\nabla \cdot (cu) - \nabla \cdot [(D_D + D_e)\nabla c] = 0$$

where c is concentration, D_e is the effective diffusion coefficient (presumably multiplied by the identity tensor $\mathbf{I}$), and $\mathbf{D_D}$ is the mechanical dispersion tensor calculated from the local Darcy velocity:

$$D_D = \alpha_L |u| + (\alpha_L - \alpha_T)\frac{uu^T}{|u|}$$

with α_L and α_T being the longitudinal and transverse dispersivity, respectively.

Water density varies as a linear function of chloride concentration. Temperature effects are not considered, and μ is treated as constant.

Abarca et al. (2019, p. 18) note that in practice that for the low groundwater velocities predicted after closure of the SFL, the diffusion term (D_e) in the transport equation dominates over the velocity-dependent dispersion ($\mathbf{D_D}$). Previous sensitivity calculations (Abarca et al., 2016) indicated little sensitivity to the dispersivity values α_L and α_T.

Tracer transport (meaning, non-reactive transport of dilute species that do not affect the flow) is also modeled. Two types of tracer transport were carried out to study solute transport in the near field:

Tracer transport I: Steady-state advective-diffusive transport using the same transport equation as for chloride, used to evaluate potential interaction between vaults.

Tracer transport II: Transient advective-dispersive transport to model transport through the backfill for solute released from the waste/backfill interface:

$$\phi \frac{\partial c}{\partial t} + \nabla \cdot (cu) - \nabla \cdot [(D_D + D_e)\nabla c] = 0$$

Model geometry

As described in Table 2, the near-field model volume is a box 1 km square by 650 m deep, with upper surface at z = –250 m. This volume is approximately centered on the vaults and extends 400 m below them.

The model includes a detailed representation of the waste vaults, access tunnels, ramp and shaft. The BHK backfill is divided into inner and outer zones to permit modeling three cases:

- base case: BHK backfill is fully intact;
- degraded case: BHK backfill is fully degraded; and
- degraded zone case: BHK backfill is degraded in an outer zone but intact in the remaining inner zone.

The thickness of the outer zone for the last case is not clearly specified but from Figures 3-6 and C-3 of Abarca et al. (2019), this appears to be represented as an annular zone on the order of 1 m in thickness.

Boundary and initial conditions

Boundary conditions for the flow model are imposed as absolute pressures specified on the outer surfaces of the model, based on residual pressures and chloride concentrations calculated by Joyce et al. (2019). Where the ramp and shaft intersect the upper surface of the model, a zero-flux boundary condition is imposed. The initial chloride concentrations in the interior of the model are also imported from the regional model.

For tracer transport modeling to study potential interactions between vaults (tracer transport I), a unit concentration is prescribed at the vault serving as the source. For modeling of tracer transport through the backfill (tracer transport II), a unit concentration is prescribed at the waste/backfill interface. In both cases I and II, the initial concentration of tracer throughout the domain is $c = 0$, and the outer surfaces of the model are assigned either a prescribed concentration (where flow is inward to the model domain) or a mass flux boundary condition (where flow is outward).

Hydraulic and transport properties

The waste vaults, access tunnels, ramp and shaft are assigned isotropic properties based on the closure specifications (Table 4). The hydraulic properties of the host rock are taken from what Abarca et al. (2019) refer to as the "regional hydrogeology model" of Joyce et al. (2019). Whether this refers to the catchment-focused model or the facility focused-model is not clear from the presentation.

Table 4: Repository and host rock material properties (adapted from Tables 3-2 and 3-3 of Abarca et al., 2019).

Model component	Material	State	Permeability k (m^2)[1]	Effective diffusivity D_e (m^2/s)	Porosity ϕ (–)
Access tunnels backfill	Crushed rock		2.0×10^{-12}	6.0×10^{-10}	0.30
Waste domain	Homogenized		2.0×10^{-14}	3.5×10^{-10}	0.30
Sealing sections	Bentonite		2.0×10^{-20}	1.4×10^{-10}	0.43
BHA backfill	Bentonite		2.0×10^{-20}	1.4×10^{-10}	0.43
BHK backfill	Concrete	Intact	1.7×10^{-16}	3.5×10^{-12}	0.11
BHK backfill	Concrete	Degraded	2.0×10^{-14}	5.0×10^{-12}	0.14
Host rock	Fractured bedrock		variable[2]	3.2×10^{-14} to 4.35×10^{-10}	variable [2]

[1] Calculated assuming water density $\rho = 1\,000$ kg/m^3 and dynamic viscosity $\mu = 0.002$ Pa·s.

[2] Host rock k and ϕ values imported from model of Joyce et al. (2019); D_e proportional to local ϕ.

The anisotropic permeability field from the "regional" model is interpolated onto the finite-element mesh for the near-field model, as implemented in COMSOL (COMSOL, 2015).

The details of the interpolation are not discussed (though from Appendix A of Abarca et al., 2019, apparently off-diagonal components of the $\boldsymbol{k}$ tensors calculated by CONNECTFLOW are not part of the data transfer). From plots of the interpolated fields (Figures 35 and 36), the interpolation apparently results in some smearing and distortion of the k values, possibly resulting in loss of continuity for high-k bands that represent the upscaled stochastic fractures. For example, ST8 in Figure 36 appears as a string of bright yellow blobs (indicating $k_{xx} \approx 10^{-15}$ m^2) separated by green (indicating $k_{xx} \approx 10^{-16}$ m^2).

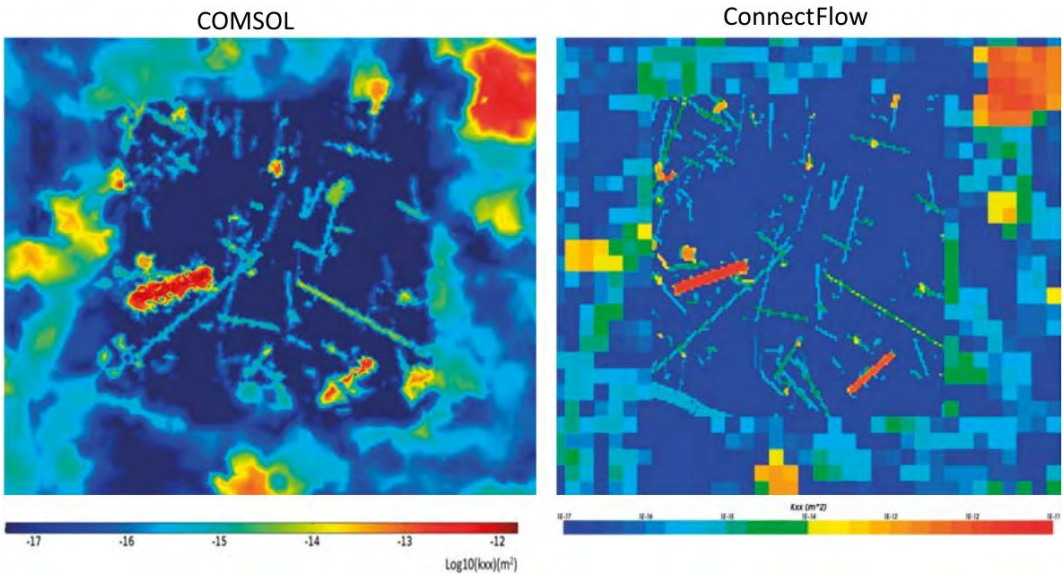

Figure 35. ConnectFlow permeability field imported in COMSOL and interpolated over the COMSOL mesh (left) and the actual permeability field in ConnectFlow (right). From Figure A-1 of Abarca et al., (2019).

Consistency between the COMSOL adaptation and the CONNECTFLOW model was checked by visual comparisons of the imported vs. calculated residual pressure and chloride concentration fields, and also by a quantitative check of the residuals (Appendix A of Abarca et al., 2019), for a model run that omitted the repository. Over most of the model domain, residual pressures were found to agree within ±2% but discrepancies of up to 8% were found in small parts of the domain. Abarca et al. (2019) conclude that this is good agreement. They do not present any information on which parts of the domain had the highest discrepancies between models, in particular, whether the discrepancies are worse in the central part of the model where the repository is placed for subsequent calculations. Groundwater flow rates are determined by pressure gradients rather than absolute values of pressure, but no check is given of the magnitude of pressure gradients.

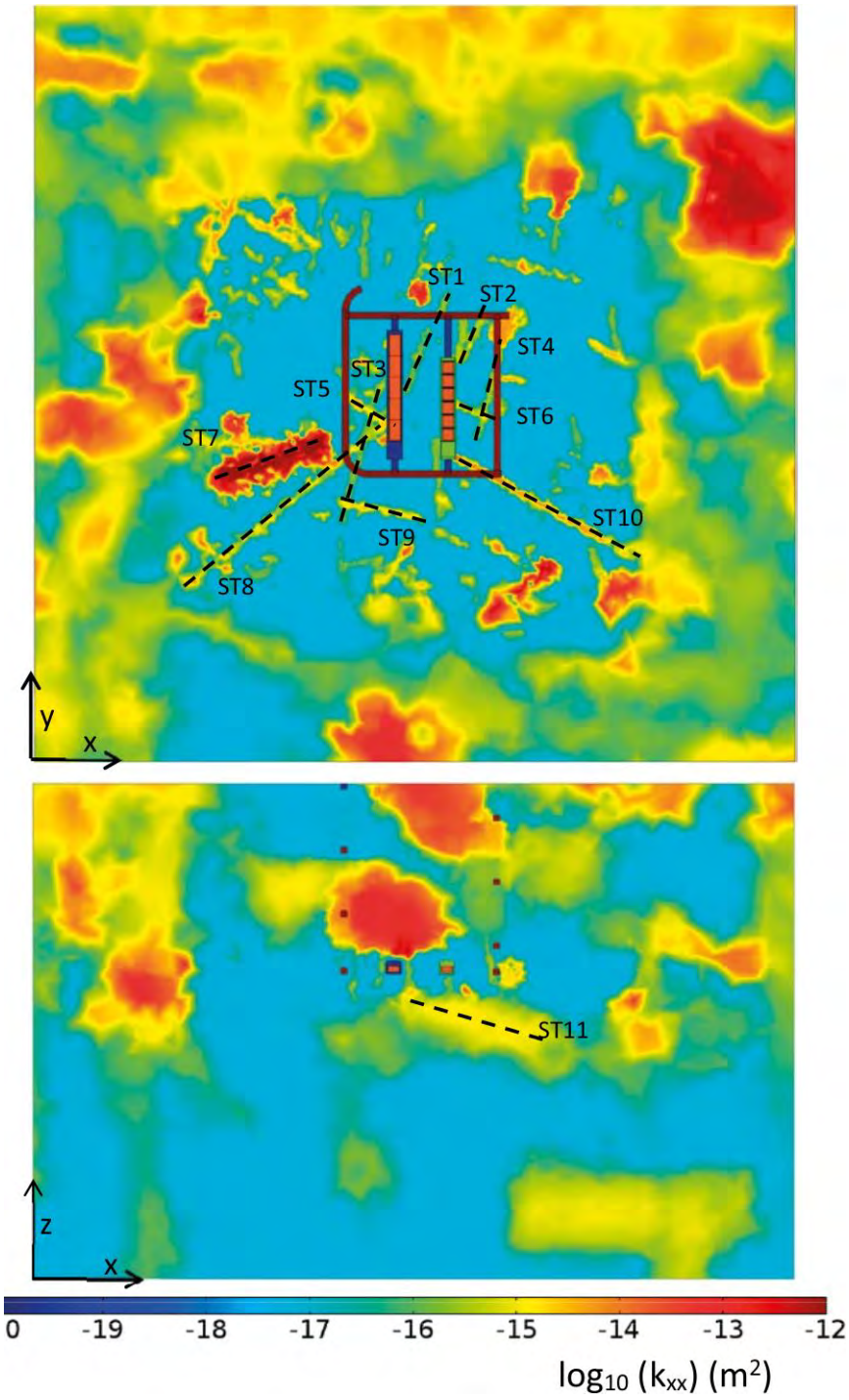

Figure 36 Rock permeability field after importing into the near-field model, showing the horizontal E-W component in a horizontal plane (top) and N-S vertical plane (bottom) intersecting the BHA and BHK vaults, with permeability values of the repository materials for the base case. The dashed lines delineate approximately the ECPM representation in COMSOL of large stochastic fractures labeled ST1 through ST11). North is oriented along the y-axis. From Figure 3-8 of Abarca et al. (2019).

Predicted flow field

Streamlines calculated by the near-field flow model show an interface between the fresh-water-driven flow system in the upper part of the model and saline water flowing upward from depth. As shown in Figure 37, this interface is 200 m or more below the repository over most of the model domain, but with localized upconing to repository depth along major deformation zones. Water reaching the vaults from the surface continues downward until it approaches this interface, then turns eastward (Figure 38).

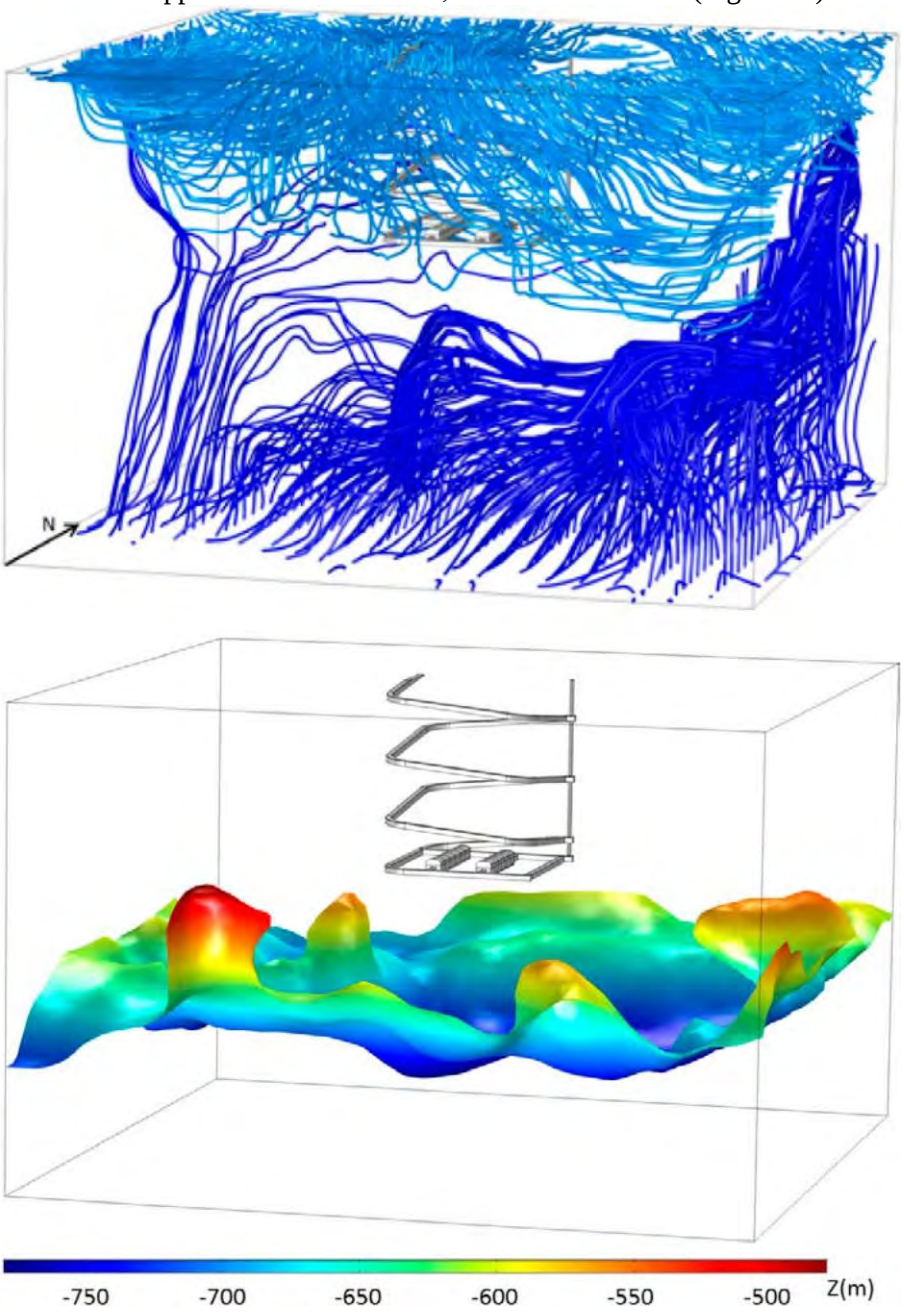

Figure 37. Flow field calculated by the near-field model, illustrated (top) by streamlines (light blue and dark blue for water entering through the top and from the bottom boundary, respectively) and (bottom) by the isosurface of salinity equal to 0.006 kg/kgs representing the location of the saline interface (colored according to its elevation to illustrate local upconing associated to deformation zones). From Figure 4-2 of Abarca et al. (2019).

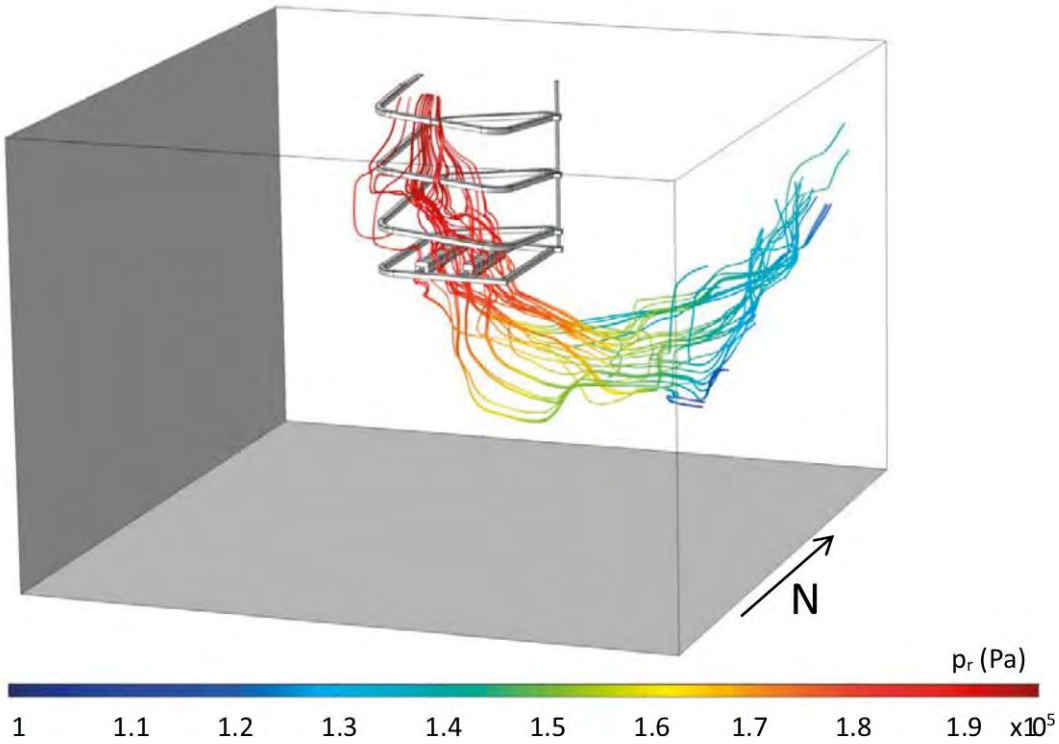

Figure 38. Groundwater flow streamlines passing through the waste control volume of the BHA and BHK vaults according to the base-case of the near-field scale model of Abarca et al. (2019, Figure 4-5).

Calculation of flow rates through vaults and waste compartments

The main quantitative results produced by the model for the SE-SFL safety evaluation are flow rates through the BHA and BHK vaults and waste. The flow Q_{vault} through each vault is calculated by integrating the inward component of the Darcy flux vector $\vec{q}$ over the interface between the rock and backfill, written by Abarca et al. (2019) as:

$$Q_{Vault} = \sum \iint_{\vec{q}\cdot\vec{n}>0} \vec{q} \cdot \vec{n}$$

where $\vec{n}$is the inward vector normal to a given point on the interface, and the integral is taken over the entire interface. The summation sign in this formula is not explained but presumably implies a summation over different facets of the closed surface formed by the interface.

Similarly the flow Q_{Waste} through each waste compartment is calculated by integrating the inward component of Darcy flux over the area of the corresponding interface between the backfill and the waste compartment. For the BHA all of the waste is enclosed in a single large compartment so there is just a single value of Q_{Waste}.

For the BHK there are six waste compartments, so the reported value is the average of Q_{Waste} over the six compartments. In situations where flow passes through more than one waste compartment (for example, if there is axial flow along the length of the vault), it is possible for the average Q_{Waste} times the number of compartments to exceed Q_{Vault}.

More detailed flow data are also provided for each of 7 sections in BHA and each of 8 sections in BHK. Each of these sections are further divided into multiple control volumes representing the waste and different parts of the associated backfill (as detailed in Appendix C of Abarca et al., 2019). The flow values are calculated by adding up flows crossing each face of a given section (or control volume) as:

$$Q_{C,face} = \iint \vec{q} \cdot \vec{n}$$

$$Q_{\mathrm{C,section,in}} = \sum_{Q_{face}<0} Q_{face}$$

$$Q_{\mathrm{C,section,out}} = \sum_{Q_{face}>0} Q_{face}$$

From the presentation on p. 23 of Abarca et al. (2019), it is not clear how situations with curving streamlines resulting in separate areas of inflow and outflow across a single face, i.e.:

$$\iint_{\vec{q}\cdot\vec{n}>0} \vec{q} \cdot \vec{n} > 0 \text{ or } \iint_{\vec{q}\cdot\vec{n}<0} \vec{q} \cdot \vec{n} < 0$$

would be accounted for in this calculation, or whether such a situation was in fact encountered for the cases considered.

Calculation of transport measures

The steady-state fraction of tracer released from one vault and passing through the second vault (tracer transport I) is calculated as the integral of inward-directed mass flux to the second vault, divided by the integral of mass flux leaving the model domain (which must be equal to the amount released from the source).

Time-dependent release of tracer from the backfill to the rock (tracer transport II) is calculated by summing the integrals of the advective, diffusive, and dispersive components of mass flux over the backfill/rock interface of the vault containing the waste from which the tracer is released.

Effects of repository design rotation and degradation of BHK backfill

Flows through the repository were calculated for three main cases:

- base case in which the BHK backfill is intact,
- degraded-zone case in which the outer zone of the BHK backfill is degraded with increased porosity and permeability according to the values given in Table 4, and
- fully-degraded case in which the entire BHK backfill is degraded.

For the first two of these cases, four different versions of the repository layout were modeled by rotating the entire layout of the repository about a vertical axis by 0° (no rotation), 90°, 180°, and 270°. For the 0° and 180° versions, the long axes of the vaults are aligned E-W; for the other two versions the vaults are aligned N-S.

Calculated flows for these cases are summarized in Tables 5 and 6 and Figures 39 and 40. Results for the base case indicate flows on the order of deciliters per year through the BHA waste and about 20 L/y through the BHA vault as a whole, with flows 2 to 3 orders of magnitude higher through the BHK waste and vault, respectively.

The degraded-zone case yields higher flows through the BHK vault as a whole, but flow through the BHK waste is reduced as the degraded zone allows more flow to bypass the waste compartments. Flows in the BHA (both through the waste and through the vault as a whole) are also slightly reduced as the higher net conductivity of the BHK diverts a portion of the flow away from the BHA.

Abarca et al. (2019) do not list numerical values of the total flows through the BHA and BHK vaults for the fully degraded case, but from graphs on p. 50 it can be seen that the flow through the BHA in this case is nearly identical to that for the degraded-zone case, while the flow through the BHK increases by about 15%. Abarca et al. (2019) also compare flows through each of 7 backfill sections for BHA and each of 8 backfill sections for BHK. The average of these flows for BHK increases by a factor of 4.8 relative to the base case and by a factor of 1.3 relative to the degraded-zone case. The corresponding average flows for BHA decrease by 6% relative to the base case and by 0.5% relative to the degraded zone.

The alternative rotations considered for the base case and degraded-zone case produce less than an order of magnitude variation in the flows. Higher flows through the vaults are obtained for the 90° and 270° rotations which have the long axis of the vaults aligned N-S, relative to the other two cases with the vaults aligned E-W.

Contradictions are apparent between the data given in tables vs. text and figures of Abarca et al., (2019). According to the text on p. 40 and the accompanying Figure 5-9 of Abarca et al., (2019), the lowest flows to the BHA vault occurs for the unrotated (0°) case. However this is contradicted by the ratios for the 180° rotation case in their Table 5-1, which indicate that the lowest flows in both BHA and BHK result from the case of a 180° rotation. A similar contradiction can be seen between Table 5-4 and Figure 5-10 of Abarca et al. (2019) for the case of a degraded zone. Values calculated based on these tables are given here in Tables 5 and 6, for comparison with Figures 39 and 40.

Table 5: Summary of computed flows through the BHA and BHK vaults for the base case and degraded-zone case. Values for 0° rotation versions of the base case and degraded-zone case taken from Tables 4-1 and 5-4 of Abarca et al. (2019). Values for the rotated cases are calculated by multiplying those values by the factors given in Tables 5-1 and 5-4 of Abarca et al. (2019). Values for the fully degraded case are estimated from Figure 6-10 of Abarca et al. (2019).

	Rotation	Base case Q_{Vault} (m^3/y)	Degraded zone Q_{Vault} (m^3/y)	Fully degraded case Q_{Vault} (m^3/y)
BHA	0°	0.022	0.021	0.021
	90°	0.079	0.075	
	180°	0.008	0.008	
	270°	0.039	0.037	
BHK	0°	1.09	3.40	3.9
	90°	1.07	3.84	
	180°	0.49	1.02	
	270°	0.97	4.69	

Table 6: Summary of computed flows through waste control volumes in BHA and BHK vaults for the base case, and degraded-zone case, and fully-degraded case. Values for 0° rotation versions of these cases are taken from Tables 4-1, 5-4, 6.1 and 6.2 of Abarca et al. (2019). Values for the rotated cases are calculated by multiplying those values by the factors given in Tables 5-1 and 5-4 of Abarca et al. (2019). Minimum and maximum values for Q_{waste} are taken over the set of 5 waste control volumes for BHA and the 6 waste control volumes for BHK.

	Rotation	Base case Minimum Q_{Waste} (m^3/y)	Degraded zone Minimum Q_{Waste} (m^3/y)	Fully degraded case Minimum Q_{Waste} (m^3/y)	Base case Maximum Q_{Waste} (m^3/y)	Degraded zone Maximum Q_{Waste} (m^3/y)	Fully degraded case Maximum Q_{Waste} (m^3/y)
BHA	0°	0.17×10^{-3}	0.16×10^{-3}	0.16×10^{-3}	0.51×10^{-3}	0.49×10^{-3}	0.49×10^{-3}
	90°	0.33×10^{-3}	0.32×10^{-3}		0.93×10^{-3}	0.90×10^{-3}	
	180°	0.05×10^{-3}	0.05×10^{-3}		0.15×10^{-3}	0.15×10^{-3}	
	270°	0.24×10^{-3}	0.23×10^{-3}		0.73×10^{-3}	0.71×10^{-3}	
BHK	0°	0.045	0.020	0.101	0.303	0.141	0.791
	180°	0.009	0.005		0.242	0.062	
	270°	0.013	0.014		0.279	0.213	

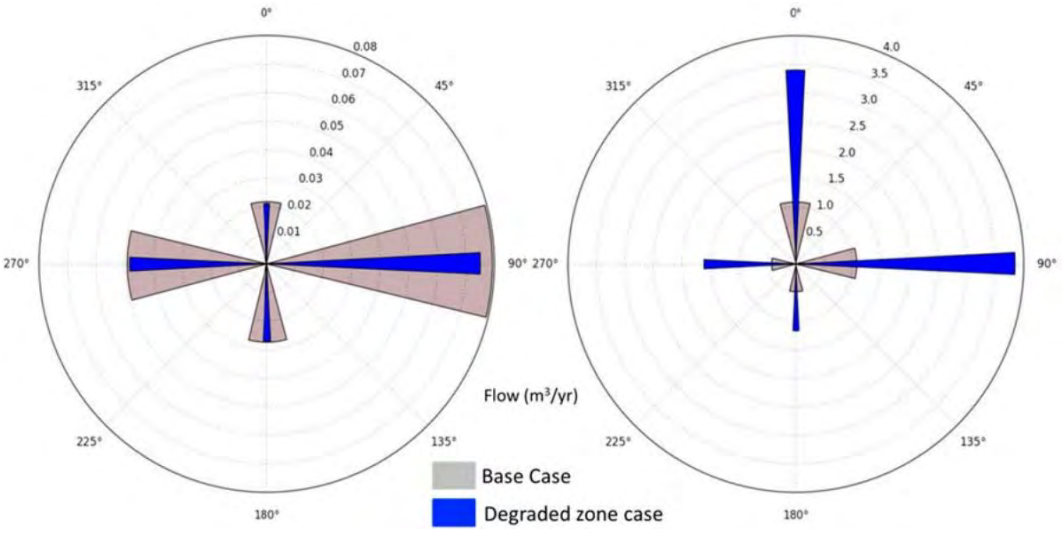

Figure 39. Groundwater flow entering the vaults BHA (left) and BHK (right) for each repository rotation angle (0°, 90°, 180° and 270°) for the base case and the degraded zone case. From Figure 5-9 of Abarca et al., (2019).

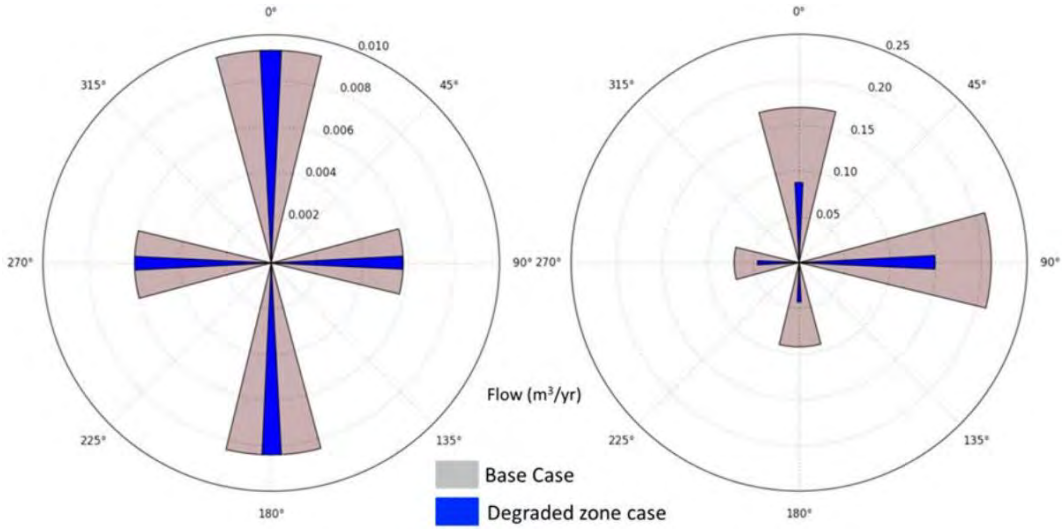

Figure 40. Groundwater flow entering the waste in BHA (left) and BHK (right) for each repository rotation angle (0°, 90°, 180° and 270°) for the base case and the degraded zone case. From Figure 5-10 of Abarca et al., (2019).

Interactions between vaults

Interactions between vaults were evaluated by steady-state tracer transport calculations ("tracer transport I" in the description of methodology by Abarca et al., 2019). The interaction is found to be very limited (less than 1‰ or 0.1%) in all versions of the base case, both for transport from BHA to BHK and vice versa (Abarca et al., 2019, Table 5-3).

The degraded-zone case produces a slight increase in transport from BHA toward BHK, with 1.5‰ for the unrotated layout of the tracer from BHA reaching BHK, and a maximum of 2.6‰ for the rotated versions. For the fully degraded case the value is 1.9‰ for

the unrotated version of the layout, so slightly higher than the corresponding version of the degraded-zone case.

Solute transport from waste compartments

Evolution of solute plumes emanating from the waste was evaluated for the same three cases (base case, degraded-zone, and fully-degraded backfill in BHK) using the transient tracer method ("tracer transport II" in the description of methodology by Abarca et al., 2019). Separate model calculations were performed for each vault.

The tracer concentration was specified as a constant value at the waste/backfill interface for the vault serving as the source, starting at time $t = 0$. The mass release from the BHA and BHK waste into the adjacent backfill varies with time (Figure 41). In the BHA, where transport through the bentonite backfill is dominated by diffusion, there is a high initial release due to the initial steep concentration gradient, combined with a relatively high diffusion coefficient ($D_e = 1.4 \times 10^{-10}$ m/s^2). This release declines steeply as the near-field concentration gradient decreases. In the BHK, the initial rate of release is lower due to the much lower diffusion coefficient in the intact concrete ($D_e = 3.5 \times 10^{-12}$ m/s^2), but rises quickly to reach a nearly steady value, controlled by advection.

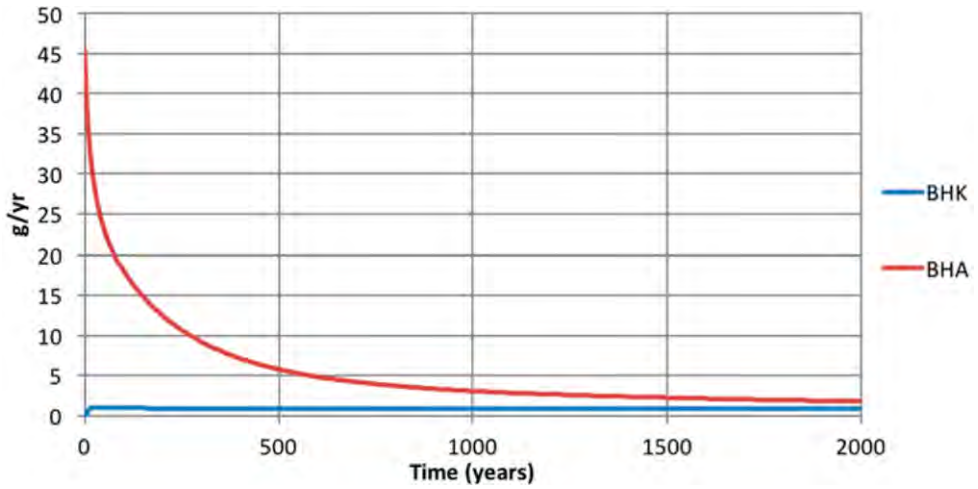

Figure 41. Mass of tracer released over time from the BHA and BHK waste for the base case. From Figure 7-1 of Abarca et al. (2020).

Mass release rates from the BHK waste are plotted for all three stages of BHK backfill degradation (intact as the base case, degraded-zone and fully degraded) are shown in Figure 42. The release rate curves are similar, with differences in magnitude reflecting the decreased flow driving advection in the degraded-zone case, and increased flow in the fully-degraded case. Abarca et al. (2019) note that the effects of BHK backfill degradation on mass release from the BHA are negligible, because diffusion dominates transport into and through the bentonite backfill.

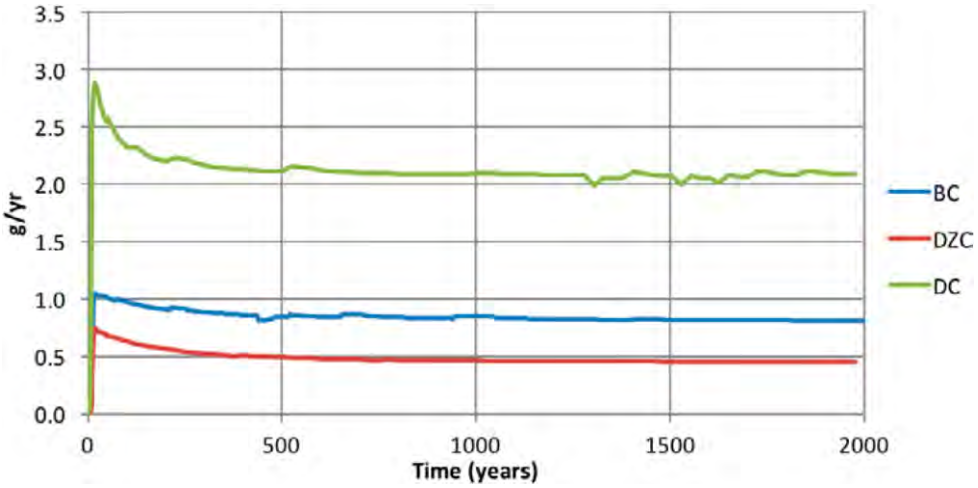

Figure 42. Mass outflow release from the BHK waste for the three concrete backfill degradation cases, the intact base case (BC), the degraded-zone case (DZC) and the fully degraded case (DC). From Figure 7-10 of Abarca et al. (2019).

The physical meaning of the units of grams per year in Figures 41 and 42, and similar plots given in Chapter 7 of Abarca et al. (2019), as well as in the text discussing these results is not clear. Section 3.4.3 of Abarca et al. (2019) states that a "unit concentration" is specified at the waste/backfill interface, which implies that the units should be arbitrary. Normally in such cases, concentrations should be presented in relative terms as c/c_o where c_o is the concentration at the source.

The finite value of initial mass release (shown as 45 g/yr for the BHA) is presumably a function of the first time step over which this was evaluated in the numerical model, and also the scale of the finite elements adjoining the waste/backfill interface.

It is not clear why the mass released from BHK waste appears to be initially zero in Figures 41 and 42, as there should also be an instantaneous release across the waste/backfill interface due to diffusion similar to that for BHA, though smaller in proportion to D_e. Based on the ratio of D_e for concrete vs. bentonite, the initial release from the BHK waste for a unit concentration should be about 2.5% that from the BHA waste, which would give a value of around 1.1 g/yr on the scale used. In Figure 42, which is plotted on a finer scale, the mass release rate for the base case does rise to approximately this value for the first time step evaluated after $t = 0$.

Breakthrough from the BHA backfill to the rock is dominated by diffusion and reaches a peak around 55 years, after which the rate of mass outflow to the rock decreases due to the declining concentration gradient (Figure 43). Breakthrough from the BHK backfill to the rock is predicted to have a very different evolution, dominated by advection, and continues to rise gradually throughout the 2000-year period for all three cases (Figure 44). The authors do not comment on why the rate of release to the bedrock is higher for the BHK, where transport is mainly by advection, than for the BHA where advective transport is negligible. Assuming that the source concentrations are the same for both cases, the only plausible explanation would seem to be the relatively high value of D_e in the bentonite.

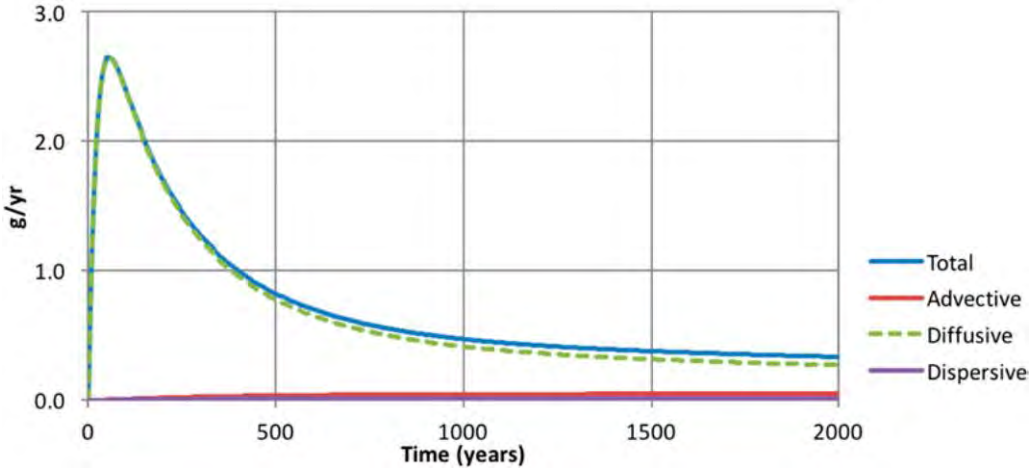

Figure 43 Breakthrough curve at the backfill/rock interface of a tracer released from the BHA waste for the base case. From Figure 7-2 of Abarca et al., (2019).

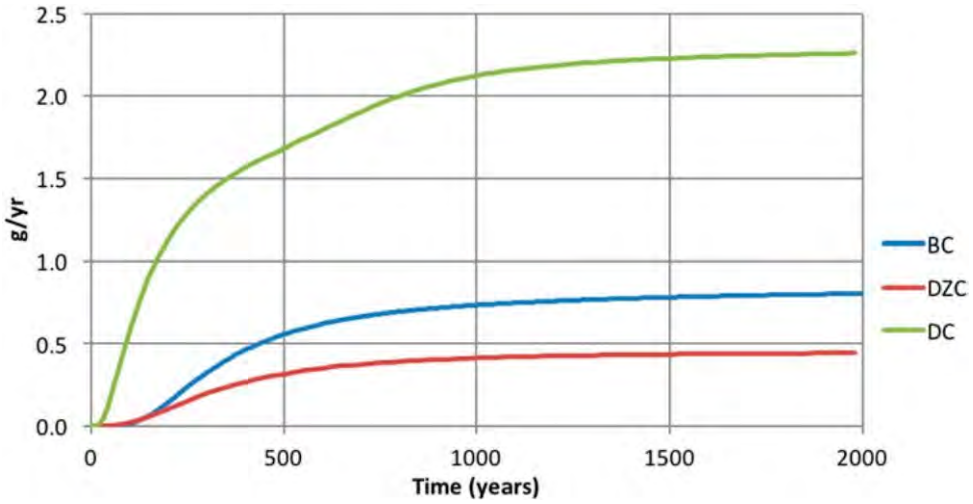

Figure 44. Total mass outflow to the rock from the BHK for the three concrete backfill degradation cases, the Base case (BC), the Degraded zone case (DZC) and the Degraded case (DC). From Figure 7-11 of Abarca et al. (2019).

2.4.5 Resaturation of vaults

Resaturation of the vault backfill in BHA and BHK is evaluated by Abarca et al. (2019, Chapter 8), by using COMSOL to solve Richards' equation for flow in a variably saturated porous medium, with hydraulic properties depending on the degree of saturation. The effective saturation S_e is a function of the soil water potential based on the empirical mathematical formulation of van Genuchten (1980). Permeability is assumed to vary by a factor proportional to S_e^3 which becomes 1 when the medium is fully saturated (when pore pressures are greater than or equal to atmospheric pressure).

The mathematical equations are given very briefly on p. 57 of Abarca et al. (2019), without full definition of all variables that appear in the equations (e.g. H_p which apparently is

pore pressure expressed as head) and without specification of the values used for several parameters (e.g. saturated water content θ_s and residual water content θ_r).

The boundary condition imposed at the rock/backfill interface, explained in Section 8.4 of Abarca et al. (2019), is a mixed boundary condition intended to represent an unsaturated fringe in the bedrock. The inflow through the boundary is $q = \alpha\Delta p = \beta k_x \Delta p$ where Δp is the difference between the calculated pressure and a prescribed, external pressure (taken from the repository-scale model for closed-repository conditions as used for the preceding flow and transport calculations), and k_x is the rock permeability. The parameter β is interpreted as representing the ratio $\beta = \rho/(\mu L)$ where L is the assumed thickness of the unsaturated fringe, ρ is water density and μ is dynamic viscosity; the parameter β has units of s/m^3.

Abarca et al. (2019) performed preliminary calculations to determine plausible bounds for β, finding that values in the range 2 to 200 were needed to match the range of Darcy velocities in the bedrock at repository depth.

The predicted saturation of the vaults as a function of time show that the results are still quite sensitive to the choice of β within this range (Figures 45 and 46). For BHA the saturation time ranges from 1600 to 15 000 years, while for BHK it ranges from 2 to 122 years. The authors note that the rock unsaturated fringe depth L is critical to calculation of the saturation time. They suggest measurement of this value around the excavated vaults, or calibration based on inflows to the vaults, but neither of these methods would be feasible prior to construction of the SFL.

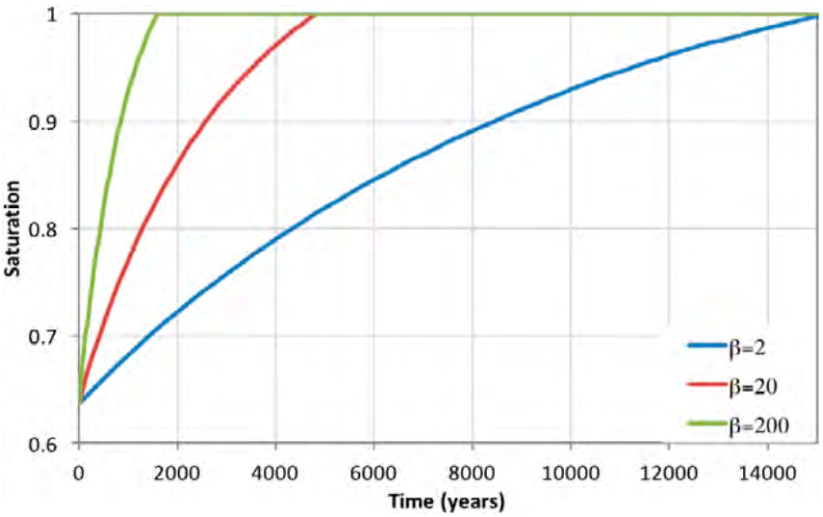

Figure 45. Temporal evolution of the volume averaged effective saturation in the BHA for β = 2, 20 and 200 s/m^3. From Figure 8-5 of Abarca et al. (2019).

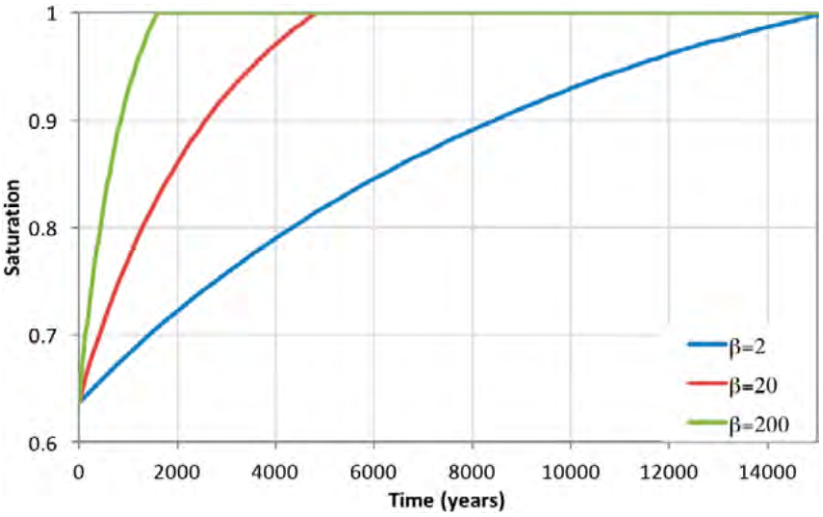

Figure 46. Temporal evolution of the volume averaged effective saturation in the BHK for β = 2, 20 and 200 s/m^3. From Figure 8-7 of Abarca et al. (2019).

3. Review findings

The main findings based on review of SKB's documentation are discussed below, beginning with observations regarding scientific quality (Section 3.1), followed by comments regarding the transparency of the documentation and related issues of presentation (Section 3.2).

3.1 Scientific quality

Review findings regarding scientific quality are organized here in terms of the following main review topics:

- Suitability of models and data for the evaluation
- Suitability of SKB's arguments on the basis of assumptions made and supporting data
- Suitability of SKB's handling of uncertainties
- Deficiencies in SKB's choice of methods, data, assumptions or handling of uncertainties

These topics are treated in sequence below.

3.1.1 Suitability of models and data for the evaluation

DFN conceptual model and implementation

The main basis for modeling flow and transport through the bedrock is a hydrogeological discrete-fracture network (DFN) model. The DFN conceptual model has a long history of application to fractured crystalline rock similar to the Laxemar site, including SKB's modeling of candidate sites for a spent-fuel repository.

The validity of this conceptual model for predicting flow and transport is not universally accepted. Black et al. (2017) have argued that an alternative, sparse-channel network concept is better able to match in-situ experiments that measured flow and transport, around underground openings on scales similar to the proposed SFL vaults. However this alternative concept is still in a development stage, while the DFN concept is still generally regarded as representing the practical state-of-the-art for groundwater flow modeling in this geological setting. As such, it can be considered appropriate for this preliminary evaluation of the SFL concept, although alternative conceptual models could need to be addressed in a license application.

The DFN statistical description model used in SE-SFL is based on a previous description developed by Rhén and Hartley (2009) and elaborated by Joyce et al. (2010). This description resulted from site investigations at Laxemar as a candidate site for a spent-fuel repository. In SE-SFL this description, and the related description of larger-scale defor-

mation zones, is used directly with no critical analysis of the underlying site data or associated uncertainties. This is reasonable considering the limited scope of SE-SFL, but for a licensing application it should be expected that the uncertainties in the underlying data to inform the models would also be evaluated.

Upscaling methodology

The DFN representation was upscaled to an equivalent continuum porous medium (ECPM) representation using ConnectFlow (Amec Foster Wheeler, 2015). The upscaling method is described only briefly by Joyce et al. (2019) but is understood from past applications to be based on block-scale flow simulations of network flow through realizations of the fracture network, evaluating flow for hydraulic gradients simulated in multiple directions to derive an effective hydraulic conductivity tensor for each ECPM block.

This approach has been verified as credible and self-consistent with the underlying DFN model, in terms of predicting large-scale flows (Jackson et al., 2000). However upscaling from a DFN to an ECPM unavoidably means a loss of detail below the 30 m to 60 m grid scale used in the ECPM representation. Further smoothing occurs in the adaptation to the near-field model of Abarca et al. (2019), due to interpolation of the permeability field from the ConnectFlow grid to a different grid in COMSOL. These steps result in successive loss of resolution which could affect the detailed flow distribution within the model.

Comparisons between the COMSOL adaptation and the ConnectFlow model showed discrepancies in residual pressures of up to 8% in parts of the domain. Local pressure gradients and calculated flow rates were not compared but could presumably be higher. Perhaps more significantly, plots of the hydraulic conductivity field around the repository by Abarca et al. (2019) do not show any distinct, high-conductivity pathways connecting from the SFL vaults to the nearest major deformation zones. Such pathways could be expected as a possibility based on the DFN description by Joyce et al. (2010) as well as evidence for presence of minor deformation zones on scales of hundreds of meters at Laxemar (Rhén et al., 2008).

Particle tracking scheme not flux-weighted

The particle-tracking scheme used for calculating flow-related performance measures by Joyce et al. (2019) uses a source term in which particles are released as 10 per fracture, rather than in proportion to flux. This can be expected to skew the distributions of performance measures toward fractures that carry low flows, which is unrealistic and non-conservative for safety evaluation.

Potential consequences of this method are addressed in Section 4.3 of this review by comparing with independent calculations based on a flux-weighted scheme. The results show that neglecting this issue leads to significant non-conservative bias in the predicted distribution of transport resistance.

The impact of this issue on dose and risk calculations in SE-SFL depends on the details of how the radionuclide transport calculations have been carried out, using the performance parameters from the hydrogeological models. This issue should be checked by other reviewers who have examined the radionuclide transport and dose calculations.

Reliability of hydrogeological and coupled hydrogeochemical models

The hydrogeological modeling reports by Joyce et al. (2019) and Abarca et al. (2019) do not discuss potential numerical issues, but generally report the results of model calculations without critical perspective. No mention is given of conventional measures such as Peclet number that are normally used to assess the potential for instabilities in numerical calculations.

Considering that the coupled application of the ConnectFlow model and IPhreeqc library by Joyce et al. (2019) is novel, it is surprising that no discussion or sensitivity analysis is given of the numerical stability of the model for the chosen iterative time-stepping scheme, or the degree to which any of the presented results could be influenced by numerical effects.

Only very limited discussion is given of the results of the hydrogeochemical modeling, mainly in graphical format without diagnostic calculations. Comparison to actual measurements are limited to only a few sampling points at repository depth, but even these show discrepancies that cannot be explained by laboratory analytical errors. The significance of these discrepancies for overall confidence in the model, for the purpose of application in SE-SFL, is not discussed.

The model for hydrogeochemical evolution appears to predict a fairly uniform, nearly linear transition in salinity from freshwater at around 400 m depth, to concentrations of approaching 45 g/ L at 1200 m depth, but the site data suggest that salinities remain relatively low until around 1000 m depth where there is a more abrupt transition.

This could be important because the boundary between fresh and saline flow systems is predicted to be within 200 m of the base of the repository. Would a deeper interface give better or worse safety performance? The depth to the saline interface would presumably affect the transport paths for radionuclides leaching from the waste in the BHA and BHK vaults, possibly in ways favorable for safety (e.g. if it results in longer transport paths allowing more groundwater/matrix interaction for retention). But it could also mean higher groundwater fluxes through the repository, resulting in a stronger source term for radionuclide release.

For future safety assessments of this concept, a clear statement should be expected about the reliability of predictions of hydrogeochemical evolution, and the implications for confidence regarding safety.

Reliability of particle-tracking algorithm for far-field transport

Joyce et al. (2019) note that some of the particles released into the ConnectFlow model become "stuck" without reaching a discharge point. From the results presented in Chapter 4 of Joyce et al. (2019), typically fewer than half of the released particles arrive at the model boundaries. This is a large fraction, raising concerns about reliability of the method.

The authors attribute the stuck particles to numerical imprecision, suggesting that this could occur in dead-end branches of the fracture network that do not carry flow in steady-state conditions, but which particles could enter (according to the particle-tracking algorithm) if small numerical errors in the finite-element pressure solution indicate a non-zero component of water flux into such a dead-end branch.

However, according to the description of the ConnectFlow particle-tracking algorithm (as recounted in Section 2.4.3), within the fracture network, flux-weighted probabilistic routing is used to determine which out-flowing branch of a fracture receives the particle from an inflowing fracture. This implies that once a particle enters a high-flow path within a fracture network, it should have a very low probability of entering a dead-end branch or a low-flow path within the network.

Possibly the high number of stuck particles in this application is partly a consequence of the separate problem regarding the boundary condition at the source (as mentioned above). This would result in some particles being forced into fractures that carry very little flow. If this is the main factor leading to the high number of stuck particles, that implies that the problem could be corrected by a more appropriate boundary condition at the source.

However if a high fraction of particles that start in high-flow fractures also become stuck in low-flow fractures, that would imply numerical problems in the method. In such a case, the reliability of the flow-related performance parameters that are calculated by this method would also be questionable.

3.1.2 Suitability of SKB's arguments on the basis of assumptions made and supporting data

The arguments in support of the safety evaluation are mainly reasonable, considering the current stage of development of the concept. However several issues may be noted as discussed below.

Analysis of glacial cases

The simplified glacial cycle evaluation case is aimed primarily to address the performance of the SFL repository concept for future colder climates, specifically periglacial, glacial, and post-glacial submerged conditions.

No hydrogeological modeling results specific to the SFL are presented. Rather, values of hydrogeological performance measures (Q_{eq}, t_w, a_w and F) for future cold periods are calculated by applying scaling factors to the corresponding performance measures that were calculated for temperate conditions by Joyce et al. (2019) and Abarca et al. (2019).

Treatment of future climate situations using the same groundwater flow patterns as for temperate climate is highly unrealistic based on studies of regional groundwater flow during glaciations (e.g. Person et al., 2007; McIntosh et al., 2011) as well as past analyses for a Swedish spent-fuel repository (Vidstrand et al., 2010; Vidstrand et al., 2014).

This simplification may be conservative for safety evaluation, insofar as longer discharge paths in periglacial/glacial climates would limit release. However the biosphere objects selected may not be representative of future periglacial or glacial conditions. A more realistic analysis should be expected as part of hydrogeological modeling in support of a license application.

Boundary condition for resaturation model

The modeling of resaturation of the vaults as a function of time shows that the results are very sensitive to the choice of the parameter β, within the plausible range. Abarca et al. (2019) note that the rock unsaturated fringe depth L (which appears as a conceptual factor in their interpretation of β) is critical to calculation of the saturation time. They suggest measurement of this value around the excavated vaults, or calibration based on inflows to the vaults, but neither of these methods would be feasible prior to licensing and construction of the SFL.

This line of argument loses sight of the fact that the rock unsaturated fringe depth L is a model-based abstraction which is likely not realistic for the actual conditions around a waste vault, where flow is controlled by discrete fractures rather than an effective continuum. Given that actual in-situ measurements will most likely not be obtainable ahead of licensing and construction, a more physically-based model of the bedrock/vault interface is needed to address the substantial uncertainties.

Consistency between different scales of models

The catchment-focused model of Joyce et al. (2019) does not include a representation of the repository, so the effective hydraulic conductivity of the portion of the model containing the repository may differ between this model and the near-field models that use this model for effective boundary conditions. This is likely a minor issue but should be addressed in any future evaluation of the concept, to eliminate the related uncertainty.

Validity of equivalent flow concept for BHK

A case with degraded concrete in the BHK vault (represented by increasing the hydraulic conductivity) results in more flow passing through the vaults, but counter-intuitively leads to lower values of equivalent flow Q_{eq} and equivalent flux U. This is explained by

the fact that these measures depend on flow rates around the vaults which are reduced because the concrete in the BHK vault does not force as much flow to be diverted around the vault.

This seems inappropriate as a representation of the source term for transport, if the waste vault in BHK acts mainly as an "advective" source with radionuclides being leached by water seepage through the vaults. It would be more appropriate where the release from the vault is governed mainly by diffusion, as is the case for BHA.

The Q_{eq} concept was originally derived (Neretnieks, 1980) to represent a bentonite-filled deposition hole in a spent-fuel repository, where mass transfer to advective flow in the bedrock is regulated by diffusion through the bentonite, similar to the situation for BHA. The application of this concept to the BHK should be examined to check that it leads to an appropriate source term for near-field release of radionuclides.

3.1.3 Suitability of SKB's handling of uncertainties

SKB acknowledge that the analysis of uncertainties in SE-SFL is simplified compared with what should be expected for a full safety assessment in support of a license application. These simplifications are mostly reasonable for the current stage of development of this concept. Several areas can be highlighted where improvement should be expected in the future.

Limited evaluation of effects of stochastic variability in base-case model

Alternative realizations of the stochastic bedrock fracturing are discussed as producing alternative flow-related performance parameters for near-field and far-field radionuclide transport. These alternative realizations would more appropriately be evaluated as representing uncertainty in parameter estimates for the main calculation case, based on the statistical description of variability represented in the DFN model.

The observed variation among realizations of the DFN model indicates that variability in connections formed by discrete fractures, together with variability in the deformation zones, could significantly affect retention in the geologic barrier. The potential consequences of discrete connections via large fractures are considered further in Section 4.2 of this report, based on independent calculations with a simplified representative model.

Uncertainty regarding future climate evolution

The treatment of future climate is highly stylized. Climate and shoreline position for the initial state are based on present-day conditions, even though closure is not expected until 2075 AD.

The use of present-day climate for the early post-closure period ca. 2075 AD is acknowledged by SKB to be unrealistic in view of current IPCC projections (IPCC, 2014). The IPCC scenario RCP 4.5 is considered to scope effects of a future warmer climate, but

considering recent climate trends, this may already be less realistic the RCP 8.5 scenario which assumes higher greenhouse gas emissions.

More pronounced changes in temperature and precipitation (including the possibility for either higher or lower annual precipitation) could result from higher-emissions scenarios. Changes in seasonality of precipitation and snow melt are not discussed, nor is the possibility for greater inter-annual variability in a future warm climate. Changes in ocean chemistry, including lower pH due to rising atmospheric CO_2, could also presumably be expected to affect groundwater chemistry at a coastal site.

Scenarios for use of well water by a single household may not be adequate to bound future situations. The case analyzed considers a well used for drinking water and garden plot irrigation by a household of five individuals. The small size of the exposed group for this case is argued to justify use of an annual risk criterion of 10^{-5} rather than 10^{-6}, according to regulatory guidance from SSM (2008). However this argument may not be applicable for a case in which a larger local population depends on water from multiple wells, or a well in which some nontraditional method (e.g. hydraulic fracturing) has been used to enhance the well yield.

With the most likely scenarios for climate evolution in the near future, a warmer climate with longer growing season, more extensive irrigation of crops using well water could be envisioned. Use of surface water to irrigate crops to address such a situation has been considered in SE-SFL, but not use of well water.

Potential impacts of a future drier climate on dose and risk should also be considered as part of the uncertainty arising from climate changes. Modeling of groundwater age distributions for large-scale flow indicates that a future drying climate would produce lower variability in water residence times (Maxwell et al., 2016), which could imply more focused discharge in a smaller number of discharge regions. The potential for changing patterns of flow in future warm climates to affect dose should be considered in future safety evaluations.

3.1.4 Deficiencies in SKB's choice of methods, data, assumptions or handling of uncertainties

Missing evaluation cases

The current preliminary design for the SFL concept does not discuss which if any types of rock reinforcement methods such as rock bolts or shotcrete could be used to stabilize the excavation during the operational period. Use of reinforcement is ordinarily required for construction of underground caverns of the size proposed, for similar rock types in the Fennoscandian Shield, both for mechanical support and for operational safety. Use of shotcrete in the BHA vault could affect groundwater chemistry as well as hydraulic conditions at the interface between the bentonite backfill and the rock, which in turn could affect resaturation times.

Deterioration of any rock supports after closure should be considered as a likely part of system evolution for the base case. For the BHK vault, eventual failure of rock bolts or other reinforcement could also affect mechanical loading of the concrete backfill by inelastic deformation of the bedrock (i.e. block failures), which apparently has not been considered in the elastic analysis of rock mechanical impacts. If inelastic deformation of the vaults leads to localized loading and fracturing of the concrete backfill, this could result in discrete flow paths that have not been considered in the analysis for SE-SFL.

The likelihood of an excavation-disturbed zone (EDZ) around the vaults is discussed as part of the base case reference evolution rather than as part of the initial state which would be expected as the starting point for all cases of evolution. An EDZ around the vaults should be expected to develop with any practical method of construction, including blast-induced fractures if drill-and-blast methods are used (as typical for excavations on this scale in Fennoscandian Shield rocks), as well as stress-induced fractures and/or extensions of pre-existing fractures. Enhanced flow in an EDZ around the vaults should therefore be modeled at least as a sensitivity case, if not as part of the base case. Quite possibly this case could yield results favorable to overall safety, if the EDZ contributes to a "hydraulic cage" effect similar to that resulting from the degraded-zone case for the BHK vault.

The possibility of void space at the concrete/bedrock interface, resulting either from imperfect backfilling or shrinkage of the concrete as it cures, is not discussed in either the main report (SKB, 2019a) or the related sections of the Initial State Report (SKB 2019b). Other mechanisms that result in through-going cracks of significant aperture, connecting directly to the waste compartment, could be of greater concern.

Earthquakes are discussed in the reference evolution rather than in the glacial-cycle case where earthquakes of significant magnitude are much more likely. Earthquakes are acknowledged to be a possibility, particularly in the early post-glacial period when the vertical compressive stress is reduced but horizontal stresses remain high, leading to potential for reverse (thrust) faulting. This possibility has not been quantitatively evaluated in SE-SFL due to the limited objectives for the current stage of evaluation for this repository concept, but an analysis should be expected as part of a full safety assessment in support of license application

Colloid transport

No quantitative assessment of potential colloid release from the BHA backfill has been made for SE-SFL, nor has the associated risk of colloid-assisted radionuclide transport been evaluated. SKB (2019a) acknowledge that this topic should be addressed further in future safety assessments for this concept.

Influence of changing groundwater chemistry (including infiltration of meteoric water or glacial meltwater as well as upconing of saline water) will need to be considered. The bentonite could act as a source of colloids to be released into the groundwater, particularly if groundwater with very low salinity should reach the BHA vault, allowing release

of colloid-sized smectite particles. This could be possible after a prolonged temperate period (as considered in the base case) or during future glaciations (as considered in the simplified glacial variant).

3.2 Transparency of presentation

SKB's reporting follows a reasonably clear structure for presentation of the safety case and supporting hydrogeological analyses, but numerous issues affecting transparency, traceability and repeatability of SKB's analysis were encountered, as noted below.

Design specifications

The closure design for the SFL is noted by SKB to be in a preliminary stage. It is described only briefly in two pages of text and figures in the Initial State Report (SKB 21019b) which are repeated verbatim in the Main Report (SKB 2019a).

A plug section with a hydraulically tight section of bentonite confined by cast concrete is also planned somewhere along the access ramp; SKB (2019a,b) give a schematic cross section of the plug design but do not specify the position of the plug along the access tunnel.

Shaft sealing procedures are not completely specified. Figure 8 of SKB (2019a) suggests that the entire shaft will be sealed, but this seems to be contradicted by the text stating that only the connections to tunnels will be sealed. SKB (2019a,b) do not state what material will be used to backfill the remainder of the shaft.

No plans or criteria are described for use of rock reinforcement methods such as rock bolts or shotcrete to stabilize the excavation during the operational period, or what the design life of those components would be. It is not clear if the rock mechanical analyses considered potential for damage to waste containment structures or concrete backfill to occur due to rock block failures following degradation of rock support systems.

Documentation of DFN model

Joyce et al. (2019) do not give a quantitative presentation of the upscaled values of hydraulic conductivity, apart from block diagrams of the model which use color to illustrate the variability of K along the edges of the model.

The statistical model for fracture transport aperture e_t is not specified by Joyce et al. (2019). This gap in SKB's documentation could not be resolved either from the SE-SFL reports or from background reports. The transport aperture model is also not specified in the previous presentation of the Laxemar DFN model by Joyce et al. (2010), which refers to Rhén et al. (2008). The consequences for transport modeling are significant (as shown by independent calculations); see also Section 2.4.1 of this review.

Hydraulic properties of the deformation zones other than transmissivity (such as porosity, thickness, and specific storage) are not documented in Joyce et al. (2019), though in most cases the relevant information could be found in Joyce et al. (2010).

The boundary conditions and initial conditions for groundwater flow and solute transport are not clearly stated by Joyce et al. (2019). They state that initial conditions and boundary conditions used were the same as those in Joyce et al. (2010), except that reference water fractions were replaced by the equivalent mass fractions of the individual solutes.

The reference water fractions on the top boundary vary with time according to the elevation of shoreline with regard to the topography of the ground surface (and presumably the time-varying salinity of the Baltic for submerged portions, though this is not clearly stated). No explanation is provided of how the mixing fractions of reference waters are backed out of the mass fractions of individual components.

The hydraulic properties of the host rock are taken from what Abarca et al. (2019) refer to as the "regional hydrogeology model" of Joyce et al. (2019). Whether this refers to the catchment-focused model or the facility focused-model is not completely clear from the presentation.

The details of the interpolation of permeabilities imported to the near-field model of (Abarca et al., 2019) are not discussed. Transport results reported by Abarca et al. (2019) are reported in inappropriate units for a case where an arbitrary concentration is applied at the waste/backfill interface. This reduces confidence in the analysis.

Mathematical definitions of the key performance measures calculated by Abarca et al. (2019) are ambiguous. In particular, it is not clear how situations with curving streamlines, resulting in separate areas of inflow and outflow across a single face, would be accounted for. Apparently, some numerical errors are included in the presentation of vault flows for the case of rotated layouts.

The DFN model of Laxemar developed for SR-Site was used without changes. This results in non-optimal location of model boundaries relative to the hypothetical location of the SFL. The boundary conditions and initial for groundwater flow are not stated by Joyce et al. (2019), so it must be assumed that prior conditions used by Joyce et al. (2010) apply.

Joyce et al. (2019) do not give a quantitative presentation of the upscaled values of hydraulic conductivity, apart from block diagrams of the model which use color to illustrate the variability of K along the edges of the model. Nor are any quantitative data or vector plots given to explain the predicted flow fields. This has been a persistent issue in SKB's analysis based on DFN modeling, arising also in past work for the spent-fuel repository candidate sites at Laxemar and Forsmark, as well as for the SFR extension at Forsmark.

Various parameters values are not documented, including the thickness of the BHK degraded zone for that case, and several parameters for the resaturation model. The relationship between fracture transmissivity and effective transport aperture, which is key for calculations of transport resistance, is not documented.

4. Independent calculations

This chapter presents independent calculations to assess key uncertainties, including (1) the upscaling of the DFN model for the sparsely fractured rock, (2) an independent assessment of flow-related transport parameters (performance measures), and (3) effects of not weighting sources by flux, for particle tracking used to calculate far-field transport resistance.

4.1 Upscaled hydraulic conductivity of sparsely fractured rock

The hydrogeological analyses by Joyce et al. (2019) and Abarca et al. (2019) do not present statistics regarding the upscaled values of effective hydraulic conductivity, as calculated from the discrete-fracture-network (DFN) model. A previous application of the same model by Joyce et al. (2010) provides only limited information (discussed further below). Therefore independent calculations have been carried out to estimate plausible ranges for upscaled hydraulic conductivity.

4.1.1 Method for estimating hydraulic conductivity

The present calculations are geometrical estimates of effective hydraulic conductivity, based on the geometry and transmissivity of fractures generated according to the DFN statistical model, without considering network effects.

Following Oda (1985), the hydraulic conductivity tensor for a rock volume V is estimated as:

$$K = \frac{1}{V}\sum_{f}\left(I - n_f \otimes n_f\right) T_f A_f$$

Where $\boldsymbol{I}$ is the identity tensor, $\otimes$ denotes the outer (tensor) product of two vectors, $\boldsymbol{n}_f$ is the normal (pole) vector for fracture f, T_f is the fracture transmissivity, and A_f is the area of the fracture that lies within the volume V. This formula is exact in the case of infinite planar fractures, in which case it is equivalent to the formula of Snow (1969).

For planar fractures of finite extent as considered here, this formula will in general overestimate the magnitude of the components of $\boldsymbol{K}$, due to network effects which limit the contribution of individual fractures to the net effective hydraulic conductivity. These effects include:

- isolated fractures that are not connected to a larger network;
- fractures in “dead-end” portions of a network that do not extend fully across the volume; and
- fractures in series, where the flow through the network is limited by the least transmissive fracture in the series.

Thus the $\boldsymbol{K}$ values calculated by this method should be seen as upper-bound estimates, compared with what would be obtained from explicit network flow calculations.

Geometrical estimation using the above formula has been carried out using the implementation in the *dfm* software (Geier, 2020). The DFN statistical models specified in Tables 3-2 through 3-5 of Joyce et al. (2019), for fracture domains HRD_C, HRD_EW007, HRD_W, and HRD_N, for each of the four specified depth zones DZ1 through DZ4, are implemented in *dfm* input files as detailed in Appendix A2.

Geometrical estimates of the effective $\boldsymbol{K}$ tensors were calculated for cube-shaped blocks on scales of 50 m and 100 m. For the 50 m block scale, 3600 blocks were simulated in each of 20 layers in an arbitrary 3000 m x 3000 m × 1000 m deep domain. For the 100 m block scale, 900 blocks were simulated for each of 10 layers in the same domain. Statistics were then calculated for each layer on each of these two scales, for the diagonal components K_{xx}, K_{yy}, K_{zz} as well as the arithmetic mean of the directional values for each block, $K_m = (K_{xx} + K_{yy} + K_{zz})/3$.

4.1.2 Results

Geometrical estimates of hydraulic conductivity for the 50 m block scale, as a function of depth in the model, are summarized in Table 7 and as statistical plots for the fracture domains HRD C, EW007, N, and W in Figures 47 through 50.

The general trend is for K_m to decrease with depth in each fracture domain, with mean values on the order of 10^{-6} m/s in the shallowest zone DZ1, decreasing to on the order of 10^{-8} m/s in the deepest zone DZ4. The decrease is nominally step-wise between depth zones, so different layers in a given depth zone have mostly very similar distributions of K_m. However in some cases a gradational transition is evident, for example the block layer at $z = -175$ m in HRD C (Figure 47), which has a higher median value of log K_m than the other layers in DZ2. These transitions result from large fractures that are centered in the shallower zone extending into the deeper zone.

Anisotropy is moderate, indicated by mean anisotropy ratios in the range 0.355 to 1.344 in Table 7. Different domains have different preferred directions of flow. In HRD C and HRD N, the preferred directions are in the x (N-S) and z (vertical) directions. In HRD W, hydraulic conductivity is generally higher in the horizontal directions than in the vertical direction, but the preferred direction in the horizontal plane varies depending on depth, with a slight preference for N-S flow in DZ1 and DZ2, shifting to preferential E-W flow in DZ4. HRD EW007 shows a more complicated variation with a switch from preferential horizontal flow in DZ1 to preferential vertical flow in DZ2, then N-S and vertical flow in DZ3 and DZ4.

Table 7: Summary of upscaled values of hydraulic conductivity K_m and anisotropy ratios for the 50 m block scale, calculated by geometric upscaling. Values of the geometric estimates are calculated from a single realization with 3600 blocks centered on each of the levels z = −75 m (in DZ1), z = −275 m (in DZ2), z = −525 m (in DZ3), and z = −725 m (in DZ4). These particular levels selected for presentation in this table are interior to the corresponding depth zones, at least 50 m from the closest neighboring depth zone.

Depth Zone	HRD	log K_m (m/s)	K_{xx}/K_m	K_{yy}/K_m	K_{zz}/K_m
DZ1	C	−6.313 ± 0.337	1.210 ± 0.127	0.543 ± 0.167	1.247 ± 0.135
DZ1	EW007	−6.708 ± 0.240	1.173 ± 0.173	1.127 ± 0.146	0.700 ± 0.219
DZ1	N	−5.765 ± 0.286	1.083 ± 0.178	0.838 ± 0.224	1.079 ± 0.236
DZ1	W	−6.420 ± 0.351	1.113 ± 0.191	0.967 ± 0.247	0.921 ± 0.266
DZ2	C	−7.022 ± 0.509	1.243 ± 0.159	0.787 ± 0.296	0.970 ± 0.321
DZ2	EW007	−6.812 ± 0.254	0.735 ± 0.216	0.958 ± 0.203	1.307 ± 0.100
DZ2	N	−6.474 ± 0.331	1.205 ± 0.133	0.793 ± 0.230	1.002 ± 0.251
DZ2	W	−6.840 ± 0.561	1.305 ± 0.171	1.198 ± 0.232	0.497 ± 0.294
DZ3	C	−7.659 ± 0.399	1.280 ± 0.123	0.951 ± 0.261	0.770 ± 0.298
DZ3	EW007	−7.560 ± 0.195	1.184 ± 0.108	0.670 ± 0.172	1.146 ± 0.182
DZ3	N	−7.297 ± 0.353	1.137 ± 0.128	0.531 ± 0.152	1.332 ± 0.099
DZ3	W	−7.325 ± 0.476	1.301 ± 0.130	1.344 ± 0.112	0.355 ± 0.180
DZ4	C	−7.914 ± 0.309	1.208 ± 0.132	0.610 ± 0.211	1.182 ± 0.204
DZ4	EW007	−7.729 ± 0.307	1.225 ± 0.115	0.679 ± 0.219	1.096 ± 0.229
DZ4	N	−8.451 ± 0.463	1.128 ± 0.170	0.584 ± 0.212	1.288 ± 0.188
DZ4	W	−8.709 ± 0.377	0.943 ± 0.273	1.264 ± 0.173	0.794 ± 0.287

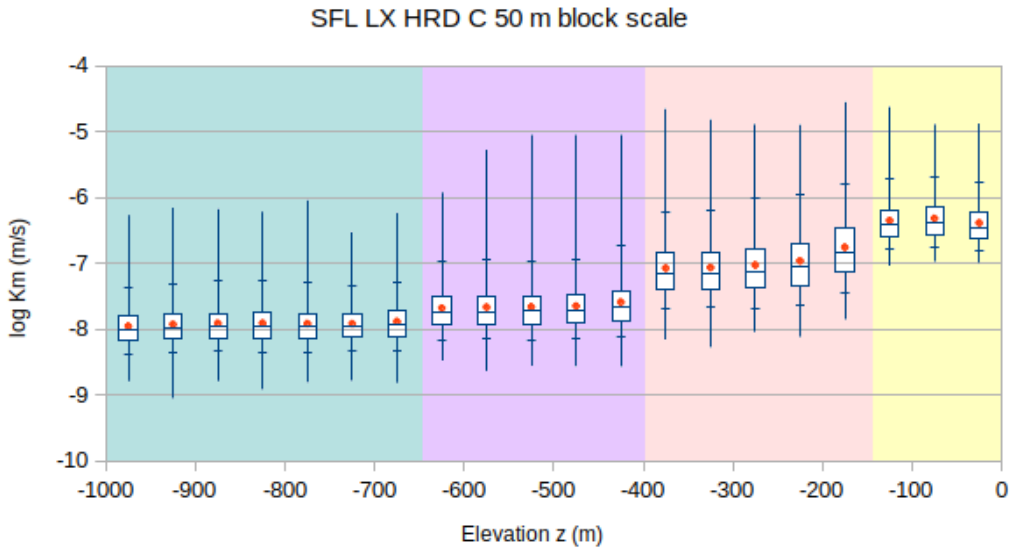

Figure 47 Box-and-whisker plot showing ranges of geometrical estimates of effective hydraulic conductivity K_m on the 50 m block scale, for fracture domain HRD C, as a function of layer elevation z. Red dots represent the mean value of log K_m for a given z, for a sample of N = 3600 blocks. The blue boxes represent the range between the first quartile (P_{25}) and third quartile (P_{75}), with the middle horizontal line indicating the median (P_{50}). Vertical blue lines below and above each box show the range from minimum to maximum values of log K_m, with tick marks to show the 5th and 95th percentiles (P_5 and P_{95}). Depth zones DZ1 through DZ4 are indicated by background color shading.

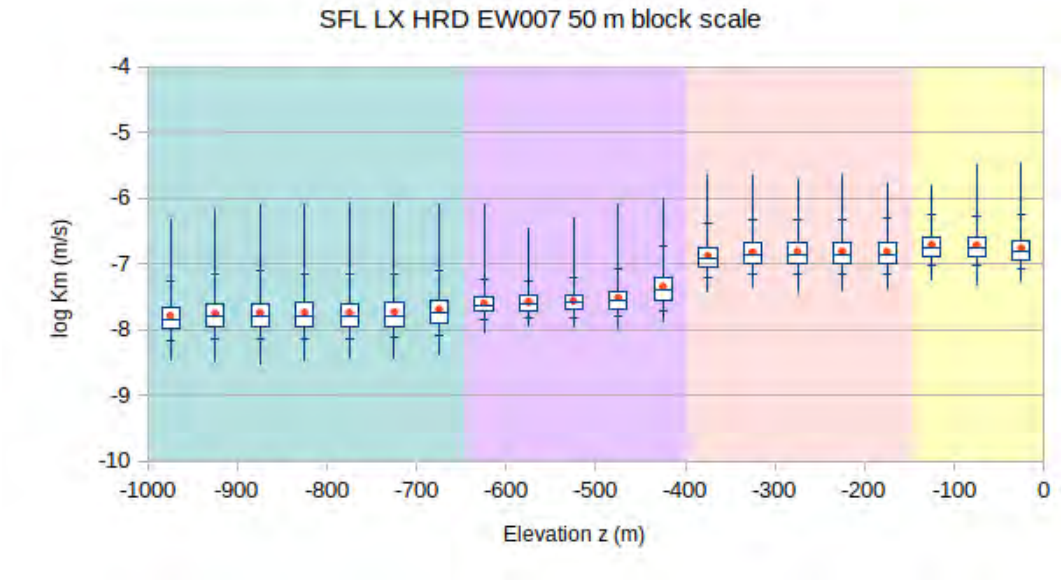

Figure 48 Box-and-whisker plot showing ranges of geometrical estimates of effective hydraulic conductivity K_m on the 50 m block scale, for fracture domain HRD EW007, as a function of layer elevation z. Red dots represent the mean value of log K_m for a given z, for a sample of N = 3600 blocks. The blue boxes represent the range between the first quartile (P_{25}) and third quartile (P_{75}), with the middle horizontal line indicating the median (P_{50}). Vertical blue lines below and above each box show the range from minimum to maximum values of log K_m, with tick marks to show the 5th and 95th percentiles (P_5 and P_{95}). Depth zones DZ1 through DZ4 are indicated by background color shading.

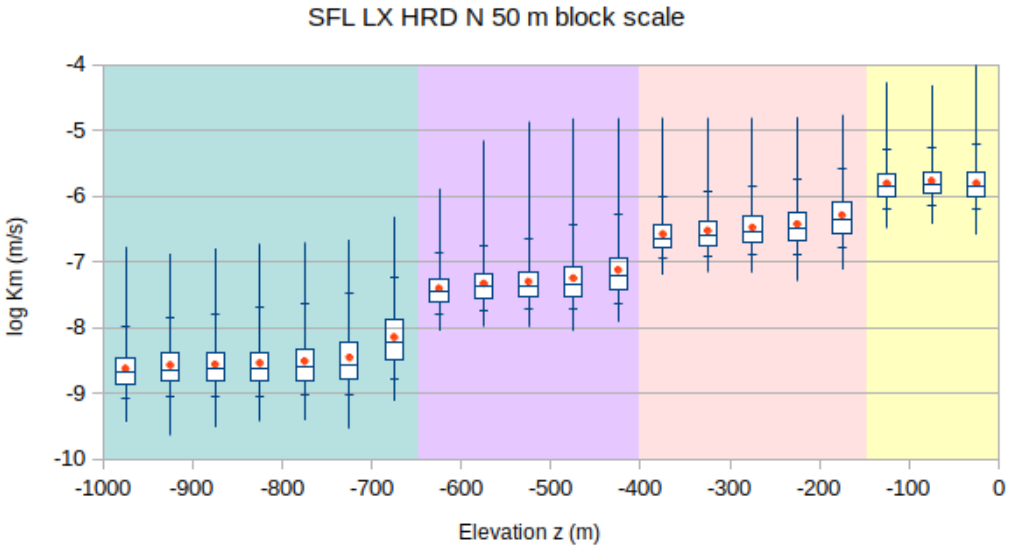

Figure 49 Box-and-whisker plot showing ranges of geometrical estimates of effective hydraulic conductivity K_m on the 50 m block scale, for fracture domain HRD N, as a function of layer elevation z. Red dots represent the mean value of log K_m for a given z, for a sample of N = 3600 blocks. The blue boxes represent the range between the first quartile (P_{25}) and third quartile (P_{75}), with the middle horizontal line indicating the median (P_{50}). Vertical blue lines below and above each box show the range from minimum to maximum values of log K_m, with tick marks to show the 5th and 95th percentiles (P_5 and P_{95}). Depth zones DZ1 through DZ4 are indicated by background color shading.

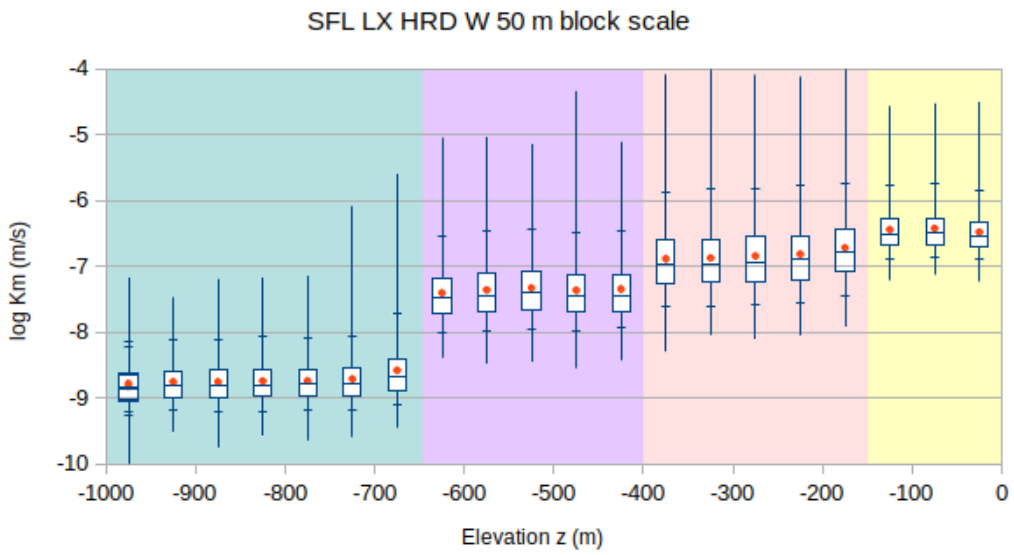

Figure 50 Box-and-whisker plot showing ranges of geometrical estimates of effective hydraulic conductivity K_m on the 50 m block scale, for fracture domain HRD W, as a function of layer elevation z. Red dots represent the mean value of log K_m for a given z, for a sample of N = 3600 blocks. The blue boxes represent the range between the first quartile (P_{25}) and third quartile (P_{75}), with the middle horizontal line indicating the median (P_{50}). Vertical blue lines below and above each box show the range from minimum to maximum values of log K_m, with tick marks to show the 5th and 95th percentiles (P_5 and P_{95}). Depth zones DZ1 through DZ4 are indicated by background color shading.

Geometrical estimates of hydraulic conductivity for the 100 m block scale (not presented here, for the sake of brevity) show only minor scale effects relative to the values calculated for the 50 m scale. The mean values of log K_m for the 100 m scale are slightly higher than the corresponding values for the 50 m scale, by 0.10 (in log space), corresponding to a factor of 1.25. The standard deviations of log K_m for the 100 m scale are on average 0.76 times the corresponding values for the 50 m scale.

The results for the 100 m block scale are compared with the corresponding results of explicit network-flow calculations by Joyce et al. (2010) in Table 8. For DZ1 where the fracture network is relatively well-connected (indicated by 100% percolation in the network-flow calculations), the geometric estimates are roughly half an order of magnitude higher than the corresponding estimates from network-flow calculations. In DZ2 and DZ3, the two types of estimates diverge more significantly, particularly for the domains HRD_C and HRD_W where the percentage of percolating blocks is below 100%.

Table 8: Upscaled values of hydraulic conductivity for the 100 m block scale, calculated based on explicit network-flow calculations (Joyce et al., 2010) and by geometric upscaling (this review). Values of K from network flow calculations have been estimated graphically from Figure 5-3 of Joyce et al. (2010). Values of the geometric estimates are calculated from a single realization with 900 blocks centered on each of the levels z = −50 m (DZ1), z = −250 m (DZ2), z = −550 m (DZ3), and z = −750 m (DZ4). Joyce et al. (2010) did not present results for fracture domain HRD_N, nor for DZ4, and did not clarify whether the presented values of K represent a particular component of the $\boldsymbol{K}$ tensor such as K_{xx}, or an average value such as K_m.

Domain	Depth zone	Percent of percolating blocks	Mean log K (m/s)	Standard deviation of log K	Mean log K_m (m/s)	Standard deviation of log K_m
C	DZ1	100%	−6.69	0.48	−6.27	0.27
EW007	DZ1	100%	−7.06	0.27	−6.69	0.18
W	DZ1	100%	−6.93	0.43	−6.36	0.28
N	DZ1	–	–	–	−5.71	0.22
C	DZ2	99%	−8.74	0.69	−6.79	0.40
EW007	DZ2	100%	−7.34	0.31	−6.76	0.18
W	DZ2	84%	−9.80	1.37	−6.58	0.44
N	DZ2	–	–	–	−6.37	0.28
C	DZ3	97%	−9.08	0.80	−7.54	0.31
EW007	DZ3	100%	−8.43	0.52	−7.54	0.14
W	DZ3	80%	−9.69	1.13	−7.15	0.35
N	DZ3	–	–	–	−7.23	0.28
C	DZ4	–	–	–	−7.83	0.21
EW007	DZ4	–	–	–	−7.66	0.21
W	DZ4	–	–	–	−8.62	0.28
N	DZ4	–	–	–	−8.35	0.37

The geometric estimates have low variability relative to the network-flow estimates, also diverging more at depth. In the shallowest zone DZ1, the standard deviations calculated by geometric estimation are 1/2 to 2/3 of the standard deviations from network-flow calculations, but in DZ3 this ratio is 1/4 to 1/3.

These discrepancies reflect the greater importance of irregular network effects in the sparser, less well-connected fracture system at depth, as represented by the DFN statistical description. In sparsely fractured rock approaching the percolation threshold, it is more likely for fractures to be isolated or to belong to dead-end paths, on a given block scale. As the number of through-going pathways decreases, greater variability can also be expected in their aggregate effect.

Considering these observations, the geometric estimates of hydraulic conductivity developed here should be used with caution, in application to estimation of performance measures for the SFL. The predicted ranges of K_m are likely to be higher and less variable than what would be obtained from explicit network flow calculations based on the same DFN statistical model, particularly for the rock at depths below 400 m.

4.2 Simple evaluation of performance measures

Independent calculations of flows to the SFL vaults and flow-related performance measures:

- equivalent Darcy flux U [m/y] at the release point from the vault into a fracture;
- flow-related transport resistance F [y/m]; and
- advective travel time t_w [y]

have been carried out based on a simplified model of the hydrogeological system. The analysis follows the simplified representative model (SRM) approach described by Geier et al. (2018), and previously applied for review of a proposed expansion of the Swedish SFR facility (Geier, 2017).

4.2.1 Approach

The main steps in the SRM approach are to identify the key components of the hydrogeological system, represent these in a simplified fashion as conductors in series and/or in parallel, and calculate their response for a reasonable boundary conditions in the recharge and discharge areas. The approach yields bounding estimates based on simple mathematics that can readily be verified without specialized software, and also allows testing alternative assumptions regarding the key components and their properties.

In the application of the SRM approach to the SFL, flows to the SFL vaults are considered to be controlled by the properties of different components of the recharge and discharge paths as shown schematically in Figure 51. In this type of crystalline bedrock environment, large-scale recharge and discharge are expected to be focused along relatively transmissive fracture zones. The SFL design calls for the facility to be located away from major fracture zones, so groundwater must pass through sparsely fractured rock first to reach the waste vaults from the nearest fracture zone carrying recharge, and then again to reach the nearest discharging zone. The flow through this system may also be limited by soils or other regolith present in the recharge and discharge areas. Local topography is here assumed to provide the main driving force for flow over most of the area, recognizing that a there also be a component of regional discharge driven by larger-scale topography.

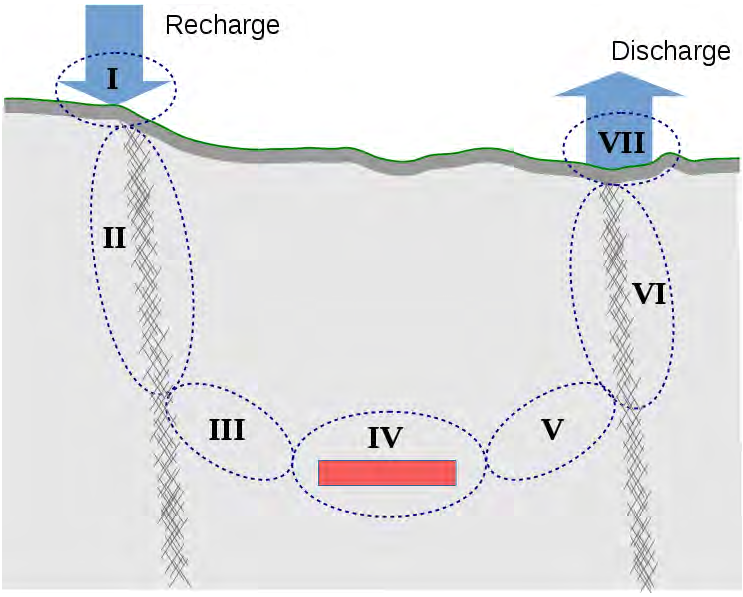

Figure 51. Simplified representative model of a recharge-discharge system for a waste storage facility in fractured crystalline bedrock with a recharge path consisting of (I) regolith in the recharge area, (II) fracture zone with relatively high transmissivity, and (III) sparsely fractured rock mass between (II) and the facility (IV), and a discharge path consisting of (V) sparsely fractured bedrock, (VI) a second fracture zone, and (VII) regolith in the discharge area

This conceptual model is further simplified as a one-dimensional system as shown in Figure 52, with flow driven by the difference in hydraulic head from the recharge to discharge areas:

$$\Delta h = h_{\text{in}} - h_{out}$$

and limited by the net effective hydraulic conductance (i.e. the effective hydraulic conductivity times area divided by length) for the different flow-path segments acting in series. For different parts of this system, alternative representations of each segment can be considered, for example representing the sparsely fractured rock mass in terms of its upscaled equivalent continuum (ECPM) properties or as a discrete connection via a "probabilistic deformation zone" (i.e. a relatively small-scale fracture zone that might not be recognized as such during site characterization).

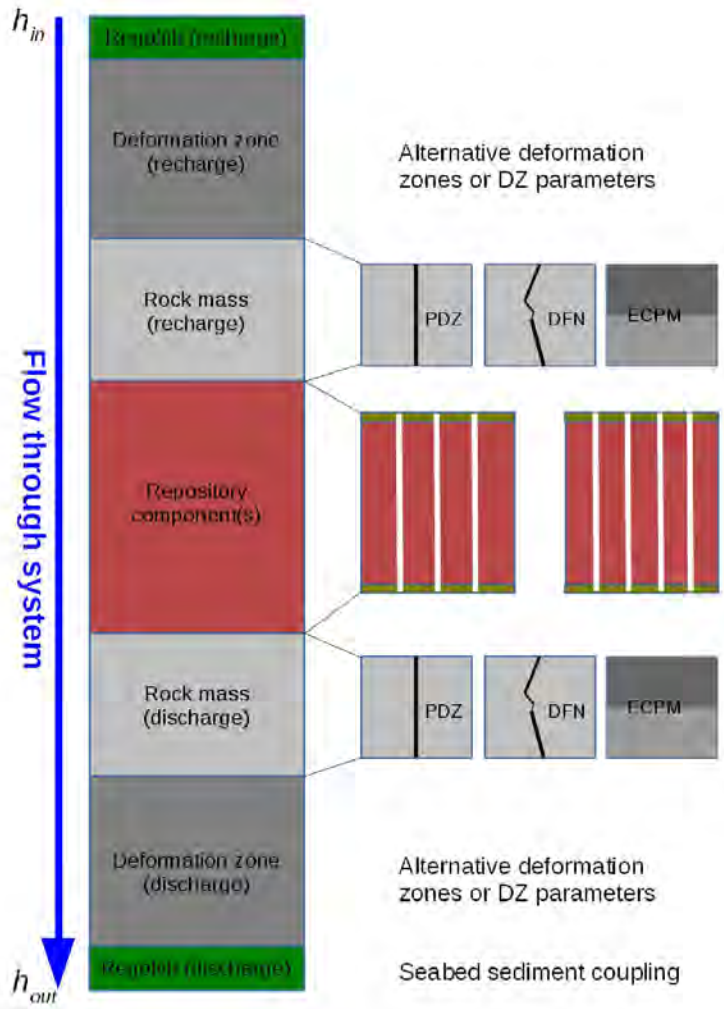

Figure 52. Schematic representation of the SRM model as a 1-D flow path, with options for different representations of each segment.

Calculations based on this approach are carried out using an open-source implementation of the standard UNIX scripting utility *awk* (https://www.gnu.org/software/gawk/manual/gawk.html), with different alternatives for each segment implemented as short scripts as listed in the digital appendix A3. The base case and alternatives for each segment are summarized in the following paragraphs.

Hydraulic gradient

The hydraulic head difference Δh between the recharge and discharge areas is chosen based on the local topographic variation between upland and low-lying areas. By inspection of maps (e.g. Figure 2-4 of Joyce et al., 2019) and elevation data on Google Earth Pro (https://www.google.com/earth/versions/), this difference is typically in the range 10

m to 15 m. The value Δh = 10 m has been used for the SRM base case and other calculation cases described below. The flow rates calculated by the SRM are linearly proportional to Δh, so the effect of higher or lower values of Δh on the main results are straightforward to calculate.

Regolith in recharge and discharge areas

Vertical hydraulic conductivity values K_v for specific regolith layers are based on values given in Table 3-8 of Joyce et al. (2019, SKB R-19-02), with comparison to earlier values given in Table 2-6 of Rhén et al. (2009, SKB R-09-24).

Recharge in more upland areas of the site is expected to be focused in local topographic depressions along the surface traces of deformation zones, where runoff pools following rain or snow-melt events, after overland flow from relatively unfractured bedrock outcrops.

For the **base case** of the SRM, the regolith in the recharge area is assumed to be the Z2 layer, with $K_v = 1.5 \times 10^{-5}$ m/s. This is indicated to be the most widespread flow-limiting layer in local topographic depressions in the more upland areas, according to Figure 3-5 of Joyce et al. (2019). A thickness of 5 m is assumed.

The regolith in the discharge area is assumed to be Z3 (gyttja), with $K_v = 2.5 \times 10^{-7}$ m/s. This is typically the lowest-conductivity layer in lower-lying lake basins and wetland areas. A thickness of 1 m is assumed.

An **alternative regolith case** to check the significance of the regolith assumes that recharge occurs through the Z1 layer with $K_v = 4.0 \times 10^{-3}$ m/s, and discharge is through Z4 (post-glacial gravel) with $K_v = 5.0 \times 10^{-2}$.

Deformation zones

Hydraulic properties of the deformation zone segments of the recharge and discharge paths are based on the parameterization for hydraulic conductor domains (HCDs) given in Table A3.3 of Rhén et al. (2008, SKB R-08-78). The transmissivity of each HCD is considered to be depth-dependent:

$$T(z) = T_0 z^B$$

where T_0 and B are empirical constants obtained by fitting to measured transmissivity values from borehole intercepts with a given HCD at different depths.

The effect of T decreasing with depth is accounted for in the SRM by evaluating T for the midpoints z_i of 50 m depth intervals, from the surface to the proposed depth of the SFL, and calculating the effective transmissivity for these segments in series:

$$T_{eff} = \frac{\sum \Delta z_i}{\sum \Delta z_i / T(z_i)}$$

Alternatively this could be calculated more exactly for the continuous case as:

$$T_{eff} = \frac{z_{max} - z_{min}}{\int_{z_{min}}^{z_{max}} \frac{dz}{T(z)}}$$

For the SRM **base case**, the deformation zone along the recharge path is assumed to be the deformation zone ZSMNS001, a major north-south striking deformation zone in an upland area close to the SFL where the models of Joyce et al. (2019) indicate recharge takes place.

The deformation zone along the discharge path is assumed to be ZSMEW002A which is expressed in the topography as a regional-scale lineament to the north of the SFL location, and receives discharge from the SFL according to particle-tracking by Joyce et al. (2019). Alternative discharge-path deformation zones, considered for variational cases, are ZSMEW007A and ZSMNW042A.

Rock mass

In the SRM **base case**, the hydraulic conductivities of both recharge and discharge segments through the rock mass are set equal to the mean *K* value for Laxemar fracture domain HRD_W (the fracture domain for the vicinity of the SFL according to Figure 2-5 of Joyce et al., 2019) and depth zone DZ3 (for $z = -400$ m to $z = -650$ m, and thus containing the proposed horizon of $z = -500$ m for the SFL). The *K* value for the base case is estimated graphically from Figure 5-3 of Joyce et al. (2010) as $K = 10^{-9.69}$ m/s = 2.0×10^{-10} m/s.

Alternative **permeameter cases** are based on random sampling of block-scale hydraulic conductivity tensors estimated by geometrical upscaling of the DFN statistical model, as presented in Section 4.1 of this report. Calculations cases are based both on HRD_W and HRD_C which may occur at depth below the hypothetical facility. In both of these cases, the values from DZ3 are used as the basis for random sampling.

Two additional **probabilistic deformation zone (PDZ) cases** consider the possibility that a minor deformation zone (MDZ), not recognized as such during site characterization, could connect directly from one or both vaults to the larger-scale deformation zones. The DFN model used for the analyses by Joyce et al. (2019) and Abarca et al. (2019) includes the possibility for discrete fractures on scales of up to 1 km, which could account for the possibility of such features. However among the limited number of realizations in their analyses, none included a discrete, high-transmissivity fracture or MDZ that connects directly from a vault to the bounding zones.

Hydraulic properties of the PDZs for these cases are based on the statistical description of minor deformation zones identified at Laxemar, as given in Tables 8-1 and 8-2 of Rhén et al. (2008, SKB R-08-78). For DZ3, the measured values of log T_{MDZ} (log m^2/s) range from –8.89 to –5.96, with a mean of –7.65 and standard deviation of 0.80, based on a sample of 21 borehole-zone intersections in DZ3 that produced flow anomalies with a differential flowmeter.

The first PDZ case, referred to as the **PDZ (maximum T) case**, assumes that a single PDZ, with transmissivity equal to the maximum value listed in Rhén et al. (2008), connects through the rock-mass segment of the recharge path. The rock-mass segment for the discharge path is treated as an effective continuum, as in the base case.

The second PDZ case, referred to as the **PDZ (random) case**, assumes that PDZs connect through the rock-mass segments of both the recharge and discharge paths. These have transmissivity values sampled randomly from a bounded lognormal distribution based on the statistics given by Rhén et al. (2008).

A more extreme case could be constructed by assuming that PDZs in both the recharge and discharge paths have transmissivity equal to the maximum value listed Rhén et al. (2008), but it would be highly unlikely that two such PDZs would be encountered in the same area and would both be undetected by site characterization. Therefore such a case has not been considered here.

Repository vaults

The BHA and BHK vaults in the SFL are represented as simple 1D conductors, with effective properties deduced from the material specifications and geometry of the vaults and waste containment structures.

In the **base case**, the simplified component model for each vault considers longitudinal flow along each of these vaults as depicted in Figure 53. For the section of the vault that contains the waste, there are two conductors in parallel, representing the encased waste and the backfill above the waste.

The net effect of the two backfilled sections at either end of the waste vault for flow is accounted for by a conductive segment placed in series with the waste-storage section. The conductance of this segment is calculated as:

$$C = \frac{K_{backfill} A_{vault}}{L_{vault} - L_{waste}}$$

where A_{vault} is the cross-sectional area of the vault, L_{vault} is the vault length, and L_{waste} is the length of the waste containment structure. $K_{backfill}$ is the hydraulic conductivity of the backfill (bentonite for the BHA, concrete for the BHK). For the base case calculations, permeability values given in Table 3-2 of Abarca et al. (2019), and converted to hydraulic conductivity values using the same values specified there for water density and dynamic viscosity. Dimensions for calculating lengths and cross-section areas are taken from Figures 3-2 and 3-3 of Abarca et al. (2019) and supporting text as noted in the scripts in the appendix.

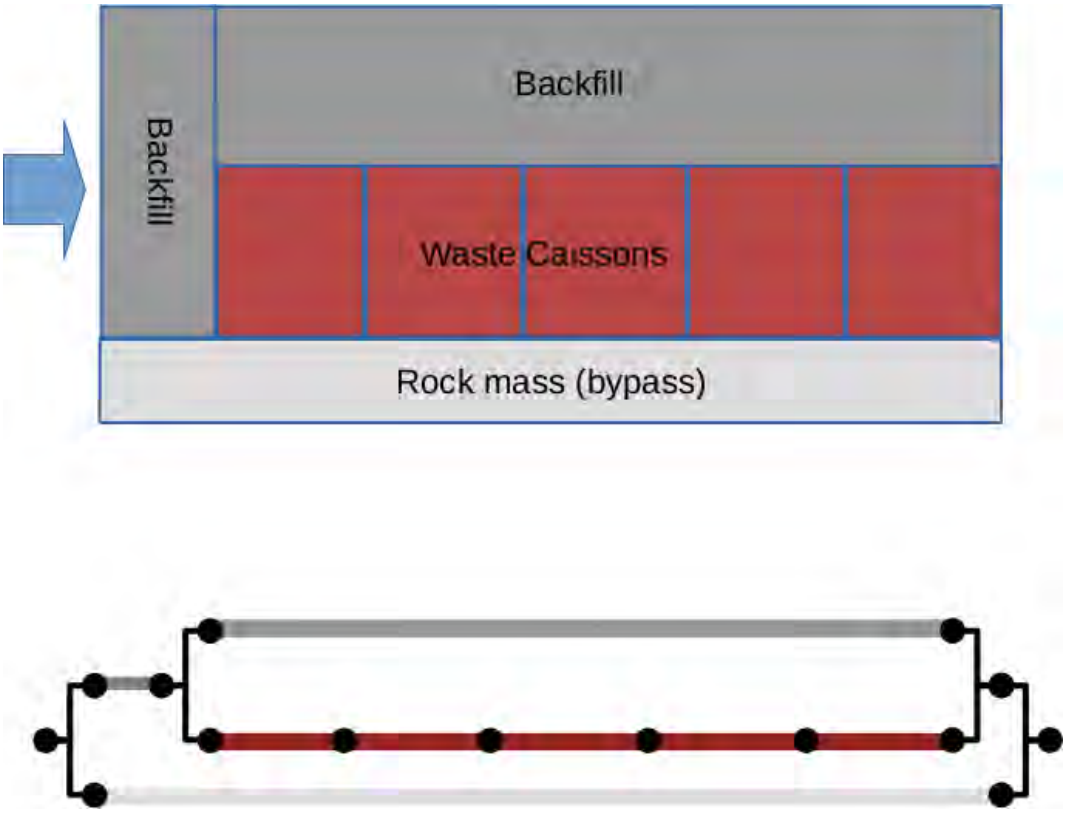

Figure 53. Simplified component model for longitudinal flow through the BHA or BHK waste vault. The upper part of the diagram shows the simplified conceptual geometry. The lower part shows the representation as linear conductors in parallel or in series.

The potential for bypass flow through the rock mass surrounding the vault is accounted for by a parallel conductance equal to:

$$C = \frac{K_{rock} A_{rock}}{L_{vault}}$$

where A_{rock} is the cross-sectional area of an annulus of thickness d_{rock} of rock around the vault.

As the detailed hydrogeological models of Joyce et al. (2019) and Abarca et al. (2019) indicate that flow through the vaults is mainly vertical rather than longitudinal, a **vertical flow case** is also considered, based on an alternative representation of the vaults as shown in Figure 54.

In this case, water enters the vault through the backfill above the waste containment structure(s), then passes partly through the waste and partly through the backfill on either side of the waste, and then finally out through the backfill below the waste (which is conceptually treated as part of the upper backfill). Flow may also bypass the section of the vault where waste is stored, either via the backfill at the ends of the vault, or by vertical flow through the rock mass on either side of the vault.

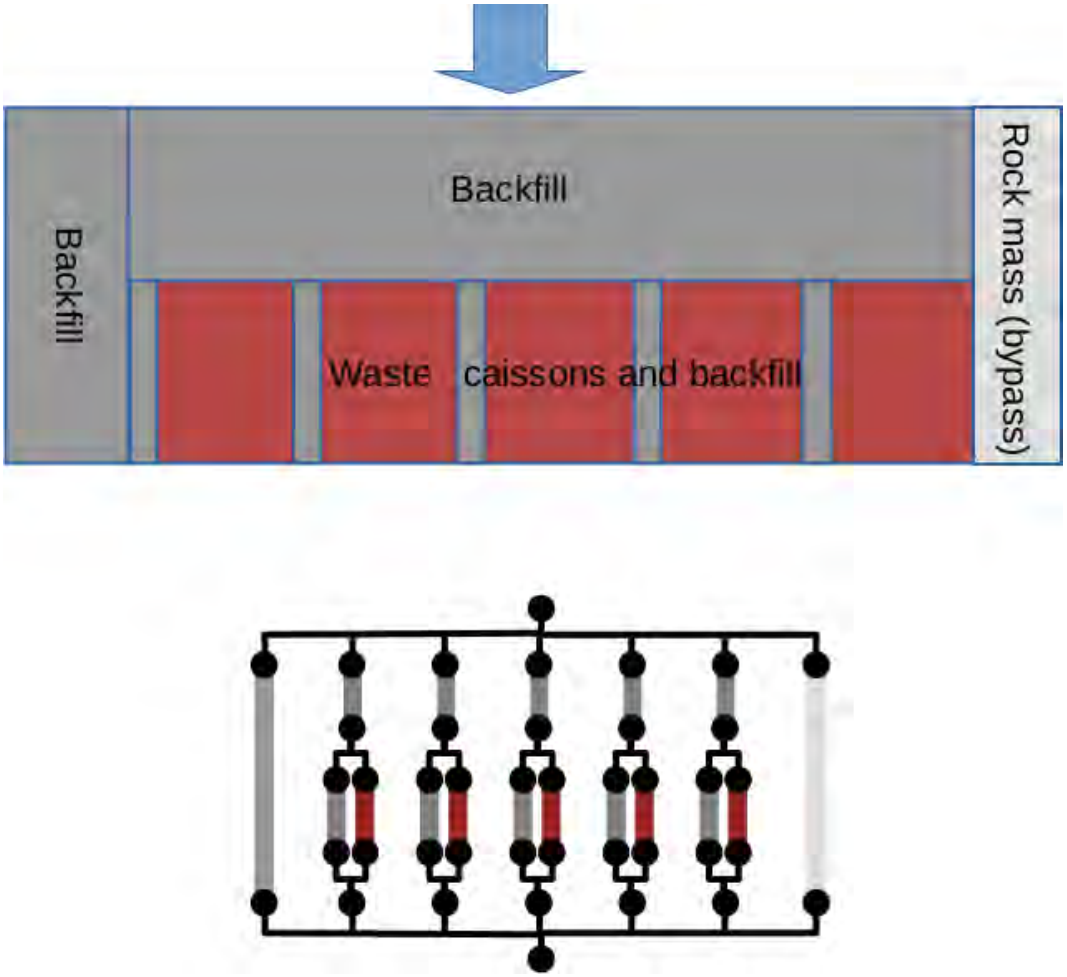

Figure 54. Simplified component model for vertical flow through the BHA or BHK waste vault. The upper part of the diagram shows the simplified conceptual geometry. The lower part shows the representation as linear conductors in parallel or in series.

Both of these representations (longitudinal flow and vertical flow) are highly simplified in comparison with the flow patterns that could result from the 3-D geometry of the vaults and waste containment structures, in combination with inhomogeneous inflow and outflow controlled by the fracture network in the surrounding rock mass, as well as possible inhomogeneity in the backfill and waste volumes.

Calculation of flow-related transport parameters for far-field transport

Flow-related performance parameters for radionuclide transport in the discharge path have been calculated based on the flow rate Q through the vaults, the effective hydraulic conductivity K_{rm} of the rock mass segment belonging to the discharge path, and the hydraulic properties of the discharging fracture zone. Travel time and transport resistance in the discharge-area regolith is neglected, on the grounds that this can be regarded as part of the biosphere (which is handled differently and using more complex models in consequence calculations for SE-SFL).

Advective travel times through the discharge-segment rock mass are calculated based on an assumption that the flow through the rock mass is dominantly through a small number of pathways (consisting of single fractures or connected fracture networks) acting in parallel. Four different models regarding the correlation between fracture transmissivity T and aperture b are considered.

Calculation cases are considered within which flow through the rock-mass segment of the discharge path is dominantly via N = 1, 2, or 4 pathways in parallel, each with identical transmissivity. The case N = 1 represents flow dominated by a single dominant, high-transmissivity feature. This leads to the highest advective velocities, shortest travel times, and least surface area for water-bedrock interaction, of these three cases.

The cases of N = 2 and N = 4 pathways are used to illustrate the effects of more distributed flow through the rock mass. In each of these cases, the transmissivity of each pathway is assumed to be identical to that of the other pathways acting in parallel. Although it is unrealistic to expect that parallel pathways will have identical hydraulic properties, this can be viewed as a bounding case, as it results in the lowest advective velocities in the main pathway, and the maximum flux-weighted transport resistance for a given number of pathways.

The transmissivity of each pathway for a given value of N is taken as:

$$T_N = \frac{1}{N}\left(\frac{A_{rm}}{W_{rm}}\right) K_{rm}$$

where W_{rm} is the nominal width of the rock mass (assumed to be on the order of the scale of the SFL vaults) and A_{rm} is the nominal cross-sectional area, as assumed in the previous SRM flow rate calculations. For the results presented here, values of W_{rm} = 100 m and A_{rm} = 50 000 m^2 were used, so effectively:

$$T_N = \left(\frac{500m}{N}\right) K_{rm}$$

The performance parameters are linear with respect to this relationship so the results of alternative values can easily be assessed.

The discharging fracture zone is considered to be a tabular aquifer with transmissivity T_{DZ}, effective width W_{DZ}, and length in the discharging direction L_{DZ}. These parameters are specified as part of the SRM for flow.

Deformation zones in granitic rock can be expected to have relatively high porosity relative to the rock mass (so lower ratios of advective velocity to flux) and higher values of wetted surface a_w (so higher transport resistance), because the flow paths are through a relatively intense network of fractures and even breccias.

To represent this, calculations cases are considered within which flow through the deformation segment of the discharge path is dominantly via N = 4, 8 or 16 pathways in parallel, each with identical transmissivity, following the same methods as for the rock mass.

Transport-path apertures b_N for a given N are calculated based on specified correlations to transmissivity T_N, depending on the variant considered. Four variants have been considered in the present calculations (b_N expressed in units of m and T_N in units of m^2/s, in all cases:

Cubic law: Theoretical relationship for parallel-plate fractures which can be written as:

$$b_N = \left(12\frac{\mu_w}{\rho_w g}\right)^{1/3} \cdot T_N^{1/3}$$

where μ_w is the dynamic viscosity of water, ρ_w is the density of water, and g is gravitational acceleration.

Äspö model: Empirical model based on data from Äspö, Sweden (Dershowitz et al. 2003):

$$b_N = 0.5{T_N}^{0.5}$$

Hjerne model: Empirical model of Hjerne et al. (2010):

$$b_N = 0.28{T_N}^{0.3}$$

"Stochastic" model: Based on the Äspö model but with a half-order-of-magnitude standard deviation:

$$b_N = 0.5 \cdot 10^{0.5N(0,1)}{T_N}^{0.5}$$

where $N(0,1)$ is a random value generated from the standard normal distribution.

These models for transport aperture are compared in Figure 55. Among the deterministic models, the cubic-law case yields the smallest apertures and the Hjerne model yields the largest apertures for the range of transmissivities considered. The stochastic model produces the widest spread of apertures, and can occasionally yield values even lower than the cubic law though its expected value for any given value of T is conforms to the Äspö model.

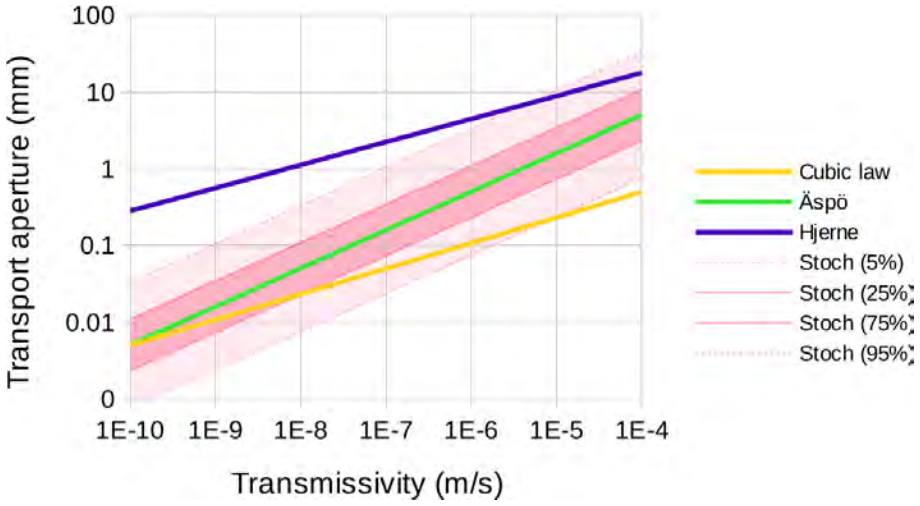

Figure 55: Comparison of the three deterministic models for transport aperture as a function of fracture transmissivity: the cubic law, the "Äspö" empirical model of Dershowitz et al. (2003), and the empirical model of

Hjerne et al. (2010). The stochastic model considered in this report follows the Äspö model but with lognormally distributed random variation (represented by the darker pink band showing the 25% to 75% confidence interval and the lighter pink band showing the 5% to 95% confidence interval).

The mean advective velocity is equal to the total flow rate through the rock mass divided by the cross-sectional area of the pathways:

$$u_{rm} = \frac{Q}{N b_N W_{rm}}$$

The advective travel time over a distance L_{rm} through the rock mass is then:

$$t_{wr,rm} = \frac{L_{rm}}{u_{rm}}$$

The transport resistance for each of the parallel pathways through the rock mass is:

$$F_{r,rm} = \frac{a_w L_{rm}}{u_{rm}}$$

where a_{w} is the flow-wetted surface per unit volume of water in the mobile zone (fractures). For a simple planar fracture $a_w = 2/b_N$ so:

$$F_{r,rm} = \frac{2 L_{rm}}{b_N u_{rm}}$$

Substituting in the above expression for u_{rm} yields:

$$F_{r,rm} = \frac{2 N L_{rm} W_{rm}}{Q}$$

From this it can be noted that, under these assumptions, $F_{r,rm}$ is not sensitive to the choice of aperture model for b_N, but only N, the assumed number of flow paths, along with the effective width and length of the rock mass through which discharge occurs.

Performance parameters for the deformation zone portion of the discharge path are calculated analogously to those for the rock mass. The mean advective velocity is equal to the total flow rate divided by the cross-sectional area of the pathways through the deformation zone:

$$u_{DZ} = \frac{Q}{N b_N W_{DZ}}$$

The advective travel time over a distance L_{DZ} through the deformation zone is then:

$$t_{wr,DZ} = \frac{L_{DZ}}{u_{DZ}}$$

The transport resistance is:

$$F_{r,DZ} = \frac{2 N L_{DZ} W_{DZ}}{Q}$$

As for the rock mass, under these assumptions $F_{r,DZ}$ is not sensitive to the choice of aperture model for b_N, but only the assumed number of flow paths, along with the effective width and length of the deformation zone through which discharge occurs.

4.2.2 Results

Conductances of vault components

The conductances of the different vault components, as calculated for flow in a given direction through the vaults, are independent of the flow magnitude and other characteristics of the recharge-discharge paths in the SRM representation. These values and the associated flow fractions (Table 9) can be useful to understand what factors control partitioning of flow through the waste and backfill components, in this simplified representation.

For flow in a longitudinal direction through the BHA vault, the conductance of the waste domain is nearly six orders of magnitude greater than that of the surrounding bentonite backfill in the same section of tunnel (9.4×10^{-8} m^2/s vs. 2.6×10^{-13} m^2/s), and nearly five orders of magnitude higher than the net conductance of the backfill sections at the ends of the vault (1.2×10^{-12} m^2/s). The result is that nearly all of the flow passing through the vault goes through the waste, but the overall flow is limited by the bentonite backfill in the ends of the tunnel. By far the main fraction (>99.9%) of flow through the system represented by this simple model is via the surrounding rock mass.

The situation in the BHK is quite different, as the conductance of the waste domain is only about six times that of the surrounding concrete backfill (1.3×10^{-7} m^2/s vs. 2.0×10^{-8} m^2/s), so only about 86% of the flow through the vault passes through the waste. The contrast in hydraulic conductivity between the concrete backfill and the surrounding rock is relatively minor, so bypass flow through the rock is less effective in shielding the BHK waste from flow.

For the case of flow in a vertical direction through the vaults, the effective conductance of both vaults is higher because the flow passing through the vault encounters a larger cross-sectional area and less thickness of backfill, than flow in the longitudinal direction. For the BHA as a whole, the calculated increase in conductance for vertical vs. longitudinal flow is about a factor of 30 (3.7×10^{-11} m^2/s vs. 1.2×10^{-12} m^2/s). For the BHK the increase is about a factor of 50 (1.4×10^{-7} m^2/s vs. 2.7×10^{-9} m^2/s). For both vaults, vertical flow provides more conductance via routes through the backfill that bypass the waste, resulting in a decrease in the fraction of the vault flow that passes through the waste (about 91% for the BHA and 24% for BHK).

Table 9: Conductances and flow fractions calculated for the SRM representations of the vaults, for flow in the longitudinal versus vertical directions. The conductances of the waste and vault are independent of other assumptions. Waste and vault flow fractions (the fractions of the total flow passing through the waste and vault, respectively) are influenced by the hydraulic conductivity *K* of the adjacent rock through which bypass flow occurs; values presented here are for *K* as in the base case.

Domain	BHA (longitudinal flow)	BHK (longitudinal flow)	BHA (vertical flow)	BHK (vertical flow)
Conductance of waste (m^2/s)	9.5×10^{-8}	1.3×10^{-7}	2.6×10^{-5}	1.7×10^{-5}
Conductance of entire vault (m^2/s)	1.2×10^{-12}	2.7×10^{-8}	3.3×10^{-11}	1.4×10^{-7}
Waste flow fraction	5.2×10^{-4}	0.41	0.0084	0.232
Vault flow fraction	5.2×10^{-4}	0.47	0.0092	0.972
Bypass flow fraction (via rock)	0.99948	0.53	0.99	0.028
Waste flow / vault flow ratio	>0.999	0.86	0.91	0.24

Flows through vaults and waste

The calculated flow rates through the BHA and BHK vaults and waste, for the base case and all alternative cases, are shown in Figures 56 through 59. For each vault, results are presented from two flow configurations:

- Vaults treated individually (i.e., flows are calculated independently for each vault, considered as if all of the flow along the recharge-discharge path passed through the single vault), and
- Vaults treated in parallel (i.e., flow along the recharge-discharge path can pass through either vault, in proportion to the vault conductance).

When the vaults are treated independently, in the base case the flow through the BHA vault is 2.6×10^{-3} m^3/y, nearly all of which passes through the waste. The flow through the waste is within a factor of two of the value of 1.55×10^{-3} m^3/y obtained in the base case of Abarca et al. (2019, Appendix B), though the latter model predicts about four times greater total flow through the vault (1.16×10^{-2} m^3/y).

As shown in Figure 56, only the case of vertical flow in the SRM produces significantly higher flow, with flows of 6.5×10^{-3} m^3/y and 5.9×10^{-3} m^3/y through the vault and waste, respectively.

The effects of the other alternatives considered are comparatively minor. When probabilistic minor deformation zone is substituted for the upscaled continuum representation of the rock mass, vault and waste flows increase by about a factor of 2. The effect of an alternative regolith is negligible. Discharge through alternative deformation zones also has negligible effect (so small that these data points are obscured by the symbol for the base case, in Figure 56).

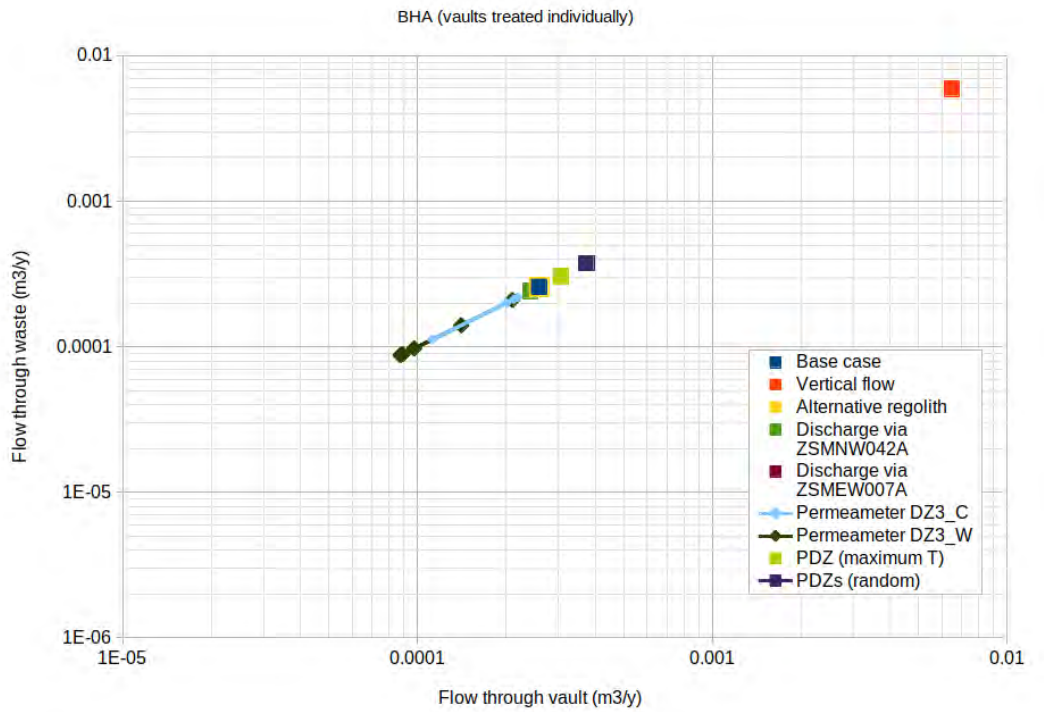

Figure 56. Flow through the vault and waste for the BHA treated independently, for the base case and alternative cases.

A surprising effect is seen for the cases based on independent estimates of rock mass *K* by geometric upscaling (labeled in Figure 56 as "permeameter" cases DZ3_C and DZ3_W). The higher *K* values result in lower flows through the BHA vault and waste. This can be understood as the result of the higher-*K* rock mass allowing a greater fraction of the flow to bypass the relatively impermeable BHA backfill.

The corresponding results for BHK treated independently are shown in Figure 57. In the base case, the flow through the BHK vault is 0.40 m^3/y, of which 0.34 m^3/y passes through the waste. The effects of the different SRM alternatives for the BHK are similar to those seen for the BHA. The case of vertical flow in the SRM produces significantly higher flow, with 1.5 m^3/y passing through the vault of which 0.36 m^3/y passes through the waste.

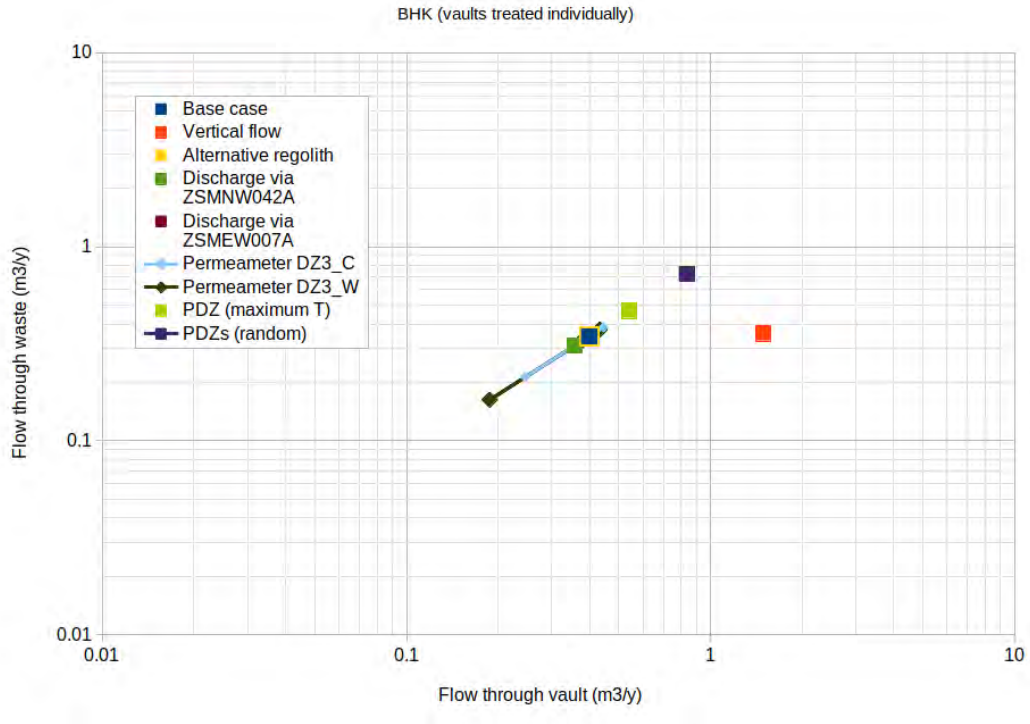

Figure 57 Flow through the vault and waste for the BHK treated independently, for the base case and alternative cases.

The corresponding values obtained by Abarca et al. (2019) are 2.29 m^3/y through the vault as a whole, and 0.92 m^3/y through the waste. Thus the BHK flows calculated by Abarca et al. (2019) are of similar magnitude but higher by a factor of 2 to 3, in comparison with the maximum flows calculated for the simplified model, giving confidence that the results from SKB's models are reasonable.

When the BHA and BHK vaults are treated together as conductors in parallel, the flows through both vaults are reduced. The greatest reductions are seen for BHA, as the BHK serves as a preferential path for flow in this system. This effect is even more pronounced for the case of vertical flow than for the case of longitudinal flow, resulting in extremely low flows on the order of 1×10^{-5} m^3/y through the BHA

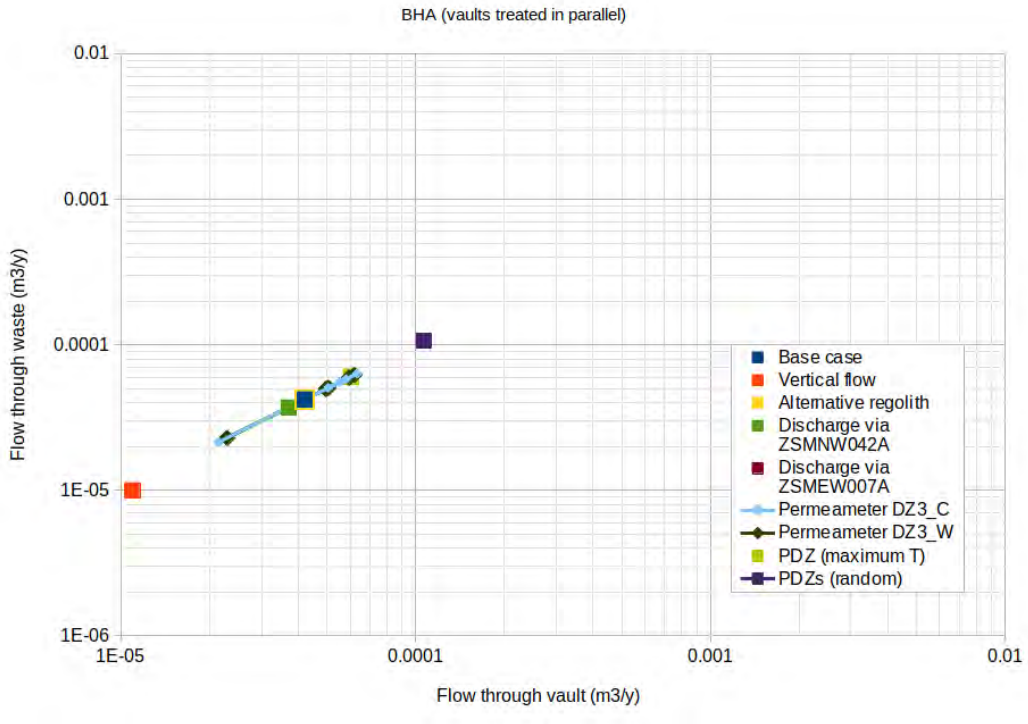

Figure 58 Flow through the vault and waste for the BHA treated in parallel with the BHK, for the base case and alternative cases.

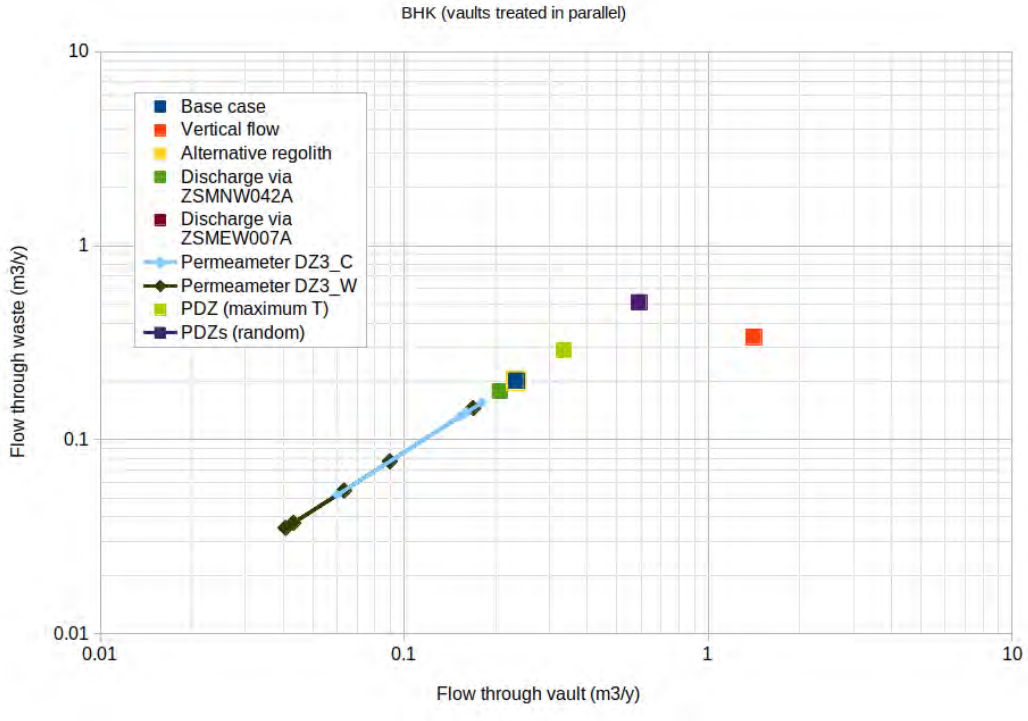

Figure 59 Flow through the vault and waste for the BHK treated in parallel with the BHA, for the base case and alternative cases.

Flow-related transport parameters

Predicted advective travel times through the rock mass (RM) and deformation zone (DZ) segments along the discharge path are summarized in Figures 60 and 61. The calculated ranges are sensitive to assumptions regarding the number of dominant fractures assumed to carry the main flow in each segment, and choice of aperture model.

The total transport time through RM and DZ segments is mainly in the range from 10 y to about 5000 y, depending on the specific assumptions of each SRM calculation case. This range is in good agreement with the results from the facility-focused model shown in Figures 4-145 and 4-153 of Joyce et al. (2019).

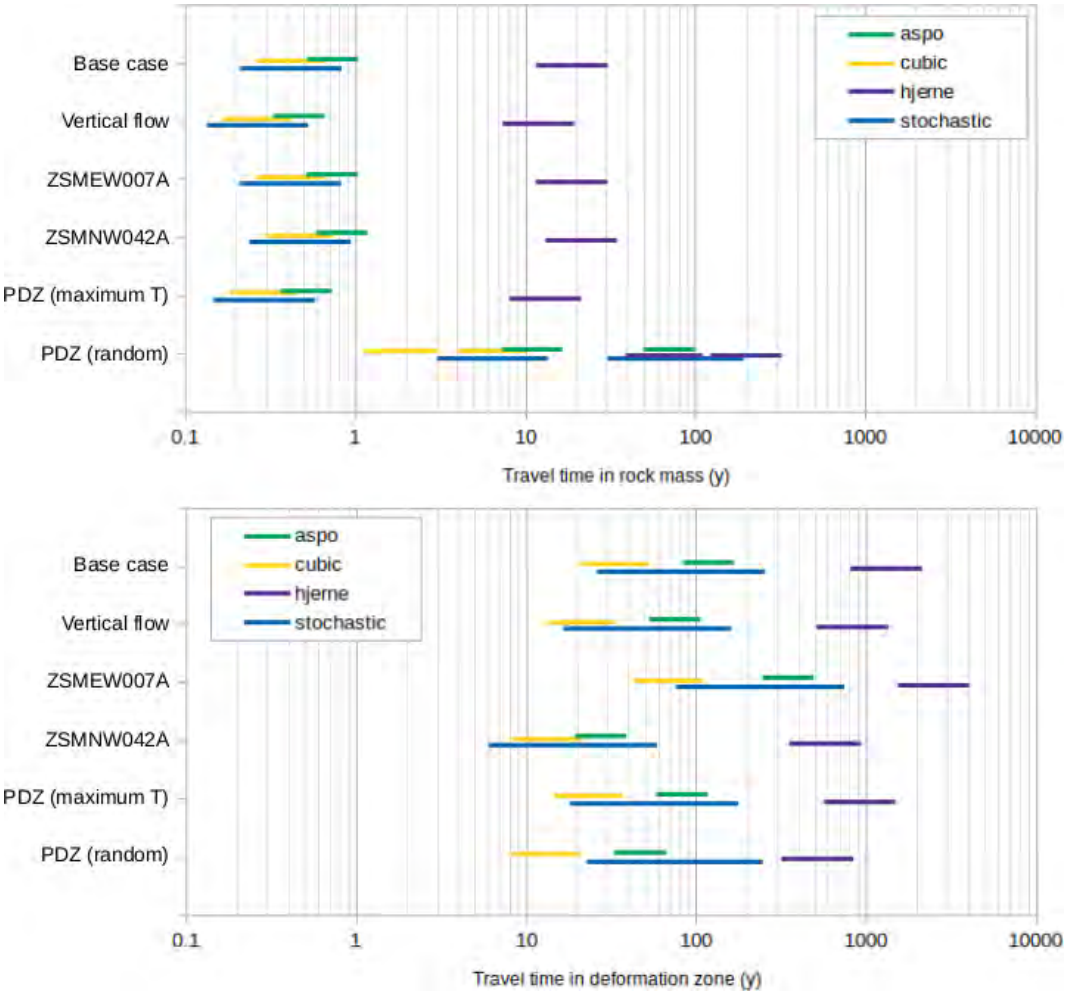

Figure 60 Ranges of travel times through the rock mass (top) and deformation zones (bottom) calculated for the base case and alternative cases including vertical flow through vaults, discharge via ZSMEW007A or ZSMNS042A, PDZ with maximum transmissivity, and PDZ with randomly sampled transmissivities (3 realizations). Colors represent the alternative aperture models (cubic-law, Äspö, Hjerne, and stochastic models). Ranges for the deterministic cases result from alternative assumptions regarding whether flow is via one to four dominant fractures in the rock mass, or 4 to 16 dominant fractures in the deformation zone.

For all of the calculation cases considered, the main portion of total travel time is in the DZ segment. This results from the relatively high pore volume associated with the deformation zones, due to the assumed higher number of dominant fractures as well as the large apertures resulting from the assumed log-linear correlations of aperture with transmissivity.

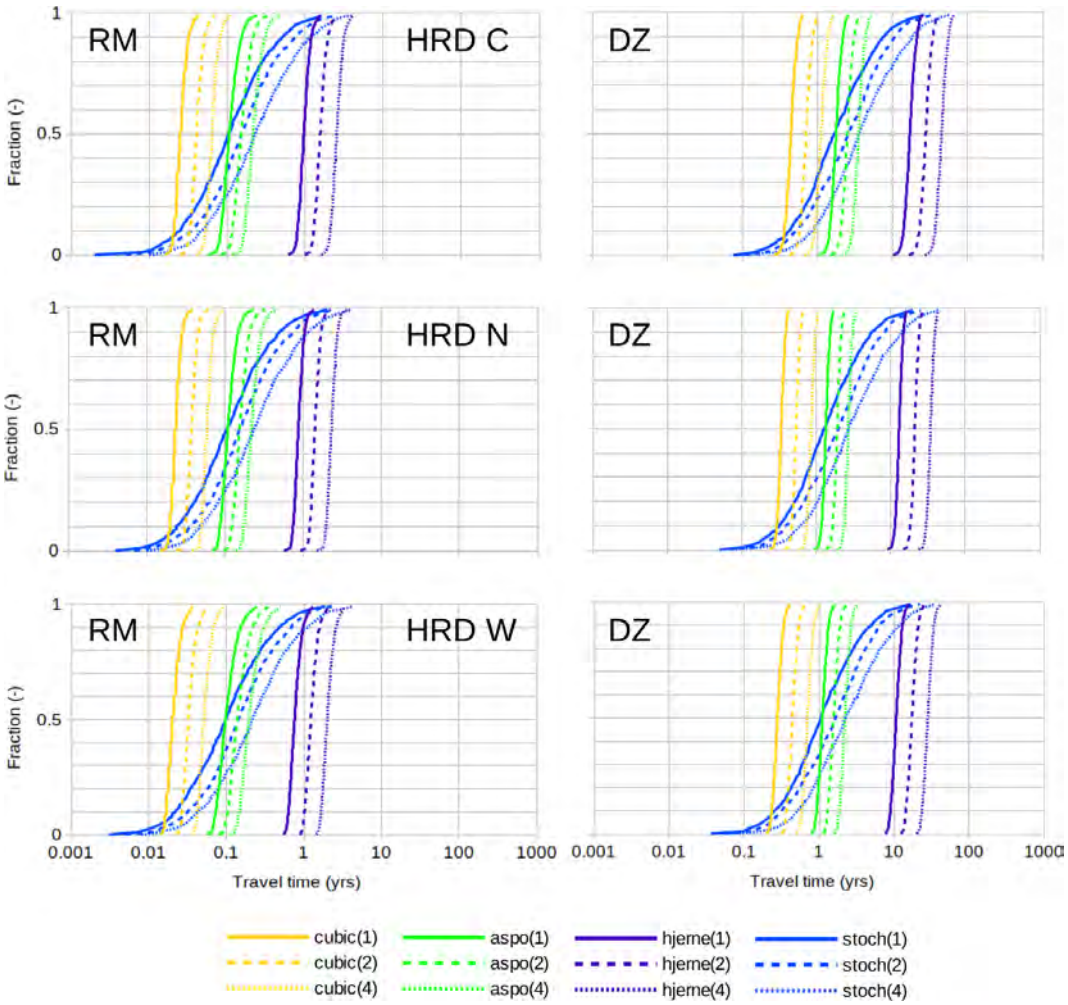

Figure 61 Distributions of travel times through the rock mass (RM) and deformation zones (DZ) calculated for the permeameter cases for domains HRD_C (top row), HRD_N (middle row), and HRD_W (bottom row). Each plots represents 1000 SRM calculations with random sampling of block-scale hydraulic conductivities upscaled as described in Section 4.1. Colors represent the alternative aperture models (cubic-law, Äspö, Hjerne, and stochastic models). Solid lines represent cases where flow is via one dominant fracture in the RM or 4 co-dominant fractures in the DZ. Dashed lines represent flow through 2 co-dominant fractures in the RM or 8 in the DZ. Dotted lines represent flow through 4 co-dominant fractures in the RM or 16 in the DZ.

Predicted transport resistance of the RM and DZ segments of the discharge path are summarized in Figures 62 and 63. The calculated ranges are sensitive to assumptions regarding the number of dominant fractures assumed to carry the main flow in each segment, but independent of the choice of aperture model (as noted above).

The total transport resistance *F* of the RM and DZ segments is dominated by the contribution of the DZ segment. For most of the cases as shown in Figure 62 this is mainly in the

range from 2×10^5 y/m to 2×10^6 y/m, but lower values result from the permeameter cases shown in Figure 63, with values as low as about 4×10^3 y/m. This latter value is lower than the range shown in Figure 4-153 of Joyce et al. (2019), which shows minimum F of about 1×10^4 y/m and median F of about 6×10^4 y/m. However Figure 4-144 of Joyce et al. (2019), which considers additional realizations of the DFN model, shows *F* values as low as 3×10^3 y/m for one realization. Thus the range of *F* values obtained here is in reasonably good agreement with the results of Joyce et al. (2019).

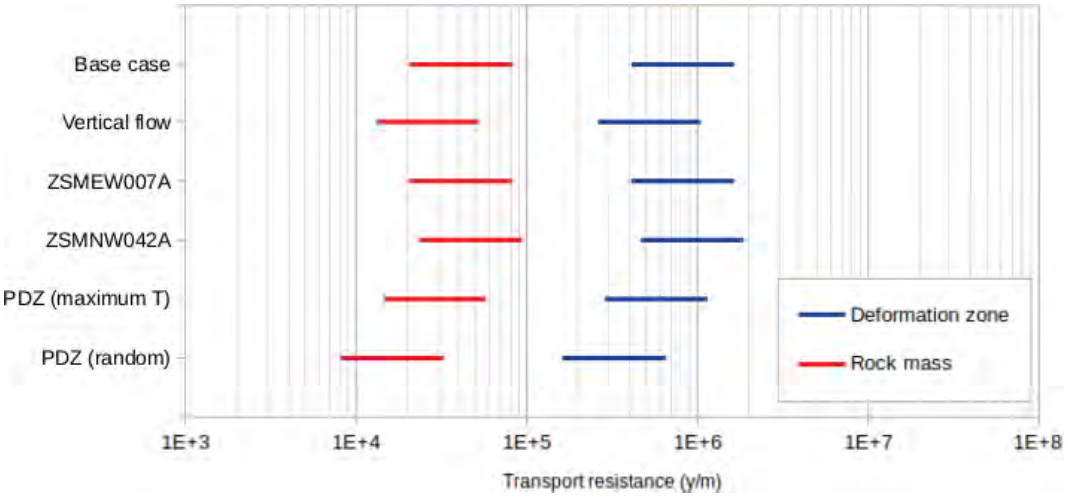

Figure 62 Ranges of transport resistance F through the rock mass and deformation zones calculated for the base case and alternative cases including vertical flow through vaults, discharge via ZSMEW007A or ZSMNS042A, PDZ with maximum transmissivity, and PDZ with randomly sampled transmissivities (3 realizations). Ranges for the deterministic cases result from alternative assumptions regarding whether flow is via one to four dominant fractures in the rock mass, or 4 to 16 dominant fractures in the deformation zone.

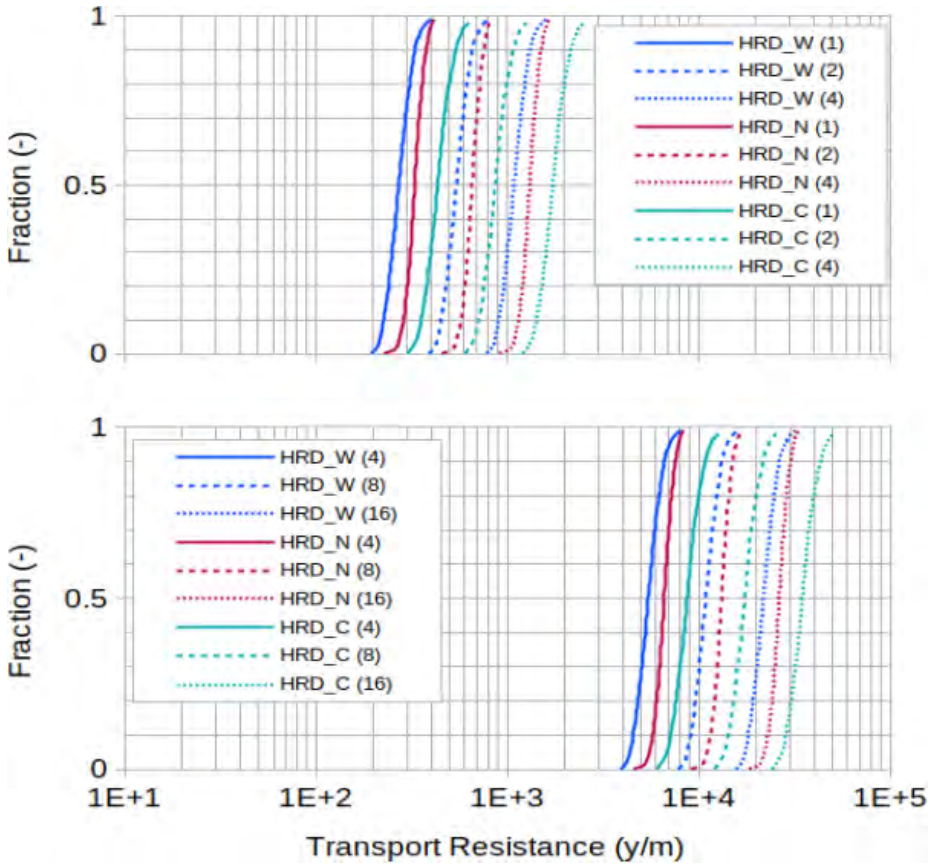

Figure 63 Distributions of transport resistance F through the rock mass (top) and deformation zones (bottom) calculated for the permeameter cases for domains HRD_C (teal), HRD_N (red), and HRD_W (blue). Each plot represents 1000 SRM calculations with random sampling of block-scale hydraulic conductivities upscaled as described in Section 4.1. Solid lines represent cases where flow is via one dominant fracture in the RM or 4 co-dominant fractures in the DZ. Dashed lines represent flow through 2 co-dominant fractures in the RM or 8 in the DZ. Dotted lines represent flow through 4 co-dominant fractures in the RM or 16 in the DZ.

Discussion of results of simplified model

The main controls on flow through the SFL vaults and waste compartments, in this SRM representation, are apparently the properties of the vaults (i.e. the waste and backfill properties, the assumed flow direction through the vaults, and interactions between vaults). Alternative assumptions regarding the geosphere components (rock mass, deformation zones, and regolith) are comparatively minor.

In the simplified flow system considered in the SRM, the rate of flow – and hence the advective velocity through the discharging deformation zone segment – is limited by the vault properties as well as the rock mass that permits bypass flow. In a more realistic representation of the 3-D flow system, higher velocities could result from flow that passes through other rock volumes and converges into the same deformation zone, resulting in more rapid transport to the surface environment and lower transport resistance. Previous modeling of a hypothetical spent-fuel repository at a similar depth under the nearby island

of Äspö, using a 3-D discrete-feature model (Geier, 1996), indicated that advective transport via deformation zones could be much faster, depending on assumptions regarding the internal architecture and heterogeneity of those zones. Considering this, the predictions here should be used with some caution, as even lower values of transport resistance could result from faster flow in the deformation zones.

The present analysis has not evaluated any cases where the hydraulic conductivity of the backfill in the vault, or of the waste containment structures, is higher than in the SFL design specification (for example, cases where through-going cracks develop in the BHK backfill or concrete walls of the caissons). Such cases could be important to consider as possibilities for review of a future license application. A case of void space between the rock and concrete might be of less concern as this might allow flow to bypass the waste compartments (similar to the effect of a degraded zone of concrete in BHK), but a through-going crack of significant aperture connecting to the waste compartment could increase flow through the waste.

4.3 Sensitivity of performance measures to weighting scheme for particle tracking

The analysis of performance measures by Joyce et al. (2019) is based on tracing transport paths by a particle tracking method that assigns an equal number of particles to each fracture that intersects the vaults, rather than apportioning particles by groundwater flux. This means that transport pathways with relatively high groundwater flux where they intersect the vaults will not be represented in proportion to the flux that they carry.

A more appropriate approach for assessing release and transport from contaminant sources is to distribute the particle sources in proportion to flux. This approach has been used, for example, in the Swedish authorities' past analysis by of a hypothetical spent-fuel repository located under the island of Äspö, approximately 4 km ENE of the location chosen for SE-SFL, as part of the SITE-94 performance-assessment project (SKI, 1996).

Flow and particle-tracking calculations for the SITE-94 project, using a multi-scale discrete model of the Äspö site (Geier, 1996) yielded predictions of near-field Darcy flux as well as effective far-field transport parameters for solute plumes originating from a randomly selected set of waste deposition holes within the hypothetical repository. In this application, multiple particles (typically 100) were released in each deposition hole intersected by one or more flowing fractures, with release proportional to the flux going from the deposition hole into each fracture. Flow-related transport properties for the resulting plume from each source were then estimated from the cumulative breakthrough curve.

The results for the base case of that model, reproduced here in Figure 64, showed a tendency for the transport resistance F to be inversely related to the near-field flux. This tendency can be expected as flow paths carrying high flux in the near field are also likely to have higher advective velocities in the far field, resulting in shorter transport times to the release point in the biosphere.

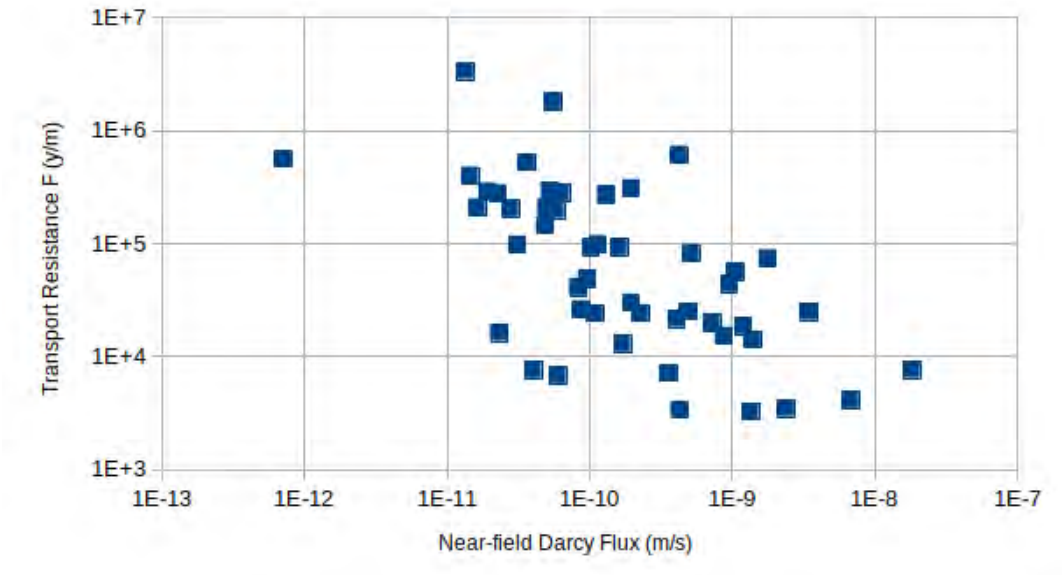

Figure 64. Transport resistance versus near-field Darcy flux for the base case variant of the SITE-94 discrete-feature model of Äspö (Geier, 1996), for the 47 deposition-hole locations that produced solute arrival to the geosphere/biosphere interface. Data for this plot are taken from an archived copy of CHC SITE 94 Data Delivery 3: Variational Cases, dated November 16, 1994, calculation case SKI0/NF0/BC0.

Joyce et al. (2019) do not give corresponding plots of the relationship between near-field flux and far-field performance parameters for the individual flow paths sampled by particle tracking for SE-SFL, but it is reasonable to expect similar tendencies.

The potential error in predicted distributions of performance parameters, due to using a fixed number of particles per fracture rather than a number proportional to flux, can be illustrated using the results for Äspö. Figure 65 compares the distribution of transport resistance for the case where each source in the SITE-94 model is given equal weight, versus the case where the results for each path are weighted in proportion to the flux at the source.

For this example, if the *F* distribution were estimated based on an equal number of particles released at each fracture intersecting a deposition hole, it would significantly underestimate the fraction of solute that encounters relatively low-*F* pathways.

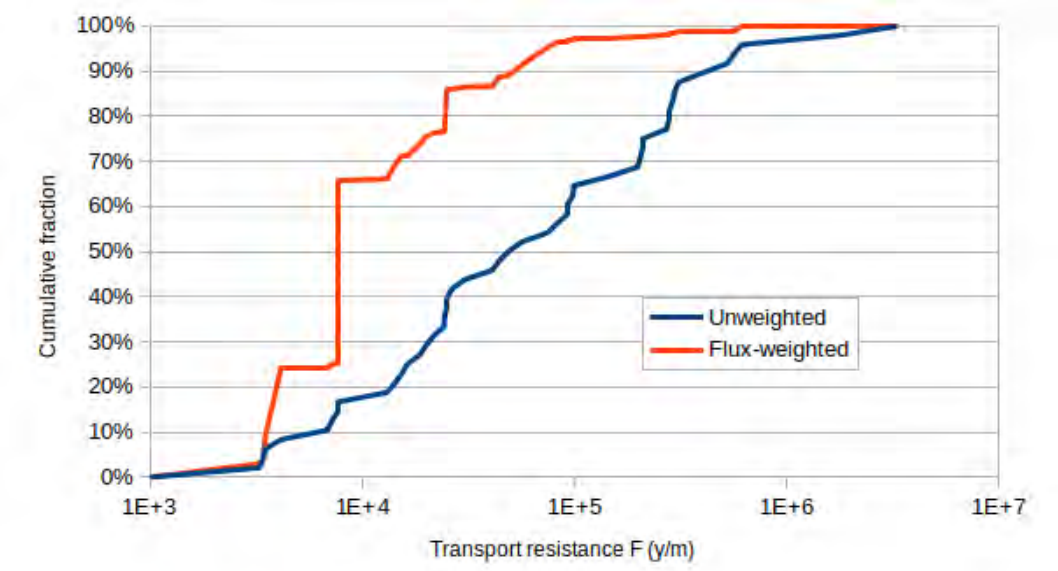

Figure 65. Cumulative distribution of transport resistance *F* weighted by near-field Darcy flux at the source, versus the unweighted case where each source is given equal weight in the cumulative distribution, for the base case variant of the SITE-94 discrete-feature model of Äspö (Geier, 1996). As in the preceding figure, the results represent 47 deposition-hole locations that produced solute arrival to the geosphere/biosphere interface. Data for this plot are taken from an archived copy of CHC SITE 94 Data Delivery 3: Variational Cases, dated November 16, 1994, calculation case SKI0/NF0/BC0.

The impact of this effect on SE-SFL depends on how the calculated flow-related performance parameters were applied in radionuclide transport calculations used to calculate

dose for the safety evaluation. According to Table C-2 of Joyce et al. (2019), the delivered data give near-field flux as well as far-field performance parameters for the path traced by each particle.

Thus information was provided that could have been used for weighting according to the near-field mass release associated with each pathway. Evaluation of the radionuclide transport and dose calculations for SE-SFL is outside the scope of this review assignment. Therefore it is recommended that this issue should be checked by other reviewers who have examined the radionuclide transport and dose calculations.

5. Conclusions

Review findings regarding scientific quality are organized here in terms of the following main review topics:

- Suitability of models and data for the evaluation;
- Suitability of SKB's arguments on the basis of assumptions made and supporting data;
- Suitability of SKB's handling of uncertainties;
- Deficiencies in SKB's choice of methods, data, assumptions or handling of uncertainties; and
- Transparency of the documentation.

Finally, suggestions are given for review topics, focusing on issues that are most likely to affect repository performance

5.1 Suitability of models and data

The methods of hydrogeological analysis, cases considered, and level of scientific development of the models used in support of the SE-SFL evaluation are generally appropriate and reasonable for the current, preliminary stage of development of the SFL concept and its hypothetical application to the Laxemar site. Independent calculations using a simplified representative model indicate that the main results in terms of flow-related performance parameters are within reasonable bounds.

The discrete-fracture network (DFN) conceptual model is a reasonable framework, consistent with the current state-of-the-art for groundwater flow modeling in this geological setting. As such, it can be considered appropriate for this preliminary evaluation of the SFL concept, although alternative conceptual models such as sparse channel networks could need to be addressed in a license application.

An existing DFN statistical description has been used, developed from previous site investigations when Laxemar was considered as a candidate site for a spent-fuel repository. This description has been used without critical analysis of the site data or the how data uncertainties might propagate to the model for SE-SFL.

The method used to upscale from the DFN representation to effective continuum properties is scientifically credible but results in some loss of detail, particularly the possibility for discrete, extensive fractures or minor deformation zones to connect directly from major deformation zones to the waste vaults.

The particle-tracking method used to estimate distributions of far-field performance parameters introduces significant, non-conservative bias by failing to account for the probability that more solute will be carried by pathways that start with fractures carrying higher flows from the vaults. The high fraction of "stuck" particles raises further concerns about numerical accuracy of the method, although to some extent this might be explained by the problem with the source term.

The coupling of reactive hydrogeochemistry to flow in the catchment-focused model represents a new and potentially powerful development in possibilities for modeling coupled process in sites such as Laxemar with fractured crystalline bedrock. However little attention has been given to demonstrating that this novel approach produces accurate and reliable results. Comparisons with hydrogeochemical data from boreholes at Laxemar indicates discrepancies between the model and reality, regarding the transition from fresh to saline water at depths below 400 m. This discrepancy could have consequences for safety which are not adequately explored.

5.2 Suitability of SKB's arguments

The arguments in support of the safety evaluation are mostly reasonable, considering the preliminary stage of development of the concept. However, some exceptions are noted.

Future periglacial and glacial situations are assessed by means of a highly simplified approach that does not account for the realistic expectation that such situations will profoundly affect spatial patterns of groundwater flow (as well as flow magnitudes as considered). While the results may be conservative in the sense that longer discharge paths in periglacial/glacial climates would limit release, the biosphere objects selected may not be realistic.

The model used to calculate resaturation of the vaults is sensitive to assumptions regarding the depth of the rock unsaturated fringe around a vault. A more physically-based model of the bedrock/vault interface is likely needed to address the substantial uncertainties ahead of licensing.

5.3 Suitability of SKB's handling of uncertainties

Uncertainty resulting from the stochastic nature of bedrock fracturing has been explored with only five realizations of the DFN model, but these indicate that variable connections formed by discrete fractures, together with variability in the deformation zones, significantly affect the potential for retention in the geologic barrier.

Uncertainties related to future climate evolution are not assessed in the level of detail that should be expected for a license application. The carbon-emission scenario chosen for analysis of future warmer climates (RCP 4.5) may not be the most realistic given the current climate trajectory. Hydrogeological effects of more extreme climate changes, resulting from higher levels of carbon emissions, could include changes in precipitation and its seasonality and inter-annual variation, as well as ocean chemistry.

Full consideration of a future warmer climate may also require consideration of scenarios beyond the case of a domestic well for a single garden-plot household. Possibilities include larger communities dependent on well water for garden plots or larger-scale irrigation, as well as changing patterns of regional flow.

5.4 Deficiencies in SKB's analysis

In addition to topics mentioned above, deficiencies were noted in several other aspects of SKB's analysis.

The BHA and BHK vaults as designed require large excavations but methods of excavation and support for these openings are not specified. Practical measures for mechanical support during the operational period could affect groundwater chemistry as well as hydraulic properties at the interface between rock and backfill. Deterioration of any such measures will also need to be considered as part of the post-closure system evolution.

An excavation-disturbed zone (EDZ) around the vaults is discussed as part of the base case reference evolution rather than as part of the initial state. An EDZ should be expected to develop with any practical method of construction, but the possibility of enhanced flow around the vaults due to an EDZ has not been included in the hydrogeological analysis. Likewise consequences of fractures forming in the BHK backfill, potentially leading to enhanced flow to the waste compartment, have not been evaluated.

Colloid transport is acknowledged by SKB as a gap in the analysis that should be addressed in future safety evaluations for this concept. In connection with such an analysis, it is noted that changes in groundwater chemistry could be important, particularly changes in salinity around the BHA vault which could affect generation of colloids from the bentonite backfill.

5.5 Transparency of documentation

SKB's reporting follows a reasonably clear structure for presentation of the safety case and supporting hydrogeological analyses, but numerous issues of transparency, traceability and completeness of documentation were encountered, as listed in Section 3.2.

Some of these issues, such as incompleteness in the design specifications, are understandable giving that the design concept is still under development and some aspects would likely not be fully specified until after a candidate site has been selected.

The documentation of the hydrogeological models and analysis of results is cursory in places. Again, many of these types of deficiencies are understandable considering the preliminary stage of development, but improvement should be expected in future rounds.

Failure to present numerical, upscaled values of hydraulic conductivity and calculated flow fields has been a persistent issue in SKB's analysis, arising in work for the spent-fuel repository candidate sites at Laxemar and Forsmark, as well as for the SFR extension at Forsmark. This type of information is fundamental for review of predictions using complex models such as those employed here. Therefore SKB should be reminded to provide such information as part of future safety evaluations.

5.6 Suggested topics for further review

Validity of the equivalent flow concept for BHK

The validity of the equivalent flow concept, as applied the BHK vault, should be examined to determine if this leads to appropriate predictions of near-field release from a vault for which release occurs by advection as well as diffusion. This issue would best be addressed by an interdisciplinary investigation involving SSM's radionuclide transport modeling experts, in consultation with hydrogeological experts.

Bias in dose estimates resulting from particle-tracking source term

A significant source of bias from the source term used in SKB's particle tracking has been identified, and confirmed based on independent calculations. What remains is to check how this has affected the radionuclide transport calculations, and calculations of dose and risk. The main issue is whether the predicted distributions of near-field Darcy flux and far-field transport resistance (and related parameters) have been treated as independent for subsequent calculations, or if these have been treated as data "tuples" sampled in a non-parametric way from the particle-tracking output files. This is again primarily an issue for SSM's radionuclide transport modeling experts, with support from hydrogeological experts.

Influence of EDZ and/or discrete fractures in BHK backfill

The potential influence of an EDZ around the vaults, and/or through-going fractures in the BHK backfill, should be evaluated to see if realistic assumptions could seriously jeopardize (or enhance) the potential for the SFL concept to meet regulatory requirements. Scoping calculations using a simple representative model (as in Section 4.2) could help to bound the significance of these issues, and evaluate whether calculations with a more detailed, discrete model are warranted.

5.7 Topics relevant for upcoming site selection process for SFL

Role of sparsely fractured rock and bypass flow

Calculations with the simplified representative model (SRM) suggest that in some situations, higher hydraulic conductivity in the bedrock around the vaults could result in reduced rather than increased flows through the waste volume, and hence better performance. Conversely, tighter rock could focus flow through the repository and worsen performance. This is contrary to SKB's expectation that identifying a site with tighter rock at repository depth could help to meet regulatory criteria.

The results from the SRM may partly be an artifact of the homogenized idealization of the rock allowing bypass flow around the vaults. Whether this same effect could be relied on for a more heterogeneous, discrete representation is an open question. This question is relevant for site selection, as the answer could clarify whether tighter rock at depth should be a key hydrogeologic criterion, compared to other possible criteria such as finding sites or rock blocks with verifiably low hydraulic gradients.

References

Abarca, E., Sampietro, D., Molinero, J., and von Schenck, H., 2019. Modelling of the near-field hydrogeology – temperate climate conditions. Report for the safety evaluation SE-SFL. SKB R-19-03. https://www.skb.com/publication/2492401/R-19-03.pdf

Amec Foster Wheeler 2015. ConnectFlow version 11.2 (proprietary software)

Black, J.H., Woodman, N.D., and Barker, J.A., 2017. Groundwater flow into underground openings in fractured crystalline rocks: an interpretation based on long channels. *Hydrogeology Journal*. https://doi.org10.1007/s10040-016-1511-y

Bosson, E., Sassner, M., Gustafsson, L-G., 2009. Numerical modeling of surface hydrology and near-surface hydrogeology at Laxemar-Simpevarp. Site descriptive modeling SDM-Site Laxemar. SKB R-08-72, Svensk Kärnbränslehantering AB.

Charlton, S.R., and Parkhurst, D.L., 2011. Modules based on the geochemical model PHREEQC for use in scripting and programming languages. *Computers & Geosciences*, vol. 37, no. 10, p. 1653-1663. https://wwwbrr.cr.usgs.gov/projects/GWC_coupled/iphreeqc/

COMSOL, 2015. COMSOL Multiphysics, version 5.1. COMSOL AB, Stockholm.

Elfwing, M., Evins, L. Z., Gontier, M, Grahm, P., Mårtensson, P., and Tunbrant, S., 2013. SFL concept study, Main report. SKB TR 13-14, Svensk Kärnbränslehantering AB.

Geier, J. E., 1996. Discrete-feature modeling of the Äspö site. Prediction of hydrogeological parameters for performance assessment. SKI Report 96:7, Swedish Radiation Safety Authority, Stockholm.

Geier, J., 2017. Hydrogeological assessment and calculations: SFR-U. In SSM Report 2017:28, Swedish Radiation Safety Authority, Stockholm.

Geier, J., 2020. DFM code Version 2.5 User Documentation.

Geier, J.E., Lindgren, G.A., and Tsang, C-F., 2018. Simplified representative models for long-term flow and advective transport in fractured crystalline bedrock. *Hydrogeology Journal*, v. 27, n. 2, p. 595-614. https://doi.org/10.1007/s10040-018-1875-2.

Gimeno, M.J., Auqué L.F., Gómez, J.B., Salas, J., and Molinero, J., 2010. Hydrogeochemical evolution of the Laxemar Site. SKB R-10-60, Svensk Kärnbränslehantering AB.

Gimeno, M.J., Auqué, L.F., and Gómez, J.B., 2019. Hydrogeochemical conditions during periods with glacial and periglacial climate conditions. Report for the safety evaluation SE-SFL. SKB R-19-08, Svensk Kärnbränslehantering AB.

Grolander, S., and Jaeschke, B., 2019. Biosphere parameters used in radionuclide transport modeling and dose calculations in SE-SFL. SKB R-19-18, Svensk Kärnbränslehantering AB.

Hartikainen, J., Kouhia, R., and Wallroth, T., 2010. Permafrost simulations at Forsmark using a numerical 2D thermo-hydro-chemical model. SKB TR-09-17, Svensk Kärnbränslehantering AB.

Hoch, A.R. and Jackson, C.P., 2004. Rock-matrix diffusion in transport of salinity. Implementation in CONNECTFLOW. SKB R-04-78, Svensk Kärnbränslehantering AB.

Hartley, L. and Joyce, S., 2013. Approaches and algorithms for groundwater flow modeling in support of site investigations and safety assessment of the Forsmark site, Sweden. Journal of Hydrology, 500, 200–216, https://doi.org/10.1016/j.jhydrol.2013.07.031.

Hjerne, C., Nordqvist, R., and Harrström, J., 2010. Compilation and analyses of results from cross-hole tracer tests with conservative tracers. SKB R-09-28, Svensk Kärnbränslehantering AB.

Hökmark, H., Lönnqvist, M., and Fälth, B., 2010. THM-issues in repository rock. Thermal, mechanical, thermo-mechanical and hydro-mechanical evolution of the rock at the Forsmark and Laxemar sites. SKB TR-10-23, Svensk Kärnbränslehantering AB.

Idiart, A., Laviña, M., and Coene, E., 2019. Modelling of concrete degradation – Hydro-chemo-mechanical processes. Report for the safety evaluation SE-SFL. SKB R-19-12, Svensk Kärnbränslehantering AB.

IPCC, 2014: Climate Change 2014. Synthesis Report. Contribution of Working Groups I, II and III to the Fifth Assessment Report of the Intergovernmental Panel on Climate Change [Core Writing Team, R.K. Pachauri and L.A. Meyer (eds.)]. IPCC, Geneva, Switzerland, 151 pp.

Jackson, C.P., Hoch, A.R., and Todman, S., 2000. Self-consistency of a heterogeneous continuum porous medium representation of a fractured medium. *Water Resources Research* v. 36, p. 189–202.

Joyce, S., Simpson, T., Hartley, L., Applegate, D., Hoek, J., Jackson, P., Roberts, D., Swan, D., Gylling, B., Marsic, N., Rhén, I., 2010. Groundwater flow modeling of periods with temperate climate conditions: Laxemar. SKB R-09-24, Svensk Kärnbränslehantering AB.

Joyce, S., Appleyard, P., Hartley, L., Tsitsopoulos, V., Woolard, H., Marsic, N., Sidborn, M., and Crawford, J., 2019. Groundwater flow and reactive transport modeling of temperate conditions. Report for the safety evaluation SE-SFL. SKB R-19-02. Svensk Kärnbränslehantering AB. https://www.skb.se/publikation/2492390/R-19-02.pdf

Laaksoharju, M., Skårman, and Skårman, E., 1999. Multivariate mixing and mass balance (M3) calculations, a new tool for decoding hydrogeochemical information. *Applied Geochemistry*, v. 14, n. 7, p. 861-871. https://www.sciencedirect.com/science/article/abs/pii/S0883292799000244

Laaksoharju, M., Smellie, J., Tullborg, E-L., Wallin, B., Drake, H., Gimeno, M., Hallbeck, L., Molinero, J., and Waber, N., 2009. Bedrock hydrogeochemistry Laxemar, Site descriptive modeling SDM-Site Laxemar, SKB R-08-93, Svensk Kärnbränslehantering AB.

Lund, B., Schmidt, P., and Hieronymus, C., 2009. Stress evolution and fault stability during the Weichselian glacial cycle. SKB TR-09-15, Svensk Kärnbränslehantering AB.

Maxwell, R. M., Condon, L.E., Kollet,, S.J., Maher, K., Haggerty, R., and Forrester, M. M., 2016. The imprint of climate and geology on the residence times of groundwater. *Geophysical Research Letters* v. 43, p. 701-708, doi:10.1002/2015GL066916.

McIntosh, J.C., Garven, G., and Hanor, J.S., 2011. Impacts of Pleistocene glaciation on large scale groundwater flow and salinity in the Michigan Basin. *Geofluids* v. 11, no. 1, p. 18-33.

Neretnieks, I., 1980. Transport mechanisms and rates of transport of radionuclides in the geosphere as related to the Swedish KBS concept. *In* Symposium on the underground disposal of radioactive wastes, Otaniemi, Finland; 2–6 Jul 1979. *Proc. Int. Atomic Energy Agency* IAEA–SM–243/108, v. 2 p. 315-338. International Atomic Energy Agency, Vienna, Austria.

Oda, M., 1985. Permeability tensor for discontinuous rock masses. *Géotechnique* v. 35 n. 4, p. 483-495. doi: 10.1680/geot.1985.35.4.483.

Person, M., McIntosh, J., Bense, V., and Remenda, V. H., 2007. Pleistocene hydrology of North America: The role of ice sheets in reorganizing groundwater flow systems. *Reviews of Geophysics*, v. 45, no. 3.

Persson, G., Asp, M., Berggreen-Clausen, S., Berglöv, G., Björck, E., Axén Mårtensson, J., Nylén, L., Ohlsson, A., Persson, H., and Sjökvist, E., 2015. Framtidsklimat i Kalmar län − enligt RCP-scenarier. Norrköping: SMHI. *Klimatologi* v. 26.

Rhén, I. and Hartley, L., 2009. Bedrock hydrogeology Laxemar. Site descriptive modeling SDM-Site Laxemar. SKB R-08-92. Svensk Kärnbränslehantering AB.

Rhén I, Forsmark T, Hartley L, Jackson C P, Roberts D, Swan D, Gylling B, 2008. Hydrogeological conceptualisation and parameterisation. Site descriptive modeling, SDM-Site Laxemar. SKB R-08-78, Svensk Kärnbränslehantering AB.

Shahkarami P, 2019. Input data report for near-field and geosphere radionuclide transport modeling in the safety evaluation SE-SFL. SKB R-19-09, Svensk Kärnbränslehantering AB.

SKB, 2006a. Long-term safety for KBS-3 repositories at Forsmark and Laxemar – a first evaluation. Main report of the SR-Can project. SKB TR-06-09, Svensk Kärnbränslehantering AB.

SKB, 2006b. Climate and climate-related issues for the safety assessment SR-Can. SKB TR-06-23, Svensk Kärnbränslehantering AB.

SKB, 2009. Site description of Laxemar at completion of the site investigation phase. SDM-Site Laxemar, SKB TR-09-01. Svensk Kärnbränslehantering AB

SKB, 2019a. Post-closure safety for a proposed repository concept for SFL. Main report for the safety evaluation SE-SFL. Updated 2020-02. SKB TR-19-01. Svensk Kärnbränslehantering AB.

SKB, 2019b. Initial state for the repository for the safety evaluation SE-SFL. SKB TR-19-03. Svensk Kärnbränslehantering AB.

SKB, 2019c. Climate and climate-related issues for the safety evaluation SE-SFL. SKB TR-19-04, Svensk Kärnbränslehantering AB.

SKB, 2019d. Radionuclide transport and dose calculations for the safety evaluation SE-SFL. SKB TR-19-06, Svensk Kärnbränslehantering AB.

SKI, 1996. SKI SITE-94 Deep repository performance assessment project. SKI report 96:36, SSM, Stockholm.

Snow, D. T., 1969. Anisotropic permeability of fractured media, *Water Resour. Res.*, v. 5, p. 1273–1289.

SSM, 2008. The Swedish Radiation Safety Authority's regulations concerning safety in connection with the disposal of nuclear material and nuclear waste. SSMFS 2008:21, Swedish Radiation Safety Authority, Stockholm.

van Genuchten M, 1980. A closed form equation for predicting the hydraulic conductivity of unsaturated soils. *Soil Science Society of America Journal* v. 44, p. 892–898. https://doi.org/10.2136/sssaj1980.03615995004400050002x

Vidstrand P, Rhén I, Zugec N, 2010. Groundwater flow modeling of periods with periglacial and glacial climate conditions – Laxemar. SKB R-09-25, Svensk Kärnbränslehantering AB.

Vidstrand, P., Follin, S., Selroos, JO. et al., 2014. Groundwater flow modeling of periods with periglacial and glacial climate conditions for the safety assessment of the proposed high-level nuclear waste repository site at Forsmark, Sweden. *Hydrogeology Journal* v. 22, p. 1251–1267. https://doi.org/10.1007/s10040-014-1164-7

Wahlgren, C-H., Curtis, P., Hermanson, J., Forssberg, O., Öhman, J., Fox, A., La Pointe, P., Drake, H., Triumf, C-A., Mattsson, H., Thunehed, H., and Juhlin, C., 2008. Geology Laxemar. Site descriptive modeling, SDM-Site Laxemar. SKB R-08-54, Svensk Kärnbränslehantering AB.

Coverage of SKB reports

The following reports have been covered in the review.

Table A1:1

Reviewed report	Reviewed sections	Comments
TR-19-01 Post-closure safety for a proposed repository concept for SFL	Chapters 4, 6, 7, and 8	Remaining chapters also considered for background and context.
R-19-02 Groundwater flow and reactive transport modeling of temperate conditions	All	
R-19-03 Modelling of the near-field hydrogeology – temperate climate conditions	All	
TR-19-03 Initial state for the repository for safety evaluation SE-SFL	Chapters 5 & 6	Checked for additional information on details of BHK and BHA vault construction and backfilling but little additional information was found.
TR-19-04 Climate and climate-related issues for the safety evaluation SE-SFL.		Selective reading focused on identification of scenarios
TR-19-06 Radionuclide transport	Appendix C	
R-19-18 Biosphere		Background on irrigation analysis

Appendix A2: Discrete-Feature Modeling Procedures

This digital appendix documents the discrete-feature modeling procedures that were used to produce upscaled estimates of hydraulic conductivity tensors based on the DFN statistical models used by Joyce et al. (2019).

Software versions

All modeling was carried out on an Hewlett-Packard Pavilion workstation running:

Linux (Ubuntu version 18.04.5 LTS, "Bionic Beaver").

Procedures were automated using scripts written in the Berkeley UNIX C shell (csh) scripting language, and were executed using the following C shell variant:

tcsh 6.20.00 (Astron) 2016-11-24

Linux core utilities (head, tail etc.) used within these scripts were from the following version:

GNU coreutils 8.28 (http://www.gnu.org/software/coreutils/)

Scripts in the *awk* programming language were executed with the following version of the Awk interpreter:

GNU Awk 4.1.4, API: 1.1 (GNU MPFR 4.0.1, GNU MP 6.1.2)

Discrete-fracture simulations and upscaling calculations were performed using *fracgen* module of the *dfm* software (Geier, 2020). The following version of this module was used:

fracgen version 2.4.2c

Fracture set definitions

Statistical properties of the fracture sets in each of the four specified depth zones DZ1 through DZ4, within each of the four fracture domains HRD_C, HRD_EW007, HRD_N, and HRD_W, are specified in the sixteen files in the subdirectory FractureSets, with names corresponding to the fracture domain and depth zone:

FractureSets/SFL-LX-HRDC-DZ1.sets
FractureSets/SFL-LX-HRDC-DZ2.sets
...
FractureSets/SFL-LX-HRDW-DZ4.sets

Grid setup

Effective hydraulic conductivity tensors were calculated for a cube-shaped blocks on scales of 50 m and 100 m, in an arbitrary 3000 m x 3000 m × 1000 m deep domain. Grids for calculations on both of these scales were generated using the *awk* script:

create_grid.awk

For the 50 m block scale, 3600 blocks were simulated in each of 20 layers. The grid for these calculations was calculated using using the tcsh command:

awk -f create_grid.awk -v D=50 > sflk50.grid

For the 100 m block scale, 900 blocks were simulated for each of 10 layers in the same domain. The grid for these calculations was calculated using the tcsh command:

awk -f create_grid.awk -v D=100 > sflk100.grid

Fracture simulations and calculation of upscaled K tensors

For each block scale (50 m and 100 m), a stochastic realization of each fracture domain (HRD_C, HRD_EW007, HRD_N, and HRD_W) was produced and upscaled to produce block-scale estimates of the K tensors by use of the csh script:

tksfl

In each case, this was executed using a csh command of the form:

tksfl *domain scale seed*

where:

domain = HRD_C, HRD_EW007, HRD_N, or HRD_W
scale = 50 or 100
seed = 1 (the seed value for the pseudo-random number generator)

Additional realizations could be generated by using different values for *seed*, but this was judged to be unnecessary based on the assumption of ergodicity (i.e., the chosen domain was large enough to represent the stochastic variability with respect to these block scales).

Each run of the tksfl script produces two output files. For example, for HRD_C and a 50 m block scale, the output files are:

SFL-LX-HRDC_50m1.dfmo
SFL-LX-HRDC_50m1_K.csv

These files are not included in this digital appendix due to their large size, but have been retained for quality assurance purposes.

Extraction of statistics

Statistics for the K tensor components and anisotropy measures for each layer of blocks (i.e., for a given block depth) were calculated using the awk scripts:

kstatistics.awk
kanisotropy.awk

for the output from each run of the tksfl script. For example, for HRD_C and a 50 m block scale, statistics were calculated with the commands:

awk -f kstatistics.awk SFL-LX-HRDC_50m1_K.csv . SFL-LX-HRDC_50m1_K_stats.csv

awk -f kanisotropy.awk SFL-LX-HRDC_50m1_K.csv . SFL-LX-HRDC_50m1_K_iso.csv

The resulting *stats.csv and *iso.csv files are included in the files in this digital appendix. Note that the latter script to produce *iso.csv files was used only for the case of a 50 m block scale.

Full list of files included in digital archive

The following is a full listing of the files in the digital archive for this appendix:

SSM-SE-SFL Hydrogeology Appendix A2.docx (this document)
tksfl
create_grid.awk
kstatistics.awk
kanisotropy.awk
FractureSets/SFL-LX-HRDC-DZ1.sets
FractureSets/SFL-LX-HRDC-DZ2.sets
FractureSets/SFL-LX-HRDC-DZ3.sets
FractureSets/SFL-LX-HRDC-DZ4.sets
FractureSets/SFL-LX-HRDEW007-DZ1.sets
FractureSets/SFL-LX-HRDEW007-DZ2.sets
FractureSets/SFL-LX-HRDEW007-DZ3.sets
FractureSets/SFL-LX-HRDEW007-DZ4.sets
FractureSets/SFL-LX-HRDN-DZ1.sets
FractureSets/SFL-LX-HRDN-DZ2.sets
FractureSets/SFL-LX-HRDN-DZ3.sets
FractureSets/SFL-LX-HRDN-DZ4.sets
FractureSets/SFL-LX-HRDW-DZ1.sets

FractureSets/SFL-LX-HRDW-DZ2.sets
FractureSets/SFL-LX-HRDW-DZ3.sets
FractureSets/SFL-LX-HRDW-DZ4.sets
SFL-LX-HRDC_100m1_K_stats.csv
SFL-LX-HRDC_50m1_K_iso.csv
SFL-LX-HRDC_50m1_K_stats.csv
SFL-LX-HRDEW007_100m1_K_stats.csv
SFL-LX-HRDEW007_50m1_K_iso.csv
SFL-LX-HRDEW007_50m1_K_stats.csv
SFL-LX-HRDN_100m1_K_stats.csv
SFL-LX-HRDN_50m1_K_iso.csv
SFL-LX-HRDN_50m1_K_stats.csv
SFL-LX-HRDW_100m1_K_stats.csv
SFL-LX-HRDW_50m1_K_iso.csv
SFL-LX-HRDW_50m1_K_stats.csv

Appendix A3: Simple Representative Model for SFL

This digital appendix documents the simple representative model (SRM) modeling procedures that were used to produce independent estimates of hydrology-related performance parameters for a hypothetical SFL located at Laxemar.

Software versions

All modeling was carried out on an Hewlett-Packard Pavilion workstation running:

Linux (Ubuntu version 18.04.5 LTS, "Bionic Beaver").

Procedures were automated using scripts written in the Berkeley UNIX C shell (csh) scripting language, and were executed using the following C shell variant:

tcsh 6.20.00 (Astron) 2016-11-24

Linux core utilities (head, tail etc.) used within these scripts were from the following version:

GNU coreutils 8.28 (http://www.gnu.org/software/coreutils/)

Scripts in the *awk* programming language were executed with the following version of the Awk interpreter:

GNU Awk 4.1.4, API: 1.1 (GNU MPFR 4.0.1, GNU MP 6.1.2)

Main command-line scripts

The calculations for the base case with horizontal (longitudinal) flow through the vaults are carried out with the following script:

run_base_case

This is executed by the csh command:

run_base_case *seed*

to just calculate flows, or

run_base_case tps *seed*

to also calculate flow-related performance parameters. Different values of the *seed* value for the pseudo-random number generator can be specified (this does not affect the base-case flows which are fully deterministic, but will affect travel-time values calculated with the stochastic aperture model).

Calculations for the case of vertical flow are carried out with the following script:

run_base_case_vertical

Calculations for the cases of alternative discharge zones ZSMEW007A and ZSMNW042A are carried out with:

run_altdisch07

run_altdisch42

and the case of an alternative regolith with:

run_altreg_case

The two minor deformation zone alternatives are carried out with:

run_PDZr_case

run_PDZs_case

All of the above scripts have command-line syntax identical to that for run_base_case.

For the case where rock-mass hydraulic conductivities are sampled from K values calculated by *dfm* upscaling of the DFN model, the script used is:

run_permeameter_case

which is invoked with the command

run_permeameter_case *case seed* tps

with *case* = HRD_C, HRD_EW007, HRD_N, or HRD_W. In order to run this script and process the results for multiple realizations, the script:

run_and_process_permeameter_case_tps *case N*

is used with *N* being the desired number of realizations (i.e. separate runs with different values of *seed* = 1, 2, …, *N*).

Main awk-language scripts

The following scripts perform the overall calculations for the SRM:

SFL_full_system.awk
SFL_parameter_estimation.awk
calc_transport_parameters.awk

The default parameters are specified in:

default_parameters.awk

The following script (invoked by run_and_process_permeameter_case_tps) is used for post-processing results of the permeameter case to produce statistical summaries and probability density functions for the flow-related transport parameters:

extract_pdfs_tps.awk

Basic mathematical functions used in the calculations are carried out by the following scripts in the subdirectory Basic:

Basic/equivalent_conductance.awk
Basic/geometry.awk
Basic/power.awk
Basic/rgasdev.awk (used to generate random Gaussian deviates)

The simple representative models of the BHA and BHK vaults are implemented in:

Vaults/SFL_vaults.awk

Transport-apertures models and calculations of flow-related transport parameters are implemented in:

Trans/aperture_models.awk
Trans/parest_math.awk

Geological system parameters

Properties of the hydraulic conductor domains (HCDs) and regolith layers are specified in:

Geosystem/hcds.awk
Geosystem/regolith.awk

Default properties for the geological parts of the flow system are specified in:

Geosystem/geosystem_default.awk

Properties for particular parts of the system are then modified depending from the default values, depending on the calculation case. For the base case these are set by:

Geosystem/geosystem_basecase.awk

The cases of alternative discharge zones ZSMEW007A and ZSMNW042A are implemented with:

Geosystem/geosystem_altdisch07.awk
Geosystem/geosystem_altdisch42.awk

The case of an alternative regolith is implemented with:

Geosystem/geosystem_altreg.awk

The two minor deformation zone alternatives are implemented with:

Geosystem/geosystem_PDZr.awk
Geosystem/geosystem_PDZs.awk

Rock mass hydraulic conductivity

Hydraulic conductivity of the rock mass for the base case (and most alternative cases) is set by the following script:

RM/K_rock_mass_basecase.awk

For the two minor deformation zone variants, the following script is invoked:

RM/T_PDZ.awk

This links to the following scripts:

RM/PDZ_Ts.awk
RM/sample_PDZ_Ts_LX.awk

which give data for the transmissivity values of known PDZs and methods for sampling from these, respectively.

For the permeameter variants, K values are sampled by one of the following scripts depending on the rock domain:

RM/K_rock_mass_sample_permeameter_DZ3_C.awk
RM/K_rock_mass_sample_permeameter_DZ3_EW007.awk
RM/K_rock_mass_sample_permeameter_DZ3_N.awk
RM/K_rock_mass_sample_permeameter_DZ3_W.awk

which link to the script:

RM/sample_permeameter_Ks.awk

as well as the K data in the respective files:

RM/permeameter_Ks_DZ3_C.awk
RM/permeameter_Ks_DZ3_EW007.awk
RM/permeameter_Ks_DZ3_N.awk
RM/permeameter_Ks_DZ3_W.awk

which were parsed from the DFM model output using:

RM/parse_permeameter_Ks.awk

Full list of files included in digital archive

The following is a full listing of the files in the digital archive for this appendix:

SSM-SE-SFL Hydrogeology Appendix A3.docx (this document)
run_base_case
run_base_case_vertical
run_altdisch07
run_altdisch42
run_altreg_case
run_PDZr_case
run_PDZs_case
run_permeameter_case
run_and_process_permeameter_case_tps
SFL_full_system.awk
SFL_parameter_estimation.awk
calc_transport_parameters.awk
default_parameters.awk
extract_pdfs_tps.awk

Basic/equivalent_conductance.awk
Basic/geometry.awk
Basic/power.awk
Basic/rgasdev.awk

Geosystem/hcds.awk
Geosystem/regolith.awk
Geosystem/geosystem_altdisch07.awk
Geosystem/geosystem_altdisch42.awk
Geosystem/geosystem_altreg.awk
Geosystem/geosystem_basecase.awk

Geosystem/geosystem_default.awk
Geosystem/geosystem_PDZr.awk
Geosystem/geosystem_PDZs.awk

RM/K_rock_mass_basecase.awk
RM/K_rock_mass_sample_permeameter_DZ3_C.awk
RM/K_rock_mass_sample_permeameter_DZ3_EW007.awk
RM/K_rock_mass_sample_permeameter_DZ3_N.awk
RM/K_rock_mass_sample_permeameter_DZ3_W.awk
RM/parse_permeameter_Ks.awk
RM/PDZ_Ts.awk
RM/permeameter_Ks_DZ3_C.awk
RM/permeameter_Ks_DZ3_EW007.awk
RM/permeameter_Ks_DZ3_N.awk
RM/permeameter_Ks_DZ3_W.awk
RM/sample_PDZ_Ts_LX.awk
RM/sample_permeameter_Ks.awk
RM/T_PDZ.awk

Trans/aperture_models.awk
Trans/parest_math.awk

Vaults/SFL_vaults.awk

Strål
säkerhets
myndigheten
Swedish Radiation Safety Authority

Authors: Richard Metcalfe, James Wilson and Steven Benbow
Quintessa Limited, Henley on Thames, UK

2021:13

2) Review of SE-SFL – Concrete degradation

Date: May 2021
Report number: 2021:13 **ISSN:** 2000-0456
Available at www.stralsakerhetsmyndigheten.se

Authors: Richard Metcalfe[1)], James Wilson[1)] and Steven Benbow[1)]
[1)]Quintessa Limited, Henley on Thames, UK

2) Review of SE-SFL – Concrete degradation

Activity number: 3034111-03
Registration number: SSSM2020-3833
Contact person at SSM: Henrik Öberg

Content

1. Introduction

1.1. Background

The Swedish Nuclear Fuel and Waste Management Company (SKB) is developing plans for a deep geological repository for long-lived low- and intermediate level radioactive waste, the SFL. It is proposed that this repository will be constructed in Swedish crystalline rock at a depth around 500 m.

The waste planned for disposal in the SFL contains mainly the long-lived wastes from the operation and decommissioning of the Swedish nuclear reactor plants, and long-lived wastes from early research in the Swedish nuclear program (legacy wastes), from medicine, industry and research including the European Spallation Source (ESS) research facility. The disposal concept for the SFL repository has been developed by SKB since the 1980s. A pre-study of the concept was undertaken (SKB TR-95-03) and a preliminary safety analysis (SKB TR-99-28) has been published.

Recently SKB has published a safety evaluation of the SFL repository (SE-SFL, SKB TR-19-01). This evaluation is part of the continuing disposal concept development. The SE-SFL focusses on a few sections of the Swedish radiation safety authority's (SSM) regulations on post-closure safety, the risk criterion, and requirements for post-closure barrier robustness. No site has been chosen for SFL and the inventory of radionuclides is only a first estimate. Based on the proposed repository concept and example site data (from SKB's site investigation program) from Laxemar, Oskarshamn municipality, the SE-SFL presents an analysis of an initial state and a reference evolution. Three reference external evolutions (present-day conditions, increased greenhouse effect and simplified glacial cycle) represent possible climate conditions and evolutions. For SE-SFL a catalogue of features, events, and processes (FEP) has been established.

Stated aims of the SE-SFL (Executive Summary of the main evaluation report, TR-19-01) are to:

- provide input to the subsequent steps in the development of SFL, including further development of the design of the engineered barriers and the site-selection process for SFL;
- evaluate conditions in the waste, barriers, and the repository environs under which the repository concept has the potential to fulfil the regulatory requirements for post-closure safety; and
- provide SKB with a basis to prioritise areas in which the level of knowledge and adequacy of methods must be improved to perform a subsequent, full safety assessment for SFL.

1.2. Purpose of this Document

This document describes a review of parts of the SE-SFL safety evaluation and presents findings of the review. The review was undertaken by Quintessa under contract to SSM, as part of SSM's regulatory oversight of SKB's planning for the SFL.

The review concerns the description of concrete degradation in the SE-SFL and focusses on the function and long-term evolution of the concrete barrier in the context of the concept performance. Included in the review are:

- an assessment of whether the models and modelling methodology employed to describe the evolution of chemical properties of the concrete are appropriate and sufficient for their purpose.
- consideration of the impact of the natural hydrogeological and hydrochemical conditions (based on example site data) on chemical concrete degradation;
- an evaluation of the parameters (hydraulic, mechanical and chemical) chosen for the performance calculations in the safety evaluation based on the modelling of concrete degradation;
- an evaluation of how interactions with other barriers (bentonite) might impact the degradation of cement; and
- a comparative discussion of SKB's methodology for treating concrete barrier degradation in the safety assessment SR-PSU.

1.3. Reviewed Reports

The following SKB reports were reviewed:

- SKB TR-19-01, SKB, 2019. Post-closure safety for a proposed repository concept for SFL. Svensk Kärnbränslehantering AB.
- SKB TR-19-03, SKB, 2019. Initial state for the repository for the safety evaluation SE-SFL. Svensk Kärnbränslehantering AB.
- SKB R-19-11, Idiart A, Shafei B, 2019. Modelling of concrete degradation – Hydro-chemical processes. Report for the safety evaluation SE-SFL. Svensk Kärnbränslehantering AB.
- SKB R-19-12, Idiart A, Laviña M, Coene E, 2019. Modelling of concrete degradation – Hydro-chemo-mechanical processes. Report for the safety evaluation SE-SFL. Svensk Kärnbränslehantering AB.
- SKB R-19-13, Idiart A, Laviña M, 2019. Modelling of concrete degradation in a one-million year perspective– Hydro-chemical processes. Report for the safety evaluation SE-SFL. Svensk Kärnbränslehantering AB.
- SKB R-19-14, Idiart A, Olmeda J, Laviña M, 2019. Modelling of concrete degradation – influence of concrete mix design. Report for the safety evaluation SE-SFL. Svensk Kärnbränslehantering AB.
- SKB R-19-15, Reactive transport modelling of montmorillonite dissolution - Report for the safe-ty evaluation SE-SFL. Svensk Kärnbränslehantering AB.
- SKB TR-14-01. Safety analysis for SFR. Long-term safety. Main report for the safety assessment SR-PSU. Revised edition. Svensk Kärnbränslehantering AB.
- SKB TR-19-02. FEP report for the safety evaluation SE-SFL. Svensk Kärnbränslehantering AB.
- SKB R-19-02, Joyce S, Appleyard P, Hartley L, Tsitsopoulos V, Woollard H, Marsic N, Sidborn M, Crawford J, 2019. Groundwater flow and reactive transport modelling of temperate conditions. Report for the safety evaluation SE-SFL. Svensk Kärnbränslehantering AB.
- SKB R-19-09, Shahkarami P, 2019. Input data report for the near-field and geosphere radionuclide transport modelling. Report for the safety evaluation SE-SFL. Svensk Kärnbränslehantering AB.

1.4. Approach

The review was conducted by means of both “top-down” and “bottom-up” approaches. The first approach began with the main review report (TR-19-01) and worked down from SKB’s stated overall objectives to the models of cement / concrete evolution that have been developed to meet these objectives. The second approach began at SKB’s detailed models of cement / concrete evolution and worked up to the high-level objectives. In this way the aim was to avoid missing any important issues.

Initially the review covered only SKB’s treatment of cement / concrete evolution. However, it became apparent that, for the BHA vaults, there is an overlap between modelling of cementitious materials and modelling of bentonite evolution, namely modelling of cement / concrete – bentonite interactions. Hence, after discussion with SSM, the review was broadened to consider these aspects.

Section 2 to Section 6 present outcomes from the “top down” approach, while Section 7 presents outcomes from the “bottom up” approach. Section 9 gives the conclusions from the review.

2. SFL Disposal Concept

2.1. Overview of the Concept

The repository design considered by the SE-SFL, and described in TR-19-11 and the other reports, consists of two parts:

- a waste vault with bentonite clay backfill for the legacy waste, which is about170 m long and has a cross-sectional area of about 20 m x 20 m (BHA); and
- a waste vault with concrete backfill for the reactor internals, which is about 135 m long and has a cross-section of about 20 m x 20 m (BHK).

The concept is shown in Figure 1.

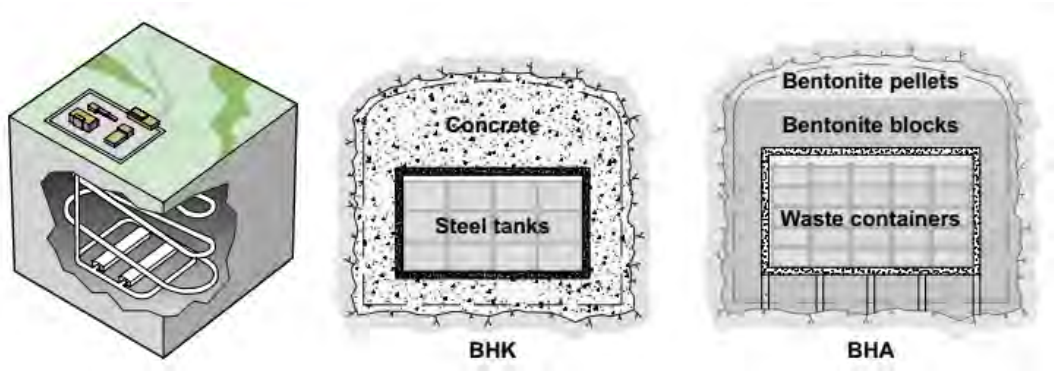

Figure 1: Preliminary facility layout and the proposed repository concept for SFL (left), with one waste vault for metallic waste from the nuclear power plants (BHK, centre) and one waste vault for waste from Studsvik Nuclear AB, Cyclife Sweden AB, and AB SVAFO (BHA, right). After SKB TR-19-01.

The main engineered barriers in BHA are:

- void-filling grouts within and between waste packages;
- a 0.5 m thick reinforced concrete structure surrounding the wastes;
- bentonite blocks between the outside of the concrete structure and the rock walls of the vault, varying from 2.3 m at the bottom, to 2.4 m on the sides and to 4 m at the top of the vault; and
- bentonite pellets, filling the 3.7 m of remaining void at the top of the vault.

The main engineered barrier in BHK are:

- void-filling grout within and between waste packages;
- a 0.5 m thick reinforced concrete structure surrounding the wastes; and
- a concrete backfill of the vault outside the reinforced concrete structure, varying in thickness from 2.4 m at the bottom, to 2.8 m on the sides, and to 8.8 m on the top of the vault.

The inventories in the BHA and BHK vaults are different. There is much more uncertainty over the inventory for BHA than for the inventory for BHK. The total radionuclide

inventory in the legacy waste in BHA is estimated to be about 4×10^{15} Bq at the time of repository closure and will be dominated by the very long-lived radionuclides Tc-99 and Cl-36. One million years after closure the radioactivity of the waste will be about 2 % of the initial radioactivity.

In contrast, the total radionuclide inventory in the BHK vault at closure is estimated to be two orders of magnitude greater than in BHA, about 2×10^{17} Bq, that is 98 % of the total radioactivity in SFL at closure. The inventory at repository closure is dominated by the relatively short-lived radionuclides Ni-63 and Co-60 and one thousand years after closure only about 1 % of the initial radioactivity remains.

2.2. Clarity of Concept Explanation

The concept seems reasonable, based on its stated goals (in TR-19-01 and elsewhere), and based on barrier systems proposed for or used in repositories elsewhere, both in Sweden (SFR) and in other countries (e.g. VLJ, in Finland). The differences in the waste inventories are reflected in the different barrier systems for the vaults. However, the documentation would benefit from a clear statement of the rationale for the different barrier designs. There is also no clear explanation of how these designs were developed; such a statement would be helpful. It would be helpful to give the reader some indication why the particular geometry was selected (as opposed to, say, a silo geometry).

The terminology regarding cementitious components of the barrier system would also benefit from refinement. “Concrete” is used to describe grout, the reinforced concrete structures surrounding the waste, and, in the case of the BHK vault, the backfill around this concrete structure. It is suggested that “vault wall” could be used to describe the reinforced concrete structure more succinctly. “Grout” and “Concrete Backfill” could then be used without ambiguity as to which part of the repository is being referred to.

3. Overall Evaluation Methodology

The overall evaluation methodology is based on the safety assessment methodologies developed by SKB for the proposed SF repository and the SFL repository at Forsmark. The methodology is summarised in Figure 2.

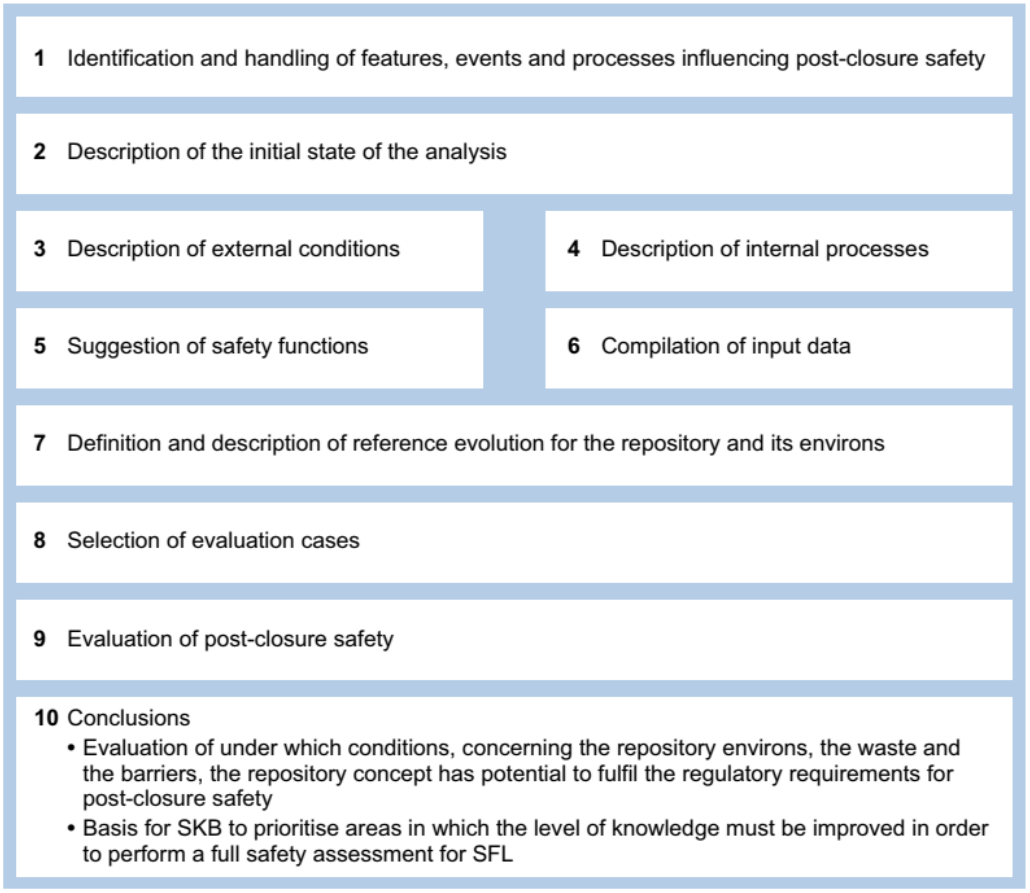

Figure 2: Overview of the methodology applied for the evaluation of post-closure safety for the proposed repository concept for SFL. After SKB Report TR-19-01.

However, the SE-SFL is simplified compared to the full safety assessments for the spent fuel (SF) repository and the SFR. These differences are described in Section 2.1 of TR-19-01, while the adaptation of the methodology for SE-SFL is described in Section 2.5 of TR-19-01. Given the generic nature of the SE-SFL these differences from the earlier full safety assessments are justified.

Of particular relevance to the present review of SKB's treatment of cementitious barrier degradation is the following statement (1st paragraph on page 35 of TR-19-01):

"*A central requirement in SSMFS 2008:21 is Section 5 that relates to barrier robustness which states that the barrier system shall be able to withstand such features, events and processes that can affect the post-closure performance of the barriers.*"

Accordingly, SKB states that a comprehensive FEP analysis is needed to evaluate if the repository barrier system can withstand future features, events, and processes (FEPs) that can affect the post-closure performance (2nd paragraph of page 35 of TR-19-11). SE-SFL

included a FEP analysis and description of the repository evolution based on the identified FEPs. The evaluation of under what conditions the repository concept has the potential to fulfil the requirements of barrier system robustness is then discussed based on the analysed evolution of the barrier system. SKB recognise, however, that some FEPs have not been considered in SE-SFL (especially FEPs related to mechanics that are deemed too site-specific to evaluate; see Section 4 below) and that there are limitations that will need to be considered in future safety analysis work.

Safety functions are stated to be (TR-19-01, page 14, first paragraph):

"*For the waste domains of BHA and BHK, the safety function is good retention, as determined by pH, redox potential, concentration of complexing agents in BHA, available sorption surface area, and the corrosion rate in BHK. For the bentonite barrier of BHA and the concrete barrier in BHK the safety functions defined are low flow in the waste vault and good retention. For the closure components and the natural bedrock barrier the safety functions are low flow*."

In SKB's safety assessment methodology, as applied to the SF and SFR repositories, safety functions are used as a basis for defining scenarios. However, in SE-SFL this was not done as there is no scenario analysis. Instead, broader "evaluation cases" are defined in place of scenarios for SE-SFL. These consist of:

- a "base case" that is a simplified, stylised representation of the repository and that assumes present environmental conditions continue throughout the assessment period; and
- a set of additional evaluation cases that evaluate the sensitivity of the released activity and consequent doses to assumptions made regarding conditions in the repository and the repository environs, chosen to illustrate conditions which are likely to improve repository performance compared to the base case, including:
  - cases with lower groundwater flow rate than at the example location; and
  - cases with alternative concrete backfill are included.

In SE-SFL the chosen future climate developments are simplified and limited in number compared with those that would be adopted in a full safety assessment, such as the SR-Site assessment for the SF repository. Three evolutionary variants are analysed:

- a variant in which the present-day climate continues throughout the analysis period of 1 million years;
- a variant in which anthropogenic global warming affects the future climate, such that the next 50000 years have an initially warmer and wetter climate than at present, followed by present-day temperature conditions; and
- a variant with simplified climatic variation according to cycles of glaciation and deglaciation, based on the overall climate development in the reconstruction of the last glacial cycle at a Swedish Baltic coastal site, in which there was early permafrost development, followed by an ice-sheet advancing over the repository site, and subsequently submerged conditions.

This third variant includes, within each cycle of glaciation and deglaciation, periods of temperate climate, periglacial conditions with permafrost, ice-sheet development, and variations in shore-level. It is assumed that the SFL is sufficiently deep that no permafrost

will reach the depth of the waste vaults. SKB recognises that the validity of this assumption will require checking at any site chosen for the SFL in future.

In summary, the general methodology is appropriate and well structured. However, the analysis does not consider all environmental FEPs that could affect cement / concrete evolution; there is no analysis of mechanical processes external to the repository. Additionally, the range of analysis cases is too small to fully establish that the cement / concrete components of the barrier system would be robust in the face of all external FEPs. For example, on the first paragraph of page 59 it is stated that "*For some of the FEPs, e.g. surface denudation, a full safety assessment for SFL will include more aspects of the FEP*." Additionally, some external FEPs are not considered by the SE-SFL, notably "mechanical evolution of the shield" and "drilled wells".

4. FEP Analysis

As stated in Report TR-19-01, commensurate with the generic nature of the SE-SFL, and consistent with its objective, scenarios were not developed systematically to represent all possible system evolutions, nor was detailed scenario analysis carried out. However, a FEP catalogue was developed for SE-SFL and used as a tool to demonstrate that all key FEPs have been considered by the SE-SFL. The FEP catalogue is summarised in Section 2.5.1 of Report TR-19-01 and described in detail in Report TR-19-02.

The FEP catalogue development process for SE-SFL was thorough and involved:

- using the SR-PSU and SR-Site FEP catalogues as a basis for development;
- re-evaluating FEPs in the NEA FEP database (including project-specific databases) that had been screened out when preparing SR-PSU and SR-Site FEP catalogues, for relevance to the SE-SFL.

The NEA FEP list used for this screening was version 2.1. This list has been superseded by version 3, which was published in 2019. It would be worthwhile for future assessments for the SFL to include a check of the SFL FEP catalogue against this latest NEA FEP list. However, the review does not believe that there would be significant changes needed to the SFL catalogue as a result of such a check.

The SE-SFL FEP catalogue comprises 281 FEP records, 234 of which are labelled “Considered” in the SE-SFL, and 47 are labelled “Not considered”. The FEPs are divided into the main categories:

- Initial state;
- Internal processes;
- Biosphere;
- External factors;
- System variables;
- Methodology; and
- Site-specific factors.

The FEPs in the main categories internal processes and system variables are subdivided into:

- Waste form;
- Concrete and steel packaging;
- BHA barriers;
- BHK barriers;
- Plugs and other closure components; and
- Geosphere.

Internal process FEPs included in the SE-SFL FEP catalogue described in Report TR-19-02 that are relevant to cement / concrete degradation are:

- BHKBa01, BHABa01 Heat transport;
- BHKBa02, BHABa02 Phase changes / freezing;
- BHKBa03, BHABa03 Water uptake and transport during unsaturated conditions;

- BHKBa04, BHABa04 Water transport under saturated conditions;
- BHKBa05, BHABa05 Gas transport / dissolution;
- BHKBa06, BHABa07 Mechanical processes (Considered only for BHK);
- BHKBa07, BHABa08 Advection and dispersion;
- BHKBa08, BHABa09 Diffusion;
- BHKBa09, BHABa10 Sorption on concrete / shotcrete;
- BHKBa10 Colloid stability, transport and filtering, BHABa12 Colloid transport and filtering;
- BHKBa11, BHABa13 Concrete degradation;
- BHKBa14, BHABa22 Metal corrosion;
- BHABa14 Dissolution / precipitation (No direct equivalent for BHK);
- BHKBa12, BHABa15 Aqueous speciation and reactions; and
- BHKBa13, BHABa20 Microbial processes

It is unclear, however, why mechanical processes are not considered for BHA.

Relevant system variable FEPs included in the SE-SFL FEP catalogue, described in Report TR-19-02 are:

- VarBHK01, VarBHA01 Geometry;
- VarBHK02, VarBHA02 Temperature System;
- VarBHK03, VarBHA03 Hydrological variables;
- VarBHK04, VarBHA04 Mechanical stresses;
- VarBHK05, VarBHA05 Material composition;
- VarBHK06, VarBHA06 Water composition; and
- VarBHK07, VarBHA07 Gas variables.

Climatic processes and effects in the SE-SFL FEP catalogue that are considered in SE-SFL and are relevant to cement / concrete barrier evolution are:

- Cli03 – Climate evolution;
- Cli05 – Development of permafrost;
- Cli06 – Ice-sheet dynamics and hydrology; and
- Cli08 – Glacial isostatic adjustment.

Detailed assessment of mechanical evolution of vaults is stated to be out of scope in R-19-02:

- VarGe07 – "*Rock stresses, as a function of time and space*" is screened out because a 3-D stress field is needed, which is very site-dependent, but there is no specific site for the SFL.
- LSGe01 – "*Mechanical evolution of the Shield*", is also screened out, although the reason is not stated (presumably it is the same as for the previous FEP, VarGeo7).
- LSGe02 – "*Earthquakes*" is screened out because effects are location-specific

In summary, the process used to develop the SE-SFL FEP catalogue has been thorough and it is unlikely that any key FEP has been missed. However, the treatment of mechanical processes is unclear. Why are mechanical processes stated to be considered only for BHK? While it is reasonable to exclude "Mechanical evolution of the Shield", it is not so

clear why “Rock stresses as a function of time and space” and “Earthquakes” are screened out. It would be possible, even in a generic evaluation, to scope the effects of mechanical evolution of the shield and earthquakes.

5. Cement / Concrete Degradation Processes

The SE-SFL, as described in the main report (Report TR-19-01) has considered all the main processes by which cement / concrete may degrade, excepting processes related to the corrosion of steel reinforcements of structural concrete.

For BHA, the evolutionary processes most likely to influence the performance of the barrier system are judged by SKB to be those processes that act on the bentonite barrier. The evolution of the cement in this vault is not considered to be a major performance-influencing factor. In contrast, in BHK, processes most likely to influence the performance of the barrier system are judged by SKB to be the evolutionary processes of cement. The most relevant of these processes is calcium leaching, which leads to a gradual loss of portlandite and C-S-H-gel. The rate of this process can be minimised by ensuring as low as possible initial connected porosity and permeability of the cement. SKB comment that the transport properties of the cement have a greater impact on the degradation rate of the cement than the composition of the cement. Chemical degradation of the concrete is recognised to potentially lead to mechanical failure. SKB's simulations indicate that mechanical failure might occur at the corners of the waste-filled parts of the vault. However, this failure was not considered in the analysis. A justification is that the net effects of concrete leaching and mechanical failure are the same, namely a loss of retardation. Since chemical degradation of the concrete is considered by the analysis, SKB argue that the effects of mechanical failure are also encompassed. SKB recognise that loading due to glaciation could result in substantial stresses on the vaults which might lead to mechanical failure of the concrete. However, since glaciation is likely to occur well after most of the radioactivity has decayed (especially that due to Mo-93 and C-14), SKB argue that mechanical effects of glaciation on the concrete barrier are unlikely to be important for long-term safety. They do, however, comment that possible earthquake effects on the repository structures have not been considered and will require further analysis in future.

A potentially important omission is that there is no mention of the evolution of the steel reinforcements that are stated to be used in the concrete walls of the vaults. For example, on page 104 of TR-19-01, there is a section on corrosion, the first paragraph of which states:

"Steel is highly prevalent in SFL; the waste in BHK is made of steel and so are the waste packages in both vaults. Some waste in BHA is also expected to be metallic."

All the discussion in TR-19-01 about steel relates to the corrosion of metallic wastes and waste containers, and how it influences the conditions in the repository (redox) and radionuclide release.

In the reviewed SE-SFL reports, only two places were found that mention corrosion of steel reinforcements:

- The second paragraph of Section 3.2.1, on page 13 of report R-19-11, recognises the heterogeneity of the initial state will depend in part on reinforcement corrosion.
- In report R-19-14, which concerns the influence of the concrete mix design on concrete degradation, Table 3-6 on page 37 gives a summary of the impact of fly ash addition (moderate levels of replacement) and limestone on the properties and durability performance of concrete. This table mentions that addition of siliceous

flyash to OPC reduces the permeability of concrete due to a refinement in the pore structure, thereby reducing Cl penetration and hence reduces potential steel corrosion in reinforcements.

In contrast, Report R-19-13, which concerns modelling of cement degradation, does not mention degradation of reinforcements at all. Similarly, Report R-19-12, which covers modelling of hydro-chemo-mechanical processes of concrete degradation, mentions the existence of steel reinforcements, but concentrates on modelling the deformation of the unreinforced concrete backfill of the BHK vault. There appears to be no consideration of degradation of reinforcements in the reinforced concrete structure.

This lack of treatment of corrosion of steel reinforcements in concrete structures in SE-SFL, contrasts with SKB's treatment of steel reinforcements in the SFR repository. Corrosion of steel reinforcements has been recognised as a potentially important issue in the main report of the SR-PSU safety assessment, TR-14-01. While many concrete barriers in the SFR have steel reinforcements, on page 174 of report TR-14-01, there is a section on the corrosion of reinforcements and other steel components. The potential deleterious consequences of steel reinforcement corrosion, namely volume expansion causing cracking of the concrete is covered by this section, which states that:

"In order to avoid the negative effects of reinforcement corrosion and corrosion of form rods, the concrete caissons in 2BMA will be designed without reinforcement and the casting process will be completed in such a way that the use of form rods can be avoided."

SKB should explain why steel reinforcement is being considered for the concrete in the SFL vaults, when a decision was taken to avoid reinforcement in the caissons of the 2BMA vault in the SFR. Additionally, further analysis and discussion of the consequences of steel reinforcement corrosion in the SFL should be undertaken.

6. Environmental Changes

6.1. Relevance to Cement / Concrete Degradation

Future changes in the environment of the SFL have the potential to influence the rate and nature of cement / concrete degradation. Three groups of environmental changes are potentially significant:

- changes in groundwater fluxes;
- changes in groundwater chemistry; and
- changes in rock stresses, caused principally by glacial loading and un-loading.

Increasing groundwater fluxes could result in increases in the rate at which the cement / concrete is leached, while also increasing the rate at which reactants (solutes such as HCO_3 and SO_4) are transported to the cement / concrete.

Changes in groundwater chemistry have the potential to influence the reaction pathways of the cement. For example, increases in SO_4 content could increase the quantity and rate of ettringite formation, with consequent increases in cracking. Similarly, increases in Cl concentrations could increase the quantity and rate at which Friedel's salt forms in cement, which may also lead to an increase in the pH of cement porewater.

Increases in vertical rock stresses could increase the potential for cementitious barriers to fail mechanically. Such failure may then result in increased permeability and consequent increased groundwater fluxes, accompanied by rates of leaching and chemical alteration.

All these variations in environmental conditions are likely to differ from one geographical location to another. Given that the SE-SFL is generic, albeit having used data obtained from Laxemar, it is appropriate to assess the degree to which the treatment of environmental changes allows general inferences to be made about cement / concrete degradation.

In Sections 6.2 to 6.6 below the environmental changes considered in the SE-SFL are summarised and their implications for the treatment of cement / concrete degradation by the SE-SFL are reviewed.

6.2. Initial Conditions

Section 4.6 of Report TR-19-01 describes the present geology of Laxemar and Section 4.6.7, commencing on page 83 of TR-19-01 covers the initial geochemical conditions in the area.

The initial state of the bedrock and groundwater considered in SE-SFL is based on the Site Descriptive Model (SDM) for the site investigation for the SF repository (SKB 2009) and new modelling performed within the SE-SFL project. The assumptions made for the initial state in SE-SFL are:

- Laxemar consists of crystalline bedrock that is dominated by well-preserved ca. 1.8 Ga intrusive rocks varying between dioritic and granitic compositions.
- Tectonic lenses, in which the bedrock is less affected by ductile deformation, are enclosed in-between ductile high-strain belts. The investigated bedrock structure chosen for SE-SFL is in such a tectonic lens.
- As part of the site investigations for the SF repository, analyses of groundwater chemistry and hydrogeochemical modelling have been shown that mixing between at least four endmember waters can explain the variations in groundwater chemistry (Laaksoharju et al., 2009 and Kalinowski, 2009):

    - an old deep saline water (Deep Saline);
    - an old marine water (Littorina Sea);
    - a modern meteoric water (Altered Meteoric); and
    - a glacial meltwater (Glacial).

- The Cl concentration at 500 m depth is between 1000 mg L^{-1} and 6000 mg L^{-1} (minimum Total Dissolved Solids, TDS around 1800 mg L^{-1}) but thereafter increases linearly to about 16,000 mgL^{-1} (maximum TDS around 30,000 mg L^{-1}) at 1100 m depth.
- Isotopic signatures indicative of glacial recharge waters are most prominent between depths of 300 m and 600 m and it is likely that in future glaciations large volumes of glacial meltwaters will penetrate to the depth of the SFL.
- The present transition from shallow oxidising conditions to deeper reducing conditions takes place in the upper 20 m and the probability of oxidising water penetrating to the depth of the SFL in future is considered low.

It is noteworthy that the spatial distribution of chemically distinct groundwaters is quite heterogeneous, reflecting largely the distribution of hydraulically conductive fracture zone. These zones tend to conduct dilute water to relatively great depth, and would allow upwelling of deep saline water should environmental conditions change. The same controls on groundwater chemistry and groundwater flow are seen widely in the crystalline shield rocks of Sweden and neighbouring countries (e.g. as described in SKB's SR-Site safety assessment for Forsmark in Sweden and Posiva's TURVA-2012 safety assessment for Olkiluoto in Finland). It follows, therefore, that general insights gained in SE-SFL should be applicable widely in Sweden. However, for this to be the case it is necessary to ensure that the SE-SFL adequately covers the full range of chemical and hydrogeological conditions seen in the Laxemar area.

6.3. Factors Driving Changes in Groundwater Flow and Chemistry

The geochemical evolution of the repository is described in Section 6.2.7 of Report TR-19-01, commencing on page 100. The evolution of groundwater chemistry at repository depth is driven primarily by:

- isostatic uplift and subsidence, respectively after and during each ice advance and retreat, which leads to sea level change and movement of the coast line;
- recharge of glacial melt water;
- permafrost development; and
- changes in meteoric water recharge.

These processes are all relevant and uncontentious.

6.4. Base Variant of the Reference Evolution

The base variant of the reference evolution assumes present-day climate conditions and accounts for the shoreline displacement after the last glacial rebound. To support the SE-SFL based on this climate evolution Joyce et al. (2019), modelled the evolution of the hydrogeological system around the example repository location from 8000 BC to 60000 AD. However, SKB recognise that the modelling in Joyce et al. (2019) takes no account of the effects of the repository itself on groundwater flow.

While the effects of the repository on groundwater flow and chemistry in the operational period will be very short-lived compared to the assessment time, it would be helpful for SKB to explore whether it could impact on longer-term cement / concrete evolution. For example, if saline water up-cones to the level of the repository, is it certain that there will be an insignificant effect on cement / concrete degradation? Possibly this will be the case, but some discussion and justification would be useful.

In the 2nd paragraph of Section 6.2.6 on page 96 of TR-19-01 the groundwater flow field through the repository is explained. Modelling of the near-field hydrogeology has been performed to evaluate the groundwater flow through the SFL vaults and waste, using an equivalent porous medium (ECPM) representation of the bedrock (Abarca et al., 2019). Assuming the hydraulic properties of saturated vaults at 2075 AD, the calculated total flow through the BHA vault of 2.2×10^{-2} $m^3\,a^{-1}$ is two orders of magnitude lower than the total flow through BHK of 1.1 $m^3\,a^{-1}$ (Abarca et al., 2019). This difference reflects the differing hydraulic conductivities of the different backfill materials in the BHA and BHK vaults. The hydraulic conductivity for the bentonite backfill in BHA is in the order of 1.0×10^{-13} m s^{-1} while that of the concrete backfill in BHK is 8.3×10^{-10} m s^{-1}.

Reflecting these different predicted groundwater fluxes, BHA is predicted to be un-saturated for a few millenia in the period when BHK is saturated; saturation of BHK is predicted to be complete within about a decade. Thus, in the BHK vault degradation of the cement / concrete will begin almost immediately post-closure, whereas in the BHA vault it will be several thousand years before any significant degradation occurs. In this latter vault, any degradation will be due to internal processes within the repository. However, it is reasonable to expect that these will be minor compared to the degradation that will occur in the presence of groundwater.

The bentonite backfill in BHA retains its hydraulic properties throughout the analysis period. However, in BHK, groundwater will gradually leach the cement minerals in the concrete backfill, as studied in detail in SKB Report R-19-13 (see also Section 7.3below). The leaching is controlled by diffusion, with a weathered zone developing at the bedrock-backfill interface, expanding inward, approaching the centre of the vault on a time scale on the order of 100000 years. The material in the degraded zone is more permeable than the concrete initially installed and therefore affects groundwater flow through the BHK vault and waste. After the highly soluble alkali hydroxides, the first concrete mineral fraction affected by leaching is portlandite and after about 85 ka post-closure, the outermost quarter of the backfill has lost its portlandite. After portlandite dissolution and leaching, the calcium-silicate-hydrate gel (C-S-H) starts leaching out and is completely lost from the outer half of the backfill after ~700 ka.

This sequence of alteration is reasonable, although the duration of each phase of alteration will be very dependent on the assumptions that are made about reaction rates and groundwater fluxes. As noted elsewhere (see Section 7), SKB's modelling does not include an adequate representation of reaction kinetics for cement phases, which may gave implications for the alteration sequence and rate of degradation of the cementitious barriers. This issue requires further investigation.

Broadly, during uplift, there is coastal retreat and increased influx of meteoric water, leading to progressively more dilute water penetrating to depth (**Figure 3**).

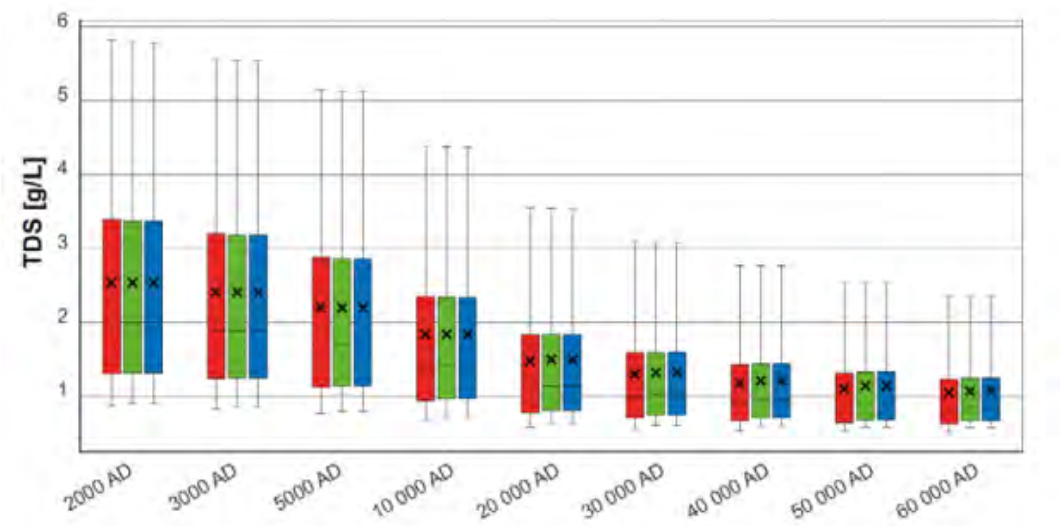

Figure 3: Time evolution of the total dissolved solids (TDS) concentration within the repository volume between elevations −530 m and −470 m for the three cases: Case 1 in red, no chemical reactions; Case 2 in green, equilibrium with quartz, calcite and iron sulphide; Case 3 in blue, equilibrium with quartz, calcite and hematite. The statistical measures are the median, the 25th and 75th percentiles (box), the mean (cross) and the 5th and 95th percentiles (whiskers). Taken from Figure 4-32 in Joyce et al. (2019) as reproduced in Figure 6-11 of Report TR-19-01.

The high salinity at depth (see Section 6.2) is enforced in the models by applying a high-salinity boundary condition below the repository. This approach prevents replacement of deep saline water with dilute water over very long time periods.

SKB state in the 6th paragraph of page 103 of Report TR-19-01 that when groundwater flows through the cementitious components of the repository, it equilibrates with the cement minerals and acquires the composition shown in Table 1.

Table 1: Chemical components in porewater of young and evolved cement. Table 6-1 reproduced from TR-19-01.

	Young cement porewater[a]	Evolved (leached) cement porewater[b]
SO_4^{2-} [mg/L]	3.84	1.92
Cl^- [mg/L]	2.13	71
Na^+ [mg/L]	644	69
K^+ [mg/L]	3237	3.9
Ca^{2+} [mg/L]	36	800
Si as SiO_2(aq) [mg/L]	22.4	0.084
Al_{tot} [mg/L]	1.08	0.054
OH^- [mg/L]	1938	612
pH	> 13	12.5
Ionic strength [M]	0.12	0.061

[a] Lagerblad and Trägårdh (1994).
[b] Engkvist et al. (1996).

While this is true, the composition of the cement-equilibrated porewater will depend on the composition of the groundwater. The SE-SFL appears to have ruled out the possibility that saline waters may react with the cement. Table 1 gives only compositions of brackish water, but as discussed above, much more saline water occurs in the vicinity of the hypothetical SFL site. Such saline water could also potentially occur at shallower depths in other sites elsewhere that might in future be considered for the SFL. Additionally, only one cement composition is considered, namely Ordinary Portland Cement (OPC), or more specifically in the case of Lagerblad and Trägårdh (1994), Degerhamn Standard Portland Cement. In future work it would be appropriate for SKB to consider a wider range of water compositions and cement compositions and their assessment of cement / concrete degradation.

As discussed in Section 1 it is noteworthy that the SE-SFL does not mention the impact of the groundwater chemistry or cement composition on the corrosion of steel reinforcements in the concrete structure around the waste.

Gas generation and its effects on groundwater flow are described on page 107 of TR-19-01. Gas generation has been evaluated only for the BHK vault, in which metal corrosion is expected to be the source of gas. An evaluation of gas has not been done for the BHA vault due to the smaller amount of metal in its waste, but SKB recognise that it needs to be studies for subsequent SFL safety assessments, since large overpressures might affect the bentonite buffer integrity.

It is expected that gas generation in BHK will cause an overpressure in the BHK vault of around 2 bar within the first 100 years after saturation (Silva et al., 2019), about an order of magnitude slower than the timescale for water-saturation of BHK. The gas gradually escapes from the vault due to its buoyancy, mainly upwards but also in the direction of groundwater flow. All steel is predicted to be corroded and hydrogen gas production to cease about 600000 years after closure. The overpressure then decreases to ≤ 0.5 bar within about 10000 years (Silva et al., 2019).

These relatively low gas pressures would seem unlikely to compromise the integrity of the concrete structures.

The predicted evolution of the concrete in the BHK vaults is summarised in Section 6.2.10 of TR-19-01, commencing on page 112. The main features of this evolution are:

1. Concrete leaching in the BHK vault starts at the concrete-backfill-bedrock interface where groundwater enters the vault.
2. The leaching front moves slowly through the backfill, towards the reinforced concrete structures containing the grouted waste.
3. The degradation sequence is outlined in Figure 4. At 100000 years after closure, only the outer zone is degraded. Here dissolution of the portlandite in the concrete is observed to a depth of c. 1 m from the interface (Report R-19-13). The permeability of this zone increases due to the mineral dissolution and conducts water around the intact inner part of the backfill.
4. The dissolution of portlandite and ettringite is followed by decalcification of calcium silica hydrate (C-S-H) and the dissolution of other hydrates.
5. Calcite and hydrotalcite precipitate to some extent in the degraded zone.
6. Portlandite completely dissolves in the outer half of the backfill after approximately 180000 years, and in the inner half after about 340000 years.
7. C-S-H starts decalcifying after portlandite is depleted, but this process proceeds even more slowly than portlandite dissolution.
8. In the outer half of the backfill, C-S-H is not completely dissolved until after ~800000 years.
9. After 1 million years of interaction with groundwater, the concrete backfill in BHK is almost fully degraded.

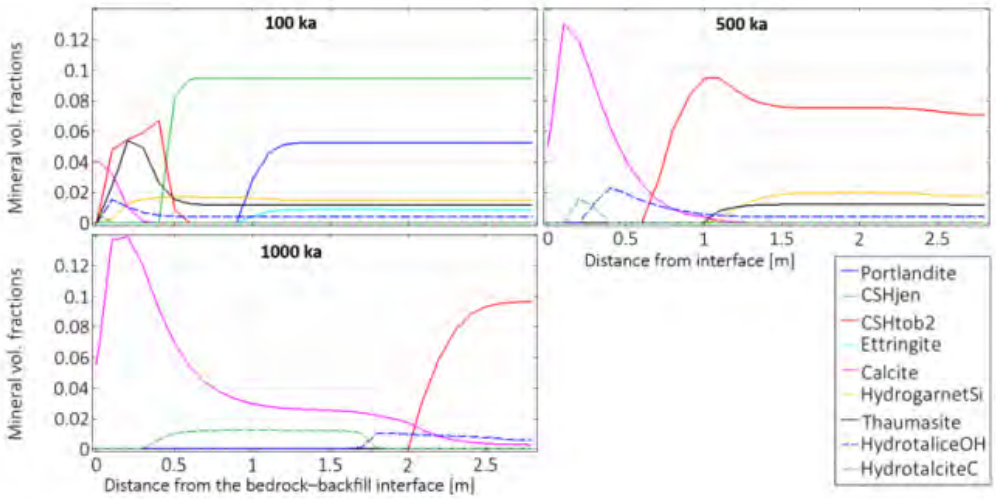

Figure 4: Mineral volume fractions after 100000, 500 000, and 1 000 000 years after closure in a 1-D profile extending horizontally from the bedrock-backfill interface. Adapted from Figure 6-2 in Report R-19-12. Reproduced from Figure 6-16 of Report TR-19-01.

This degradation sequence is reasonable, but the SE-SFL does not consider in depth the possible effects of different groundwater salinity and composition, and cement composition on this evolutionary sequence, particularly the durations of the various stages.

6.5. Increased Greenhouse Effect Variant of the Reference Evolution

Section 6.3 of Report TR-19-01, starting on page 115, describes the increased greenhouse effect variant of the reference evolution.

It is stated that a small decrease in total groundwater recharge is expected in a warmer and wetter climate, owing to decreased snow accumulation and hence less spring snowmelt.

In the increased greenhouse effect variant of the reference case, groundwater chemical conditions in the BHK and BHA vaults are expected to be the same as in the base variant of the reference evolution, which assumes that present climatic conditions continue throughout the assessment period.

Given the nature and stated objective of the SE-SFL this treatment of conditions at the repository level is reasonable. However, the same reservations concerning the limited consideration of spatial and temporal variations in groundwater chemistry and limited cement composition, as for the base variant (Section 6.4) apply.

6.6. Simplified Glacial Cycle Variant of the Reference Evolution

The simplified glacial cycle variant of the reference evolution is described in Section 6.4 of Report TR-19-01, which commences on page 119. This variant includes simplified glacial-cycle cold-climate conditions, permafrost growth, and an ice-sheet overriding the Laxemar site. Owing to isostatic subsidence caused by the ice sheet after the glacial period the SFL is covered by sea.

Permafrost is assumed to occur at the site c.17000 years after repository closure when next solar radiation will be at a minimum at high northern latitudes. A second periglacial period starts c.50000 years after repository closure, again corresponding to a second period of low summer solar irradiation. This second periglacial period is followed by glacial conditions, with an ice sheet up to 2500 m thick overriding the repository site. During this period, the ice sheet is assumed to become sufficiently thick to cause substantial isostatic bedrock depression.

The regional hydrogeological evolution during glaciation and deglaciation is covered in Section 6.4.5 of Report TR-19-01, which commences on page 122. The corresponding geochemical evolution is covered by Section 6.4.7 of Report TR-19-01, which commences on page 133.

During periods of permafrost, the ground freezes by up to a few hundred metres, below which unfrozen bedrock is encountered. In the SE-SFL, the repository is assumed to be sufficiently deep that it will never be frozen. In the frozen bedrock, groundwater advection is negligible, but may be significant in some unfrozen parts of the bedrock. Local water flow can be even greater in these unfrozen rock volumes than under temperate conditions.

The flow decreases during submerged conditions and increases during the 2000-year periods when the ice-front advances and retreats over the repository. The maximum flow occurs when the ice-front is above the repository during its advance.

Freezing of the groundwater will cause exclusion of salts and may lead to temporarily increased groundwater salinities. The effect of this process is stated not to have been considered explicitly in the SE-SFL evaluation.

Advances and retreats of ice over the site are predicted to change groundwater salinity (Figure 5). Increased groundwater flow, combined with the low salinities of glacial meltwaters, will result in periods when groundwater salinity in and around the repository is markedly lower than during temperate periods.

The hydrogeological models predict up-coning of deep groundwater in front of the advancing or retreating ice margin, causing higher salinities at the repository depth. Generally, the ice margin is thought to pass the site relatively quickly meaning that the periods of increased salinity will also be short. The up-coning of saline water will be decreased if the ice sheet passes over permafrost.

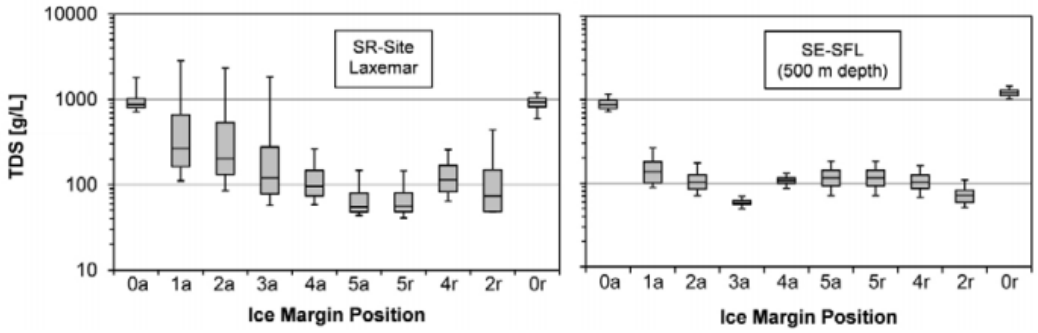

Figure 5: The calculated TDS concentrations for the different stages of the glacial period, where the x-axis shows the six time periods of advancing ice (0−5a) over frozen ground (permafrost), followed by four time periods of ice retreat (r) with submerged conditions in front of the ice margin. Results for groundwaters within the candidate Spent Fuel Repository volume at 500 m depth at Laxemar (left, Gimeno et al., 2010), and within the SE-SFL bedrock volume at 500 m depth (right, Gimeno et al., 2019). The statistical measures are the median, the 25th and 75th percentiles (box), and the 5th and 95th percentiles (whiskers). Figure 6-24 reproduced from Report TR-19-01.

Again, given the nature and stated objective of the SE-SFL this treatment of conditions at the repository level is reasonable. However, the same reservations concerning the limited consideration of spatial and temporal variations in groundwater chemistry and limited cement composition, as for the base variant (Section 6.4) and increased greenhouse effect variant (Section 6.5) apply. However, in the case of the simplified glacial cycle variant there is even greater potential for the salinity and chemistry of groundwater and groundwater fluxes to vary over time.

6.7. Summary of Review Findings about Environmental Change

SKB's modelling does not take account of the effect of the repository on groundwater flow and chemistry. These effects due to the operational period will be very short-lived compared to the assessment time frame. Nevertheless, it would be helpful to explore whether they could impact on longer-term cement / concrete evolution.

The general sequence of cement / concrete alteration assumed in SE-SFL (Report TR-19-01) is reasonable, the duration of each phase of alteration will be very dependent on the

assumptions that are made about reaction rates and groundwater fluxes. As noted elsewhere (see Section 7), SKB's modelling does not include an adequate representation of reaction kinetics for cement phases, which may gave implications for the alteration sequence and rate of degradation of the cementitious barriers. This issue requires further investigation.

Section 6.4.9 of TR-19-01, on page 125, covers evolution of the barrier system in the BHA vaults during glacial periods. It is concluded that the evolution of the BHA barriers during a period of glaciation is generally not expected to deviate from the evolution described in the base variant. However, this conclusion relies on the integrity of the bentonite barrier being maintained. If this is not the case, for example if increased groundwater fluxes beneath an ice sheet results in erosion of the bentonite allowing the concrete structure to be exposed to flowing groundwater, then this conclusion may not be valid. Greater discussion of this issue would be helpful.

Section 6.4.9 of TR-19-01, also on page 125, covers the evolution of the BHK barrier. Key points that are made are:

- The groundwater flux at the bedrock - concrete backfill interface will generally affect the rate of cement mineral dissolution and influence the concrete degradation rate.
- Glaciation may introduce dilute groundwater into the repository.
- Simulations of concrete degradation in BHK have found only minor effects when exposing the concrete to glacial groundwater (SKB Report R-19-11).
- An extensive ice sheet above the repository will be accompanied by increased vertical in-situ stresses on repository components.
- Simulations indicate that during periods when an ice sheet lies above the repository mechanical damage may occur in the concrete backfill, close to the waste domain, and locally at the interface between the backfill and the bedrock (Report R-19-12).

These general conclusions regarding the degradation of cement are reasonable for the assumed evolution, including the evolution of chemical conditions. However, SKB have assumed that saline groundwater will not flow into the repository and appear to have considered only a single cement composition. In future work, SKB should give greater consideration to the spatial variability of groundwater salinity and chemistry and to the possible use of different cement compositions. It is also important that some consideration is given to the corrosion of steel reinforcements in the concrete structures surrounding the grouted waste. This issue is not mentioned at all in the SE-SF (Report TR-19-01.

In Section 9.3.2 of Report TR-19-01 on page 196, SKB conclude that hydrochemistry only has a minor effect on the performance measures for the repository and that it should therefore not be necessary to include coupling between hydrogeology and groundwater chemistry in future studies. However, the justification for this statement is weak.

7. Models and Modelling Methodology

7.1. SKB Report R-19-11: Modelling of concrete degradation - Hydro-chemical processes

7.1.1. Background

The report describes initial benchmark using the iCP software to reproduce modelling by Höglund (2014) of BMA vaults in the SFR repository concept using "PHAST" (coupling of HST3D with PHREEQC).

Having described the benchmarking models the report presents models for concrete degradation in the BHK vault of the proposed repository concept for SFL. A range of sensitivity cases are described using 2D models to evaluate the influence of various assumptions on the results, and to determine an optimal approach for 3D modelling (including simplification of chemistry). Cases consider boundary conditions, assumptions of concrete and waste being homogenous or heterogeneous media, variation in groundwater composition (glacial meltwater variant), the coupling of physical and chemical processes, initial concrete composition. The model description concludes with the 3D model of the BHK compartment and a 3D model of the entire vault. A discussion on computational requirements for different levels of model complexity is provided.

7.1.2. iCP Reactive Transport Benchmark (SFR)

The approach is to build on the modelling of SFR by Höglund (2014). Initially, a benchmark case is presented where the "Large20" simulation of the 2BMA vault described by Höglund (2014) is replicated using the iCP software (Nardi et al., 2014) which allows for coupling of PHREEQC and COMSOL (noting that Höglund used PHREEQC and PHAST).

The approach to building on previous models is reasonable given similarities between the SFR modelling and that needed for SFL and much of the previous work by Höglund (2014) is relevant. It would be possible to build models for SFL without consideration of previous work, but the approach adopted was presumably intended to build confidence in the new models, which is understandable.

The four fractures (0.1 mm thickness) included in Höglund's conceptual model were excluded as they had little effect on model outcomes. Porosity and transport were not coupled as in Höglund's approach, in which concrete degradation was simulated by increasing transport over time in a stepwise manner. Note that Table 7.7 in Höglund shows constant porosity, as tortuosity is set to increase in a series of stages over time, along with increases in hydraulic conductivity. This approach was included in the benchmark with smoothing of the transitions. Time-dependent changes in boundary conditions were also applied as in Höglund (2014) with different transitions ("smooth" and "less smooth") to avoid discontinuities and convergence issues.

A horizontal inflow of groundwater is assumed as a boundary condition (left side of the model) which is referred to as constant inlet flow (top and bottom are no flow boundaries). A constant hydraulic head is imposed on the right boundary, the flow on the left boundary increases over time in a stepwise manner. The report discusses how Péclet numbers were calculated as a function of time for each model domain (values much less than 1 suggest diffusion dominated transport, values much greater than 1 suggest advective transport dominates). The equation (4-1, page 18) shows that the characteristic length Lc (m) is related in the work to the finite element size h (m) calculated in COMSOL. It is noted that using element size as the characteristic length is not based on physical reasons, and selecting a reasonable characteristic length for the entire domain is not an easy task. Issues surrounding the use of grain size (up to a few centimetres in length, with small resulting Péclet numbers) are noted. An alternative is selecting a representative length based on concrete walls is mentioned (1-3 m). The choice of element size in the range of 0.03 to 0.6 m is suggested as a reasonable compromise. Péclet numbers calculated for the model are provided (Table 4-3, pg. 19).

As in Höglund, the models assume local chemical equilibrium (reaction kinetics are excluded), MintqCem-2001 was used as the thermodynamic database. The same initial concrete composition and porewater composition were used as in Höglund (2014). The same secondary solids were included as in Höglund. The report describes an approach whereby iCP calculates porosity in a way which is equivalent to the approach in Höglund (2014), but it is not coupled to chemical reactions. Therefore, efforts were made to ensure the treatment of processes in the benchmark case was as close to the original model as possible.

It is noted that iCP uses the sequential non-iterative approach (SNIA) to solve the reactive transport problem, with communication times between PHREEQC and COMSOL having to be defined by the user. Within each timestep, the two models (COMSOL and PHREEQC) may divide time into sub-steps to reach convergence of the multiphysics and chemical parts of the simulation. PHREEQC only subdivides the time step where reaction kinetics are considered (which they are not in the benchmark case). Two different sets of timesteps were used. The report outlines how communication time steps are set up for a given finite element mesh using two criteria: Von Neumann criterion and Courant number.

The report identifies convergence issues relating to using the same chemical set-up as Höglund (2014), and the issue was found to relate to the inclusion of iron [dissolved Fe and $C_3FH_6(C)$]. It is suggested that it is not essential for iron to be included given the low dissolved concentration present in porewater and the small amounts of Fe-bearing solids initially present in the system. To consider the implications of removing iron, a new PHAST simulation was developed to allow more accurate comparison between PHAST and iCP model approaches. This appears to be a reasonable work-around. Although it seems a little odd that convergence problems did not occur in the original PHAST modelling where iron species were included.

New PHAST simulations were produced using two time-stepping schemes (“course” and “fine”) to explore the implications for model outputs. The benchmark models (new PHAST) and iCP are compared to those in Höglund for a point within the concrete structure (termed “GH” in Höglund, 2014). The time discretisation in the new PHAST models affects the timing of mineral dissolution-precipitation reactions. The finer time discretisation gives a reasonable match to the calculated porosity at point “GH” compared to

Höglund's model. The outputs from the new PHAST simulation with finer temporal discretisation are therefore compared to the iCP model outputs. Some differences in Darcy velocities are noted, and it is suggested that these may be due to underlying numerical algorithms (PHAST uses finite difference). It is noted that comparisons of the two approaches have been made in the literature.

The chemical evolution of the iCP and new PHAST model are compared, and a reasonably good agreement is reported.

Overall, this work has been very thorough in attempting to replicate the modelling by Höglund (2014) to show that different software (and different underlying numerical approaches to transport) can give similar results. The issue of non-convergence associated with iron is considered, but the reasons for the problem are not apparent. However, many models of concrete degradation neglect iron-bearing solids to simplify the chemical aspects of the system being examined (e.g. Wilson et al., 2018).

7.1.3. 2-D reactive transport modelling

Purpose

The 2-D reactive transport modelling aimed to perform a preliminary assessment of potential cement degradation processes of cement and concrete barriers due to groundwater interaction. The potential for alteration due to the reaction between waste forms and barriers is not mentioned and is presumably out of scope.

Approach

The choice of software used for the geochemical modelling (iCP) and any implications associated with using a Sequential Non-Iterative Approach (SNIA, a type of operator splitting), rather than an approach that includes the full coupling of transport and chemical processes (globally implicit approach) are not mentioned. The exclusion of reaction kinetics would presumably simplify the coupling of transport and chemical processes. (operator splitting approaches require managing mass balance errors, e.g. Valocchi and Malmstead, 1992; Carrayrouet et al., 2004).

Many models are presented to consider different assumptions and approaches. The following are considered:

- concrete heterogeneity;
- fixed or open boundary conditions; and
- groundwater boundary condition (constant inlet flow vs. constant hydraulic head); groundwater type ("old meteoric" and glacial meltwater compositions); and coupling of processes, considering either Kozeny-Carman or modified Kozeny-Carman relation for porosity-permeability coupling.

However, the potential for variation in salinity of the groundwater is not discussed.

Porosity-diffusion coupling is not mentioned initially but is discussed later in the text. The potential for salinity variation is considered in part, but most models consider the one water composition from Pękala et al (2015) (which does not seem to be available). The potential for salinity changes is not considered.

It is noted that the boundary condition assumptions have implications for process-couplings, uncoupled simulations were produced for two different solute transport boundary implications. A modified Kozeny-Carman relationship was used that was "more aggressive".

Heterogenous vs Homogenous Hydraulic Conductivity

The modelling considers homogenous and heterogeneous hydraulic conductivity and the issue of cracking of concrete is noted. The uncertainty associated with the extent of cracking and effect on flow led to different approaches being explored. In models where a heterogenous hydraulic conductivity is assumed, a distribution of values is used based on Gaussian distribution and a successive transformation of a multi-Gaussian field (where there is greater connectivity of cracks and more rapid concrete degradation is expected).

Boundary Conditions

The report states that where advection is considered to dominate over diffusion, an open boundary condition at the inlet is used, but where diffusive transport is dominant, a fixed concentration boundary conditions can be used instead. It is assumed that groundwater in contact with the concrete backfill is flushed out before the out-diffusion from the latter leads to changes in groundwater composition.

Feedback between Physical and Chemical Processes

The report states that porosity is the main control of hydraulic and transport properties and the models are described as using the Kozeny-Carman relationship (a commonly used approach) and a modified version in which hydraulic conductivity ranges between values for the initial state and that in which cement paste has completely degraded.

The process couplings are common approaches and considering potential variation in transport properties is valid.

BHK cross-section modelling (2-D)

The geometry is a cross-section of the BHK vault, based on a 3-D groundwater flow model (Abarca et al., 2016) and comprises three domains: host rock, concrete backfill and waste domain. The backfill is conceptualised as a monolith of concrete, which is the same as that considered by Höglund (2014) for the SFR models. The model only considers flow in the host rock. It is noted that there could be reactions between host rock and concrete but that this phenomenon is excluded to simplify models and reduce sources of uncertainty.

The approach will simplify the models and therefore the degree of uncertainty within them (in terms of variation in parameter values). However, there is a degree of uncertainty introduced in terms of the representativeness of the models. It is not expected that complex 2-D models of the concrete would consider cement-rock interaction, but this simplification could have implications for the accuracy of calculated water flows. For example, the potential for fractures to become sealed by cement-rock alteration products is not considered but could impact on water flow. It is noted that calcite precipitation in the host rock could

"*positively impact the long-term performance of the concrete by decreasing mass transfer of solute by advection and diffusion from the rock to the concrete structure*".

Furthermore, it is stated that:

"*Thus, neglecting these processes in this study is considered to be a conservative assumption*".

It would be beneficial for the safety evaluation (in general) to include a clear summary of what processes are being simulated, those which could occur but are not being simulated, and how processes relate to safety evaluation assumptions and associated calculations.

There are a few detailed technical points which can be made on the conceptual model:

- Cement / concrete-rock interaction is known to lead to rock alteration and precipitation of zeolites, feldspathoids and possibly layer silicates, not just calcite.
- In general, fractures in the rock and other media are likely to undergo a degree of sealing due to precipitation of secondary solid formation in fractures, which would reduce flows and therefore the flux of water to the repository. However, a potential scenario could be envisaged whereby this affects water flow in some places, but does not necessarily lead to reduced flow either because:
  - (1) flow is simply diverted to other fractures;
  - (2) fracture surfaces are "armoured" with secondary solids but remain transmissive to a degree.
- The assumption of no calcite precipitation in the rock could be conservative, but there needs to be a clear conceptual approach outlined which separates "expected evolution" as ascertained from modelling (and other studies, such as analogues) and the evolution that is explicitly considered in safety evaluation calculations. For example, a model (or other data) may suggest a reduction in flow due to clogging of pores in concrete / fractures, but the "benefit" is not considered in radionuclide transport and biosphere dose calculations. Considering what may or may not be conservative in terms of dose calculations in models designed to elucidate expected behaviour of the system, could introduce a form of bias into the safety evaluation.

The report describes material properties and that they may evolve in coupled simulations. The coupling, as would be expected, is based on porosity changes induced by mineral dissolution-precipitation reactions. Porosity changes affect hydraulic conductivity K (m s^{-1}), and the effective diffusion coefficient D_e (m^2 s^{-1}). Initial values appear like those reported elsewhere (e.g. Savage and Stenhouse, 2002) for intact concrete.

The models used thermodynamic data from CEMDATA07. This is a recognised database that draws on data which has published in the peer-review literature. However, the reason for the use of this database rather than others that include many relevant solids and have been produced especially with radioactive / hazardous waste disposal in mind (e.g. THERMODDEM, ThermoChimie) are not mentioned. Also, it is not clear what data are used for secondary aqueous species. The report refers to a report by Jacques (2009) where the CEMDATA07 values are incorporated into PHREEQC (apparently the PSI / Nagra version). It would assist the reader if the version of PHREEQC database used was stated, as several versions are available.

The models consider a "full" and "simplified" treatment of chemistry (based on Höglund, 2014). Models also consider glacial meltwater in addition to a reference "granitic" water composition. The simplified system is considered given the complexity of models that include complex geometries (e.g. 3D) and all chemical species. The glacial water has a pH

of 5.8, which is quite low, but this one of the "reference" water compositions, and its applicability is another issue.

The models assume chemical local equilibrium as in previous work by Höglund, (2014). This approach has been used in older modelling of complex systems, but in recent years there has been a move to include mineral dissolution-precipitation kinetics, even though: (1) measured data may be unavailable for dissolution rates of some cement solids and analogue approaches have to be used; and (2) the kinetics of secondary solids precipitation is mostly not clear and a transition-state-theory (T-S-T) equation that considers both precipitation and dissolution based on saturation index is used, or precipitation is assumed to be near-instantaneous. The possible implications of this assumption for model outcomes are not considered.

The simplified chemistry includes Portlandite, C-S-H gel (two compositions) along with calcite, ettringite and gypsum as secondary solids. Alkali species are simulated using an ion-exchange approach.

The two C-S-H compositions (tobermorite-like and jennite-like) included in the models from CEMDATA are included in the database as end members of an ideal solid solution. It is not clear whether a solid-solution assumption was used in the simulations. It appears that they were included as discrete solids. This needs to be made clear.

The simplified system would provide an adequate representation of leaching and carbonation, and to an extent, sulphate attack (note later comments on thaumasite which is included as a primary solid, although it is often considered as a product of sulphate attack).

The primary cement solids present are stated to be the same as in Höglund (2014), which are in turn, based on a consideration of hydration behaviour of Portland cement by Höglund (1992). It should be noted that a different hydrated cement solid assemblage has been suggested elsewhere (Cronstrand, 2007, 2014). However, the potential for different primary solids to be present and the implications of cement compositional variation are considered in a subsequent report (SKB R-19-14).

The primary cement solids in the full model are said to be like Höglund (2014), but there are significant differences. Table 2-7 in Höglund (2014) includes C_3FH_6 (tri-calcium ferrite hydrate), C_3AH_6 (hydrogarnet), monosulphate (presumably monosulfoaluminate), ettringite (zero concentration), C-S-H gel, portlandite, calcite (and NaOH and KOH to represent alkalis). However, model outputs in Höglund (2014) suggest that ettringite was included rather than monosulphate as a primary solid. The report (R-19-11, Table 5-6) lists the following as primary solids: portlandite, C-S-H (jen), ettringite, hydrogarnet_Si, thaumasite, hydrocalcite-OH. Therefore, C_3FH_6 is not included. Hydrotalcite and thaumasite are not included as primary solids in Höglund (2014).

The potential secondary cement solids include monocarboaluminate, hydrogarnet, hydrotalcite, monosulfoaluminate and hemicarboaluminate. In general, these are hydrated cement solids that are considered to form during the initial hydration of cement clinker, rather than being typical products of cement leaching, carbonation, or sulphate attack. However, the inclusion of carbonate-bearing versions of hydrated cement solids as potential secondary alteration products does consider the role of increasing carbon availability due to that present as dissolved carbonate in intruding groundwater. The potential varia-

tion in salinity in the groundwater is not discussed, and Friedel's salt (a product of chloride attack) is not included in the models. The dissolved Cl concentration is greater than that in the modelling by Höglund (2014) (by a factor of ~4) and in that system, a small amount of Friedel's salt precipitated as a cement alteration product.

The base case simulation (homogenous concrete, fixed concentration boundary conditions) shows limited degradation over 100,000 years due to limited groundwater flow (Darcy velocity ~1 x 10^{-11} m s^{-1}), the initial diffusion coefficient in concrete being very low (3.5 x 10^{-12} m^2 s^{-1}), and the large concrete volume. Alteration limited to ~half the thickness of the wall of the concrete backfill (1-1.25 m) with porosity increasing from 0.11 to 0.25 going towards the rock. This leads to an increase in hydraulic conductivity (up to 16 times the initial value) and effective diffusivity (3 times the initial value). The increase in porosity is due to Portlandite dissolution and partial C-S-H degradation. Near the water inlet, there is a greater loss of primary solids, including ettringite and hydrogarnet. The alkalis are gradually released with Ca replacing in the ion exchange model used to simulate alkali leaching. Most secondary solids do not precipitate (note that the initial dissolved sulphate concentration is higher than that in the groundwater), only C-S-H ("tob2"), hydrotalcite-C and calcite precipitate. As previously noted, hydrotalcite is usually a solid considered to be a primary component of Portland cement (e.g. Lothenbach et al., 2011). However, the overall evolution is consistent with expected Portland cement-based concrete behaviour.

In summary, sensitivity cases show that:

- Simplified chemistry leads to slightly different porosity evolution (full chemistry is more prone to porosity change due to the amount of reactive mineral being larger; maximum porosity increase is 0.21 compared with 0.25 in the base case). The overall evolution of the system is broadly similar in the simplified case so it is suggested it can be used for 3D simulations.
- A comparison of the base case with one where there is no permeability-porosity coupling highlights the increase in hydraulic conductivity and effective diffusivity with coupling. The modified Kozeny-Carman approach suggested by Höglund (2014) did not give significantly different results.
- Boundary condition assumptions are explored, "open" at the "inlet" (typical for advective flow) vs. fixed concentration. Also, constant inlet flow vs. hydraulic head gradient cases were considered.
- Overall, the models show that a fixed concentration boundary is a more "aggressive" scenario with increased degradation when there is the coupling of porosity with diffusion and hydraulic conductivity. The "open" boundary condition show degradation being limited to the side of the concrete closest to the inlet, a fixed boundary assumption leads to more symmetric degradation (almost independent of flow field).
- The glacial water (simplified chemistry) gives a similar evolution compared to using the base case "old meteoric" water composition.

All these findings appear reasonable in terms of the overall evolution in the base case and differences (or lack thereof) in the sensitivity cases. However, the potential for salinity variation and Friedel's salt formation is not addressed.

Cases where heterogeneity is included in concrete hydraulic conductivity, a multivariant Gaussian distribution is applied, with K_{max} and K_{min} of 10^{-6} m s^{-1} and 10^{-11} m s^{-1}, with a

value of 10^{-7} m s^{-1} in the waste domain. Coupling is considered for the full chemical system with open boundary conditions. The models show preferential flow pathways leading to a heterogenous dissolution process, but pH is largely unaffected. The shortcoming of this approach is that "clusters" of enhanced hydraulic conductivity tend to form, rather than interconnected flow paths or channels. Therefore, a model is presented called "SGSIM" which is based on a transformation of a multi-Gaussian field that results in connected zones of higher permeability.

This is an interesting approach and does give a more "connected" higher K field, but how representative this might be of degraded concrete is unclear, as observations of the evolution of large concrete structures are not readily available.

The model shows portlandite dissolution throughout the full thickness of the concrete backfill along the resulting preferential flow path after 78 500 y, with a reduction in portlandite present in the waste form. These results seem reasonable.

3D model of BHK vault

A 3-D model of the vault is described in which the simplified chemical system is adopted, using pressure field data from Abarca et al. (2016) for boundary conditions. The flow velocity field is calculated in the model and evolves as hydraulic properties of the concrete and waste domains evolve (as in previous coupled 2-D models). Compartment and entire vault scale models are described.

The finite element meshes are described and the time stepping between the two codes (COMSOL and PHREEQC) is the same as in 2-D models. The total simulation time is 50,000 y. A Dirichlet-type fixed concentration boundary was applied over the whole boundary of the concrete domain for solute transport. Diffusive and advective solute transport are considered.

In the compartment scale model, the application of a heterogeneous velocity field results in non-uniform concrete degradation fronts. Portlandite was completely dissolved at the concrete-rock interface with significant heterogeneity compared to the simpler 2D model. Higher flow velocity also led to increased degradation with a front moving into the concrete barrier. Heterogeneous dissolution is also seen for other primary solids such as C-S-H, as is the precipitation of secondary calcite and ettringite (although the latter forms in very small amounts). The pH evolution is related to portlandite behaviour (pH~12 until it is completely lost). After 50,000 y ~43.5% of the portlandite volume is lost which is about twice that in the 2D model. Overall, the precipitation of calcite does not compensate for the loss of volume of primary solids.

The vault-scale model shows the total volume of portlandite dissolved after 8500 y is 23.6% of the initial amount, which is slightly higher than 22.1% in the compartment scale model. The overall evolution appears to be like the compartment scale model.
The complexity of these model and the attempt to simulate alteration at a whole vault scale should be commended. Considering the differences between 2D and 3D models is a valid approach.

7.1.4. Summary of Review Findings

Benchmark Modelling (SFR)

The reproduction of the work by Höglund (2014) demonstrates that the iCP software approach can replicate the simulation of concrete degradation constructed using PHAST. This approach provides evidence to support the repeatability of the work and provides a degree of confidence in the codes used. As noted by Report R-19-11, there were convergence issues in the model for the chemical system described by Höglund (2014) which appears to arise due to the inclusion of iron species. Therefore, models were produced that excluded iron.

This approach is reasonable if the aim is to mostly consider major alteration pathways and pH evolution and has been made in other published models of cement degradation (e.g. Wilson et al., 2018). The reason for iron causing problems is not clear.

Report R-19-11 also notes that there are some differences between the iCP models and PHAST models, which is ascribed to COMSOL flow model smoothing algorithm and computational approaches (finite element vs. finite difference) in 2-D simulations. The overall conclusions seem reasonable, the COMSOL-related issue is explored, and the complexity of the models means it is unlikely that a full quantitative account of the all the factors resulting in the differences between model outputs can be given.

In addition, the simulations assume local chemical equilibrium rather than having a kinetic treatment of mineral dissolution-precipitation reactions. The previous models assume changing material properties over time (porosity, hydraulic conductivity, tortuosity) in concrete and grout. The models described by Höglund (2014) include a reasonable set of potential secondary solids, but there is no Mg-silicate (M-S-H gel or a proxy for it) or $Mg(OH)_2$. The models use CEMDATA thermodynamic data (a well-known dataset, based on numerous publications by Lothenbach and co-workers), including discrete end member C-S-H gel approximation. Cement-rock interactions are not being explicitly considered, and minerals that form in rock affected by hyperalkaline fluids (such as feldspathoids, zeolites) are not included.

Modelling of the BHK Vault

The reason for using the iCP framework (COMSOL-PHREEQC coupling, operator splitting approach) rather than a different approach (e.g. fully coupled or globally implicit approach) is not provided. Possible implications of the iCP approach being selected are not provided. For future work supporting a safety assessment, the choice of code and the overall approach used for process coupling should be justified.

The BHK cross-section model (Section 5) excludes cement-rock interaction to simplify the models to reduce uncertainty. The report mentions calcite is expected to precipitate in the bedrock, with porosity reduction, thereby decreasing mass transfer. The exclusion of this process is therefore considered to be conservative in terms of concrete longevity. Although calcite is a likely secondary solid, several other aluminosilicates could also precipitate which could also act to reduce porosity. The potential for advective flow paths to become clogged is not given much attention, whereas this is something that has been widely considered in elsewhere, especially in relation to natural analogues (e.g. Savage 2011).

The overall full chemical system considered is broadly appropriate (calcite, brucite, lower Ca/Si C-S-H, ettringite and gypsum), however the initial concrete composition (taken

from Höglund, 2014) is different to that used in other studies (e.g. Cronstrand, 2014) and this has been noted elsewhere (Metcalfe et al., 2017).

The Höglund composition is based on the reported clinker composition of the cement, with hydrated solids being assigned using the approach outlined by Höglund (1992). Both cement compositions include portlandite and C-S-H, the leaching of which dominates the degradation process and porewater pH evolution. However, the concentration of other primary solids being different could have some implications, possibly for later stage leaching (past the simulation time of the models) that is no longer dominated by portlandite and high Ca/Si C-S-H gel. However, the implications for different hydrated cement compositions are considered by Report R-19-14:

- Anläggningscement (i.e. CEM I 42.5 N – SR 3 MH/LA) with a water / cement (w/c) ratio of 0.47.
- Anläggningscement with a w/c ratio of 0.63 and 320 kg m^{-3} concrete.
- Anläggningscement with a w/c ratio of 0.63 and 280 kg m^{-3} concrete.
- Bascement Slite (i.e. CEM II/A-V 52.5 N) with a w/c ratio of 0.47 and 12.3 wt% fly ash.
- Anläggningscement containing limestone and dolomite addition with w/c of 0.49.

It is not clear whether the solid-solution approach included in CEMDATA for C-S-H was applied to the two compositional end members used in the models. The discrete composition approach provides a reasonable fit to measured cement leaching data, although with "lower resolution" compared with solid solution approaches (e.g. Walker et al., 2016). The primary cement solids in the full chemistry model are said to be like Höglund (2014), but there are some significant differences which are not fully described or discussed.

The identity of secondary aqueous species included in the models is not provided. Presumably, they are automatically considered as in a PHREEQC water speciation calculation?

Several potential secondary solids are included in the model including the following hydrated cement solids: hydrogarnet(OH), monosulfoaluminate, hemicarboaluminate, hydrotalcite(C). These solids are not typically associated with common concrete degradation pathways. The choice of some potential secondary solids is not typical. Presumably, the models consider that hydrotalcite could become richer in carbonate, but the approach to hydrogarnet is not clear. In addition, it is not clear why thaumasite is included as a primary solid and monosulfoaluminate is a secondary solid. The opposite of this would be more typical.

Al-bearing cement solids could be altered to other cementitious solids, but it is noted that Al could also precipitate as zeolites or calcium-aluminium-silicate-hydrate (C-A-S-H) minerals. Also, Mg could precipitate as secondary M-S-H or aluminosilicate minerals. However, reactions involving these solids are probably less important to the overall evolution of concrete and the changes in porosity than those arising due to portlandite and C-S-H gel leaching (and carbonation).

The different modelling assumptions assist in understanding the importance of different process couplings and model assumptions. The approach used to consider heterogeneous flow in the 2-D models is interesting and provides insights into how concrete properties

could vary (noting that distribution of hydraulic conductivity in degraded concrete is unknown, so models are "illustrative" rather than predictive, as the "real" behaviour is not known).

The implications of potential processes that are not included in the simulations, such as rock fracture / concrete crack infilling, should have been discussed. However, the overall picture given by the models is consistent with what would be expected in a concrete repository, with leaching and carbonation processes dominating.

The complexity of the 2-D and 3-D models is impressive, but the lack of mineral dissolution-precipitation kinetics in the models is not justified. There are uncertainties associated with kinetic data for cement solids and possible cement-rock alteration products, but some data exist for key cement solids and many potential secondary minerals, and that analogue approaches can approximate values where data are missing (e.g. Watson et al., 2016; Wilson et al., 2018). The assumption of local equilibrium for all minerals (which will dissolve and precipitate at different rates) would also lead to temporal and spatial variability in alteration paths that may not necessarily be captured using a local equilibrium assumption. This has been observed in models of cement-bentonite interfaces (Marty et al., 2009).

A more in-depth justification for the exclusion of reaction kinetics would have strengthen the report. There is also little justification for the use of the iCP framework (COMSOL and PHREEQC coupling) in preference to other codes. The potential implications of different approaches to coupled modelling are not mentioned (e.g. operator splitting vs global solve). The inclusion of a brief overview of the iCP approach and associated verification and justification of its use for the SE SFL modelling would have be helpful. For future work supporting a safety assessment, a greater justification would arguably be required.

7.2. SKB Report R-19-12: Modelling of concrete degradation – Hydro-chemo-mechanical processes

7.2.1. Background

The work builds on modelling described by Idiart et al on the BHK vault (Report R-19-11), to include a consideration of the effect of chemical processes on the mechanical behaviour of the system. A hydro-chemo-mechanical (HCM) model is developed and implemented in iCP using the previous work as a starting point. The models aim to determine the effect of calcium leaching on mechanical stability using 2-D cross-section representations of the repository. The simulations include an implementation of the regularised mechanical damage model by Mazars (1986) in COMSOL. The effect of sulphate-rich groundwater potential reaching the repository is also assessed, as sulphate attach may result in expansion due to precipitation of sulphate-bearing minerals in the cement matrix. Both leaching / carbonation and sulphate attack are major concrete / cement alteration pathways, and it is appropriate for these to be considered in the models.

7.2.2. Approach

Regarding sulphate attack, the potential for the formation of ettringite and gypsum is identified, and the potential for thaumasite formation is also discussed. Possible implications related to volume changes and stresses in concrete are also discussed. The report notes the issue of expansion in laboratory studies not being representative of that occurring under field conditions where the material is subject to significant loading. The report also discusses coupling between damage and transport properties (e.g. Archie's Law, Kozeny-Carmen equation). As noted by Report R-19-12, the impact of mechanical damage on transport properties is not straight forward, given that permeability and diffusivity are functions of the level of micro-and macro-cracking of concrete with transport properties being influenced by crack patterns, which in turn are related to the type of loading (compressive / tensile, thermal, drying and shrinkage etc.). The authors note several studies of the impact of mechanical damage on water and especially gas permeability, with data then being used to determine intrinsic permeability and then water permeability values. Report R-19-12 notes that that data on effective diffusion coefficient values and mechanical damage are limited, but that two relationships have been used in previous modelling work, but that they have not been derived from experimental data.

In short, the authors are aware of the processes and limitations associated with the available data.

The models described in Report R-19-12 include fluid flow, solute transport, chemical reactions, and mechanical deformations. Several simulations were produced to explore implications of model input assumptions and process coupling on model outputs. The calcium leaching HCM models consider the coupling between porosity and transport properties (effective diffusion coefficient, hydraulic conductivity) but the impact of mechanical damage on transport is not considered. The base case model (500m deep repository, oriented in direction of major horizontal stress) suggest that mechanical damage is only likely to occur at the corners of the concrete backfill at the corners of the waste domain. Chemical degradation close to the rock results in softer material with a higher capacity to sustain deformations from the rock, which may have a positive effect on the intact concrete. A series of other cases are presented, however, even under the most adverse conditions, mechanical damage (varying between 0 and 1) is localised near waste domains and is < 0.1 suggesting that the mechanical stability of the repository is not compromised. The impact of mechanical processes on hydraulic conductivity and diffusion and therefore chemical degradation, is not significant, except for glacial-induced stresses at 700 m or a case where there is a very low rock stiffness.

Models of sulphate attack consider one-way coupling (mechanical calculations use reactive transport outputs) and full coupling of mechanical damage and sulphate attack. It is noted that there are uncertainties in model parameterisation with implications of sulphate attack measured under laboratory conditions not accounting for loading of the solid. The authors note that ettringite data on expansion are applied to thaumasite given a lack of measured laboratory data. The simulations show localised expansion due to sulphate attack (assuming higher potential concentrations of dissolved sulphate that may arise). The effect of groundwater flow leads to asymmetric damage. The models suggest that no regions are subject to tensile stresses throughout the simulated time (100,000 y). The fully coupled model increased the degradation rate compared to the one-way case with complete chemical degradation after 14,500 y in one region and by the end of the simulation,

sound concrete is only observed in the innermost metre of the backfill. However, as recognised by the authors, the assumptions associated with the model are numerous and subject to significant uncertainty.

7.2.3. Summary of Review Findings

Overall, the report includes a thorough review of available data on the chemical concrete degradation phenomena and potential mechanical implications.

The results of chemical degradation can be used to determine potential mechanical damage using an existing mechanical modelling approach.

Coupling of mechanical and chemical processes (which is the same as those used in previous models) is a complex, non-trivial task and the authors appear to have made significant progress in their efforts. However, as they note themselves, there are significant uncertainties associated with the models.

Note that the approach for C-S-H gel is the same as in Report R-19-11, namely two discrete C-S-H compositions from CEMDATA are used. In the CEMDATA database, C-S-H is considered as a solid solution, it is not clear whether a solid-solution approach was applied in the work described in Reports R-19-11 and R-19-12.

Further review of the mechanical aspects of the report by an expert in this subject area is recommended; both the reviewers are experts in chemical aspects.

7.3. SKB Report R-19-13: Modelling of Concrete Degradation in a One-million-year Perspective - Hydro-Chemical Processes

7.3.1. Background

The report describes 1-D reactive transport models of concrete degradation in BHK (rock vault in proposed SFL repository concept). The "iCP" software (Nardi et al., 2014) has been used to generate models in which there is the coupling of chemical processes simulated in PHREEQC with physical processes simulated using COMSOL. The focus of the work is on evaluating porosity, effective diffusivity, and hydraulic conductivity of the BHK concrete over a 1-million-year timespan. The values of porosity, effective diffusivity, and hydraulic conductivity of the concrete are used in safety evaluation calculations (Shahkarami, 2019).

7.3.2. Approach

The modelling considers groundwater flow representative of the horizontal flow across the backfill. The conceptual model is based on Case 1 (base case) in Report R-19-11. A comparison with analytical solutions based on a shrinking core model (Levenspiel, 1972) and previous results of 2D reactive transport simulations (Report R-19-11) is made.

As outlined by Report R-19-13, the radionuclide transport model using in the SE SFL safety evaluation requires the following time-dependent properties for concrete and outer and inner backfill: pH, porosity, effective diffusivity, hydraulic conductivity. The values required led to the following approach:

- The evolution on the left side of the waste domain provides representative parameters for entire out and inner backfill (most degraded region)
- The diffusion coefficient and hydraulic conductivity correspond to values obtained using a series model, separately over the inner and outer backfill.
- Local values are calculated.
- Porosity and pH values are calculated based on the weighted mean at different distances from the backfill outer boundary.

The equivalent effective diffusion coefficient resulting from 1-D reactive transport modelling is calculated over 1 million years, using the equation:

$$D_e^{eq} = \frac{L}{\int_a^b \frac{1}{D_{e(x,t)}} dx}$$

Where $D_{e(x,t)}$ is the local effective diffusion coefficient, a (m) and b (m) correspond to the x coordinate of the boundaries where the integration is calculated, and L (m) is the calculated backfill thickness (b-a). Thus, L is 1.4 m for the control volumes (thickness of inner and outer backfill) and 2.8 m for the complete backfill. A similar approach is used for hydraulic conductivity. Porosity is calculated using the equation:

$$\varphi = \frac{\int_a^b \varphi(x,t) dx}{L}$$

And pH is calculated using:

$$pH = \frac{\int_a^b pH(x,t) dx}{L}$$

The parameterisation of the model is the same as that of the base case (case 1) in Report R-19-11. Porosity can evolve in the model due to dissolution and precipitation of solids affecting hydraulic conductivity and effective diffusion coefficient. The models assume chemical equilibrium. The reason for this approach and the potential implications of not including reaction kinetics are not discussed (see review in Report R-19-11).

The input groundwater data, mineral assemblage and potential secondary solids are the same as in the previous modelling work (they include lower Ca/Si C-S-H gel, monocarboaluminate, OH-hydrogarnet, monosulfoaluminate, calcite, brucite, hemicarboaluminate, gypsum, hydrotalcite(C), and SiO_2(am). The primary cement solids are the same as in the previous work reported in Report R-19-11, based on Höglund (2014). Alkali species (KOH, NaOH) are modelled using the ion exchange approach as in Report R-19-11.

As noted for Report R-19-11, there are some significant differences between the primary cement solid assemblage in the concrete and the source reference that is based on Höglund (2014).

Similar to Report R-19-11, some of the potential secondary cement solids are a little unusual. However, the main degradation pathway (leaching, carbonation) is not affected by this, as the primary degradation path is portlandite dissolution and C-S-H leaching. Note that Cl-attack and possible evolution of groundwater salinity are not considered. Hydraulic conductivity is coupled to porosity using the Kozeny-Carman relationship. The effective diffusion coefficient is coupled with porosity using Archie's law (exponent n = 2.5). These are standard approaches. The exponent results in effective diffusion (D_e) reduction not being a linear function of porosity, which is an assumption that some workers have used elsewhere.

The porosity of the concrete is 0.11, D_e = 3.5 x 10^{-12} m^2 s^{-1}, K_0 = 8.3 x 10^{-10} m s^{-1} (from Report R-19-11, from Pękala et al., 2015, which is taken to be consistent with Höglund, 2014). These are like values given for "structural" concrete (e.g. SFR vault database has structural concrete values as follows: porosity = 0.125, D_e = 2.5 x 10^{-12} m^2 s^{-1}, K = 9.5 x 10^{-11} m s^{-1}, Savage and Stenhouse, 2002). The hydraulic conductivity of concrete with penetrating cracks could be higher (possibly ~10^{-8} m s^{-1} (e.g. Höglund and Bengtsson, 1991; Skagius et al., 1999).

The spatial discretisation included equally spaced, 0.1 m - long finite elements (28 elements in total). There is limited discussion on this assumption. The approach used to set time-stepping between COMSOL and PHREEQC is like that described in Report R-19-11. The authors describe how two criteria are used to set up step size, considering the Von Neumann criterion for preventing numerical oscillation, the second is the Courant number (time step size to be much smaller than the time for water to travel to adjacent grid points). The initial Peclet number is ~75 suggesting a larger contribution of advective solute transport, but diffusion is non-negligible.

The boundary conditions for solute transport are fixed at the "left boundary" (groundwater interface) and a no concentration gradient is applied at the right boundary. A constant hydraulic head gradient is applied in the model to give an initial Darcy flow of 1.03 x 10^{-11} m s^{-1}. As degradation proceeds, the hydraulic conductivity gradually increased from left to right (thereby increasing Darcy velocities).

7.3.3. Results

The results include dissolution of primary Portlandite and ettringite followed by C-S-H decalcification, as is typical for cement degradation. After portlandite dissolution, other primary solids dissolve and there is the precipitation of calcite and hydrotalcite-C. There is almost the complete degradation of cement after 1 million years. The "inner backfill" is virtually unaffected for the first 100,000 y, with only alkalis (NaOH, KOH) leaching. However, the outer backfill by this time had undergone significant portlandite dissolution over a thickness of 1m. Complete portlandite dissolution occurred by 180,000 y in the outer backfill. This occurs by 340,000 in the inner backfill. Complete dissolution of C-S-H in the outer backfill only occurs after ~800,000 y.

Porosity increases from 0.11 to ~0.3 due to dissolution of primary solids, with an increase to 0.3 representing a complete loss of cement paste from the concrete (the rest being aggregate which is assumed to be chemically inert).

The report states that the increase in porosity reported did not account for calcite precipitation, which is a conservative assumption. It would have been useful to have porosity values that included calcite precipitation. Plots showing volume fractions of solids over space and time are given and it appears that the volume fraction of calcite is as high as ~0.14 at ~0.2 m into the concrete from the interface with the rock (upstream side of the modelled domain).

In determining the likely evolution of the system, the precipitation of calcite is an important finding, even if the porosity (and other transport parameter values linked to it) are not assumed to be affected in radionuclide transport calculations. A clearer picture of expected evolution assists in making decisions when parameterising radionuclide transport calculations and introducing assumptions that are intended to introduce a degree of caution.

On a related note, if porosity clogging were investigated further, a consideration of the approach to spatial discretisation would be required. Note that approaches to both reaction kinetics and mesh refinement can affect model outputs (e.g. Marty et al., 2009).

The evolution of pH, porosity, effective diffusivity, and hydraulic conductivity of concrete in the outer and inner backfill are reported using the post-processing approach previously described. Concrete porewater pH decreases from 13 to 12.5 after leaching of alkalis, after ~10,000 y in both domains. After 1 million years, pH in the outer backfill is ~8.6 (close to groundwater value), the inner region has a pH of ~9.8 by this time.

Changes in porosity are also given, with steady increases in both regions (calcite precipitation effects therefore not represented). The same is true for effective diffusion coefficients and hydraulic conductivity.

The model outputs are compared with previous 2-D reactive transport models (Report R-19-11) and analytical solutions. There are some differences between the 1-D and 2-D models which used different discretisation (triangular elements ~0.6 m in 2D model vs. 0.1 m spaced elements in the 1-D model). This resulted in relatively slower degradation in the 1-D model. It is also noted that the Darcy velocity varies to a degree in the 2-D model whereas it is all in the same direction in the 1-D model. The analytical Shrinking Core Model (SCM) is compared to the models, with a poor fit to 1-D models and a reasonable fit to 2D model data. It is noted that in the 1-D model the constant increase in Darcy velocity with time leads to an advective-dominated degradation process (constant head gradient boundary condition). The 2-D models show a more diffusive-dominated degradation over the first 100,000 years.

7.3.4. Summary of Review Findings

Overall, the modelling is consistent with approaches used elsewhere, except for the exclusion of dissolution-precipitation kinetics (see comments on previous reports)

The rate data for cement solids are not extensive, but values do exist and have been used in other studies. The implications of reaction kinetics are not considered and discussion on the implications of the approach is lacking.

There are some issues surrounding the justification of the primary hydrated cement solid assemblage (as in previous work by the authors).

A clearer presentation of porosity evolution both with and without secondary calcite precipitation and a discussion on expected evolution and that which may be assumed in radionuclide transport calculations may have been useful.

7.4. SKB Report R-19-14: Modelling of Concrete Degradation - Influence of Concrete Mix Design

7.4.1. Background

The concrete composition considered in models of the BHK vault of the SFL repository were assumed to be the same as that in the SFR repository (Report R-19-11). Alternative compositions have also been identified, and their performance assessed using 1-D and 2-D models.

Models were used to predict the hydrated cement solid assemblage, with thermodynamic models coupled to the kinetically controlled dissolution of cement clinker and mineral additions (where present).

The different concrete compositions include:

- Anläggningscement (i.e. CEM I 42.5 N – SR 3 MH/LA) with a w/c ratio of 0.47.
- Anläggningscement with a w/c ratio of 0.63 and 320 kg m^{-3} concrete.
- Anläggningscement with a w/c ratio of 0.63 and 280 kg m^{-3} concrete.
- Bascement Slite (i.e. CEM II/A-V 52.5 N) with a w/c ratio of 0.47 and 12.3 wt.% fly ash.
- Anläggningscement containing limestone and dolomite addition with w/c of 0.49.

Modelling of cement hydration used data and an approach that is more up to date than those used by Höglund (2014). The effect of the water-to-cement ratio is also discussed. The composition of each hydrated assemblage is used in reactive-transport models using the same approach as those of Report R-19-11 and Report R-19-12. The report describes 15 numerical models of the BHK vault using 1-D and 2-D geometries.

7.4.2. Literature Review

A literature review is provided on how the different mix designs are expected to alter the chemical and physical properties of the concrete and this is used to suggest initial transport properties of the intact composition for each mix.

The review of the effect of adding fly ash to Portland cement clinker appears thorough. A minor observation is that the section on sulphate attack (last part of 3.1, page 24) lacks references to sulphate attack processes and is somewhat brief.

The review of the effect of limestone addition on OPC and fly ash (FA) blended cement appears thorough. However, Section 3.2.1. on workability and bleeding lacks references. The consideration of water-to-cement ratio on concrete properties appears thorough. Table 3-6 is an especially useful summary for the reader.

7.4.3. Thermodynamic Modelling of Cement Hydration

Recent advances in the thermodynamic modelling of cement hydration are outlined. It is noted that rates of clinker dissolution and supplementary materials are included in models with the assumption that precipitation of hydrated cement solids is much faster and as such, an equilibrium assumption can be made.

Dissolution rates of clinker are taken from Parrot and Killoh (1984) which have been applied in other studies of cement hydration, as stated in the report. Numerical calculations were undertaken using PHREEQC and the CEMDATA07 database (which has been used in many previous studies).

It is noted that there are relatively few data on the nature of hydrated cement blends that include limestone and dolomite. A wide compositional range of potential hydration products is included in the models including C-A-S-H and M-S-H (Table 4-8) considering possible solid solution behaviour. The behaviour of alkalis is considered using an ion-exchange approach which is reasonable and consistent with previously published studies (e.g. Savage et al., 2011a).

A verification of cement hydration modelling included replicating hydration calculations by Lothenbach and Winnefeld (2006) for OPC. The authors consider that there is good agreement of their results with the previous work and consider sources for the relatively minor differences (given the chemical complexity of the models). The inclusion of this model provides a degree of confidence for the "blind" models of concrete hydration. The models of CEM1 and CEMII hydration produce sensible results which agree with previously published models. Likewise, the cement with added limestone and dolomite.

7.4.4. Reactive Transport Modelling

Five concrete compositions from thermodynamic modelling are considered. The conceptual models used are like those in previous studies (Report R-19-11; Report R-19-13).

To simplify the models, hydrated iron-bearing solids are not included given previous issues of convergence and solid-solutions are simplified into single dominant solids. C-S-H and C-A-S-H compositions are not changed.

Secondary solids allowed to precipitate include: brucite, CAH_{10}, hydrotalcite-C, tricarboaluminate, C_4AH_{13}, C_2AH_8 straetlingite, syngenite, thaumasite, dolomite and SiO_2(am). Calcite is not listed (Table 5-4) but appears to be in the models (it is a primary solid in one concrete composition).

Calcium aluminates and straetlingite are reasonable cement potential alteration products, the inclusion of carbonate-bearing cement solids is reasonable, although calcite is generally assumed to be the main product of hydrated cement reacting with dissolved carbonate in groundwater. Brucite is a reasonable choice of solid considering the potential for Mg-attack, other solids such as M-A-S-H or M-S-H could also have been considered, and possibly Mg-rich clays (which have been considered as possible late-stage products of leaching elsewhere, e.g. Wilson et al., 2018). Syngenite can occur in K-rich systems but is possibly less relevant.

The report states that calcite clogging could lead to sealing which may not be a conservative assumption. It is useful that the models consider the difference in results where calcite can clog porosity (and therefore reduce solute transport) and a case where calcite clogging is considered. The inclusion of clogging (which does seem to be a real effect as far as can be ascertained from analogue and some experimental data) should be considered. Understanding the potential for this process is useful, as it provides an argument that excluding mineral precipitation in calculations of degraded concrete matrix porosity for radionuclide transport is likely to be cautious (all else being equal).

The 2-D model for case 1 (100,000 y run time) show similar concrete degradation compared with previous models described in Report R-19-11, with a mineral dissolution front that moves into the concrete from the concrete-rock interface upstream of the direction of water flow. Primary portlandite, jennite-like C-S-H and OH-hydrogarnet dissolve, tobermorite-like C-S-H precipitates (lower Ca/Si) but there is loss of C-S-H at the interface with the rock. Monocarboaluminates and monosulfoaluminates are dissolved completely upstream, but OH-hydrogarnet remains stable after 100,000 y and a small amount precipitates near the interface with the rock. Ettringite and straetlingite (C-A-S-H mineral) precipitate as secondary solids, followed by thaumasite and calcite.

This is an interesting reaction sequence, and the choice of primary solids is much better constrained than in the initial work reported in Report R-19-11. It would be interesting to see how the inclusion of reaction kinetics (even with some approximate values) affect the temporal / spatial patterns of alteration. It is noted that without calcite precipitation, the porosity in leached zones would be increased from 0.11 to 0.3, which is the maximum possible in the simulation (presumed inert concrete components, i.e. aggregate and sand, comprise a volume fraction of 0.7).

The pH in the model decreases from 13.33 to 12.5 due to alkali leaching in unaltered areas, whereas at the concrete-rock interface upstream, it decreases to 8.5 (i.e. that of intruding groundwater). Maximum calculated values for effective diffusivity and hydraulic conductivity at the concrete-host rock interface are: $D_e = 4.5 \times 10^{-11}$ $m^2 s^{-1}$, $K = 2.9 \times 10^{-8}$ $m\ s^{-1}$. The D_e and K values are similar (within an order of magnitude) compared to Stage (III) degraded structural concrete in the SFR assessment that has a porosity of 0.25 (Savage and Stenhouse, 2002).

Case 2 considers the same cement as Case 1, but with higher w/c ratio (0.63 rather than 0.47) and two cement clinker proportions in the concrete mix. The degradation of concrete in these two variant cases is remarkably similar to that seen in Case 1, but smaller amounts of cement hydrate lead to increase values in transport properties and an increased rate of degradation. The differences between the two variant cases are small. The model that includes cement with fly ash addition (Case 3) shows the significant formation of C-A-S-H (high Ca/Si) with less straetlingite. Ettringite forms to give larger volumes than case 1, along with a small amount of thaumasite.

In Case 4, the significant replacement of cement with limestone (26.9 wt.%) and dolomite (6.9 wt.%) in the concrete mix results in calcite being present as a primary cement solid. In this case, the portlandite dissolution front advances into the concrete at a slower rate with porosity increases being less marked than in the other cases.

The 1-D model for Case 1 (1-million-year timescale) shows primary solid dissolution and calcite precipitation which is extensive near the upstream interface (up to ~0.23 vol fraction at ~0.2 m depth) with rock and small volumes forming further away after several hundreds of thousands of years. After 1 million years there is completely degradation of the concrete with only a small fraction of tobermorite-like C-S-H in the last 0.5 m. Small amounts of hydrotalcites and brucite also remain. The pH decreases to ~12.5 due to alkali leaching before 100,000 y. After portlandite is lost, pH ~10.5 due to lower Ca/Si C-S-H and then once this is lost, the pH is that of intruding groundwater. Porosity increases with the movement of the dissolution front downstream from the concrete-rock interface, after 1 million years, the concrete has a porosity of 0.29 except for last 0.5 m where it is 0.21. Maximum $D_e = 4.5 \times 10^{-11}$ $m^2 s^{-1}$ and maximum $K = 2.9 \times 10^{-8}$ $m\ s^{-1}$. Minimum D_e and K values downstream boundary are 1.9×10^{-11} $m^2 s^{-1}$ and 7.9×10^{-9} $m\ s^{-1}$, respectively. These values are broadly like those given elsewhere (e.g. Savage and Stenhouse, 2002).

The Case 2 1-D model shows similar results compared to Case 1, but with variation in the timing of the advance of the degradation front. In Case 3 (fly ash addition), a slower rate of degradation occurs, after 500,000 y, jennite-like C-S-H is still present in the inner backfill (upstream) and there is still some portlandite in the last few centimetres of the model domain. After 1 million years a significant amount of low Ca/Si C-S-H and C-A-S-H gels remain in the inner backfill (pH ~ 10.5). The loss of portlandite occurs 100,000 y later than in Case 1. In Case 4, the replacement of limestone with dolomite results in a decreased rate of degradation occurs, with thaumasite precipitation occurring (volume fraction up to 0.07) and less straetlingite precipitation. In Case 4, pH = 12.5 -12 for the whole duration unlike Case 1, in which pH of groundwater values occurred. Values of D_e, K, porosity, and Darcy velocity are provided for inner and outer backfill regions (at points and spatially averaged) for each case. Péclet numbers show that the simulations are initially dominated by advection and that the relative impact of diffusion over advection increases with time (as porosity increases). However, advection dominates throughout.

Overall, the variation in cement composition does not have a significant effect on performance over 100,000 y (2-D models) and degradation is not extensive. The depth of the alteration front is sensitive to concrete composition, but the key factors appear to be initial porosity and transport properties.

The 1-D models (1-million-year timescale) show greater differences in terms of depth of alteration front. In all cases, the full thickness of the concrete backfill is nearly completely degraded with calcite precipitation being extensive. The addition of limestone filler to the concrete mix results in best performance which appears to be a result of an initially lower porosity compared with the other concrete compositions.

7.4.5. Summary of Review Findings

The review on the properties of the alternative cement compositions is thorough.

The review of cement hydration processes and model approaches is thorough.

The models of cement hydration use recognised published thermodynamic data and the results look plausible. The hydrated cement compositions are used in reactive-transport simulations.

The reactive transport simulations do not include kinetics but have relevant process couplings. Clogging is discounted in outputs of porosity (and coupled transport parameters – D_e, K).

Overall, the modelling looks reasonable, but the report would have been improved by more discussion on the choice of thermodynamic data and possible implications / justification for excluding reaction kinetics in reactive transport simulations.

The potential evolution of large cracks / fractures (including clogging with secondary solids) is not discussed here, but it is noted that the nature of secondary mineral formation is such that large volume expansion due to sulphate attack seems unlikely.

7.5. SKB TR-19-03 Initial State for the Repository for the Safety Evaluation SE-SFL

It is stated in Section 7.3.5 that the grout composition has not been decided on, but an example from SFR is given (Table 7-8). The grout appears to comprise the same cement as the concrete (Portland cement) and Sika Plastiment, but no pozzolanic material. It is unclear if there has been a consideration of whether the assumed grout will fill voids adequately in the BHK waste vaults. Other repository systems have adopted compositions that include pozzolanic material (e.g. fly ash or blast furnace slag) to give the required properties. There could be interactions between the cement present in the grout present on the top of containers / filling voids between waste drums and the cement component of the concrete backfill. However, it seems unlikely that the reaction of these two cementitious materials would have greater implications than the leaching and degradation of cement paste present in the concrete backfill by intruding groundwater.

The choice of grout in the BHA vaults may have implications for future investigations of cement-bentonite interactions if the cement includes additives which are not present in the cement component of the concrete backfill.

7.6. SKB R19-09: Input Data for Radionuclide Transport

Porosity in the BHK concrete is taken from Figure 6-8 of Report R-19-13 (1-D model output data). The values are summarised in Table B-2 of Idiart and Laviña (2019) **"**with minor modifications**".** However, it is not clear what these modifications are.

The effective diffusivities in the BHK compartments depend on concrete degradation state and values are taken from Report R-19-13, Table B-2. Values are required for intact backfill, inflow compartments, outflow, and side compartments (Table 2-34).

The two datasets appear consistent.

Table 2-34. Effective diffusivities in the BHK backfill compartments during the repository evolution.

Compartment	Effective diffusivity [m²/s]	Timeframe [a]
BHK – Intact concrete backfill	3.50E-12 – 3.71E-12	2.08E+03 – 1.72E+05
BHK – Inflow compartment	3.50E-12 – 1.15E-11	2.08E+03 – 1.72E+05
BHK – Inflow compartment	1.15E-11 – 3.74E-11	1.72E+05 – 7.82E+05
BHK – Inflow compartment	3.74E-11 – 3.86E-11	7.82E+05 – 1.00E+06
BHK – Outflow and side compartments	3.71E-12 – 1.29E-11	1.72E+05 – 3.92E+05
BHK – Outflow and side compartments	1.29E-11 – 1.44E-11	3.92E+05 – 7.82E+05
BHK – Outflow and side compartments	1.44E-11 – 2.27E-11	7.82E+05 – 1.00E+06

Table B-2. Porosity and effective diffusion coefficient representative values for inner and outer backfills. Values tabulated for each leaching event.

Time (years)	Porosity outer backfill	Porosity inner backfill	D_{ef} (m²/s) outer backfill	D_{ef} (m²/s) inner backfill	Leaching event
0	0.11	0.11	3.5E−12	3.5E−12	Initial values
170 000	0.18	0.11	1.5E−11	3.71E−12	CH in outer b
390 000	-	0.19	-	1.29E−11	CH in inner b
780 000	0.28	0.20	3.74E−11	1.44E−11	C-S-H in outer b
1 000 000	0.29	0.24	3.86E−11	2.27E−11	Final values

7.7. Summary of the Review of Chemical Modelling of Concrete in the BHK Vaults (SKB Reports R-19-11, R-19-12, R-19-13, R-19-14)

Initial benchmark modelling of previous work by Höglund (2014) on SFR provides added confidence in subsequent modelling for SE-SFL (BHK vault) using the iCP approach.

Little information on the iCP approach (COMSOL-PHREEQC coupling) is provided in the reports and they do not include a justification of why it was used in preference to other codes or types of coupled-model approaches. In addition, there is no discussion in the reports on the different approaches available for coupled process modelling (e.g. sequential vs. globally implicit) and the implications of using one approach in preference to another. There needs to be some discussion on this in future work that supports safety assessments. A little more background on the iCP approach would have been useful.

The initial BHK vault modelling (R-19-11) used assumptions from Höglund (2014) to specify initial hydrated cement solid assemblage. The approach is based on the approach by Höglund (1992). Much work has been undertaken which supersedes this. However, thermodynamic models of cement hydration are used to improve the initial hydrated cement composition and to consider hydrated compositions of other cement compositions. These are then modelled in Report R-19-14. The review of cement hydration and subsequent modelling is very thorough, and the simulations presented in SKB R-19-14 cover a range of possible hydrated cement compositions.

The geochemical modelling does not include a representation of dissolution-precipitation kinetics. For the very spatially complex models (2-D and 3-D), this presumably reduces model complexity. However, published papers of cement degradation and cement-rock interactions typically include some consideration of reaction kinetics, even though the data available for modelling are somewhat limited, and analogue estimation approaches

must be used for many solids. The implications of assuming local equilibrium rather than adopting a kinetic treatment, are not clear. This is an aspect of the modelling where further consideration may be useful.

There is a lack of discussion on reasons for the selection of secondary solids in the models, those in R-19-11 in particular, are a little odd. However, the main concrete degradation pathway of leaching (and carbonation) is included along with the potential for sulphate attack which is considered in SKB reports R-19-12, R-19-13, and R-19-14. The modelling mostly includes one groundwater composition (dissolved Cl concentration of 4.5×10^{-3} M), there is no consideration of potential variation in salinity (noting that in in more saline systems, Friedel's salt may form as an alteration product – this was seen as a minor secondary solid in SFR modelling). Friedel's salt is a Cl-bearing solid ($Ca_4Al_2Cl_2O_6 \cdot 10H_2O$) that can form in saline cementitious systems. It tends to result in cement porewater pH being buffered at ~13 (e.g. Wilson et al., 2017a, 2018), which could have implications for contaminant behaviour.

The 3-D geochemical models are impressive. They show the behaviour that would be expected to occur but are not directly used to generate inputs for safety evaluation calculations. However, the comparison of 1-D models with 2-D and 3-D models is interesting, as they show how model assumptions result in relatively small differences in predicted evolution of the concrete backfill.

1-D models are used to calculate "inner" and "outer" concrete zone hydraulic properties, including porosity, hydraulic conductivity, and effective diffusion over a 1-million-year timescale. The data are then used in radionuclide transport calculations. The models include a standard approach for the coupling of porosity to effective diffusion and hydraulic conductivity. In the calculated outputs, it is assumed that secondary solids such as calcite do not contribute to porosity evolution, thereby ensuring that porosity increases over time, with no reduction due to carbonate precipitation. It is stated that this is "conservative", which is probably the case in terms of solute transport through the backfill. However, a clearer comparison of "with" and "without" calcite cases would be useful, as would a clearer discussion on the expected repository evolution and the assumptions made in radionuclide transport calculations. This helps remove any indication of bias in the modelling approaches.

The potential for fractures at rock-concrete interfaces to become clogged with secondary solids is not mentioned, even though this is a phenomenon that could, to some extent, reduce water flow through the BHK vault.

The observed concrete degradation pathways (mostly leaching and carbonation, and a degree of sulphate attack) are consistent with known cement degradation pathways. However, the potential for Cl attack, which is also likely to be of less importance than leaching / carbonation, is not considered.

It is suggested that a hydraulic cage could develop in the BHK vaults due to loss of cement solids and porosity increase. However, the porosity increase could be counteracted, to a degree, by calcite precipitation in the "upstream" regions of advective flow. The potential for clogging of fractures in host rock and formation of secondary solids at the cement-rock interface needs to be considered in the analysis of hydraulic cage development. It is not clear whether the hydraulic cage would form if there was some porosity reduction due to secondary solids precipitating.

Porosity, effective diffusion, and hydraulic conductivity data from 1-D models simulating 1 million years are used to calculate averaged "inner" and "outer" backfill values to be used in radionuclide transport calculations as part of the safety evaluation. In a more developed safety assessment, further discussion would be needed to justify the direct use of the these calculated values, including associated assumptions, likely bounds of uncertainty and a qualitative statement of associated conservatisms and implications of processes that were not explicitly simulated (such as cement-rock interactions, the potential for clogging of fractures, concrete cracking behaviour, the potential for crack healing due to secondary mineral formation, implications of calcite precipitation in some concrete regions etc).

The potential effects of waste containers and grout present on the concrete backfill do not appear to have been considered. The possibility of Fe from container corrosion impacting cementitious materials has been considered elsewhere and it is unlikely to lead to any issues (Metcalfe et al., 2017). The current grout composition considered in the safety evaluation includes the same cement as the structural concrete. If a different grout is used, there could be some interaction between the two cementitious materials, but this is unlikely to be very important compared with the bulk evolution of the concrete backfill due to leaching and degradation caused by intruding groundwater.

7.8. SKB Report TR-19-01: Treatment of Bentonite Evolution in BHA Vaults in the SE SFL Safety Evaluation

7.8.1. Repository Design

In the executive summary (page 10) and Section 4.3.2, it is stated that compared to the BHK vault, the BHA vault is designed for low activity but less well-known material compositions and radionuclide inventory. The waste vault comprises a concrete structure in which waste is deposited and grouted. This is surrounded by a thick layer of bentonite with high dry density and the top of the vault is to be filled with bentonite pellets. The bentonite is assumed to have similar properties to the buffer material in the Spent Fuel Repository.

The radionuclide transport calculations show that BHA is very efficient for retaining radionuclides with C-14, Mo-93 and Ni-59 activities reducing significantly in the near field and for the long-lived radionuclides Tc-99 and Cl-36 a substantial part decays in the near field (pg. 16).

The choice of materials is understandable, but it is not clear from the safety evaluation (TR-19-01) whether options assessment / optimisation work was undertaken to specify the materials present and their quantities in the BHA vault.

7.8.2. Safety Functions

Section 5.2, page 86 states that for the bentonite barrier of BHA, the following safety functions and associated indicators (in parentheses) are identified:

- low flow in the waste vault (hydraulic conductivity); and
- good retention (diffusivity, available sorption surface area).

Low flow in the waste vault implies that the hydraulic conductivity of the bentonite barrier needs to be limited to make diffusion the main transport process. Good retention is maintained if the diffusivity is low, and the area available for sorption is high.

The low hydraulic conductivity of bentonite and transport being diffusion-limited are the properties that result in bentonite being chosen as a barrier material.

Page 87 states that:

"*In the FEP processing, it is stated that mechanical processes in the BHA barriers are not considered in SE-SFL. Consequently, no quantitative mechanical analysis of the bentonite barrier is performed within SE-SFL. Mechanical processes in the bentonite could however influence the post-closure performance of BHA and should be considered in subsequent safety analysis*".

The reviewers agree that a mechanical analysis may be required in future work.

Page 87 further states that:

"It is also noted that phase changes / freezing is not considered since it is assumed that the depth of the repository is chosen to avoid permafrost. The production of gas is likely to be small in BHA and therefore no safety function related to gas is associated with the bentonite barrier in BHA. Since colloid transport is not considered in SE-SFL the capacity of the bentonite to filter colloids is not included as a safety function indicator related to good retention. If colloid transport in future analysis should show to be of importance, such a safety function indicator could be considered".

It is agreed that the potential for colloid formation will need to be considered in a more detailed safety assessment.

The safety functions for both BHK and BHA include low flow in the waste vault and good retention. For BHK, the additional properties of high pH and low redox conditions are noted.

7.8.3. Bentonite Performance

In Section 6.2.9 (page 108 to 112) the potential evolution of the bentonite is considered, including the saturation of the bentonite from its initial unsaturated state. It is recognised that this saturation may be heterogeneous. The potential for piping and erosion is also noted, but it has not been considered in detail. However, a simple calculation is given (Appendix 1) based on the empirical formula by Sandén and Börgesson (2010). It is calculated that the cautiously estimated maximum loss of bentonite is about 7230 kg for piping from a single fracture, which is a volume of ~4.7 m^3, or <0.01 % of total backfill volume. Although several fractures could be present (10 fractures would result in ~16,180 kg total loss) local erosion is considered to be more problematic than global effects. As the small amount of bentonite loss expected per fracture is small, it is unlikely that erosion via piping would have a significant impact on bentonite performance. However, bentonite erosion processes are complex and difficult to model in a mechanistic way. Work

has been ongoing on the issue of bentonite erosion (e.g. BELBaR project), and it would be prudent to consider erosion in more detail in future work.

The evolution of swelling and swelling pressure is described, including consideration of processes of backfill homogenisation, the mechanical interaction between backfill and waste, movement of waste compartment inside the vault and homogenisation after the loss of bentonite mass. The need to consider homogenisation processes and mechanical properties in future safety assessments has been recognised.

The potential for bentonite-groundwater interaction resulting in ion exchange is noted (Ca replacing Na in smectite interlayers after resaturation) but it is considered that complete equilibrium is unlikely to be reached due to a large amount of bentonite porewater and small expected groundwater flows. It is stated that the composition of the exchanger will have a limited effect on the hydro-mechanical properties of the bentonite as long as the target density is met. It is noted that processes such as ion exchange (and the dissolution-precipitation behaviour of accessory minerals) might need to be reconsidered in future analysis. For a more detailed safety assessment, it would seem reasonable to expect the potential changes to bentonite swelling arising due to ion exchange to be considered. Calculating exchange composition and examining bentonite properties for different dominant smectite interlayer cations is not challenging.

The potential for bentonite alteration to occur due to groundwater interactions is not mentioned in the section on bentonite-groundwater interactions, but some consideration is given to it in the section on bentonite-waste package interactions. It is noted that smectite in natural sediments undergoes illitisation, but that temperatures are unlikely to be high enough for this to occur over a 1-million-year timescale in the repository. The available evidence does indeed support this assertion. However, other bentonite alteration pathways are possible, although the extent of alteration is likely to be minor. For example, water with significant dissolved Mg could, in theory, result in the alteration of montmorillonite to saponite (e.g. Wilson et al., 2017b). A preliminary analysis shows that the granitic groundwater composition used in cement modelling (Table 4-2 of report R-19-13) has solute activities that coincide with saponite stability fields (Figure 6). The water composition is oversaturated with respect to gibbsite (saturation index of 0.5), and close to quartz saturation (saturation index of -0.1). As stated by Wilson et al., (2017b), the replacement of montmorillonite by saponite, should not result in significant loss of swelling capacity, but there could be small changes if the later charge associated with the altered smectite is different to that of the primary montmorillonite.

The potential for bentonite to react with concrete components is noted by SKB and potential cement-bentonite interactions are being considered in a modelling study (not completed at the time of production of TR-19-01) which considers alkaline cement porewater reacting with montmorillonite, the dissolution of which, is going to be simulated using a kinetic approach. It is stated that cement solids are being simulated using a local equilibrium approach. As with the concrete modelling, there are kinetic data available for some cement solids and potential alteration products, and why they should be discounted is not clear.

As outlined in Section 3.4.3 of the "initial state" report (TR-19-03) grout is to be emplaced on top of waste containers and between steel drums. The grout composition has not yet been decided, but the grout composition comprises cement, ballast, water, and plasticiser (Table 7-8, Section 7.3.5). This grout is part of the inventory of cementitious

materials that could interact with bentonite, along with concrete structures. Therefore, the composition may need to be considered in the assessment of bentonite-cement interactions.

SKB recognise that the effect of bentonite transformation on the safety functions "low flow in the waste vault" and "good retention" will need to be analysed. The reviewers agree that this is necessary.

The potential for colloid generation and release if glacial meltwater reaches repository depth is also noted but has yet to be analysed. The need for this to be considered in future safety analysis is recognised by SKB.

As outlined on page 182 of TR-19-01, it is assumed that the repository is situated deep enough not to be frozen during permafrost conditions. Generally, the effect of decreased temperature on the barrier evolution is advantageous, since chemical processes, including corrosion and material degradation, slow down. The potential for bentonite freezing and a decrease in barrier performance is recognised in TR-19-01 and it is stated that: in a future safety assessment for a selected site, the potential for freezing of pore water in SFL needs to be analysed in more detail.

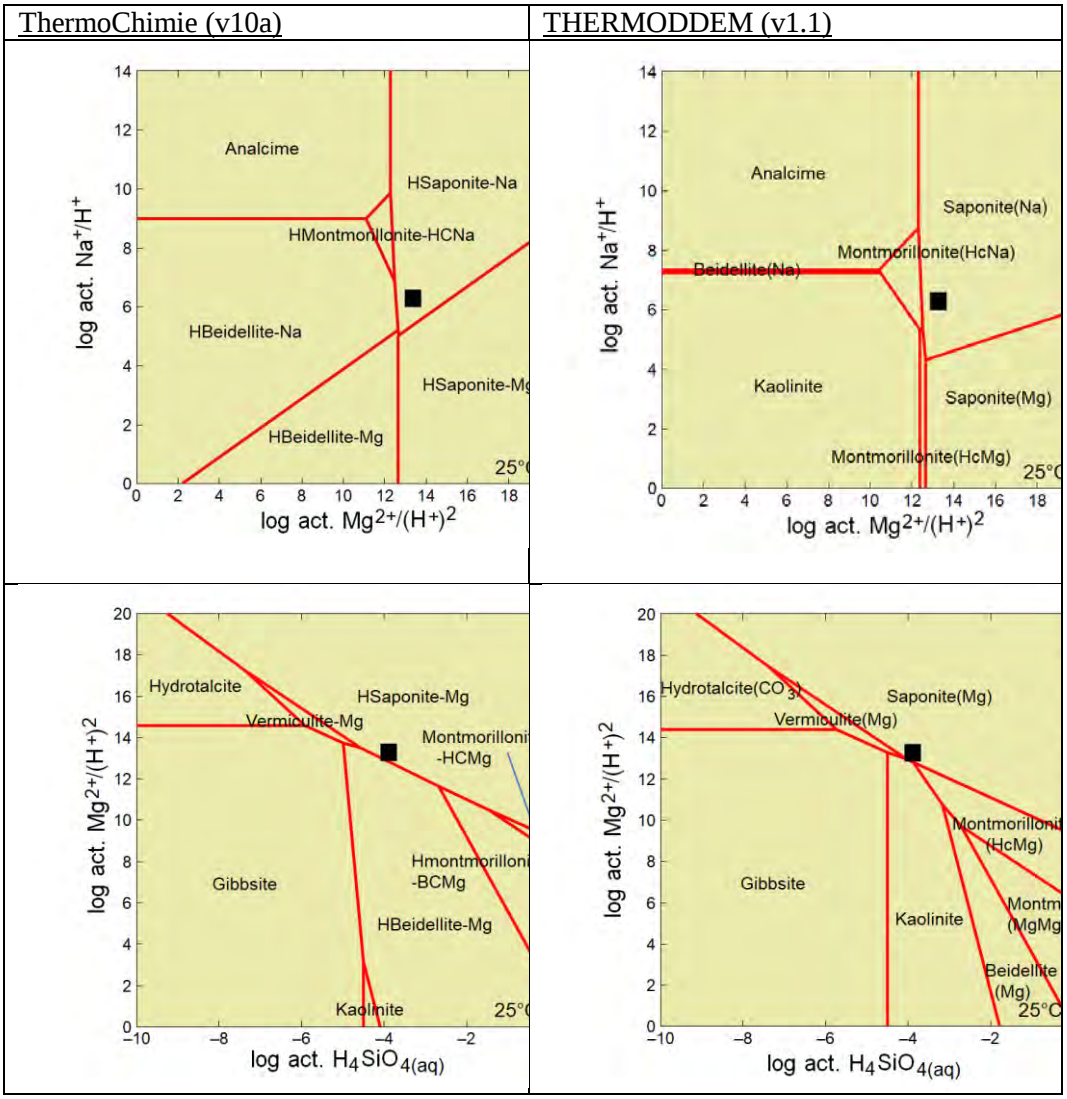

Figure 6: Activity diagrams for the system Al_2O_3-MgO-Na_2O-SiO_2-H_2O showing stability fields for clays and analcime (representative Na-rich framework silicate), high-temperature chlorite and mica minerals, along with less soluble Al-hydroxides (boehmite and diaspore) are suppressed. Both databases include high-charge montmorillonite compositions (denoted by "HC" in both databases). ThermoChimie includes hydrous and hydrous compositions, hydrous end members are denoted by the suffix "H". Aluminium activity is buffered by gibbsite, dissolved silica buffered by quartz log a Na^+ = -2.36. Solute activities for the granitic water used in geochemical modelling (Table 4.2 of Report R-19-13) are shown by black squares.

7.8.4. Summary of Review Findings

The choice of bentonite for the BHA vault where the inventory is less certain is understandable, but it is not very clear from the safety evaluation (TR-19-01) how options assessment work was undertaken to specify the materials present and their quantities for each vault.

The potential for bentonite to undergo erosion, especially piping, is recognised but detailed analysis has not yet been undertaken (noting that much work has been undertaken in the last few years on this issue, including outputs from the BELBaR project).

The need to consider homogenisation processes and mechanical properties in future safety assessments has been noted by SKB.

The potential for cement-bentonite interactions has been identified and modelling was underway at the time the report was produced. It was recognised that future work will need to consider the implications of bentonite alteration for safety functions.

The potential for bentonite to undergo alteration due to reaction with groundwater solutes is recognised as a potential process, and it is noted that illitisation reactions are unlikely to occur due to a lack of heat-producing wastes. However, there is, in theory, the potential that there could be a (probably minor) amount of alteration to other clays, such as saponite. This is predicted by thermodynamic modelling of the granitic water used in cement modelling and has been predicted by reactive transport modelling of a shale-bentonite interface (Wilson et al., 2017b). However, the conversation of one swelling clay (montmorillonite) to another swelling clay (such as saponite) is unlikely to have a significant impact on the swelling capacity of the bentonite, unless the layer charge distribution changes significantly. Therefore, the omission of this process is unlikely to be problematic regarding barrier functions but should be noted as a possible process when demonstrating an understanding of system behaviour.

As noted in the SE-SFL assessment additional work on bentonite evolution is needed in future safety assessments.

7.9. SKB Report R-19-15: Reactive Transport Modelling of Montmorillonite Dissolution

7.9.1. Background

The report describes a study of the alteration of the bentonite backfill of the BHA vault in the SFL repository by the interaction with cementitious materials. Two sets of 1-D reactive transport models of bentonite degradation in the BHA vault are developed and implemented using iCP, an interface between COMSOL Multiphysics and PHREEQC. The first set of models considers only the bentonite system, treating concrete as a boundary condition. The second set explicitly considers the interaction between the concrete and bentonite barriers. The goal of the work was to assess the extent of montmorillonite dissolution in the bentonite barrier because of the interaction with the cementitious fluids from the concrete barrier over a time span of 100 000 years. The different aspects of the modelling approach, results, and suggested implications are reviewed in turn.

7.9.2. Report Introduction

The authors provide a comprehensive review of previous work in cement-bentonite modelling including predicted bentonite / cement alteration products. However, as detailed in the model input data (see subsequent discussion), there are some additional solids that

could have been considered for inclusion in the models to explicitly represent both concrete and bentonite domains (rather than a bentonite domain in contact with a cement porewater boundary condition).

7.9.3. Methodology

To simulate the interaction of bentonite with an alkaline plume, 1-D reactive transport models of the BHA bentonite backfill have been developed and implemented in iCP (Nardi et al. 2014), an interface between COMSOL (2015) and PHREEQC (Parkhurst and Appelo 2013). The reactive transport code PHAST (Parkhurst et al. 2010) was also used as a verification exercise. Simplified models include bentonite reacting with cement porewater, and a full analysis considers explicitly the cement-based materials (waste domain and concrete structure) together with the bentonite backfill.

Although there is some uncertainty associated with kinetic data for cement solids and some secondary minerals associated with cement-rock or cement-bentonite interactions, models published in the international scientific literature have tended to include reaction kinetics as they influence the spatial and temporal evolution of materials interfaces (e.g. Marty et al., 2009; Marty et al., 2014).

The report states that solute transport is diffusion-driven, based on a Fickian approach with a single bulk porosity. The authors suggest that this assumption is valid since the repository is expected to be water saturated in a time scale that is much shorter than the expected dissolution rates of montmorillonite. Once saturated, solute transport is mainly driven by diffusion due to the very low permeability of the bentonite backfill. Degradation of the concrete domains determines the alkaline water interacting with the bentonite backfill. These are reasonable assertions.

As a simplified analysis, the cementitious system is replaced by a fixed concentration boundary condition, thus only representing the bentonite domain explicitly in the model. The composition of the cementitious porewater at the boundary is determined by equilibrium with Portland cement. This approach is consistent with published studies that are concerned mainly with bentonite evolution. Of course, this approach does not provide an indication of the effect of bentonite on cement evolution. This is considered in the "full analysis". The dissolution of montmorillonite is set as a kinetically controlled reaction. This is essential to understand likely bentonite evolution, as dissolution / alteration of smectite clay is known to be very slow (as it is for many layer silicates). The dissolution rate used in the models is the "Sato-Oda" rate expression (Nakabayashi 2014), which considers the dependency on pH, temperature, and the proximity to thermodynamic equilibrium.

In the full analysis, all chemical reactions in the cement-based materials are considered under thermodynamic equilibrium. The assumption of local equilibrium in cement was an approach used in earlier studies, but more recently, attempts have been made in published modelling studies to include reaction kinetics, even though data for precipitation rates are limited. If specific precipitation data are unavailable, a typical transition state theory approach that includes both dissolution and precipitation depending on saturation state can be used, even though the approach has limitations (e.g. Watson et al., 2013; Marty et al., 2014; Watson et al., 2016; Wilson et al., 2018). Even though kinetic data are uncertain, such an approach would give some insights into the likely significance of reaction kinetics for cement-bentonite interactions.

The authors state that the dissolution of bentonite minerals depends on several factors. The relative importance of these factors, especially those that are subject to a high degree of uncertainty, is studied through a set of sensitivity cases. The parameters that have been analysed are:

- the effective diffusion coefficient of aqueous species in the bentonite barrier and concrete domain;
- the reactive montmorillonite surface area;
- the set of primary and secondary minerals;
- the concrete porewater composition;
- bentonite chemical composition; and
- boundary condition at the rock-bentonite interface.

It is reasonable to investigate uncertainties in these parameters, however, there are some detailed aspects of the modelling that are problematic (see comments below).

In the report a total of 21 reactive transport simulation cases are described and the results of the simplified and full analyses are presented. Of the 21 cases, some include only montmorillonite and / or thermodynamic equilibrium is assumed (cases 1, 12, 13). However, these model cases are arguably of limited relevance in terms of developing an expected system evolution scenario, because:

- Bentonite reactions involving some accessory minerals can be important (carbonates in particular affect porewater chemistry, e.g. Savage et al., 2011b); and
- montmorillonite dissolution is not rapid, even under far from equilibrium conditions.

The models include different sets of potential alteration products based on other modelling studies. There is a wide compositional range of zeolites, which has resulted in most published studies including several simplified compositions, with variation in silica content, as less siliceous variants could form further from the cement interface as suggested by Savage et al. (2007).

7.9.4. Conceptual Model

The reactive transport simulations include a model cross section through the BHA vault that includes waste packages, concrete structure, and bentonite blocks. The 1-D model domains are specified to ensure the correct waste-to-concrete volume ratio and represent a “conservative” assumption in terms of volume-thickness of the bentonite backfill. Although the view towards conservatism is understood, it is perhaps better to include a more realistic model representation, with model outputs then confirming whether the model assumptions really are conservative in terms of barrier performance.
As shown in the diagram of the proposed BHA vaults, the system includes a proportion of cement grout in addition to concrete. The grout, which has a slightly higher cement paste content is not mentioned but including it as concrete is reasonable (cement / ballast ratio is ~0.2 for concrete, and ~0.25 for grout, according to the composition given in Table 7-8, initial status report, SKB TR-19-03). The porosity of the cement and effective diffusion coefficients are taken from previous studies and are reasonable.

The reference case assumes that there is no coupling between porosity and diffusivity, which is stated to be:

"*justified by the fact that changes in porosity and related properties due to mechanical stresses will probably also play an important role*".

It is, however, stated that porosity changes are monitored and reported.

Porosity evolution and diffusivity are often coupled in reactive transport simulations (Archie's Law) and the above justification for not including this coupling is weak. Even though the coupling between the mechanical behaviour of cement and the cement's chemical evolution is complex, it is still amenable to investigation by scoping calculations. A model case whereby processes are decoupled could just justified, but it would be more complete to represent porosity evolution in one case, even given the uncertainties associated with modelling bentonite as a porous medium, with total water content being assumed equal to total water porosity. Pore clogging is a process which although somewhat uncertain in compacted bentonite, has been observed in some mudrocks and has been simulated in many modelling studies of cement-clay interaction (see review by Savage and Cloet, 2018); the potential for pore clogging has also been considered in concrete degradation models (e.g. Wilson et al., 2017a, 2018).

The physical properties of the bentonite are taken from relevant documents. ThermoChimie is used as the thermodynamic database. A brief justification of the choice of database would be useful for some readers, but this database is reputable and includes a wide range of relevant solids and aqueous species. The model includes a discrete endmember C-S-H gel approach as this is included in ThermoChimie (v10), which is a suitable approximation of more complex solid-solution behaviour, as is the assumed bentonite composition which is based on SKB documentation. A simplified bentonite composition is assumed which is reasonable.

Regarding mineral dissolution in the models, calcite and gypsum are assumed to dissolve / precipitate under thermodynamic equilibrium, but the reason for this is not clear, as kinetic data exist for these minerals (see Palandri and Kharaka, 2004; Marty et al., 2015). The assumption of instantaneous equilibrium is not clearly justified by the authors. In contrast, montmorillonite, illite, quartz, and feldspar dissolution is kinetically controlled. The authors provide a review of the kinetic data for montmorillonite, including the uncertainties associated with rate data and reactive surface area approaches.

The rate data chosen for montmorillonite are based on Sato et al. (2004) and Oda et al. (2014). Dissolution rate is calculated using combined data (T = 25 and 30 ˚C) and plotted as a function of pH and compared to values calculated using the rate data from Rozalén et al. (2008, 2009). As shown in Figure 4-5 of the report, the slope of dissolution rate vs. pH is broadly similar for the "Sato-Oda" (modified by Nakabayashi, 2014) and the "Rozalén" datasets. The dissolution rates reported in units of mol m^{-2} s^{-1} are higher for the Sato-Oda data by a factor of ~4 to 5 (about half a log unit) between pH 9 and 12, with some non-linearity in the data at pH 7-9 (noting that some scatter in measured rates is common). Typical BET surface areas for montmorillonite are 30-120 m^2 g^{-1} whereas edge site values are typically ~5 to 8 m^2 g^{-1} (Rozalén et al., 2008).

The authors review the approaches available for reporting measured dissolution rate data as a function of surface area. As the authors assert, there is some uncertainty associated

with what is most appropriate to use when reporting rate data normalised to surface area for clays. There has been much work on what is the most appropriate way to represent surface area terms in rate data. The authors also discuss recent work that aims to understand how reactive surface area varies as a function of bentonite density. All this material is relevant for providing the reader with a picture of the difficulties in measuring reactive surface area for clays.

In most laboratory measurements of mineral dissolution rate, a given mass of sample is dispersed in water under a range of conditions to provide an apparent dissolution rate as a function of pH. The surface area is then measured on the same material, typically using either BET (N2 sorption) or a direct measurement of edge site area (ESA) using techniques such Atomic Force Microscopy (AFM) (e.g. Rozalén et al., 2008). The measured dissolution rate data are then reported in the form of a "surface area – normalised" set of rate data, which for clays, is possibly not the best approach available, as different reactive surface area measurements will give different values, which can lead to confusion (Rozalén et al., 2008).

In addition to issues of ensuring the correct surface area term is used for the rate data being considered within a model, there are clearly uncertainties associated with the applicability of rate data from clay mineral suspensions to compacted bentonite. Montmorillonite dissolution rates measured for compacted systems (e.g. Yamaguchi et al., 2007) are much lower, often by one, two or more orders of magnitude, depending on pH (Savage and Cloet, 2018). However, for reactive transport models of bentonite alteration, montmorillonite dissolution rates measures using mineral suspensions with a reported surface area used to produce the normalised values expressed as mol m^{-2} s^{-1} is probably as good as one can expect, given there are few studies on compacted bentonite. If the rate is known to be smaller under compacted conditions, variant model cases can be constructed in which the surface area term is reduced by one or two orders of magnitude. This will affect the extent of montmorillonite alteration.

In Report R-19-15, a surface area of 800 m^2 g^{-1} is used for montmorillonite, as it is stated that it is within the range of total surface area. However, this value is rarely used when reporting surface area normalised rates and it is extremely high compared with other values used for converting measured dissolution rates from mol g^{-1} s^{-1} to mol m^2 s^{-1}. For example, Rozalén et al. (2008) give rates that are ~4-5 times slower than Sato-Oda, which are normalised to a BET surface area value of 111 m^2 g^{-1} (Figure 7).

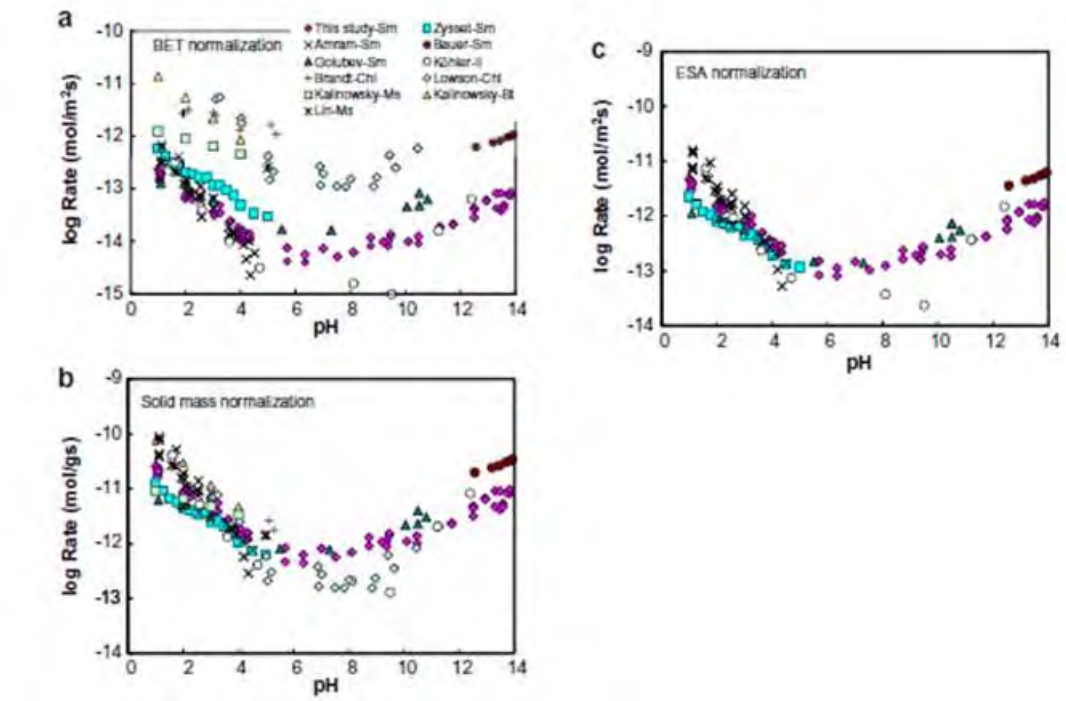

Figure 7: Dissolution of smectites and other layer silicates normalised to BET (a), mass (b), edge site surface area (c) (ESA = 6.5 $m^2 g^{-1}$) from Rozalén et al. (2008).

In contrast, Nakabayashi (2014) models montmorillonite dissolution using the Sato-Oda data and a montmorillonite surface area that is initially specified to be 7 $m^2 g^{-1}$ and then is modified by a factor of 0.02 when comparing predicted rates to those measured in the laboratory. Therefore, the reactive surface area used in Report R-19-15 appears to be inconsistent with the material on which rates were measured and may significantly overpredict montmorillonite dissolution rate in the reference case. It is noted that other models are presented that assume a surface area of 30 $m^2 g^{-1}$ (more consistent with BET data) and assuming 0.03$m^2 g^{-1}$, after Terada et al. (2019), who suggest that reactive surface area is reduced in compacted bentonite due to a "masking" effect resulting from contact of reactive sites with planar surfaces of neighbouring particles.

For minerals that can be considered "equant" in terms of grain morphology (i.e. are not planar like layer silicates), reported rate data are commonly used with surface area being specified for spherical grains of a specified diameter. Report R-19-15 gives sources of kinetic data for quartz, illite and feldspar kinetic data (Table 4-4) but the rate values and assumed surface areas are not clear.

In R-19-15, a local equilibrium approach is described for secondary minerals such as zeolites, cement solids (ettringite), carbonates, silica polymorphs etc. This is not justified by the authors, and it is unclear why a kinetic approach was not adopted. Although precipitation and growth rate data are lacking for many minerals, especially more complex silicates, a typical approach is to use a Transition-State-Theory approach, where minerals are allowed to dissolve and precipitate at a rate depending on degree of saturation, for example:

$$\frac{dS}{dt} = A(S)(k_1(a_{H+})^{n_1} + k_2 + k_3(a_{H+})^{n_3} + k_4(f_{CO_2})^{n_4})\left(1 - \frac{Q}{K}\right) \qquad \text{Equation 1}$$

where S is the quantity of solid (mol), t is time (s), $k_{1,2,3,4}$ are rate constants (mol m^{-2} s^{-1}) for acid, neutral, base and carbonate mechanisms, A(S) is the reactive surface area (m^2) which varies depending on mineral abundance, n is a dimensionless catalysis constant for acid (n_1), base(n_3) and carbonate-dependent rates (n_4), Q is the ion activity product for the solid of interest, aH^+ is the activity of the hydrogen ion, f CO_2 is the fugacity of carbon dioxide and K is the equilibrium constant for the mineral of interest. The mineral reactive surface area is a function of mineral abundance, specific surface area A_{sp} ($m^{-2}g^{-1}$) and molecular weight, W (g mol^{-1}), and is given by $A(S) = A_{sp}$ WS (e.g. Wilson et al., 2018 and references therein).

In summary, kinetic data used in the models for montmorillonite are not clearly described and it is unclear whether the values used are appropriate or justifiable in the reference case. However, variant cases consider variation in surface area, with values potentially being more realistic. Furthermore, the kinetic data used for minerals other than montmorillonite is not clearly presented in the report (values are not tabulated, surface area assumptions are not provided). Minerals for which kinetic data exist (both primary and secondary) and would normally be simulated using a kinetic approach, are treated using a local equilibrium assumption and the reason for this, is not justified.

In the simplified analysis (bentonite only), the bentonite porewater has a pH of 7.19 (Table 6-1), which seems low for a bentonite porewater compared to some studies, where a value of ~8 (or higher) is generally more typical where calcite is present.

The models include clinochlore (Mg-rich chlorite) as a potential bentonite alteration product, which is an unusual choice, as it tends to occur in low-grade metamorphic systems. Saponite, which is included in the models as well, is arguably more appropriate. Another option would be to include a Mg-bearing 1:1 clay mineral end member, as in models of iron-bentonite interactions (e.g. Wilson et al., 2015). Mg-rich alteration products could also potentially include Magnesium-(Aluminium)-Silicate-Hydrate (M-(A)-S-H) solids, which are not considered. Until recently, thermodynamic data for these solids were lacking, but analogues have been considered in cement degradation models (e.g. sepiolite, Wilson et al., 2018).

7.9.5. Results Overview

Report R-19-15 states that all the models suggest a significant dissolution of montmorillonite, of between 20 and 70 % of the initial montmorillonite mass. It is also stated that recent studies of the reactive surface area of montmorillonite in compacted bentonite in the dry density range of interest to repository conditions suggest that this parameter may be lower than expected. However, as discussed earlier in this review, the approach taken for the kinetic input data are problematic.

7.9.6. Results: Simplified Models (Bentonite Domain, Cement Porewater Boundary)

In the simplified reference case, the alteration pathways are broadly as expected from bentonite reacting with cementitious pore fluids, with zeolites forming along with C-S-H gel and ettringite. Report R-19-15 states that zeolites form first, then illite and C-S-H. Given that these minerals are all assumed to precipitate instantaneously, it is difficult to determine whether this is realistic or not. However, the increasing Ca/Si ratio of C-S-H

nearer to the cement porewater boundary is consistent with expected behaviour. Montmorillonite is completely dissolved throughout the bentonite after 100,000 years. The model cases show an expected pattern in terms of amount of alteration and assumed effective diffusion coefficient. In many cases, a closed boundary is assumed at the interface of the boundary and the rock, and a model case which does include it, shows some differences compared to the other models. It is arguable that the model that has the groundwater boundary is more realistic in some ways, but the models do not show significant variation and the emphasis is on the cement-bentonite interface.

Cases are presented where the concrete porewater boundary is assumed to correspond to cement in which portlandite has been leached out such that the porewater is equilibrated with C-S-H gel (Ca/Si = 1.2) resulting in a pH of 11.42. In this model, the lateral extent of montmorillonite alteration is less extensive, ettringite is lacking and the only zeolite that forms is Ca-heulandite. This case provides an interesting contrast to the assumption of fresh cement pore fluids contacting the bentonite throughout the simulated timeframe, using only a bentonite model domain.

The case in which crystalline C-S-H minerals are included rather than C-S-H gel shows less alteration, and different extents of alteration occur depending on assumed secondary minerals. As noted in Report R-19-15, the secondary minerals included in the model will affect solute activity evolution as they dissolve and precipitate, and this will affect the saturation state of montmorillonite and rate of dissolution. However, rates of mineral dissolution-precipitation (which using a T-S-T approach (equation 1) vary as a function of saturation index) would also influence the evolution of the system, and this is not accounted for in the models.

The authors note that the reference case with kinetics suggests that the rate limiting factor for alteration is diffusion rather than reaction rates. The case where local equilibrium is assumed rather than reaction kinetics for primary montmorillonite shows good agreement with the reference case, thereby highlighting the role of diffusion. While diffusion is a key factor controlling the rate at which alteration occurs through the bentonite, the relative rates of precipitation of different minerals is not considered in the model, and previous work, such as Marty et al. (2009) suggests that excluding kinetics will give different model outputs, including predictions of porosity evolution. The lateral extent of the alteration zone is also influenced by many factors including model mesh, transport-porosity coupling and pore clogging (Marty et al., 2014) which are not accounted for in the study. Therefore, the report could give the impression that reaction kinetics are of less relevance to the evolution of clay / bentonite barriers in contact with cementitious materials, which is not the case.

7.9.7. Results: Full Analysis

The “full analysis” with concrete and bentonite domains, but only montmorillonite present in the bentonite, shows much less dissolution than where a cement boundary condition was applied. The authors correctly point out that this is much less than the simple model reference case. However, all previous work on cement-bentonite or cement-mudrock interactions show a relatively narrow zone of alteration, the width of which varies depending on model assumptions (e.g. Marty et al., 2014). Therefore, the relevance of this analysis is questionable.

Report R-19-15 states that the model including both bentonite and concrete domains with mineral dissolution and secondary solid precipitation has 30% of total montmorillonite mass being degraded after 100,000 years. The overall results appear plausible in terms of pH evolution and overall reaction pathways, but the bentonite porewater has a relatively high dissolved chloride concentration (~1.4×10^{-1} M, Table 6-1), which would probably result in formation of Friedel's salt in the concrete domain (see Wilson et al., 2017a; 2018) and this has not been considered. The precipitation of this solid has implications for porewater pH, as it results in pH ~13.

For the concrete domain Report R-19-15 describes the partial dissolution of portlandite and precipitation of ettringite as sulphate diffuses into the concrete from the bentonite porewater. Major changes at the interface are reported, with loss of primary solids and precipitation of calcite and K-saponite. There was extensive alteration of bentonite with zeolite precipitation throughout the backfill, but with higher concentrations nearer the interface. There was also the precipitation of calcite and clinochlore. There was a lack of ettringite and C-S-H gel precipitation in the bentonite, which did occur in the simplified model, due to the fresh cement porewater boundary condition. These findings are all broadly consistent with previous work, but the lack of process couplings makes it hard to ascertain what the implications for solute transport and alteration may be. The authors report that pore clogging would be expected based on observed porosity evolution in both concrete and bentonite domains, with calcite being a major contributor in the full analysis. The clogging occurs over a timescale of ~2000 years in the full analysis.

The cases that explore the implications of variation in model inputs are also discussed, including those in which montmorillonite reactive surface area is changed from the reference value. A reduction to more realistic values results in much less alteration. The implications of effective diffusion coefficient in concrete are also considered, showing that this is an important parameter in terms of lateral extent of alteration. The effect of concrete composition is also considered, with a case including cement for which KOH and NaOH had been leached out which results in less bentonite alteration over the 100,000-year timeframe.

The implications of bentonite backfill composition and modelling assumptions are also considered by different model case assumptions. In the full model, ion exchange is included, in a variant case it is assumed that Ca-montmorillonite is present as this is likely to become the dominant interlayer form. There are some relatively minor differences reported in model outputs.

Different sets of secondary zeolites are considered in some models, In the section where this is discussed (Section 7.6.2, page 52), it is stated that:

"Precipitation kinetics are excluded given the lack of reliable data".

This issue has not been properly addressed in the report. Many previous studies use a T-S-T approach with the same equation for dissolution / precipitation (e.g. equation 1). It is clear that precipitation rates are rather uncertain, but variation in surface area and rates can be explored in variant cases if needed. This approach could have been used instead of other variant cases, such as considering multiple sets of zeolite minerals. Some supporting thermodynamic modelling using ThermoChimie may have helped constrain the

choice of zeolites for the model, noting that many previous studies relied on less extensive datasets with less supporting information being available than at present from experimental and other studies.

7.9.8. Analytical Estimation of Montmorillonite Dissolution Depth

The report considers two analytical models to calculate evolution of montmorillonite dissolution depth as a function of time, including a "shrinking core model" (SCM) (Levenspiel, 1972) and a concrete degradation model based on Neretnieks (2014). The SCM includes a linear relationship between dissolution depth and the square root of time, which is consistent with reactive transport models except for the early stages of evolution (the first few thousand years). As the authors suggest, this provides an additional degree of confidence in terms of the depth of alteration but is not a surprising result.

The model by Neretnieks (2014) includes an SCM approach which can be used to calculate depths of portlandite and montmorillonite dissolution as a function of time (assuming a pseudo steady state approximation). However, as the authors note, model outputs are quite sensitive to assumed mineral compositions and as such, the model is limited in terms of how much confidence can be placed on calculated values.

7.9.9. Discussion and Conclusions

Report R-19-15 summarises the models and their results, noting that the full analysis reference case (both concrete and bentonite domains with secondary solids) predicts complete loss of the montmorillonite within 0.25 m of the interface after 100,000 years, with some alteration occurring throughout the bentonite. The authors note that decreasing the reactive surface area from 800 to 30 $m^2 g^{-1}$ does not significantly impact the conclusion and that similar behaviour is predicted in the local equilibrium model. It is noted that the value of 0.03 $m^2 g^{-1}$ is used, the amount of alteration is significantly reduced.

However, as previously noted, the reference reactive surface area appears too large and is inconsistent with the surface-normalised rate data that are used in the reactive transport simulations. The reactive surface value of 30 $m^2 g^{-1}$ used as an alternative is more consistent with the lower end of reported BET surface area measurements that typically accompany rate data that are surface area normalised in mineral suspension studies (e.g. Rozalén et al., 2008). The reactive surface area value of 0.03 $m^2 g^{-1}$, is much smaller than those used in most studies, but might be more appropriate for a compacted clay. The limited data available suggest that rates may be ~1-2 orders of magnitude lower in compacted bentonite, compared with montmorillonite suspensions (see Savage and Cloet, 2018).

In summary the "reference case" is unlikely to provide a good representation the repository system, because of inconsistencies in the input kinetic data. A far simpler, and more transparent approach would have been to use the surface area data provided with the dissolution rate data (to which the values were normalised) and consider a reduced dissolution rate in a compacted system by reducing the reactive surface area value by a factor of 10 or 100.

The authors note the important influence of diffusion rate on bentonite alteration depth, but the interpretation of the relative importance of diffusion rate and reaction kinetics is

not clearly demonstrated by the study. This limitation is due to the lack of clarity related to how consistent the surface area data is with the adopted rate, and a lack of representation of secondary mineral precipitation.

The authors note the importance of treatment of boundary conditions and whether concrete domains are included, along with the choice of secondary solids. The authors also note that the models are limited as process couplings such as porosity-diffusion are not included, which is justified based on the likely importance of mechanical effects. This is not very well explained, and the coupling of mechanical and chemical processes is not very well understood. Many published models include such process couplings (but these seem to generally avoid operator splitting) and the assertion that process couplings should not be considered as others may be more important, is not at all convincing.
The authors also state that kinetic data for zeolite precipitation are lacking, which is true, but methods are still nevertheless available to simulate dissolution / precipitation, and although the exact rates of precipitation are not well constrained, reactive transport models that use a typical T-S-T approach have managed to replicate the broad evolution of industrial analogue systems, such as Tournemire (e.g. Watson et al., 2013), natural analogues systems such as Maqarin (e.g. Watson et al., 2013) and saline alkaline lakes (Savage et al., 2010).

7.9.10. Summary of Review Findings

The report includes a review of previous cement-bentonite models which is thorough.

The report described several 1-D reactive transport models of a cement-bentonite interface within the BHA vault concept; models include: bentonite only (cement-equilibrated porewater boundary); or concrete and bentonite domains. The models include coupling of physical and chemical processes using iCP, an operator splitting approach. Whilst this is a recognised approach, there is no discussion of other approaches (i.e. global solve) and implications of the coupling strategy for model outputs. A brief consideration would be useful, as other modelling strategies are available. Some potential alteration products are not considered in the models, namely Friedel's salt (product of cement-Cl interaction), and Mg-bearing solids such as M-(A)-S-H (or a proxy for it).

The models include relevant processes. However, the authors made the decision to decouple porosity from effective diffusion coefficients and the attempt to justify this based on uncertainty in mechanical processes is unconvincing. Although the process of pore clogging in bentonite is uncertain (as numerous models exist for bentonite porosity, given that the water present is mostly in smectite interlayers, rather than pores), it is generally given some consideration in reactive transport models, at least as a variant case(s). In addition, pore clogging has been reported in some cement / concrete studies.

The model includes dissolution kinetics for montmorillonite. The simplest approach is to take reported rate data measured in the laboratory and its associated surface area value that was used to produce surface area normalised reaction rates. Instead, the authors use one rate equation (from a PhD thesis), with a different reactive surface area, that is arguably extremely high. It is noted that the variant cases with reduced surface area are probably more realistic.

A kinetic treatment is provided for some other primary minerals, but not all, with no justification as to why this approach was adopted, especially as data are available (see compilations by Palandri and Kharaka, 2004; Marty et al., 2015).

Secondary minerals are allowed to precipitate under local equilibrium conditions (i.e. an instantaneous approach). It is true that rate laws and data for some secondary solids are not available or are uncertain, but the use of a typical T-S-T equation for dissolution / precipitation with exploration of assumptions in surface area or rate values can provide some insight into alteration processes. Also, this approach has managed to broadly replicate the evolution of clay minerals in models of analogue systems.

The authors suggest that because the model case assuming local equilibrium gives similar system evolution compared to the reference case with montmorillonite kinetics, bentonite alteration is diffusion limited. While it is true that diffusion is a major control on reactant availability, and therefore potential for bentonite alteration, using a model that excludes precipitation kinetics to support the argument that diffusion rates are the primary control, could be interpreted as being somewhat biased.

The number of model cases is arguably excessive, and some are of limited applicability. Resources may have been better deployed by developing a more coherent reference case that included a more consistent kinetic dataset, using a classic T-S-T approach for all minerals / cement solids. Even if absolute rate values / reactive surface areas are somewhat uncertain, different groups of solid will precipitate (and crystallise) at different rates, for example C-S-H precipitation is likely to be much more rapid than zeolite / smectite formation.

The model results are broadly consistent with other published models. However, the treatment of reaction kinetics is somewhat weak, and the exclusion of some process couplings further weakens the models. The wide range in calculated volume loss of the montmorillonite reflects the very wide range of surface area values in the models. The potential for diffusion being reduced to some extent by porosity reduction is not considered.

Overall, the models are of limited applicability to safety evaluation calculations, other than they show some broad consistency in terms of reactive pathways elicited from previous experimental and modelling studies (namely the dissolution of primary cement solids and bentonite minerals and the development of a zone of alteration dominated by lower Ca/Si C-S-H, secondary clays, and zeolites).

8. Cement Evolution Models

8.1. Issues with SKB's Cement Evolution Models

The review described in previous sections has identified several key areas of uncertainty in SKB's numerical modelling of concrete degradation, notably:

1. SKB's modelling uses an operator splitting approach (sequential modelling of chemical processes and transport processes in each timestep) and the significance of the associated uncertainties (as compared to a fully coupled approach) are unclear from the modelling presented by SKB.
2. SKB's modelling assumes instantaneous reactions (all phases are in equilibrium). The significance of not incorporating reaction kinetics requires investigation.
3. The implications of including additional potential secondary solids, such as those typically associated with the later stages of cement-rock interaction, needs clarification.
4. Only two groundwater compositions are used in SKB's modelling. A wider range of water compositions might occur in Swedish sites that could be considered to host the SFL. The significance for concrete degradation models of using different Swedish water compositions to those considered by SKB in the SE-SFL require clarification.
5. In its modelling of cement degradation, SKB has used thermodynamic data from the CEMDATA database. However, there are other thermodynamic data available and it would be beneficial to establish whether these could produce different results to those of SE-SFL.

To assess whether these areas of uncertainty are significant, some independent modelling was undertaken and is described in the following sections.

8.2. Independent Modelling Approach

Independent modelling was undertaken in four steps:

1. A 1-D fully coupled model of concrete evolution was developed, using Quintessa's QPAC code;
2. The QPAC model was used to explore the significance of representing reactions kinetics using the model;
3. The QPAC model was used to explore the significance of using different water compositions; and
4. The significance of using different thermodynamic databases was assessed using a combination of QPAC and the Geochemist's Workbench (GWB) software.

Quintessa's QPAC software is a general-purpose modelling tool for solving systems of partial differential and algebraic equations. Rather than using an operator splitting approach to represent coupling between transport and chemical processes, the software fully couples these processes. QPAC has been used on many projects to investigate cement-water interactions (e.g. Wilson et al., 2017a). QPAC has also been used on several previous review assignments for SSM (e.g. Benbow et al., 2015). Version 4.2 of the software was used in the work described here.

GWB is a commercial software package for geochemical modelling, which is widely used (Bethke, 2010). Version 2021 of GWB was used.

It was not attempted to reproduce the models developed by SKB, which would require a considerably larger study. Instead, the approach was to set up a QPAC model that represented the same minerals and reactive transport processes as included in SKB's model presented by Idiart et al. (2019; SKB report R-19-14). These models were run with and without reaction kinetics being represented for secondary phases, using different input groundwater compositions and with different thermodynamic data constraints.

The reactive transport models produced in QPAC are 1-D and use the model geometry and cement composition of Case 1 (reference concrete) in report R-19-14. The cement composition is based on SKB's clinker hydration modelling. The models include the same transport properties, and vault cross section given in the 1-D simulations described by Idiart et al., in SKB Report R-19-14.

8.3. Conceptual Model

The conceptual model is a 1-D section of the BHK vault (2.8 m in width) as in of report R-19-14 (Figure 8).

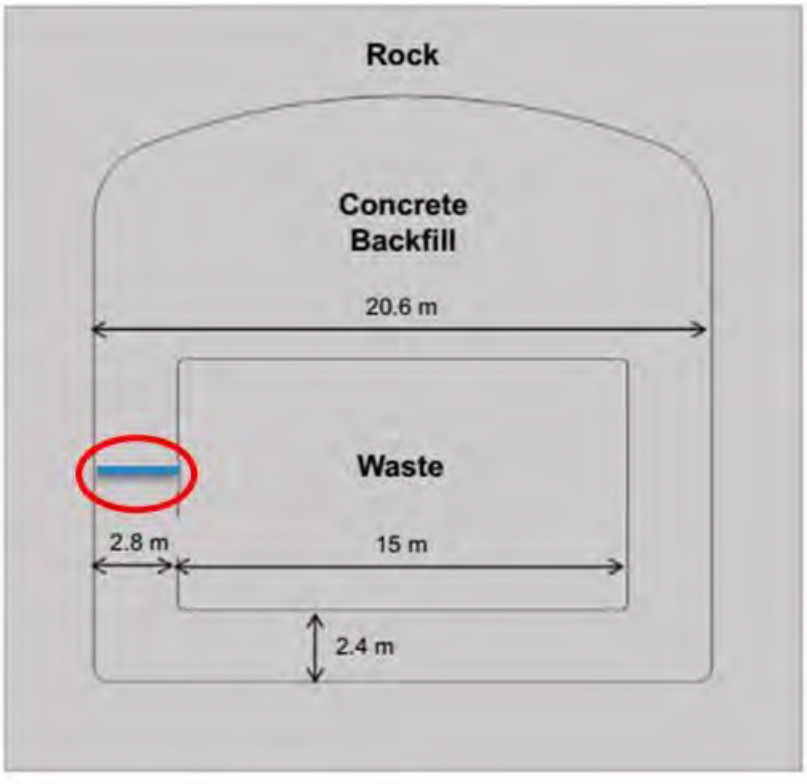

Figure 8: 2D cross section of the BHK vault, dimensions in metres (m) reproduced from R-14-19. The 1-D models are of the 2.8 m thick concrete backfill (outlined in red).

Two model discretisations (finite volume) were used (Figure 9):

- a regular grid including 28 cells, equally spaced (as in R-14-19), used in all models except one; and
- a "geometric" distribution (30 cells) used in one model, in which cell width is smaller near to the groundwater boundary (left hand side of modelled domain).

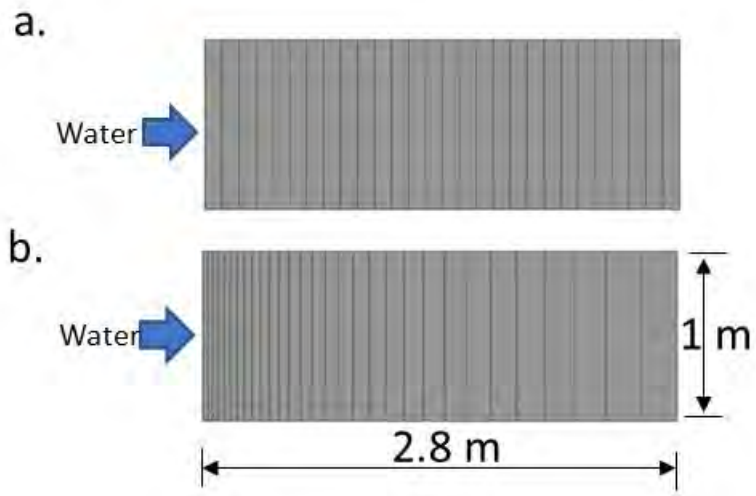

Figure 9: Model discretisations. a. a regular grid, as used in all except one model. b. a geometric grid used in one model. The compartments are 1 m wide perpendicular to the plane of the page.

The right-hand boundary is treated as a zero-concentration gradient boundary in all cases. One model case includes a "geometric" grid (smaller width compartments near the groundwater interface).

The models include the following processes:

- dissolution / precipitation reactions for cement solids and alteration products;
- advective transport of water and solutes; and
- diffusive transport of solutes.

Diffusion is coupled to porosity using a linear Archie's law approach (equation 1), and porosity-permeability coupling is based on a Kozeny-Carmen relationship (equation 2). The simulations were produced using the Quintessa code QPAC, which has been used to construct many published reactive-transport models.

Archie's Law takes the form:

$$D_{\text{eff}} = D_{\text{pore}} \cdot \theta^{c-1} \quad (1)$$

where effective diffusion (D_{eff}) (mol m^{-2} s^{-1}) is equal to porewater diffusion (D_{pore}) multiplied by porosity θ (-) and c is the "cementation factor" (here taken to be 2).

The Kozeny-Carman Relationship is:

$$K = [K_{ref} \left[\frac{\left(1-\theta_{ref}\right)^2}{\left(\theta_{ref}\right)^3}\right] \times \left[\frac{(\theta)^3}{(1-\theta)^2}\right] \quad (2)$$

where K is hydraulic conductivity (m s^{-1}), K_{ref} is the initial hydraulic conductivity at the initial reference porosity θ_{ref} and θ (-) is porosity.

One of the models includes alkali leaching, using a different approach to that of R-14-19. In R-14-19 alkali partitioning between the solid phases and mobile aqueous phase is modelled using a cation exchange model proposed by Savage et al. (2011a), which is based on data from Hong and Glasser (1999) (but uses modified equilibrium constants). The independent modelling used the K_d data from Hong and Glasser, (1999), with Na^+ and K^+ sorption / desorption occurs as C-S-H undergoes leaching.

QPAC allows users to specify reactions kinetics. The following Transition State Theory (T-S-T) expression was used for dissolution-precipitation reactions:

$$\frac{dS}{dt} = A(S)(k_1\ (a_{H^+})^{n1} + k_2 + k_3\ (a_{H^+})^{n3} + k_4\ (f_{CO_2})^{n4}(1 - Q/K) \qquad (3)$$

where S (mol) is the abundance of the solid of interest, t is time (s), $k_i, i = 1, \ldots, 4$ are the rate constants (mol m^{-2} s^{-1}) for acid, neutral, base and carbonate mechanisms, $A(S)$ is the mineral reactive surface area (m^2) (which is a function of the mineral abundance), n is a dimensionless catalysis constant for acid (n_1), base (n_3) and carbonate (n_4) – dependent rates, Q is the ion activity product, a_{H^+} (-) is the activity of the hydrogen ion, f_{CO_2} is the CO_2 fugacity, and K is the equilibrium constant for mineral dissolution. The mineral reactive surface area is a function of the mineral abundance, S, its specific surface area, A_{sp} (m^2 g^{-1}), and its molecular weight, W (g mol^{-1}), and is given by $A(S) = A_{sp}WS$. Values of rate constants (k_i) vary as a function of T, as do catalysis constants (n). In one model case a "local equilibrium" approach is simulated by specifying only one k term, which is set to an arbitrarily high value.

The "B-dot" extended Debye-Hückel approach was used for solute activity-concentration conversions as it is applicable over a relatively wide range of ionic strength values (up to ~1 M in NaCl-dominated systems, e.g. Bethke, 2010).

8.4. Input Data

8.4.1. Thermodynamic Data

The independent geochemical models were constructed using the thermodynamic database THERMODDEM (v1.1, GWB format, downloaded from BRGM website[1]) as this database includes many cement solids and potential cement or cement-rock alteration products. SKB's model reported in R-19-14 uses the CEMDATA07 dataset for cement (which includes much of the data from Lothenbach and co-workers, e.g. Jacques et al., 2009; Lothenback et al., 2008), supplemented by data for magnesium-silicate-hydrate (M-S-H) phases, K_2SO_4 and Na_2SO_4 that are included in the more recent CEMDATA18 dataset (Lothenbach, 2019). However, CEMDATA07 and CEMDATA18 are unavailable in a format that can be readily applied with the QPAC software used for reactive transport modelling.

[1] https://thermoddem.brgm.fr/databases/geochemists-workbench

It is noteworthy that report R-19-14 is not clear about the source of thermodynamic data for aqueous species. Presumably the thermodynamic data from the CEMDATA compilation were added to one of the thermodynamic databases distributed with PHREEQC, but which one is not stated.

In the THERMODDEM database used here, C-S-H is represented using many discrete C-S-H phases with different compositions (i.e. a "discrete solid phase" (DSP) approach). These phases have a wide range of Ca/Si ratios (1.6 – 0.7). Data are also provided for C-A-S-H and M-S-H compositions which can be considered as potential cement alteration products, depending on intruding groundwater composition (Section 8.4.4). The database uses the character "." in mineral names, this has been replaced with "_" to allow the database to run with the QPAC code. In contrast, the CEMDATA approach uses an ideal binary solid-solution model for C-S-H, that comprises "tobermorite-like" $[(CaO)_{0.83}(SiO_2)(H_2O)_{1.3}]$ and "jennite-like" $[(CaO)_{1.67}(SiO_2)(H_2O)_{2.1}]$ endmember compositions. This approach has been incorporated into one of the models to compare it again the DSP approach (Section 8.4.7).

The log K data used for the two C-S-H solid solution endmember compositions have been recalculated using reported ΔG_f data for the C-S-H end members (Lothenbach et al, 2019) and ΔG_f for "basis" aqueous species consistent with the THERMODDEM database. These latter ΔG_f values are available online in the THERMODDEM database tool (BRGM, 2020; https://THERMODDEM.brgm.fr/).

As discussed in Section 8.4.5, another database that could be used instead of THERMODDEM is the Andra database "ThermoChimie" (Andra, 2021). This latter database also includes several cement solids and minerals that could form due to cement-rock interactions. However, as shown in Section 8.4.5, this database is likely to result in a broadly similar cement degradation pathway.

8.4.2. Concrete Composition

The concrete is based on the calculated hydrated composition given in SKB Report R-19-14 for Anläggningscement (CEM I 42.5 N – SR 3 MH/LA, Idiart and Shafei, 2019) with a w/c ratio of 0.47. The initial assemblage of hydrated cement solids present in the concrete is taken from SKB's thermodynamic modelling of cement hydration in R-19-14 (Table 2). The composition of the concrete used in the modelling is given in Table 3. The concrete has a porosity of 0.11, with an inert volume fraction of 0.704 (Table 5-6 of Idiart and Shafei, 2019).

Table 2: Hydrated concrete composition (from R-19-14). C-S-H simulated using ideal solid solution, "C-S-H Jennite" = $(CaO)_{1.67}(SiO_2)(H_2O)_{2.1}$, "C-S-H Tobermorite" = $(CaO)_{0.83}(SiO_2)(H_2O)_{1.3}$

Primary Solid	mol L^{-1} (total volume)
Portlandite	1.422
Hydrotalcite OH	0.016
Monocarboaluminate	0.033
Monosulfoaluminate	0.081
Hydrogarnet OH	0.111
C-S-H "Jennite" (End Member, EM)	1.1
C-S-H "Tobermorite" (EM)	0.161
Porosity	0.11
Inert Fraction	0.694
Exchanger Composition	
CaX_2	0.04286
K_2X_2	0.01657
Na_2X_2	0.00292

Table 3: Concrete composition used in 1-D models (based on the cement composition in Table 2). Quartz is assumed present as an inert aggregate. Solid phase compositions are from the THERMODDEM database.

Primary Solid	Composition	vol.%
Portlandite	$Ca(OH)_2$	4.44
Hydrotalcite OH	$Mg_4Al_2O_7 \cdot 10H_2O$	0.34
Monocarboaluminate	$Ca_4Al_2CO_9 \cdot 10.68H_2O$	0.82
Monosulfoaluminate	$Ca_4Al_2SO_{10} \cdot 12H_2O$	2.38
Hydrogarnet OH (C3AH6)	$Ca_3Al_2(OH)_{12}$	1.57
C-S-H (1.6)	$Ca_{3.2}Si_2O_{8.2682}H_{2.1364} \cdot 2.3446H_2O$	9.04
Inert fraction (quartz)	[SiO_2 inert]	70.40
Porosity	-	11.00

8.4.3. Transport Data

Transport data were taken from SKB report R-19-14 (Idiart et al., 2019):

- Hydraulic conductivity, K (m s^{-1}):· 8.3 x 10^{-10}
- Effective Diffusion coefficient, De (m^2 s^{-1}):· 3.5 x 10^{-12}
- Calculated permeability (for coupling) (m^2): 7.53 x 10^{-18}
- Head gradient (-) (1.24 x 10^{-1}) applied based on the reported flux q (m s^{-1})[1.03 x 10^{-11}] and hydraulic conductivity, K.

The calculated head gradient was compared to that given in Figure 5-4 of SKB R-19-14, which suggests a head gradient nearer to 1 x 10^{-2}. This latter value was adopted in one of the model cases.

8.4.4. Water Composition

Model water compositions were produced using PHREEQCi (v3, Parkhurst and Appelo, 2013) and the THERMODDEM database (v.1.2, BRGM, 2021). The reference groundwater composition is that reported by Idiart et al. (2019) in SKB report R-19-14 with charge balance correction being made by adjusting the Cl^- concentration (Table 4). This groundwater is the so-called "old meteoric groundwater" endmember from Idiart and Shafei (2019), which quotes Pękala et al. (2015). While not relevant to the validity of the model outputs, it should be noted that the designation of this groundwater as "old meteoric groundwater" may be erroneous, since it is based on the "altered meteoric Laxemar" groundwater composition given by Laaksoharju et al. (2009), rather than the "old meteoric + glacial" water specified by the same authors.

Only this single water composition was used in the models developed by Idiart et al. in SKB report R-19-14. However, there is considerable variability in groundwater chemistry in Swedish crystalline bedrock. At the present generic stage of studies, it is uncertain what groundwater composition will be encountered at a future SFR site. The question therefore arises as to the general applicability of the cement leaching / alteration behaviour modelled by Idiart et al.

Laaksoharju et al. (2009) give the compositions of five groundwater "endmembers" in the Laxemar area, based on a statistical analysis of sampled groundwaters from this area:

1. deep saline water (TDS 76,000 mg L^{-1});
2. Littorina seawater (TDS 12,000 mg L^{-1});
3. Glacial water (TDS 2 mgL^{-1});
4. Old meteoric plus glacial water (TDS 2 mg L^{-1}); and
5. Altered meteoric water (460 mg L^{-1}).

Endmembers 3. and 4. in this list have the same solute composition, but are distinguished by their stable isotopic compositions, the glacial water (3.) being depleted in heavy isotopes (^{18}O and ^{2}H) compared to the old meteoric water plus glacial water (4.). Water 5. is the basis for the groundwater composition used in the modelling presented in report R-19-14.

It is beyond the scope of this review to consider the full range of possible groundwater compositions that might be encountered at a future SFL site. Generally, the more dilute the groundwater, the faster will be the leaching of cement phases for a given groundwater flux. Therefore, it is to be expected that leaching with water 3. or 4. would proceed more rapidly than that with water 5. However, generally the more saline a water, the more concentrated will be solutes that can react with cement phases. The mineral products produced by reactions between groundwater and cement will depend both on salinity and proportions of dissolved constituents.

For comparison, with the models developed by Idiart et al., additional models were developed using:

- a very low-salinity water based on the glacial groundwater endmember reported by Laaksoharju et al. (2009); and
- a more saline groundwater based on a "Littorina Sea" water composition reported by Laaksoharju et al. (2009).

These water compositions are given in Table 4. It is noted that these compositions are theoretical endmember compositions based on statistical analysis of sampled groundwaters. However, using them in the calculations gives an initial indication of the likely significance of different groundwater compositions that plausibly could be encountered in future SFL site.

Laaksoharju et al. (2009) do not provide a pH value for the first of these two waters. Therefore, a value of 7.75 was used since this is appropriate for a sub-glacial water that has interacted substantially with bedrock (Harper et al., 2015). Unlike the reference water, the low-salinity water based on the glacial groundwater endmember was charge-balanced on dissolved carbonate. However, the water based on the Littorina Sea endmember composition given by Laaksoharju et al. (2009) was charged-balanced using chloride.

The most saline endmember reported by Laaksoharku et al. (2009) was not used in the independent modelling. The reason is the high salinity of this water, which causes the extended Debye-Hückel approach used to calculate activities of aqueous species to be somewhat inaccurate. However, it cannot be ruled out that such saline waters may occur at a future SFL site. Should this be the case it will be necessary to consider further the implications for cement degradation pathways.

The initial cement porewater was calculated assuming the groundwater composition with primary cement solids buffering solute activities (with the corrected Cl concentration from groundwater speciation and charge balance on H^+ at T = 25°C, P = 1 bar).

Table 4: Model water compositions.

Parameter	Reference Groundwater	Glacial Groundwater	Saline Groundwater [buffering solids]	Cement (no alkalis) [buffering solid]	Cement (alkalis) [Buffering sold]
pH	8.6	7.75	7.6	12.47	13.15
Solute concentrations (mol kg^{-1})					
Al	1.21E-06	7.93E-09 [Kaolinite]	7.55E-09 [Kaolinite]	4.34E-05 [C_3AH_6]	2.34e-04 [C_3AH_6]
C	6.91E-04	1.92E-03	2.65E-03 [Calcite]	1.59E-07 [monocarboaluminate]	1.15e-06 [monocarboaluminate]
Ca	5.26E-04	9.32E-04 [Calcite]	3.77E-03	2.04E-02 [Portlandite]	2.055e-03 [Portlandite]
Cl	4.73E-03 (reported 4.53E-3)	1.41E-05	1.87E-01 (reported 1.83E-01)	4.73E-03	4.73e-03
K	7.60E-05	1.02E-05	3.43E-03	7.60E-05	1.70e-01
Mg	1.48E-04	4.11E-06	1.84E-02	3.24E-09 [Hydrotalcite]	6.38e-10 [Hydrotalcite]
Na	4.79E-03	7.39E-06	1.60E-01	4.79E-03	3.300e-02
S(VI)	3.73E-04	5.20E-06	9.26E-03	2.95E-05 [Monosulfoaluminate]	9.234e-04 [Monosulfoaluminate]
Si	1.42E-04	1.86E-04 [Quartz]	1.82E-04 [Quartz]	1.96E-06 [$C_{1.6}SH$]	1.935e-05 [$C_{1.6}SH$]

8.4.5. Secondary Minerals and Cement Solids

The secondary minerals included in the independent models described here are slightly different from those considered in R-19-14. In this independent modelling C-A-S-H and M-S-H solids are included, along with additional products of cement-rock interaction, such as zeolites and smectites (beidellite and saponite), and Friedel's salt which can form due to Cl ingress (Table 5).

The solids also include those which could form due to carbonation, reaction with dissolved Mg^{2+} and sulphate ("external" sulphate attack). Representative zeolites included in the models are based on reported occurrence in models and experiments (e.g. Savage et al. 2007; Savage, 2011; Savage and Cloet, 2018) and a theoretical cement leaching / degradation pathway (Figure 10). It has been suggested in the literature that relatively more siliceous zeolites (e.g. clinoptilolite, phillipsite) are likely to form in lower pH regions distant from the cement-rock interfaces, whereas C-A-S-H, illite and the more aluminous zeolites (e.g. analcime, heulandite) are more likely to form at higher pH, and hence closer to cement-rock interfaces (Savage et al., 2007). The zeolites phillipsite, chabazite and zeolite-P have also been found in experimental systems and have been included in modelling studies (e.g. Marty et al., 2009). Experiments to simulate cement-rock interaction have reported gismondine and zeoliteP with the latter forming under lower T conditions (Lothenbach et al., 2017). Straetlingite (associated with aluminous cement blends, e.g. Lothenbach et al., 2011), carbonated hydrotalcite, and silicious katoite are also included as potential secondary solids. The THERMODDEM database includes discrete solids for a range of C-S-H, Magnesium-Aluminium-Silicate-Hydrate (M-A-H) and C-A-S-H compositions (Table 6).

Table 5: Secondary solid compositions (THERMODDEM v1.2, BRGM, 2021).

Solid	Composition
C-S-H	see list of discrete solid compositions, Table **6**
M-S-H	see list of discrete solid compositions
C-A-S-H	see list of discrete solid compositions
Brucite	$Mg(OH)_2$
Calcite	$CaCO_3$
Dolomite	$CaMg(CO_3)_2$
Hydrotalcite-CO_3	$Mg_4Al_2(OH)_{12}(CO_3)\cdot 2H_2O$
Ettringite	$Ca_6Al_2(SO_4)_3(OH)_{12}\cdot 26H_2O$
Thaumasite	$CaSiO_3CaSO_4CaCO_3\cdot 15H_2O$
Gypsum	$CaSO_{4.2}H_2O$
Friedel's salt	$Ca_4Al_2Cl_2O_6\cdot 10H_2O$
Katoite_Si_1	$Ca_3Al_2(SiO_4)_1(OH)_8$
Straetlingite	$Ca_2Al_2SiO_2(OH)_{10}\cdot 2.5H_2O$
SiO_2(am)	SiO_2
Ca-Saponite (hydrated)	$Ca_{0.17}Mg_3Al_{0.34}Si_{3.66}O_{10}(OH)_2\cdot 4.799H_2O$
Na-Saponite (hydrated)	$Na_{0.34}Mg_3Al_{0.34}Si_{3.66}O_{10}(OH)_2\cdot 4.297H_2O$
K-Saponite (hydrated)	$K_{0.34}Mg_3Al_{0.34}Si_{3.66}O_{10}(OH)_2\cdot 4.061H_2O$
Ca-Beidellite (hydrated)	$Ca_{0.17}Al_{2.34}Si_{3.66}O_{10}(OH)_2\cdot 4.24H_2O$

Solid	Composition
Na-Beidellite (hydrated)	$Na_{0.34}Al_{2.34}Si_{3.66}O_{10}(OH)_2 \cdot 2.756H_2O$
K-Beidellite (hydrated)	$K_{0.34}Al_{2.34}Si_{3.66}O_{10}(OH)_2 \cdot 1.627H_2O$
Chabazite	$Ca(Al_2Si_4)O_{12} \cdot 6H_2O$
ZeoliteP(Ca)	$Ca_2Al_4Si_4O_{16} \cdot 9H_2O$
Analcime	$Na_{0.99}Al_{0.99}Si_{2.01}O_6 \cdot H_2O$
Illite	$K_{0.85}Al_{2.85}Si_{3.15}O_{10}(OH)_2$
Ca-Heulandite	$Ca_{1.07}Al_{2.14}Si_{6.86}O_{18} \cdot 6.17H_2O$
Na-Heulandite	$Na_{2.14}Al_{2.14}Si_{6.86}O_{18} \cdot 6.17H_2O$
Ca-Clinoptilolite	$Ca_{0.55}(Si_{4.9}Al_{1.1})O_{12} \cdot 3.9H_2O$
Na-Clinoptilolite	$Na_{1.1}(Si_{4.9}Al_{1.1})O_{12} \cdot 3.5H_2O$
K-Clinoptilolite	$K_{1.1}(Si_{4.9}Al_{1.1})O_{12} \cdot 2.7H_2O$
Ca-Phillipsite	$Ca_{0.5}AlSi_3O_8 \cdot 3H_2O$
Na-Phillipsite	$NaAlSi_3O_8 \cdot 3H_2O$
K-Phillipsite	$KAlSi_3O_8 \cdot 3H_2O$

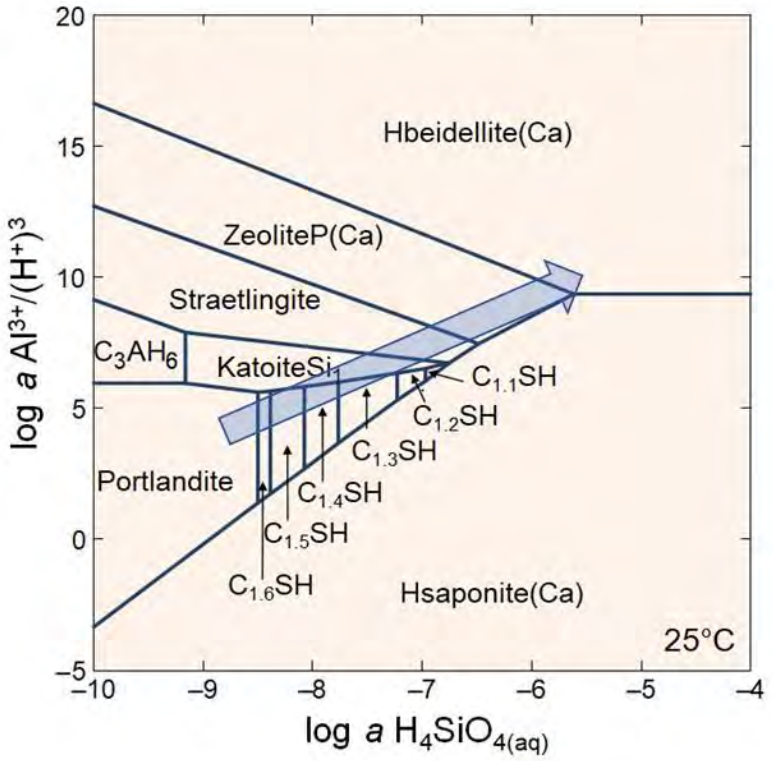

Figure 10: Activity diagram for the system Al_2O_3-CaO-MgO-SiO_2-H_2O showing a potential reaction pathway for cement leaching (minerals associated with higher-temperature igneous / metamorphic rocks are excluded as are crystalline C-S-H minerals). Gismondine (which occurs in place of zeoliteP) was excluded as it is more likely to form under higher temperature conditions. The activity of Ca^{2+} is buffered by Portlandite, the activity of Mg^{2+} is buffered by hydrotalcite. The arrow shows likely reaction progress associated with cement leaching by groundwater. The diagram was constructed using the Act2 model of Geochemist's Workbench and the THERMODDEM database (v1.1, BRGM, 2021).

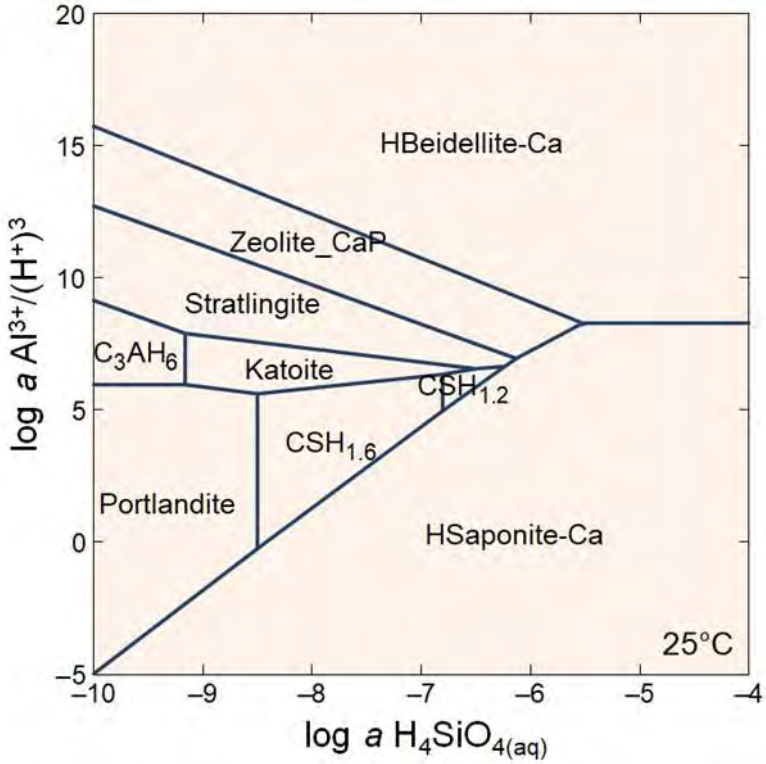

Figure 11: Activity diagram for the system Al_2O_3-CaO-MgO-SiO_2-H_2O constructed using the same assumptions as for Figure 10, but using the ThermoChimie database ("ThermoChimie_GWB_oxygen_v10a", Andra, 2021).

The activity diagram in Figure 10 was replicated in Figure 11 using the ThermoChimie thermodynamic database and making the same assumptions (solute buffers, T/P, the exclusion of higher-temperature solids and crystalline C-S-H). Figure 11 has similar stability fields compared with those associated with the diagram produced using THERMODDEM, although some slight differences in positions of boundaries can be observed (c.f. Figures Figure 10 and Figure 11). Therefore, were reactive-transport models to be constructed using ThermoChimie (which is not used in the coupled analysis reported here) they would likely to produce broadly similar outputs to those generated using THERMODDEM. However, as noted in Section 8.4.1, the thermodynamic data used in R-19-14 included a binary ideal solid solution to represent C-S-H gel from CEMDATA. Therefore, a model case was produced that included this solid solution approach rather than the DSP approach which is included in both THERMODDEM and ThermoChimie databases.

Table 6: Compositions of Discrete Cement Solids in THERMODDEM (C-S-H, C-A-S-H, M-S-H).

Cement Solid	Composition
C-S-H discrete solids	
C1_5SH	$Ca_3Si_2O_{7.9783}H_{1.9566}\cdot 2.2848H_2O$
C1_4SH	$Ca_{2.8}Si_2O_{7.687}H_{1.774}\cdot 2.2274H_2O$
C1_3SH	$Ca_{2.6}Si_2O_{7.3957}H_{1.5914}\cdot 2.1702H_2O$
C1_2SH	$Ca_{2.4}Si_2O_{7.1203}H_{1.4406}\cdot 2.0692H_2O$
C1_1SH	$Ca_{2.2}Si_2O_{6.8821}H_{1.3642}\cdot 1.867H_2O$
C1_SH	$Ca_2Si_2O_{6.6436}H_{1.2872}\cdot 1.7542H_2O$
C0_9SH	$Ca_{1.8}Si_2O_{6.4048}H_{1.2096}\cdot 1.7014H_2O$
C0_8SH	$Ca_{1.6}Si_2O_{6.1698}H_{1.1396}\cdot 1.6122H_2O$
C0_7SH	$Ca_{1.4}Si_2O_{5.9496}H_{1.0992}\cdot 1.378H_2O$
C-A-S-H discrete solids	
C1_6A0_01SH	$Ca_{3.2}Al_{0.04}Si_2O_{8.3296}H_{2.1392}\cdot 2.3446H_2O$
C1_5A0_01SH	$Ca_3Al_{0.04}Si_2O_{8.0399}H_{1.9598}\cdot 2.2858H_2O$
C1_4A0_01SH	$Ca_{2.8}Al_{0.04}Si_2O_{7.7502}H_{1.7804}\cdot 2.2294H_2O$
C1_3A0_01SH	$Ca_{2.6}Al_{0.04}Si_2O_{7.4606}H_{1.6012}\cdot 2.1732H_2O$
C1_2A0_01SH	$Ca_{2.4}Al_{0.04}Si_2O_{7.1845}H_{1.449}\cdot 2.0794H_2O$
C1_1A0_01SH	$Ca_{2.2}Al_{0.04}Si_2O_{6.9455}H_{1.371}\cdot 1.885H_2O$
C0_8A0_01SH	$Ca_{1.6}Al_{0.04}Si_2O_{6.2343}H_{1.1486}\cdot 1.63H_2O$
C0_7A0_01SH	$Ca_{1.4}Al_{0.04}Si_2O_{6.0128}H_{1.1056}\cdot 1.4156H_2O$
C0_7A0_025SH	$Ca_{1.4}Al_{0.1}Si_2O_{6.1077}H_{1.1154}\cdot 1.5092H_2O$
C0_8A0_025SH	$Ca_{1.6}Al_{0.1}Si_2O_{6.331}H_{1.162}\cdot 1.6746H_2O$
C0_7A0_05SH	$Ca_{1.4}Al_{0.2}Si_2O_{6.2658}H_{1.1316}\cdot 1.6968H_2O$
C0_8A0_05SH	$Ca_{1.6}Al_{0.2}Si_2O_{6.4921}H_{1.1842}\cdot 1.7636H_2O$
M-S-H discrete solids	
MSH06	$Mg_{0.82}SiO_{2.385}(OH)_{0.87}$
MSH12	$Mg_{1.07}SiO_{2.075}(OH)_{1.99}$

8.4.6. Kinetic Data

Mineral dissolution / precipitation rate values were taken from Palandri and Kharaka (2004) (Table 7) and other recent modelling publications (Wilson et al., 2017a, 2018). Surface areas (Table 8) are those used to produce surface-area normalised rates, and if those data unavailable, geometric assumptions were made by (spherical particle approach). Surface areas were updated from previous published work using reported molal volume data and relative formula weight values from THERMODDEM (rather than density values reported from other data sources). One variant case was produced a using simplified T-S-T expression with a single rate (k) set at 1 x 10^{-3} mol m^{-2} s^{-1} and surface area at 1 m^2 g^{-1} to mimic the attainment of local equilibrium.

Table 7: Kinetic Data for acid, neutral, base / carbonate mechanisms (Equation 3).

Solids	Acid		Neutral	Base		Carbonate		Analogue	Ref.
Primary	log *k*1	*n*1	log *k*2	log *k*3	*n*3	log *k*4	*n*4		
Portlandite	-	-	-12	-	-	-	-	-	
Hydrotalcite OH	-	-	-12	-	-	-	-	Talc	2
Monocarboaluminate	-	-	-12	-	-	-	-	Ettringite	1
Monosulfoaluminate	-	-	-12	-	-	-	-	Ettringite	1
Hydrogarnet OH (C3AH6)	-	-	-12	-	-	-	-	Ettringite	1
C-S-H (1.6)	-	-	-12	-	-	-	-	-	1
Secondary									
C-S-H discrete solids	-	-	-12	-	-	-	-	-	1
C-A-S-H discrete solids	-	-	-12	-	-	-	-	-	1
M-S-H discrete solids	-	-	-12	-	-	-	-		1
Brucite	-4.73	0.5	-8.24	-	-			-	2
Calcite	-0.3	1	-5.81	-	-	-3.48	1	-	2
Dolomite	-3.19	0.5	-7.53	-	-	-5.11	0.5	-	2
Hydrotalcite-CO3	-	-	-12	-	-	-	-	Talc	1
Ettringite	-	-	-12	-	-	-	-		1
Thaumasite	-	-	-12	-	-	-	-		1
Gypsum	-	-	-2.79	-	-	-	-		2
Friedel's salt	-	-	-12	-	-	-	-		1
M-S-H (06, 12)	-	-	-12	-	-	-	-		1
Katoite_Si1	-	-	-13.8	-16.34	-0.36	-	-		3
Straetlingite	-	-	-13.8	-16.34	-0.36	-	-		4
Amorphous SiO_2	-	-	-12.77	-	-	-	-		2
Saponite (Na, Ca, K)	-12.37	0.35	-14.54	-15.66	-0.18	-	-		3
Beidellite (Na, Ca, K)	-12.37	0.35	-14.54	-15.66	-0.18	-	-		3
Chabazite	-	-	-13.8	-16.34	-0.36	-	-		4
ZeolitePCa	-	-	-13.8	-16.34	-0.36	-	-		4
Analcime	-	-	-11.4	-13.9	-0.36	-	-		3
Illite	-11.78	0.56	-15	-20.07	-0.55	-	-		3
Heulandite (Ca, Na)	-	-	-13.8	-16.34	-0.36	-	-		4
Clinoptilolite (Ca, Na, K)	-	-	-13.8	-16.34	-0.36	-	-		4
Phillipsite (Ca, Na, K)	-	-	-13.8	-16.34	-0.36	-	-		4

References

1. Baur et al. (2004)
2. Palandri and Kharaka (2004)
3. Wilson et al. (2017a)
4. Wilson et al. (2018)

Table 8: Surface area data.

Solid	Asp ($m^2 g^{-1}$)	Data / Analogue	Ref.
Primary			
Portlandite	10.7	0.25 μm spheres	-
Hydrotalcite OH	12.3	0.25 μm spheres	-
Monocarboaluminate	11.2	0.25 μm spheres	-
Monosulfoaluminate	12.0	0.25 μm spheres	-
Hydrogarnet OH (C3AH6)	9.5	0.25 μm spheres	-
C-S-H (1.6)	41.0	BET data	1
Secondary			
M-S-H	41.00	C-S-H analogue	
C-A-S-H	41.00	C-S-H analogue	
Brucite	10.13	1 μm spheres	
Calcite	2.21	1 μm spheres	
Dolomite	2.10	0.25 μm spheres	
Hydrotalcite-CO3	11.94	0.25 μm spheres	
Ettringite	9.80	BET data	1
Thaumasite	9.80	Ettringite analogue	
Gypsum	10.39	0.25 μm spheres	
Friedel's salt	9.80	Ettringite analogue	
Katoite_Si1	9.23	0.25 μm spheres	
Amorphous SiO_2	11.59	0.25 μm spheres	
Saponite (Na, Ca, K)	111.00	Montmorillonite analogue	2
Beidellite (Na, Ca, K)	111.00	Montmorillonite analogue	2
Illite	130.00	BET	2
Straetlingite	12.60	0.25 μm spheres	
Heulandite (Ca, Na)	10.10	Clinoptilolite analogue	
Clinoptilolite (Ca, Na, K)	10.10	reported	3
Phillipsite (Ca, Na)	10.10	Clinoptilolite analogue	
Gismondine	10.10	Clinoptilolite analogue	
Chabazite	10.10	Clinoptilolite analogue	
ZeolitePCa	10.10	Clinoptilolite analogue	
Analcime	0.25	BET	2

References

1. Baur et al. (2004)
2. Wilson et al. (2017a)
3. Wilson et al., (2018)

8.4.7. Model Cases

To address the issues posed in Section 8.1, several model cases have been specified (Table 9). In all model cases except one, a kinetic approach was used for mineral dissolution-precipitation. In one case, a "rapid" rate was applied to simulate the assumption of local equilibrium attainment. Alkali leaching was included in one of the models.

Table 9: Summary of coupled model cases.

Identifier	Description
Model 1 (kin)	Full dissolution / precipitation kinetics, no alkali leaching, DSP approach to C-S-H leaching (a) regular grid (b) "geometric" grid
Model 2 (LE)	Local equilibrium simulation (see text)
Model 3 (alt C-S-H)	As Model 1 with alternative C-S-H leaching
Model 4 (alkalis)	As Model 3 with alkali release from C-S-H (solid solution approach)
Model 5 (glacial water)	As Model 1, but with water based on glacial water
Model 6 (saline water)	As Model 1, but with saline water

8.5. Model Outputs

8.5.1. Independent Modelling

The main model outputs of interest include the overall bulk evolution of the solids, particularly the rate of dissolution front movement through the concrete, the changes in pH, and the volume change of the solid phase assemblage, with consequent porosity change. Initially, a comparison is made between the independent models to ascertain the role played by reaction kinetics (which are not included in the SKB approach). Model 1a and Model 2 give broadly similar outputs. In the first few hundred to 1000 y, the distribution of solids in the cement paste change, with significant dissolution of primary hydrogarnet and monosulphate, and replacement by Si-katoite and monocarboaluminate (Figure 12).

By 1000 years, portlandite has partially dissolved close to the groundwater boundary, with a slight increase in the amount of monocarboaluminate present (Figure 13). By 10,000 y, the amount of portlandite loss and C-S-H leaching is similar with both models showing portlandite dissolution (mostly within ~ 0.2 m of groundwater boundary), incongruent C-S-H dissolution (represented by dissolution / reprecipitation of discrete C-S-H solid phases with successively lower Ca/Si ratios), ettringite precipitation and the precipitation of small amount of calcite (Figure 13). Model 1a (kinetic treatment and Model 2 (local equilibrium simulation) give similar outputs after 10,000 y of reaction time, with only minor differences in C-S-H composition (lower Ca/Si in Model 2 near to the groundwater boundary).

M1a (kinetics, regular grid), 1,000 y	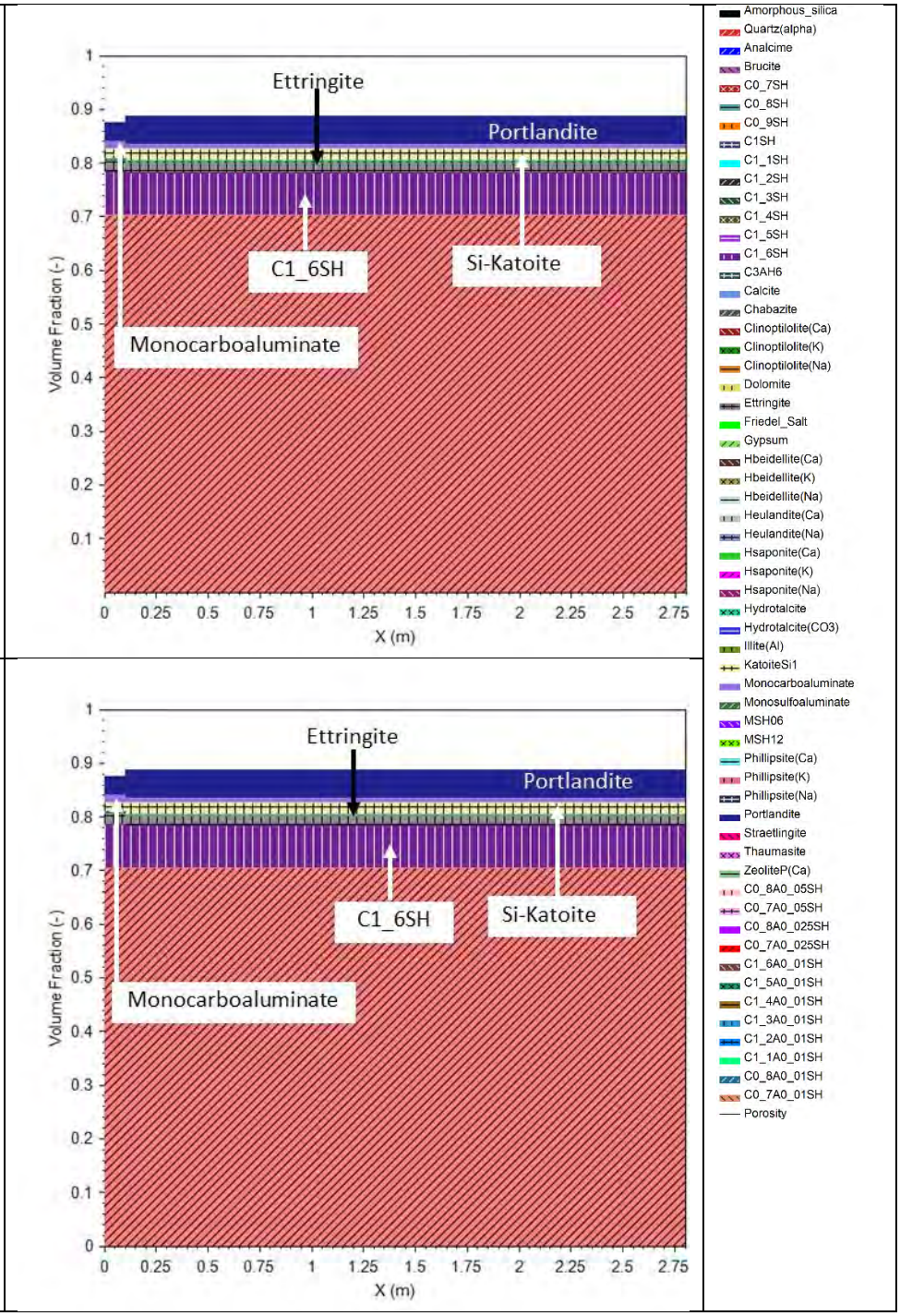
M2 (local equilibri-um, regular grid), 1000 y	

Figure 12: Volume fraction plots from Models 1 (above, kinetic approach) and Model 2 (below, local equilibrium simulation) after 1,000 years.

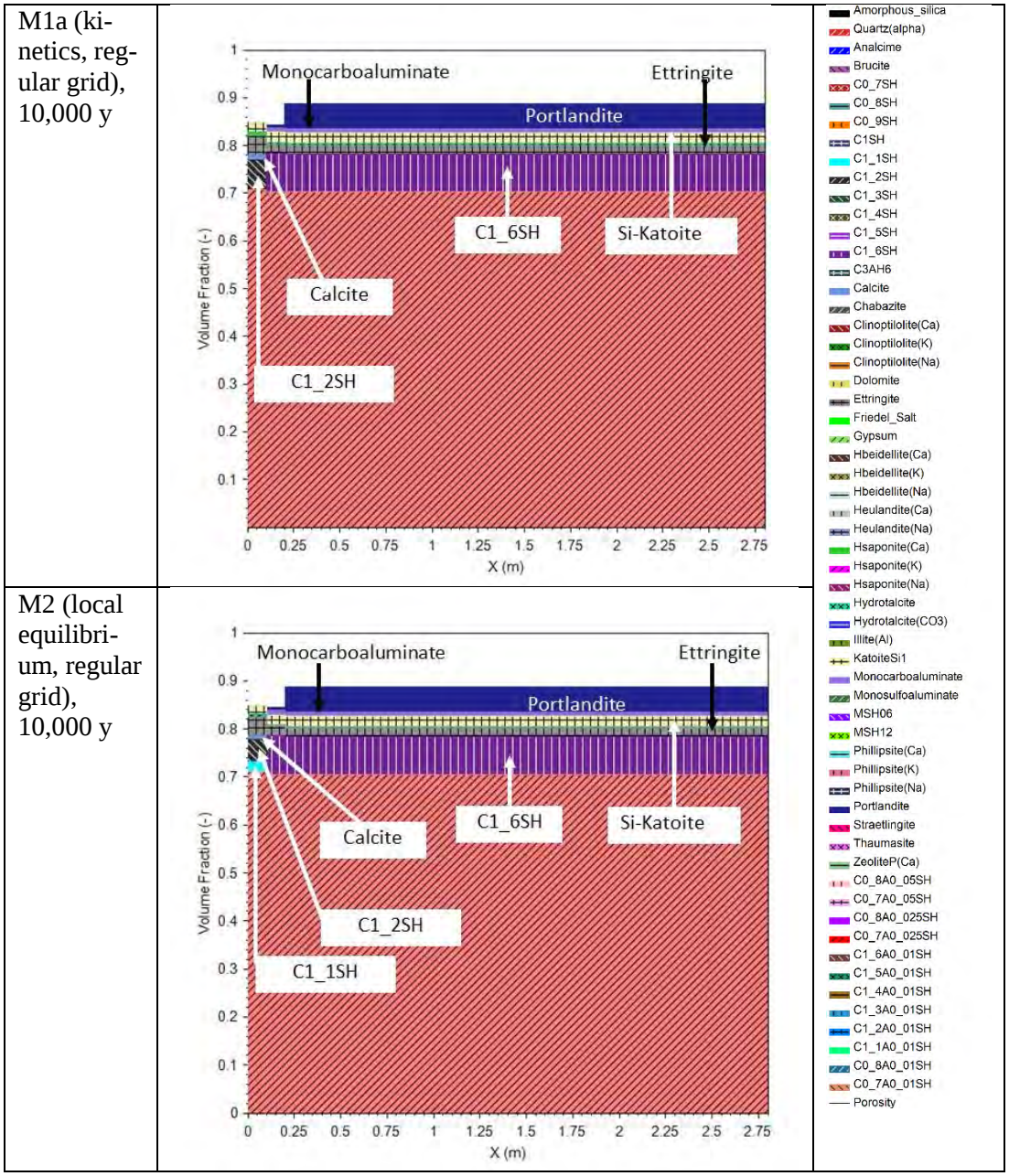

Figure 13: Volume fraction plots from Models 1 (above, kinetic approach) and Model 2 (below, local equilibrium simulation) after 10,000 years.

By 100,000 y, loss of portlandite and C-S-H leaching is quite extensive, with portlandite being completely dissolved up to ~0.75 m from the groundwater boundary (Figure 14). From 10,000 y to 100,000 y, the portlandite dissolution front was followed by a front of C-S-H leaching, (Ca/Si ratio decreasing from 1.5 to the edge of the remaining portlandite to 1 in Model 1, and 0.9 in Model 2, in the second model cell from the groundwater boundary). C-S-H was completely lost in the first model cell, with secondary products adjacent to the groundwater boundary comprising calcite, ettringite, Ca-saponite, chabazite and zeoliteP in Model 1, and straetlingite in Model 2 (Figure 14).

M1a (kinetics, regular grid), 100,000 y	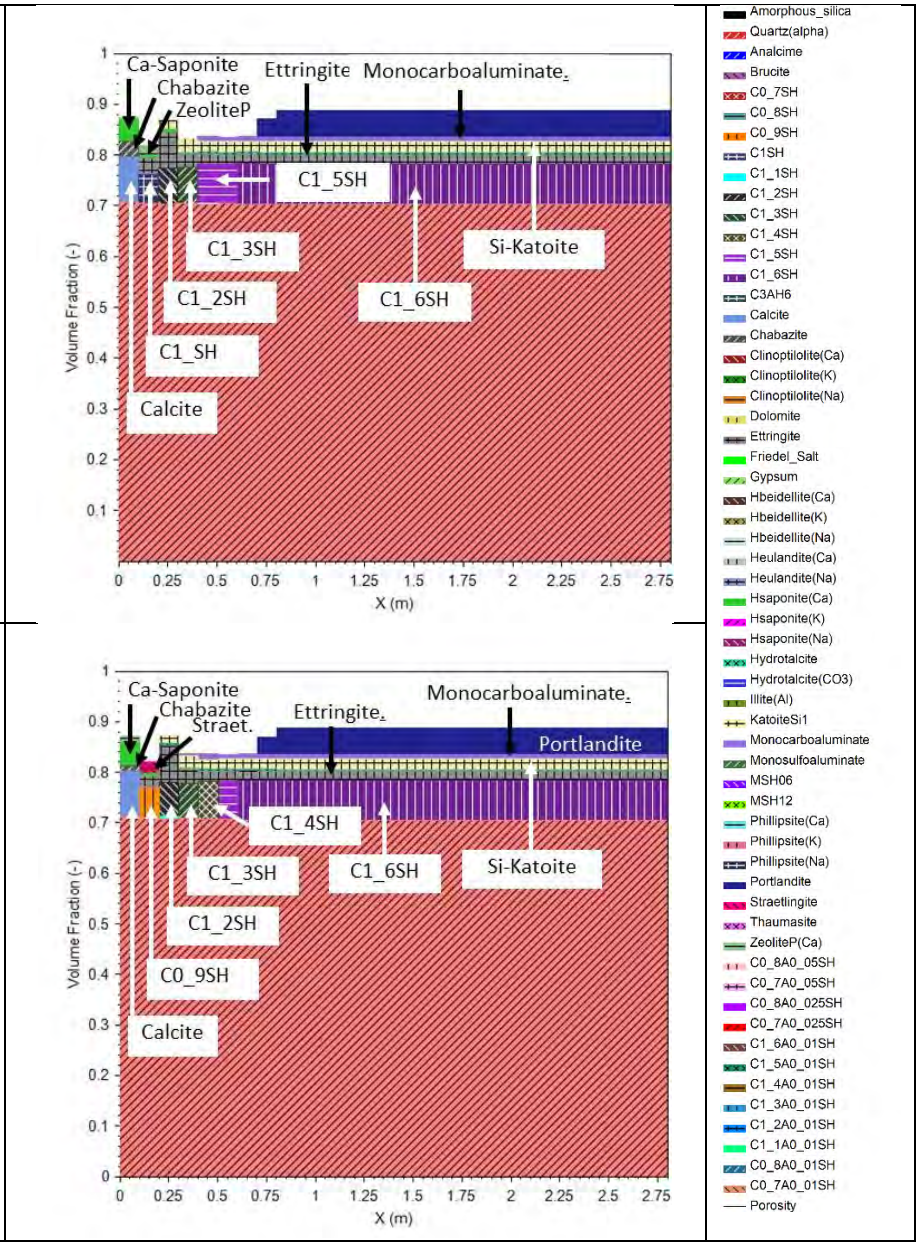
M2 (local equilibrium, regular grid), 100,000 y	

Figure 14: Volume fraction plots from Models 1 (above, kinetic approach) and 2 (below, local equilibrium simulation) after 100,000 years.

By the end of the Model 1a and Model 2 simulations (1 million y), the portlandite dissolution front moves further from the groundwater inflow, reaching a distance of 1.7 m from it (Figure 15). C-S-H leaching continues in a front following that of portlandite dissolution, with Ca/Si now ranging from 1.3 closer to the groundwater inflow, and 1.6 where portlandite remains. Ettringite, calcite and Ca-saponite continue to precipitate, and there is also the precipitation of very small amounts of straetlingite (and zeoliteP) occurring in the cell adjacent to the groundwater boundary and a loss of porosity (Figure 15). The differences between Model 1 and 2 simulations continue to be very small even after 1 million years, with minor differences in the amounts of straetlingite present. The porosity of the model cell next to the groundwater boundary gradually decrease throughout the simulations. By 800,000 y, almost all porosity has been lost (only 0.05 vol.% remain in Model 1) with 0.09 vol.% remaining in Model 2 by 1 million years (Figure 15).

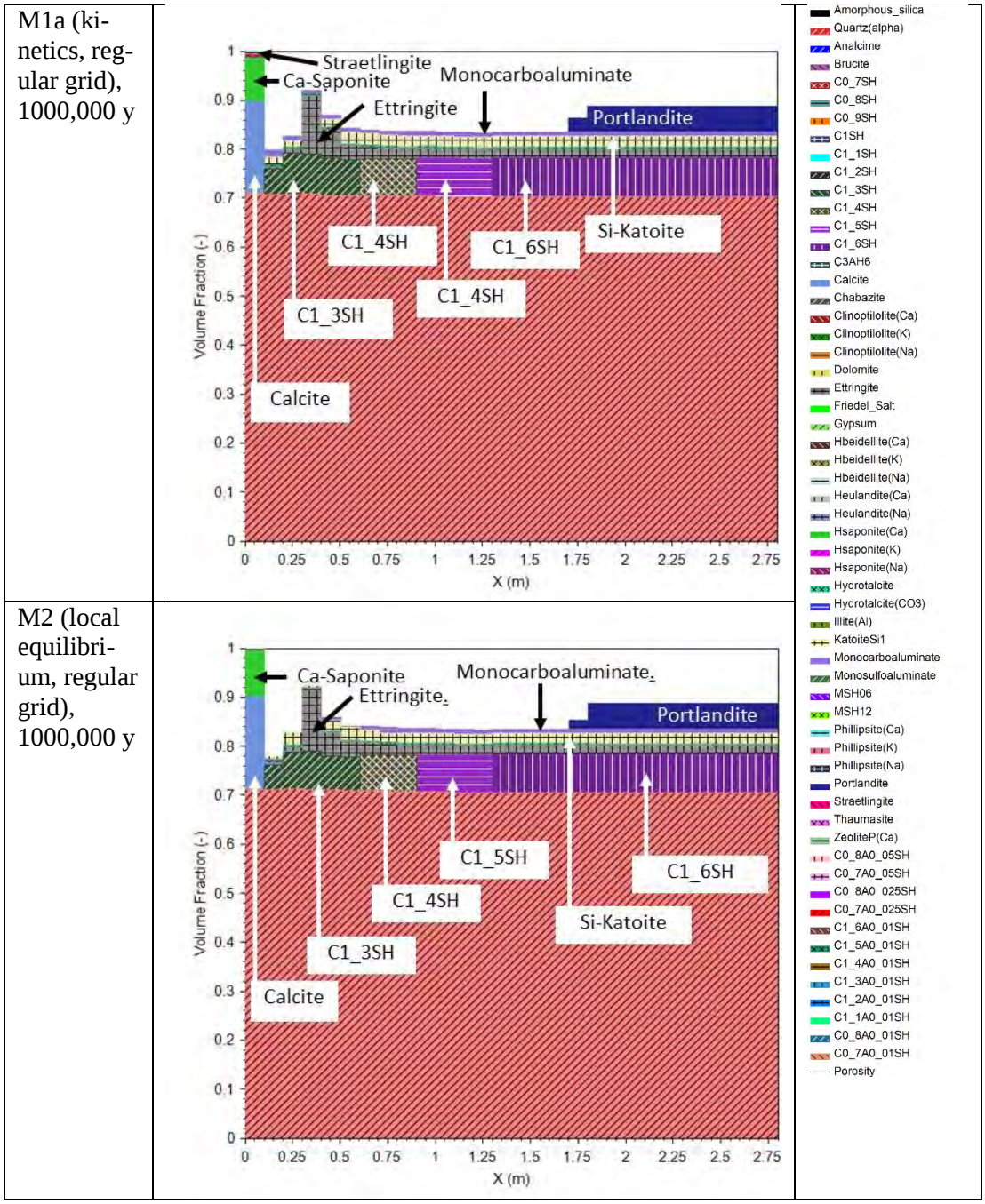

Figure 15: Volume fraction plots from Models 1 (kinetic approach) and 2 (local equilibrium simulation) after 1,000,000 years.

The pH of the cement porewater in Model 1a (and other models with similar solids) reflects the solids present, with pH decreasing from ~12.5 when portlandite is completely dissolved to values as low as ~11 due to C-S-H buffering. The pH gradually decreases over time, with the decrease being more extensive closer to the groundwater inflow over the first ~250,000 y. However, once the porosity of the model cell next to the groundwater inflow becomes very small, the potential for advective transport decreases due to the

decrease in porosity, and pH actually begins to rebound, due to back-diffusion as the primary solids remaining far from the groundwater interface continue to dissolve.

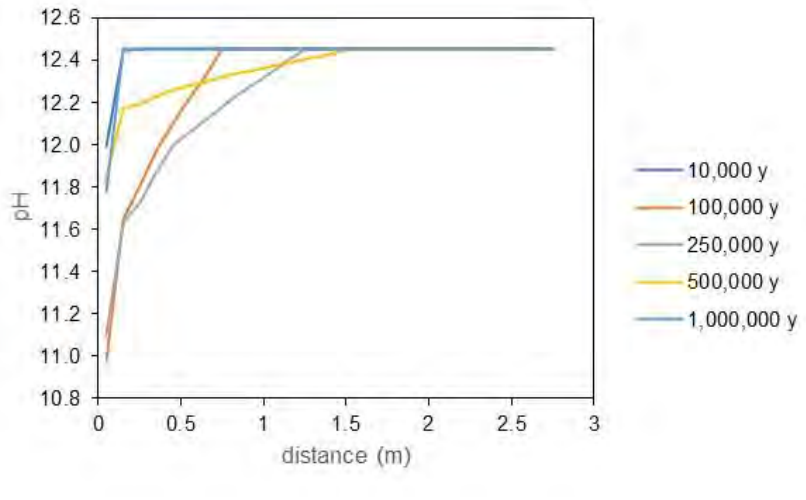

Figure 16: pH profiles associated with Model 1a at key times (years).

The minimum and maximum porosities across the modelled domain are similar in both Model 1a and Model 2 at any given time. By the end of the modelled 1 million years the porosity distribution across the domain is almost identical in both models (Figure 15). However, at earlier times, there is a tendency for a greater proportion of the domain to have relatively high porosity when there is instantaneous equilibrium (Model 2) than when reaction kinetics are simulated (Model 1a) (e.g. Figure 14).

Thus far, the results have focused on the effect of kinetics. The effect of model discretisation was also investigated by specifying the alternative grid in Model 1b (Figure 9). The effect of this is shown in Figure 17, where the narrower model cells towards the groundwater boundary have a greater amount of secondary calcite and therefore a greater reduction in porosity. In fact, Model 1b, fails to progress past ~250,000 y as the cell next to the groundwater boundary becomes completely full of secondary solids, especially calcite and Ca-saponite, thereby preventing further solute transport. With this model it would have been possible to slow precipitation of calcite such that some pore space remains, and solute transport could continue, but this was not considered further.

These results show that the regular grid is conservative from the perspective of the stated function of the cementitious engineered barrier to minimise water fluxes through it.

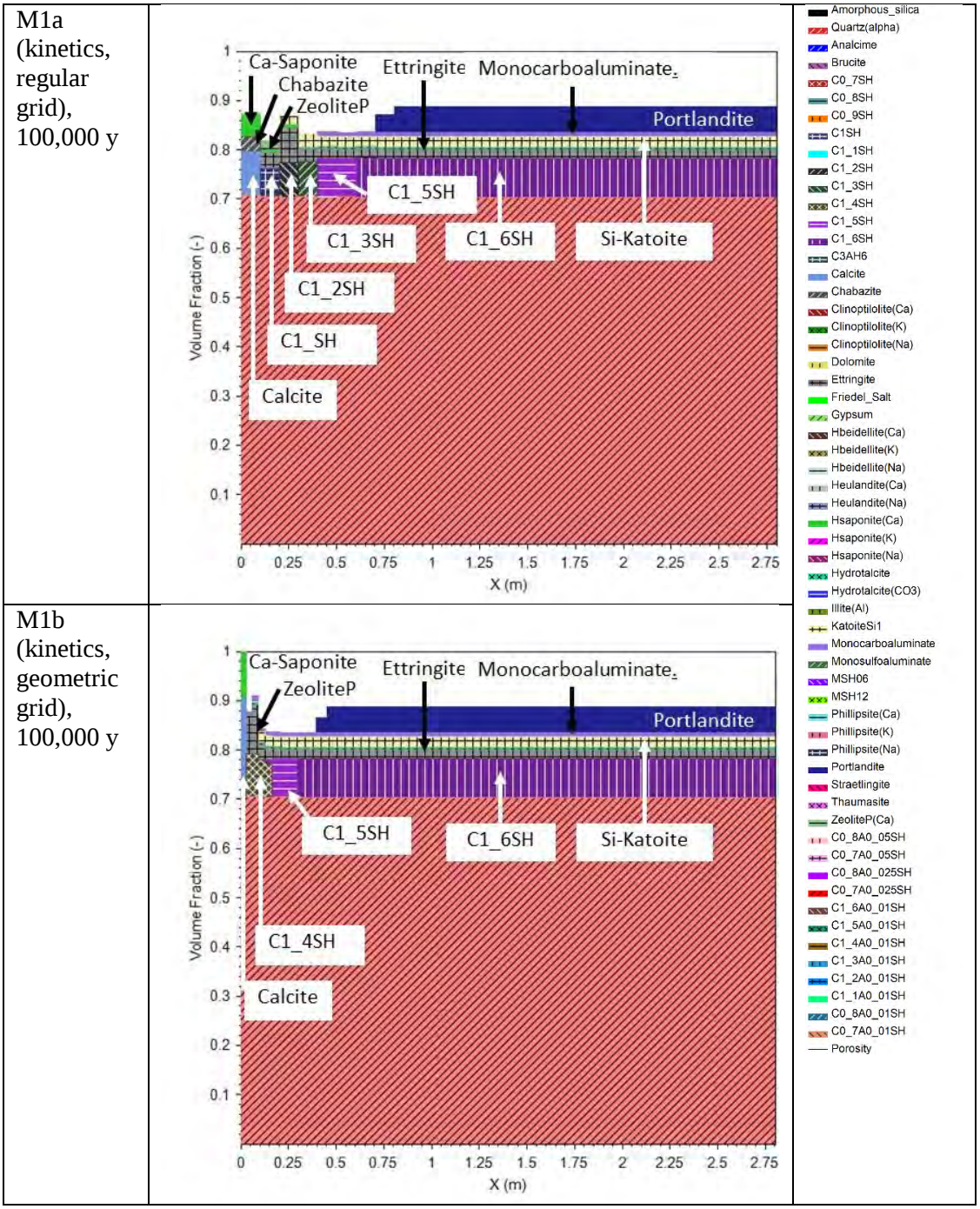

Figure 17: Comparison between mineral assemblages for Model 1a (upper, regular grid) and Model 1b (lower, geometric grid).

In Model 3, an alternative C-S-H representation is used to determine whether this has any significant effects on model outputs. In this alternative approach the C-S-H phases are represented by an ideal solid solution consisting of a jennite-like endmember and a tobermorite-like endmember. As shown in Figure 18, the proportions of other cement solids and the extent of leaching is remarkably similar in both models, suggesting that either a DSP or ideal solid solution approach can be applied to cement degradation over long time scales relevant to safety assessment. It is also noteworthy that the distribution of porosity

across the modelled domain is very similar whichever of the two C-S-H representations is used.

M1a (kinetics, regular grid), 100,000 y

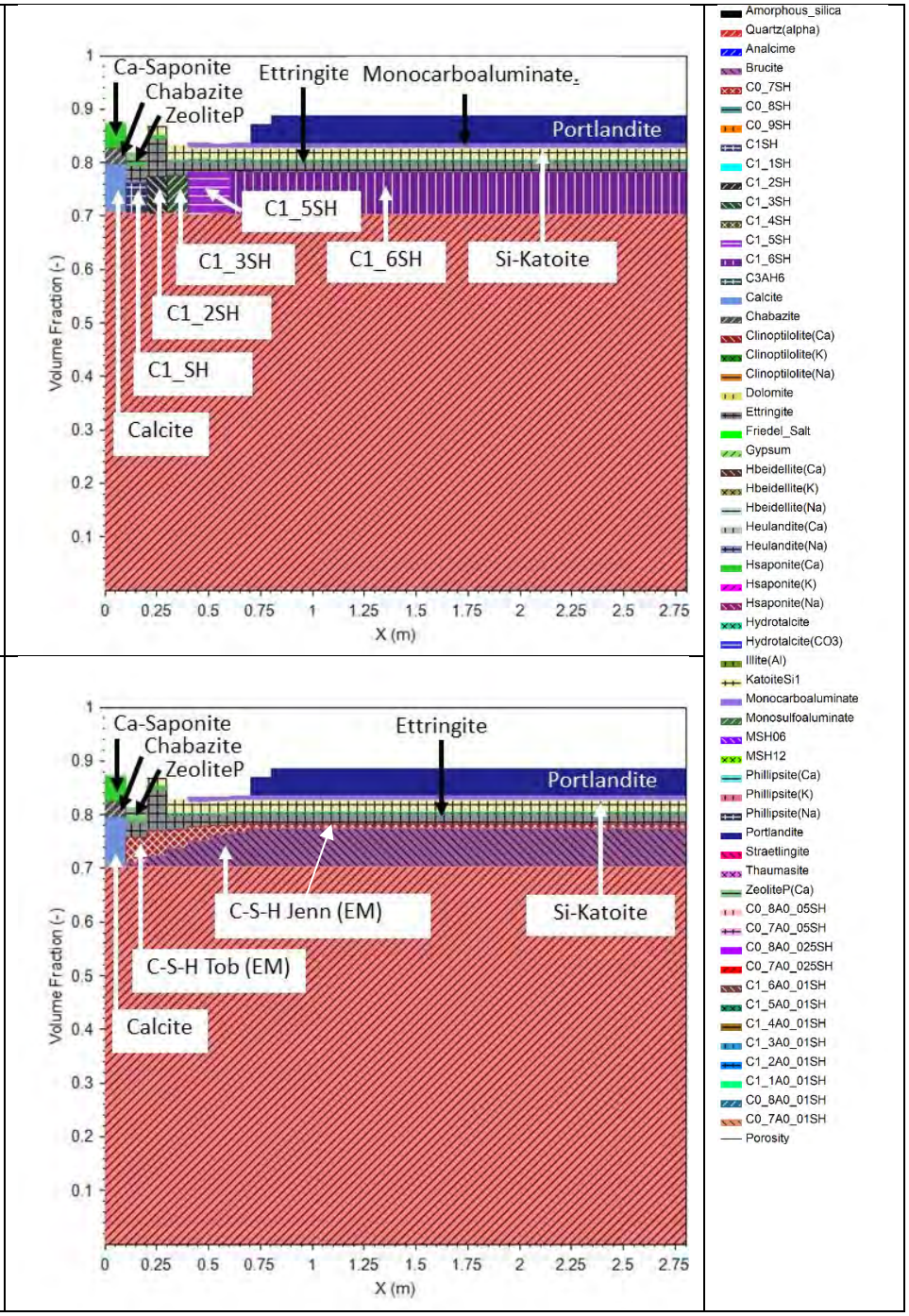

M3 (as M1a with alternative C-S-H leaching). 100,000 y

Figure 18: Volume fraction plots for Model 1a (upper, DSP approach for C-S-H gel) and Model 3 (lower, ideal binary solid-solution approach for C-S-H gel) after 100,000 years.

The models described thus far are simplified in that they do not include the leaching of alkali species notionally sorbed to C-S-H gel, which tends to be a relatively short-lived initial period of cement evolution (considering safety assessment timescales). A comparison of Model 3 (no alkalis, alternative C-S-H representation) with an identical model into

which Na and K desorption from C-S-H was included (Model 4) suggests that in terms of the extent of alteration over long time scales such as 100,000 y, there is little difference when alkalis are excluded (Figure 19).

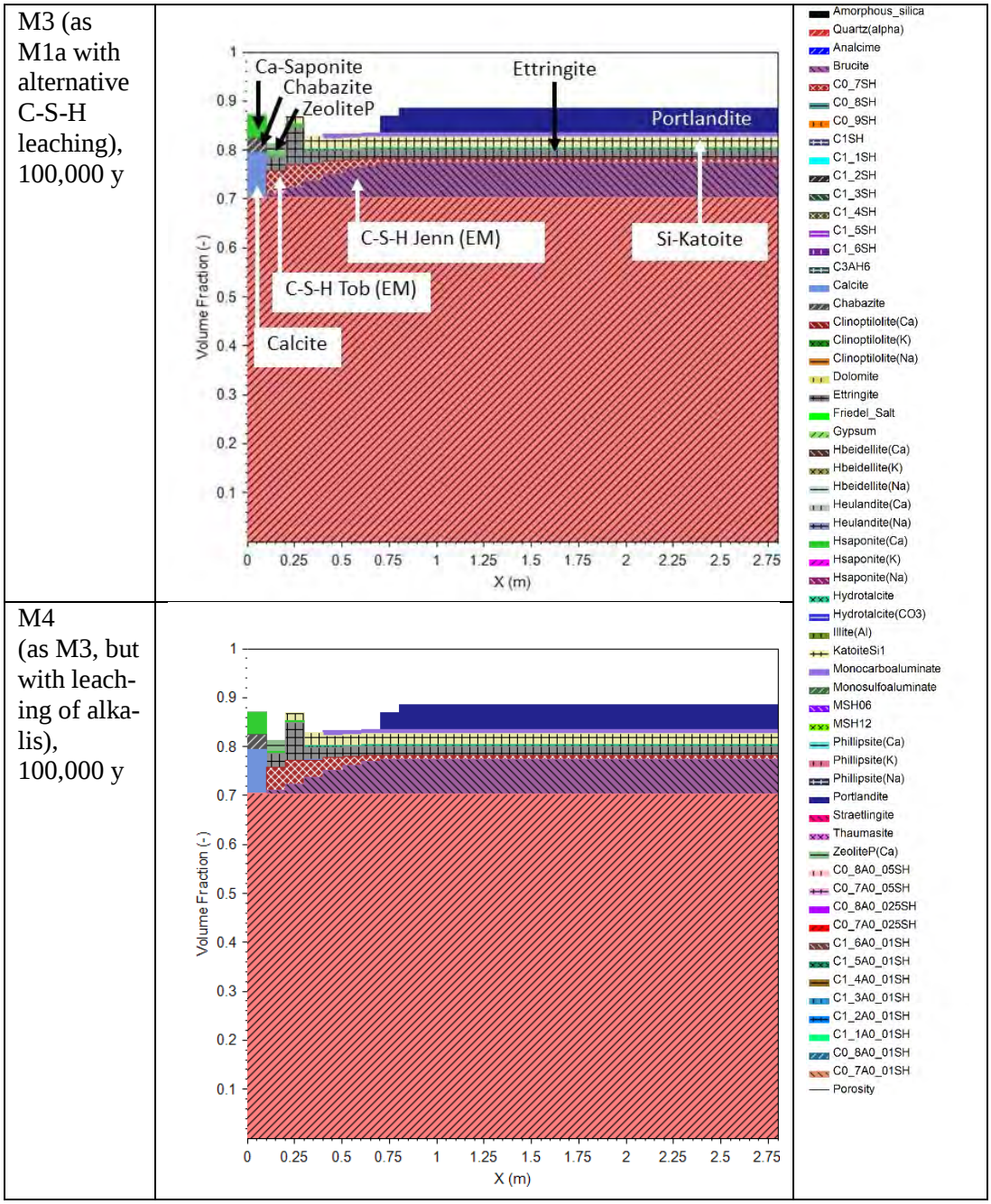

Figure 19: Volume fraction plots for Model 3 (upper, alternative C-S-H representation) and Model 4 (alternative C-S-H representation with alkalis) after 100,000 years.

The simulations of Idiart et al. (2019) in SKB report R-19-14 consider only a single groundwater reference groundwater composition, corresponding to an "old meteoric groundwater" endmember from Idiart and Shafei (2019) (see Section 8.4.4).

To investigate the potential impact of a lower salinity water than the reference water used by Idiart et al. in SKB report R-19-14, Model 5 used a groundwater composition based on a glacial groundwater endmember given by Laaksoharju et al. (2009) (see Section 8.4.4). The results of Model 1a and Model 5 are compared in Figure 20 and Figure 21.

M1a (kinetics, regular grid, reference groundwater), 100,000 y

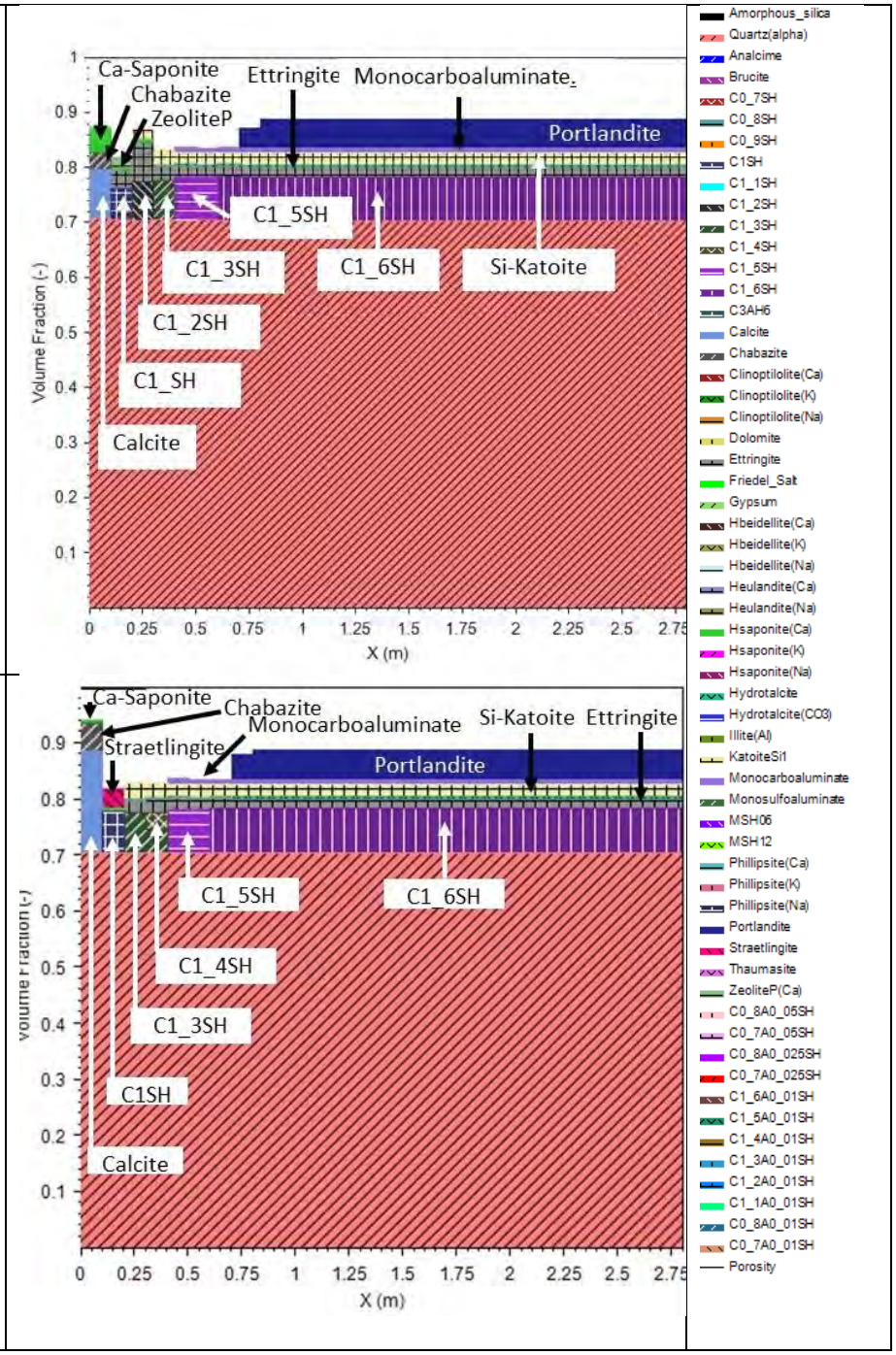

M5 (kinetics, regular grid, glacial water), 100,000 y

Figure 20: Volume fraction plots for Model 1a (upper, reference groundwater) and Model 5 (lower, glacial groundwater) after 100,000 years.

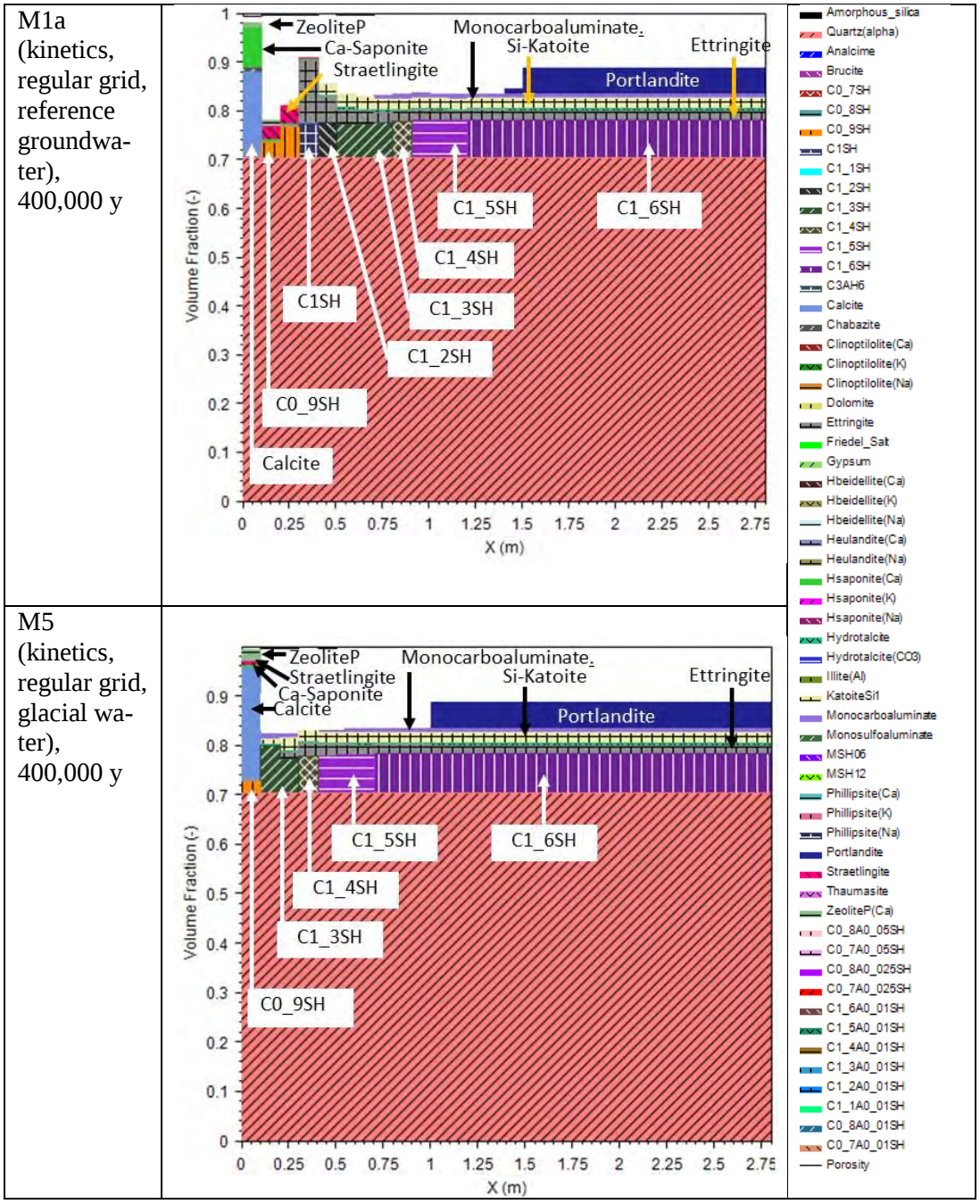

Figure 21: Volume fraction plots for Model 1a (upper, reference groundwater) and Model 5 (lower, glacial groundwater) after 400,000 years.

In the case of Model 5, with the glacial water, there is much greater precipitation of calcite adjacent to the groundwater inflow than in Model 1a. The result is that the pore space in the compartment next to the inflow becomes completely clogged shortly after 400,000 y, causing the model to stop. A consequence of more rapid pore sealing adjacent to the inflow in Model 5 than in Model 1a is that leaching of portlandite and C-S-H phases does not proceed as far in Model 5 as in Model 1a (Figure 21).

On the other hand, there is greater precipitation of ettringite in Model 1a than in Model 5 between 0.25 and 0.5 m (Figure 20 and Figure 21). This difference is matched by a corresponding smaller porosity between 0.25 m and 0.5 m in Model 1a than in Model 5. The enhanced formation of ettringite in Model 1a reflects the greater concentration of SO_4 in the reference groundwater used by Idiart et al. (2019) than in the glacial water considered for comparison in the independent modelling.

Apart from these difference in porosity between the two models, in other respects the variations in porosity across the modelled domain are generally similar in Model 1a and Model 5.

To investigate the possible significance of inflowing groundwater being more saline than the reference groundwater considered by Idiart et al. (2019), Model 6 has saline inflowing water based on the Littorina Seawater endmember given by Laaksoharju et al. (2009). Outputs form Model 6 are compared with those from Model 1a in Figure 22, Figure 23 and Figure 24.

In Model 6 the porosity adjacent to the groundwater inflow is smaller than in Model 1a at any considered time. The porosity of domain immediately next to the groundwater inflow becomes completely clogged in Model 6 shortly after 300,000 y, resulting in the model stopping. The low-porosity zone next to the groundwater inflow in Model 6 progressively expands over time into the modelled domain. This decreased porosity is due largely to the formation of ettringite and to a lesser extent thaumasite.

Another marked difference between Model 1a and Model 6 is that in the former there is no Friedel's salt, whereas in the latter Fridel's salt forms at the expense of Si-Katoite and to a lesser extent portlandite. This formation of Friedel's salt reflects the much higher chloride concentration of the groundwater based on Littorina Seawater used in Model 6, compared to the reference groundwater used in Model 1a.

As a consequence of the more rapid decrease in porosity next to the groundwater inflow in Model 6 compared to Model 1a, groundwater fluxes decrease more rapidly in Model 6 than in Model 1a. There is therefore less rapid leaching of C-S-H and portlandite in Model 6 than in Model 1a (Figure 23 and Figure 24).

M1a (kinetics, regular grid, reference groundwa-ter), 10,000 y	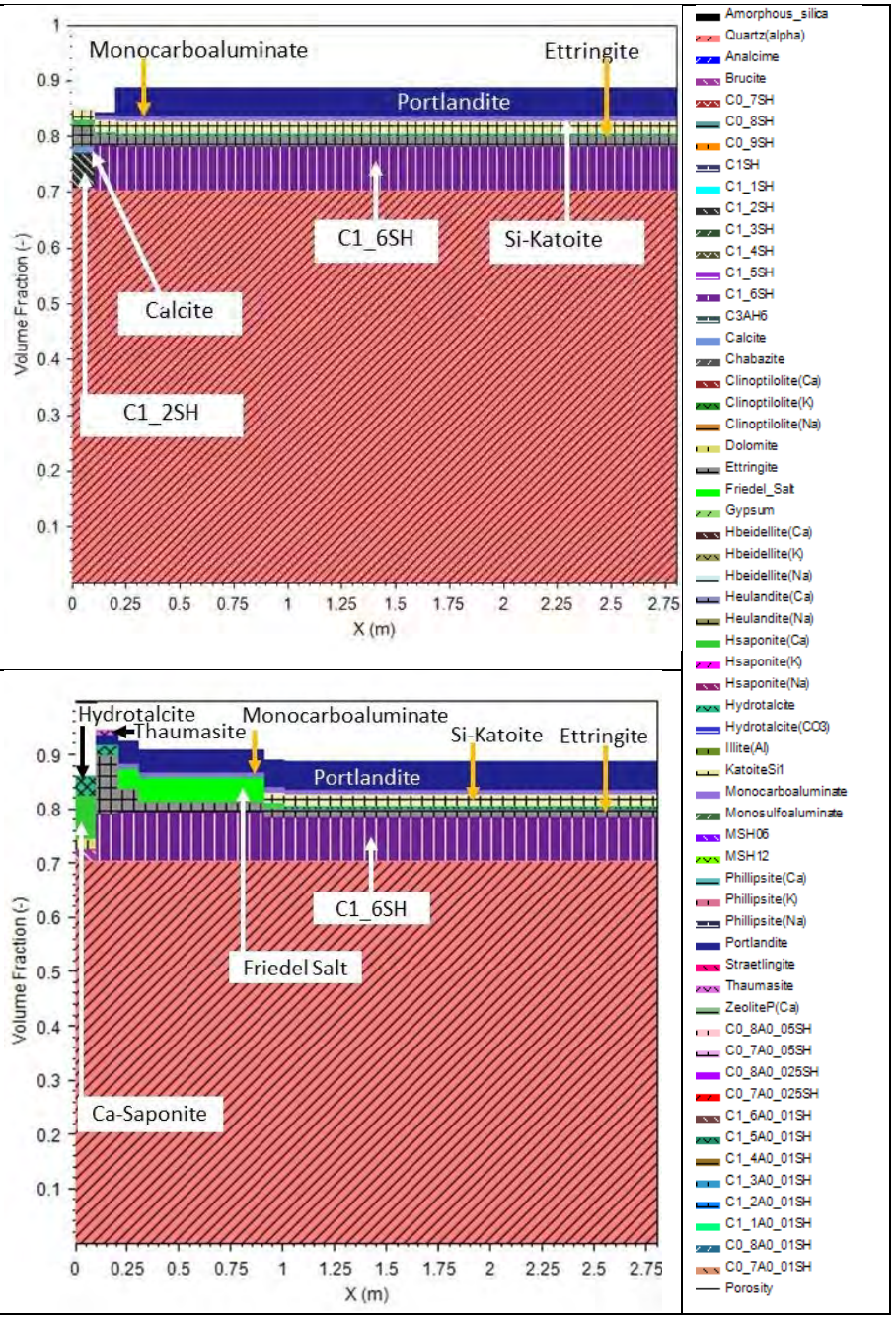
M6 (kinetics, regular grid, Littorina Seawater), 10,000 y	

Figure 22: Volume fraction plots for Model 1a (upper, reference groundwater) and Model 6 (lower, saline water (Littorina seawater)) after 10,000 years.

M1a (kinetics, regular grid, reference groundwa-ter), 100,000 y	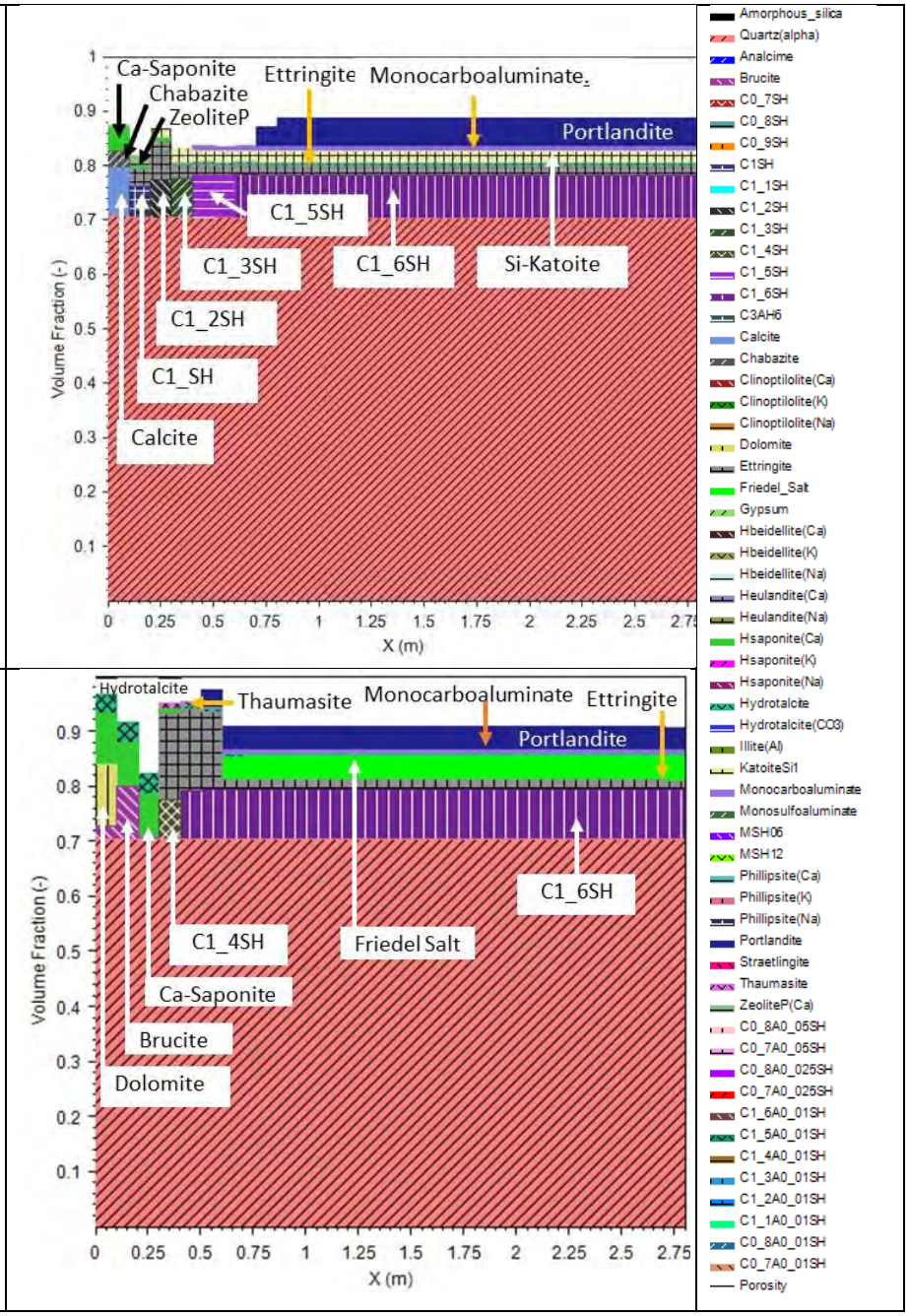
M6 (kinetics, regular grid, Littorina Seawater), 100,000 y	

Figure 23: Volume fraction plots for Model 1a (upper, reference groundwater) and Model 6 (lower, saline water (Littorina seawater)) after 100,000 years.

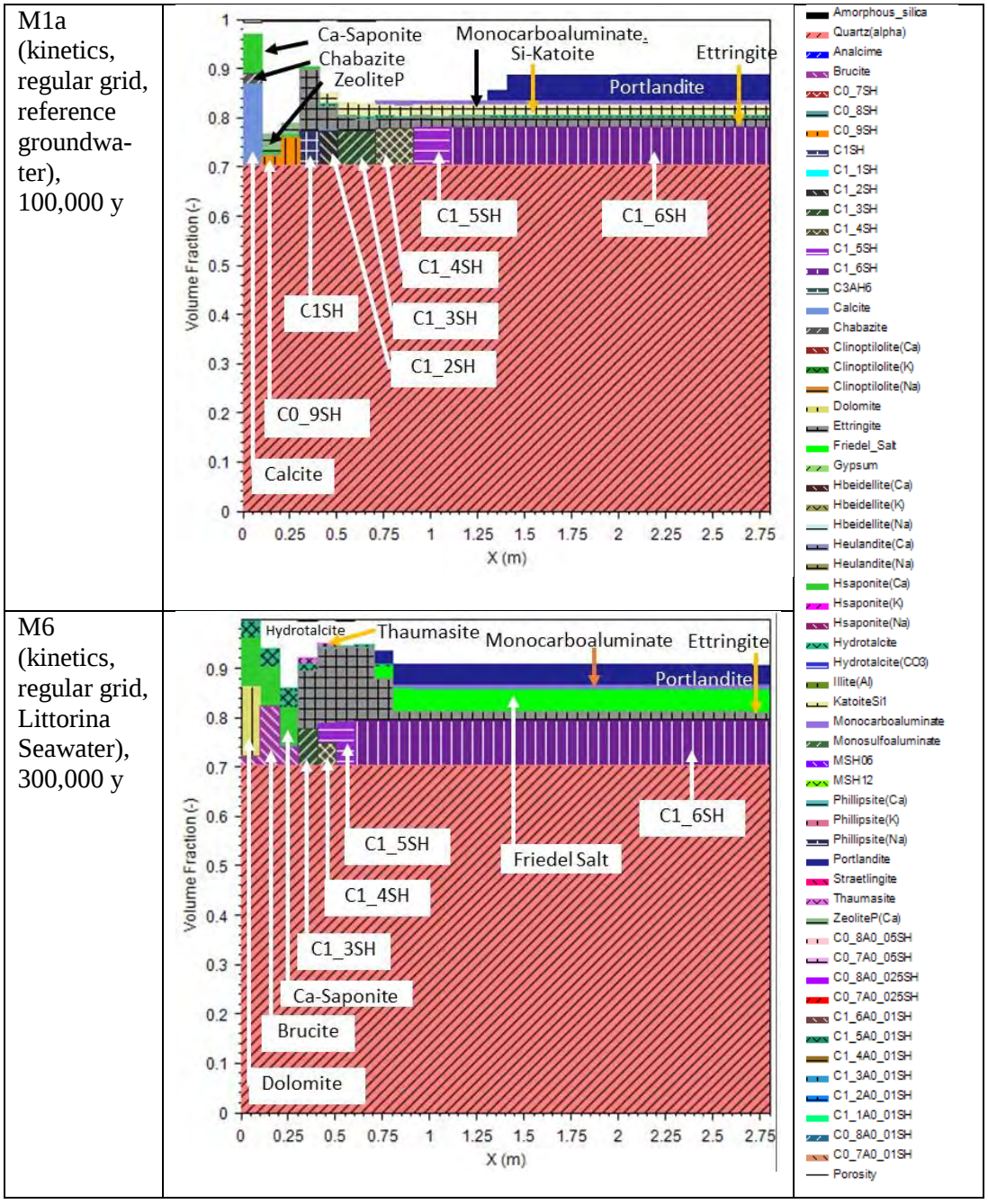

Figure 24: Volume fraction plots for Model 1a (upper, reference groundwater) and Model 6 (lower, saline water (Littorina seawater)) after 300,000 years.

The less rapid decrease in water flux in Model 1a compared to Model 5 and Model 6, means that Model 1a is conservative from the perspective of the stated function of the cementitious engineered barrier to minimise water fluxes. That is, from this perspective the model of Idiart et al. (2019) in SKB report R-14-19 can be considered conservative. However, in Model 6 relatively large quantities of ettringite are formed compared to Model 1a. Since ettringite has a very large molar volume (710.320 cm^3 mol^{-1} compared with 456 cm^3 mol^{-1} for jennite) its formation is likely to be accompanied by cracking of the concrete. From this perspective, Model 1a is not conservative. Of course cracking would also likely result in increased hydraulic conductivity of the cement. However, it was outside

the scope of the study reported here to investigate these effects. Should groundwater at a future SFL site be saline and sulphate-rich, it will be necessary to assess the possible effects of ettringite formation.

Formation of Friedel's Salt in Model 6 is unlikely to be directly detrimental with respect to the performance (pH-buffering capacity and hydraulic conductivity) of the concrete, but its presence illustrates that Cl can penetrate through the concrete. Were steel reinforcements to be used in the concrete they might be more likely to corrode in the presence of saline water like the Littorina Seawater-based groundwater specified in Model 6. Corrosion would likely result in loss of strength and would be accompanied by expansion which could cause the concrete to crack. Again, it will be necessarily to investigate the potential for such effects if the groundwater at a future SFL site is saline and chloride-rich.

8.5.2. Comparison of Independent Models Outputs to SKB Models

The independent models M1-4 show broadly similar behaviour, therefore M1a is taken as a representative model for comparative purposes. Idiart et al. (2019) provide plots of mineral volume fractions over the model domain at key times (Figure 25). They report that portlandite is completely lost to a depth of 1.4 m after 200,000 y, at which time decalcification of the C-S-H gel begins. Portlandite and the "jennite-like" C-S-H gel end member are completely depleted after 0.5 million years, with "tobermorite-like" C-S-H being lost in the first 0.8 m from the concrete-rock interface, with a large amount of calcite precipitating near the host rock interface. Straetlingite and ettringite also form as secondary solids along with a small amount of brucite, and hydrotalcite mostly persists in the simulation. Straetlingite precipitation occurred as hydrogarnet was lost after portlandite dissolution being complete. After 1 million years, the cement degradation is almost complete with only a small amount of tobermorite-like C-S-H end member left. The pH of the porefluid in the model reflects the dissolution-precipitation behaviour of the solids, with reduction occurring after the loss of Portlandite (200,000 y) and pH does not decrease below 10.5 if C-S-H was present, after which time values gradually decreased towards the value of the intruding groundwater.

Although the expected cement evolution pathways of leaching, carbonation and sulphate attack were predicted by both the SKB models and those described in Section 8.5.1, there are some important differences between them (c.f. Figure 25 and Figure 26).

The independent models have portlandite dissolution being extensive over the model domain throughout the timescales considered. Idiart et al. (2019) report portlandite being lost to a distance of 1.4 from the groundwater inflow after 200,000 y, whereas in the independent model portlandite was lost for only 1.1m after this time. In the model of Idiart et al. (2019), portlandite was lost after 1 million years, but some portlandite remained in the independent model after this time. This appears to be a result of the model of Idiart et al. (2019) not accounting for porosity being reduced by precipitation of phases such as calcite resulting in decreased water fluxes. Additionally, the independent models include secondary solids that have been postulated as very late-stage alteration products (smectites, such as saponite) and Ca-saponite occur as a secondary solid. Zeolite minerals are also included in the independent models, with chabazite and zeoliteP forming in small amounts. Such minerals would be expected to occur over post closure timescales due to cement-rock interaction.

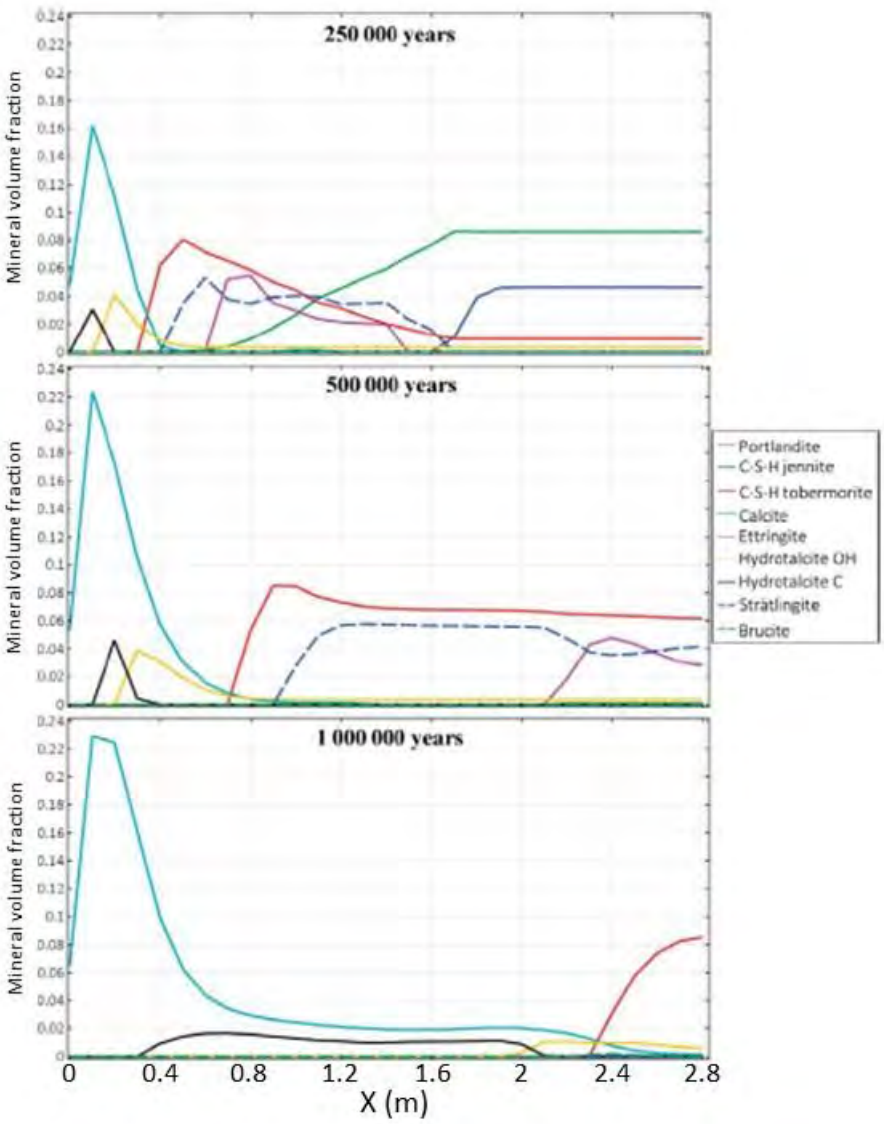

Figure 25: Volume fraction data for 1-D model of BHK vault evolution described by Idiart et al. (2019) (Case 1).

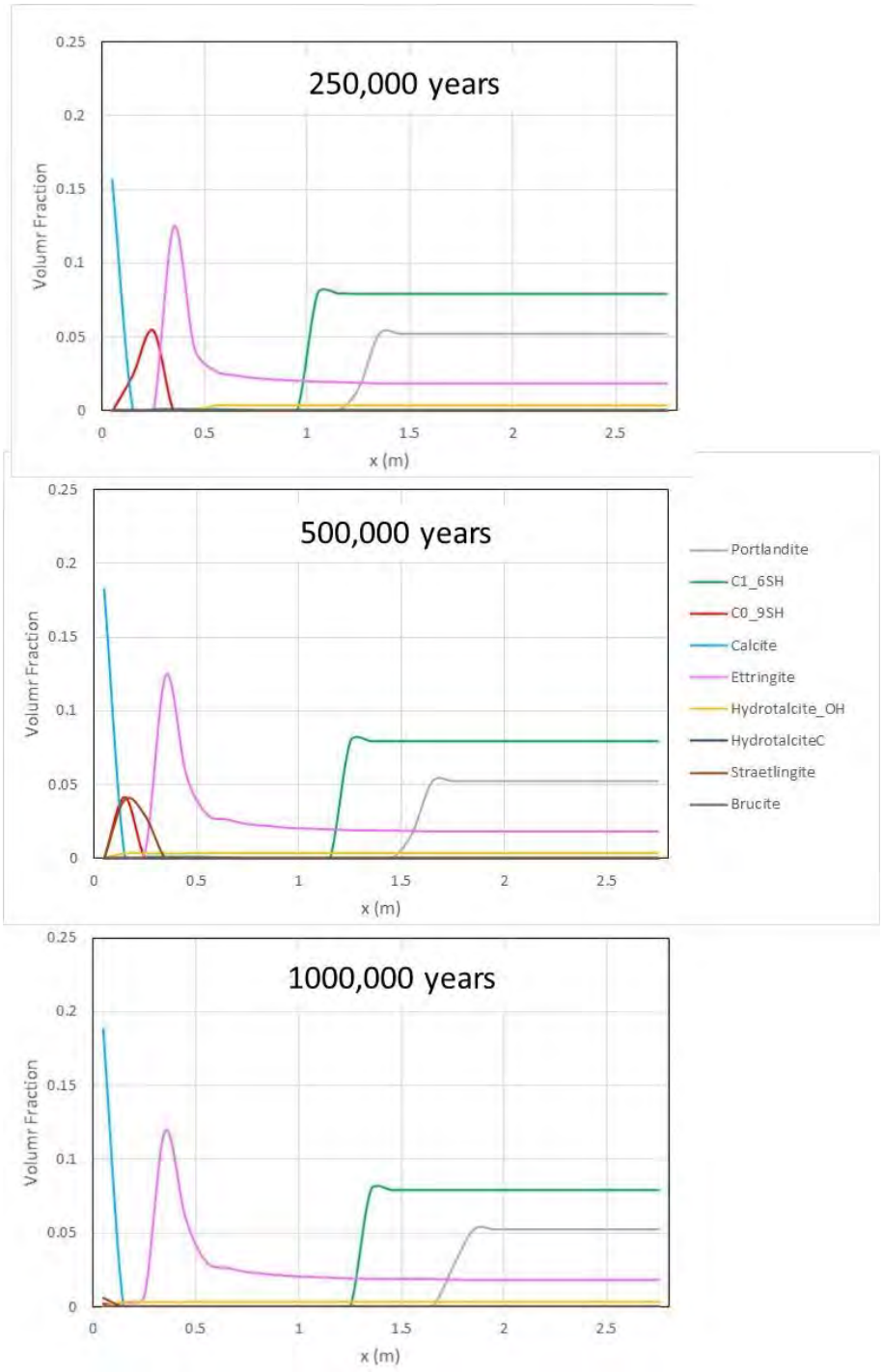

Figure 26: Volume fractions of solid phases calculated by the independent Model 1a. Only the phases corresponding to those shown by Idiart et al. (2019) (Figure 25, above) are shown. The independent modelling also predicted other solid phases not shown in the output from Idiart et al. (2019). N (see Figure 12, Figure 13, Figure 14, and Figure 15).

Reflecting the different evolving solid phase assemblages in the two models there are significant differences in pH evolution between the model of Idiart et al. (2019) and the independent Model 1a (Figure 27 and Figure 28). In particular, in the model of Idiart et al. (2019), pH at the groundwater inflow is close to that of the reference groundwater (pH =

8.6) at all times plotted, other than at the start of the simulation (Figure 27). The low-pH water penetrates progressively deeper into the concrete over time. This is possible owing to the loss of portlandite at later times and the relatively high degree of leaching of C-S-H phases.

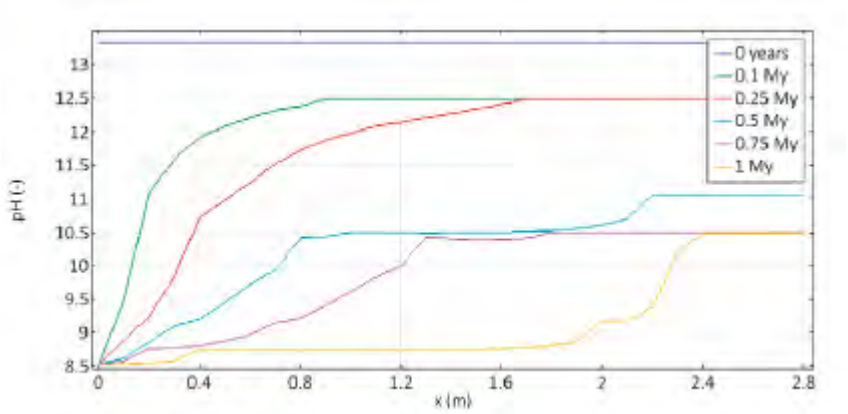

Figure 27: pH profiles for 1-D model of BHK vault evolution described by Idiart et al. (2019) (Case 1).

In contrast, in the independent Model 1a the pH remains substantially alkaline throughout the modelled domain over the considered period of 1 million years (Figure 28). Although relatively low pH is attained adjacent to the groundwater inflow, the pH never gets lower than pH = 11 here. These relatively alkaline conditions, compared to those in the model of Idiart et al. (2019) are maintained because important pH-buffering phases, notably portlandite and high Ca/Si C-S-H phases are not leached as rapidly in the independent model. This slower leaching in turn reflects the clogging of pores adjacent to the inflow by secondary phases.

Although in the independent Model 1a the pH next to the groundwater inflow initially decreases, at late times, when pore clogging is most advanced, the pH near the inflow increases again (Figure 28). This increase is caused by back-diffusion of OH^- from deeper in the concrete.

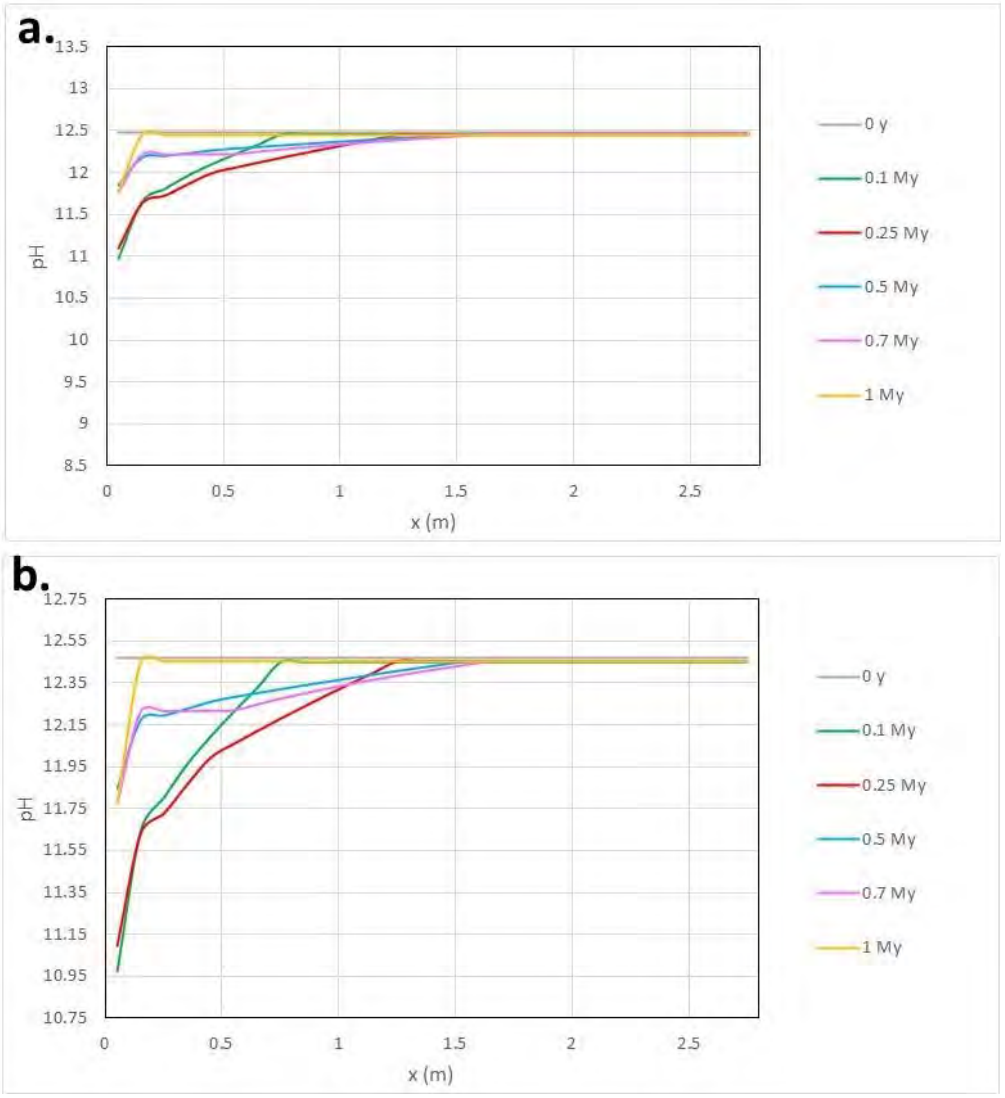

Figure 28: pH calculated by the independent Model 1a. a. is plotted with the same pH scale as given by Idiart et al. (2019) for their Case 1 (see Figure 27). b. shows the same results but with an expanded pH scale.

The differences in the pH evolution between the model of Idiart et al. (2019) and the independent Model 1a correspond to different porosity evolutions in the two models (Figure 29 and Figure 30). Whereas in the model of Idiart et al. (2019), there is progressive increase in porosity, spreading from the groundwater inflow across the domain (Figure 29), in Model 1a the porosity evolution is more complex (Figure 30). However, in Model 1a there is a marked decrease in porosity adjacent to the groundwater inflow, and a progressive increase in porosity with time across the modelled domain between 0.5 m and 1.8 m. This latter increase in porosity is much smaller than in the model of Idiart et al. (2019).

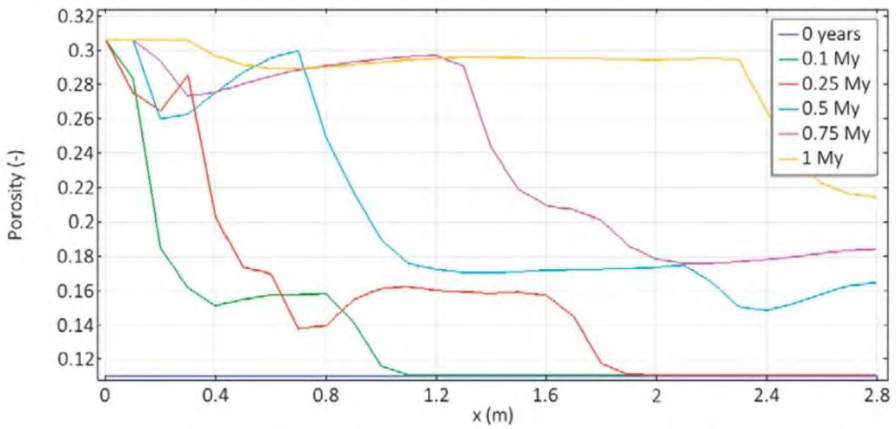

Figure 29: Porosity profiles for the 1-D model of BHK vault evolution described by Idiart et al. (2019) (Case 1).

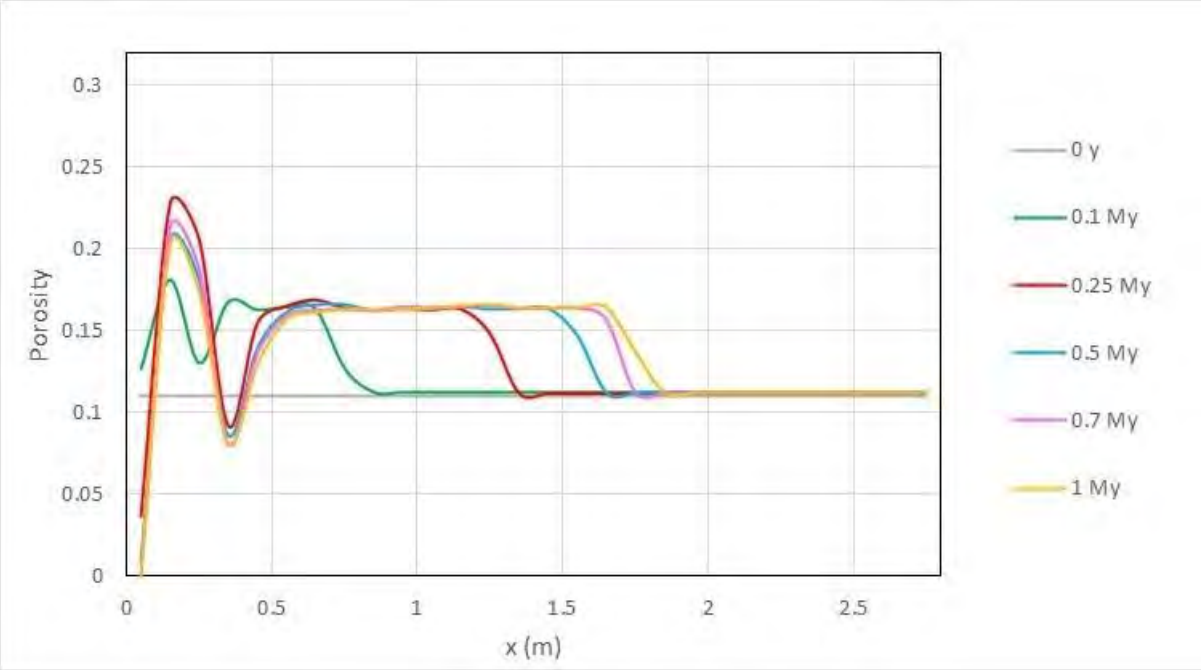

Figure 30: Porosity calculated by the independent Model 1a.

9. Assessment of SKB's Conclusions

9.1. General Conclusions

SKB's stated aims for the SE-SFL evaluation are:

- provide input to the subsequent steps in the development of SFL, including further development of the design of the engineered barriers and the site-selection process for SFL;
- evaluate conditions in the waste, barriers, and the repository environs under which the repository concept has the potential to fulfil the regulatory requirements for post-closure safety; and
- provide SKB with a basis to prioritise areas in which the level of knowledge and adequacy of methods must be improved to perform a subsequent, full safety assessment for SFL.

These objectives have been met to a large degree, although SKB does not indicate firm criteria for judging the success of the SE-SFL; it would be possible for SKB to provide additional detailed modelling and evaluation work to go even further towards meeting these objectives.

Overall, the modelling of cement degradation in the assessment is impressive, but arguably is too detailed for the present generic (not site-specific) state of the SFL programme. It would have been appropriate for SKB to have produce less sophisticated models, but to run more cases to evaluate uncertainties. Rather than 3-D and 2-D coupled models, simple 1-D models that explore uncertainties in key processes more rigorously would have been more useful. Particularly, models that incorporate reaction kinetics for both dissolution and precipitation reactions of all the major phases would have been useful.

SKB conclude that cementitious components of the barrier system in both the BHA and BHK vaults contribute to the retention function being met. However, in BHA, the main function of the cementitious components (grout and concrete structure in this respect) is to provide a sorbent for certain radionuclides, rather than to restrict advection. Only if the bentonite barrier in BHA was to fail, for example due to piping erosion, would the concrete structure have a function to reduce groundwater flow. Greater discussion of the impact of bentonite barrier failure on cement / concrete degradation would be beneficial.

SKB's modelling does not take any account of the effect of the repository on groundwater flow and chemistry. While the effects of the repository on groundwater flow and chemistry in the operational period will be very short-lived compared to the assessment time frame, it would be helpful to explore whether it could impact on longer-term cement / concrete evolution. For example, if saline water up-cones to the level of the repository, is it certain that there will be an insignificant effect on cement / concrete degradation?

The groundwater system in the Laxemar area is very heterogeneous in terms of groundwater chemistry and groundwater flow, reflecting the distribution of relatively few hydraulically conductive fracture zones in an otherwise non-conductive rock mass. There is generally an increase in groundwater salinity from fresh water at the surface, to brackish water at the repository depth and then to saline water about 500 m below the repository. However, dilute waters can penetrate to relatively great depth in hydraulically conductive

fracture zone, while there is potential for up-coning of saline water in such zones if there is an upwards head gradient, such as might be caused by construction of the repository, or in front of an ice sheet. Similar heterogeneous patterns of groundwater flow and chemistry are found throughout the Baltic Shield. It is therefore reasonable to suppose that such heterogeneity might also occur at any actual site for the SFL that might be selected in future. It is therefore important that the SE-SFL should capture this variability. However, it appears that, at least as far as cement / concrete degradation is concerned, SKB has only considered dilute groundwater. A wider range of groundwater compositions should be considered in future.

Another issue that is not considered in the SE-SFL is the corrosion of steel reinforcements in the concrete structures that surround the grouted waste in both the BHK and BHA vaults. This corrosion has the potential to cause expansive cracking of the concrete. However, it is not considered at all by the SE-SFL. Future assessments should consider this issue.

In TR-19-11. SKB conclude that the results of the radionuclide transport and dose calculations indicate that the conditions assumed in the base case yield doses that are too high to comply with the risk criterion for the BHA and BHK inventories underlying SE-SFL.

SKB suggest that for BHK an optimised concrete backfill material that has low hydraulic conductivity, porosity, and diffusivity improves the potential for the repository to meet regulatory requirements. It is noted that the properties of the concrete developed for the extension of SFR potentially yields a sufficiently good nearfield performance. Improved concrete properties should also improve the ability of the concrete to withstand degradation due to cement leaching. The effect on gas transport also needs to be considered.

The present reviewers concur with the need to optimise the concrete backfill material in the BHK vault. However, it would be beneficial to go further and to consider the potential benefits of alternative cement / concrete formulations for the concrete structures and grout in both vaults. Future modelling could usefully consider different cement compositions to establish which is optimum in the light of potential future changes in chemical conditions.

9.1. Summary of Concrete Degradation Modelling Review ("Bottom-Up" Approach)

Idiart and co-workers (Reports R-19-11, R-19-12, R-19-13, and R-19-14) have produced a suite of reports that describe several geochemical models of concrete degradation in the BHK vault included in the SFL concept for which the SE-SFL safety evaluation has been produced. There are some key themes that emerged from the detailed technical review of these documents, from the perspective of each report having been reviewed as a "stand-alone" document (Report TR-19-01).

The reports present a substantial body of material which is generally informative and of a high standard. The 3-D reactive-transport models are especially impressive. However, the inclusion of a small amount of additional discussion would have improved some aspects of the modelling reports. There are also some issues that need to be addressed, some

of which are potentially important for supporting the SE SFL safety evaluation. Additionally, some of the comments relating to earlier reports are addressed by further work described in later reports. Each of these issues and comments are summarised here.

- The most important point relating the detailed modelling, is the lack of discussion or justification of the iCP approach in the reports. The iCP software couples two separate software packages: COMSOL (transport processes); and PHREEQC (geochemical processes). Although a reference to a paper on the iCP approach is provided, there is no discussion in the reports on the different approaches available for coupled modelling, such as the implications for the sequential (operator-splitting) approach being used rather than a globally implicit approach as adopted in other codes. This comment is not meant to criticise operator-splitting approaches *per se*, but rather asks the question of what the implications of this approach (compared with other approaches) could be, or at least to recognise that other approaches are available (which may help the reader that is less familiar with geochemical modelling).
- The second major point is that reaction kinetics for cement solids are not included in the geochemical simulations. Although cement leaching and degradation processes could be more rapid than those seen in other barrier materials (such as bentonite), recently international literature has presented attempts to represent the kinetics of dissolution-precipitation reactions in simulations of cement degradation. It is recognised that input data are often not plentiful, and approximations are often necessary (e.g. Wilson et al., 2017a, 2018), but nevertheless simulations with kinetics can provide insights into the likely significance of kinetics for cement degradation. Although kinetic data are somewhat uncertain, the relative rates of dissolution / precipitation of different types of secondary solid could affect spatial / temporal patterns of cement alteration. These effects may not be captured assuming local-equilibrium as in the models described in SKB's reports.
- The third major point to be made for the modelling reports, is the lack of discussion of processes of crack development / healing and how this affects water flow and solute transport. The models, as with most of those published to date, considers the concrete as a porous medium, with dissolution-precipitation reactions occurring throughout the bulk of the material. Specific models of fracture / crack evolution are not necessarily required to support the safety evaluation, but some discussion on their potential to occur, and their possible implications would be useful to provide a more complete picture of concrete evolution (see Metcalfe et al., 2017). However, it is recognised that considerable efforts were made to consider heterogenous transport behaviour (R-19-11).

The models include the main cement alteration reactions that are likely to occur in the repository given the reference material and representative groundwater. The main concrete degradation pathway of leaching (and subsequent carbonation) is included, along with the potential for sulphate attack which is considered in SKB reports R-19-12, R-19-13, and R-19-14. However, there is little discussion or justification for the selection of secondary solids in the models. The modelling mostly includes one groundwater composition (dissolved Cl concentration of 4.5×10^{-3} M) and there is no consideration of potential variation in salinity (noting that in more saline systems, Friedel's salt may form as an alteration product and that this was seen as a minor secondary solid in SFR repository models, Höglund, 2014). In addition, in the models it is not clear whether the C-S-H gel end member compositions are treated as solid-solutions as described in the thermodynamic database used for cement solids (CEMDATA).

Several points can be made that are possibly less important in terms of modelling strategy but may have implications for how the models are described in the safety evaluation. One of these is the overall description of approach taken to calculate concrete porosity (and other properties) by averaging values in an "inner zone" and "outer zone" (Report R-19-13). These values are then used in radionuclide calculations, without including pore clogging (due to calcite precipitation) that is observed in the models. It is stated in the modelling reports that this approach is "conservative", which it may well be in terms of radionuclide fluxes. However, a clearer comparison of "with" and "without" calcite cases would be useful, as would a clearer discussion on the expected repository evolution and the assumptions made in radionuclide transport calculations. This helps negate any question of bias having been introduced into the modelling approaches. Additionally, the potential for fractures at rock-concrete interfaces to become clogged with secondary solids is not mentioned, even though this is a potential phenomenon that could, to some extent, impede water flow through the BHK vault. Although clogging is predicted in the models, the safety evaluation mentions the potential for a hydraulic cage to form (SKB Report TR-19-01) and how the model assumptions have influenced this suggestion is not very clear.

An example of an issue that arises in the earlier models but is subsequently resolved in later reports, is the primary cement solid assemblage included in the models. The work reported in Report R-19-11 uses a primary hydrated cement solid assemblage based on a rather old reference (used in SFR repository modelling). This hydrated assemblage predates much recent work that has been undertaken on the nature of cement hydration. However, a very comprehensive review of cement hydration is provided in later work which also includes thermodynamic models of hydration processes (R-19-14). The calculated hydrated assemblages consider variation in water / cement ratio and the effect of including different additives in cement blends (fly ash, or limestone and dolomite). The long-term evolution of the different cement compositions is then simulated.

9.2. Summary of Bentonite Degradation Modelling Review ("Bottom-Up" Approach)

In addition to modelling concrete degradation, SKB has undertaken simulations of interaction between bentonite in BHA vaults and cementitious materials (Report R-19-15). However, this modelling was not described in the safety evaluation (Report TR-19-01).

Two sets of 1-D reactive transport models of bentonite degradation in the BHA vault are developed and implemented using iCP, as interface between COMSOL Multiphysics and PHREEQC:

- a first set considering only the bentonite system, treating concrete as a boundary condition; and
- a second set explicitly considering the interaction between the concrete and bentonite barriers.

The goal of the work was to assess the extent of montmorillonite dissolution in the bentonite barrier due to the interaction with cementitious fluids from the concrete barrier over a time span of 100 000 years. The second set of simulations is most relevant to this goal

since these simulations are much more representative of the system than the first set. However, as with the concrete modelling potential implications of the process coupling approach that is used is not discussed.

There are several issues associated with the conceptual model and model input data. Regarding the conceptual model, the sizes of the 1-D model domains are specified to ensure the correct waste-to-concrete volume ratio and represent a "conservative" assumption in terms of volume-thickness of the bentonite backfill. The reasons for stating this arrangement to be conservative are understood. However, it would have been better to include a more realistic model representation, with model outputs, to confirm whether the model assumptions really are conservative in terms of barrier performance. Alternatively, an additional case could have been developed that included a higher cement / bentonite ratio.

The review states that the BHA vault includes a proportion of cement grout in addition to concrete. The grout, which has a slightly higher cement paste content, is not really mentioned but it appears to have been included. This approach is reasonable given the cement / ballast ratio is ~0.2 for concrete, and ~0.25 for grout, according to the composition in Table 7-8 of the initial status report, TR-19-03.

The reference case assumes that there is no coupling between porosity and diffusivity. The authors state that this is:

"justified by the fact that changes in porosity and related properties due to mechanical stresses will probably also play an important role".

However, these properties are often coupled in reactive transport simulations (using Archie's Law) and this justification is not convincing. Although Report R-19-12 provides a good attempt to couple mechanical behaviour with chemical processes, the authors recognise the uncertainty of the process couplings. Therefore, it is not appropriate to use the extent to which these couplings influence system behaviour to justify the exclusion of processes that reactive transport models often include. The inclusion of a variant model case that discounted porosity-diffusion coupling to consider its importance would have been more reasonable, especially given the uncertainties associated with modelling bentonite using a "total porosity" approach.

The model includes clinochlore (Mg-rich chlorite) as a potential secondary solid, which is arguably less likely to form in the repository than other Mg-rich clays or M-S-H. These latter phases are known to form under repository temperatures which are relatively lower than those at which Mg-chlorite forms. Additionally, the relatively high chloride content of the model bentonite porewater (~1.4×10^{-1} M), could lead to Friedel's salt formation in the concrete, which was not considered in the simulations. Should it occur, Friedel's salt formation may be accompanied by very high pH (13), which could impact on the rate of montmorillonite dissolution.

Calcite and gypsum present in the bentonite are assumed to dissolve / precipitate under thermodynamic equilibrium, but the reason for this is not clear. Kinetic data exist for these minerals (see Palandri and Kharaka, 2004; Marty et al., 2015) and the assumption of instantaneous equilibrium is not clearly justified by the authors.

In contrast, in the models, montmorillonite, illite, quartz, and feldspar dissolution is kinetically controlled in the bentonite. Where concrete domains are included, cement solids are

treated using a local equilibrium approach. The number of model cases is arguably excessive, and some are of limited applicability. Resources may have been better deployed by developing a more coherent reference case that included a more consistent kinetic dataset, using a classic T-S-T approach for all minerals and hydrated cement solids. Even though absolute rate values / reactive surface areas are uncertain, indisputably different types of solids will precipitate (and crystallise) at different rates and capturing the relative rates of mineral transformations is valuable. For example C-S-H precipitation is likely to be much more rapid than zeolite or smectite mineral growth.

The dissolution rate data available for montmorillonite are comprehensively reviewed in the report. However, the approach taken in the models is inconsistent in terms of the surface-area normalisation of measured dissolution rates. The work in Report R-19-15 uses a very high montmorillonite surface area of 800 $m^2 g^{-1}$ in the reference model. The reactive surface area reported in Report R-19-15 also appears to be inconsistent with the material on which rates were measured and it could lead to montmorillonite dissolution being overestimated to a significant degree in the reference model. Surface area data should have been used with the dissolution rate data to which the measured dissolution rates were normalised. It would have been useful to explore the significance of a reduced dissolution rate in a compacted system used a reactive surface area reduced by a factor of 10 or 100 in a variant case.

The model results are broadly consistent with other published models. However, the treatment of reaction kinetics is weak, and the exclusion of some process couplings also detracts from the work. The wide range in calculated volume loss for primary montmorillonite (30-70% depending on model assumptions) reflects the excessively wide range of surface area values in the models, and the potential for diffusion being reduced to some extent by porosity reduction is not considered.

Overall, given these limitations, the models are of limited applicability to safety evaluation calculations, other than showing some broad consistency in terms of reactive pathways elicited from previous experimental and modelling studies.

9.3. Summary Conclusions from Independent Cement Modelling

The independent models developed as part of the review suggest that in the case of the concrete being simulated, the assumption of local equilibrium made in the SKB models has little effect on predicted general cement degradation pathways. The longevity of the cement solids and pH evolution (given the safety assessment timeframe of interest, 1 million years) is predicted to be the same whether reaction kinetics are specified, or local equilibrium is always assumed.

The independent modelling has shown that using either the THERMODDEM or Thermo-Chimie thermodynamic databases should produce similar results. Additionally, for the model cases compared, broadly similar results were obtained using different thermodynamic databases in the independent modelling and by Idiart et al. (2019) in SKB report R-19-14: THERMODDEM v 1.1 in the independent modelling; and a PHREEQC-compatible version of the CEMDATA07 thermodynamic database, augmented by data from CEMDATA18 and other sources in SKB R-19-14.

Although there are some important differences between the models presented by SKB and the independent models reported herein, the overall degradation pathways that are

key for performance assessment have been captured in both models. However, many of the key model assumptions that could have been of interest were not considered within the SKB models, and justification for the approaches taken (treatment of reaction rates, numerical approach to process couplings, identity of secondary solids, model cell sizes) are limited.

A key difference between the results of the independent model and SKB's model is that compared to the models of SKB the independent models predict a greater degree of pore clogging in the concrete adjacent to the groundwater inflow. A consequence is that generally for a given time water fluxes through the concrete are smaller in the independent model than in SKB's model. The smaller water fluxes in the independent model are reflected in lower degrees of leaching of cement phases across the modelled domain, with pH being generally buffered to higher values.

The differences between the independent model and the model of Idiart et al. (2019) in report R-19-14 are likely to be due primarily to differences in the mineral phases in the two models. Possibly, differences in thermodynamic data between the models could be partly responsible for the different model outcomes, although this cannot be judged rigorously because Idiart et al. (2019) do not give details of the source of thermodynamic data for aqueous species.

The modelling in Idiart et al. (2019) considers only a single groundwater composition, an altered meteoric water. However, at a future SFL site groundwater with a substantially different composition to the one considered by Idiart et al. (2019) could plausibly occur. The independent models suggest that different water compositions may result in significantly different solid phase evolutions and consequent porosity and pH evolutions.

For the alternative water compositions considered by the independent modelling (one based on a glacial water endmember and one based on a Littorina Seawater endmember), there is a greater pore clogging. Therefore, the use by Idiart et al. (2019) of a reference groundwater composition based on altered meteoric water is conservative from the perspective of the cementitious engineered barrier functioning to minimise water fluxes. However, the alternative model representing groundwater based on the Littorina Seawater produces significant quantities of ettringite; after 300,000 y ettringite occurs throughout the model domain, but particularly between 0.25 m and 0.75 m from the inflow, where it composes about 0.18 vol% of the solid phase assemblage. Formation of this phase is accompanied by a net volume increase of the solid phase assemblage, raising the possibility that concrete cracking might occur. From this perspective, models developed using the reference water based on altered meteoric water are not conservative. Should groundwater at a future SFL site be saline and sulphate-rich, it will be necessary to assess the possible effects of ettringite formation.

The alternative model representing groundwater based on Littorina Seawater also predicts the formation of substantial quantities of Friedel's salt, which does not form in any of the other models. While formation of Friedel's salt is unlikely to be directly detrimental with respect to the performance, its presence illustrates that Cl can penetrate through the concrete. Were steel re-inforcements to be used in the concrete they might be more likely to corrode in the presence of saline water like the Littorina Seawater-based groundwater. Corrosion would likely result in loss of strength and would be accompanied by expansion which could cause the concrete to crack. Again, it will be necessarily to investigate the

potential for such effects if the groundwater at a future SFL site is saline and chloride-rich.

It cannot be ruled out that groundwater substantially more saline than the Littorina Seawater endmember may be encountered at a future SFL site. If this is the case, the evolution of the concrete may depart significantly from the evolutions predicted by Idiart et al. (2019) and by the independent models reported here. It could be challenging to model cement evolution in more saline water than the Littorina Seawater endmember because conventional thermodynamic models become increasingly inaccurate as the ionic strength of the water increases above 1.

10. References

Abarca E, Sampietro D, Miret M, von Schenck H, 2016. Initial modelling of the near-field hydrogeology. Exploring the influence of host rock characteristics and barrier properties. Report for the safety evaluation SE-SFL. SKB Report R-16-02. Swedish Nuclear Fuel and Waste Management Co, Stockholm, Sweden.

Abarca, E., Sampietro, D. and Molinero, J. 2019. Modelling of the near-field hydrogeology – temperate climate conditions. Report for the safety evaluation SE-SFL. SKB Report R-19-03. Swedish Nuclear Fuel and Waste Management Co, Stockholm, Sweden.

Andra. 2021. ThermoChimie database webpages https://www.ThermoChimie-tdb.com/ (last accesses 25.01.2021).

Baur, I., Keller, P., Mavrocordatos, D., Wehrli, B., Johnson, C.A. 2004. Dissolution precipitation behaviour of ettringite, monosulfate, and calcium silicate hydrate, Cement and Concrete Research, 34, 341-348.

BELBaR Project Website: https://igdtp.eu/activity/belbar-bentonite-erosion-effects-long-term-performance-engineered-barrier-radionuclide-transport/

Benbow, S.J., Metcalfe, R. and Burrow, J. 2015. Independent modelling of engineered barrier evolution and coupled THMC: canister corrosion calculations in SR-Site. SSM Technical Note 2015:49 ISSN: 2000-0456.

Bethke, K. 2010. Geochemical and biogeochemical reaction modelling, 2nd Edition. Cambridge University Press.

Carrayrou, J., Mosé, R., Behra, P. 2004. Operator splitting procedures for reactive transport and comparison of mass balance errors. Journal of Contaminant Hydrology, 68, 239-268.

COMSOL, 2015. COMSOL Multiphysics® v. 5.2. COMSOL AB, Sweden.

Cronstrand, P. 2007. Modelling the long-time stability of the engineered barriers of SFR with respect to climate changes. SKB Report R-07-51. Swedish Nuclear Fuel and Waste Management Co, Stockholm, Sweden.

Cronstrand, P. 2014. Evolution of pH in SFR 1, SKB Report R-14-01. Swedish Nuclear Fuel and Waste Management Co, Stockholm, Sweden.

Gimeno, M.J., Auqué, L.F., Gómez, J.B., Salas, J., Molinero, J. 2010. Hydrogeochemical evolution of the Laxemar Site. SKB R-10-60, Swedish Nuclear Fuel and Waste Management Co, Stockholm, Sweden.

Gimeno, M.J., Auqué, L.F. and Gómez, J.B, 2019. Hydrogeochemical conditions during periods with glacial and periglacial climate conditions. Report for the safety evaluation SE-SFL. SKB Report R-19-08, Swedish Nuclear Fuel and Waste Management Co, Stockholm, Sweden.

Harper. J., Hubbard, A., Ruskeeniemi, T., Claesson Liljedahl, L., Kontula, A., Hobbs, M., Brown, J., Dirkson, A., Dow, C., Doyle, S., Drake, H., Engström, J., Fitzpatrick, A., Follin, S., Frape, S., Graly, J., Hansson, K., Harrington, J., Henkemans, E., Hirschorn, S., Humphrey, N., Jansson, P., Johnson, J., Jones, G., Kinnbom, P., Kennell, L., Klint, K.E., Liimatainen, J., Lindbäck, K., Meierbachtol, T., Pere, T., Pettersson, R., Tullborg, E-L. and van As D. 2015. The Greenland Analogue Project: data and processes. SKB Report R-14-13, Swedish Nuclear Fuel and Waste Management Co, Stockholm, Sweden.

Hong, S-Y and Glasser, F.P. 1999. Alkali binding in cement pastes Part I. The C-S-H phase. Cement and Concrete Research, 29, 1893–1903.

Höglund, L.O. 1992. Some notes on ettringite formation in cementitious materials; influence of hydration and thermodynamic constraints for durability. Cement and Concrete Research, 22, 217-228.

Höglund, L.O. 2014. The impact of concrete degradation on the BMA barrier functions. SKB Report R-13-40. Swedish Nuclear Fuel and Waste Management Co, Stockholm, Sweden.

Höglund, L.O. and Bengtsson, A. 1991. Some chemical and physical processes related to the long-term performance of the SFR repository. SKB Report SFR 91-06. Swedish Nuclear Fuel and Waste Management Co, Stockholm, Sweden.

Idiart, A. and Laviña, M. 2019. Modelling of concrete degradation in a one-million-year perspective – hydro-chemical processes. SKB Report R-19-13. Swedish Nuclear Fuel and Waste Management Co, Stockholm, Sweden.

Idiart, Laviña, M., Coene, E. 2019. Modelling of concrete degradation – Hydro-chemo-mechanical processes. Report for the safety evaluation SE-SFL. SKB Report R-19-12. Swedish Nuclear Fuel and Waste Management Co, Stockholm, Sweden.

Idiart A, Olmeda J, Laviña M, 2019. Modelling of concrete degradation – influence of concrete mix design. Report for the safety evaluation SE-SFL. SKB Report R-19-14. Swedish Nuclear Fuel and Waste Management Co, Stockholm, Sweden.

Idiart, A. and Shafei, B. 2019. Modelling of concrete degradation – hydro-mechanical processes. SKB Report R-19-11. Swedish Nuclear Fuel and Waste Management Co, Stockholm, Sweden.

Jacques, D., 2009. Benchmarking of the cement model and detrimental chemical reactions including temperature dependent parameters. Project near surface disposal of category A waste at Dessel. NIROND-TR 2008–30 E, ONDRAF/NIRAS, Belgium.

Joyce, S., Appleyard, P., Hartley, L, Tsitsopoulos, V., Woollard, H., Marsic, N., Sidborn, M and Crawford, J, 2019. Groundwater flow and reactive transport modelling of temperate conditions. Report for the safety evaluation SE-SFL. SKB Report R-19-02. Swedish Nuclear Fuel and Waste Management Co, Stockholm, Sweden.

Kalinowski B (ed) 2009. Background complementary hydrogeochemical studies. Site descriptive modelling SDM-Site Laxemar. SKB Report R-08-111. Swedish Nuclear Fuel and Waste Management Co, Stockholm, Sweden.

Laaksoharju, M., Smellie, J., Tullborg, E-L, Wallin, B., Drake, H., Gascoyne, M., Gimeno, M., Gurban, I., Hallbeck, L., Molinero, J., Nilsson, A-C, and Waber, N.H. 2009. Bedrock hydrogeochemistry Laxemar - Site descriptive modelling SDM-Site Laxemar. SKB Report R-08-93. Swedish Nuclear Fuel and Waste Management Co, Stockholm, Sweden.

Lagerblad, B. and Trägårdh, J, 1994. Conceptual model for concrete long time degradation in a deep nuclear waste repository. SKB Report TR 95-21. Swedish Nuclear Fuel and Waste Management Co, Stockholm, Sweden.

Levenspiel, O. 1972. Chemical reaction engineering, 2nd edition. Wiley, New York.

Lothenbach, B., Matschei, T., Möschner, G. and Glasser, F.P., 2008. Thermodynamic modelling of the effect of temperature on the hydration and porosity of Portland cement. Cement and Concrete Research, 38, 1–18.

Lothenbach, B. and Winnefeld, F., 2006. Thermodynamic modelling of the hydration of Portland cement. Cement and Concrete Research, 36, 209–226.

Lothenbach, B., Scrivener, K. and Hooton, R.D. 2011. Supplementary Cementitious Materials. Cement and Concrete Research, 41, 1244-1256.

Lothenbach, B., Bernard, E., Mäder, U. 2017. Zeolite formation in the presence of cement hydrates and albite. Physics and Chemistry of the Earth, 99, 77-94.

Lothenbach, B., Kulik, D. A., Matschei, T., Balonis, M., Baquerizo, L., Dilnesa, B. and Myers, R. J. 2019. Cemdata18: a chemical thermodynamic database for hydrated Portland cements and alkaliactivated materials. Cement and Concrete Research, 115, 472-506. https://doi.org/10.1016/j.cemconres.2018.04.018

Marty, N. C. M., Tournassat, C., Burnol, A.A., Giffaut, E., Gaucher, E.C. 2009. Influence of reaction kinetics and mesh refinement on the numerical modelling of concrete / clay interactions. Journal of Hydrology, 364, 58-72.

Marty, N., Munier, I., Gaucher, E.C., Tournassat, C., Gaboreau, S., Vong, C.Q., Giffaut, E., Cochepin, B., and Claret, F. 2014. Simulation of Cement / Clay Interactions: Feedback on the Increasing Complexity of Modelling Strategies. Transport in Porous Media, 104/2, 385- 405.

Marty, N.M., Claret, F., Lassin, A., Tremosa, J., Blanc, P., Madé, B., Giffaut, E., Cochepin, B. Tournassat, C. 2015. A database of dissolution and precipitation rates for clayrocks minerals. Applied Geochemistry, 55, 108–118.

Mazars J 1986. A description of micro- and macroscale damage of concrete structures. Engineering Fracture Mechanics, 25, 729–737.

Metcalfe, R., S. Benbow, J. Wilson and D. Savage. 2017. Review of Geochemical Aspects of SR-PSU – Main Review Phase. Chapter 3 in SSM's external experts review of SKBs safety assessment SR-PSU – hydrogeology, geochemistry and bentonite. SSM report 2017:28, Swedish Radiological Safety Authority, Sweden.

Nakabayashi, R. 2014. Evaluation of bentonite/hyperalkaline-fluids interaction in compacted system by X-ray computed tomography. PhD thesis. Hokkaido University, Japan.

Nardi, A., Idiart, A., Trinchero, P., de Vries, L. M., and J. Molinero. 2014. Interface COMSOL-PHREEQC (iCP), an efficient numerical framework for the solution of coupled multiphysics and geochemistry. Computers & Geosciences, 69, 10-21.

Neretnieks, I., 2014. Development of a simple model for the simultaneous degradation of concrete and clay in contact. Applied Geochemistry, 43, 101–11.

Oda, C., Walker, C., Chino, D., Ichige, S., Honda, A., Sato, T., Yoneda, T. 2014. Na-montmorillonite dissolution rate determined by varying the Gibbs free energy of reaction in a dispersed system and its application to a coagulated system in 0.3 M NaOH solution at 70 °C. Applied Clay Science, 93-94, 62-71.

Palandri, J.L., Kharaka, Y.K. 2004. A Compilation of Rate Parameters of Water-mineral Interaction Kinetics for Application to Geochemical Modelling. USGS Open File Report 2004-1068. United States Geological Survey, Menlo park, California, USA.

Parkhurst, D.L and Appelo, C.A.J., 2013. Description of input and examples for PHREEQC Version 3 - A computer program for speciation, batch-reaction, one-dimensional transport, and inverse geochemical calculations. Techniques and Methods 6–A43, U.S. Geological Survey, Denver, Colorado.

Parkhurst, D.L., Kipp, K.L., Charlton, S.R. 2010. PHAST version 2: a program for simulating ground-water flow, solute transport, and multicomponent geochemical reactions. Techniques and Methods 6–A35, U.S. Geological Survey, Denver, Colorado.

Parrot, L.J. and Killoh, D.C. 1984. Prediction of cement hydration. British Ceramic Proceedings 35, 41–53.

Pękala, M., Olmeda, J., Grivé, M., Bruno, J. 2015. Assessment of redox state and its impact on the solubility and speciation of selected radionuclides in the SFL repository. Final report. Amphos 21. SKB doc 1533627 v 1.0, Svensk Kärnbränslehantering AB.

Rozalén M L, Huertas F J, Brady P V, Cama J, García-Palma S, Linares J, 2008. Experimental study of the effect of pH on the kinetics of montmorillonite dissolution at 25 °C. Geochimica et Cosmochimica Acta, 72, 4224-4253.

Rozalén M L, Huertas F J, Brady P V, 2009. Experimental study of the effect of pH and temperature on the kinetics of montmorillonite dissolution. Geochimica et Cosmochimica Acta, 73, 3752-3766.

Sandén, T. and Börgesson, L. 2010. Early effects of water inflow into a deposition hole. Laboratory test results. SKB Report R-10-70. Swedish Nuclear Fuel and Waste Management Co, Stockholm, Sweden.

Sato, T., Kuroda, M., Yokoyama, S., Tsutsui, M., Fukushi, K., Tanaka, T., Nakayama, S. 2004. Dissolution mechanism and kinetics of smectite under alkaline conditions. In Proceedings of International Workshop on Bentonite–Cement Interaction in Repository Environments, Tokyo, 14-16 April 2004. A3-38.

Savage, D. and Stenhouse, M. 2002. SFR 1 Vault Database. SKI Report 02:53.

Savage, D., Walker, C., Arthur, R.C., Rochelle, C.A., Oda, C., Takase, H. 2007. Alteration of bentonite by hyperalkaline fluids: a review of the role of secondary minerals. Physics and Chemistry of the Earth, 32, 287-297.

Savage, D., Benbow, S., Watson, C., Takase, H., Ono, K., Oda, C., and Honda, A. 2010. Natural systems evidence for the alteration of clay under alkaline conditions: an example from Searles Lake, California. Applied Clay Science, 47, 72-81.

Savage, D. 2011. A review of analogues of alkaline alteration with regard to long-term barrier performance. Mineralogical Magazine, 75(4), 2401-2418.

Savage, D., Soler, J.M., Yamaguchi, K., Walker, C., Honda, A., Inagaki, M., Watson, C., Wilson, J., Benbow, S., Gaus, I. and Rueedi, J. 2011a. A comparative study of the modelling of cement hydration and cement-rock laboratory experiments. Applied Geochemistry, 26, 1138-1152.

Savage, D., Arthur, R., Watson, C., Wilson, J. and Stromberg, B. 2011b. Testing geochemical models of bentonite pore water evolution against laboratory experimental data, Physics and Chemistry of the Earth, 36, 1817-1829.

Savage, D. and Cloet, V. 2018. A Review of Cement Clay Modelling. Nagra Report NAB 18-24. National Cooperative for the Disposal of Radioactive Waste. Wettingen, Switzerland.

Savage, D., Wilson, J., Benbow, S., Sasamoto, H., Oda, C., Walker, C., Kawama, D., Tachi, Y. 2019. Natural systems evidence for the effects of temperature and the activity of aqueous silica upon montmorillonite stability in clay barriers for the disposal of radioactive wastes. Applied Clay Science, 179, 105146.

Shakarami, P. 2019. Input data report for the near-field and geosphere radionuclide transport modelling. Report for the safety evaluation SE-SFL. SKB Report R-19-09. Swedish Nuclear Fuel and Waste Management Co, Stockholm, Sweden.

Silva, O., Coene, E., Moliner, J., Laviña, M. and Idiart, A, 2019. Gas release from the BHK vault – Multiphase flow modelling of the near-field. Report for the safety evaluation SE-SFL. SKB Report R-19-06. Swedish Nuclear Fuel and Waste Management Co, Stockholm, Sweden.

Skagius, K., Pettersson, M., Wiborgh, M., Konsult, K. 1999. Compilation of data for the analysis of radionuclide migration from SFL 3-5. SKB Report R-99-13. Swedish Nuclear Fuel and Waste Management Co, Stockholm, Sweden.

SKB, 2009. Site description of Laxemar at completion of the site investigation phase. SDM-Site Laxemar. SKB Report TR-09-01. Swedish Nuclear Fuel and Waste Management Co, Stockholm, Sweden.

Terada, K., Tani, A., Harada, S., Satoh, H., Hayashi, D. 2019. Monte Carlo analysis of montmorillonite particle structures and modeling of dissolution rate reduction. Materials Research Express, 6, 035514.

Valocchi, A.J., and Malmstead, M. 1992. Accuracy of operator splitting for advection-dispersion-reaction problems. Water Resources Journal, 28(5), 1471-1476.

Walker C.S., Sutou, S., Oda, C. Mihara, M. and Honda A. 2016. Calcium silicate hydrate (C-S-H) gel solubility data and discrete solid phase model at 25 °C based on two binary non-ideal solid solutions. Cement and Concrete Research, 79, 1-30.

Watson, C., Wilson, J., Savage, D., Benbow, S. and Norris, S. 2016. Modelling reactions between alkaline fluids and fractured rock: the Maqarin Natural Analogue. Applied Clay Science, 121–122, 46–56.

Watson, C., Savage, D., Wilson, J., Benbow, S., Walker, C., and Norris, S. 2013. The Tournemire industrial analogue: reactive transport modelling of a cement-clay interface. Clay Minerals, 48, 167-184.

Watson, C., Wilson, J., Savage, D., Benbow, S. and Norris, S. 2016. Modelling reactions between alkaline fluids and fractured rock: the Maqarin Natural Analogue. Applied Clay Science, 121–122, 46–56.

Wilson, J.C., Benbow, S., Watson, C., Sasamoto, H., and Savage, D. 2015. Fully-coupled reactive transport models of the iron-bentonite interface. Applied Geochemistry, 61, 10-28.
Wilson, J.C., Benbow, S. J., Metcalfe, R. 2017a. Understanding the long-term evolution of cement backfills: alteration of NRVB due to reaction with groundwater solutes. Report 202387/002 Issue A for RWM, Harwell, UK.

Wilson, J.C., Benbow, S., Metcalfe, R., Lueng, H. 2017b. Reactive transport modelling of a shale-bentonite interface in a hypersaline system. Applied Geochemistry, 76, 60-73.

Wilson, J.C., Benbow, S. and Metcalfe, R. 2018. Reactive transport modelling of a cement backfill for radioactive waste disposal. Cement and Concrete Research, 111, 81-93.

Yamaguchi, T., Sakamoto, Y., Akai, M., Takazawa, M., Iida, Y., Tanaka, T., Nakayama, S. 2007. Experimental and modeling study on long-term alteration of compacted bentonite with alkaline groundwater. Physics and Chemistry of the Earth, 32, 298-310.

APPENDIX 1

Coverage of SKB reports

Following reports have been covered in the review.

Table A:1

Reviewed report	Reviewed sections	Comments
[*insert SKB report number and title*]	[*insert reviewed sections*]	[*insert comments, if any*]
SKB TR-19-01, SKB, 2019. Post-closure safety for a proposed repository concept for SFL. Svensk Kärnbränslehantering AB.	All. Focus on Sections 1, 2, 3, 4, 5, 6, 9 and 10	
SKB TR-19-03, SKB, 2019. Initial state for the repository for the safety evaluation SE-SFL. Svensk Kärnbränslehantering AB.	All, Focus on Sections 1, 2, 4, 5 and 7	
SKB R-19-11, Idiart A, Shafei B, 2019. Modelling of concrete degradation – Hydro-chemical processes. Report for the safety evaluation SE-SFL. Svensk Kärnbränslehantering AB.	All	
SKB R-19-12, Idiart A, Laviña M, Coene E, 2019. Modelling of concrete degradation – Hydro-chemo-mechanical processes. Report for the safety evaluation SE-SFL. Svensk Kärnbränslehantering AB.	All	
SKB R-19-13, Idiart A, Laviña M, 2019. Modelling of concrete degradation in a one-million year perspective– Hydro-chemical processes. Report for the safety evaluation SE-SFL. Svensk Kärnbränslehantering AB.	All	
SKB R-19-14, Idiart A, Olmeda J, Laviña M, 2019.	All	

Modelling of concrete degradation – influence of concrete mix design. Report for the safety evaluation SE-SFL. Svensk Kärnbränslehantering AB.	
SKB R-19-15, Reactive transport modelling of montmorillonite dissolution - Report for the safety evaluation SE-SFL. Svensk Kärnbränslehantering AB.	All
SKB TR-14-01. Safety analysis for SFR. Long-term safety. Main report for the safety assessment SR-PSU. Revised edition. Svensk Kärnbränslehantering AB.	Sections 1, 2, 3, 4, 5, 6, 7.1, 7.2 and 7.3
SKB TR-19-02. FEP report for the safety evaluation SE-SFL. Svensk Kärnbränslehantering AB.	All
SKB R-19-02, Joyce S, Appleyard P, Hartley L, Tsitsopoulos V, Woollard H, Marsic N, Sidborn M, Crawford J, 2019. Groundwater flow and reactive transport modelling of temperate conditions. Report for the safety evaluation SE-SFL. Svensk Kärnbränslehantering AB.	All
SKB R-19-09, Shahkarami P, 2019. Input data report for the near-filed and geosphere radionuclide transport modelling. Report for the safety evaluation SE-SFL. Svensk Kärnbränslehantering AB.	Sections 2.2, 2.6, 3.1

Strål
säkerhets
myndigheten
Swedish Radiation Safety Authority

Authors: George Towler, Rebecca Newson and Laura Limer
Quintessa Limited, Henley on Thames, UK

2021:13

3) Review of SE-SFL – Radionuclide transport in the near-field

Date: May 2021
Report number: 2021:13 **ISSN:** 2000-0456
Available at www.stralsakerhetsmyndigheten.se

Authors: George Towler[1)], Rebecca Newson[1)] and Laura Limer[1)]
[1)]Quintessa Limited, Henley on Thames, UK

3) Review of SE-SFL – Radionuclide transport in the near-field

Activity number: 3034111-04
Registration number: SSSM2020-3834
Contact person at SSM: Jinsong Liu

Content

1. Introduction

In Sweden, long-lived low- and intermediate level radioactive waste (L/ILW) is planned to be disposed of in a repository (SFL) in crystalline bedrock at a depth around 500 m. The long-lived wastes derive from operation and decommissioning of the Swedish nuclear reactor plants, as well as from early research in the Swedish nuclear programme (legacy wastes), from medicine, industry and research including the European Spallation Source (ESS) research facility. The disposal concept for the SFL repository has been under development by SKB since the 1980s. A pre-study of the concept has been carried out (SKB TR-95-03; Wiborgh, 1995) and a preliminary safety analysis (SKB TR-99-28; SKB, 1999) has been published previously.

The recently released safety evaluation of the SFL repository (SKB TR-19-01; SKB, 2019a) is a continuation of this conceptual development. SSM have contracted independent experts to support their review and understanding of SKB's recent safety evaluation in several topic areas. This report describes the findings of Quintessa Ltd's review of the topic area "near-field transport of radionuclides".

1.1. Objectives and Scope

SKB's Safety Evaluation for SFL (SE-SFL) has been undertaken in support of ongoing concept development. It has not been undertaken in support of a licence application.

SE-SFL describes the developing SFL concept, the potential long-term safety performance, key factors that affect the performance, and the associated uncertainties. The main issues identified by SSM for the topic area "near-field transport of radionuclides" are associated with building confidence in the work SKB has undertaken and the conclusions SKB has drawn. The outputs from review of these main issues are also relevant to having confidence in the future work identified by SKB to develop the SFL concept further.

The main issues considered in the near-field radionuclide transport review are:

- the soundness of the conceptual models in reasonably representing the design concept of the repository and the expected evolution of the engineered barriers with time;
- the correctness of the mathematical formulations and the numerical algorithms of the models;
- the appropriateness of the way the models are implemented, including discretisation of the modelling domain, and handling of numerical round-off, truncation and other errors (if any); and
- the reasonableness of SKB's modelling results, as function of both space and time.

The scope of the review includes undertaking independent modelling of radionuclide transport in the near field of the SFL repository, using well-developed and adapted software that provides a similar implementation of the conceptual model to the tool used by SKB. The independent modelling focusses on the main issues listed above, especially

checking the correctness of mathematical formulations and the appropriateness of implementation of the models.

The review focusses on the following SKB reports, and report sections:

- SKB TR-19-01. SKB, 2019a. Post-closure safety for a proposed repository concept for SFL.
    - Chapter 4, Initial state of the repository and its environs, and Chapter 7, Evaluation of post-closure safety for the repository design at the example location.
- SKB TR-19-06. SKB, 2019b. Radionuclide transport and dose calculations for the safety evaluation SE-SFL.
    - Section 4.3, Near-field model.
- SKB R-19-05. Wessely O, Shahkarami P, 2019. Radionuclide transport and dose calculations for the safety evaluation SE-SFL.
    - The entire report.
- SKB R-19-09. Shahkarami P, 2019. Input data report for near-field and geosphere radionuclide transport modelling. Report for the safety evaluation SE-SFL.
    - The entire report.

Additional SKB reports and other publications are consulted on an ad hoc basis, where relevant.

1.2. Report Structure

Section 2 describes the review approach. The review has followed the steps of the IAEA ISAM approach (IAEA, 2004). Sections 3 to 7 of this report each correspond to a step in the ISAM approach. Section 8 presents our independent modelling and Section 9 presents the review conclusions. SKB reports are referenced in this review report by their report number, while other reports are referenced by their author. A complete reference list is provided in Section 11.

2. Review Approach

The IAEA ISAM approach (IAEA, 2004) is a systematic, stepwise approach for developing safety assessments (Figure 1). The ISAM approach is recognised as a best practice approach, and SKB have used a comparable approach to develop the SE-SFL assessment (Figure 2-2 of TR-19-01). The near-field radionuclide transport review has been undertaken systematically following the ISAM approach.

The ISAM approach has been used to help ensure the review considers the context of SE-SFL; the reviewers understand the nature of the wastes, the repository design, assumed site conditions, evolution scenarios, etc; and the conceptual and assessment models are reviewed systematically. However, it is noted that while this review needs to be aware of the context, repository design, etc, these aspects are outside the scope of this review area. Aspects of SE-SFL that need to be understood by this review, and key topics and activities for the near-field radionuclide transport review, are described in Table 1 for each step of the ISAM approach.

Please note that Steps 8, 9 and 10 of the ISAM approach are not relevant to the scope of this review.

Figure 1: The IAEA ISAM approach (IAEA, 2004)

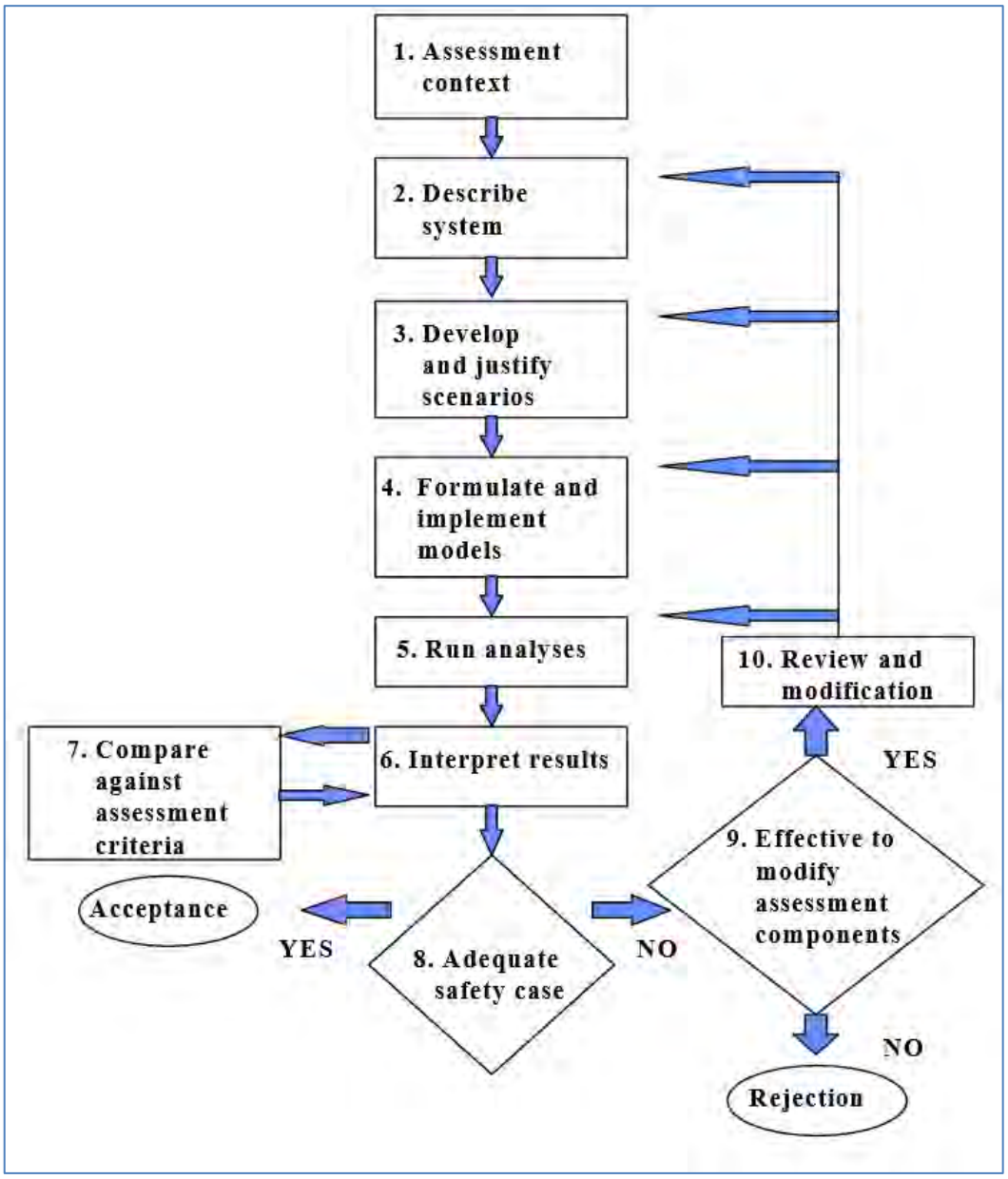

Table 1: Context that needs to be understood and key near-field radionuclide transport review topics and activities, for each step of the ISAM approach

ISAM Step	Context for the near-field radionuclide transport review	Key topics and activities for the near-field radionuclide transport review
1. Assessment Context	▪ Objectives of the Safety Evaluation ▪ SKB's expectations and accepted limitations ▪ SKB's approach and key assumptions / simplifications	▪ No specific topics or activities
2. Describe System	▪ Assumed site and characteristics ▪ Waste types and packaging ▪ Engineering design ▪ Construction methods ▪ Underpinning detailed models, e.g. groundwater flow models	▪ Radionuclide forms and release mechanisms ▪ Gas generation ▪ Radionuclide transport pathways and processes
3. Develop and Justify Scenarios	▪ Climate and landscape evolution scenario(s) ▪ Impacts on flows / pathways ▪ Impacts on physical and geochemical conditions at the repository horizon	▪ Conceptualised physico-chemical and mechanical evolution, including couplings ▪ Degradation of barriers, evolution of flows ▪ Reference evolution and variants ▪ Links to other review areas that are examining long-term barrier performance and degradation in more detail
4. Formulate and implement models	▪ This is the focus of the near-field radionuclide transport review. Wider context not required.	▪ Representation of key features in the assessment model and their discretisation ▪ Radionuclide transport process included the assessment models ▪ Representation of degradation of barriers and evolution of flows ▪ Mathematical models and assumptions ▪ Review key parameter values ▪ Build independent models
5. Run analyses	▪ Not applicable	▪ Run independent models

6. Interpret results	▪ This is the focus of the near-field radionuclide transport review. Wider context not required.	▪ Review SKB's model results
		  ▪ Evolution of distribution of activity over time
		  ▪ Near-field radionuclide fluxes – behaviours of different radionuclides, magnitude of fluxes, evolution of fluxes
		  ▪ How do fluxes for variants to the reference evolution, and sensitivity cases compare with the reference evolution base variant?
		  ▪ How do the fluxes per unit inventory compare with SFR?
		▪ Independent modelling
		  ▪ Comparison of fluxes with SKB's results
		  ▪ What is the relative importance of different transport processes and barriers?
		  ▪ Impact of model configuration and parameterisation on the model results

7. Compare against assessment criteria	▪ This is the focus of the near-field radionuclide transport review. Wider context not required.	▪ Treatment and impact of uncertainties. ▪ Key areas for future development of the repository design and safety assessment

As noted previously, the scope of this review includes independent modelling. The independent modelling provides more detailed insight and understanding for steps 4, 5 and 6 of the ISAM approach. Although the independent modelling has been undertaken in parallel with review of SKB's reports, for clarity, the findings of the review of SKB's reports are presented first, followed by our independent modelling work and the results. This avoids potential confusion between review of SKB's work and our independent modelling.

3. Assessment Context

SKB do not have a specific assessment context section in TR-19-01. Relevant contextual information is included in Section 1 (Introduction) and Section 2 (Methodology) of TR-19-01. More detailed aspects of the assessment methodology are described in the subsequent sections in the context of the objectives of SE-SFL.

A useful overview of the assessment context is provided by the Executive Summary of TR-19-01. Early work focussed on cost calculations (SKB, 1993) and understanding the potential performance of the near field as a barrier to radionuclide release, including sensitivity to repository location (Wiborgh, 1995; SKB, 1999). This early work made assumptions about the design of SE-SFL and did not consider alternatives. Potential solutions for management and disposal of the Swedish long-lived low- and intermediate-level waste were examined in a concept study (Elfwing et al., 2013). Among the alternatives considered, a system was proposed as a basis for further assessment of post-closure safety. This system is evaluated in SE-SFL.

SE-SFL is not a safety assessment underpinning a regulatory submission, and SKB have highlighted this, by using the term Safety Evaluation. The purpose of SE-SFL is to input into the next steps in the development of SFL. These steps include further design of the engineered barriers and the selection of a site to host the repository. More specifically, SKB's two main objectives are:

- *"Evaluate the conditions in the waste, barriers and repository environments under which the repository concept has the potential to fulfil the regulatory requirements for post-closure safety.*
- *Provide SKB with a basis to prioritise areas in which the level of knowledge and adequacy of methods must be improved in order to perform a subsequent, full safety assessment for SFL."*

The objectives for this review (Section 1.1), and therefore the review outputs presented in the following sections, reflect this context.

Some additional contextual information at the start of TR-19-01 would be beneficial. In particular, a little more description of the work that has been undertaken to arrive at the current facility concept, and the planned future programme to develop the SFL facility would be beneficial. For example, while we have only consulted Elfwing et al. (2013) very briefly, it would be useful to note that Elfwing et al. (2013) examined alternative repository concepts and barrier materials, and assessed their performance against a range of criteria, leading to current concept for SFL. Additional contextual information of the planned future programme to develop the SFL facility would help the reader understand the types and ranges of concept variations and uncertainties that need to be explored within SE-SFL to inform the next steps; and what does not need to be done as part of SE-SFL, but SKB plan to do subsequently.

It would also be helpful to have additional overarching discussion of which aspects of SE-SFL need to be underpinned by real site information and why, which aspects can be treated more generically, and which aspects are judged not to be important so simplifying cautious assumptions can be made. This would provide a 'framework' for detailed choices described later in TR-19-01 and other SE-SFL reports.

An assessment timeframe of 1,000,000 years has been chosen. Section 2.3.2 of TR-19-01 explains that this timeframe has been chosen considering the regulatory requirements and guidance for a full safety assessment, and because the wastes are long-lived. During this assessment timeframe, the radiotoxicity of the reactor internals decreases to less than 0.01% of its initial value, and the radiotoxicity of the legacy wastes decreases to a couple of percent of its initial value. To provide some context to the radiotoxicity of total inventory at closure, SKB note this is around ten times the corresponding value for the extended SFR and less than the corresponding value for a single copper canister in the Spent Fuel Repository.

4. System Description

4.1. Assumed Site and Characteristics

A site has not been selected for SFL. SKB reviewed the information collected by its site investigation programme for the Spent Fuel Repository and extension to SFR and decided to use a dataset from a single location (the Laxemar site). This approach was chosen to ensure all the geological and hydrogeological data are consistent and are representative of a site that may be suitable to host the SFL facility.

We note that another potential advantage of this approach is that a real site could contain features such as larger water bearing fractures that cannot be respected when constructing large vaults. Such features might significantly affect localised barrier evolution, e.g. bentonite resaturation and cement alteration. These localised impacts could potentially significantly affect the performance of a whole vault. The potential disadvantage of this approach is that the evaluation is not truly generic, and it is potentially more difficult to explore bounding parameter ranges while ensuring internal consistency is retained.

The following sections of this review report reveal that while SKB have used real site data to describe site and geological conditions, their conceptual and assessment models of barrier degradation and repository performance do not fully examine the effects of localised features, and are therefore more generic. A logical next step to help further achieve SKB's objectives (described in the previous section) would be to use the site-specific information to examine the effects of realistic geosphere features on the evolution and performance of the repository.

The Laxemar site was chosen as a volume of bedrock that is potentially suitable to host a radioactive waste disposal facility. The site had already been identified and characterised during investigations for the Spent Fuel Repository (Section 1.2 of TR-19-01). Hydraulic conductivity data from the locations investigated by the site investigation programme for the Spent Fuel Repository are shown in Figure 2. The hydraulic conductivity data have been derived from injection tests at measurements scales of 20-25 m. These lengths scales are comparable to the width and height of the SFL repository vaults. Relatively high conductivity regions (associated with fractures and fracture zones) are more frequent at Laxemar compared with Forsmark (the location of SFR and chosen for the Spent Fuel Repository) and many of the other sites that have been studied by SKB.

Groundwater flow rates tend to increase as hydraulic conductivities increase, although hydraulic conductivity is not the only factor; the head (pressure) gradients driving flow are equally important. The rates of barrier degradation and advective transport of radionuclides will tend to increase as flow rates increase. Therefore, use of site data from Laxemar may be cautious, as it may lead to higher fluxes of radionuclides in groundwater compared with data from other sites that are potentially suitable to host a radioactive waste disposal facility. However, TR-19-01 does not make it clear whether the sites studied by SKB's spent fuel programme are representative of conditions often found in Sweden, or if they represent a relatively small number of locations with the most favourable conditions. Therefore, the ease of finding a site with suitable conditions is uncertain.

Laxemar is located on the Baltic coast. Section 4.5.1 of TR-19-01 describes the geography and its evolution since the last ice age. The land has emerged from the sea since the last glaciation. Around 12,000 BC, the land was 50-100 m below sea level. The land started to emerge from the sea around 9,400 BC. The regional topography is 'mildly uneven' with a maximum elevation of around 50 m above sea level and is still rising at a rate of around 1 mm y^{-1}. The example location is below a local hill in the landscape, which has an average peak elevation of 21.5 m above present mean sea level (Section 6.2.1 of TR-19-01). The landscape of the Laxemar site is not being influenced by ongoing glacial rebound, but closer to the shoreline of the Baltic Sea, new terrestrial areas, lakes and wetlands form as the land rises from the sea. The lakes and wetlands are successively covered by peat.

The regolith is thin and mainly located in the valleys, whereas the higher-altitude areas are dominated by exposed bedrock or thin layers of till and peat. Section 4.5.1 of TR-19-01 describes the reogolith in more detail. Glacial till is the most common Quaternary deposit and covers half of the terrestrial part of the Laxemar-Simpevarp area. Sandy gravelly till overlies the bedrock in the whole area, also in most areas with exposed / shallow bedrock (which may have a regolith depth of up to c. 0.5 m). The exceptions are some of the exposed / shallow bedrock areas, in which organic soil and a thin vegetation layer directly overlies the bedrock.

Figure 2: Hydraulic conductivity data collected by site investigation programmes for the Spent Fuel Repository (Figure 4-12 of TR-19-01)

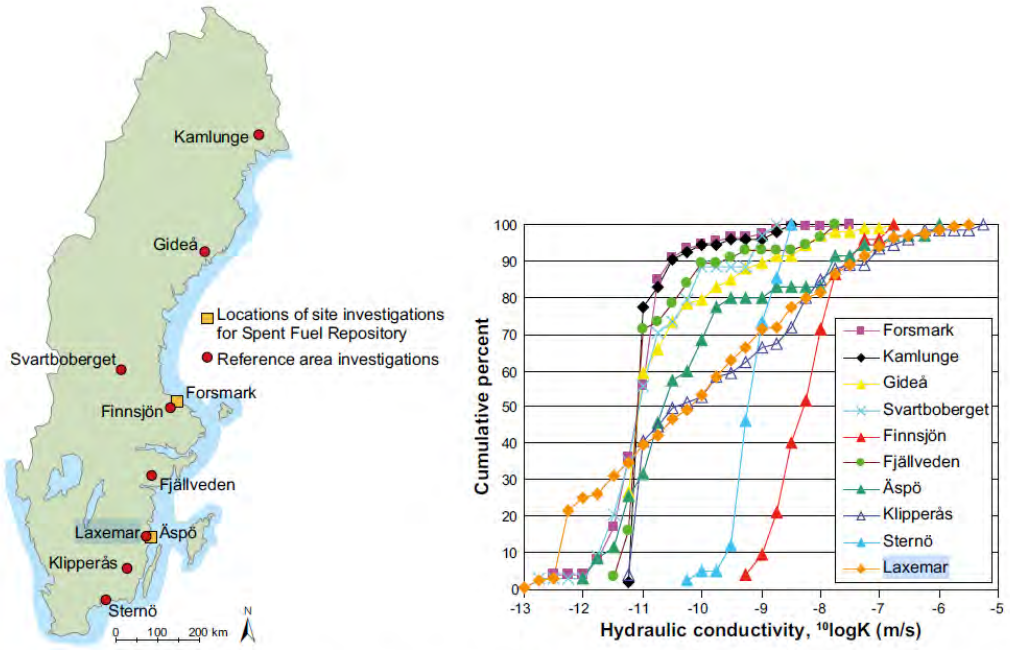

Figure 4-12. Left, map showing Sweden and locations of site investigations for the Spent Fuel Repository (yellow rectangles), and reference area investigations (red dots). Right, plot of cumulative distributions for measured hydraulic conductivity (K) on a scale of 20−25 metres, for site investigation and reference areas. The data represents the bedrock between deterministic deformation zones in the depth interval 400 to 700 m (SKB 2011b).

4.2. Waste Types and Packaging

4.2.1. Waste Types

The wastes proposed for disposed to SFL can be divided into two categories: reactor core components; and legacy wastes (Executive Summary of TR-19-01).

The reactor core components are mainly made from metal, although there will also be some waste concrete from the reactor bioshields, and some secondary wastes from reactor dismantling and size reduction (cutting) of reactor core components, including swarf, filters, abrasives and decommissioned segmentation equipment. The activity in the metal components from close to the reactor core is dominated by neutron activation products, while surface contamination dominates in components that were located further from the core. The reactor core components will be segregated into long-lived wastes (for disposal to SFL) and short-lived wastes (for disposal to SFR). However, the details of the separation procedure have not yet been specified, and cautiously SE-SFL assumed the entire radionuclide inventory is disposed to SFL (Section 4.2.1 of TR-19-01).

Legacy wastes is a broader category of wastes that originate from Studsvik Nuclear AB (SNAB) and Cyclife Sweden AB. They include existing and future wastes from research, as well as wastes from decommissioning (Section 4.2.1 of TR-19-01). The waste mainly consists of ion-exchange resins, precipitation sludge, exchanged components from the research reactor at Studsvik, tools, instruments, consumable laboratory ware, ashes, glove boxes and radiation sources. In addition, there are wastes from other producers involved in medicine, industry and research.

4.2.2. Packaging

Reactor Core Components

Reactor core components are stored in large carbon steel steel tanks (Figure 3), and it is planned to use these tanks for final disposal of these wastes, assuming they will comply with the Waste Acceptance Criteria (WAC) for SFL, which will be established later in the repository development process.

SKB plan to fill the void spaces in the metal tanks using cementitious grout. Section 4.2.2 of TR-19-01 explains that the wastes will not be finally conditioned (i.e. grouted) until WAC have been developed for SFL, and it is confirmed that the tanks are compliant with the WAC. The wastes must be retrievable until it is confirmed that the tanks are compliant with the WAC.

Some open void space will remain in the packages after they have been grouted, presumably due to some ullage space at the top of the tank, and any voids the grout cannot penetrate. Table 3-19 in TR-19-03 gives a total voidage of 1200 m^3. There are 606 tanks (Section 3.5.1 of TR-19-03), so the typical voidage in a tank is 2 m^3. Each tank has an exterior volume of 9.87 m^3, so the void volume is around 20% of the tank volume.

Figure 3: Steel tank (Figure 4-1 of TR-19-01)

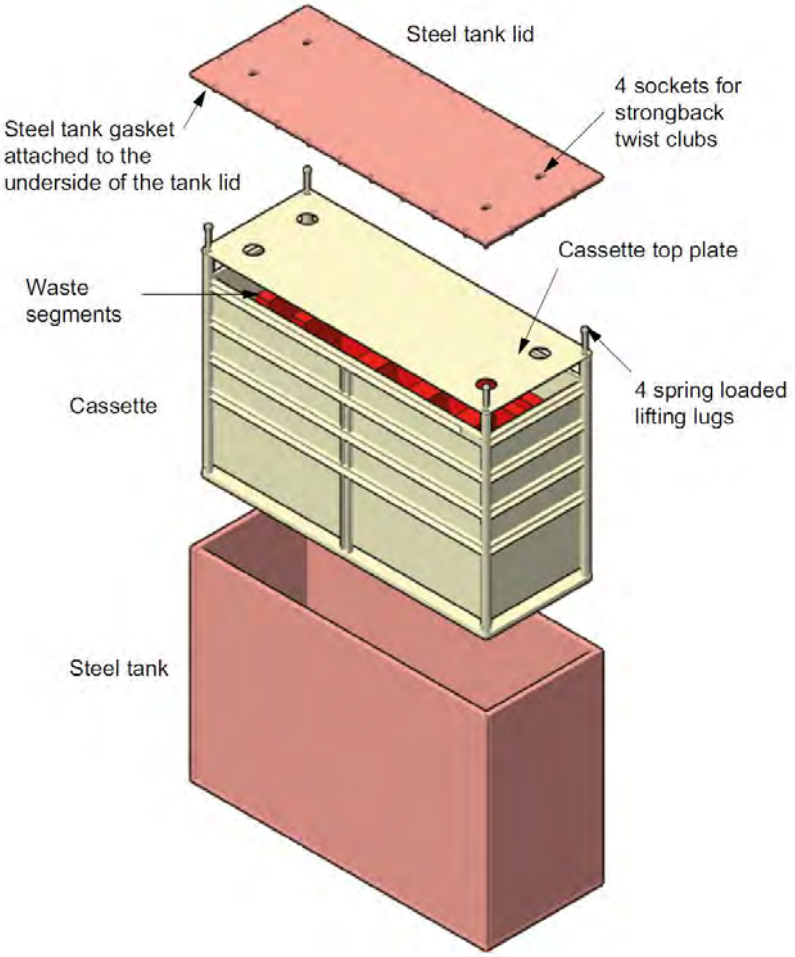

The amount of voidage is important as it can affect radionuclide transport and very long-term mechanical stability of the engineered barriers. For example, as the containers corrode and weaken, they may not be able to support the loads on them. If there is voidage in the containers they may be crushed, leading to cracking of any surrounding cementitious backfill and a reduction in barrier performance. The potential for this to occur depends on the rock loads and the thickness and strength of the backfill. As voidage increases the potential for damage to the surrounding backfill increases.

The main tank walls range from 50 mm to 200 mm thick, so they should be very strong and resist mechanical loads for a long period of time. For example, under high pH conditions the corrosion rate could be 1×10^{-8} m/y (Section 2.5.4 of R-19-09). At this corrosion rate it would take 2.5×10^{6} y to corrode 50 mm of metal (assuming corrosion from both sides). The tanks would be placed in a vault (BHK) with concrete backfill (Section 4.3). As the concrete backfill and conditioning grout degrades and the pH decreases the corrosion rate will increase. Nevertheless, the tanks will likely provide mechanical support until the backfill has significantly degraded, at which point any mechanical movements should not significantly further damage the containment properties of the backfill.

Such effects have been studied in SE-SFL, and the Section S10.1 of the Executive Summary of TR-19-01 notes:

"Chemically induced changes in the performance of the concrete barrier could potentially degrade the mechanical performance of the barrier, both in terms of stiffness and strength. Further, the concrete backfill of BHK may also be affected by mechanical stress from the rock adjacent to the repository (Sections 6.2.10, 6.4.10). Simulations indicate that limited mechanical damage may occur internally in the concrete backfill, at the corners of the waste domain. The effect of this degradation is not explicitly considered in the radionuclide transport calculations. However, the calculations account for the damage due to leaching, which is likely to have a similar effect on radionuclide releases and doses. An exception is the case that considers glaciation-induced stresses. In that case, mechanical damage can be substantial, extending over large regions of the concrete backfill (Section 6.4.4). However, since glaciation is likely to occur only well after tens of thousands of years (Section 6.4.1), when Mo-93 and C-14[1] *have substantially decayed, it is likely that any mechanical effects on the concrete barrier will not have substantial adverse impacts on radionuclide releases and doses."*

Legacy Wastes

Section 4.2.4 of TR-19-01 describes the packaging for legacy wastes. Most of the legacy waste currently stored at the Studsvik site is in 200 L drums containing a mixture of waste and concrete. To provide for safe storage and handling, these drums have recently been placed in new 280 L drums. Solidified sludge is stored in steel drums containing the mixers used in the solidification process. Ashes, general waste and scrap metal are stored in steel drums with inner 100 L steel drums surrounded by concrete. Some of the waste at the Studsvik site is also stored in steel and / or concrete moulds.

SKB plan to dispose of the wastes in 200 L drums, 280 L protection drums and standard moulds with overpacks. These waste packages will be grouted into a steel disposal container (Figure 4). The lids of the 280 L protection drums will be removed before grouting, to allow grout to fill the void between the wall of the 280 L protection drum and the 200 L drum. Reinforcement bars will be placed over the waste packages to prevent cracking of the top layer of the grout.

[1] SE-SFL shows that Mo-93 and C-14 are key radionuclides for potential doses from reactor decommissioning wastes.

Figure 4: Steel disposal containers loaded with waste packages, a) standard moulds, b) standard 200 L drums, C) 280 L protection drums (Figure 4-2 of TR-19-01)

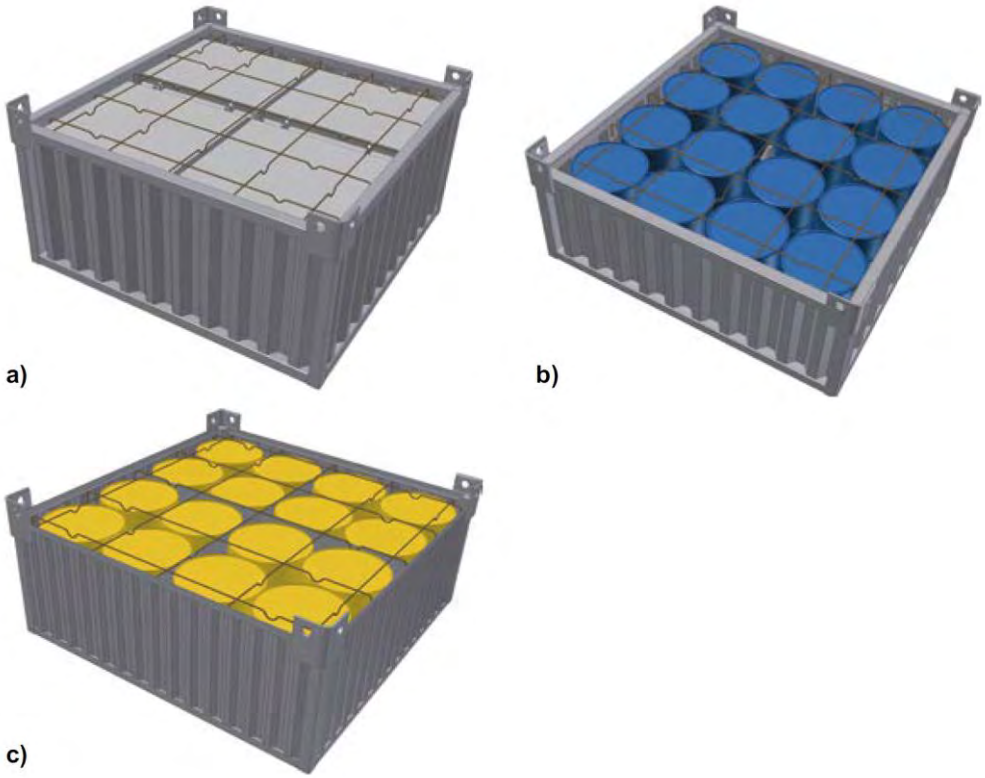

The BHA wastes include some aluminium (Figure 4-3 of TR-19-01) and this has a large surface area (Table 4-2 of TR-19-01). Under alkaline conditions this aluminium could corrode quite quickly. The legacy wastes would be placed in a vault (BHA) with bentonite backfill (Section 4.3). If uncorroded aluminium remains at the start of the post-closure phase, ongoing gas generation could influence resaturation and homogenisation of surrounding bentonite backfill.

The legacy wastes contain similar voidage to the reactor component wastes (1300 m^3 in Table 3-20 of TR-19-03). In the repository, the waste packages may be under significant load due to the swelling pressure of the surrounding bentonite backfill. As SKB anticipate the bentonite will not degrade significantly throughout the 1 x 10^6 y assessment timeframe (further discussed in Section 5.2.1), it would be useful to check that any compaction of the waste packages would not adversely affect the bentonite density and performance.

4.3. Repository Design

The repository comprises two parallel, horizontal disposal vaults (BHK for reactor core components and BHA for legacy wastes) plus associated access tunnels, ramp and shaft.

The steel tanks will be placed into six concrete caissons in the BHK vault (Figure 5). The residual void space inside the caissons will be backfilled with grout, and then the vault will be backfilled with concrete.

The BHA vault contains a reinforced concrete structure supported by granite pillars (Figure 6). The disposal containers will be placed into the concrete structure, then residual void space inside the caisson will be backfilled with grout. Finally, the vault will be backfilled with bentonite blocks, and the crown space will be filled with bentonite pellets. The bentonite blocks will slide between the pillars supporting the concrete structure.

Figure 5: Schematic cross-section layout of BHK (Figure 4-6 of TR-19-01). Legend: 1) Theoretical tunnel contour. 2) Concrete backfill. 3) Grout. 4) Concrete structure (0.5 m). 5) Steel tanks. 6) Concrete. Approximate dimensions: A = 20.6 m, B = 19.6 m, C = 15 m, D = 2.8 m, E = 2.4 m, F = 8.8 m.

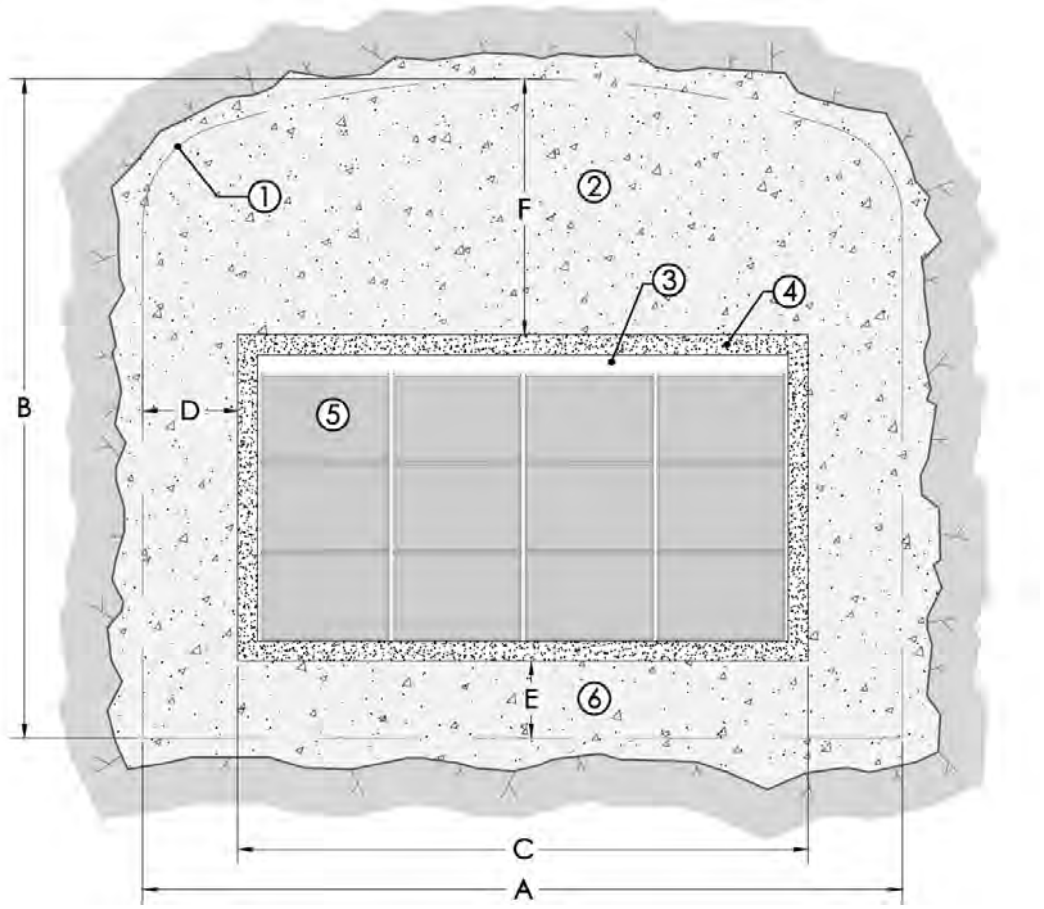

Figure 6: Schematic cross-section layout of BHA (Figure 4-7 of TR-19-01). Legend: 1) Theoretical tunnel contour. 2) Bentonite Pellets. 3) Grout. 4) Concrete structure (0.5 m). 5) Granite pillars. 6) Waste packages. 7) Bentonite blocks. Approximate dimensions: A = 20.6 m, B = 18.5 m, C = 16 m, D = 2.3 m, E = 2.4 m, F = 4 m, G 3.7 m.

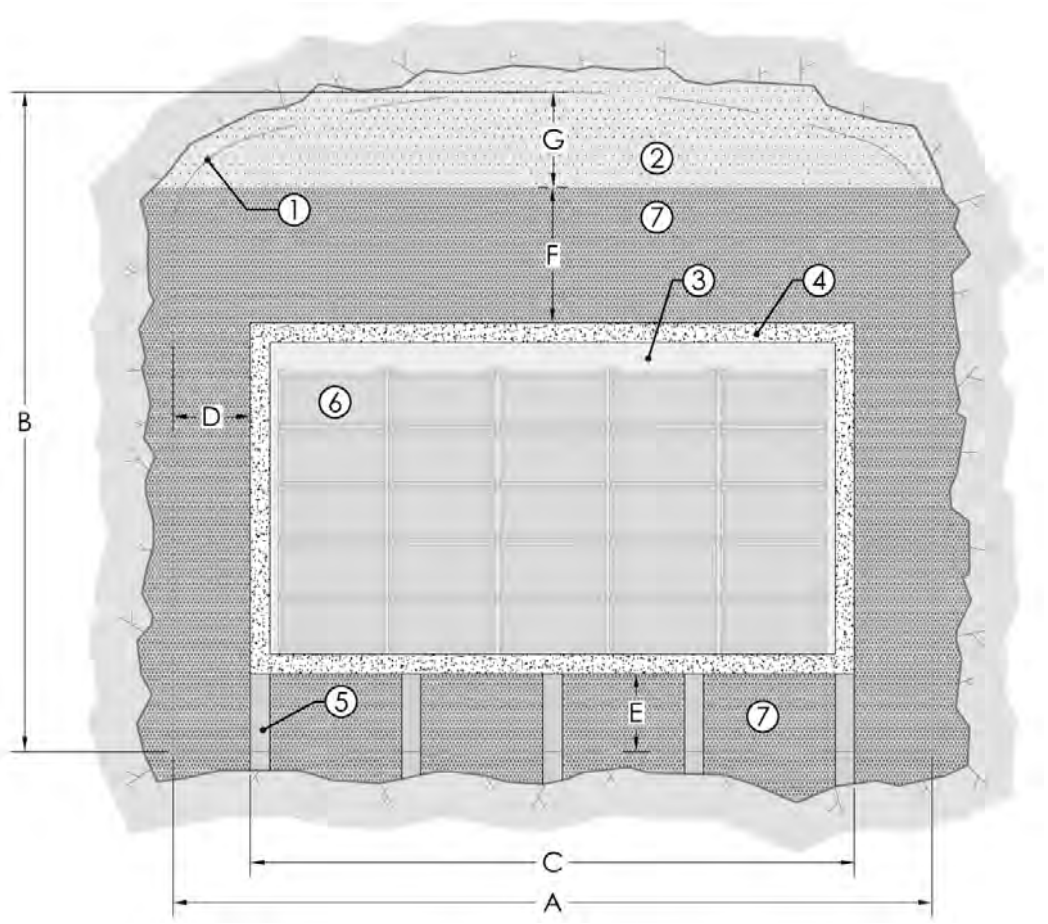

4.4. Construction Methods

The methods that would be used to construct the repository are outside the scope of this review. However, the methods that would be used are important as they will affect the properties and performance of the barriers, and the potential for localised defects that could affect the performance. These include localised construction defects, and defects that develop as the newly installed backfill evolves to achieve its design properties, e.g. curing of concrete and resaturation of bentonite. The potential for physical defects is greater than the potential for chemical defects, although physical defects can affect chemical conditions and processes, for example if flows of water through cementitious materials are mainly within localised fractures rather than spread throughout the pore structure. This can result in localised degradation of the cement and reduced chemical conditioning of water in the fractures.

SKB plan to backfill the BHA vault using bentonite blocks and pellets. SKB, other waste management organisations and regulators have undertaken significant research into the behaviour of bentonite backfills. An important topic is resaturation of bentonite blocks

and pellets to achieve the desired bentonite density, hydraulic properties, swelling pressures. Mechanical stresses can develop during resaturation as volumes of the backfill close to water-bearing fractures resaturate and swell ahead of the rest of the backfill. These mechanical forces could potentially lead to displacement or even damage of waste packages and containing structures.

Controlling the resaturation behaviour and achieving the target properties is challenging for a disposal hole containing a single spent fuel canister. We anticipate this will be much more challenging for a large vault, where it will not be possible to avoid larger fractures that may be more significant sources of water. However, it may be possible to mitigate these effects, for example by grouting water-bearing features to reduce inflow of water, and potentially such measures might also be used to minimise infiltration during the operational phase.

Development of differential stresses could potentially lead to displacement and cracking of the concrete structure containing the waste packages, and also cracking of the grout fill inside the structure. There might also be damage to some of the waste packages. However, this might not be too significant for performance because so long as the bentonite backfill achieves the required properties there will be negligible flow of water through the bentonite backfill into the concrete structure and wastes. We also note that little credit is taken for physical containment provided by the waste packages, concrete structure and grout fill in the SE-SFL assessment models. This is consistent with the purpose of the concrete in the waste domain, which is to, "*reduce the corrosion rate due to high pH and to enhance sorption of radionuclides*" (Section 6.2.9 of TR-19-01).

The resaturation behaviour of the bentonite is discussed in Section 6.2.9 of TR-19-01. SKB have recognised in section 6.2.9 of TR-19-01 that processes such as bentonite erosion and piping could occur and have the potential to reduce the bentonite density and hence swelling pressures. The potential issues noted above have been recognised and some scoping calculations have been undertaken. However, they have not been specifically studies for SE-SFL and SKB note that these issues would have to be studied as part of any future safety assessment.

SKB plan to backfill the BHK vault using concrete. The documents studied as part of this review do not describe the backfilling process and any potential challenges to achieving the assumed backfill properties. There is significant global experience in the use of concrete and developing concrete formulations for different applications across multiple construction sectors, which gives confidence in achieving the assumed properties. However, we anticipate it will be necessary to manage issues that could lead to cracking and shrinkage.

Cracking could increase water flow through the backfill. As water flows through the cracks it will react with the cement minerals in the fracture surfaces. Small aperture cracks may become clogged and sealed with secondary minerals. However, large aperture cracks may remain open and the fracture surfaces may become 'armoured' with secondary minerals. This will reduce chemical conditioning by the cement.

The water content of the backfill mix will affect the flow properties, and the risk of shrinkage and cracking. Wetter mixes that readily flow, and are more suitable for pumping into a vault, tend to result in greater shrinkage and cracking compared with dryer mixes which would have to be 'placed' into position. Wetter mixes also result in weaker

concrete that is less able to withstand mechanical loads and stresses. It may be necessary to consider the use of superplasticisers in the backfill (and also in waste grouts) to improve flow without adding more water. However, some of these additives can increase radionuclide mobility, so it will be important to demonstrate this is not an issue for the chosen additives.

As the backfill cures, heat will be generated. The larger the amount of backfill that is emplaced during a 'pour', the more heat will be generated, and the greater the risk that the backfill will crack as it heats and cools. The thermal stresses might also affect the concrete caissons and their grout fill. This is a driver for emplacing the backfill as a succession of small pours. However, the interfaces between successive pours might not be perfectly sealed, and will therefore be pathways for increased water flow. Therefore, the impact of heat generated during curing of the backfill and bleed water will need to be managed to optimise the properties of the final backfill mass.

It will be difficult to fully prevent cracking and shrinkage, but this may not be detrimental to the performance of the backfill. It is important that there is confidence that the properties assumed in any future safety assessment are consistent with the planned backfill mix and installation method.

Overall, the planned construction methods and building confidence that the required barrier properties can be achieved will be an important part of a future safety assessment.

4.5. Underpinning Detailed Models

The conditions at the repository horizon are important for the performance of the repository. SKB have argued that SE-SFL should use real site data to ensure it is representative of the conditions and features that could be expected to be encountered. Therefore, we spent some time getting a good overview of the underpinning detailed assessment modelling, as it is relevant to reviewing the conceptualised evolution of the near field, configuration and parameterisation of the near-field radionuclide transport models and selection of sensitivity cases.

Regional Groundwater Flow Models

Two regional groundwater flow models have been developed: a catchment focussed model and a repository focussed model (Section 6.2.5 of TR-19-01).

The catchment focussed model uses an Equivalent Porous Medium Approach (ECPM) based on an upscaled Discrete Fracture Network (DFN) realisation. The repository is not represented in the catchment focussed model, but there is additional refinement in the assumed location of the repository. The model accounts for density-driven flow, solute transport by advection and dispersion, matrix diffusion, and hydrogeochemical processes. The catchment-focussed model is used to calculate groundwater density and pressure values at specified time slices for use in the facility focussed model.

The facility focused model considers the same domain as the catchment focussed model. The facility focussed model also uses an ECPM approach, except in the volume of rock around the repository, where a DFN representation is used. Five realisations of the facility focussed model were run to test sensitivity to stochastic variability of the fracture net-

work between known deformation zones that are larger than 1 km in length. The first realisation (r1) used deterministic properties for the fracture network between the deformation zones, while the other four realisations used stochastic properties.

The facility-focussed model calculates a steady-state, density-dependent pressure solution for the considered time slice. Hydrogeochemical processes are not modelled in the facility-focussed model, but their effects on flow are included through the imported spatially variable water density.

The facility focussed model was used to calculate particle tracks and properties relevant to contaminant transport for a set of time slices from 8000 BC to 60,000 AD. SKB found that groundwater-recharge locations and extents vary very little after 2000 AD, responding mainly to the shoreline displacement. The small hill above the assumed repository location is an area of groundwater recharge.

Particle tracks for 2000 AD show that the recharge area for particles passing through the repository is located above and slightly west of the repository. Therefore, once the vaults have resaturated recharge will come from almost directly above the repository. The particle tracks generally continue further downwards after passing through the repository and thus the model suggests insignificant cross flow between the vaults. Discharge locations are found mostly in depressions and stream valleys, and primarily to the north and east of the repository towards the sea (Figure 7).

Figure 7: Detailed groundwater flow modelling particle tracks (Figure 6-5 of TR-19-01. Based on Figure 6-4 of TR-19-01 the plan area shown in this figure is approximately 2 km by 2 km)

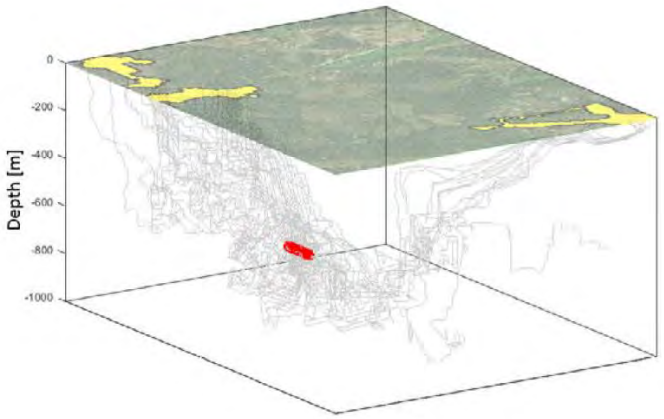

Figure 6-5. *Subset of 100 particle tracks (grey traces) from waste vault BHA (red) to the surface. Yellow areas at the surface represent biosphere objects that are used in the biosphere modelling and into which most particles discharge. Figure identical to Figure 4-9 in the* ***Radionuclide transport report****.*

The discharge locations also show only very small changes after 2000 AD, but a few more distant locations appear to the east as the shoreline regresses. The deformation zones have a significant influence on the particle tracks, resulting in a clustering of the discharge locations. However, a few particle tracks discharge far from other discharge locations. The five realisations of the fracture network result in similar recharge and discharge areas for 2000 AD, but there are some differences and not all realisations discharge to all of the areas.

Particle tracks from the facility focussed model have been used to derive parameters for the geosphere radionuclide transport model. The transport-related properties change relatively little after 2000 AD.

The distributions of the geosphere transport parameters are wide and show substantial tailing, except for the particle-track lengths, which range over less than two orders of magnitude. The five realisations of the fracture network that were simulated for 2000 AD result in substantial variation of the transport-related properties, especially for the F-factor (the sum of flow related transport resistances over all fracture segments). SKB attribute the variation to the presence of large sub-vertical fractures with depth-dependent properties that intersect the vaults in some realisations, including realisation r1, which is the main realisation considered in SE-SFL. SKB note the relatively large differences between the realisations indicate that the full variability of the bedrock properties may not be captured with only five realisations; a higher number of realisations may be warranted in future safety assessments. Section 6.2.7 of TR-19-01 describes the geochemical evolution modelled using the catchment focussed model. At 2000 AD, the shoreline has migrated eastwards from its initial location at 8000 BC. The glacial water present at 8000 BC in the upper part of the bedrock has to a large extent been flushed out by 2000 AD and been replaced by altered meteoric water.

SKB compared the calculated geochemical evolution for the five realisations of the fracture network. They found there is a correlation between the permeability and the modelled chemical results. Higher permeability in and around the repository volume, corresponding to low flow-related transport resistance leads to more and deeper flushing of saline waters, with more fresh meteoric water entering from the top of the model. Realisation r1, which is the main realisation considered in SE-SFL, is one of the two realisations with higher permeability in and around the repository volume.

Flushing is a slower process at depths below 600 m, consistent with the salinity profile shown in Figure 4-9 of Réhn and Hartley (2009), which shows salinity increasing with depth, and also consistent with the decreasing intensity of flowing features with depth, resulting in a trend of decreasing hydraulic conductivity with depth (Réhn and Hartley, 2009).

Implications of the Regional Groundwater Flow Model Results for SE-SFL

In Section 4.1 it was noted that relatively high conductivity regions (associated with fractures and fracture zones) are more frequent at Laxemar compared with Forsmark (the location of SFR and chosen for the Spent Fuel Repository) and many of the other sites studied by SKB's investigation programme for the Spent Fuel Repository. Realisation r1 of the Laxemar repository focussed model has been used to underpin parameterisation of a detailed local model of groundwater flows through the repository (described below), and to parameterise the geosphere transport calculations (outside the scope of this review). Realisation r1 is one of the realisations with higher permeability in and around the repository volume. Since the flow rates used in SE-SFL are based on a higher conductivity realisation of a location with higher frequency of fracture zones, this suggests the flow rates used in SE-SFL may be towards the upper end of the range that might be expected. Higher flow rates are cautious in the sense that they result in more rapid transport radionuclides from the near field and more rapid repository barrier degradation.

The Laxemar site has been studied and modelled in detail. The authors of this review are not familiar with the Laxemar site and have not studied the Site Descriptive Model (SDM) or detailed groundwater flow modelling in detail (they are outside the scope of this review). However, the authors observe that the particle tracks shown in Figure 7 above (Figure 6-5 of TR-19-01) are slightly surprising. As expected, the small hill above the repository is a zone of groundwater recharge, and groundwater discharges to the adjacent lowland areas. The elevation difference between the recharge and discharge locations is less than 20 m over a lateral distance of c.1 km. It is surprising that this elevation difference is sufficient to drive flow to depths of c.600 m. We have briefly tried to understand the reasons for this.

Figures 7-3 and 7-4 of Réhn and Hartley (2009) show an observed small decrease in environmental head with depth. The model results show a similar, although slightly weaker, vertical environmental head gradient. This explains why the pathlines extend to a depth of c.600 m.

It is beyond the scope of the current review to examine the literature on Laxemar further to see if the cause of the observed vertical head gradient has been investigated and identified with confidence. For example, whether there is any evidence the groundwater system is under-pressured at depth following the last deglaciation and the groundwater system is evolving; or if equilibrium local flow systems extend to c.600 m depth because the wider regional topography is too flat to superimpose a deeper regional flow system? (An example of the latter concept is illustrated in Figure 8.5 of Fetter, 1994).

Even though the pathlines extend to c.600 m depth, hydrogeological ‘activity’ at depth is low and flows at the repository horizon are small (e.g. Figure 6-8 of TR-19-01). For a future safety assessment, it would be beneficial to present some additional high level information explaining the conditions at depth, including whether they are in equilibrium or evolving, and the factors influencing the pathlines.

Repository Groundwater Flow Model

A local model of the repository and the surrounding volume of rock in which flow may be influenced by the repository has been developed using an ECPM approach. Hydraulic properties of the bedrock, including the position of higher permeability fractures that intersect the vaults as well as boundary and initial conditions, are taken from realisation r1 of the regional, repository focussed, groundwater flow model (Section 6.2.5 of TR-19-01) at 2000 AD (Section 2.3 of R-19-05). The properties of higher permeability features in realisation r1 of the regional groundwater flow model have been upscaled for use in the ECPM approach (Figure 6-8 of TR-19-01).

The backfill materials in the BHK and BHA vaults are the main barriers limiting groundwater flow through the vaults. Therefore, for constant climate and landscape conditions, i.e. no changes to the regional groundwater flows, future evolution of the flows through the vaults is mainly in response to degradation of these materials.

The bentonite backfill in the BHA vault is assumed not to degrade over the assessment timescales. The regional groundwater flow model results indicate there is a very small

flow along the long-axis of the vault. The flow rate along the long-axis of the BHA vault changes with time in response to changing flows through the BHK vault, but it is always very small.

The concrete backfill in the BHK vault is assumed to degrade and three cases are considered (Section 2.3 of R-19-05):

- Intact Case (IC): All the concrete backfill is intact.
- Degraded Zone Case (DZC): Leaching of the outer half of the concrete backfill creates a more permeable zone.
- Degraded Case (DC): The entire concrete backfill is leached and becomes more permeable.

Degradation of the concrete results in an increase in flow through the BHK vault. This draws water away from the BHA vault, resulting in a decrease in the already very low flows through the BHA vault.

In the DZC case, the degraded concrete acts as a hydraulic cage. This results in lower flows through the wastes in the BHK vault compared with the IC case. However, the flows through the wastes increase to a maximum once the backfill has fully degraded (DC case).

The pattern of concrete degradation assumed in the DZC case is underpinned by the results of the reactive transport modelling e.g. Section 6.3 of R-19-12 (Idiart et al., 2019a). The reactive transport modelling assumes a uniform flow field, excluding the effects of local features in the rock and backfill. In this generalised flow situation, the reactive transport modelling shows there is alteration / degradation around the entire perimeter of the vault, although the greatest alteration / damage occurs where the majority of flow into the vault occurs (Figure 8). (Note that in Figure 8 flow is assumed to be across the vault, from left to right). Water flowing into the vault leaches and reacts with the cement in the concrete. This buffers the water chemistry and reduces alteration of the downstream concrete.

Figure 8: Reactive transport modelling results showing alteration / degradation of concrete backfill in the BHK vault (Figure 6-7 of R-19-12). Note in the reactive transport modelling flow is assumed to be across the vault from left to right.

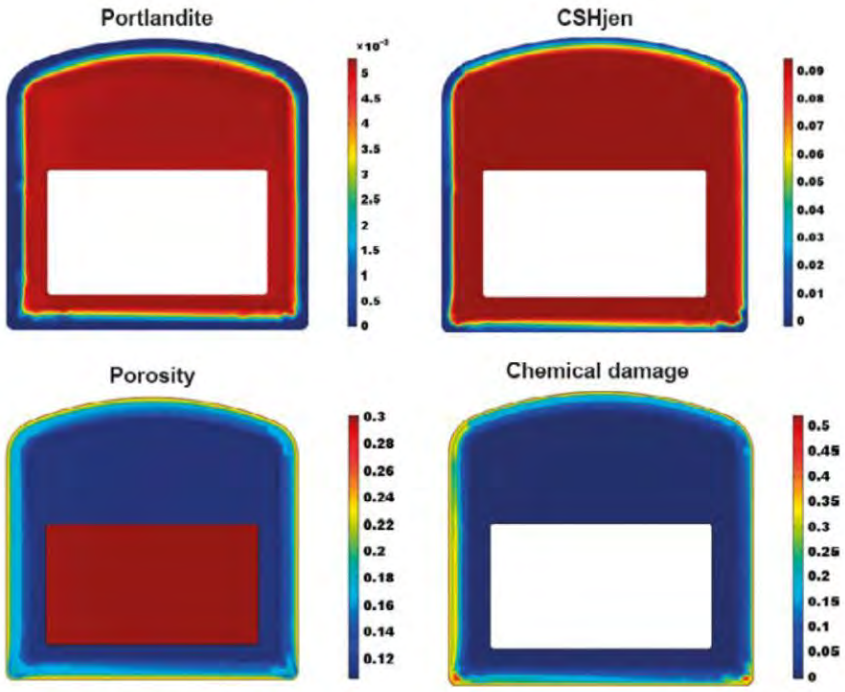

Figure 6-7. *Base Case reactive transport results after 100 000 years: 2D spatial distribution of portlandite and CSHjen volume fractions (top), and porosity and chemical damage (bottom).*

Since flow is expected to be mainly vertically downwards through the BHK vault (Figure 9), there is expected to be preferential degradation of the backfill at the top of the vault compared with the bottom of the vault. This is consistent with the shape of the degraded zone assumed in the DZC case, as illustrated by the pattern of flows in Figure 9. It is also consistent with the radionuclide transport calculations, which assume the concrete back-fill in the top of the vault degrades faster than the backfill in the bottom and sides of the vault (further discussed in Section 6.2.2 of this review report).

Figure 9: Darcy flows through the two cross-section of the BHK vault (Figure 2-11 in R-19-05)

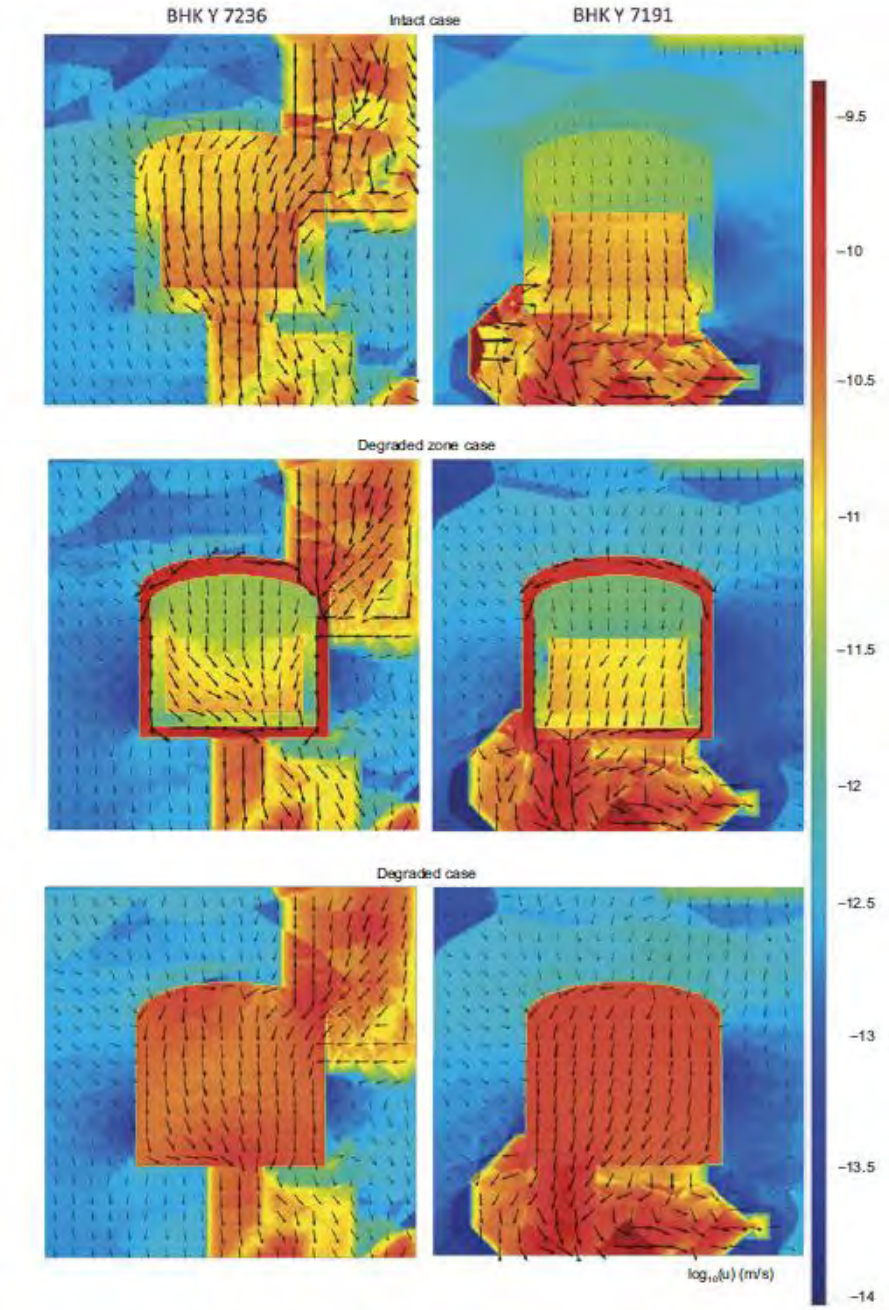

Figure 2-11. Darcy flux through two cross-sections of the BHK vault. The colour scale illustrates the logarithm of the magnitude of the Darcy flux (m/s). (Abarca et al. 2019).

Figures 2-8 and 2-9 in R-19-05 show there are significant variations in flows through the waste and backfill and along the length of the BHK vault. These variations are influenced by the pattern of water bearing features that intersect the backfill. Higher flows in water bearing features that intersect the repository are also illustrated in Figure 9, with high flows occurring in feature ST14 which is present in the left-hand cross-section (BHK Y 7236).

Potentially, the pattern of concrete degradation and the effectiveness of long-term barrier performance could be complicated by such features. Most of the flow into and out of the vault could be associated with these features. Areas of high flow would be associated with localised, relatively rapid concrete degradation. Therefore, flow and transport could potentially preferentially occur in localised volumes of the backfill that degrade significantly more quickly than the majority of the backfill. This would result in the backfill providing a weaker barrier to radionuclide transport compared with a situation where the backfill degrades homogeneously.

These effects could be particularly important because it may be difficult to avoid intersections with more permeable features due to the length of the vault, although there could be the opportunity to minimise such intersections by optimising the repository layout. For example, this could include optimising the vault depths (BHK and BHA could be at different elevations), vault orientations (BHK and BHA might not be parallel) and vault lengths (either vault could be split into a several shorter vaults). For any future safety assessment, it could be beneficial to explore whether a transient coupled model of flow and concrete degradation, which includes localised areas of higher flow, would lead to significantly different patterns of near-field flow and barrier degradation compared with the three steady state cases currently modelled.

The near-field radionuclide transport model developed for SE-SFL represents each vault using a 'Waste' compartment surrounded by backfill compartments. (This is further described in Section 6). If the results of a transient coupled model of flow and concrete degradation showed significant spatial variations in the rates of concrete barrier degradation and flows along the length of the vault, then the near-field radionuclide transport model would need additional discretisation to represent these spatial variations.

Note that a separate review task is examining SKB's conceptualisation and modelling of cement barrier degradation in SE-SFL in more detail than considered here.

5. Scenarios and Conceptual Models

5.1. Scenarios

The SR-PSU FEP Database was used to identify all the factors that may influence post-closure safety for the SFL repository concept at the example location of Laxemar (Section 3.1 of TR-19-01). FEPs that may influence post-closure safety were included in the reference evolution. Three variants of the reference evolution have been identified (Section 6.1 of TR-19-01):

- The *base variant* assumes present day climate and landform with no evolution.
- The *increased greenhouse effect variant* assumes present day climate and landform until 2075 AD, with increased temperatures and precipitation thereafter (Section 4.4.1 of TR-19-01). This variant includes shoreline regression and a succession resulting in new land areas beyond the present shoreline (Section 6.2.2 of TR-19-01), although this does not affect the near-field evolution.
- The *simplified glacial cycle variant* follows reconstruction of the last glacial cycle, with periods of temperate climate, periglacial conditions with permafrost, ice-sheet development and variations in shore level (Section 6.4 of TR-19-01). The simplified glacial cycle is shown in Figure 10, and is repeated every 100,000 years throughout the 1,000,000 year assessment timeframe.

These are a sensible set of scenarios for understanding the performance of the repository, and radionuclide transport in the near field, given the context and objectives of SE-SFL. This approach allows the performance and evolution of the repository to be understood for present day conditions, with the potential additional complexities associated with climate evolution being added later. We anticipate any future safety assessment would explore more ‘realistic’ evolution scenarios, for example an initial period of anthropogenic warming followed by a long-term return to natural glacial cycles.

Figure 10: Evolution of climate and climate-related conditions 100,000 years into the future for the simplified glacial cycle climate case for Laxemar (Figure 6-20 of TR-19-01)

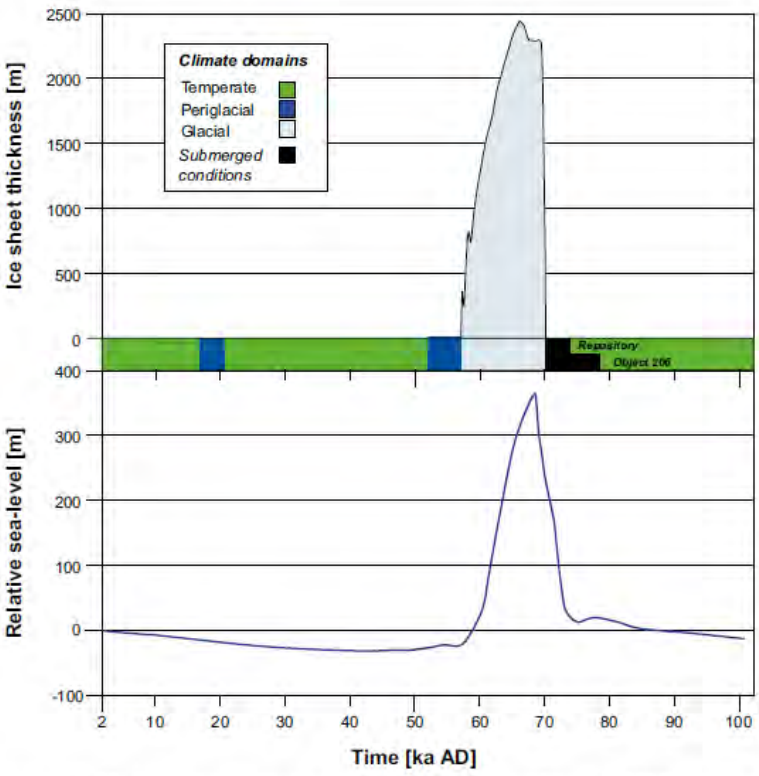

Figure 6-20. Evolution of climate and climate-related conditions 100 000 years into the future for the simplified glacial cycle climate case for Laxemar, shown as a succession of climate domains and submerged periods (top panel). The durations of the glacial climate domain and the subsequent submerged conditions are derived from the glacial maximum stadial (corresponding to MIS 2) in the Laxemar Reference glacial cycle of SR-Can (SKB 2006c). The submerged period following deglaciation shows the duration of water-covered conditions for the locally elevated (21.5 m above present sea level) area immediately above the repository and for biosphere object 206 which receives most of the discharge from the repository. The relative sea-level curve (bottom panel) has its zero line at the present sea level. In SE-SFL, the evolution from 2000 AD to 102 000 AD is repeated every 100 000 years until one million years after repository closure to represent the effects of repeated Late Quaternary glacial–interglacial cycles. Reproduced from Figure 4-3 in the ***Climate report****.*

5.2. Conceptual Models

This section summarises SKB's conceptual model of evolution of the repository and radionuclide transport from the near field. Sections 5.2.1 to 5.2.3 describe evolution of the BHA and BHK vaults, summarising SKB's conceptual model for each variant of the reference evolution. Sections 5.2.4 and 5.2.5 summarise SKB's conceptual model of radionuclide release and transport from the near field. A separate review task is examining SKB's conceptualisation and modelling of the cementitious materials in more detail, in particular concrete backfill in the BHK vault. Evolution of the geosphere and biosphere are outside the scope of this review, although these aspects are also considered in SE-SFL.

5.2.1. Reference Evolution – Base Variant

BHK

SKB conceptualise that the vault will rapidly resaturate once it has been backfilled. (This is further described in Section 5.2.4). Initially the backfill will have low permeability, so there will be little flow through the backfill and waste. The porewater in the vault will be chemically conditioned to a high pH by cement in the backfill, caissons and grout (the waste-domain). The metal wastes and containers will corrode very slowly under the high pH conditions, so the rate of gas generation from anaerobic corrosion of metals will be low.

Geochemical conditions at repository depth are naturally reducing. Conditions in the waste-domain would be even more reducing due to corrosion of the metal wastes and containers. High pH, reducing conditions minimise the mobility of many radionuclides, and cement minerals form a substrate for sorption of radionuclides.

SKB consider that the concrete backfill, caissons and grouted wasteform will gradually degrade through leaching of the cement minerals and reaction of the cement minerals with solutes in inflowing groundwater. For the assumed location at Laxemar, the main direction of groundwater flow would vertically downwards through the BHK vault (see Section 4.5). Therefore, SKB conceptualise that the concrete in the top of the vault would degrade faster than the concrete in the bottom and sides of the vault (Section 6.2.10 of TR-19-01).

Flow through the backfill and waste-domain, and chemical degradation of the backfill and waste-domain, are coupled. Evolution of the flows through the vault is described by the repository scale modelling. As described in more detail in Section 4.5, the repository scale modelling considers three cases: an initial case where all the backfill is intact; a Degraded Zone Case (DZC), where the outer part of the backfill is degraded; and a Degraded Case (DC), where all the backfill is degraded.

As gas is slowly generated it will rise buoyantly through the vault and then through fractures in the rock. Gas will be released as it is slowly generated, so it will not have a significant effect on evolution of the vault. (This is further described in Section 5.2.4).

After one million years the backfill has almost fully degraded. However, the pH in the wastes remains sufficiently high throughout the assessment timeframe that corrosion rates do not change. Section 6.2.8 of TR-19-01 states that it would take around 640,000 years to fully corrode all the metal waste in BHK, and as noted in Section 4.2.2 of this report, it would take even longer to fully corrode the metal tanks. Therefore, corrosion of the metal tanks would promote reducing conditions in the vault throughout the assessment timeframe.

Sorption of radionuclides onto the backfill and waste-domain decreases as cement is leached from the vault, and the amount of cement in the vault decreases. For some radionuclides, the ‘strength’ of sorption (as described by sorption distribution coefficients) changes as the cement is chemically altered. Four cement degradation states are conceptualised (State I, II, IIIa and IIIb), with sorption distribution coefficients specified for each

state (Table 2-18 of R-19-09). However, conditions in the vault remain sufficiently reducing that there are no changes to radionuclide redox states that would affect sorption onto cement minerals (Section 2.5.5 of R-19-09).

The concrete is 70% aggregate. The porosity of the concrete is initially low but increases up to 0.3 as the cement is gradually lost and only the aggregate remains (Section 6.2.10 of TR-19-01).

The groundwater at Laxemar contains sulphate, which can react with the cement forming ettringite and gypsum. These minerals have high specific volumes, so their formation can result in cracking of the concrete. Section 6.2.10 of TR-19-01 discusses the potential for formation of these minerals, concrete cracking and barrier performance:

"*Sulfate concentrations of up to 6 mM have been measured in boreholes at a depth of 500 m in the Laxemar area (Kalinowski 2009). According to the simulations of Idiart et al. (2019a), this concentration is sufficiently high to cause ettringite-induced chemo-mechanical degradation, with the possible risk of a significantly increased hydraulic conductivity and diffusion coefficient, locally but across the entire barrier thickness, within 14 500 years. However, the results are associated with high uncertainties due to conservative assumptions, including the choice of a conservative mechanical-damage model. Furthermore, the porosity decrease due to ettringite is partly compensated by a porosity increase due to mineral leaching. A reduction in the overall concrete leaching rate due to ettringite formation is possible but has not been quantified within SE-SFL*."

SE-SFL does not include cracking of the concrete due to reaction with sulphate bearing groundwaters. The concrete is conceptualised as a single porosity medium, with the porosity increasing over time as the cement minerals are leached. However, cracking is potentially an important consideration for long-term barrier performance. Therefore, sulphate in groundwater is potentially an important factor for future site selection.

The wastes in the BHK vault do not contain potential complexants, e.g. EDTA[2], or materials that could degrade forming complexants, e.g. formation of ISA[3] from cellulosic materials in a Ca^{2+} rich alkaline environment (Section 2.5.6 of R-19-09). Transport of radionuclide sorbed to colloidal material is also assumed to be negligible (in both BHK and BHA) as calcium ions from the concrete structures and grouted wasteform will suppress colloid formation (Section 6.2.8 of TR-19-01).

Radioactive decay and chemical processes will not generate sufficient heat to significantly alter temperatures in the BHK vault, and influence evolution of the conditions.

BHA

SKB conceptualise that the vault will take more than a thousand years to resaturate once it has been backfilled with bentonite. (This is further described in Section 5.2.4). Flow will be into the vault while it is resaturating. Once fully resaturated the bentonite backfill will have very low permeability, and there will be little flow through the vault.

[2] ethylenediaminetetraacetic acid
[3] iso-saccarinate

Geochemical conditions at repository depth are naturally reducing, so conditions in the bentonite would be reducing. Many radionuclides are less mobile under reducing conditions than under oxic conditions, and many radionuclides sorb strongly onto the bentonite backfill.

SKB consider that the bentonite backfill is unlikely to degrade significantly over the assessment timeframe, although they have not yet evaluated all the potential degradation processes. Section 6.2.9 of TR-19-01 describes the processes SKB have undertaken initial evaluations of and the processes still to be considered.

Bentonite – groundwater interaction could lead to exchange Na for Ca and a reduction in the swelling pressure. However, due to the large amount of backfill and the small amount of groundwater it interacts with, equilibrium will probably not be reached during the assessment timeframe, and SKB anticipate this will not significantly affect the hydro-mechanical properties of the bentonite. Similarly, a scoping calculation indicates piping and erosion would not result in significant mass loss, or impact on the performance of the bentonite.

Radioactive decay and degradation of the wastes will not generate sufficient heat to significantly alter temperatures in the vault. Since there are no thermal gradients, SKB consider the extent of bentonite – groundwater reactions, leading to precipitation and / or dissolution of accessory minerals, will be small, and will not affect the backfill performance.

TR-19-01 notes that at the time of writing SKB were undertaking reactive transport modelling explore the potential for alteration of the bentonite backfill (montmorillonite depletion) though reaction with cement porewater, from the concrete structure and grouted wastes. The model results showed that alteration was limited to a few tens of cm adjacent to the concrete structure.

Overall, SKB have conceptualised that there would be no significant degradation of bentonite for SE-SFL, and this is reflected in the parameterisation of the assessment models. They have not yet assessed bentonite mass loss as colloids, which is another process that could lead to degradation of the bentonite, but note this would need to be considered for a full safety assessment. As noted in Section 4.2.2, it would also be useful to check that any compaction of the waste packages would not adversely affect the bentonite density and performance.

Similar to the BHK vault, there will be high pH, reducing conditions in the concrete structure and cementitious wasteform (the waste-domain). Corrosion rates will be low under the high pH conditions, and gas generation will be low, except (as noted previously), the potential for relatively rapid generation of gas at early times from any aluminium wastes that have not corroded before closure. Corrosion of metal wastes and containers will result in highly reducing conditions in the concrete structure and wastes.

Although SKB consider that the bentonite backfill in the BHA vault will not degrade, they do consider degradation of the concrete structure and cementitious wasteform. SKB assumes that groundwater flow through the waste compartment will be along the long axis of the waste compartment. Section 6.2.8 in TR-19-01 notes that in the BHA vault the very low-permeability bentonite backfill may reduce the leaching rate of the waste-domain concrete, leading to a slower pH decrease compared with BHK, but this has not been studied within SE-SFL.

The assumptions made in the assessment calculations are clarified in Table 2-19 of R-19-09. Cement in the caissons and grouted wastes is assumed to degrade to State II at the same rate as the waste and concrete structure in the BHK vault. However, while the wastes and caissons in BHK continue to degrade to State IIIa and then IIIb, cement in BHA does not degrade sufficiently to reach State IIIa within the 1,000,000 year assessment timeframe.

These conceptualised degradation times imply transport of solutes that chemically degrade the cement is initially diffusion dominated in both vaults, so the waste-domain degrades at the same rate in both vaults. As the cement backfill in the BHK vault degrades, flow through the vault increases, the flux of solutes increases, and degradation of the waste-domain accelerates. However, the bentonite backfill in the BHA vault does not degrade, so transport of solutes into the waste-domain is always by diffusion, and the degradation of the waste-domain does not accelerate.

Highly reducing conditions would persist for a shorter time than in the BHK vault because metal corrosion will finish earlier in BHA than in BHK. However, consistent with BHK, cessation of metal corrosion will not affect the redox states or sorption of the radionuclides.

Organic wastes are assumed to degrade in the Ca^{2+} rich alkaline environment forming ISA, which can then complex with radionuclides increasing their mobility (Section 6.2.8 of TR-19-01; and Section 2.5.6 of R-19-09). Production of ISA will cease once all the cellulosic material in the waste has degraded, and ISA will gradually diffuse out of the vault. ISA can also be microbially degraded, but SKB assume this will not be significantly under the high pH conditions, which will limit microbial activity.

For SFR, SKB calculated that 90% of ISA will remain in the vault after 20,000 years (Section 6.2.8 of TR-19-01). Conceptually ISA would be released more slowly from the BHA vault than from SFR. Therefore, SKB's assessment models cautiously assume complexation occurs in the BHA vault throughout the assessment timeframe, and the extent of complexation does not decrease with time as ISA diffuses from the vault (Section 7.4.2 in TR-19-01). Radionuclides that complex with ISA in the wastes are assumed to remain complexed as they are transported through the caissons and bentonite backfill (Section 2.5.6 of R-19-09).

Consistent with the conceptual model for the BHK vault, transport of radionuclides sorbed onto colloidal material is also assumed to be negligible as calcium ions from the concrete structures and grouted wasteform will suppress colloid formation. Radionuclides could also be transported sorbed onto any colloids that form from the bentonite backfill, however, as noted above, loss of colloidal material from barriers has not been studied in SE-SFL.

5.2.2. Reference Evolution – Increased Greenhouse Effect Variant

This variant includes the effect of global warming, resulting from anthropogenic influence on climate combined with natural climate variability. At Laxemar, this results in a warmer and wetter climate compared with the present situation, followed by present day

climate conditions. Isostatic rebound is anticipated to be greater than sea-level rise, so the shoreline is expected to continue to regress from the Laxemar site.

Assessment models assume present day climate conditions until 2075 AD. At 2075 AD there is a step change to warmer and wetter conditions, which persist for 23,000 years. At 25,075 AD there is then a step change back to present day climate conditions (Section 6.3.1 of TR-19-01).

This variant mainly impacts the biosphere. It is not expected to significantly impact Thermo-Hydro-Mechanical-Chemical conditions in the repository or the geosphere at depth. Therefore, there are no changes to the near-field groundwater flow or radionuclide transport models for his variant.

5.2.3. Reference Evolution – Simplified Glacial Cycle Variant

This variant includes an early period of permafrost development ~17,000 years after repository closure, followed by a cycle of permafrost, glaciation, submerged conditions and isostatic rebound / shoreline regression starting at ~50,000 years. This glacial cycle is based on reconstruction of the last stadial period of the Weichselian glacial cycle at Lexemar around 20,000 years ago (Section 6.4.1 of TR-19-01). This glacial cycle is repeated every 100,000 years throughout the 1,000,000 year assessment timeframe.

At 500 m depth the repository is below the level of permafrost / ground freezing. Therefore, advection and diffusion of dissolved radionuclides will continue during the glacial cycle.

There may be enhanced flows through the repository during periods of ice sheet advance and retreat. However, gradients driving flow are anticipated to be low during the time of peak glaciation, and very low during submerged conditions (Section 6.4.5 of TR-19-01). Mechanical ice sheet loading by a glacier can affect the properties of the host rock through stress-induced transmissivity changes, hydraulic jacking and stability of fractures. However, these processes have not been assessed for SE-SFL (Section 6.4.4 of TR-19-01). In the assessment calculations, flows through the repository are based on the flows calculated for 2000 AD, multiplied by scaling factors to represent the effects of the glacial cycle (Section 6.4.6 of TR-19-01).

Ice sheet advance and retreat are associated with ‘injection’ of low salinity meltwaters. These can penetrate to repository depth, and affect the geochemical conditions in the repository. SKB’s groundwater flow models show that ice-sheet loading can also cause upconing of more saline waters from depth. The combined effect for the volume of bedrock assumed to host the repository in SE-SFL is around a factor of ten decrease in salinity while the repository is behind the ice sheet margin (Section 6.4.7 and Figure 6-24 of TR-19-01).

Temperatures changes at repository depth will be small (a few degrees) so they should not have a significant impact on evolution of the waste (Section 6.4.8 of TR-19-01) or barriers, including corrosion of metal wastes.

SKB anticipate that oxygen in the glacial meltwater will be consumed by reaction with minerals in the geosphere before it reaches repository depths. Therefore, although there

may be decreases in salinity in the repository associated with periods of icesheet advance and retreat, conditions should remain reducing. Section 6.4.8 of TR-19-01 notes that sorption distribution coefficients are expected to decrease only slightly during the short periods of increased flow associated with icesheet advance and retreat. Section 6.4.5 of TR-19-01 states that these periods of increased flow last 2,000 years, with maximum flow occurring during ice sheet advance. Given the short duration of the periods with increased flow, the geochemical conditions in the repository, and the sorption distribution coefficients, are assumed to be the same as the base variant, and do not change over time (Section 6.4.8 of TR-19-01).

In the BHA vault, reduced salinity and increased flows associated with injection of glacial meltwaters could increase bentonite erosion through release of colloid material. The potential impacts have not been quantified for SE-SFL, and there is assumed to be no impact on the properties of the bentonite. However, SKB note this would need to be considered in a future safety assessment (Section 6.4.9 of TR-19-01). Since the repository is assumed to be deep enough that it is not affect by permafrost, degradation of the bentonite backfill through freezing is not considered.

SKB have examined the impacts of reaction with glacial meltwaters on chemical degradation of the concrete backfill in the BHK vault. The effects were found to be minor. SKB's simulations of mechanical ice sheet loading indicate the loads may cause damage to the concrete backfill close to the waste domain and locally at the interface between the backfill and the bedrock (Section 6.4.10 of TR-19-01). The backfill at the interface with the bedrock would already have undergone some degradation by this time, so mechanical damage might not further reduce the performance. However, these effects are not included in the assessment models.

5.2.4. Radionuclide Release and Transport Pathways

Radionuclides are assumed to be present as surface contamination on the wastes in the BHA vault. They are immediately available for transport on contact with water. Radionuclides are also present as surface activity on the wastes in the BHK vault, but much of the inventory is present as induced activity in the matrix of the metal wastes. Radionuclides present in the matrix of the metal wastes only become available for transport congruent with corrosion of the wastes.

SKB's conceptual model includes transport of radionuclides dissolved in water by advection and diffusion. Flows through the BHA vault are always very small, so transport is diffusion dominated. Initially flows through the BHK vault are also very small, and transport is diffusion dominated. However, flows increase as the concrete degrades and becomes more permeable, so advection becomes increasingly important. These transport mechanisms are further discussed in Section 5.2.5.

Degradation of the waste can result in gas generation. Key gas generating processes are anaerobic corrosion of metals, and microbial degradation of organics. The former is likely to be most important for SFL due to the prevalence of metals in the forms of wastes and containers. In addition, the high pH environment will suppress microbial activity and therefore microbial generation of gas.

Gas generation can have the following impacts.

- It can affect flows of water into and out of the vaults, including resaturation of the vaults, and therefore transport of radionuclides in water.
- Anaerobic corrosion of metals consumes water, and in very low permeability environments this can potentially limit aqueous radionuclide transport by desaturating the wastes / vault. (Note the amount of water present in the wastes and backfill at closure can be an important factor affecting the availability of water to support corrosion reactions).
- Release of bulk gases, such as H_2 generated by anaerobic corrosion of metals, from the repository can advect trace radioactive gases (especially carbon-14 labelled gases).

SKB's radionuclide transport calculations assume the vaults are fully saturated at all times, although they have modelled post-closure resaturation of the vaults. Ignoring any operational impacts, such as drying of the rock surrounding the vaults, SKB calculate that it will take 2 to 120 years for BHK to resaturate and 1,600 to 15,000 years for BHA to resaturate (Figure 6-9 of TR-19-01). BHA resaturates more slowly than BHK due to the lower permeability of the backfill. For both vaults a key uncertainty affecting the resaturation time is bedrock characteristics. Therefore, resaturation might take longer for a site with lower numbers of higher conductivity fractures than Laxemar. Note that these resaturation calculations did not include consumption of water by gas generating reactions, or the effect of the gas pressure on flows of water into the vaults.

SKB have undertaken multiphase flow calculations to examine the impacts of gas generation on water flows for the BHK vault. These are summarised in Section 6.2.8 of TR-19-01. (Note we have not consulted the underpinning references that describe the multiphase flow modelling in detail as part of this review). The multiphase flow modelling showed that a small gas overpressure develops in BHK, but gas is readily released from the BHK vault, and has a negligible effect on water saturation and groundwater flow in the BHK vault. SKB have not undertaken multiphase flow calculations for BHA due to the smaller amount of metal in the vault, but note that since large overpressures might affect the integrity of the bentonite buffer they would need to be studied for any future safety assessment.

SKB's safety assessment models assume the vaults resaturate instantaneously, and gas generation does not affect water flow or transport of dissolved radionuclides. The work SKB has undertaken so far supports this approach for the BHK vault, but further work would be beneficial for the BHA vault. For example, if it takes several thousand years for the BHA vault to resaturate, the associated inflow of water could reduce the fluxes of radionuclides diffusing out of the vault. Conversely, if high gas pressures develop in the wastes, this could drive water, and dissolved radionuclides, out of the vault. Ideally any future multiphase flow modelling for the BHA vault would account for the availability of water to support corrosion reactions, and the potential for higher rates of gas generation during the resaturation phase due to corrosion of aluminium wastes (Section 4.2.1).

The potential for generation of C-14 gas is noted in Section 6.2.8 of TR-19-01. One potential generation route is through degradation of organic wastes by methanogenic bacteria. SKB consider the high pH conditions in the repository will suppress the activity of all microbes, and there is no evidence that methanogens are metabolically active at the anticipated pH. As the cement degrades the pH will start to decrease, microbial activity could start to increase, and methanogens could become active. However, the timescales for the

pH to decrease to levels where methanogens become active are sufficiently long that C-14 will have decayed to negligible levels.

Recent research (Wormald, 2019) has shown that methanogens can be active at higher pHs than previously thought, including at the pH anticipated in SFL at early times. In addition to tolerance to high pH conditions, the research highlights the importance of niches in which local conditions different from the bulk average. Niches can reflect both material type, e.g. within organic materials, and modification of local conditions by microbes, e.g. microbial production of acids leads to local lowering of the pH. In SFL, niches might also be associated with areas of potentially enhanced local cement degradation, e.g. where water flows into the vault from a fracture in the host rock, or adjacent to any fractures through the backfill and grouted wasteform.

C-14 present as an activation product in irradiated metals can be released congruently with corrosion of the metals. C-14 may be present in elemental forms or as metal carbides. On dissolution, the metal carbide may form hydrocarbons (such as methane or acetylene) or small organic molecules. In assessment calculations for the C-14 gas pathway, the UK's Radioactive Waste Management (RWM) organisation have cautiously assumed all the C-14 present in irradiated metals either decays to stable N-14 before the metals corrodes, or if it has not decayed, is released as C-14 methane gas, congruent with corrosion of the metal wastes (RWM, 2016).

A state-of-the-art review, undertaken as part of the International CArbon-14 Source Term (CAST) project, has highlighted uncertainty in the form of release of C-14 from irradiated steels (Swanton et al., 2018). There is evidence for release of C-14 in C1 to C5 hydrocarbons (C1 = methane), but also as dissolved organic and inorganic species. Inorganic species (i.e. carbonate and biocarbonate) would react with cement minerals forming carbides, therefore attenuating release of C-14. Organic species could either remain in solution, resulting in advective and diffusive release of C-14, or they could be microbially metabolised forming C-14 gas.

In the reports reviewed, SKB have not discussed the form of C-14 in irradiated metals, or the form of C-14 released from corroding metals. SKB have assumed all C-14 is released to water, and is then transported by advection and dispersion, without solubility limitation or sorption (Section 2.5.5 of R-19-09). This approach is cautious in the context of potential impacts from release and transport of C-14 in groundwater.

Release of C-14 gas from corrosion of irradiated metal wastes is not considered. This includes direct release, or release of organic species that are subsequently microbially metabolised. However, this could potentially be an important transport pathway for a portion of the C-14 inventory, so it may be appropriate to consider this in more detail for a future safety assessment.

5.2.5. Radionuclide Transport Mechanisms

The grouted wasteform, concrete structures / caissons, concrete and bentonite backfills are porous media. The degraded concrete is conceptualised as a single porosity medium, i.e. cracks do not form. Dissolved radionuclides are transported by flow of groundwater through the pores; and diffusion in the porewater, driven by concentration gradients. Groundwater flow through the BHA vault is always low due to the very low permeability

of the bentonite, and transport is diffusion dominated. Groundwater flow is very low through the intact concrete, so transport in the intact concrete is diffusion dominated. The permeability of the degraded concrete is much higher than the intact concrete, so groundwater flow is much higher through the degraded concrete and transport is advection dominated.

The diffusive fluxes of radionuclides from intact concrete backfill and (undegraded) bentonite backfill into fractures in the rock are affected by two factors. These are illustrated in Figure 11 for the BHA vault.

1. The cross-section area of the fractures is small, so there is only a small area for diffusion out of the backfill into the fractures. The average diffusive pathlength through the backfill to a fracture is greater than the direct pathlength that would be possible if the rock were a porous medium. Focusing of the diffusive fluxes towards the fractures will affect the concentration gradients in the backfill, and therefore the diffusive fluxes. These geometrical effects can be described as a resistance to diffusion into the fracture.
2. There will be concentration gradients in the fractures, with radionuclide concentrations decreasing away from the interface between the backfill and the rock. The concentration gradients will affect the diffusive fluxes of radionuclides into the fractures. The concentration gradients will be affected by the groundwater flow rates in the fractures. The higher the flow rates, the faster radionuclides will be advected away from the backfill-rock interface, the lower the concentrations at the interface, and the higher the diffusive fluxes.

Figure 11: Conceptual model of advective and diffusive transport in the BHA vault

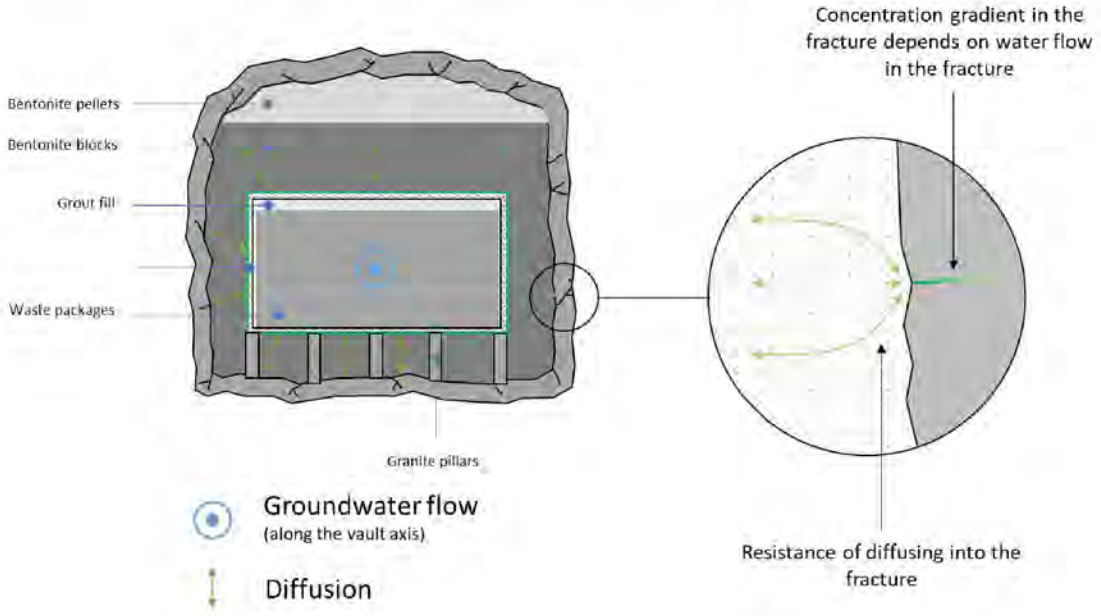

R-19-05 describes mathematical models for radionuclide transport in porous and fractured repository materials. These models are further considered in the next section of the review report.

6. SKB's Assessment Models

6.1. Mathematical Models

SKB report R-19-05 describes development of radionuclide transport models for the near field. This includes the mathematical models, and the approach to discretising the model domain to represent the repository in a compartmental model. The compartmental models are implemented using the Ecolego software[4].

The mathematical models and compartmental models developed by R-19-05 form the basis for the mathematical and assessment models used in SE-SFL. However, they are not used directly. For example, as noted above, in SE-SFL degraded concrete is assumed not to be fractured, so the mathematical models for radionuclide transport described in R-19-05 are not used in SE-SFL. In addition, the assessment models developed in R-19-05 represent the six concrete caissons in the BHK vault separately, while only a single combined caisson is represented in the assessment models used in SE-SFL (TR-19-06 and R-19-09). These inconsistencies introduce some confusion when the assessment reports refer to R-19-05 for additional information.

The mathematical models presented in R-19-09 and TR-19-06 are not entered directly into the assessment models. Equations for the transfer fluxes (Bq y^{-1}) between compartments need to be divided by the amount in the compartment, to give equations for fractional transfer rates (y^{-1}).

SKB's assessment models use a compartmental modelling approach. A key assumption of this approach is that conditions, including radionuclide concentrations, are uniform throughout the volume represented by the compartment (i.e. 'fully mixed'). R-19-05 introduces the concept of the Peclet number, which describes the ratio of advection to diffusion. Section 4.2 of R-19-05 notes:

"When the Péclet number is smaller than one, Pe < 1, the effect of diffusion exceeds that of advection in determining the overall mass flux. This suggests that diffusion dominates in the domain and the concentration may become equilibrated over a certain course of time, similar to a well-mixed tank. By contrast, a large Peclet number, Pe >> 1, indicates that transport mainly occurs by advection, similar to a plug flow reactor. However, advection only displaces the fluid in the absence of turbulent effects and can hardly add to the radionuclide mixing. Therefore, the full-mixing assumption is not expected to be satisfied in the backfill where transport occurs mainly by advection. Alternative models to address radionuclide transport within these domains are therefore required."

These arguments are not clear. Consider a simple 1D system in which a radionuclide is diffusing away from a source. There is no advection. The concentration decreases with increasing distance from the source. If the 1D system is represented by a 1D chain of compartments, the actual radionuclide concentration can decrease across the volume represented by a compartment. However, in the compartmental model the radionuclide concentration is considered to be homogeneous (fully mixed) throughout the volume represented by each compartment. Therefore, the compartmental modelling approach introduces some additional mixing, which is termed numerical dispersion.

[4] https://www.ecolego.se/

The more compartments there are in the 1-D chain, the smaller the amount of numerical dispersion. It has been demonstrated (Quintessa, 2019) that discretising the 1D transport pathway between the source and receptor using five compartments, reduces numerical dispersion such that the modelled diffusive flux out of the fifth compartment is very similar to the flux calculated analytically (Figure 12). The error in the peak flux is equal to $1/N^2$, where N is the number of compartments. Therefore, for a chain of five compartments the error is 4%.

Figure 12: Analytical solution for the diffusive flux through a barrier compared with the results of an AMBER model where the barrier is represented using five compartments (Quintessa, 2019)

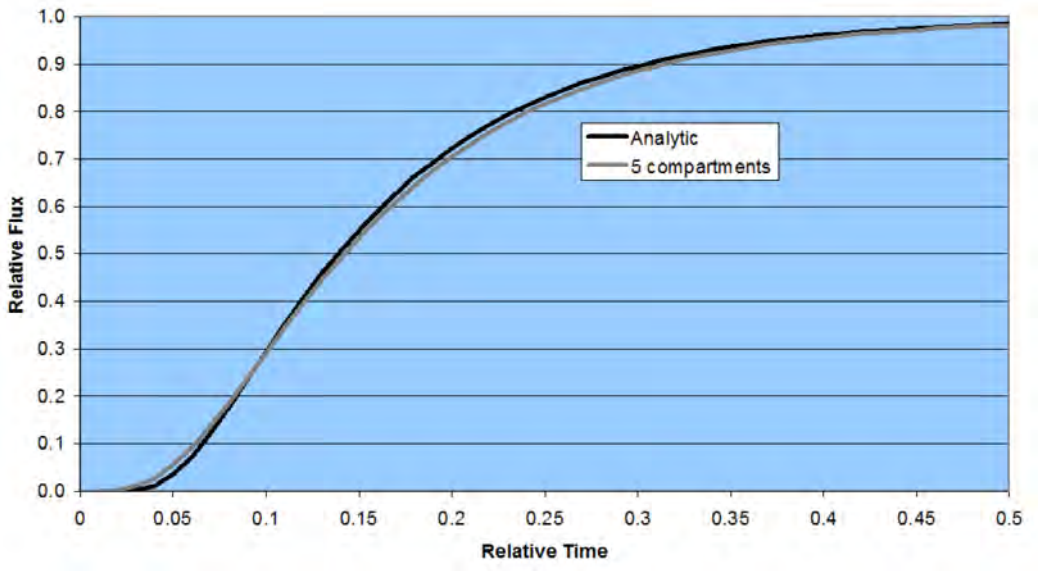

Now consider a simple 1D system in which a radionuclide is being transported away from a source by advection. Diffusion still occurs but is negligible compared with advection. Although diffusion is not significant, mechanical dispersion will result in a degree of contaminant mixing. Again, the concentration decreases with increasing distance from the source, and if system is represented by a 1D chain of compartments, the actual radionuclide concentration can decrease across the volume represented by a compartment. However, in the compartmental model the radionuclide concentration is considered to be homogeneous (fully mixed) throughout the volume represented by each compartment, so again the compartmental approach introduces some numerical dispersion.

Fick's law is used to model diffusion. Mechanical dispersion is also typically modelled as a Fickian process, i.e. using the same mathematical model as diffusion. Therefore, in an advection dominated system the Peclet number describes the ratio of advection to mechanical dispersion. Two approaches are available to represent mechanical dispersion in a compartmental model. The first approach is to use a large number of compartments such that numerical dispersion is negligible, and then represent mechanical dispersion using appropriate transfer rates between compartments. The second approach is to adjust the number of compartments, so the amount of numerical dispersion is equal to the amount of mechanical dispersion. The second approach is used in SE-SFL (Section 4.3.2 of TR-19-06).

For a compartmental model, the Peclet number, Pe, is equal to twice the number of compartments (Section 3.3 of R-19-05). SKB have assumed a Peclet number of 10 for SE-SFL (Section 4.3.2 of TR-19-06). This is given by using a chain of five compartments.

In summary, using a chain of five compartments appropriately represents diffusive transport through low permeability barrier materials. Once the barrier materials have degraded, and their permeability has increased so transport becomes advection dominated, a chain of five compartments results in an amount of numerical dispersion that matches the mechanical dispersion when the Peclet number is 10. A Peclet number of 10 is a common assumption for the ratio of advection to mechanical dispersion anticipated in a porous medium (Gelhar et al., 1992).

R-19-05 presents two models for radionuclide transport in degraded concrete: the Fractured-Backfill (FB) model; and the Degraded Backfill (DB) model. Note that both models assumed the degraded concrete is fractured, but they assume different fracture patterns. In each model, there are three stages of concrete degradation: intact (IC), partially degraded (degraded zone, DZC), and fully degraded (DC).

The FB model assumes that water only flows through fractures in the degraded concrete. The DB model assumes flowing water can spread out of the fractures into the degraded concrete. This increases the contact area between the degraded material and the intact material and increases the contact time, allowing more radionuclides to diffuse from the intact material into the degraded material.

When the outer part of the concrete backfill is degraded (DZC), water flows through the degraded backfill and around the intact inner backfill. Radionuclides diffuse through the intact inner backfill into fractures in the degraded outer backfill. This situation is analogous to the initial situation where the inner and outer backfill are both intact, and radionuclides diffuse through the intact backfill into fractures in the host rock.

The conceptual model for the situation where both the inner and outer concrete are degraded (DC) is not clear. Figures 4-8 and 4-10 of R-19-05 illustrate the FB and DB fracture models, respectively. In both models, radionuclides diffuse from the waste package into fractures in the backfill. This implies that the waste package (which in this context comprises the caissons and grouted wastes packages) is intact, because otherwise transport out of the waste package would be advection dominated. However, Figures 4-8 and 4-10 of R-19-05 also show advection from the porous degraded backfill, between the fractures, into the waste package, implying that the waste package is degraded. As noted above, this implies transport out of the waste package would be advection dominated, so the diffusion model is not important. In addition, these figures do not make conceptual sense. If flow is through the degraded porous backfill between the fractures, rather than mainly within the fractures, then radionuclides would also be expected to diffuse into the degraded porous backfill, rather than only into the fractures.

Section 4.2.3 of R-19-05 states that the DB model is used in SE-SFL. The transport parameters are derived using the results of the repository groundwater flow model described in Section 4.5. The flow rates from the repository groundwater flow model are sufficiently low, and the residence time of the water is sufficiently long, that diffusion is able to even out radionuclide concentrations throughout the degraded materials. Therefore, the degraded concrete can be treated as a homogeneous porous medium.

The FB and DB models are not discussed in TR-19-01, TR-19-06 and R-19-09. This makes it difficult to understand how the models developed in R-19-05 are used in the assessment. The parameters included in R-19-09 indicate the degraded concrete is simply treated as a porous medium in the assessment model, which is consistent with the conclusions of R-19-05.

It should be noted that this result is based on water flow rates calculated by the repository groundwater flow model. The repository groundwater flow model used an ECPM approach and calculates Darcy and pore velocities in the backfill. It conceptualises the degraded concrete as a porous medium with a porosity of 0.14 (Table 3-3 of Abarca et al., 2019), rather than a fractured medium. We assume the Darcy velocities calculated by the repository groundwater flow model have been used to calculate the fracture flow velocities given in Table 4-2 and Table 4-3 of R-19-05, which then leads to the result that diffusion is able to even out radionuclide concentrations throughout the degraded materials. However, this requires assumptions about the nature of the fractures in the backfill, which are not provided.

6.2. SKB's Assessment Models

6.2.1. BHA

SKB's conceptual model of the BHA vault and its representation in the assessment model are summarised in Figure 13.

Radionuclides are considered to be present as surface contamination on the wastes, so they are immediately available for transport on contact with water. The waste domain, which includes the concrete structure, waste packages, and grout fill is represented using a single compartment. This approach assumes that radionuclides are homogeneously distributed throughout the waste domain, and therefore underestimates the containment provided by the wasteform, grout fill and walls of the concrete structure. Containment provided by the features in the waste domain is further underestimated because all the radionuclides are assumed to have an effective diffusivity equal to diffusivity of radionuclides in free water (Section 2.6.1 of R-19-09).

Although the containment provided by the waste domain is likely to be underestimated, the containment provided by the waste domain may be small compared with the containment provided by the bentonite backfill, and therefore this may not be significant. However, in any future safety assessment. it would be beneficial to better understand the containment provided by the waste domain as it forms part of a multi-barrier system.

As noted in Section 5.2.1 the concrete / cementitious grout in the waste domain is assumed to degrade over time. The sorption distribution coefficients and porosity of the concrete evolve in response, but it appears that the porosity of the waste grout is constant for reasons that are not explained by SKB. The bentonite backfill is assumed not to degrade, and therefore has the same transport properties throughout the assessment timeframe.

ISA is generated in the BHA vault through degradation of cellulosic wastes. ISA forms complexes with radionuclides, increasing their mobility. SKB's assessment models cautiously assume the concentration of ISA in the vault does not decrease with time, and radionuclides remain complexed as they are transported through the backfill into the geosphere.

Chains of five compartments are used to represent the bentonite backfill. The inflow and outflow compartments represent bentonite backfill at the ends of the vault. The side compartments represent the bentonite backfill surrounding the waste packages along the length of the vault. Note there are no transfers between inflow and side compartments, or between side and outflow compartments, to represent tangential transport of radionuclides. However, these tangential transfers should be negligible.

Chains of five compartments are used to ensure numerical dispersion (Section 6.1) is negligible compared with transport by diffusion. Diffusion from the outermost backfill compartments into fractures in the rock is affected by the geometrical resistance of diffusing into the fractures (R_{plug}) and the resistance due to the concentration gradient in the fractures, which depends on the flow rate in the fractures (R_{Qeq}) – see Figure 11.

There is a very small flow of water along the axis of the vault. In the assessment model, all the water that flows through the backfill at the upgradient end of the vault is assumed to flow through the waste. Transport is diffusion dominated within the bentonite. Transport from the bentonite into fractures in the rock is also diffusion dominated for most of the bentonite-rock interface. However, the AMBER model results (Section 8) indicate that where water flows out of the end of the vault, transport across the backfill-rock boundary is slightly advection-dominated for some radionuclides.

Figure 13: Summary of SKB's conceptual model for the BHA vault and representation in their assessment model

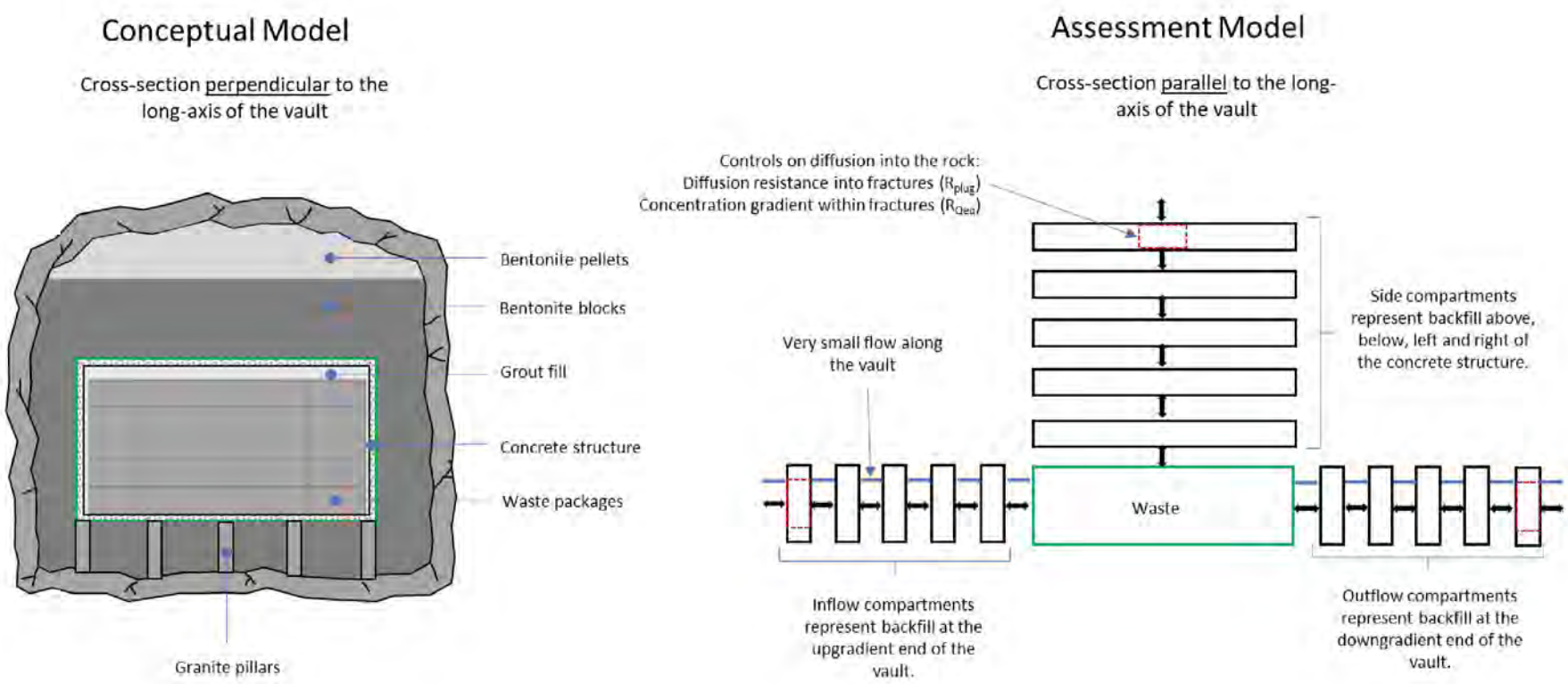

6.2.2. BHK

SKB's conceptual model of the BHK vault and its representation in the assessment model are summarised in Figure 14 to Figure 16 for intact concrete backfill, degraded outer concrete backfill (DZC) and fully degraded concrete backfill (DC) respectively.

Radionuclides are present as contamination on the surfaces of the wastes, and as induced activity in metal wastes. Radionuclides present as surface contamination are immediately available for transport on contact with water, but radionuclides present in the matrix of metal wastes only become available for transport as the metal corrodes. The inventory of induced radioactivity is split between metal wastes of four different thicknesses. These metal wastes corrode at the same rate, but it takes longer to corrode the thicker wastes than the thinner wastes, so radionuclides are released from the thicker wastes over a longer time period than from the thinner wastes.

The waste domain, which includes the concrete caissons, waste packages, and grout fill is represented using a single compartment. This approach assumes that radionuclides are homogeneously distributed throughout the waste domain, and therefore underestimates containment provided by the wasteform, grout fill and walls of the concrete caissons. Containment provided by the features in the waste domain is further underestimated because all the radionuclides are assumed to have an effective diffusivity equal to the diffusivity of radionuclides in free water (Section 2.6.2 of R-19-09).

As discussed for the BHA vault the containment provided by the waste domain is likely to be underestimated. The containment provided by the waste domain in the model may be more significant for the BHK vault than the BHA vault, so this might be more of a conservatism than for BHA. In any future safety assessment. it would be beneficial to better understand the containment provided by the waste domain as it forms part of a multi-barrier system.

The concrete and cementitious grout in the waste domain are assumed to degrade over time. The porosity, sorption distribution coefficients, and flows through the wastes evolve in response. Degradation of the concrete / grout in the waste domain is controlled by flow of water through the domain, which in turn depends on degradation of the concrete backfill.

The concrete backfill is assumed to degrade over time. The three stages described in Section 4.5 are represented in the assessment model, i.e. intact concrete (IC), degraded outer zone (DZC) and full degraded (DC). Flow through the intact concrete is small, and diffusion is the dominant transport process. Flows are much greater through the degraded concrete, so advection is the dominant transport process in the degraded concrete.

It is unclear whether the assessment models and detailed underpinning models are internally consistent regarding the timings of events such as changes in groundwater flow rate, timing of the changes between IC, DZC and DC states, and the timing of the changes in the concrete degradation state (i.e. between I, II, IIIa and IIIb), because the cement degradation models do not appear to use the same groundwater flow field as the radionuclide transport models.

Water flows predominantly downwards through the vault. Most of the inflow through the roof of the vault leaves through the floor of the vault, but a small proportion flows laterally though the side walls. In the assessment model, all the water that flows through the inner backfill is assumed to flow through the waste.

Similar to the BHA vault, chains of five compartments are used to represent the backfill. However, for the BHK vault the inflow compartments represent the backfill above the wastes, the side compartments represent the backfill to the side of the wastes, and the outflow compartments represent the backfill below the wastes. Again, use of five compartments reduces numerical dispersion to a negligible level when transport is diffusion dominated. When transport is advection dominated, five compartments results in an amount of numerical dispersion that is equal to the amount of mechanical dispersion anticipated by SKB. There are no transfers between inflow and side compartments, or between side and outflow compartments, to represent tangential transport of radionuclides. Therefore, radionuclides that migrate upwards or sideways through intact backfill into the degraded backfill, cannot subsequently be advected downwards in the degraded backfill.

Figure 14: Summary of SKB's conceptual model for the BHK vault with intact backfill and representation in their assessment model

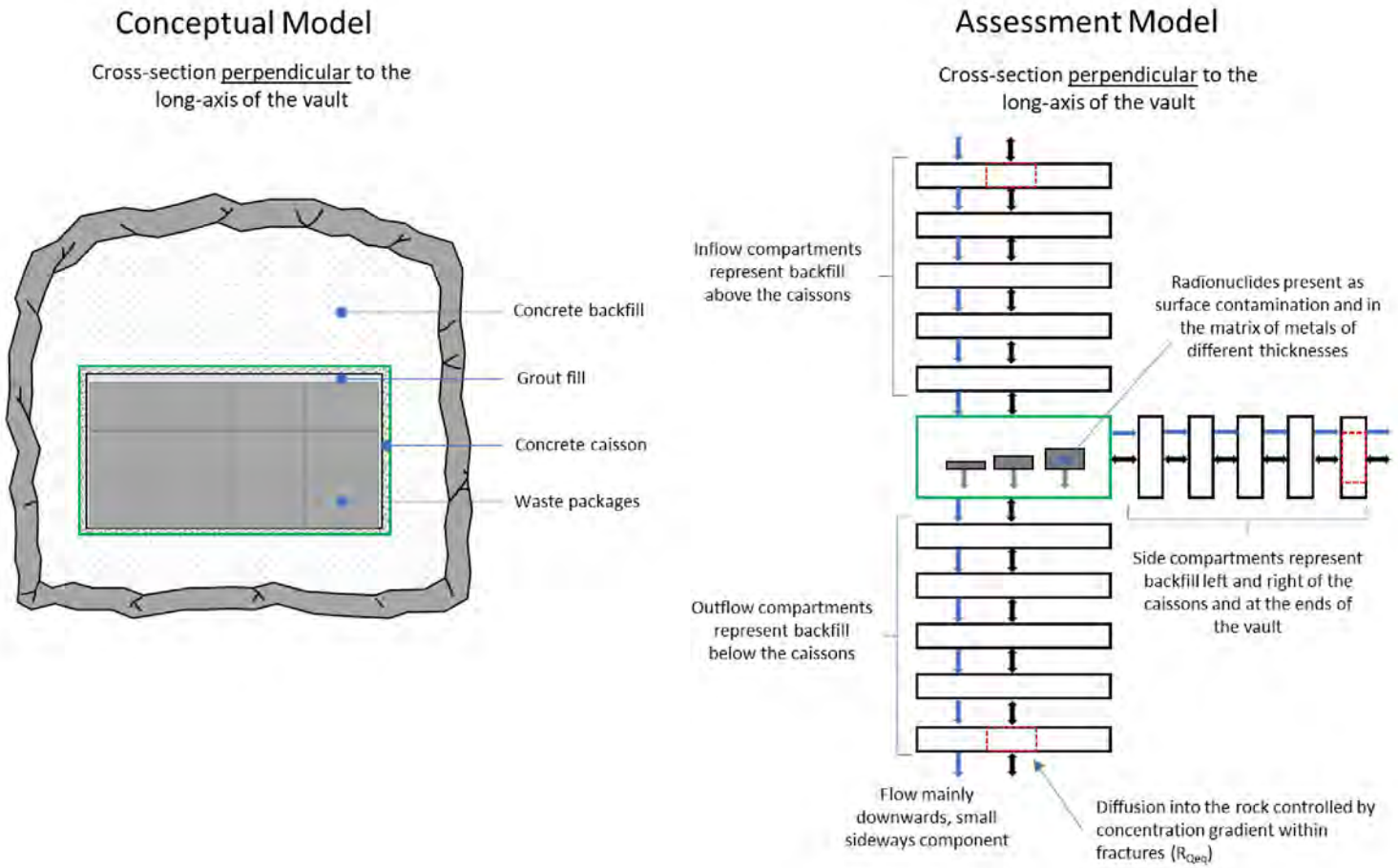

Gradual degradation of the concrete backfill is considered within each concrete degradation state. This illustrated in Figure 17 which shows evolution of the diffusion transport resistance of the backfill compartments. The concrete above the waste domain is exposed to the inflowing water. The inflowing water reacts with the cement in the concrete, chemically degrading the cement, and altering the chemistry of the water so it is in equilibrium with the cement. Therefore, the concrete backfill above the waste domain degrades more rapidly than the concrete below and to the side of the waste domain.

Although gradual degradation of the concrete is considered during each degradation stage, there are discontinuities in the radionuclide transport properties between degradation stages. This is illustrated by the step changes in diffusion transport resistance at 87,000 y and 782,000 y in Figure 17.

The evolution of the properties of the backfill is complex. It combines elements of a simplified assessment model, in which three stages of backfill degradation are considered, and a more realistic representation with continuously evolving properties. This is an area that could potentially be further developed in the future to provide a more realistic description of the evolving properties of the backfill, with the properties evolving continuously over time without any discontinuities. However, this may not be straightforward as it may require updates to the underpinning flow and concrete degradation models.

During the first concrete degradation stage, when all the backfill is intact, the backfill compartments represent all the backfill between the waste zone and the vault wall. However, in the intermediate stage where the outer concrete has degraded (DZC), the same compartments seem to only represent the intact backfill, although this is not completely clear from SKB's documents. The degraded outer backfill does not appear to be represented. The compartment volumes do not change, but the diffusion lengths are reduced by a factor of two, reflecting the outer half of the backfill being degraded (Section 2.8.2 in R-19-09).

During the third degradation stage, when all the concrete has degraded (DC), the same compartments again represent all the backfill. Again, the compartment volumes do not change, but the diffusion lengths revert to their original values.

This approach is conceptually complex. With the transition from the initial intact stage to the intermediate stage where the outer concrete is degraded (DZC), radionuclides that were present in compartments that represent the outer backfill are suddenly present in compartments that represent in the inner backfill. With the transition from the intermediate stage where the outer concrete is degraded, to the final stage where all the concrete is degraded (DC), radionuclides that were present in compartments that represent the inner backfill are suddenly present in compartments that represent in the outer backfill.

It would be interesting to test alternative approaches before developing a full safety assessment. For example, this might involve using chains of ten compartments, with the outer five compartments representing the outer backfill, and the inner five compartments representing the inner backfill. (Additional mechanical dispersion transfers could be added to the model to retain a Peclet number of 10 if required). However, this could also be linked to any improved representation of the evolving properties of the concrete backfill, potentially underpinned by updates to the near-field groundwater flow and concrete

degradation models. For example, potentially chains of five compartments could be retained, but each compartment would have a unique set of continuously evolving transport parameters that reflect the location of the volume of backfill represented by the compartment in the vault.

Diffusion from the outermost backfill compartments into fractures in the rock is affected by the resistance due to the concentration gradient in the fractures, which depends on the flow rate in the fractures (R_{Qeq}) – see Figure 11. However, it is assumed there is not any geometrical resistance of diffusing into the fractures (R_{plug}). Section 2.9.6 of R-19-09 notes that, "*since the concrete has a higher permeability than bentonite, the seeping water can have access to a larger volume within the concrete compared to the limited surface area provided by the fracture aperture. Therefore, the plug resistance* R_{plug} *is neglected in the BHK concrete backfill*".

During the intermediate (DZC) stage, the outermost backfill compartments represent the outer part of the intact backfill. Therefore, diffusion is into the degraded backfill, not into the rock. Diffusion is still considered to be into a fractured medium, with the values for R_{Qeq} being given in Table 2-36 of R-19-09. It is not clear if this fractured medium is the degraded outer backfill or the rock.

Elsewhere in SE-SFL, the degraded outer backfill is conceptualised as a porous medium. Therefore, it is possible that the outer backfill is neglected and R_{Qeq} relates to the rock. Alternatively, R_{Qeq} might relate to highly fractured concrete backfill (the DB model described in R-19-05). The values of R_{Qeq} in Table 2-36 of R-19-09 are the same for the intact and degraded concrete stages, but are different for the degraded outer backfill stage. This change in parameter values could reflect diffusion into degraded backfill rather than rock, or it could reflect a change in the flow rate in the rock in response to the evolving permeability of the outer backfill. These potential confusions and the assumptions that are implemented in the model need to be clarified.

Figure 15: Summary of SKB's conceptual model for the BHK vault with degraded outer backfill and representation in their assessment model

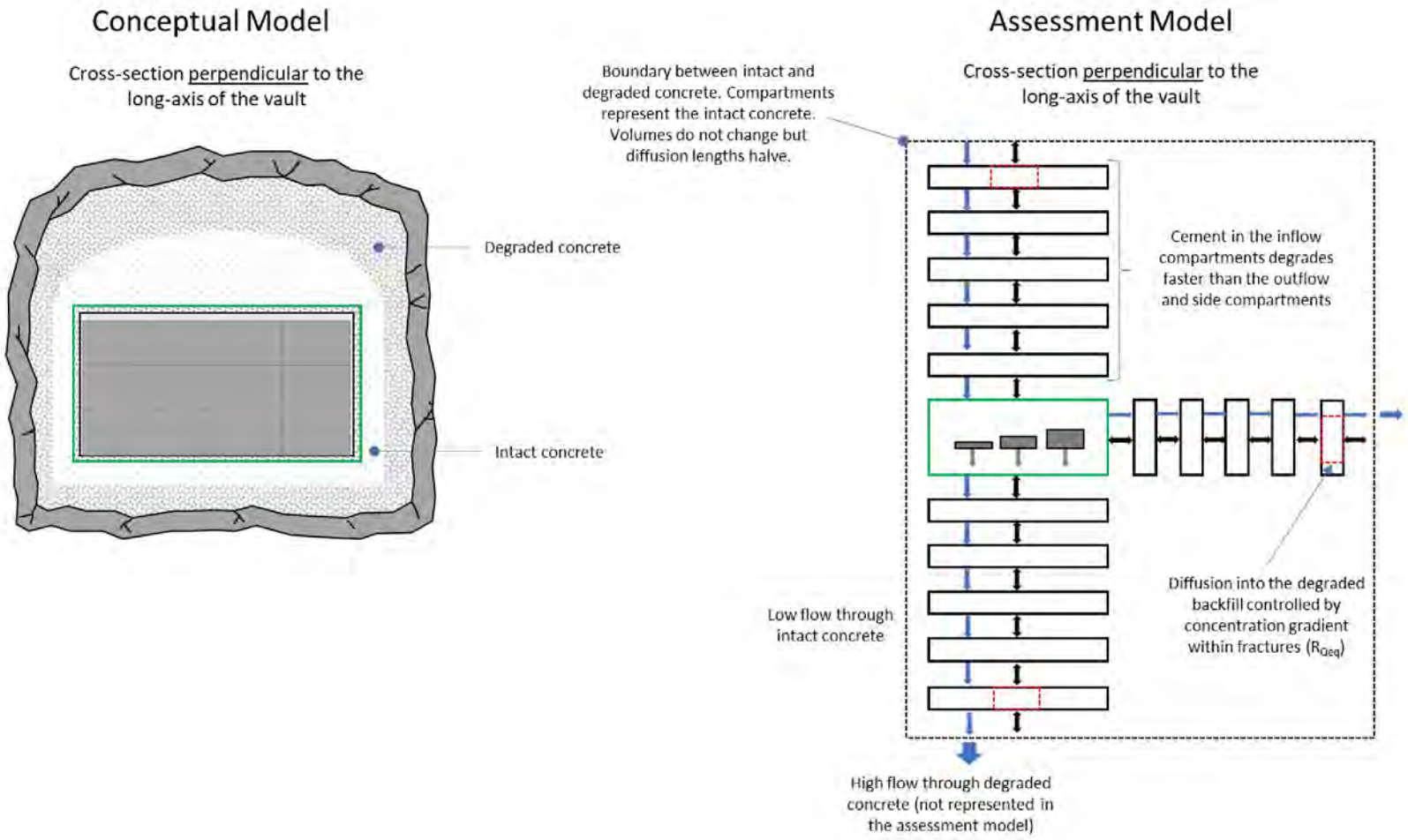

Figure 16: Summary of SKB's conceptual model for the BHK vault with completely degraded backfill and representation in their assessment model

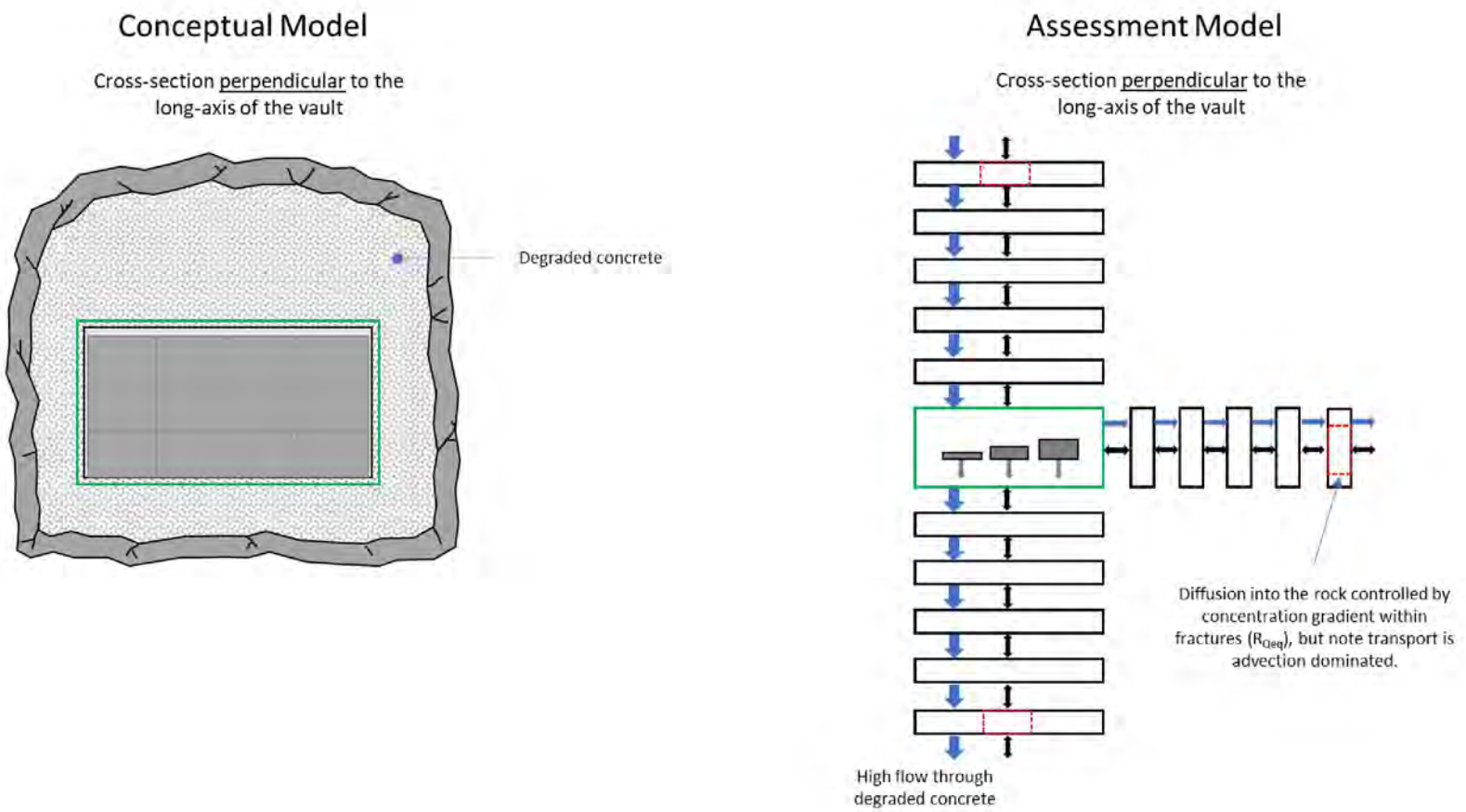

Figure 17: Diffusion transport resistance of the concrete backfill in the BHK vault (Figure 2-14 in R-19-09)

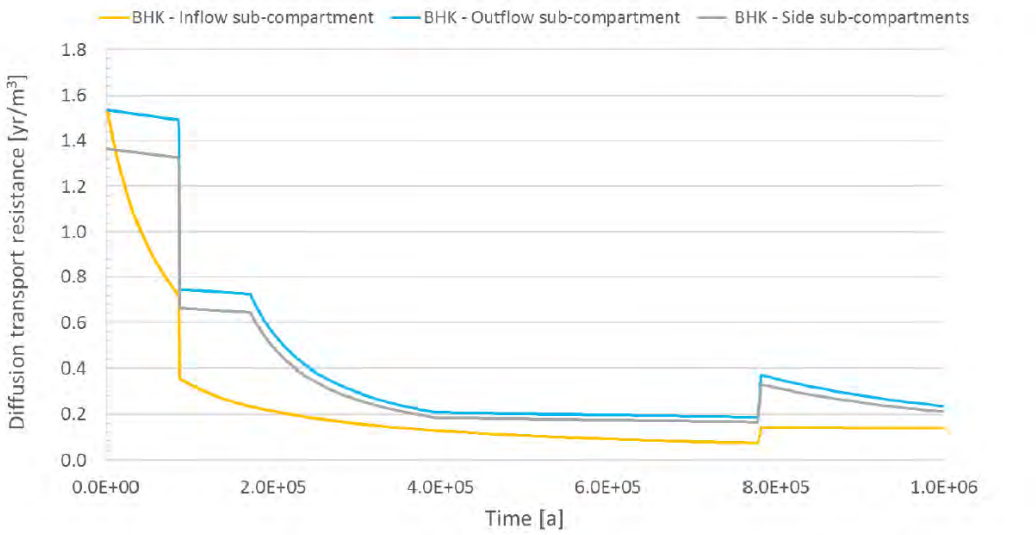

7. SKB's Model Results

This section discusses the near-field radionuclide fluxes calculated by SKB and considers whether they are logical and consistent with SKB's conceptual models. Independent modelling to reproduce the near-field radionuclide fluxes calculated by SKB is discussed in Section 8.

In this section, we also undertake a simple comparison of the radionuclide fluxes from the near field calculated in SE-SFL with the near-field fluxes calculated by SKB in their SR-PSU safety assessment for SFR (SKB, 2015). The objective is to compare the containment performance of the two facilities, to build confidence the near-field fluxes calculated in SE-SFL are consistent with the conceptualised performance of the repository.

7.1. SE-SFL Near-Field Radionuclide Fluxes

Radionuclide fluxes from the near field to the geosphere are presented in Figure 7-11 of TR-19-01 for the present-day evaluation case. They are reproduced here as Figure 18. The results are conceptually reasonable, with the fluxes being dominated by radionuclides do not sorb, or only sorb weakly, and have half-lives longer than a few thousand years.

The fluxes from the BHA vault are the simplest to understand because transport is diffusion dominated, and the properties of the bentonite backfill do not change over time.

Ag-108m, C-14, Cl-36 and Tc-99 diffuse though the bentonite backfill establishing an equilibrium concentration profile in a few thousand years. C-14 diffuses faster than Cl-36 and Tc-99, so it reaches an equilibrium concentration profile more quickly. This behaviour can be explained by a simple 1-D diffusion calculation.

Fetter (1994) gives the analytical solution for 1-D diffusion of a non-sorbing tracer with a constant source concentration (C_o). At time t, the concentration C at a distance L is given by:

$$\frac{C}{C_o} = \frac{1}{2}\left[erfc\left(\frac{L}{2\sqrt{D_e t}}\right)\right] \quad (1)$$

where D_e is the effective diffusivity (m^2/s).

When C/C_o is equal to 1%, $L = \sim 3.29\sqrt{D_e t}$.

The time taken for the concentration at the bentonite-rock interface to reach 1% of the concentration in the waste is calculated for C-14 and Cl-36.

C-14 and Cl-36 do not sorb onto bentonite backfill (Table 2-31 of R-19-09). However, C-14 is a cation/neutral species and Cl-36 is an anion so they have different effective diffusivities.

For C-14, taking L = 2.3 m (the thickness of the bentonite backfill) and D_e = 1.2E-10 m^2/s (Table 2-32 in R-19-09) gives t = 129 y.

For Cl-36, taking L = 2.3 m and D_e = 1.0E-11 m^2/s gives t = 1550 y.

In the absence of radioactive decay, or depletion of the source inventory, once an equilibrium concentration profile has been established the flux would remain constant. This is most clearly illustrated by the results for Cl-36 and Tc-99 which have long half-lives (301,000 y and 211,000 y respectively). However, the fluxes of these radionuclides do slowly decrease over time due to due to decay and source depletion.

C-14 decays more quickly than Cl-36 and Tc-99, so as soon as the concentration profile in the backfill starts to approach equilibrium the peak flux from the near field to the geosphere occurs, and then the flux starts to fall. Ag-108m behaves similarly to C-14, but the peak flux decreases even faster than for C-14 reflecting the shorter half-life of Ag-108m.

Figure 18: Radionuclide fluxes from the near-field to the geosphere in the present day evolution case (Figure 7-11 of TR-19-01)

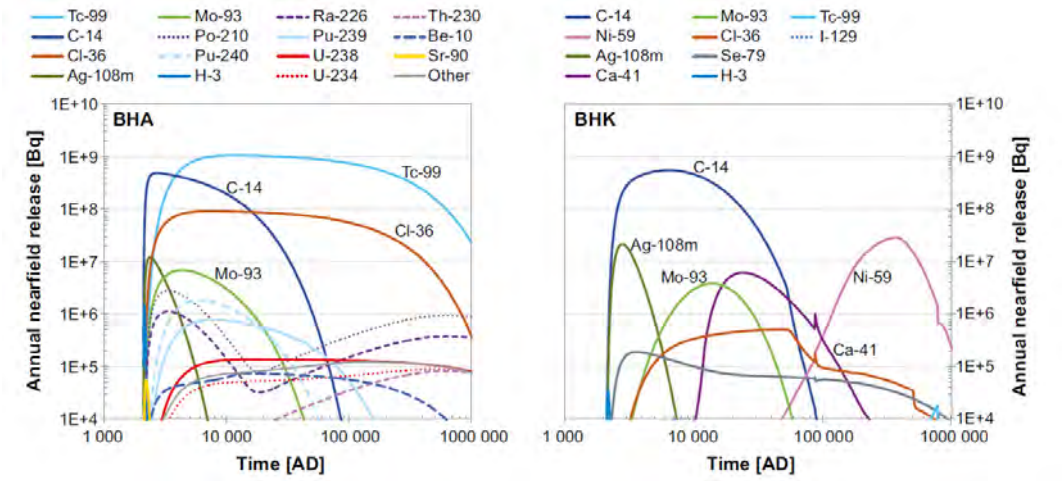

SKB's models discretise the bentonite backfill into a chain of 5 compartments. This discretisation should be sufficient to reduce numerical dispersion to a level where it is not significant, noting that the error in the peak flux compared with the analytical solution is equal to 1/N^2 where N is the number of compartments (Quintessa, 2019). This provides confidence that the apparently rapid transport of C-14, etc through the bentonite and intact concrete backfills is not due to numerical dispersion.

SKB's models have been successfully reimplemented in the AMBER code, producing similar results (Section 8). A sensitivity analysis was undertaken using the AMBER implementation of the BHA model build further confidence that the apparently rapid transport of C-14, etc through the bentonite and intact concrete backfills is not due to numerical dispersion.

In the AMBER model sensitivity analysis:

- the advective flow rate was set to zero m^3/y; and
- upgradient (inflow) and downgradient (outflow) backfill compartments were removed, so only sideways diffusion was included in the model.

The flux of C-14 from the near-field into the geosphere was compared for a model that discretised the bentonite backfill into 5 compartments, and a model that discretised the bentonite backfill into 10 compartments (Figure 19). Consistent with expectations, increasing the discretisation had negligible effect on the diffusive flux.

Figure 19: Sensitivity of diffusive fluxes of C-14 to number of compartments using AMBER

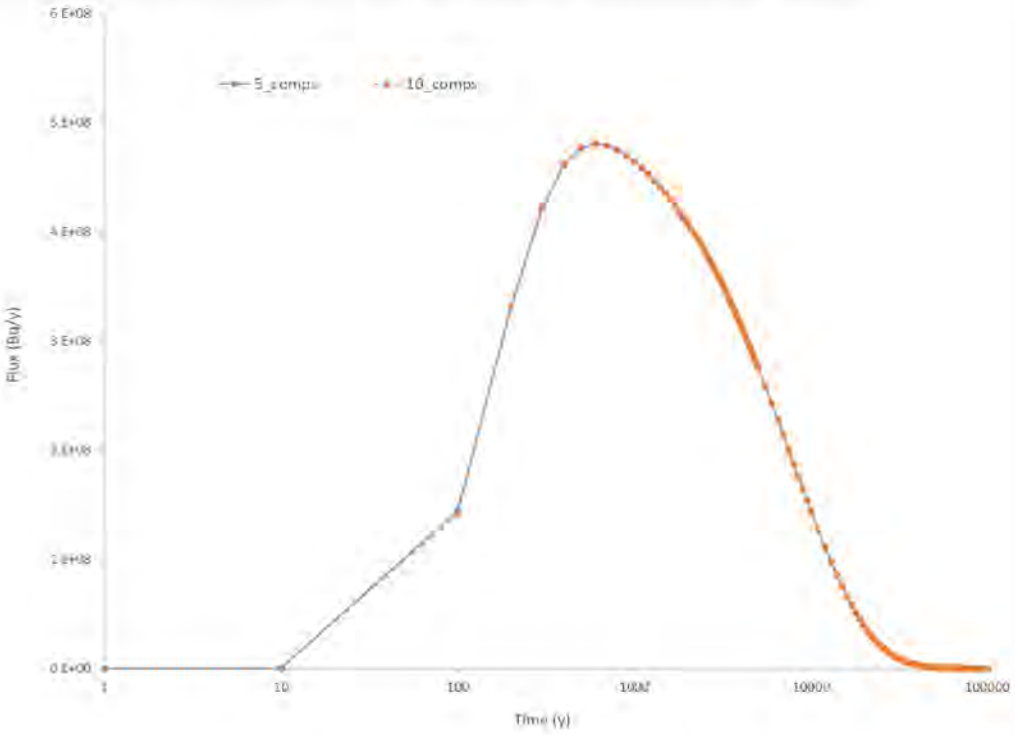

The fluxes from BHK show slightly different behaviour to BHA, reflecting gradual release of radionuclides from irradiated metal wastes congruent with corrosion, and degradation of the cementitious backfill. For example, similar to the BHA vault the flux of C-14 from the near field to the geosphere increases rapidly following closure. However, while the flux from the BHA vault reaches an early peak and then decreases, the flux from the BHK vault continues to increase but at a slow rate, reflecting ongoing gradual release from the corroding metal wastes. Consequently, the peak flux of C-14 from the BHK vault occurs later than the peak flux of C-14 from the BHA vault.

Cl-36 is present as surface contamination and induced activity in the BHK vault. The decreases in the fluxes of Cl-36 at around 50,000 years and 500,000 years correspond to cessation of releases of Cl-36 from 1 mm thick metals wastes and 1 cm thick metal wastes respectively, when the metals become fully corroded.

There are small spikes in the fluxes of Cl-36, Ca-41 and Se-79 around 90,000 y and a small spike in the flux of Tc-99 around 800,000 y. These spikes correlate with the changes in the backfill diffusion lengths and flow rates associated with the transitions from the IC to the DZC, and from the DZC to the DC respectively. Although SKB's approach to representing the DZC is conceptually complex, it only results in small numerical artefacts.

The key radionuclides for doses from the BHA vault are Cl-36, Mo-93, Tc-99 and the U-238 decay chain (Figure 20). (Note U-238+ is used to denote the combined dose from radionuclides in the U-238 decay chain). Cl-36 and Mo-93 do not form complexes with ISA, but sorption of Tc-99 is reduced by a factor of 10,000 in the near field (Table 2-20 of R-19-09). Complexation with ISA also reduces sorption of radionuclides in the U-238 decay chain by factors ranging from 10 to 10,000.

SKB's assessment models assume ISA is not lost from the BHA vault by diffusion, and therefore there is no decrease in complexation over time. If the near-field models were updated to include diffusion of ISA from the BHA vault, and decrease in complexation with time, it is unlikely the early peak fluxes of Tc-99 and U-238 from the vault would change. However, the relationship between the peak fluxes from the vault and the peak doses in the biosphere is complex. Therefore, although a more realistic representation of complexation might not change the peak fluxes of Tc-99 and U-238 from the BHA vault, it might affect the peak doses. This is further explored in the following.

The complex relationship between the peak fluxes from the vault and the peak biosphere doses is shown by Figures 7-13 and 7-14 of TR-19-01, which show: fluxes from the near-field to the geosphere and fluxes from the geosphere to the biosphere; and biosphere doses, respectively. Inspection of these figures reveals that Tc-99 and radionuclides in U-238 decay chain are significantly retarded by matrix diffusion and sorption in the geosphere (Figure 7-13 of TR-19-01). There is significant ingrowth of radionuclides in the U-238 decay chain in the geosphere. Retardation and decay / ingrowth in the geosphere affect the timing of the peak fluxes to the biosphere, and the magnitudes of the fluxes. The doses are also affected by evolution of the biosphere. The dose per unit flux to the biosphere changes as the biosphere evolves. Therefore, assumptions around complexation in the near field and retardation in the geosphere that affect when radionuclides arrive at the biosphere will also change the doses.

SKB have undertaken a sensitivity analysis where they excluded complexation in the BHA vault. This reduced the very long-term doses from Tc-99, the U-238 decay chain and other radionuclides by several orders of magnitude. This confirms the potential for more realistic representation of diffusion of ISA out of the vault to have an impact on the very long-term doses.

Table 3-24 of TR-19-03 gives the dissolved ISA concentration in the BHA vault at different times. These values can be used to scope the potential impact of diffusion of dissolved ISA out of the vault on radionuclide fluxes. After 109,000 y the ISA concentration has decreased by a factor of 2.5, and after 1,080,000 y the ISA concentration has decreased by a factor of 20. Section 2.5.6 of R-19-09 states that, except for Pb and Pd, the sorption reduction factors increase by a factor of ten with each ten-fold increase in the ISA concentration above the no effect level. Therefore, if diffusion of dissolved ISA out of the BHA vaults was included in the models, it might not have a large effect on the very long-term doses, because the sorption reduction factors might remain high for several hundred thousand years.

Overall, the reference case – base variant fluxes from the near field to the geosphere are logical and consistent with the described conceptual and numerical models. There are some small numerical artefacts resulting from simplifications in the assessment model, but these are not important.

Figure 20: Doses from BHK and BHA for the reference evolution – base variant (Figure 7-14 of TR-19-01)

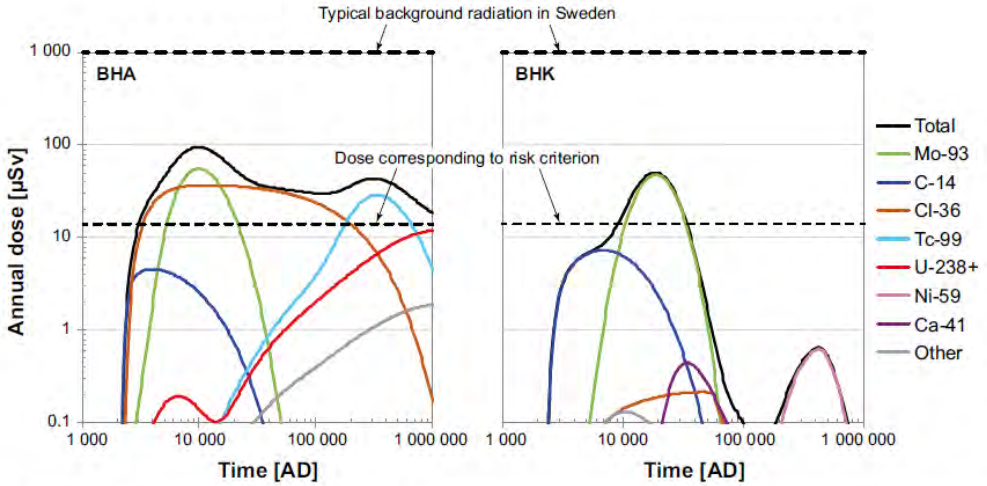

Figure 7-14. *Annual doses from BHA and BHK from draining and cultivating the mire ecosystem in biosphere object 206. The total dose (black line) is shown together with the contributions from individual radionuclides (coloured lines). Dashed black lines show the dose corresponding to the regulatory risk limit (14 μSv). Figure corresponds to Figure 5-18 in the* ***Radionuclide transport report****.*

SKB have explored a wide range of sensitivity cases. Some of these cases affect the radionuclide fluxes from the near field to the geosphere. We have reviewed the results for the sensitivity cases that are relevant to the scope of this review. For each case, the changes in the fluxes are logical and consistent with the changes to the model inputs.

We note the simplifications included in the 'alternative concrete backfill in BHK' sensitivity case will underestimate potential improvements in performance from an alternative backfill. In this case, the backfill is assumed to be less permeable than in the reference evolution. This will decrease flows through the vault and therefore advection of radionuclides. These effects have been included in the assessment models. The reduced flows also mean the backfill should degrade more slowly and will therefore perform well for longer. This effect has not been included in the assessment models.

7.2. Comparison Against SFR

The SFL repository for long-lived L/ILW is intended to provide better containment of radionuclides than the SFR repository for short-lived L/ILW. SKB have not compared the performance of SFL and SFR. A simple comparison was undertaken as part of this review firstly to confirm the SFL repository does provide better containment of radionuclides than SFR, and secondly because it is interesting to compare the overall behaviour of the two repositories.

The radionuclide fluxes from the near field to the geosphere, per unit inventory disposed, reflect the containment performance of the repository. The fluxes per unit inventory disposed, from SFL and SFR are compared for a selection of key radionuclides in Figure 21 to Figure 24. For both repositories the fluxes per unit inventory disposed have been calculated using the disposed inventory at 2075 AD. The radionuclide fluxes from SFR were taken from Towler and Penfold (2017).

Some key differences in the assessments need to be noted when interpreting the figures.

- The assessment timeframe in the SR-PSU safety assessment for SFR is 100,000 years, while the assessment timeframe in the SE-SFL safety evaluation for SFL is 1,000,000 years.
- The results for SFL assume no climate or landscape evolution, while the results for SFR do include climate and landscape evolution.
    - There are no releases from SFR for the first 1000 years as the repository is under the sea.
    - Beyond c.50,000 years the fluxes from SFR are affected by development of periglacial conditions, but the impact on fluxes is not significant.

SFR contains a silo and vaults of different designs. The fluxes per unit inventory disposed have been calculated for the silo and 1BMA vault in SFR. The silo and 1BMA vault contain the most hazardous wastes and therefore have more highly engineered near-field barriers than the other vaults. The silo comprises a concrete cylinder. The gap between the cylinder and the rock is filled with bentonite. Waste packages are grouted into the silo. The 1BMA vault comprises concrete caissons. Wastes packages are grouted into the caissons. The caissons are surrounded by macadam backfill.

In SR-PSU the concrete caissons in the 1BMA vault are an important barrier to radionuclide release. In the assessment models the caisson walls are each represented using 5 compartments, to ensure numerical dispersion does not result in unrealistically high calculated fluxes of radionuclides through the walls. The different waste types, containers and grout fill inside the caissons are also represented using separate compartments. In contrast, in SE-SFL, the wastes, containers, grout fill and concrete structures / caissons are represented using a single compartment, in which radionuclides are assumed to be well mixed. Therefore, the barriers provided by the containers, grout fill and caissons / concrete structures are largely neglected in the SE-SFL assessment calculations.

C-14 is present in the SFR silo and 1BMA vault, and the SFL BHA vault, in organic forms (C-14org, Figure 21). This form of C-14 does not sorb onto bentonite or cement / concrete (Table 2-18 and Table 2-31 in R-19-09). Therefore, the differences in the fluxes per unit inventory largely reflect differences in advective and diffusive transport.

In SE-SFL the vaults are assumed to resaturate instantaneously, so C-14org starts to be released earlier from the BHA vault than from SFR. For both SFR and the BHA vault, the peak flux occurs shortly after releases start. The peak flux per unit inventory disposed is around an order of magnitude lower for the BHA vault than the SFR silo and 1BMA vault. This illustrates the better containment provided by the BHA vault compared with the SFR, even though the barriers provided by the concrete structures, containers and grout fill have mostly been neglected.

C-14 is present in the SFL BHK vault as induced activity (C-14ind) in metals. C-14ind present as surface contamination is immediately available for transport, but C-14ind present in the matrix of metals wastes is only becomes available as the metal corrodes. Once released from the metal wastes, it is assumed C-14ind does not sorb onto cement / concrete (Table 2-18 in R-19-09), consistent with C-14org.

C-14ind present as surface contamination, and thin pieces of metal that fully corrode relatively quickly starts to be released from the vault at early times. However, the peak flux

per unit inventory disposed is around an order of magnitude lower than the BHA vault, because the majority of the C-14ind inventory is present in thicker pieces of metal that take many thousands of years to fully corrode.

There is potentially a small inconsistency in parameterisation of the behaviour of C-14ind in the assessment calculations. The assumed form of C-14ind is not specified, but it is treated as C-14inorg for diffusion, and as C-14org for sorption (Table 2).

Figure 21: Comparison of the near-field C-14 fluxes, per unit inventory disposed, for SFL and SFR

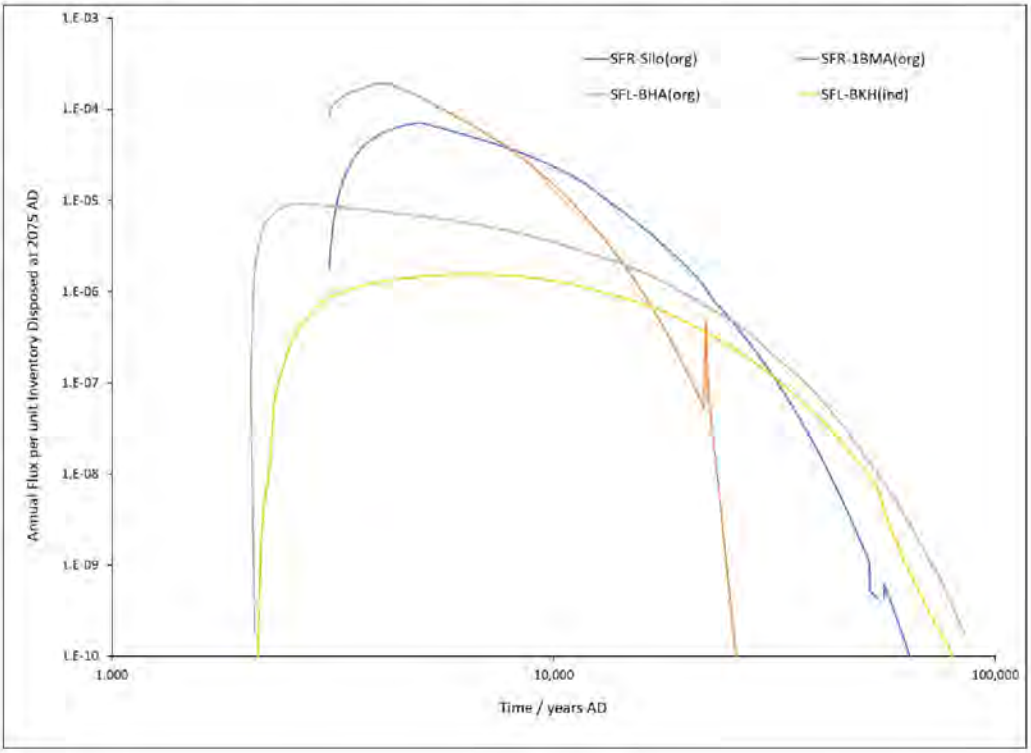

Table 2: Comparison of the transport properties of different forms of C-14

C-14 Form	R-19-09				
	Table 3-3		Table 2-32	Table 2-31	Table 2-18
	Assumed charge	Dominant or important species	Effective diffusivity (m^2 s^{-1})	Kd bentonite (m^3 kg^{-1})	Kd cement State I (m^3 kg^{-1})
C-14inorg	Anion	HCO_3^-	1.0E-11	Not specified	2
C-14ind	Anion	Not specified	1.0E-11	Not specified	0
C-14org	Neutral	CH_4, CO_2H	1.2E-10	0	0

Cl-36 does not sorb onto the bentonite backfill and only sorbs weakly onto cement and concrete (Table 2-18 and Table 2-31 in R-19-09). Therefore, like C-14org and C-14ind, differences in the fluxes per unit inventory largely reflect differences in advective and diffusive transport. The peak fluxes per unit inventory disposed are around one to two orders of magnitude lower from SFL than SFR, which is broadly consistent with the differences seen for C-14 (Figure 22).

Cl-36 has a long half-life, so greater retention in the vault results in releases of Cl-36 from SFL being spread over a much longer time period than releases from SFR. This effect is not seen for C-14 due to its shorter half-life, so more of the C-14 decays in the vault rather than being released at later times.

Cl-36 is present as surface contamination and induced activity in the BHK vault. As noted previously, the decreases in the fluxes of Cl-36 at around 50,000 years and 500,000 years correspond to cessation of releases of Cl-36 from 1 mm thick metals wastes and 1 cm thick metal wastes respectively, when the metals become fully corroded.

Figure 22: Comparison of the near-field Cl-36 fluxes, per unit inventory disposed, for SFL and SFR

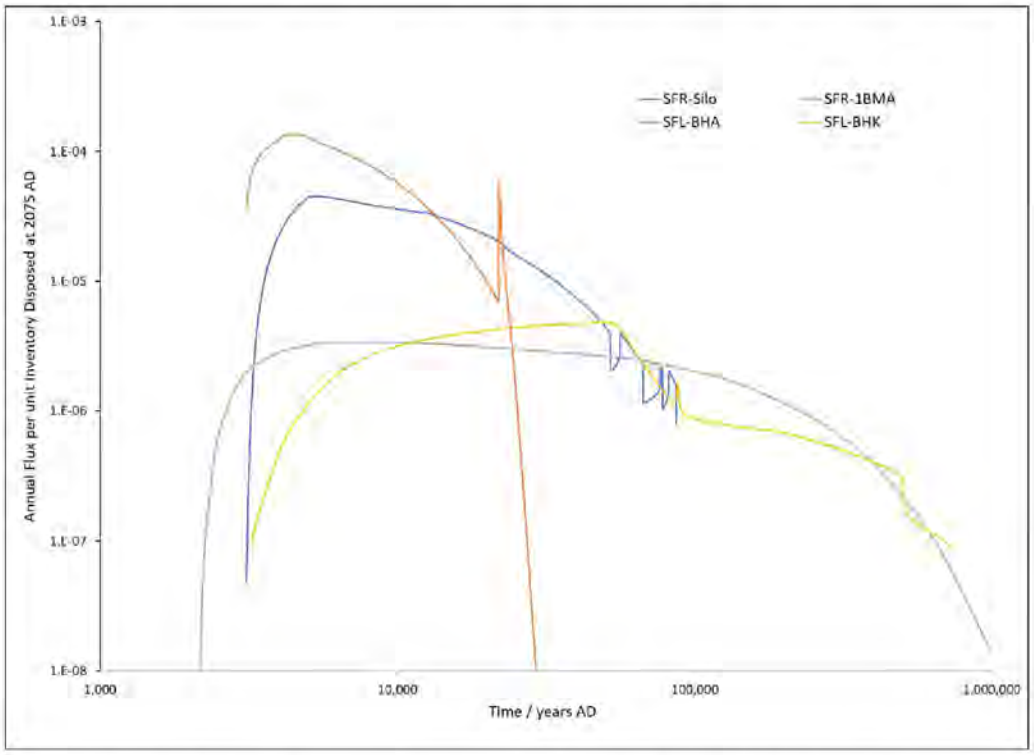

Mo-93 also does not sorb onto the bentonite backfill and only sorbs weakly onto cement and concrete, albeit more strongly than Cl-36 (Table 2-18 and Table 2-31 in R-19-09). Relatively less Mo-93 is present as surface contamination and in very thin metal wastes compared with Cl-36. The lower availability of Mo-93 at early times and slightly higher sorption onto cement / concrete, compared with Cl-36, result in the peak flux per unit disposed inventory being lower for Mo-93 than Cl-36, and the peak occurs later (Figure 23).

The flux of Ni-59 from the BHA vault is too small to appear in SKB's results figures (see Figure 7-11 in TR-19-01), so the flux per unit inventory disposed does not appear in Figure 24. In the BHK vault, Ni-59 is present as surface contamination and induced activity. Ni-59 sorbs moderately onto cement / concrete, so the peak flux per unit disposed inventory is lower for Ni-59 than Mo-93, and the peak occurs later.

Overall, SFL provides better containment of radionuclides than SFR, consistent with expectations. This is due to slower transport of dissolved radionuclides by diffusion and advection, and because a significant proportion of the inventory in the BHK vault is present

as induced activity in metals. These radionuclides only become available for transport as the metal corrodes. Corrosion is slow in the high pH conditions in the BHK vault.

Figure 23: Comparison of the near-field Mo-93 fluxes, per unit inventory disposed, for SFL and SFR

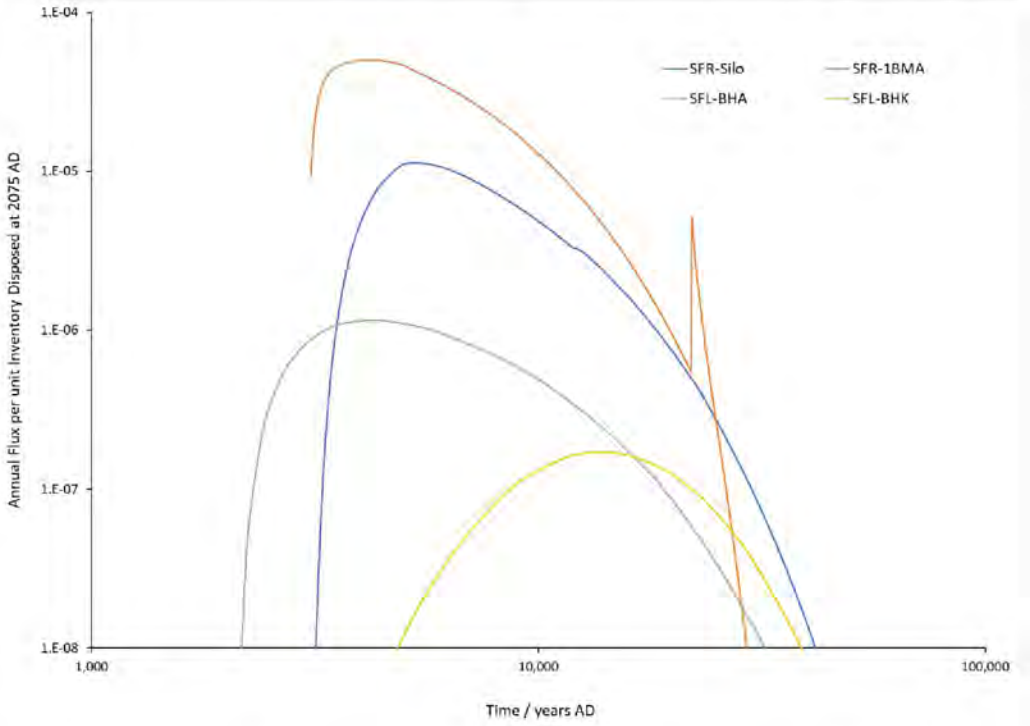

Figure 24: Comparison of the near-field Ni-59 fluxes, per unit inventory disposed, for SFL and SFR (N.B. the flux per unit inventory disposed in BHA is low so it does not appear in the figure)

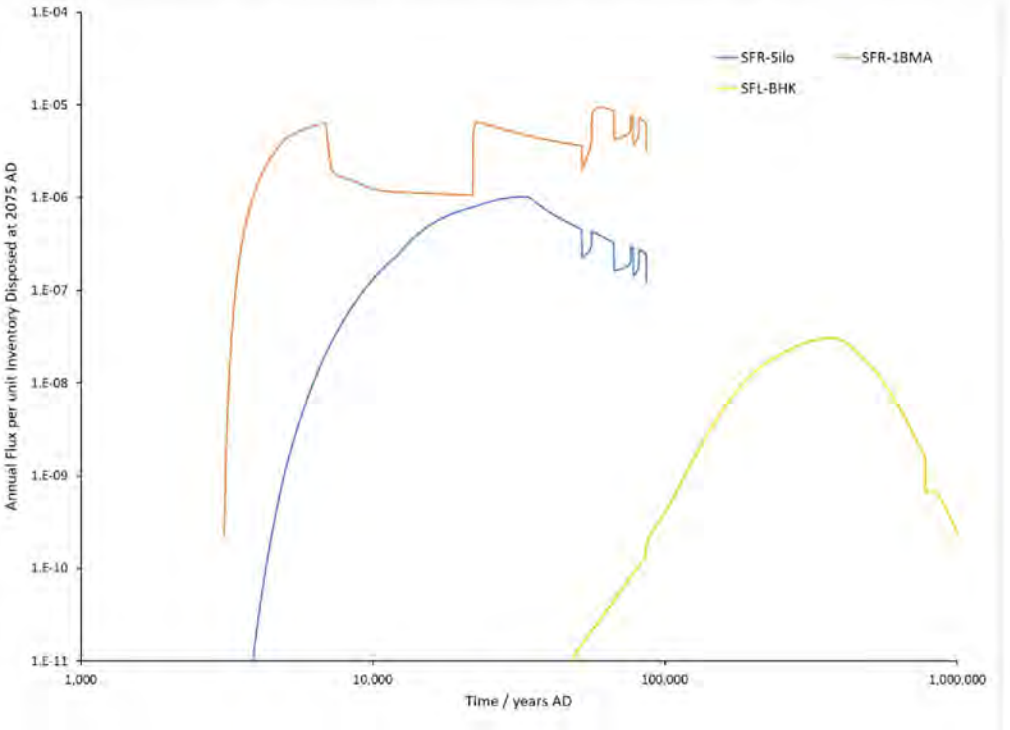

8. Independent Modelling

To further understand and build confidence in the near-field radionuclide transport calculations undertaken by SKB, the Ecolego models have been independently re-implemented in Version 6.4 of the AMBER code (Quintessa, 2019).

The re-implemented models are based on the reference 'present-day evaluation case' for each of the BHA and BHK vaults. The configuration and parameterisation of the AMBER models is described in Section 8.1, with reference to the SKB reports that describe the Ecolego implementation.

Section 8.2 compares the calculated radionuclide fluxes from the near field from the AMBER models with SKB's results. The re-implemented models are then used to further explore sensitivities and uncertainties in the calculations.

8.1. Implementation

8.1.1. Model Configuration

The compartment structure for the BHA and BHK vaults is described in Section 2.1.2 of R-19-05. The same structure has been used in the AMBER re-implementation.

BHA

For the BHA vault, all of the wastes, waste packages, grout and concrete structures are represented by a single homogenous compartment. This is a highly simplified representation and ignores known heterogeneity within the vault.

In the radionuclide transport review for SR-PSU (Towler and Penfold, 2017), it was determined that modelling all caissons with a single compartment is a reasonable approximation but will underestimate the retardation for radionuclides transported between compartments along the length of the vault. For the SFL BHA vault, flow is predominantly along the length of the vault, but the groundwater flow rate is small and transport is expected to be dominated by diffusion. The main transport path for radionuclides out of the vault is therefore expected to be diffusion out of the larger 'side' area.

The bentonite backfill surrounding the waste compartment is represented by 15 compartments; 5 in the 'inflow' or upstream direction, 5 in the 'outflow' or downstream direction, and 5 'side' compartments representing the top, bottom and long sides of the vault. The discretisation of 5 compartments in each direction is used to provide an amount of numerical dispersion equivalent to the analytic dispersion for advective transfers with a Peclet number of 10 (e.g. Appendix B of Quintessa, 2019). The geometry of the backfill is simplified and treated as a cuboid; the additional bentonite pellets used to backfill the vault roof are neglected. This is a cautious assumption.

The compartment structure for the BHA model as re-implemented in AMBER is shown in Figure 25.

Figure 25: Configuration of compartments in the BHA vault. Transfers are coloured by type: diffusion only (red), or advection and diffusion (blue). Backfill compartments are coloured in green. The geosphere fracture compartment (sink) is not shown.

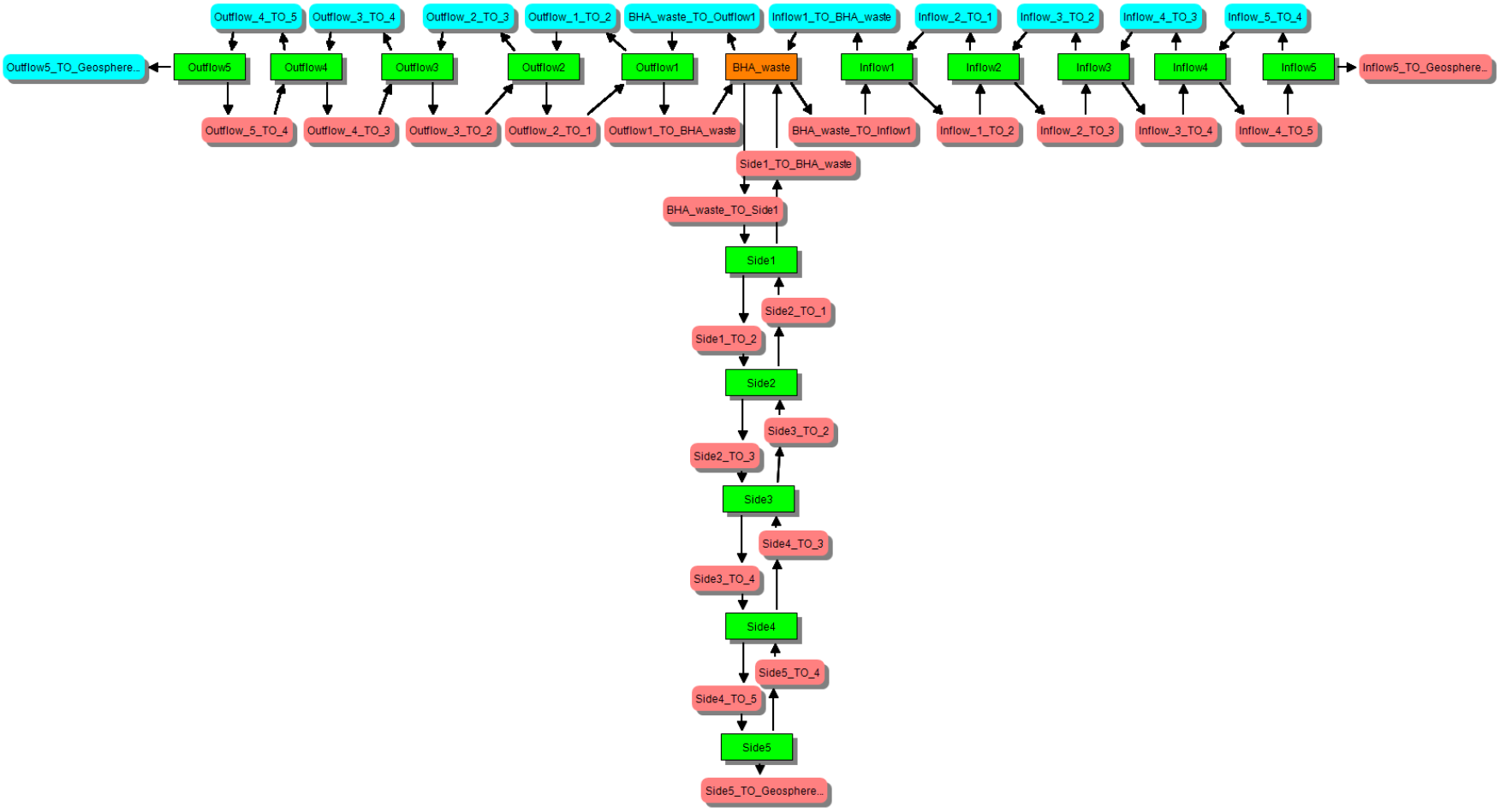

BHK

In the BHK vault, the packaged wastes are assumed to be disposed of in six concrete caissons. By assuming that the distances between the caissons are negligible, in the BHK vault it is assumed that all of the wastes, waste packages, grout and concrete structures are represented by a single homogenous compartment. As noted above, such an assumption will underestimate the retardation for radionuclides transported between compartments along the length of the vault.

The waste that is planned to be disposed of in the BHK vault contains metallic components with neutron induced activity. In the near-field model, the metallic waste components are categorized into four different groups with increasing thickness (R-19-09, Section 2.5.3). There is also assumed to be some surface contamination, giving five categories of waste in total. Both the inventory associated with the surface contamination and the metals of 0-1 mm thickness are assumed to be instantly released, whereas the inventory associated with the other metals is assumed to be released congruent to the corrosion of those metals. The model configuration for the BHK waste compartment is shown in Figure 26; the process by which the release from those metals is modelled is described in the next section.

Figure 26: Configuration of contaminant release in the BHK vault. Transfers are coloured by type: congruent release with corrosion (yellow), diffusion only (red), or advection and diffusion (blue).

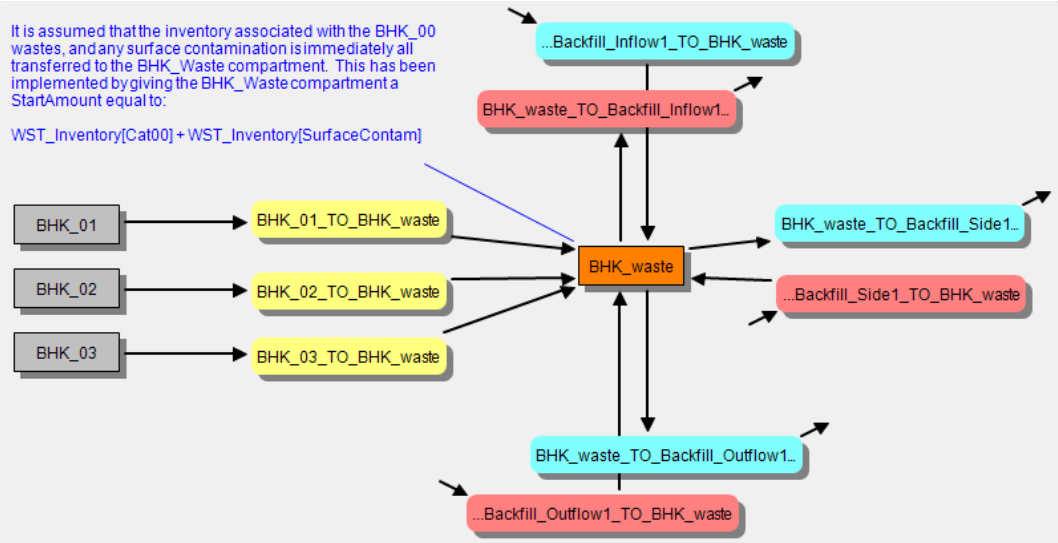

For the SFL BHK vault, flow is predominantly vertically downwards through the vault, with limited flow through the sides of the vault. As the concrete in the waste and backfill in the vault degrades, both the flow and the diffusive resistances are assumed to change. In particular, there are three states of concrete degradation taken into account for the repository and near-field modelling:

- Intact Case (IC): The concrete backfill is intact and has initial state properties, 2075–87 083 [y].
- Degraded Zone Case (DZC): The outer half of the concrete backfill is degraded, 87 083–782 168 [y].
- Degraded Case (DC): The entire concrete backfill is degraded, 782 168–1 002 075 [y].

Similar to the BHA vault, the concrete backfill surrounding the waste compartment in the BHK vault is represented by 15 compartments; 5 in the 'inflow' or upstream direction, 5 in the 'outflow' or downstream direction, and 5 'side' compartments representing the short and long sides of the vault. These 'side' compartments are taken to have dimensions such that they represent all four sides of the vault in a single set of compartments. These compartments are taken to have the same dimensions as each other, with their height equal to that of the waste itself, H_{Waste} (m), and the area normal to the side direction, $Area_{SideBackill}$ (m^2), calculated as the sum of the four side backfill faces shown in blue in Figure 27:

$$Area_{SideBackill} = H_{Waste}\left(2L_{Waste} + 2W_{Waste} + 4\left(\frac{W_{Vault} - W_{Waste}}{2}\right)\right) \qquad (2)$$

where and L_{Waste} is the length of the long sides of the waste (m), and W_{Vault} and W_{Waste} are the lengths of the short sides of the vault and waste respectively (m). The last term is referred to as D by SKB (see Equation 2-16 of R-19-09).

Figure 27: Schematic to show area of side backfill assumed for the assessment

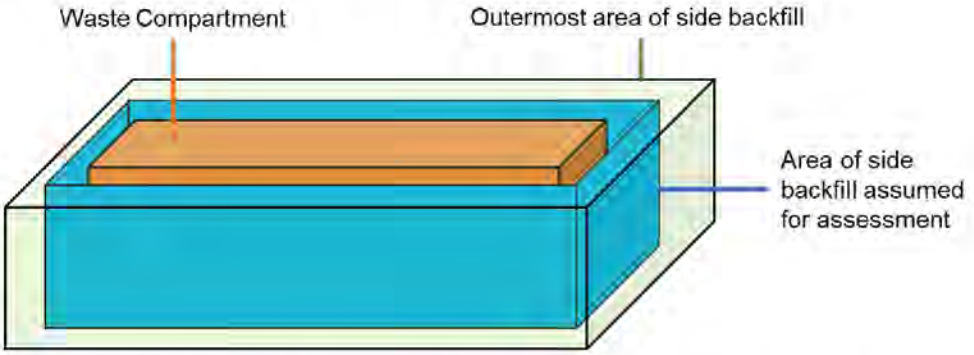

The geometry of the backfill is simplified and treated as a cuboid; the additional concrete backfill used to backfill the vault roof is neglected, with the assumption that the waste compartment is surrounded with a backfill of uniform thickness, equal to half that of the difference of the width of the tunnel and the width of the waste compartment. This is a cautious assumption.

The compartment structure for the backfill in the BHK vault as implemented in AMBER is shown in Figure 28.

Figure 28: Configuration of backfill for the BHK vault. Transfers are coloured by type: diffusion only (red), or advection and diffusion (blue). Backfill compartments are coloured in green. The geosphere fracture compartment (sink) is not shown.

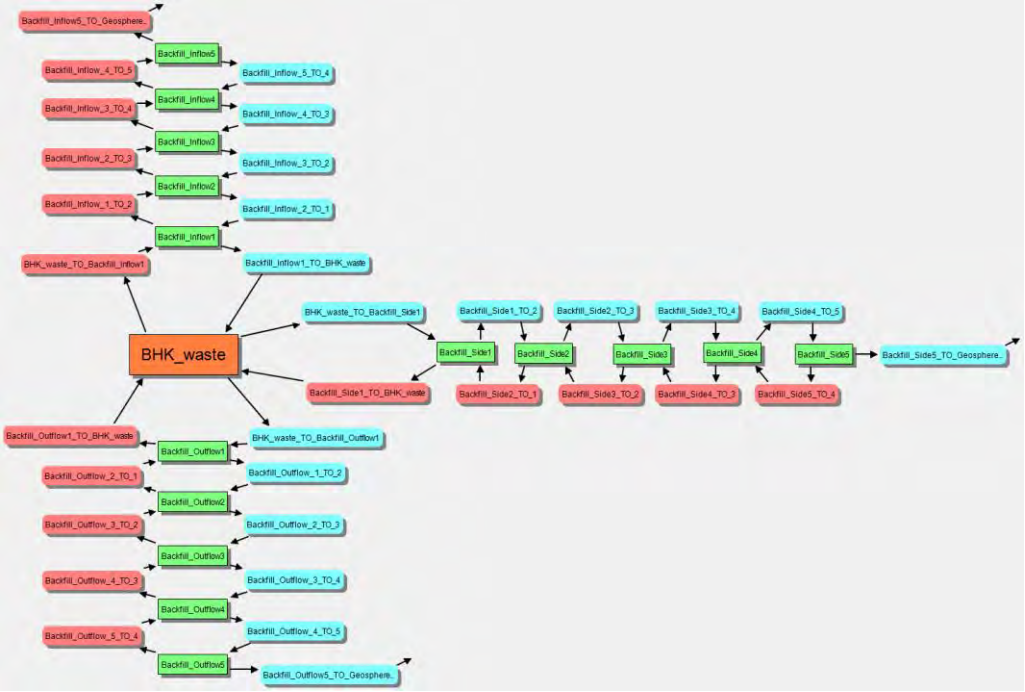

8.1.2. Processes

The key processes represented in the near-field models are release of radionuclides from the BHK wasteforms, advection of radionuclides with groundwater, diffusion of radionuclides in groundwater, sorption and complexation of radionuclides, and degradation of concrete. Solubility limitation is not considered in either BHA or BHK.

Radionuclide Release from BHK Metallic Waste

As noted above, the BHK metallic waste components are categorised into four different groups with increasing thickness (Section 2.5.3 of R-19-09). Each category of metallic waste is assumed to corrode at the same rate (Table 3), with radionuclides released from the wastes congruent to the corrosion of the metals. Although not stated explicitly by SKB, the corrosion must be assumed to occur on both sides of the lengths of metallic wastes to achieve the assumed release times.

Table 3: Thickness of metallic waste components, corrosion rate and assumed release time (R-19-09 Sections 2.5.3 and 2.5.4)

Metal category	Metal thickness	Underlying thickness range	Corrosion rate, Corr	Release time [y]
00	0 mm	0-1 mm	10 nm/y	Instant release
01	1 mm	1-5, 5-10 mm	10 nm/y	5E+4
02	10 mm	10-11, 11-20 mm	10 nm/y	5E+5
03	20 mm	20-60 mm, 109 mm, 216 mm, 300 mm	10 nm/y	1E+6

Thus, at any given time, the fraction of metallic waste category MCi, available for radionuclide release, $F_A^{MCi}(t)$ [-], is given by:

$$F_A^{MCi}(t) = \frac{2Corr}{Thickness_{t0}^{MCi}}\,t \tag{3}$$

where $Corr$ [nm/y] is the corrosion rate, and $Thickness_{t0}^{MCi}$ [mm] is the initial thickness of metallic waste category MCi. The change in the available fraction of metallic waste available over time, $\frac{d}{dt}F_A^{MCi}$ [-], is given by:

$$\frac{d}{dt}F_A^{MCi} = \frac{2Corr}{Thickness_{t0}^{MCi}} \tag{4}$$

The radionuclide release rate from the BHK metallic wastes ($\lambda_{MCi,Release}$ [/y]) is then modelled as:

$$\lambda_{MCi,Release} = \frac{d}{dt}F_A^{MCi}/\left(1 - F_A^{MCi}\right) \tag{5}$$

For a stable isotope, Equation (4) gives a constant flux from the metallic wastes during the period over which the metal is corroding.

Advection and Diffusion

The equations for radionuclide transport by advection and diffusion are provided in the SE-SFL documentation. Equation (2-2) in R-19-09 gives the total transfer rate from compartment k to a neighbouring compartment j, N_{kj}^i [Bq/s]:

$$N_{kj}^i = \frac{c_k^i - c_j^i}{R_{kj}^i + R_{jk}^i} + Q_{kj}c_k^i \tag{6}$$

where c_i [Bq/m^3] is the pore water activity concentration of radionuclide i in compartment k, Q_{kj} [m^3/s] is the water flow rate from compartment k to compartment j, and R_{kj}^i [s/m^3] is the diffusion resistance against the transport of radionuclide i from compartment k toward compartment j.

This transport equation is not in the form required for use in the AMBER model. Transfer rates in AMBER are specified as the fraction of the inventory in a particular compartment

that are transferred to another compartment per unit of time, λ_{ij} [/s]. The transport equation above therefore needs to be expressed in terms of the activity in each compartment. It is assumed that the porewater activity concentration c_{k^i} can be expressed as:

$$c_k^i = \frac{a_k^i}{V_k(\epsilon_k^i + K_{d,k}^i \rho_{b,k})} \tag{7}$$

where a_k^i is the activity of radionuclide i in compartment k [Bq], V_k is the volume of compartment k [m^3], ϵ_k^i is the available porosity for radionuclide i in compartment k [-], $K_{d,k}^i$ is the sorption coefficient for radionuclide i [m^3/kg] and $\rho_{b,k}$ is the bulk density of the sorbing material [kg/m^3]. The term $(1 + K_{d,k}^i \rho_{b,k}/\epsilon_k^i)$ is the retardation factor and the term $V_k(\epsilon_k^i + K_{d,k}^i \rho_{b,k})$ is the capacity of compartment k for radionuclide i, M_k^i [m^3].

The transport equation can therefore be expressed as three separate terms: a forward diffusive transfer from compartment k to compartment j ($\lambda_{kj_{diff}}$ [/y]), a backward diffusive transfer from compartment j to compartment k ($\lambda_{jk_{diff}}$ [/y]), and an advective transfer ($\lambda_{kj_{adv}}$ [/y]):

$$\lambda_{kj_{diff}} = \frac{1}{R_{kj}^i + R_{jk}^i} \cdot \frac{1}{M_k^i} \tag{8}$$

$$\lambda_{jk_{diff}} = \frac{1}{R_{kj}^i + R_{jk}^i} \cdot \frac{1}{M_j^i} \tag{9}$$

$$\lambda_{kj_{adv}} = \frac{Q_{kj}}{M_k^i} \tag{10}$$

Equation (9) is the standard equation for transport by advection, consistent with that used in SR-PSU. For diffusion, the general expression for the 'diffusion resistance' R_{kj}^i is given by Equation (2-3) of R-19-09 as:

$$R_{kj}^i = \frac{l_{kj}/2}{A_{kj} \cdot D_{e,k}^i} \tag{11}$$

where A_{kj} [m^2] is the contact area between the compartments k and j, l_{kj} [m] is the diffusion length of compartment k in the direction of compartment j, and $D_{e,k}^i$ [m^2/s]is the effective diffusivity of radionuclide i in the compartment j. Substituting this into the expression for the diffusive transfer rate gives:

$$\lambda_{kj_{diff}} = \frac{2A_{kj}}{\frac{l_{kj}}{D_{e,k}^i} + \frac{l_{jk}}{D_{e,j}^i}} \cdot \frac{1}{M_k^i} = \frac{2A_{kj} \cdot D_{e,avg}^i}{(l_{kj} + l_{jk}) \cdot M_k^i} \tag{12}$$

where $D_{e,avg}^i$ is the harmonic mean of the effective diffusivity for the transfer between compartments k and j. This is the standard equation for transport by diffusion, consistent with that used in SR-PSU. If the distances l_{kj} and l_{jk} are instead defined as the distances from the mid-point of each compartment to the interface between the compartments, the factor of 2 can be removed from the numerator (e.g. Equation 2-26 of R-19-09).

These equations for advection and diffusion in porous media are used to define radionuclide transport through the waste and backfill compartments of both BHA and BHK. Although the BHK degraded concrete is conceptually assumed to be fractured in R-19-05, it is modelled as a homogeneous porous medium where the full cement pore volume is accessible for transport and retardation (as discussed in Section 6.2.2).

At the interface between the backfill and the host rock, a different form of the diffusion resistance is used. This incorporates two elements; a 'plug resistance' describing the resistance due to diffusion from a large volume of bentonite into thin fractures, and an 'equivalent flow rate' resistance which describes the rate at which radionuclides can diffuse from the backfill to water seeping in the fracture; this approach has been used previously to model solute transport between seeping water in fractured rock and a copper canister embedded in a clay buffer (Neretnieks et al, 2010). For BHK, R-19-05 argues that the plug resistance can be assumed to be negligible since the concrete backfill has a higher permeability than bentonite so the seeping water can have access to a larger volume within the concrete than the limited fracture area. The model for the plug resistance for BHA is given in Equation 2-35 of R-19-09, taken from a 1986 report. The derivation of this mathematical model relies on approximations of the fracture geometry and flow regime, so there are some uncertainties in the constants used.

To calculate the backfill-rock diffusion resistances for each vault, data are required on the apertures and lengths of each fracture intersecting the vaults. The individual fracture data are not reported directly by SKB, so the calculations have not been verified, but the resulting diffusion resistances are provided in Table 2-35 of R-19-09 for BHA and Table 2-36 for BHK. The values will depend on the assumed fracture network intersecting the vaults.

It is assumed that the fractures are a zero-concentration boundary, so there is no reverse diffusion back into the vault.

Backfill Degradation

In BHA, the backfill is composed of bentonite which is assumed not to degrade. Degradation of the cement in the waste compartment (concrete structure and grout) is considered. The porosity of the concrete structure increases with time as the cement degrades; however, the porosity of the grouted wastes appears to be treated as constant. The sorption coefficients of cement in both the concrete and grout evolve with time according to the degradation stage of the concrete. Table 2-19 in R-19-09 provides the times for each degradation state; in BHA, only state II is reached within the assessment timeframe due to the low flows and protective bentonite buffer. However, since the K_d values are linearly interpolated between each degradation state, it is not clear whether the K_d remains constant from the time at which state II is reached (10,000y) until the end of the assessment timeframe (1,000,000y) or whether the K_d is linearly interpolated from state II to state IIIa over some unspecified timeframe. This makes limited difference to the results since there is not much change in the K_d of most elements between state II and state IIIa and the change is assumed to occur over a very long timeframe.

In BHK, the backfill is composed of concrete which is assumed to degrade over time, with the inflow backfill concrete (i.e. the backfill above the waste compartment) assumed to degrade more rapidly than the concrete to the sides or in the outflow direction (i.e. underneath the waste compartment). As in BHA, degradation of the cement in the waste

compartment (concrete caissons and grout) is considered. The porosity of the concrete caissons in the waste compartment and the backfill increase with time as the cement degrades; as with BHA, the porosity of the grouted waste appears to be treated as constant. The sorption coefficients of cement in both the concrete and grout in the waste compartment, and of the cement in the concrete backfill, evolve with time according to the degradation stage of the concrete. Table 2-19 in R-19-09 provides the times for each degradation state; in BHK, all states of concrete degradation are attained, with more rapid degradation of the concrete in the inflow backfill compartments as compared to the concrete in the waste, outflow or side backfill compartments. The effective diffusivities in the BHK backfill are assumed to evolve during the repository evolution, with a timeframe in line with the times associated with changes in the groundwater flow.

In both BHA and BHK, as the porosity of the cement containing structures increases, so the fraction of cement in those structures is assumed to decrease. It is assumed that the sorption of radionuclides in the concrete containing structures is scaled by the fraction of cement in those structures. This means that the effective sorption coefficients assumed in the modelling are dependent both upon the assumed degradation state of the cement (Table 2-19 in R-19-09) and evolution of the fraction of cement in the concrete, which evolve over different timescales.

Further, in the BHK vault, the degradation of the cement is assumed to affect the groundwater flow rates, but the times assumed for the transition between these flow regimes are different again to the times assumed for the cement degradation states as affecting the K_d values, and the times associated with the evolution of the concrete porosity. Figure 29 summarises these timescales and illustrates an apparent inconsistency between the evolution of the concrete properties and the evolution of the groundwater flow field that is determined by the hydraulic properties of the concrete. We anticipate the apparent inconsistency does not affect the conclusions drawn from the modelling. However, it would be beneficial for SKB to include a similar figure in any future safety assessment and explain the relationships between the timings. This would build confidence that different areas of modelling are consistent.

Figure 29: Summary of the different timescales on which changes in parameters occur. Changes in the groundwater flow regime are step changes smoothed over 100 y. Other parameters are determined by linear interpolation so the times indicated are points at which the slope in the linear interpolation changes.

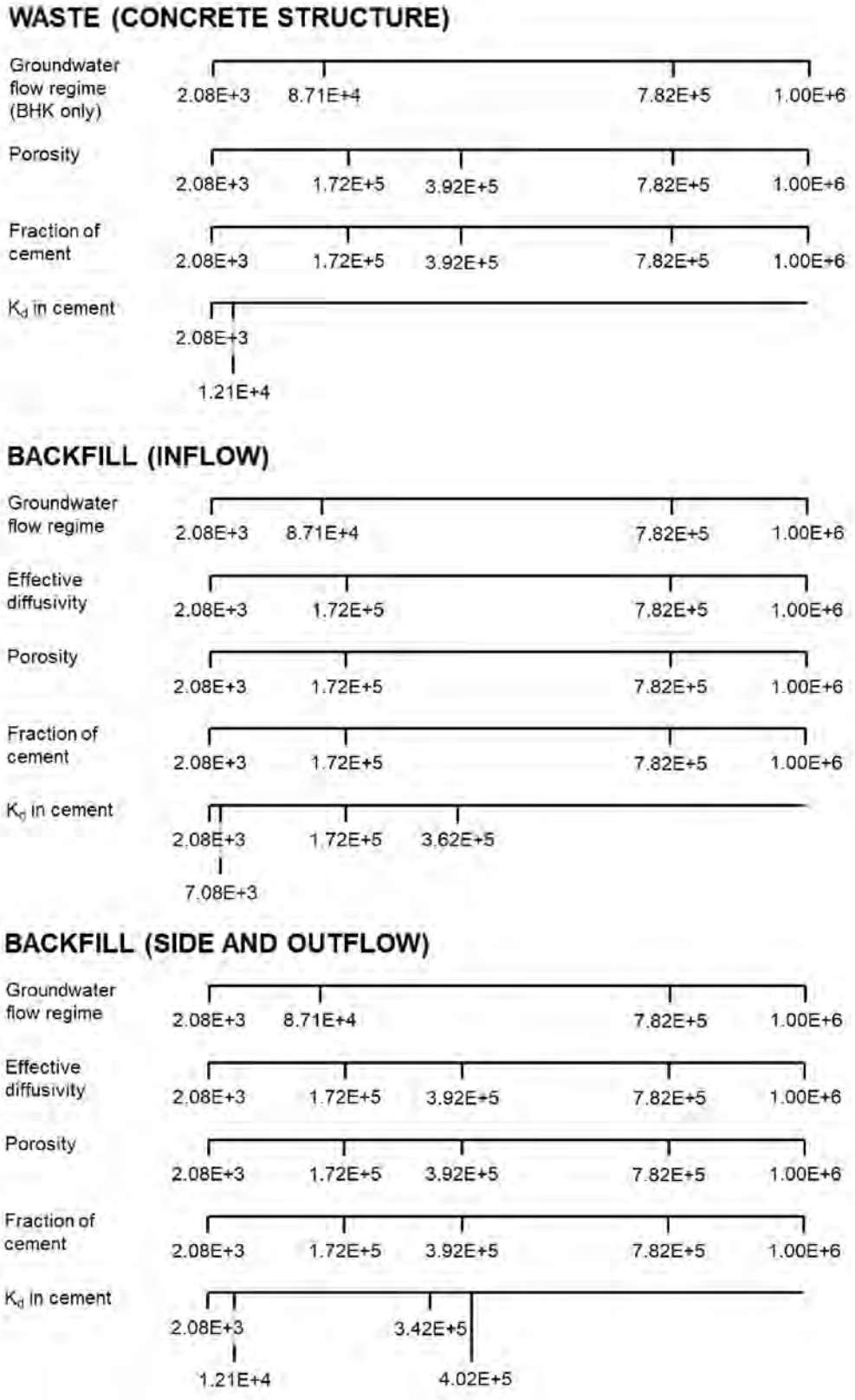

8.1.3. Data

The data are taken from the values provided in R-19-09.

Radionuclide Decay

The radionuclide decays and half-lives are provided in Section 2.4 of R-19-09. There are small changes to the half-lives used in SR-PSU for some radionuclides (e.g. Mo-93, Se-79). There are three different forms of Carbon-14 considered in the assessment: C-14org (organic), C-14inorg (inorganic) and C-14ind (induced). All the C-14 in the BHA vault is assumed to be in organic form and all the C-14 in the BHK vault is assumed to be in induced form; the inorganic form of C-14 is not used in either model. Little is known of the speciation of the induced C-14 in BHK, so it is generally assumed to behave similarly to the organic C-14.

Only the radionuclides with the largest fluxes from the near field are included in the AMBER model. From Figures 5-7 (BHA) and 5-10 (BHK) in TR-19-06, these are:

- Ag-108m (BHA and BHK)
- Be-10 (BHA)
- C-14ind (BHK)
- C-14org (BHA)
- Ca-41 (BHK)
- Cl-36 (BHA and BHK)
- H-3 (BHA and BHK)
- I-129 (BHA and BHK)
- Ni-59 (BHK)
- Mo-93 (BHA and BHK)
- Po-210 (BHA)
- Pu-239 (BHA)
- Pu-240 (BHA)
- Ra-226 (BHA)
- Se-79 (BHK)
- Sr-90 (BHA)
- Tc-99 (BHA and BHK)
- Th-230 (BHA)
- U-234 (BHA)
- U-238 (BHA)

Radionuclides in the waste inventory which are parents of the above radionuclides will contribute to the ingrowth of those radionuclides, so also need to be included in the model:

- Am-243
- Cm-243
- Cm-244
- Cm-246
- Pu-242

Waste Inventory

The waste inventory is taken from Section 2.3 in R-19-09. For BHA, the total inventory is assigned to the waste compartment; it is assumed to be instantly released from the waste materials to the pore water in the waste domain upon the repository closure. This is a cautious assumption.

For BHK, the inventory is assigned to four categories of metallic waste components, and also to surface contamination. The inventory associated with the 0 mm thickness metallic waste category and the surface contamination is assumed to be instantly released from the waste materials to the pore water in the waste domain upon the repository closure. This is a cautious assumption. The inventory associated with the other three categories of metallic waste components is assumed to be released congruent with corrosion of the metals, as described above (see also Figure 26).

Dimensions

The assumed dimensions of BHA and BHK vaults are given in Section 2.2 of R-19-09. Each of the waste and backfill compartments is represented as a cuboid.

In BHA, the inflow/outflow backfill compartments are adjacent to the short sides of the waste compartment and the side compartments are adjacent to the long sides and top/bottom of the waste compartment. The cross-sectional area of the BHA waste compartment is not a square, so the length of the waste compartment in the direction of the 'side' backfill cautiously uses the height of the concrete structure (8.4 m), which is smaller than its width (16 m). To calculate the diffusive resistance for transport from the waste compartments (Equation (11)), the length of the waste compartment in the inflow/outflow/side directions is divided by a factor of 2.5. This is justified in R-19-09 Section 2.6.1 as resulting in a release rate comparable to an analytical solution with a zero-concentration boundary. The results of the reimplemented model suggest that the fluxes from the BHA vault are insensitive to this parameter. The resulting diffusion lengths are 56 m for transport along the inflow/outflow direction and 3.36 m for the side direction. The interface areas for diffusion are simply the total cross-sectional areas of the concrete structure in each direction; 6,832 m^2 normal to the 'side' direction and 134.4 m^2 normal to the inflow/outflow directions.

As previously stated, the dimensions of the BHA backfill cautiously ignore the additional bentonite pellets in the roof. The diffusion length is set to the thickness of the backfill below the concrete structure; 2.3 m. Since the backfill in each direction is discretised into five compartments, each is assigned a diffusion length of 0.46 m. It is not clear from the documentation whether this length is divided by a factor of 2 to calculate the diffusive resistance between compartments (as in Equation (11)), but the results of the re-implementation suggest this has been done. The cross-sectional area for diffusion is constant for each backfill compartment; this is an average of the waste compartment area and the backfill area (i.e. calculated by adding half the backfill thickness to the waste compartment dimensions; 195.8 m^2 normal to the inflow/outflow direction and 8,120 m^2 normal to the side direction). This is a simplified approximation that will tend to over-estimate the diffusion area in the inner backfill and under-estimate the diffusion area in the outer backfill. The compartment volumes given in Table 2-4 of R-19-09 are products of the compartment areas and thicknesses; with the exception of the inflow/outflow backfill

compartments. These have an area of 195.8 m^2 and a total thickness of 2.3 m, but are assigned a volume of 616 m^3 rather than the expected 450.34 m^3. One fifth of this total volume is assigned to each individual compartment. The AMBER calculated fluxes are insensitive to the volume of the inner/outer backfill, as the majority of the contaminant transport is through the side compartments, but it remains unclear why SKB have assumed a larger volume of backfill than expected from the given areas and thicknesses.

In BHK, the inflow/outflow backfill compartments are adjacent to the top/bottom of the waste compartment and the side compartments are adjacent to the long and short sides of the waste compartment. The cross-sectional area of the BHK waste compartment is not a square. However, the length of the waste compartment in the direction of the 'side' backfill cautiously uses its width (15 m), which is smaller than the length (90 m); see Figure 30. To calculate the diffusive resistance for transport from the waste compartments (Equation (11)), the length of the waste compartment in the inflow/outflow/side directions is divided by a factor of 2.5. The resulting diffusion lengths are 3.36 m for transport along the inflow/outflow direction and 6 m for the side direction. The interface areas for diffusion are simply the total cross-sectional areas of the concrete structure in each direction; 1,764 m^2 normal to the 'side' direction and 1,350 m^2 normal to the inflow/outflow directions.

Figure 30: Dimension used for the waste compartment length to calculate diffusion between the waste compartment and the side backfill.

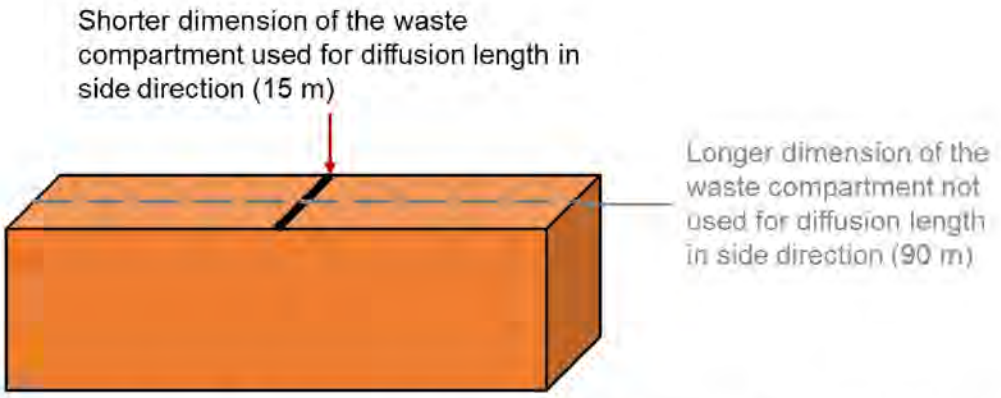

As previously stated, the dimensions of the BHK backfill cautiously ignore the additional concrete in the roof. The diffusion length is set to the thickness of the backfill to one side of the concrete structure; 2.8 m. Since the backfill in each direction is discretised into five compartments, each is assigned a diffusion length of 0.56 m. Further, although the dimensions of the BHK backfill compartments themselves are assumed to remain constant with time, the diffusion distance is not. In particular, as noted in Section 2.8.2 of R-19-09, during the Degraded Zone Case the diffusion length of the backfill compartments is assumed to be half the thickness of the compartment, whereas in for the other time periods (IC and DC), it is assumed to be the full thickness of the backfill compartment. As with BHA, it is not clear from the documentation whether this length is divided by a factor of 2 to calculate the diffusive resistance between compartments (as in Equation (11)), but the results of the re-implementation suggest this has been done.

The cross-sectional area for diffusion is constant for each backfill compartment; this is an average of the waste compartment area and the backfill area (i.e. calculated by adding half the backfill thickness to the waste compartment dimensions; 1,652 m^2 normal to the

inflow/outflow direction and 1,858 m^2 normal to the side direction). As noted above, the area normal to the side direction is calculated as the sum of the four side backfill faces shown in blue in Figure 27. This is a simplified approximation that will tend to over-estimate the diffusion area in the inner backfill and under-estimate the diffusion area in the outer backfill.

Material Properties

In BHA, the waste compartment is assigned homogenous properties incorporating the waste, grout, containers and concrete structure. The effective diffusivity of all radionuclides in the compartment is set to the diffusivity of radionuclides in water, 2×10^{-9} m^2/s. This is cautious and does not account for the likely diffusion resistance of the materials in the waste compartment.

The average porosity/density of the BHA waste compartment is calculated from the relative proportions of grout and concrete in the waste compartment; the wastes and containers themselves are not considered. The resulting densities appear to be very low. Section 2.5.2 in R-19-09 states that there is 8.649×10^6 kg of unsaturated grout in the BHA waste domain, with a volume of 15,429 m^3 (excluding the volume of the concrete structure). This suggests a dry bulk density of only 561 kg/m^3, which seems unusually low, with a porosity of 31%. The porosity of the grouted waste is assumed to be constant, whereas the porosity of the concrete structure evolves from 11% to 24% over the assessment timeframe (Table 2-16 in R-19-09).

The material properties of the BHA bentonite backfill are taken from the properties of bentonite assumed in previous SKB assessments. The porosity data is taken from the properties of the bentonite in the KBS-3 concept (SKB, 2010). The effective diffusivity data are taken from SR-Can assessment (Ochs and Talerico, 2004). The sorption coefficients are taken from the SR-PSU assessment (SKB, 2014). These properties are assumed to remain constant throughout the entire assessment timeframe. The total physical porosity is 43%. For anions, the diffusion available porosity is reduced to 17%. Likewise, the effective diffusivity for anions in bentonite is reduced from 1.2×10^{-10} m^2/s to 1.0×10^{-11} m^2/s. It is not clear which elements SKB have assumed that anion exclusion applies to in the near field (whereas for the geosphere model, this information is supplied in the data report R-19-09). Ochs and Talerico (2004) provides this information but does not include the full list of radionuclides considered in SE-SFL. For the remaining radionuclides, it is assumed that Be, H and Po are cations/neutral species and Mo is an anion, consistent with their properties in the geosphere. From the near-field flux results (Section 8.2), it appears that SKB have modelled C-14org without anion exclusion in BHA whereas Ochs and Talerico (2004) suggests that it is treated as an anion.

In BHA, there is assumed to be a significant concentration of complexing agents (primarily ISA), which can reduce the sorption of some radionuclides. The concentration of ISA is assumed to reach a saturation concentration of 20 mM immediately after repository closure and remain at this concentration for the full assessment timeframe. This is cautious since it ignores the effect of ISA being transported away from the vault, although the simple scoping arguments presented previously indicate this may only have a small impact on the very long-term fluxes and doses. The resulting sorption reduction factors for the BHA wastes and backfill are listed in Table 2-20 of R-19-09; these are as high as 10,000 for some radionuclides.

In BHK, the waste compartment is assigned homogenous properties incorporating the waste, grout, containers and concrete structure. The effective diffusivity of all radionuclides in the compartment is set to the diffusivity of radionuclides in water, 2×10^{-9} m^2/s. This is highly cautious and does not account for the likely diffusion resistance of the materials in the waste compartment.

The average porosity/density of the BHK waste compartment is calculated from the relative proportions of grout and concrete in the waste compartment in the same manner as for the BHA waste compartment; the wastes and containers themselves are not considered. Section 2.5.2 in R-19-09 states that there is 5.415×10^6 kg of unsaturated grout in the BHK waste domain, with a volume of 9,220.4 m^3 (excluding the volume of the concrete structure). This suggests a dry bulk density of only 587 kg/m^3, with a porosity of 28%. The porosity of the grouted waste is assumed to be constant, whereas the porosity of the concrete structure evolves from 11% to 24% over the assessment timeframe (Table 2-16 in R-19-09).

The material properties of the concrete backfill in BHK (porosity, effective diffusivity and sorption) are all assumed to evolve over time as the concrete degrades, but as noted above the timescales for this differ for different parts of the backfill. The porosity of the backfill to the sides and in the outflow direction of the groundwater flow is assumed to evolve in a similar manner to that of the concrete structure in the waste compartment (Figure 31). The porosity of the backfill in the inflow direction is assumed to undergo a more rapid degradation. The effective diffusivities of the backfill compartments are assumed to evolve in a similar manner (Figure 2-13 of R-19-09). The breakpoints in the linear interpolation of the porosity and effective diffusivities are based on times when portlandite and C-S-H gels have completely leached in a control volume (Idiart and Laviña, 2019).

The sorption coefficients assumed for the concrete in the wastes in both the BHA and BHK vaults, and the concrete in the backfill in the BHK vault, are assumed to evolve with both the degradation state of the cement in the compartment, and also the fraction of cement in the concrete (see Sections 2.5.2 and 2.7.3 of R-19-09). There are four different states of cement degradation, with Table 2-18 of R-19-09 giving the breakpoints of the linear interpolation of sorption coefficients between these different states of chemical degradation (Idiart and Laviña, 2019), and Table 2-19 of R-19-09 providing the timing at which those breakpoints are reached for the differing waste and backfill compartments. It is not entirely clear as to how the pH evolution reported in Appendix B of Idiart and Laviña (2019), has been used to derive the time periods listed in Table 2-19.

The sorption coefficients based upon the degradation state of the cement are then multiplied by the fraction of cement in the concrete to obtain the K_d values used in the transport calculations. As an example, the evolution of the K_d values used for Ca in the backfill in the inflow, outflow and side directions is shown in Figure 32; note that the same K_d values are used for the outflow and side directions.

Figure 31: Evolution of porosity of the material types in the BHK vault

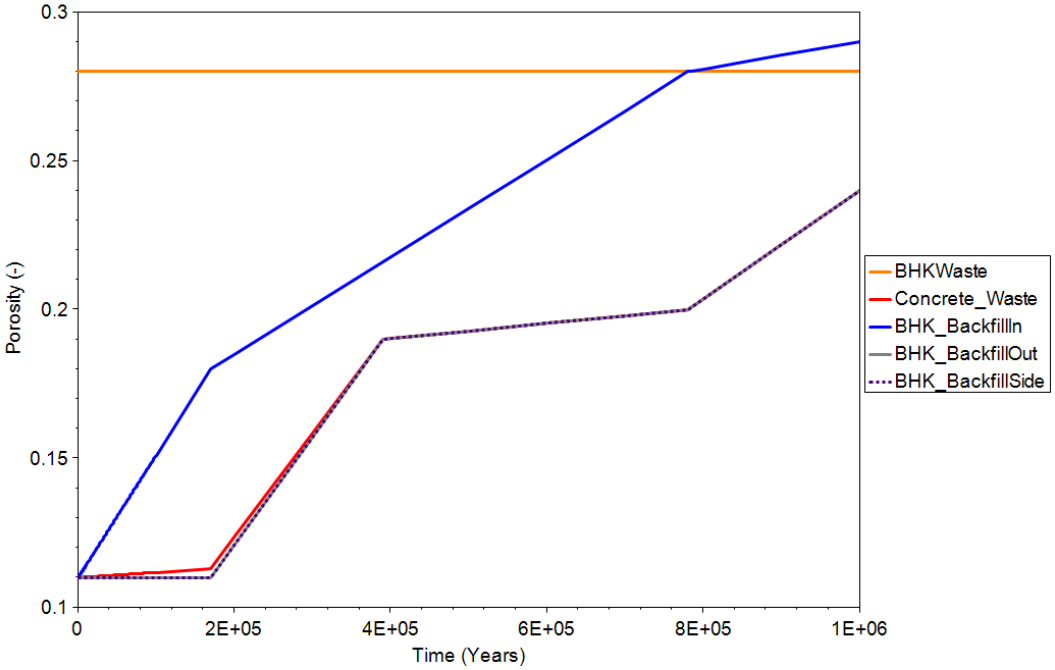

Figure 32: Evolution of Kd for Ca in the backfill in the (a) inflow direction; and (b) the outflow and side directions. These graphs show the evolution of the assumed porosity (dark blue) and fraction of cement in the concrete (light blue) in these backfill compartments, the sorption coefficient of the cement taking into account the cement chemical degradation state (orange line), and the Kd used in the transport calculations (red line), which scales the Kd by the fraction of the cement in the concrete. These graphs also show the breakpoints in the linear interpolation of the evolution of Kd and porosity based on chemical cement degradation states.

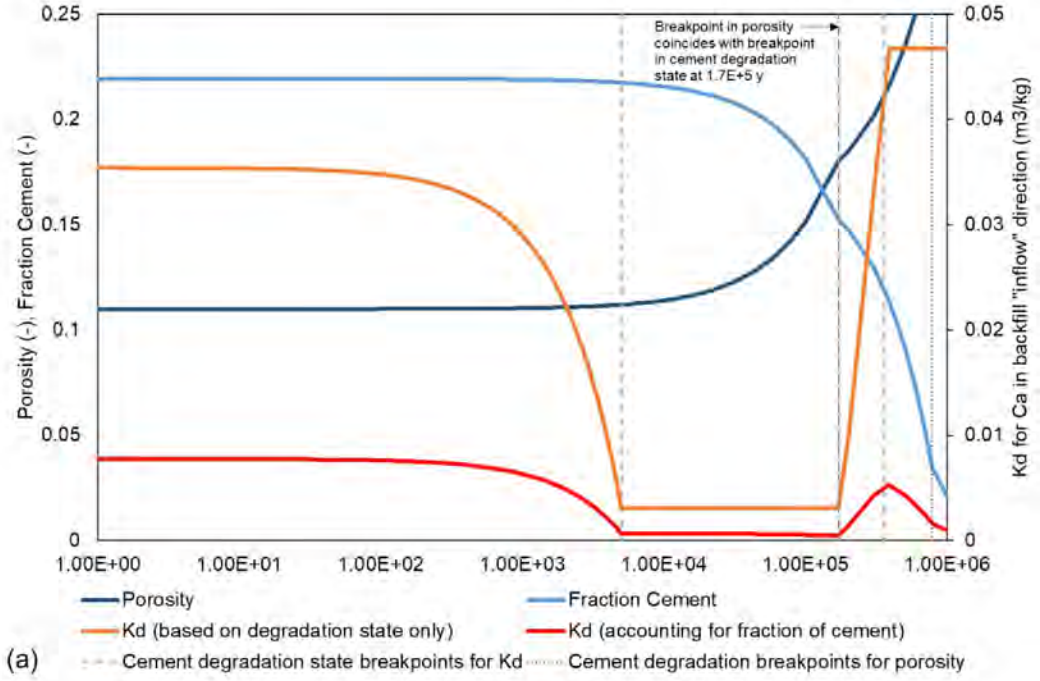

(a)

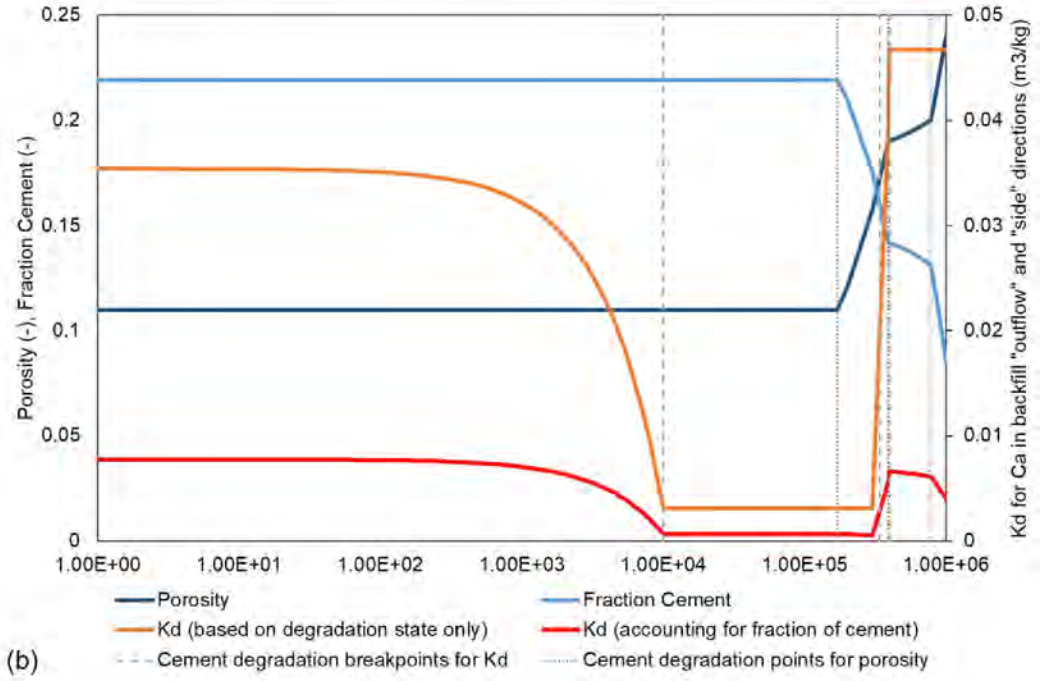

(b)

Flows

For BHA, all flow is assumed to be horizontal along the length of the vault (R-19-09, Section 2.6.3). The flow information is provided by the repository-scale model in which the BHA vault is divided into 7 sections. For the simplified near-field model, the groundwater flow through each control volume is summed to give the total flow through the single waste compartment; this method 'double counts' the flow between the control volumes but the overall flow remains small, at 1.55×10^{-3} m^3/a. All flow through the backfill is assumed to flow through the wastes. The flows are assumed to be constant with time since the bentonite backfill, which provides the main resistance to flow, is assumed to have a constant low hydraulic conductivity.

For BHK, flow is predominantly vertically downwards through the vault, with limited flow through the sides of the vault (R-19-09, Section 2.6.4). The flow information is provided by the repository-scale model in which the BHK vault is divided into eight sections. As the concrete in the waste and backfill in the vault degrades, local groundwater flow conditions are assumed to change. The repository-scale model has therefore been run for the three stages of degradation assumed:

- Intact Case (IC): The concrete backfill is intact and has initial state properties, 2075–87 083 [y].
- Degraded Zone Case (DZC): The outer half of the concrete backfill is degraded, 87 083–782 168 [y].
- Degraded Case (DC): The entire concrete backfill is degraded, 782 168–1 002 075 [y].

The data used to derive the groundwater flow rates in the simplified model are given in Tables 2-25 to 2-27 of R-19-09. For the simplified near-field model, the groundwater flow out of the bottom of each control volume is summed, together with the flow out of the longer sides, to give a total flow out of the waste compartment. The side flow is taken to be the largest magnitude flow either in or out of the short sides of the control volumes. SKB argue that the absolute value of the flows is used because the sign only indicates the direction of the flow. Noting an inconsistency in the logic, in as much as direction matters for the outflow but not the side flow, consideration has therefore been given as to how the outflow rates might have differed. Whilst the effects of SKB's assumption are minimal for the magnitude of the outflow in the intact concrete (IC) and degraded concrete (DC) states, there is a potential for the groundwater flow in the DZC timeframe to have been underestimated (Table 4).

Table 4: Effect of alternative assumptions on outflow [m^3/y]

Timeframe	**IC**	**DZC**	**DC**
Downward flow [m^3/y]	6.33E-01	3.34E-01	1.30E+00
Flow out of long sides [m^3/y]	6.26E-02	7.84E-03	1.57E-01
Flow into long sides [m^3/y]	6.35E-02	1.35E-01	1.29E-01
Flow used by SKB	6.96E-01	3.42E-01	1.45E+00
Alternative flow direction	6.97E-01	4.69E-01	1.42E+00

The inflow is not specified. However, using the logic SKB have presented for their side and outflow rates in the near-field simplified model, for the independent calculations we

have assumed that the absolute value of the sum of the groundwater flow rates into the control volumes is the inflow rate.

8.2. Results

8.2.1. BHA

Comparison with SKB's results

Figure 33 shows a comparison between the calculated radionuclide fluxes from the near field in the re-implemented AMBER model and SKB's Ecolego model. Consistent with the Ecolego results the timescale used is year AD. This figure is equivalent to Figure 5-7 in TR-19-06, with the additional AMBER results; only the 15 radionuclides with the highest fluxes are shown. The results have been extracted from TR-19-06 using Graph Grabber (Quintessa, 2020).

Figure 33: Comparison of calculated activity release from BHA near-field in the present-day evaluation case. SKB's Ecolego results are shown with dashed lines and cross markers (reproduced from Figure 5-7, TR-19-06) and the re-implemented AMBER results are shown with solid lines and circular markers.

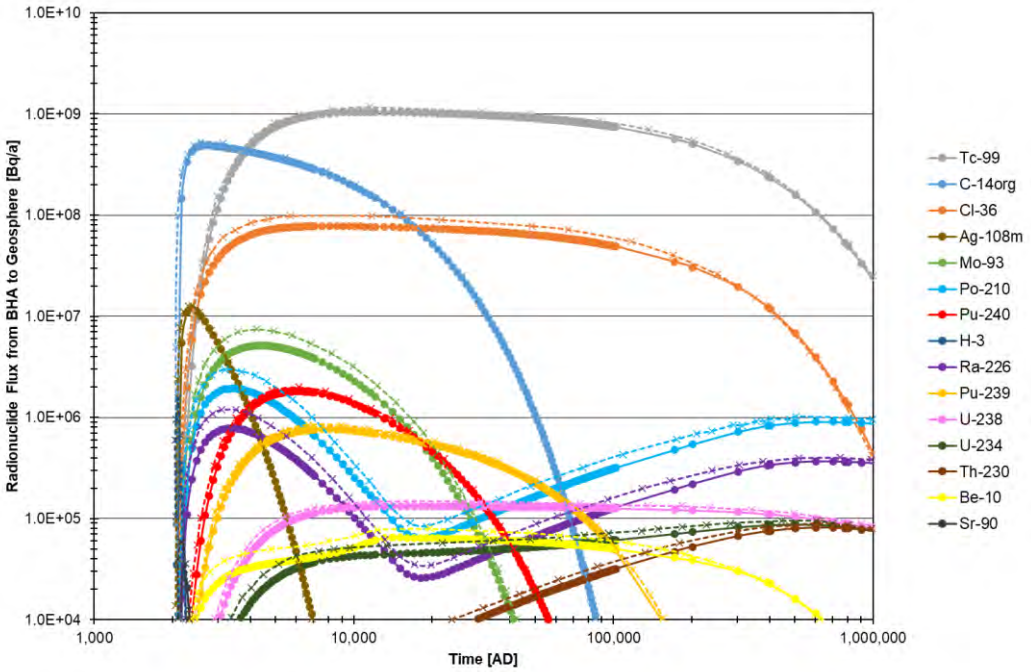

It can be seen that there is generally good agreement between the original and re-implemented models. In general, the fluxes calculated by the AMBER model are slightly lower than those calculated by SKB; with a difference in the peak fluxes of up to 40% (for Sr-90). The error in the peak fluxes for radionuclides with sharp initial spikes is imprecise due to the difficulty of reading the fluxes from the results figures in TR-19-06, and possible differences in the report times used by AMBER and Ecolego; the peak flux of Sr-90 is calculated to occur approximately 120 years after closure.

The radionuclides with the highest near-field fluxes (those included in Figure 33) are all non-sorbing (C-14org, Cl-36, Ag-108m, Mo-93, H-3) or very weakly-sorbing in bentonite. In the case of radionuclides such as Tc-99, this is because of complexation causing a significant reduction in sorption (by a factor of 10,000). Other radionuclides which have a high initial inventory but are more strongly sorbing are significantly retarded in the bentonite buffer, reducing their peak near-field flux.

The small discrepancy between the AMBER and Ecolego results is seen in both non-sorbing and weakly-sorbing radionuclides but appears to be greatest in the sorbing radionuclides. The timing of the near-field fluxes is mainly controlled by the bentonite backfill, which provides the largest resistance to transport. In BHA, the transport through the bentonite backfill is dominated by diffusion, although advection between the vault and the fractured rock is also significant. Decreasing the assumed diffusion lengths of the backfill compartments by a factor of two does increase the peak AMBER fluxes to a magnitude more similar to SKB's for some radionuclides, but also brings the timings of the peak flux earlier than SKB's. There is some uncertainty in the volume of the inflow/outflow backfill compartments but the fluxes are insensitive to this volume, since most transport is through the larger side compartments.

This suggests that the discrepancy between the AMBER and Ecolego results is related to the properties of the waste compartment. The near-field fluxes are insensitive to the diffusion length and volume of the waste compartment but are affected by the amount of sorption onto the cement in the waste compartment. The results suggest that AMBER is calculating more retention in the waste compartment than Ecolego. The sorption coefficients of cement are clearly specified in R-19-09 and the flux discrepancy is seen in both complexing and non-complexing radionuclides which implies that there is a disagreement in the density or porosity of the grouted waste or concrete structure. The density of the grouted waste used in the AMBER model is 561 kg/m^3 (Section 8.1.3); this is very low, suggesting most of the grouted waste volume is taken up by non-sorbing, non-grout material.

Figure 34 shows near-field fluxes from the AMBER model without any grout (grouted waste assigned a density of 0 kg/m^3), which are closer to the fluxes reported by SKB. This emphasises that the grout provides very little resistance to transport with SKB's cautious modelling assumptions. Alternatively, Figure 35 shows near-field fluxes from the AMBER model where the bulk density of the concrete structure is reduced from 2344 kg/m^3 (as specified in Section 2.5.2 of R-19-09) to 514.5 kg/m^3 (the density of the cement powder and water only). Again, the fluxes are more similar to those reported by SKB. This is conceptually confusing because the cement sorption coefficients are already multiplied by the fraction of cement in the material in AMBER, so that fraction is effectively being applied twice with this reduced density. Further clarity from SKB about the properties of the waste compartment is required.

In Figure 34 and Figure 35 there is still a small discrepancy between the AMBER and Ecolego results for U-234 and Th-230, suggesting there may be a small error in this decay chain. Further verification and testing of the AMBER model has not suggested a reason for this.

Figure 34: Comparison of calculated activity release from BHA near-field in the present-day evaluation case, with no grout in the waste compartment. SKB's Ecolego results are shown with dashed lines and cross markers (reproduced from Figure 5-7, TR-19-06) and the re-implemented AMBER results are shown with solid lines and circular markers.

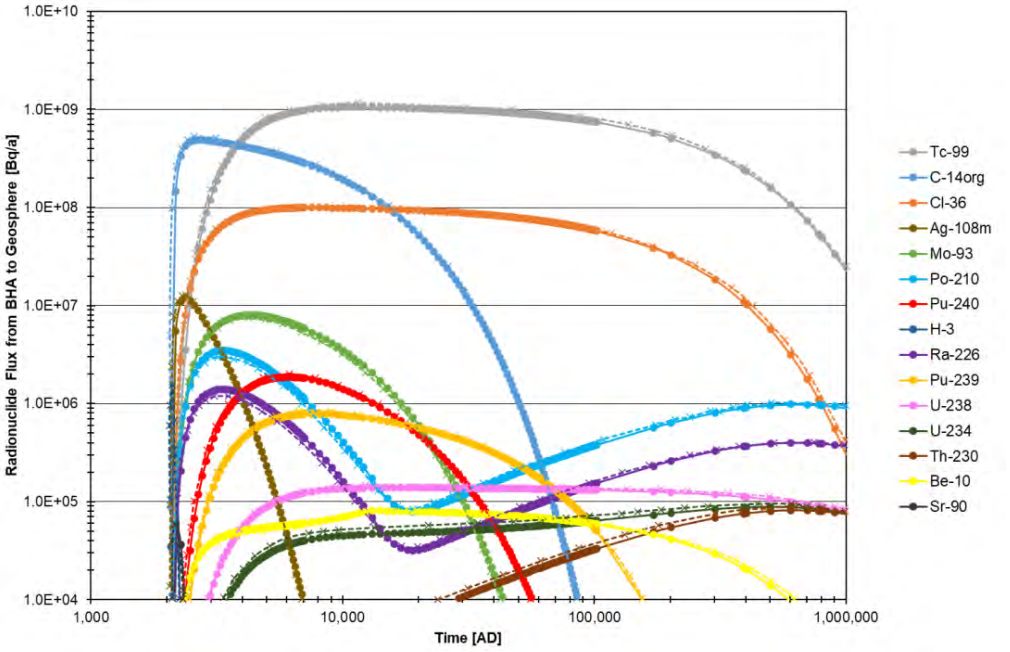

Figure 35: Comparison of calculated activity release from BHA near-field in the present-day evaluation case, with reduced concrete structure density. SKB's Ecolego results are shown with dashed lines and cross markers (reproduced from Figure 5-7, TR-19-06) and the re-implemented AMBER results are shown with solid lines and circular markers.

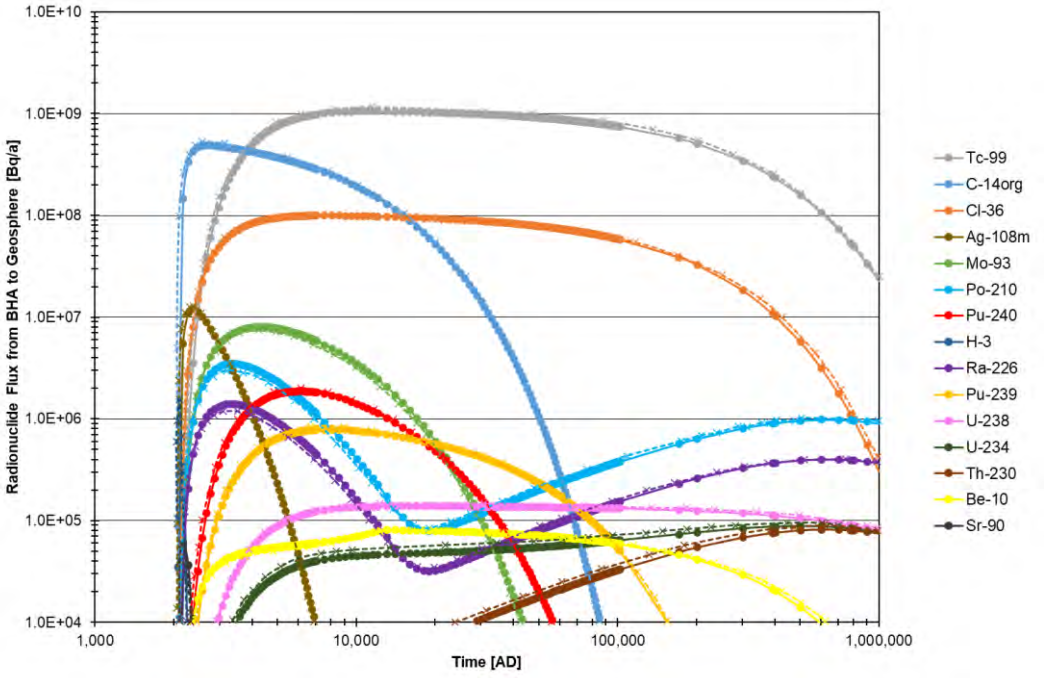

The following sub-sections further investigate the sensitivities in the near-field model.

Sensitivity case - No effect of complexing agents

The amount of complexing agent in the BHA waste is not well known. The base case cautiously assumes a concentration of ISA which remains at saturation levels throughout the assessment timeframe. SKB assess the impact of this assumption in the sensitivity case *No effect of complexing agents in BHA*. In this case, the sorption reduction factors (SRFs) are set to 1 for each radionuclide. This sensitivity case has been reimplemented in AMBER and the calculated near-field fluxes compared with the Ecolego results in Figure 36. The non-sorbing or weakly-sorbing elements (C-14org, Cl, Ag, Mo and H) are assigned SRFs of 1 in the presence of ISA, so the radionuclide fluxes of these elements are unchanged from the base case. Tc-99 has the highest near-field flux in the base case, but Tc has a very high SRF of 10,000. The peak flux of Tc-99 drops by almost 10 orders of magnitude from 1 x 10^{9} Bq/y in the base case to 3 x 10^{-1} Bq/y in this sensitivity case (not shown in Figure 36). Likewise, the SRF for Pu, U and Th is 10,000 and the other radionuclides in the U-238 chain also have a SRF greater than 1 (1,000 for Po, 100 for Cm and Pb, 10 for Ra). This demonstrates that the relative importance of contaminants in the BHA inventory is strongly affected by assumptions about the concentration of ISA in the vault.

Figure 36: Comparison of calculated activity release from BHA near-field in the *No effect of complexing agents in BHA* case. SKB's Ecolego results are shown with dashed lines and cross markers (reproduced from Figure 5-7, TR-19-06) and the re-implemented AMBER results are shown with solid lines and circular markers. 'U-238 chain' is the sum of U-238, U-234, Th-230, Ra-226, Pb-210 and Po-210.

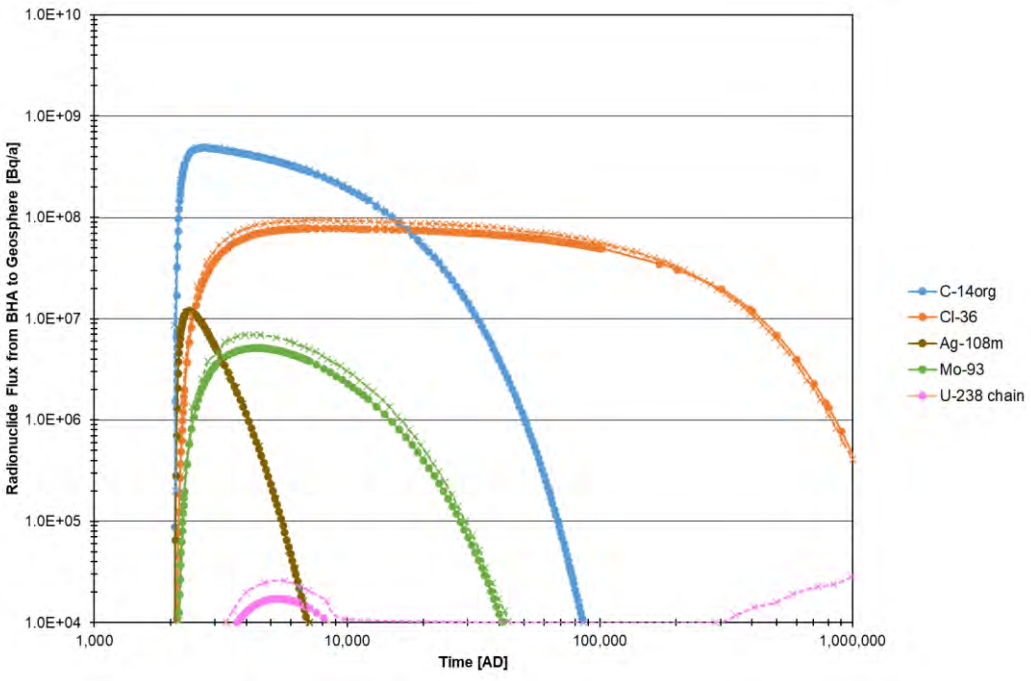

Sensitivity case - No anion exclusion

As discussed in Section 8.1.3, the diffusion-accessible porosity and effective diffusivity in bentonite are reduced for anionic species. It is not clear which elements this applies to, with particular uncertainty about the treatment of C-14. Figure 37 shows the near-field fluxes calculated by AMBER with and without anion exclusion for organic C-14 and Mo-93. Other elements are modelled as cations or neutral species. Figure 37 demonstrates that

SKB have modelled Mo-93 with anionic exclusion in the near field but organic C-14 is modelled without anion exclusion, in contradiction to Ochs and Talerico (2004).

Figure 37: Comparison of calculated activity release from BHA near-field in the present-day evaluation case. SKB's Ecolego results (reproduced from Figure 5-7, TR-19-06) are compared with AMBER results with and without anion exclusion for organic C-14 and Mo-93.

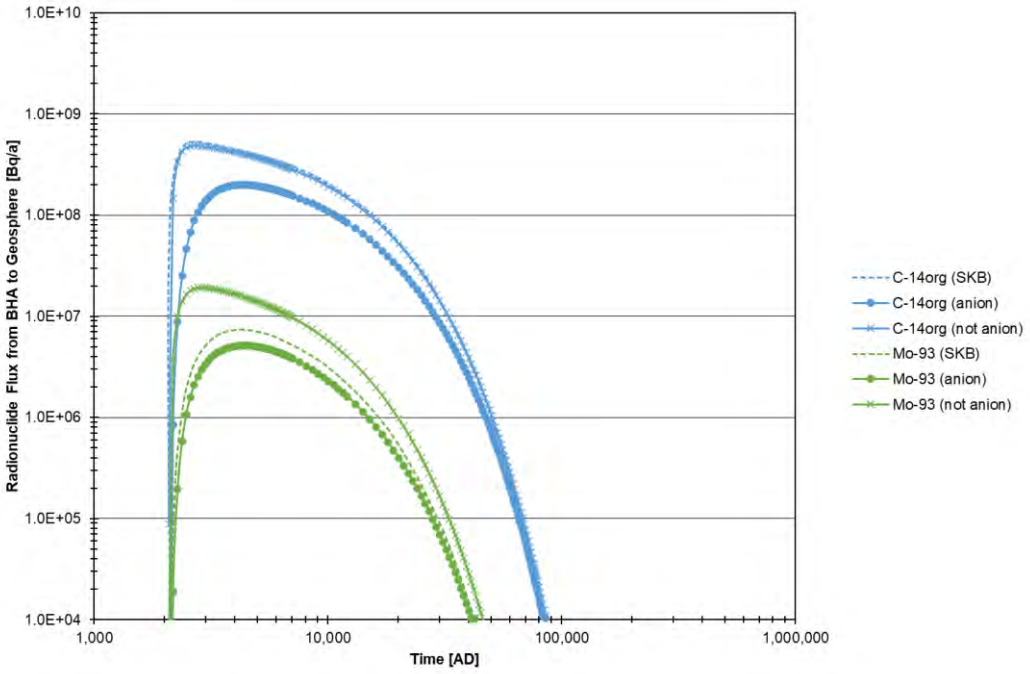

8.2.2. BHK

Comparison with SKB's results

Figure 38 shows a comparison between the calculated radionuclide fluxes from the near-field in the re-implemented AMBER model and SKB's Ecolego model. This figure is equivalent to Figure 5-10 in TR-19-06, with the additional AMBER results; only the 10 radionuclides with the highest fluxes are shown. Again, the results have been extracted from TR-19-06 using Graph Grabber (Quintessa, 2020).

It can be seen that there is generally good agreement between the original and re-implemented models; with a difference in the peak fluxes of up to 135% (for H-3), but mostly less than 10% (for Mo-93). The error in the peak fluxes for radionuclides with sharp initial spikes is imprecise due to the difficulty of reading the fluxes from the results figures in TR-19-06, and possible differences in the report times used by AMBER and Ecolego.

The small discrepancy in the calculated fluxes of Ni-59 arises from the fact that the AMBER implementation of the model has a non-zero advective transfer moving through the 'inflow' backfill compartments, included for a more complete representation of the groundwater flow, whereas the SKB implementation does not. This was confirmed by running a variant of the AMBER implementation of the BHK vault with that advective flow turned off (Figure 39).

The radionuclides with the highest near-field fluxes (those included in Figure 38) are generally either non-sorbing (C-14ind, Ag-108m) or very weakly-sorbing (Cl-36, Ca-41, Mo-93) in concrete. The one exception is Ni-59. Ni-59 is assumed to be weakly sorbed in concrete when it is in State I, but the sorption increases by almost an order of magnitude as the concrete degrades to State II and beyond.

Figure 38: Comparison of calculated activity release from BHK near-field in the present-day evaluation case. SKB's Ecolego results are shown with dashed lines and cross markers (reproduced from Figure 5-10, TR-19-06) and the re-implemented AMBER results are shown with solid lines and circular markers.

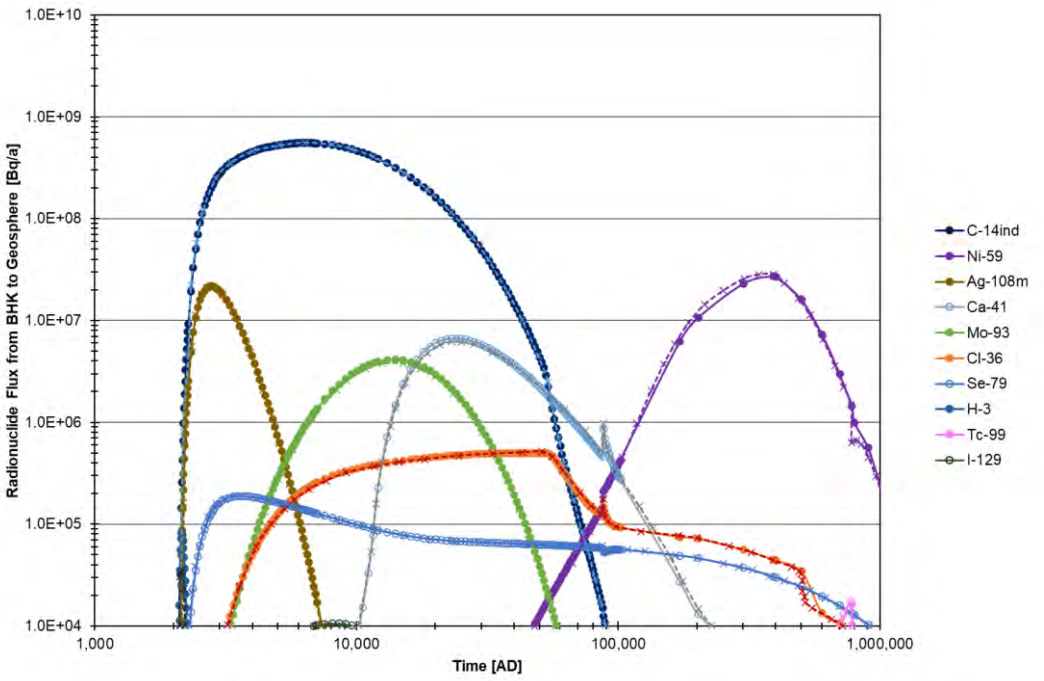

Figure 39: Comparison of calculated activity release from BHK near-field in the present-day evaluation case, with no advective flow assumed in the inflow backfill in the independent calculations. SKB's Ecolego results are shown with dashed lines and cross markers (reproduced from Figure 5-10, TR-19-06) and the re-implemented AMBER results are shown with solid lines and circular markers.

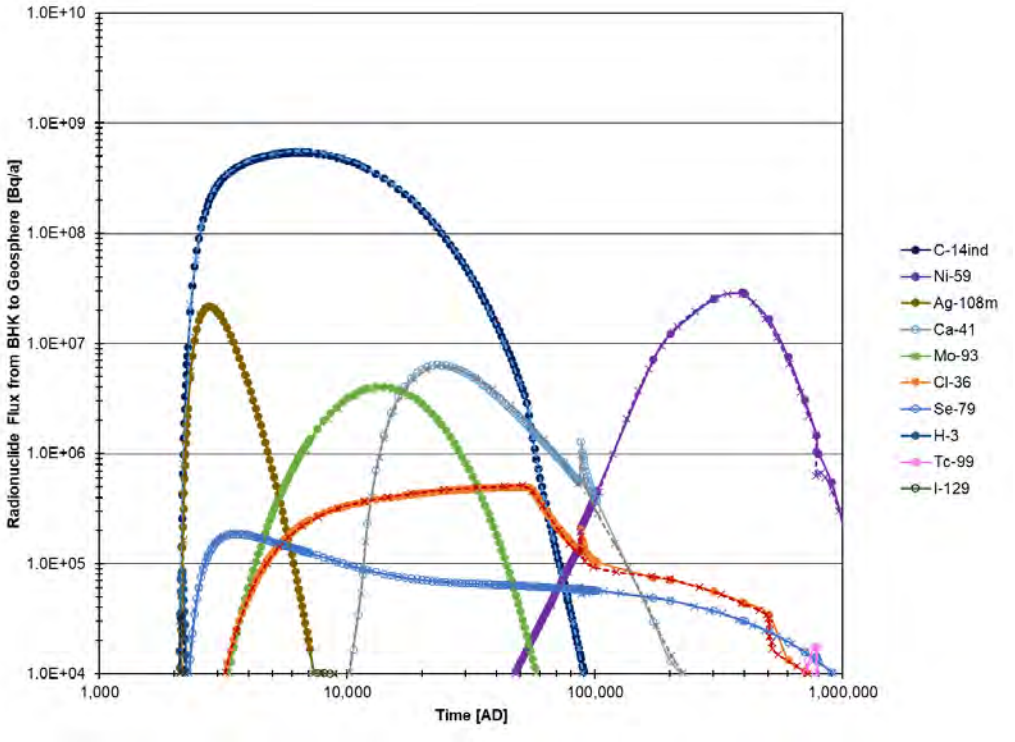

SKB state that the spikes in the results around 87,000 yAD and 780,000 yAD are associated with the abrupt transitions in groundwater flow introduced to represent the transition between intact concrete, degraded zone concrete and fully degraded concrete (Section 5.2.8 of TR-19-06).

On transitioning between the intact and degraded zone concrete states at around 87,000 yAD, the groundwater flows are assumed to be reduced by approximately a factor of two. However, what is observed in the calculated fluxes of radionuclides from the near field at that time is a spiked increase in the release of radionuclides. At the time of transitioning between the two groundwater flow rates, it is also assumed that the effective diffusion length of the backfill compartments halves, as a means of approximating the degraded concrete. Thus, at this time, the diffusive transfer rates increase, as shown in Figure 40. The net effect is an increase in the release rate, i.e. the decrease in the diffusion length is more significant than the decrease in the flow rate.

The transitions in transfer rates for sorbing radionuclides, such as Ca-41 (Figure 41), are further complicated by changes in the sorption coefficients (see Figure 32). This is what leads to the spikes, or in the case of Ni-59 sudden increase, in the calculated fluxes around 87,000 yAD.

At the transition between the degraded zone concrete and fully degraded concrete, the diffusive transfers decrease by a factor of two as the effective diffusive lengths return to their original values, and the advective flows increase. This is why there is a sudden drop in the calculated fluxes of Ni-59 and Tc-99 at around 870,000 yAD.

Figure 40: Advection and diffusion rates out of the near-field for a non-decaying, non-sorbing, tracer (1/y)

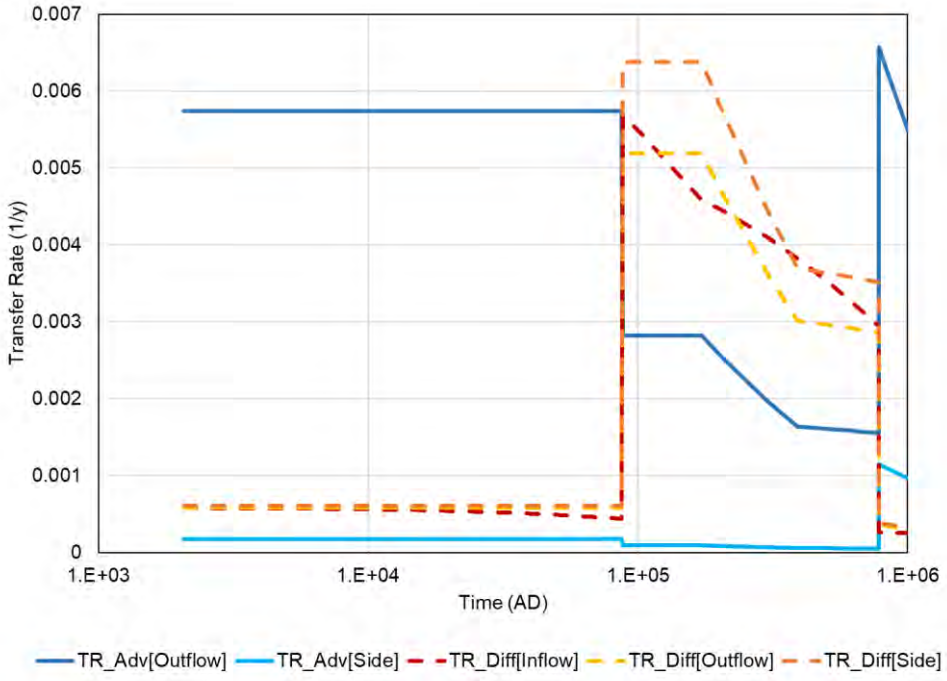

Figure 41: Advection and diffusion rates out of the near-field for Ca-41 (1/y)

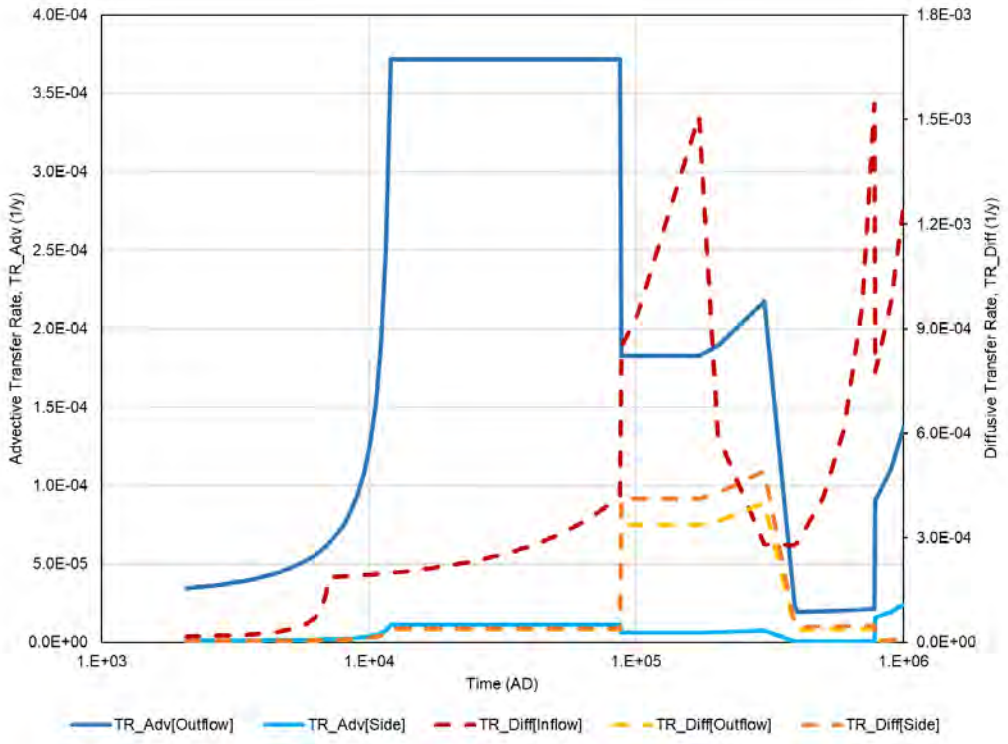

Sensitivity Case - Inventory

Section 2.3.2 of R-19-09 details the radionuclide inventory in the BHK vault at the initial state. In comparing the data contained in Tables 2-8 to 2-12 of R-19-09 with those presented in Section 3.8.1 and Appendix 1 of the Initial State Report (TR-19-03), it is not clear as to whether the 'Contamination' inventory presented in Table 3-26 of TR-19-03 should be used for the surface contamination; it is implied that those values are derived from Herschend (2014). In particular, many of the numbers presented in that table do not agree with the values reported for surface contamination in Table 2-12 of R-19-09 for surface contamination, which are taken from Herschend (2016). These inventory data are reproduced in Table 5 below.

Table 5: Surface Contamination Inventory in BHK [Bq]. Data from Table 2-12 in R-19-09 has been used for the base case, and data from Table 3-26 in TR-19-03 have been used to explore the sensitivities around this aspect of the inventory

Radionuclide	**Table 2-12 (R-19-09)**	**Table 3-26 (TR-19-03)**	**Radionuclide**	**Table 2-12 (R-19-09)**	**Table 3-26 (TR-19-03)**
Ag-108m	5.37E+11	5.40E+11	Ni-59	3.07E+12	3.00E+12
Am-243	1.08E+09	1.10E+09	Pb-210	0	0
Be-10	5.94E+04	0	Po-210	0	0
C-14ind	8.68E+10	0	Pu-239	1.14E+10	1.10E+10
C-14org	0	0	Pu-240	0	1.50E+10
Ca-41	2.85E+11	0.00E+00	Pu-242	1.10E+10	1.10E+10
Cl-36	2.60E+09	0.00E+00	Ra-226	0	0
Cm-243	1.37E+08	1.40E+08	Se-79	1.01E+09	1.00E+09
Cm-244	1.25E+10	1.30E+10	Sr-90	4.68E+11	4.70E+11
Cm-246	6.34E+06	6.30E+06	Tc-99	5.19E+09	5.00E+09
H-3	4.10E+13	0	Th-230	0	0
I-129	1.69E+08	1.70E+08	U-234	0	0
Mo-93	8.03E+09	7.20E+09	U-238	0	0

The calculated fluxes of Cl-36 and Ca-41 from the near-field are affected by the alternative surface contamination inventory assumptions (Figure 42).

The Cl-36 associated with the surface contamination accounts for only 2% of the total inventory in the base case, which is why the peak calculated flux does not differ, only the nature of the early flux. In contrast, 88% of the Ca-41 inventory is associated with the surface contamination in the base case, with the majority of the remaining 12% associated with the thickest metallic waste components. This is why the calculated peak flux with the alternative surface contamination inventory is both lower in magnitude, and later than the peak flux in base case.

Figure 42: Comparison of calculated activity release from BHK near-field for alternative surface contamination inventory assumptions. Both calculations have been undertaken using AMBER. The solid lines represent the fluxes calculated using the surface contamination inventory data as presented in Table 2-12 of R-19-09. The dashed lines represent the fluxes calculated using the alternative surface contamination inventory reported in Table 3-26 of TR-19-03.

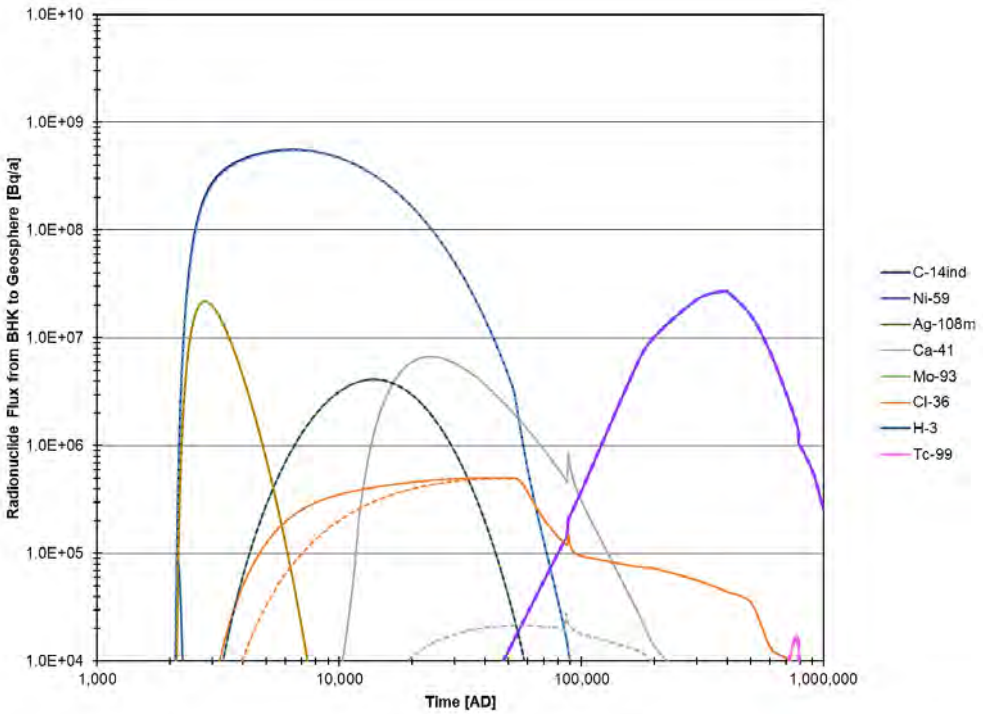

Sensitivity Case – Groundwater Flow

As noted in Section 8.1.3, there is some inconsistency with how SKB have applied the repository scale groundwater modelling results to the simplified near-field model. As part of the independent modelling, we have run a variant calculation, using the alternative outflow rates as given in Table 4; see Figure 43. There is a slight increase in the calculated peak flux of Ni-59 from the near field, which is not dissimilar to the impact of disregarding the advective flow in the inflow backfill (Figure 44).

Figure 43: Comparison of calculated activity release from BHK near-field for alternative outflow rate assumptions. Both calculations have been undertaken using AMBER. The solid lines represent the fluxes calculated using the outflows as given in Table 2-28 of R-19-09. The dashed lines represent the fluxes calculated using the alternative outflows as given in Table 4.

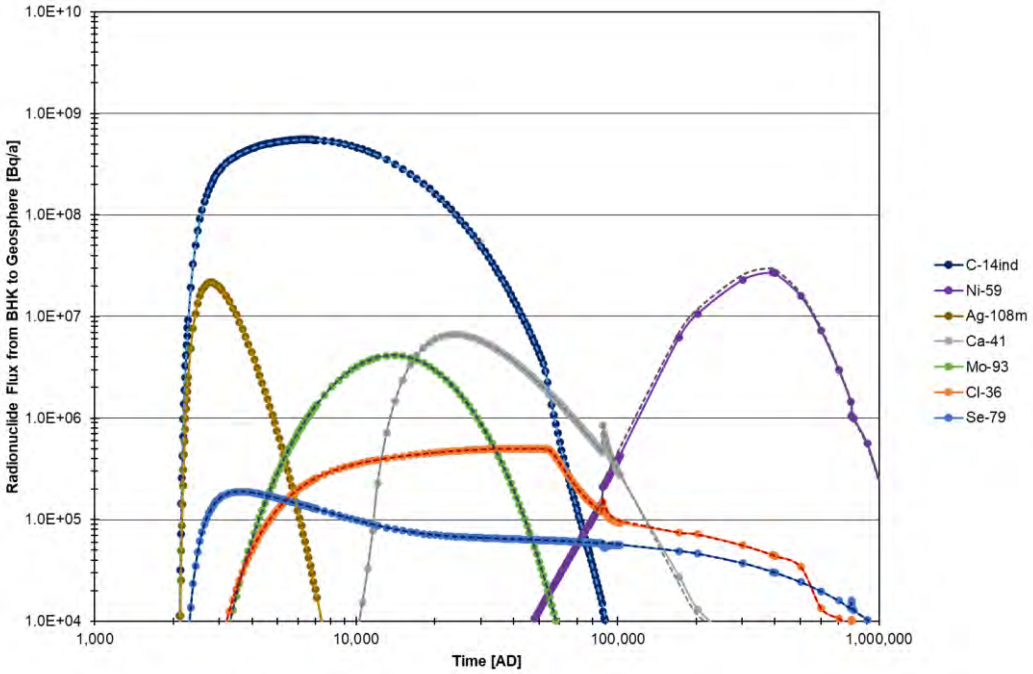

Figure 44: Comparison of calculated Ni-59 release from BHK near-field for alternative outflow rate assumptions, with (purple) and without (grey) advection in the inflow backfill. The solid lines represent the fluxes calculated using the outflows as given in Table 2-28 of R-19-09. The dashed lines represent the fluxes calculated using the alternative outflows as given in Table 4. SKB's results are also shown with a blue dashed line.

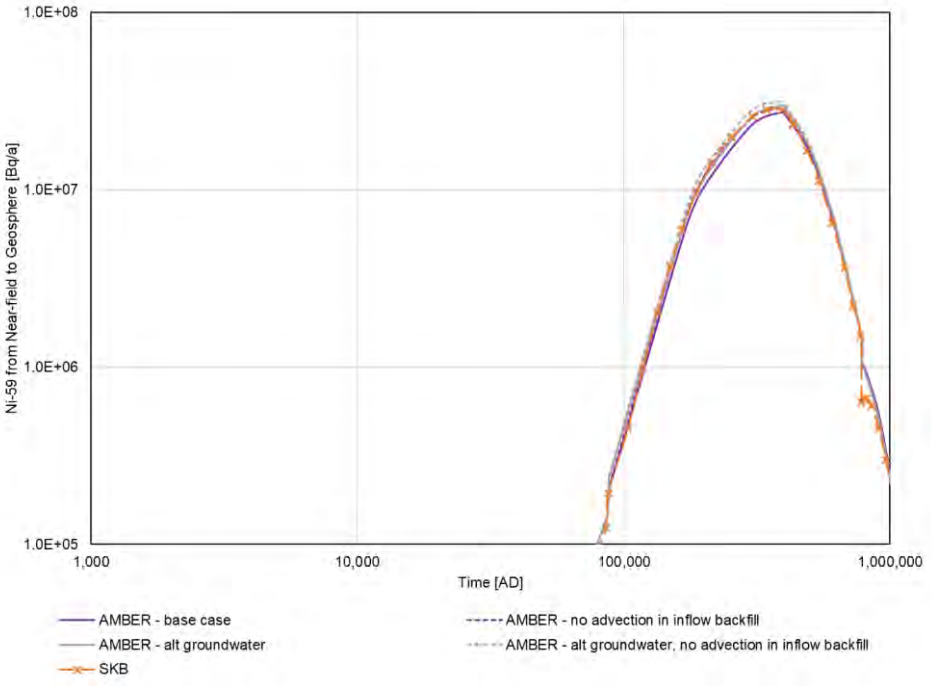

Sensitivity Case – Metallic Waste Corrosion Rate

The near-field model assumes that the metallic components corrode at a constant rate during the time of interest for SE-SFL. In the base case, the corrosion rate is set to 10 nm/y (Table 3), which is considered to be representative of stainless steel under anoxic alkaline conditions. As an alternative scenario, SKB consider a constant corrosion rate for all the metallic waste components an order of magnitude lower than the base case. This sensitivity case has been reimplemented in AMBER and the calculated near-field fluxes compared with the Ecolego results in Figure 45; the two implementations of the model show generally good agreement. However, the decline in the calculated flux of Ca-41 from the near-field is more rapid in the AMBER implementation of the model than SKB's calculations in Ecolego.

Figure 45: Comparison of calculated activity release from BHK near-field in the *Lower Steel Corrosion Rate in BHK* case. SKB's Ecolego results are shown with dashed lines and cross markers (reproduced from Figure 6-3, TR-19-06) and the re-implemented AMBER results are shown with solid lines and circular markers.

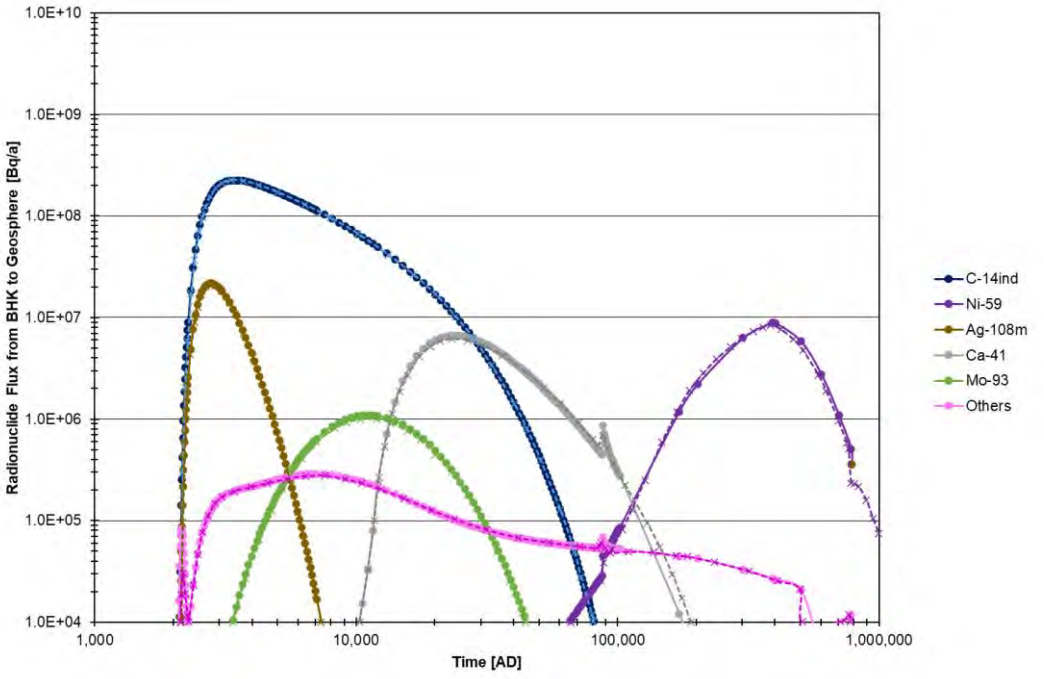

Sensitivity Case – Concrete Degradation

The gradual degradation of concrete is assumed to lead to an increase in the groundwater flow rate over time, with advection ultimately becoming the dominant transport mechanism in BHK. SKB have considered a sensitivity scenario in which the BHK concrete backfill is replaced with a new concrete backfill, which exhibits enhanced resistance against groundwater flow (Idiart et al., 2019b). This scenario is represented by assuming a lower flow rate through the BHK vault up until the time at which the concrete is considered to be fully degraded. SKB arbitrarily reduced the groundwater flow rates by a factor of 10 until the time when the concrete is fully degraded. Note that the time at which the concrete is assumed to be fully degraded was not varied for this sensitivity case. Furthermore, the concrete porosity and effective diffusivity are both scaled by a factor of 0.5 provided the concrete is intact or partly degraded. The reduction in assumed porosity means that the fraction of cement in the concrete is assumed to be higher up until the concrete is

fully degraded (Figure 46). As noted in R-19-09, SKB have assumed that, when the concrete is completely degraded, the water flow, porosity and effective diffusivity will be similar to those in the base case. In the independent calculations, therefore, it is assumed that once the concrete is fully degraded that these parameters will be as for the base case.

Figure 46: Effect of Alternative Concrete in BHK assumptions on the evolution of the fraction of cement (-) in all concrete containing compartments. The solid lines are the base case, and the dashed lines are the alternative grout.

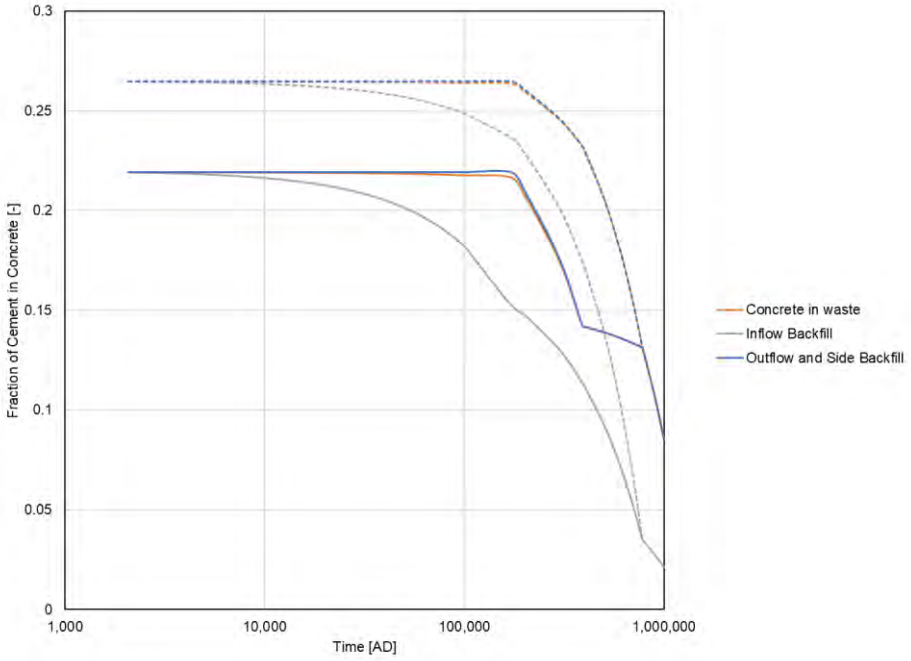

In defining this sensitivity case, although SKB have accounted for the lower permeability of the concrete affecting the assumed flow of water, and physical properties of the concrete, no consideration has been given as to how an alternative concrete might affect the timescales over which the system might evolve. A decrease in the groundwater flow rates would alter the rate of cement leaching and thus the chemical evolution of the system. This means that the breakpoint times associated with changes in groundwater flow rates, porosity, effective diffusivity and sorption coefficients, as shown in Figure 29, would reasonably be expected to occur at later times. This sensitivity case has been reimplemented in AMBER and the calculated near-field fluxes compared with the Ecolego results in Figure 47. The independent calculated fluxes for Mo-93 and Ca-41 are generally lower than those calculated by SKB. However, despite the flux being initially lower than SKB's, the independent calculated peak near-field flux of Ni-59 is 63% greater than the peak flux calculated by SKB, and occurs later than the peak flux calculated by SKB (~500,000 yAD rather than ~440,000 yAD). The sorption coefficients for all sorbing elements will be greater in this sensitivity calculation as consequence of assuming a lower porosity in the cement, as can be seen in Figure 48, but this phenomenon does not explain the differences seen in Figure 47.

Figure 47: Comparison of calculated activity release from BHK near-field in the *Alternative Concrete Backfill in BHK* case. SKB's Ecolego results are shown with dashed lines and cross markers (reproduced from Figure 6-6, TR-19-06) and the re-implemented AMBER results are shown with solid lines and circular markers.

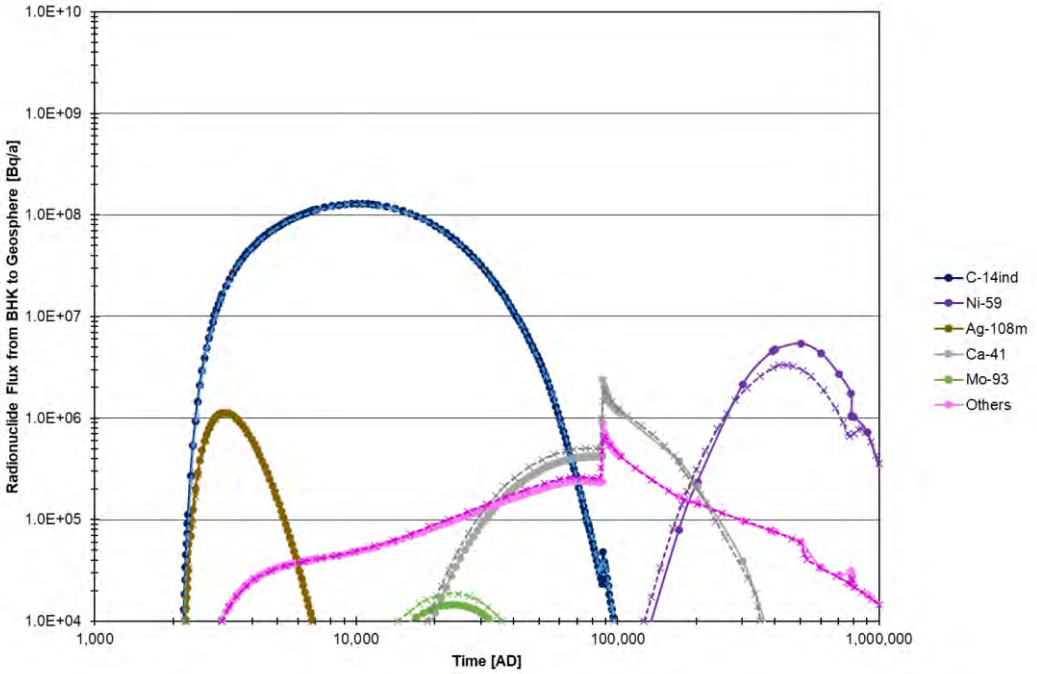

Figure 48: Effect of Alternative Concrete in BHK assumptions on the evolution of porosity (-) and fraction of cement (-) assumed in the backfill concrete in the outflow and side directions, and the sorption coefficient for Ni in the same backfill (m^3/kg). The solid lines are the base case, and the dashed lines are the alternative grout.

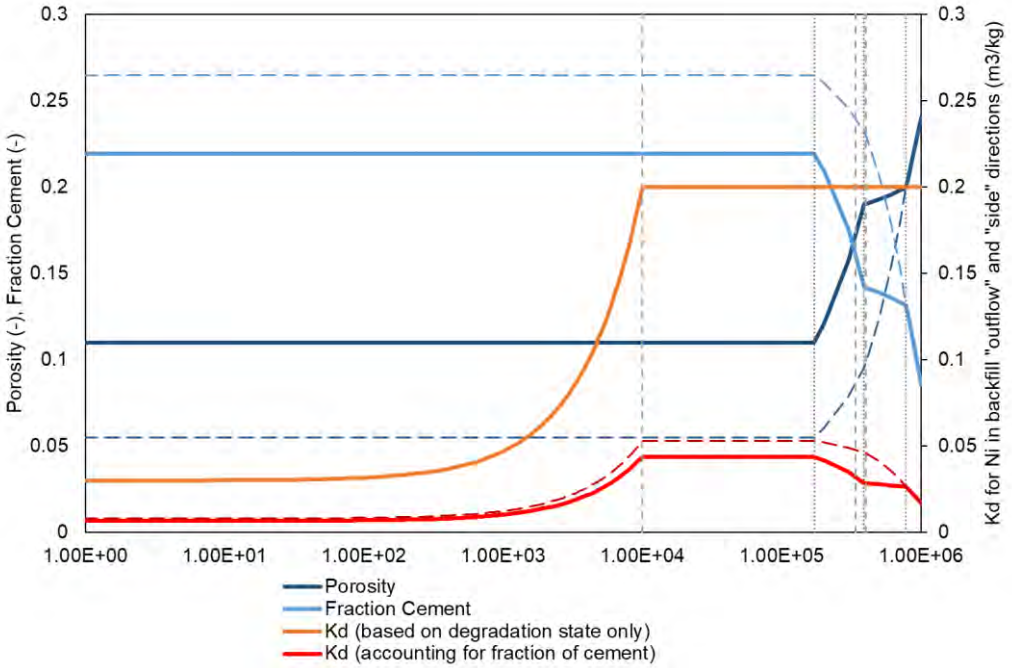

9. Review Conclusions

SKB has undertaken a large amount of work in developing SE-SFL, addressing all the major areas that would form part of a full safety assessment. This includes developing detailed understanding of site and repository conditions and their evolution, and representing the key features, events and processes in assessment models. Furthermore, SKB has identified areas where additional work would be needed for any future safety assessment. However, SE-SFL is primarily intended to help SKB develop the SFL concept and is not intended to be a full safety assessment. In particular, SKB's two main objectives for SE-SFL are:

- *"Evaluate the conditions in the waste, barriers and repository environments under which the repository concept has the potential to fulfil the regulatory requirements for post-closure safety.*
- *Provide SKB with a basis to prioritise areas in which the level of knowledge and adequacy of methods must be improved in order to perform a subsequent, full safety assessment for SFL."*

SKB has largely achieved these objectives in the context of modelling radionuclide releases from the near field. The assessment models include the main features, events and processes that are likely to be important for safety, the key assumptions have been documented, and some high-level scoping sensitivity analyses have been undertaken to understand important uncertainties. The assessment model results should help guide future site selection and safety assessment development. The results should also help SKB review and confirm the concepts for the BHA and BHK vaults, e.g. choice of bentonite backfill for the BHA vault in preference to concrete backfill. We recommend that future steps in the concept development process should evaluate a wider range of more specific uncertainties and sensitivities than the simple scoping sensitivity analyses that have been undertaken at this stage, e.g. sensitivity to the assumed bentonite properties.

The assessment models have been documented in detail, and we have been able to reimplement SKB's models, closely matching SKB's results. However, there is scope to improve the documentation, for example SKB's conceptual model of concrete degradation and the way the conceptual model has been implemented in the assessment models is not always clear. In some areas, we had to reimplement the models to be confident in our understanding.

There are two aspects of the near-field models which could be improved:

1. Representation of long-term degradation of the cementitious barriers, in particular the concrete backfill in the BHK vault. The repository-scale groundwater flow model, which is used to calculate flows through the vault for use in the assessment model, considers three steady state situations: intact backfill (IC), degraded outer backfill (DZC) and fully degraded backfill (DC). It would be preferable if this model could represent continuous evolution, coupled to degradation of the cementitious backfill, and the evolving backfill hydraulic properties. This need not be a full reactive transport model, but could potentially be a simpler representation, e.g. cement degradation and properties could potentially be coupled to the amount of water that has flowed through the cement (e.g. Berner, 1992).

2. The effects of localised water bearing features in the rock on backfill degradation have not been explored. Potentially localised degradation could result in poorer performance compared with the uniform backfill degradation assumed in SE-SFL.

The assessment models include many cautious assumptions. Therefore, they are likely to underestimate the performance of the repository. If SKB plan to use the models to optimise the repository design, then it would be appropriate to develop the models further so they have more realistic assumptions, as multiple cautious assumptions can significantly affect the model results and mask the effects of design changes. For example, limited credit is given to the grout and concrete structure of the caissons in retarding radionuclide transport. Cautious assumptions can also result in the engineering performance requirements being more stringent than necessary. The calculated engineering requirements may be difficult to achieve, with corresponding implications for cost.

In SE-SFL, SKB assume the bentonite buffer in the BHA vault does not degrade. They have undertaken some simple scoping assessments in support of this, and highlight that further work is required to examine these processes and a wider range of phenomena. This would be an important part of developing a future safety assessment as robust evidence would be needed to build confidence the bentonite backfill would not degrade over the 1,000,000 y assessment timeframe. This includes looking at the potential for heterogeneous resaturation and localised physicochemical degradation where the backfill is in contact with water bearing features in the rock.

SSM identified four main issues to be considered in this review. The conclusions for each issue are presented below.

The soundness of the conceptual models in reasonably representing the design concept of the repository and the expected evolution of the engineered barriers with time.

SKB's conceptual models reasonably represent the design concept of the repository and the expected evolution of the repository with time. However, as noted above, a potentially important issue that has not been explored is the effects of water bearing features in the rock on localised backfill degradation. Potentially this could be important for the overall vault performance. It may not be possible to optimise the repository layout to avoid such features, so it is important that their potential impacts are understood.

The conditions in the geosphere are an important factor for the longevity and performance of the near-field barriers. SKB decided to base the properties of the geosphere on a real site to ensure all the geological and hydrogeological data are consistent and are representative of a site that may be suitable to host the SFL facility. SKB reviewed the information collected by its site investigation programme for the Spent Fuel Repository and extension to SFR. They decided to base the geosphere on a volume of rock at the Laxemar site that was considered suitable to host the spent fuel repository.

The geosphere at Laxemar has less favourable conditions than most of the other candidate sites for the spent fuel repository, and the assessment calculations are based on one of the less favourable realisations of hydrogeological modelling. This suggests the assumed conditions are cautious. However, the information we have reviewed does not discuss whether the sites studied by SKB's spent fuel programme are representative of conditions

often found in Sweden, or if they are representative of a relatively small number of locations with the most favourable conditions that were potential candidates to host the spent fuel repository. If SKB's siting programme for SFL is going to include different locations to those studied by the spent fuel programme, it is difficult to judge whether it could be easy or difficult to find a site with suitable conditions.

SKB have identified a number of Features, Events and Processes that are likely to be of secondary importance, but have not been assessed, or have only been partially assessed, at this stage. This includes bulk gas generation in the BHA vault, and the potential impacts of gas on resaturation and the buffer. We note that better understanding of the generation, release and fate of bulk gasses is also needed because of the potential for advection of trace radioactive gases in bulk gas.

SKB argue against the potential for development of C-14 gas. However, there is evidence for abiotic release of $^{14}CH_4$ gas from irradiated metals as they corrode, and recent work indicates the potential for some microbial activity under the anticipated conditions in the repository. This includes localised microbial activity in niches where conditions differ from the bulk average (Wormald, 2019). Therefore, there is the potential for generation of C-14 gas in both vaults.

SKB reasonably anticipate that ISA will form from cellulosic wastes under the high pH conditions in the BHA wastes. ISA can form complexes with some radionuclides increasing their mobility. The pH needs to be above 12.5 for ISA to form (Humphreys et al., 2010). SKB assume ISA is stable in the bentonite backfill but degrades in the geosphere. The main mechanism of ISA degradation would be by microbes (Humphreys et al., 2010). The bentonite backfill should buffer the pH to ~8, which is favourable for microbial activity. However, the high swelling pressure and small pore spaces in the bentonite could limit microbial activity, and therefore limit degradation of ISA in the backfill. SKB's sensitivity analyses show that if ISA did not form then very long-term doses from the BHA vault could be significantly reduced.

It might be possible to reduce the stability of ISA in the vault by optimising the formulation of the concrete structures and grout fill using lower pH cement formulations. Although it will not be possible to reduce the pH in waste packages that have already been grouted, it may be possible to reduce the overall pH sufficiently that ISA is no longer stable. In addition, a lower pH in the waste caisson would reduce the potential for deleterious interactions at the boundary between the caisson and the bentonite backfill.

Finally, as noted above, SKB assume there is no degradation of the bentonite backfill in the BHA vault throughout the 1,000,000 y assessment timeframe. Further evidence and arguments are needed to build confidence in this conceptual model.

The correctness of the mathematical formulations and the numerical algorithms of the models.

The underpinning detailed models are important for describing the long-term evolution and performance of the engineered barriers and parameterising these aspects of the assessment models. A separate review task is examining SKB's conceptualisation and modelling of the cementitious materials, in particular concrete backfill in the BHK vault. However, as noted above, the detailed models, and therefore the assessment models,

could be improved by further developing the repository scale groundwater model to include coupled degradation of the cementitious materials.

The near-field assessment models are described in TR-19-06 and R-19-09. Standard mathematical models are used, including well established mathematical models for diffusion of radionuclides through a porous medium into a fractured medium, e.g. through porous bentonite backfill into fractured rock. However, note that this mathematical model relies on approximations of the fracture geometry and flow regime, so there are some uncertainties in the constants used.

R-19-05 is an underpinning model development report, but only some aspects of this report are used in the assessment models. R-19-05 develops models for radionuclide transport in fractured degraded concrete backfill. Degraded concrete backfill is assumed to be a porous medium in SE-SFL. However, it is not clear if there is complete consistency in the conceptualisation and treatment of the nature of the degraded concrete backfill throughout SE-SFL. In the situation where the outer backfill in the BHK vault has degraded (DZC), it is unclear if the fracture equivalent flow rate applied to diffusion from the outermost intact backfill compartment represents diffusion into degraded backfill, or directly into fractures in the rock.

The fracture models developed in R-19-05 are available if needed in the future to assess the potential performance of sites where the groundwater has sufficiently high sulphate concentrations that formation of ettringite and gypsum could lead to cracking of concrete.

The appropriateness of the way the computer models are implemented, including discretisation of the modelling domain, and handling of numerical round-off, truncation and other errors (if any).

Overall, the conceptual and mathematical models are appropriately implemented. However, there are some aspects that could potentially be improved.

- The approach used to represent the situation where the outer part of the concrete backfill in the BHK vault has degraded (DZC) is not clearly explained. It was necessary to reimplement the models to understand this. Initially the five backfill compartments represent the intact concrete backfill between the waste-domain and the vault wall. Once the outer backfill has degraded, the compartments only represent the intact inner backfill. Finally, once all the backfill has degraded, the compartments represent the degraded backfill between the waste-domain and the vault wall. Alternative approaches might provide a simpler representation of the conceptual model and more confidence in the results. SKB's approach leads to some artefacts in the model results, but these are small. It would be useful to explore alternative approaches for any future safety assessment, and / or further explain and justify the chosen approach.
- As described previously, the underpinning repository groundwater flow model considers three steady state conditions. This leads to transport parameters that combine continuous evolution with step changes at the flow transitions. If the repository flow model could be improved to represent transient evolution, coupled with degradation of the backfill, this would remove the step changes in the transport parameters.
- In the BHK vault, water flows in through the roof of the vault, and then downwards, primarily through the outer degraded concrete, and around the intact inner concrete. The assessment model does not include tangential transfers that connect

the backfill above the waste-domain to the backfill to the side of the waste domain, or the backfill to the side of the waste domain to the backfill below the waste-domain.

- Loss of ISA from the BHA vault is not included in the assessment models. An improvement could be to include loss of ISA. SKB's underpinning detailed calculations indicate it would take hundreds of thousands of years for the concentration of ISA to decrease significantly by diffusion out of the vault. Therefore, not representing loss of ISA from the BHA vault in the assessment models is only likely to result in radionuclide fluxes from the near field being overestimated in the very long-term.
- There appear to be some inconsistencies between the underpinning cement degradation modelling, the groundwater flow modelling and the assessment models. The cement degradation modelling appears to have considered a similar but different flow regime to the one implemented in the assessment models. For example, the direction of groundwater flow in the cement modelling is at right angles to that derived from the groundwater flow modelling and near-field modelling. We have not examined the underpinning models in detail as they are beyond the scope of this review, and they are being examined by a parallel review. Therefore, we have not assessed whether this difference is important. However, such differences further indicate the potential to improve the assessment of coupled flow and cement degradation.

The assessment models include a number of cautious assumptions, which will tend to underestimate the performance of the repository, e.g. little credit is taken for containment by the waste-domain. Even with a favourable geological setting and high specification barriers the peak calculated doses exceed the dose that equates to the regulatory risk criterion. This result will tend to drive SKB to consider methods of increasing the performance of the engineered barriers. This illustrates the point noted previously that care is needed to ensure the cautious assumptions do result in unnecessarily stringent engineering performance requirements.

SKB have undertaken a sensitivity analysis to examine the potential performance of an alternative concrete formulation for the performance of the BHK vault. The alternative formulation significantly improved the performance, with doses falling below the dose that equates to the regulatory risk criterion. However, we note the implementation of the sensitivity case was cautious, and therefore underestimated the performance improvement. While the case accounted for the decrease in flow through the BHK vault, it did not consider that the decrease in flow would increase the durability of the concrete. Therefore, it is likely the rate of barrier degradation was overestimated, and the performance was underestimated.

We have verified SKB's implementation of its models in the Ecolego code by re-implementing the models in a different compartment modelling code (AMBER). The calculated near-field fluxes closely match SKB's, suggesting the documentation in R-19-09 accurately describes the implementation to a large extent. No significant errors have been found. There are some small discrepancies between the re-implemented AMBER results and SKB's results which may result from ambiguities in descriptions of SKB's implementation. For example, SKB's model appears to calculate a lower amount of retention in the BHA waste domain than the re-implemented results would suggest, which may be due to ambiguity in the description of the amount of cement in the waste domain. In this and

most other areas where there are ambiguities, the results are insensitive to the associated parameters (see Section 8).

The reasonableness of SKB's modelling results, as function of both space and time.

SKB's modelling results are reasonable, explainable and consistent with their conceptual models. As noted above, we have reimplemented SKB's models and closely matched their results. On initial inspection, the fluxes of radionuclides that are poorly sorbed increase surprisingly quickly post-closure. The reimplemented models give the same behaviour, and the results of some scoping analytical calculations confirm that fluxes of radionuclides that are poorly sorbed could increase quickly post-closure.

There are some artefacts in SKB's model results (e.g. small spikes in the calculated fluxes of radionuclides from the near field caused by changes to the BHK vault backfill diffusion length between the IC and DZC cases, and the DZC and DC cases), and these are reproduced by the reimplemented models. These can be explained and do not seem to be significant for overall performance. We have compared the containment performance provided by SFL against the performance provided by SFR. Consistent with expectations, SFL provides significantly better containment of radionuclides than SFR, even though the assessment models include a number of cautious assumptions.

10. Acknowledgement

The authors are indebted to Sarah Watson at Quintessa for the review of the report with many helpful comments and suggestions.

11. References

Abarca E, Sampietro D, Molinero J, von Schenck H. 2019. Modelling of the Near-field Hydrogeology – Temperate Climate Conditions. SKB R-19-03.

Berner UR. 1992. Evolution of pore water chemistry during degradation of cement in a radioactive waste repository environment. Waste Management, Vol 12, pp.201-219.

Elfwing M, Evins L Z, Gontier M, Grahm P, Mårtensson P, Tunbrant S. 2013. SFL concept study. Main report. SKB TR-13-14, Svensk Kärnbränslehantering AB.

Fetter, C W. 1994. Applied Hydrogeology. Third Edition. Prentice Hall.

Gelhar LW, Welty C, Rehfeldt KR. 1992. A critical review of data on field- scale dispersion in aquifers. Water Resources Research 28, 1955–1974.

Herschend B, 2014. Long-lived intermediate level waste from Swedish nuclear power plants. Reference inventory. SKB R-13-17, Svensk Kärnbränslehantering AB.

Herschend B, 2016. Initial state SFL. SKBdoc 1441724 ver 1.0, Svensk Kärnbränslehantering AB. Internal document.

Humphreys P, Laws N, Dawson J. 2010. A Review of Cellulose Degradation and the Fate of Degradation Products under Repository Conditions. SERCO/TAS/002274/001, Issue 2.

IAEA. 2004. Improvement of Safety Assessment Methodologies for Near Surface Disposal Facilities. Volume I: Review and Enhancement of Safety Assessment Approaches and Tools. IAEA-ISAM-1. International Atomic Energy Agency, Vienna, Austria.

Idiart A, Laviña M, 2019. Modelling of concrete degradation in a one-million-year perspective – Hydro-chemical processes. Report for the safety evaluation SE-SFL. SKB R-19-13, Svensk Kärnbränslehantering AB.

Idiart A, Laviña M, Coene E. 2019a. Modelling of concrete degradation – Hydro-chemo-mechanical processes. Report for the safety evaluation SE-SFL. SKB R-19-12, Svensk Kärnbränslehantering AB.

Idiart A, Olmeda J, Laviña M. 2019b. Modelling of concrete degradation – Influence of concrete mix design. Report for the safety evaluation SE-SFL. SKB R-19-14, Svensk Kärnbränslehantering AB.

Kalinowski B (ed). 2009. Background complementary hydrogeochemical studies. Site descriptive modelling SDM-Site Laxemar. SKB R-08-111, Svensk Kärnbränslehantering AB.

Neretnieks I, Liu L, Moreno L. 2010. Mass transfer between waste canister and water seeping in rock fractures: Revisiting the Q-equivalent model. SKB TR-10-42, Svensk Kärnbränslehantering AB.

Ochs M, Talerico C. 2004. SR-Can. Data and uncertainty assessment. Migration parameters for the bentonite buffer in the KBS-3 concept. SKB TR-04-18, Svensk Kärnbränslehantering AB.

Quintessa. 2019. AMBER 6.4 User Guide. QPUB-AMBER-2, Quintessa Limited.

Quintessa. 2020. GraphGrabber 2.0.2 User Guide. QRS-4007AT7-1-UG, Version 2.0.2.

Rhén I and Hartley L. 2009. Bedrock hydrology Laxemar. Site descriptive modelling SDM-Site Laxemar. SKB R-08-92, Svensk Kärnbränslehantering AB.

Radioactive Waste Management (RWM). 2016. Geological Disposal. Gas Status Report. NDA Report no. DSSC/455/01.

Shahkarami P. 2019. Input data report for near-field and geosphere radionuclide transport modelling. Report for the safety evaluation SE-SFL. SKB R-19-09, Svensk Kärnbränslehantering AB.

SKB. 1993. Plan 93. Costs for management of the radioactive waste from nuclear power production. SKB TR 93-28, Svensk Kärnbränslehantering AB.

SKB. 1999. Deep repository for long-lived low- and intermediate-level waste. Preliminary safety assessment. SKB TR-99-28, Svensk Kärnbränslehantering AB.

SKB, 2010. Data report for the safety assessment SR-Site. SKB TR-10-52, Svensk Kärnbränslehantering AB.

SKB, 2014. Data report for the safety assessment SR-PSU. SKB TR-14-10, Svensk Kärnbränslehantering AB.

SKB. 2015. Safety analysis for SFR Long-term safety. Main report for the safety assessment SR-PSU. Revised edition. SKB TR-14-01, Svensk Kärnbränslehantering AB

SKB. 2019a. Post-closure safety for a proposed repository concept for SFL. Main report for the safety evaluation SE-SFL. SKB TR-19-01, Svensk Kärnbränslehantering AB.

SKB. 2019b. Radionuclide transport and dose calculations for the safety evaluation SE-SFL. SKB TR-19-06, Svensk Kärnbränslehantering AB.

SKB. 2019c. Initial state for the repository for the safety evaluation SE-SFL. SKB TR-19-03, Svensk Kärnbränslehantering AB.

SKB. 2019d. Biosphere synthesis for the safety evaluation SE-SFL. SKB TR-19-05, Svensk Kärnbränslehantering AB.

Swanton SW, Baston GMN and Smart NR. 2018. Review of Steel Corrosion and Carbon-14 Release from Irradiated Steels – State of the Art Review. Amec Foster Wheeler report to RWM, AMEC/201265/001 Issue 5.

Towler G and Penfold J. 2017. SR-PSU Main Review Phase: Radionuclide Transport Modelling. In SSM's external experts' review of SKB's safety assessment SR-PSU – consequence analysis: Main review phase, SSM 2017:30.

Wessely O, Shahkarami P. 2019. Radionuclide transport and dose calculations for the safety evaluation SE-SFL. SKB R-19-05, Svensk Kärnbränslehantering AB.

Wiborgh M (ed). 1995. Prestudy of final disposal of long-lived low and intermediate level waste. SKB TR-95-03, Svensk Kärnbränslehantering AB.

Wormald R. 2019. Environmental Limits of Methanogenesis and Sulphate Reduction. Doctoral Thesis, University of Huddersfield. http://eprints.hud.ac.uk/id/eprint/35063/

Appendix 1. Coverage of Reviewed Reports

SKB Report Number	Coverage
TR-19-01	Chapters 4 and 7 reviewed in full. Other chapters reviewed as required.
TR-19-06	Chapter 4.3 reviewed in full. Other chapters reviewed as required.
R-19-05	All chapters reviewed in full. Appendices briefly consulted.
R-19-09	All Chapters.
Other	Specific information as recorded in this review report.

Strål
säkerhets
myndigheten
Swedish Radiation Safety Authority

Authors: Walke R.C., Towler G.H., Newson R.K and Penfold J.S.S.
Quintessa Limited, Henley on Thames, UK

2021:13

4) Review of SE-SFL – Biosphere dose assessment

Date: May 2021
Report number: 2021:13 **ISSN:** 2000-0456
Available at www.stralsakerhetsmyndigheten.se

Authors: Walke R.C., Towler G.H., Newson R.K and Penfold J.S.S.
Quintessa Limited, Henley on Thames, UK

4) Review of SE-SFL – Biosphere dose assessment

Activity number: 3034111-02
Registration number: SSM2020-5391
Contact person at SSM: Maria Nordén

Content

1. Introduction

In Sweden long-lived low- and intermediate level radioactive waste is planned to be disposed in a repository (SFL) in the Swedish crystalline bedrock at a depth around 500 m. The waste contains mainly the long-lived wastes from the operation and decommissioning of the Swedish nuclear reactor plants, as well as the long-lived wastes from early research in the Swedish nuclear program (legacy wastes), from medicine, industry and research including the European Spallation Source (ESS) research facility. The disposal concept for the SFL repository has been developed by SKB since the 1980s. A pre-study of the concept has been carried out (SKB TR-95-03) and a preliminary safety analysis (SKB TR-99-28) was previously published. The recently published safety evaluation of the SFL repository (SE-SFL, SKB TR-19-01) is a continuation of this conceptual development with the purpose of providing input to consecutive steps in the development of the repository. The focus of SE-SFL is on a few sections of the Swedish Radiation Safety Authority's (SSM) regulations on post-closure safety, the risk criterion and requirements for post-closure barrier robustness.

SSM have contracted independent experts to support their review and understanding of SKB's recent safety evaluation in several topic areas. This report describes the findings of Quintessa Ltd's review of the topic area "biosphere dose assessment".

1.1. Objectives and scope

The review includes an assessment of the overall quality of SKB's documentation for the biosphere component of the SE-SFL study. The main issues identified by SSM for the topic area "biosphere dose assessment" are:

- consideration whether the dose assessment methodology applied in SE-SFL as a whole is appropriate and sufficient for its purpose, with a specific focus on SKB's methodology for defining biosphere objects;
- consideration whether the approach of landscape models and surface hydrological modelling used by SKB are appropriate and sufficient for its purpose, with a specific focus on assessing differences in accumulation of radionuclides depending on the size of the biosphere object; and
- consideration whether SKB's parameter derivation is appropriate and sufficient for its purpose.

The biosphere model as employed in SE-SFL is a development of that used in the safety assessment SR-PSU (SKB, 2015) for the expansion of the facility for disposal of low- and intermediate level radioactive waste, SFR. Therefore, the review includes an evaluation of the development of the methodology in SE-SFL by comparing it to the methodology used in SR-PSU, with specific regards to comments raised by SSM and its external experts during the review of the license application for the expansion of SFR.

The review focusses on the following SKB reports:

- the Main Report (SKB TR-19-01);
- the Biosphere Synthesis report (SKB TR-19-05);
- the Radionuclide Transport and Dose report (SKB TR-19-06); and
- the Biosphere Parameters report (SKB R-19-18).

Additional SKB reports and other publications have been consulted, as required.

1.2. Review approach and report structure

The review has been conducted through detailed review of the Main Report and the Biosphere Synthesis report, along with reference to supporting documentation, notably the Radionuclide Transport and Dose report, and the Biosphere Parameters report.

The approach to the review is reflected in the structure of the report:

- the context for the assessment is discussed in Section 2, along with review of the way in which uncertainty about the evolution of the biosphere is reflected in the evaluation cases considered by SKB;
- SKB's approach to identifying and characterising biosphere objects, including hydrogeological interpretation, and selection of potential exposure groups (PEGs) is reviewed in Section 3;
- the radionuclide transport and exposure modelling is considered in Section 4;
- SKB's approach to parameter uncertainty and derivation of key parameters are reviewed in Section 5; and
- The report concludes with overall discussion in Section 6.

References are provided in Section 7.

Coverage of the SE-SFL reports is summarised in Appendix 1 and a summary of review findings relating to previous biosphere modelling undertaken by SKB is provided in Appendix 2.

Developments in SKB's approach to representing the biosphere since the SR-PSU assessment have been of particular interest. Previous feedback from SSM and its external experts on the biosphere components of the SR-Site and SR-PSU assessments was collated as input to the review and is summarised in Appendix 2.

Note that SKB reports are typically referenced by Technical Report (TR) or Report (R) number.

2. Context, methodology and evaluation cases

The context for the SE-SFL is summarised and reflected upon in Section 2.1. SKB's overall methodology for biosphere assessment is then discussed in Section 2.2. SKB's selection of the evaluation cases included in the assessment is then discussed in Section 2.3.

2.1. Assessment context

SKB have been developing concepts for deep geological disposal of long-lived low- and intermediate-level radioactive waste. At present, no specific disposal site has been selected. A concept based on steel tanks and a high-pH concrete backfill has been developed for metallic wastes from nuclear power plants (the BHK vault) and a concept based on bentonite clay backfill has been developed for other long-lived low- and intermediate-level radioactive waste (the BHA vault). A main purpose of the SE-SFL study is to evaluate *the potential for the proposed repository concepts to meet applicable criteria on radiation protection after closure*. It is targeted towards understanding the radiological hazards associated with the wastes and with development of associated disposal concepts; it is explicitly not part of a licence application. As such, there is no intention in SE-SFL to evaluate regulatory compliance in full. Assessment of compliance with full regulatory requirements is not therefore part of the expert review.

SSM's regulations (2008) require that a repository should be designed so that the annual risk of harmful effects to humans after closure does not exceed 10^{-6} for a representative individual in the group exposed to the greatest risk. This equates to an annual dose of 14 μSv for scenarios that have a probability of occurring of one, and has been taken by SKB to be the main radiation protection criterion for the assessment. If the exposed group only consists of a few individuals, then guidance to the regulations indicates that a risk criterion of 10^{-5} per year can be considered, explicitly referring in this context to the example where drinking water from a drilled well is the dominant exposure pathway.

In a proof-of-concept type study, focus on assessing potential doses to humans as the primary protection objective is entirely justified by reference to calculated doses for humans and non-human biota relative to their associated dose criteria in previous assessments, including SR-PSU (TR-14-09). SKB acknowledge that future assessments for SFL that aim to demonstrate full compliance with regulatory criteria will need to include explicit assessment of doses to non-human biota.

SKB's representation of the biosphere in SE-SFL represents a further iteration of the approach developed notably through the SR-Site assessment for a deep geological repository for spent nuclear fuel at Forsmark (TR-11-01) and, subsequently, the SR-PSU assessment for a shallow geological repository for short-lived and low-level radioactive waste, also at Forsmark (TR-14-01). Those assessments draw extensively on information drawn from detailed site characterisation and associated interpretative modelling. That extensive information, coupled with potential radionuclide releases to a surface environment subject to post-glacial uplift and associated transition from a marine, coastal through to fully terrestrial setting, has resulted in a relatively complex approach to model-

ling the biosphere. The Biosphere Synthesis report for SE-SFL runs to 275 pages and references a range of further, more detailed reports for providing a full description of the approach.

SKB's approach to representing the biosphere in SE-SFL is, therefore, rather complicated for a proof-of-concept type study. Nonetheless, SKB is able to draw on the understanding developed through its previous related assessments to help inform the potential for the SE-SFL concept to meet regulatory requirements, and to help identify important radionuclides, and associated transport and exposure pathways.

SKB have used the SE-SFL assessment as an opportunity to explore potential further developments in its approach to representing the biosphere in post-closure assessments. As such, the biosphere component represents a hybrid between a formal assessment and a research study. The documentation includes extensive analysis of uncertainties, processes and pathways. The regulatory review provides an early opportunity for SSM to understand and comment on SKBs plans for developments in its approach to representing the biosphere in future formal licence applications.

SKB have taken the opportunity to base the SE-SFL assessment on a hypothetical location for the repository at the Laxemar site, which was extensively characterised ahead of the SR-Site assessment as a potential location for the proposed spent fuel repository. This allows SKB to draw on extensive understanding of a real site in support of a generic assessment. This helps to build confidence in the internal consistency of the system description and its overall evolution.

Previous studies have shown that it can be difficult to develop coherent and internally consistent descriptions of a completely generic environment; this was demonstrated in the context of a generic post-closure biosphere assessment in Birkinshaw et al. (2005). Use of data characterising a specific site helps to avoid such uncertainties, but at the potential cost of constraining the conditions for which the assessment is valid. To help mitigate this cost in SE-SFL, SKB explore potential consequences of radionuclide releases to regions of the biosphere with a variety of characteristics, representative of environments encountered at both Laxemar and Forsmark. They also explore potential consequences of different regional climate.

2.2. Methodology

SKB's approach to representing the biosphere sits as an integral part within the overall SE-SFL assessment methodology. Consideration of the biosphere is needed both in terms of defining boundary conditions for the overall disposal system, as well as in providing a key metric of performance and long-term protection of human health and the environment. SKB's overall approach to the SE-SFL study reflects its experience developed through previous post-closure safety assessments, as well as understanding drawn from safety assessment studies in other countries and international guidance, notably the Nucear Energy Agency (NEA) MeSA guidance (NEA, 2012). In support of its approach to consideration of the biosphere, SKB references recent international collaborative work on enhancing the International Atomic Energy Agency (IAEA) BIOMASS methodology (Lindborg, 2018). Indeed, experience of moving to site-specific studies in Sweden in the context of biosphere assessment for geological disposal of radioactive waste has helped shape the development of international guidance through, for example, placing greater

emphasis on the iterative nature of assessments and the central role played by site understanding. The degree of interaction between different national programmes and developing international guidance is well described and acknowledged in Section 2.1 of the Biosphere Synthesis report.

SKB's approach to the biosphere is reflected in the structure of the Biosphere Synthesis report.

- The Biosphere Synthesis report starts out by describing the overall context and methodology (Section 2).
- The Laxemar site is then described (Section 3), along with its expected future development (Section 4).
- Sub-catchment areas of greatest interest for potential radionuclide releases to the surface (termed biosphere 'objects') are then identified (Section 5).
- The screening of features, events and processes (FEPs) of relevance is then presented, along with an analysis potential exposure pathways and identification of distinct PEGs (Section 6).
- The biosphere objects are then described in the context of each of the evaluation cases (Section 7).
- The model for evaluation radionuclide transport and exposure (termed BioTEx) is then presented, with reference back to the SR-PSU approach that forms the basis of BioTEx (Section 8).
- Notable developments in the biosphere modelling approach since the SR-PSU assessment are then described (Section 9).
- Parameterisation of the biosphere for the SE-SFL assessment is then summarised (Section 10), with reference to the supporting Biosphere Data report.
- Analysis of the main present-day evaluation case is then presented (Section 11), along with analysis of other evaluation (Section 12) and sensitivity cases (Section 13).
- Supporting reviews of the behaviour of key elements in the biosphere are summarised (Section 14), as is supporting, more detailed, modelling of radionuclide behaviour within individual biosphere objects (Section 15).
- The Biosphere Synthesis report concludes with discussion of the results and findings in the specific context of the uncertainties inherent in assessing the biosphere on extremely long time scales (Section 16) and a final summary (Section 17).

SKB's methodology is logical and can be broadly mapped onto the phases of the enhanced BIOMASS methodology, as illustrated in Figure 1.

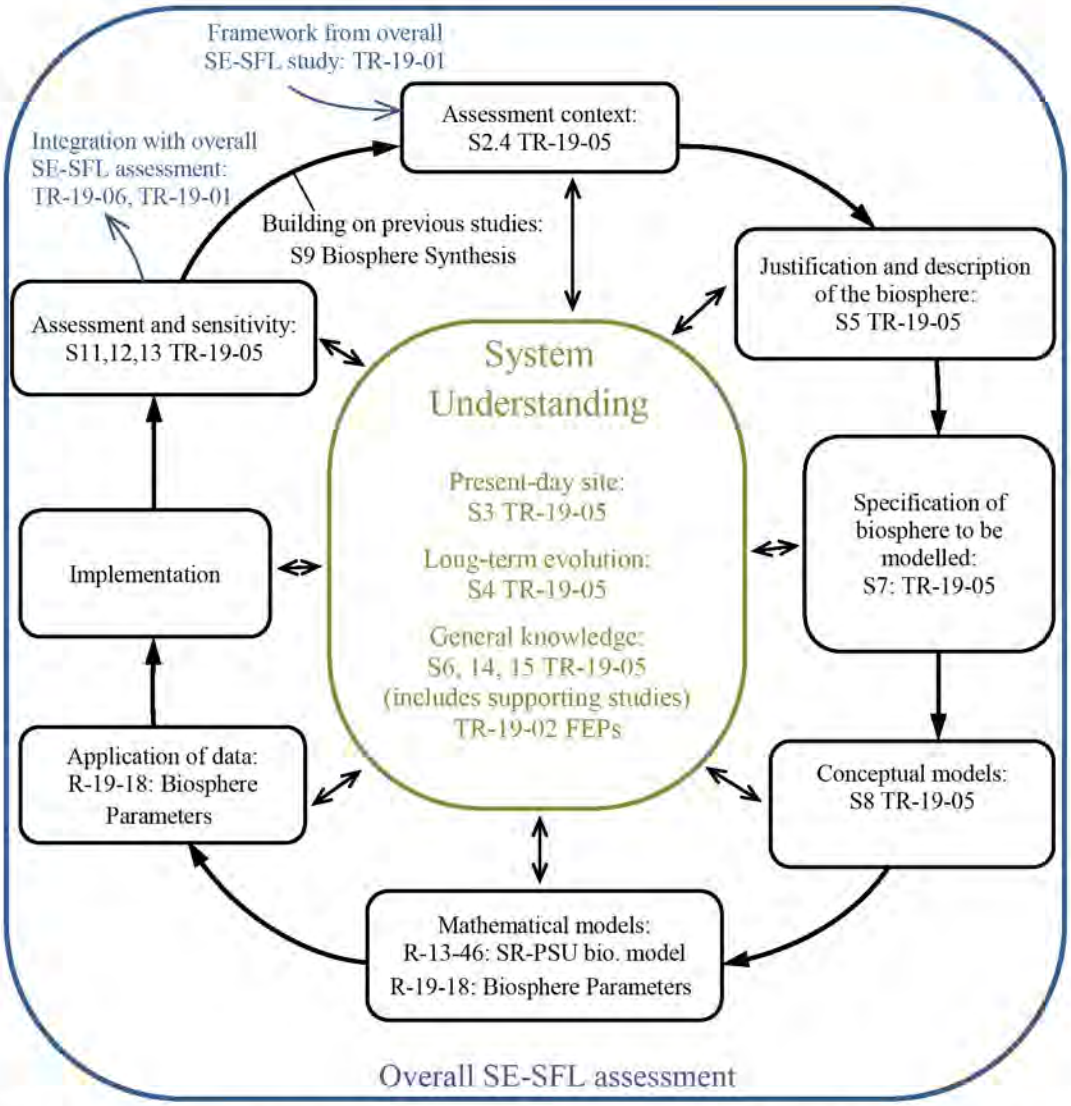

Figure 1: Mapping of SE-SFL biosphere methodology to the enhanced BIOMASS guidance (the latter based on Lindborg (2018)). Note that specific sections in the SKB reports are identified by "S" (e.g. "S2.4 TR-19-05" refers to Section 2.4 of TR-19-05).

2.3. Evaluation cases

It is notable that the title of Section 6 of the Biosphere Synthesis report implies that it includes a description of the SE-SFL evaluation cases. However, this description is missing from Section 6 and the evaluation cases are in fact introduced earlier in Section 2.4 instead, with reference back to the Main Report. It is helpful to present the evaluation cases in the broader context of the overall assessment, so their introduction in Section 2.4 of the Biosphere Synthesis report is well placed.

In the Main Report, SKB describe the *reference evolution* for the overall disposal system, including three *variants*:

- a base variant of the reference evolution;
- an increased greenhouse effect variant of the reference evolution; and

- a simplified glacial cycle variant of the reference evolution.

There is, therefore, no single *reference evolution*. The base variant assumes constant present-day conditions. This is acknowledged by SKB as being unrealistic, but has been selected for the proof-of-concept level study as a baseline for comparison. The increased greenhouse effect variant is based on the Intergovernmental Panel on Climate Change (IPCC) emission scenario RCP4.5. RCP4.5 represents an intermediate level of radiative forcing due to greenhouse gas emissions. Further information is given in the Climate Report for SE-SFL (TR-19-04), which has not been reviewed in detail in the present report.

It is noted that SKB and Posiva have been undertaking research to update long-term global climate modelling and associated downscaling (Lord et al., 2019a,b). The SKB and Posiva study built on long-term climate modelling undertaken as input to Working Group 6 (WG6) of the IAEA's collaborative programme on Modelling and Data for Radiological Impact Assessments (MODARIA; IAEA, 2020)[1]. These studies are referenced in the climate report (SKB, 2020) supporting the next iteration of safety assessment studies for a spent fuel repository at Forsmark (the Preliminary Safety Assessment Report, PSAR), but are not referenced in the SE-SFL Climate Report. For SE-SFL, the simplified glacial cycle is instead based on a reconstruction of the Weichselian glacial cycle, consistent with the approach adopted in the SR-Site assessment. Developments in understanding climate on long timeframes is recognised by SKB as an issue for review in future assessments in the executive summary to the SE-SFL Main Report.

To help distinguish the proof-of-concept level SE-SFL study from a formal assessment in support of a licence application, SKB have used the term *evaluation cases* to describe the cases carried through to quantitative assessment, distinct from formal scenarios envisaged in regulatory requirements. The SE-SFL evaluation cases are listed in Figure 2, which also identifies those that explore specific uncertainties associated with the biosphere. These evaluation cases are conveniently summarised in Table 8-1 of the Main Report, and those relating to biosphere conditions are also summarised in Table 7-1 of the Biosphere Synthesis report (reproduced as Table 1).

[1] The MODARIA WG6 work was undertaken on behalf of the UK geological disposal programme (Lord et al., 2015; 2017).

Table 1: Summary of the biosphere cases evaluated in SE-SFL (Table 7-1 of the Biosphere Synthesis report)

Table 7-1. Short description of biosphere conditions in SE-SFL evaluation cases. Biosphere object refers to the area where the release was discharged to the surface, Ecosystem to the state or states of the area during the simulation and Hydrology indicates if groundwater flows have been modified in the calculations (as compared with the *present-day* evaluation case). Succession indicates whether the ecosystems states were modelled in sequence (if not, ecosystem properties are time-independent). Abbreviations of potentially exposed groups are the same as in Table 6-2. Lx and Fm refers to Laxemar and Forsmark, respectively. Note that most ecosystem parameter values were the same in all evaluation cases (e.g. K_d and *CR* values). However, some ecosystem parameters were adjusted for a warmer climate (1) and some were adjusted for colder conditions (2) (see text for details).

Evaluation case	Short description	Geosphere release	Biosphere object	Ecosystem	Hydrology	Succession	Pot. exp.group
Present-day	Present-day conditions	Base case	206	Mire, Agri	Present day	No	HG, IO, DM, GP
Alternative discharge area							
Without landscape development	Effects of ecosystem type, and object properties	Base case	Nine in Lx, Six in Fm	Sea, Lake, Mire, Agri	Present day (object specific)	No	HG, IO, DM, GP
With landscape development	Effects of relative sea-level change and succession	Base case	Three in Lx, Six in Fm	Sea, Lake, Mire	Function of sea depth (object specific)	Yes	HG, IO, DM, GP
Increased greenhouse effect	Effects of global warmingand irrigation	Base case	206	Mire[1], Agri[1]	Global warming ± irrigation	No	HG, IO, DM, GP
Alternative regional climate	Effects of different regional climate	Base case	206	Mire, Agri	Regional variation	No	HG, IO, DM, GP
Initially submerged conditions	Effects of initially submerged conditions	Function of sea depth	206	Sea, Lake, Mire	Function of sea depth	Yes	HG, IO, DM, GP
Simplified glacial cycle	Effects of permafrost and passage of inland ice	Function of ice-front and sea depth	206, 207, 201	Sea, Lake[2], Mire[2]	Talik, function of ice-front and sea depth	Yes	HG, IO, DM, GP
Drilled well	Drilled well for drinking and small-scale irrigation	Base case	geosphere well	Kitchen garden	Present day Lx	No	GP

In addition to the evaluation cases, the Biosphere Synthesis report examines three further *sensitivity cases*:

- an *aged soil* case that explores potential implications of radionuclide releases to aged agricultural soils;
- an *alternative K_d and CR values* case that explore results if a generic, rather than site-specific, soil sorption (K_d) and soil-to-plant uptake (CR) dataset is used; and
- a case that explores sensitivities relating to a new method for interpolating *groundwater flow* characteristics for use in the assessment model.

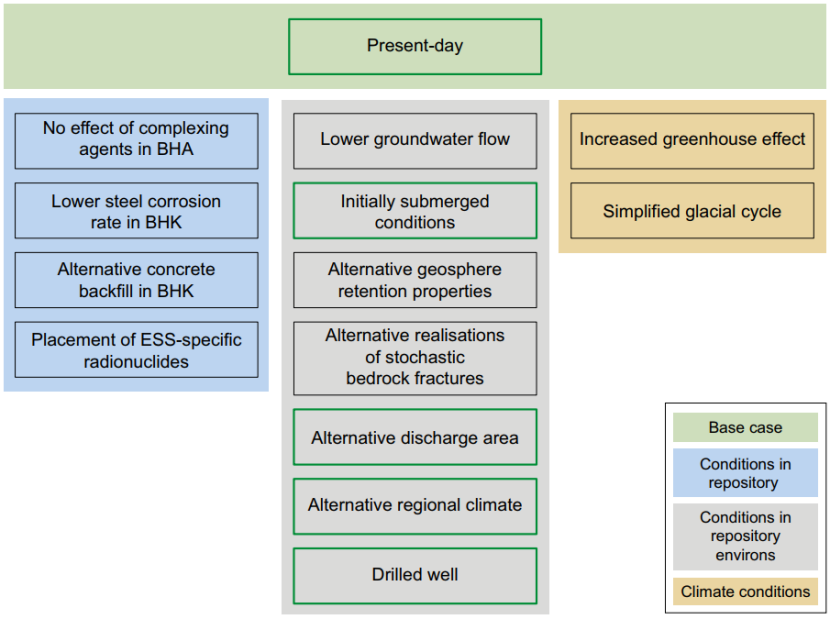

Figure 2: Evaluation cases included in SE-SFL; alternative cases motivated by consideration of uncertainties associated with biosphere conditions and explored in the Biosphere Synthesis report are outlined in green. Based on Figure 2-5 of the Biosphere Synthesis report, but with the alternative climate cases also highlighted, since results for those cases are also presented in the Biosphere Synthesis report.

Some review observations concerning the evaluation cases are provided below.

The *simplified glacial cycle*, *increased greenhouse effect* and *alternative regional climate* evaluation cases all included variation in climate that affected groundwater recharge. The effect on groundwater flows in the biosphere model are explicitly represented in SE-SFL, however, the effect on groundwater flows at the repository depth and between the repository and near-surface are not explicitly represented. This is somewhat surprising, given the importance of groundwater flow in transporting radionuclides to the biosphere and the emphasis that is placed on an integrated approach to the overall assessment. It adds to the qualitative uncertainty that needs to be borne in mind when evaluating the validity of the results for these cases.

Groundwater flows at depth were varied in the *initially submerged conditions* case, as illustrated by the scaling factor in Figure 12-15 of the Biosphere Synthesis report.

The location of groundwater discharges from depth to the biosphere changes through the course of the simplified glacial cycles, reflecting the presence or absence of permafrost, ice sheets and submerged conditions. This pattern is nicely summarised in Figure 7-6 of the Biosphere Synthesis report.

3. Biosphere objects and exposure

SKB's approach for identifying biosphere objects is reviewed in Section 3.1. The hydrogeological interpretation of biosphere objects is then explored in Section 3.2. Exposure assumptions are reviewed in Section 3.3. Finally, SKB's approach to considering groundwater wells is reviewed in Section 3.4.

3.1. Identification of biosphere objects

SKB have developed regional groundwater flow models for both the Laxemar site and the Forsmark site. SKB have used the groundwater flow models for Laxemar and Forsmark to undertake particle tracking calculations. The results of the particle tracking calculations reveal potential groundwater flow and contaminant transport pathways from an assumed repository location to the biosphere. For both Laxemar and Forsmark, the particle tracking results indicate that radionuclides released from the repository would be transported in groundwater which eventually discharges to the topographically low-lying areas in the landscape.

Section 5.1 of the Biosphere Synthesis report defines a biosphere object as:
"an area that potentially, at any time during the considered assessment period, could receive a discharge of radionuclide-containing groundwater associated with the repository".

Section 7.3.4 of the Main Report notes that biosphere objects are delimited as being:
"geographically bounded so as to represent clearly defined ecosystems with reasonably homogenous properties".

SKB used a two-step process to identify potential biosphere objects at Laxemar:

1. Identification of biosphere objects across the whole Laxemar area, based on the locations of groundwater discharge.
2. Identification of biosphere objects using particle tracking from an assumed repository location within the Laxemar area.

Note that the biosphere objects identified using particle tracking from an assumed repository location within the Laxemar area are a sub-set of the biosphere objects across the broader area. Once the objects had been identified, the object boundaries were defined; mainly based on the present landscape and site conditions. The present-day landscape and land use will be influenced by the hydrogeological conditions, but the boundaries of the biosphere objects may not exactly align with the area of deep groundwater discharge.

In SE-SFL, SKB have used a specific biosphere object, identified using particle tracking (i.e. biosphere object 206), as a basis for assessment of potential doses, and to explore sensitivities. However, to reflect that a specific site and location have not yet been chosen, SKB have also undertaken sensitivity analyses using all the biosphere objects identified from the wider Laxemar landscape, plus the biosphere objects from Forsmark considered in the SR-PSU assessment (SKB, 2015). This approach means that a variety of biosphere objects and associated characteristics are considered in SE-SFL. This is a good

approach, consistent with the current stage of development of the SFL concept. However, it would be useful for SKB to comment on whether there could be additional ecosystems that have not been explored at this stage, but which might become relevant if a location is chosen for SFL that has significantly different characteristics to Laxemar and Forsmark, e.g. an inland location.

The following further describes and discusses SKB's approach to identifying biosphere objects at Laxemar, then the range of biosphere objects considered in SE-SFL is discussed.

3.1.1. Identification of biosphere objects across the whole Laxemar area

Groundwater discharge areas across the whole of the Laxemar area were identified using a regional hydrological model, developed using MIKE SHE software. The MIKE SHE model has not been reviewed as part of this work, but we note it is related to the regional groundwater flow model, developed using ConnectFlow software, that is referred to in Section 3.1.2, below. Three different realisations of the stochastic bedrock fracture network model used in the regional groundwater flow (ConnectFlow) model were fed into the regional hydrological (MIKE SHE) model, with one realisation giving a more favourable model calibration (see Section 2.2.2 in Bosson et al., 2009).

Section 5.2.1 of the Biosphere Synthesis report explains how the groundwater flow field calculated by MIKE SHE was used for particle tracking calculations. Particles were released uniformly across the base of the model. They were found to discharge to the topographic lows (exemplified by the presence of streams and lakes) and the coast (Figure 3). Two studies have been undertaken using the Laxemar MIKE SHE model, with similar results.

Nine discharge areas, containing four different ecosystem types were selected for further consideration. Five of the discharge areas are located in valley bottoms. At present, the valley bottoms are predominantly used for agriculture, therefore five of the biosphere objects are associated with agriculture.

A range of factors are considered when defining the boundaries of each biosphere object, associated with each discharge location. Section 5.2.2 of the Biosphere Synthesis report notes that the approach is the same as that used in SKB's previous safety assessments, and provides a summary of the factors considered: "*biosphere objects were outlined based on topography to represent clearly defined ecosystems, reflecting reasonably homogenous biotic properties (e.g. type of vegetation, and rates of primary production and decomposition) and abiotic characteristics (e.g. regolith stratification and groundwater hydrology)*".

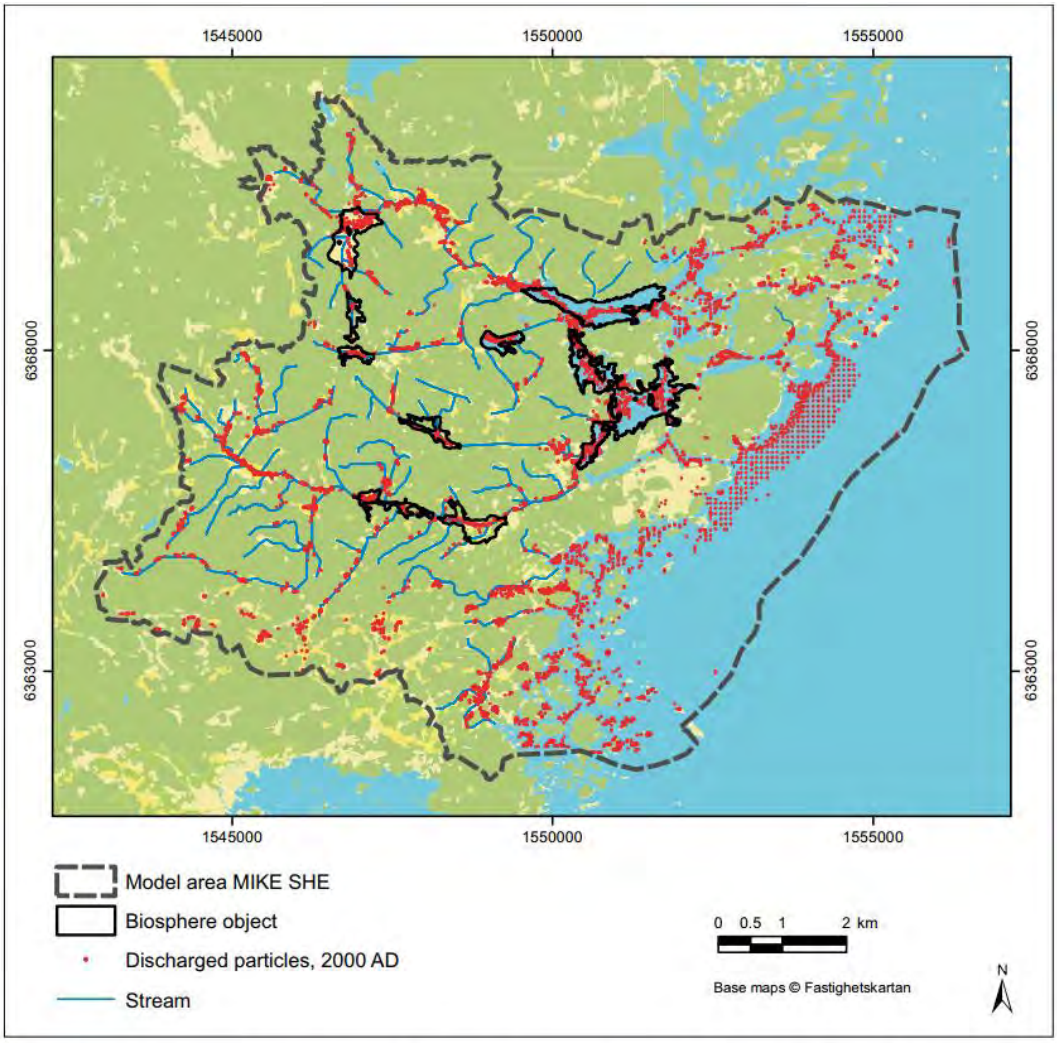

Figure 5-1. *The location at the surface of discharge particles released at a depth of 150 m below sea level in the bedrock. The MIKE SHE simulation was run for 5 000 years using present conditions (2000 AD). Redrawn from Sassner et al. (2011). The selected biosphere objects are indicated by black contour lines in the figure.*

Figure 3: Surface discharge locations calculated using MIKE SHE (after Figure 5-1 of the Biosphere Synthesis report)

To understand what this means, and the judgements SKB have made when defining the boundaries of each biosphere object, it is necessary to understand SKB's conceptual model of landscape development. Their conceptual model of landscape development is described in Section 4.3 of the Biosphere Synthesis report and is summarised as follows. Following deglaciation, the landscape is initially submerged and isostatic rebound results in relative sea-level fall and regression of the shoreline. As land 'emerges' from the sea, the conceptualised main transitions are (Figure 4):

- formation of a sea bay, with the shape of the bay controlled by the bedrock topography;
- transition into an isolated freshwater lake;
- sedimentation of the lake leading to formation of a mire;
- eventually the mire may transition into a raised bog;

- the mire or bog stage may be drained and used for agriculture, and
- the bog or abandoned agricultural land may become forested.

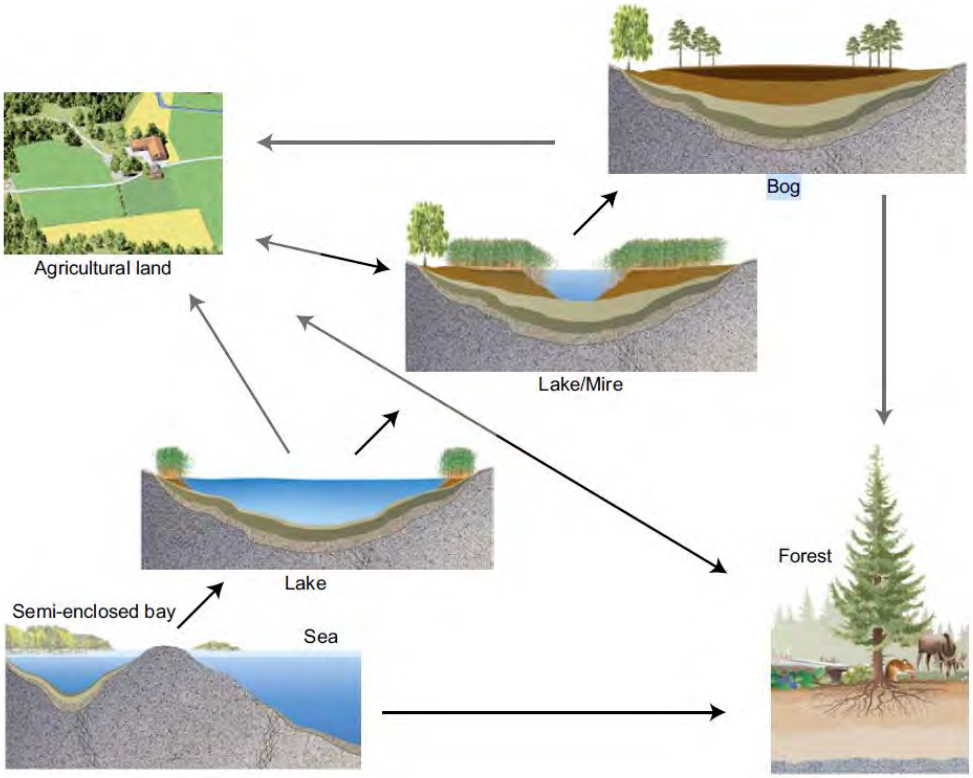

Figure 4-4. *A schematic illustration of the major ecosystems that may be found at certain points during a temporal sequence, in which the original sea bottom slowly becomes land due to relative sea-level decrease. Black arrows indicate natural succession, whereas grey arrows indicate human-induced changes to provide new agricultural land or improved forestry. Agricultural land may be abandoned and will then develop into forest or, if the hydrological conditions are suitable, into a fen. A forest may be "slashed and burned" and used as agricultural land.*

Figure 4: Conceptual model of landscape evolution (Figure 4-4 from the Biosphere Synthesis report)

This conceptualised landscape evolution sequence leads to a common set of regolith deposits in the bedrock basins. SKB have developed a coupled Regolith-Lake Development Model (RLDM) that represents basin sedimentation and thickness of different strata during the conceptualised evolution sequence shown in Figure 4. The conceptualised evolution sequence, and the RLDM, are underpinned by interpretation of the development of the landscape at Laxemar and Forsmark since the last glaciation to the present, and the regolith layers that have been deposited during this period.

The stratigraphy and thickness of the present-day regolith is described by a Regolith Depth Model (RDM) that interpolates point data on the thickness of regolith layers into a 3D model. This is illustrated in Figure 5. The depositional environments of the regolith layers are summarised in Table 2. Note that all the regolith deposits at Laxemar were deposited during the last phase of the last glaciation, or during the subsequent post-glacial period. Older regolith deposits were removed from Laxemar by the last glaciation. More

generally, preservation of regolith deposits predating the last glaciation is rare in Sweden (Section 3.3.2 of the Biosphere Synthesis report).

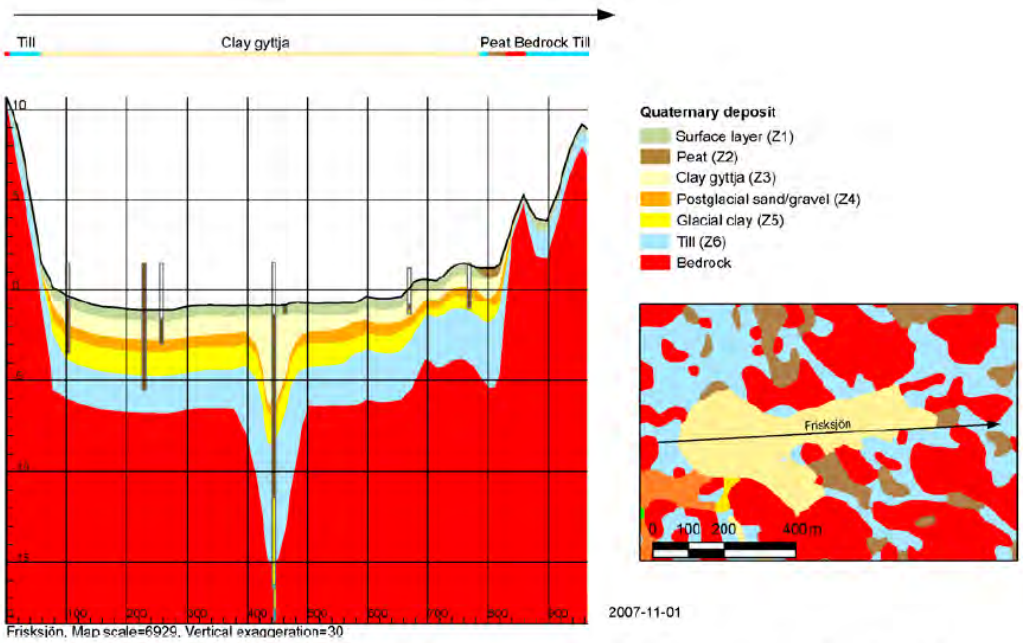

Figure 3-4. The Regolith Depth Model (RDM) showing a vertical profile with stratigraphy and total regolith depth along a profile across Lake Frisksjön (see Figure 3-1 for location). The uppermost layer, Z1, is influenced by the impact from surface processes, e.g. roots and biological activity. The next layer (Z2) consists of peat. After that follows layer Z3, which is characterised by clay gyttja, followed by layer Z4 that consist of sand/ gravel, glaciofluvial sediment or artificial fill. Layer Z5 correspond to glacial clay and the bottom layer Z6 correspond to till (figure from Nyman et al. 2008).

Figure 5: Regolith Depth Model (RDM) (Figure 3-4 of the Biosphere Synthesis report)

Table 2: Regolith layers and depositional environments (after Section 3.3.2 of the Biosphere Synthesis report)

Layer	**Environment**
Z1 - Surface	Present-day – location specific
Z2 – Peat	Mire
Z3 – Clay gyttja	Shallow bay or lake
Z4 – Post-glacial sand / gravel	Erosion and redeposition of sand and gravel by waves and currents in the coastal environment
Z5 – Glacial clay	Deposited as the ice sheet retreated
Z6 – Till	Deposited as the ice sheet moved from the north-west

The boundaries of biosphere objects 204, 206, 210 and 213 were simply described by the boundary of the present-day agricultural land, e.g. Figure 6. However, some objects were more complicated (Section 5.2.2 of the Biosphere Synthesis report). Object 212 includes agricultural land, but also an area of deciduous forest at the same elevation, which SKB interpreted as a coherent area reflecting previous land use, i.e. land that was previously cultivated but is now forested. For the sea basins, 201 and 208, the biosphere object was defined based on the size of the future lake basin, determined from SKB's digital elevation model, accounting for the bathymetry of the basin and the vertical position of the

lake threshold, i.e. the elevation contour where the lake would become isolated from the sea.

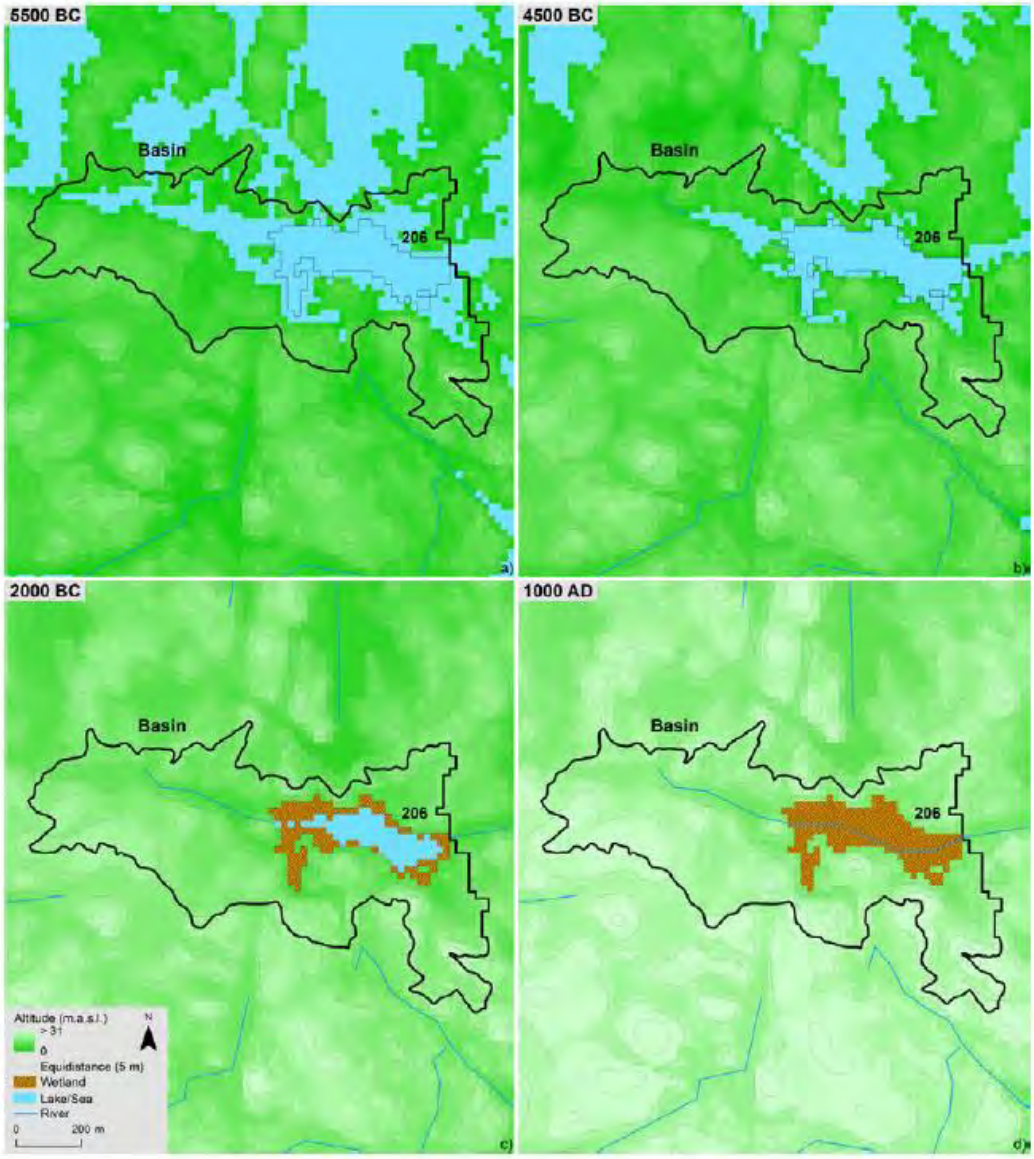

Figure 5-8. Illustration of the development of biosphere object 206, (a) from a sea basin just before the start of lake isolation, (b) at lake isolation, (c) into a lake, and finally into (d) a mire. The biosphere object is presently agricultural land (Figure 5-2) with the delimitation identical to the mire seen in (d). The black line outlines the original sea basin, which coincides with the watershed for this object. Grey contour lines follow constant elevation, with a five meter difference between lines.

Figure 6: Development of basin 206, and identification of biosphere object 206 (brown) (Figure 5-8 of the Biosphere Synthesis report)

Radionuclides discharged to the biosphere objects will be retained in the object for a period of time, depending on the hydrological conditions in the object, and the element specific sorption characteristics. Radionuclides that do not completely decay within the object may be transported out of the object through discharge to the atmosphere (i.e. C-14), transport in ground or surface water, or extraction of resources for use outside the object.

Section 7.3.4 of the Main Report notes that doses are not calculated for downstream objects, because in the SR-Site and SR-PSU biosphere modelling it was, "*found that the dose consequences from biosphere objects receiving the release through groundwater discharge were generally higher than doses from down-stream areas having received radionuclides by dispersion through the landscape*". This statement is accurate, although results for Mo-93 appear to have been greater in a down-stream object in SR-PSU (see also discussion in Section 3.1.3). However, care is needed when extrapolating findings between assessments, given potential for different landscape contexts and differing profiles of radionuclide releases and associated mobility for different types of waste and disposal concepts.

3.1.2. Identification of biosphere objects from an assumed repository location within the Laxemar area.

Regional groundwater flow model results were used for particle tracking calculations from the BHA and BHK vaults for an assumed repository location within the Laxemar area. Figure 7 shows the assumed location of the SFL repository. The regional groundwater flow model is underpinned by a stochastic fracture network model, and particle tracks are shown for five different realisations of the stochastic fracture network model. For both vaults, the majority of particles discharge to biosphere objects 204, 206 and 210. In three of the five realisations, the greatest number of particles discharged to biosphere object 206, so this was used as a primary basis for assessment of potential doses and as a baseline for the exploration of associated sensitivities.

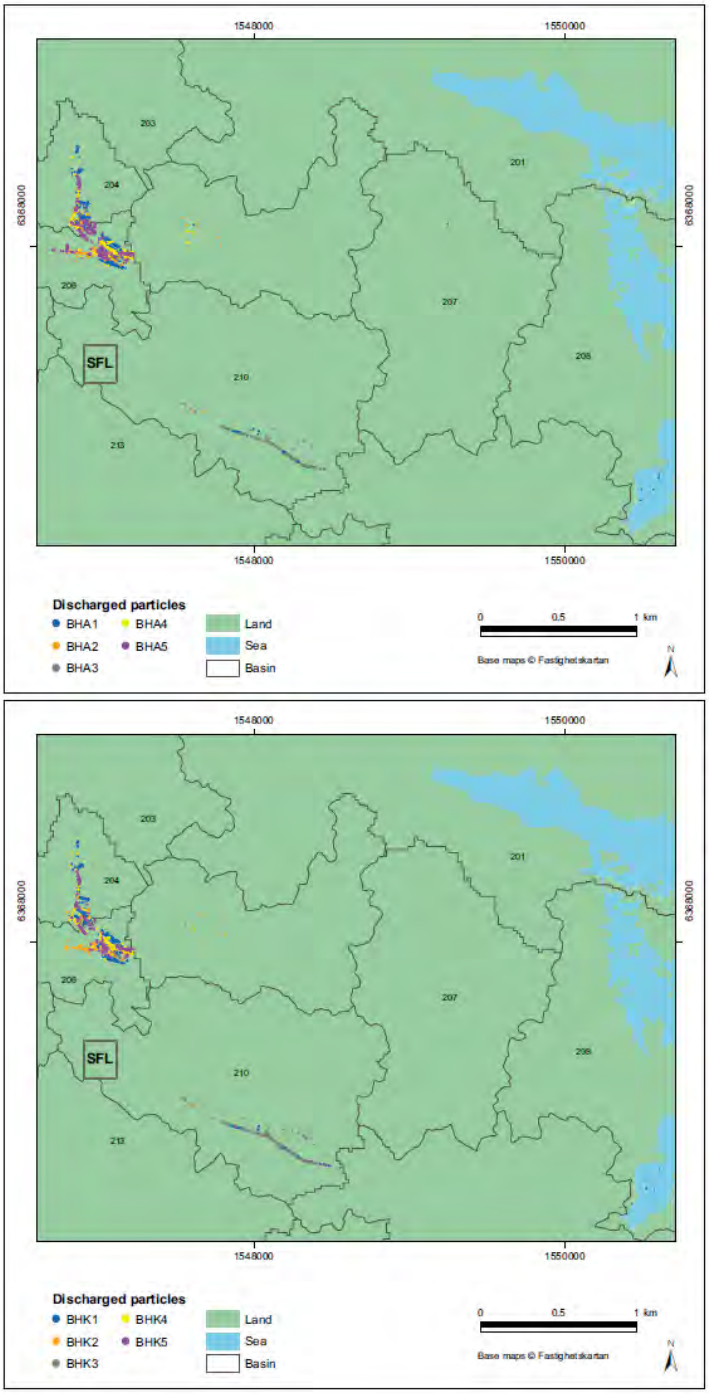

Figure 5-3. Distribution of potential discharge from a hypothetical repository in Laxemar. The discharge is based on particle tracking from the two waste vaults BHA (above) and BHK (below) in five different realisations of the stochastic fracture networks. Locations of particles are on the surface of the bedrock before entering the regolith. This is from where the transport starts in the biosphere assessment. The outlined areas correspond to the former sea basins of the biosphere objects. Note that for objects 204, 206 and 210 (which are the first objects along three different streams) the area of the basin coincides with area of the watershed for the lake. The example location for the SFL repository is indicated with a square.

Figure 7: Particle tracks from the assumed SFL repository location (Figure 5-3 of the Biosphere Synthesis report)

3.1.3. Discussion of biosphere object identification

SKB have considered a comprehensive range of biosphere objects and evolution cases based around the typical progression from sea bay, to lake, mires and potential agricultural land. SKB's landscape evolution model is generally relevant to Laxemar, Forsmark, and presumably many other potential sites in coastal areas. Sensitivity to the size, geometry and regolith characteristics of the biosphere objects has been explored for this typical configuration, especially for agricultural ecosystems. In SR-PSU, releases to objects progressing directly from marine to mire ecosystems was also considered. The analysis and exploration of uncertainties for the marine-lake-mire systems is robust and the results should significantly help SKB further develop its approach to defining biosphere objects.

At Laxemar, SKB note that particle-tracking studies show discharge areas being located along streams, as well as in lakes and mires (see Figure 3 and Section 5.2.1 of the Biosphere Synthesis report). The Main Report identifies riparian wetlands along streams as being important and distinct from the typical mires (Section 4.5.4 of the Main Report). These areas are flooded at least once a year and affected by overbank sedimentation. SKB comment that such areas *may be of importance for the retention of various substances that otherwise are transported by the water directly to the sea*. The stream and riparian context at Laxemar is somewhat different from Forsmark, as maybe the case for other sites, particularly inland. SKB's modelling approach for biosphere objects is relatively flexible, for example allowing for a surface water component to be retained following terrestrialisation. However, should assessment of further sites with stream and riparian contexts be needed, then it would be beneficial to include more explicit consideration of such systems in developing and justifying the biosphere modelling approach. This would help build confidence that the associated processes are adequately represented and/or to demonstrate that a lake-mire system is more pessimistic.

Review of SKB's SR-PSU safety assessment for SFR (Walke et al., 2016) highlighted the potential significance of discharges to lakes, particularly for C-14. Discharge to lakes (e.g. biosphere object 207) has been considered in SE-SFL. The results highlight the importance of discharge to lakes for C-14, and doses from lakes were similar to doses from agriculture ecosystems (Figure 12-4 of the Biosphere Synthesis report), but lower than from drained mires (Figure 12-2 of the Biosphere Synthesis report). A focus on the present-day configuration at Laxemar means that SKB only considered three of the nine biosphere objects (objects 207, 201 and 208) as either being lakes (alternative discharge area evaluation case), or with explicit landscape development through a lake stage (alternative discharge areas with landscape development evaluation case). It is notable that a lake stage in biosphere object 206 is omitted from the evaluation, even though the landscape modelling indicates that it will have been a lake in the past (e.g. see Figure 6). Indeed, explicit modelling of biosphere objects with landscape development at Laxemar focuses on the relatively large biosphere object 201 (more than six times the size of biosphere object 206). This focus is not explicitly explained, but is likely a result of greater focus on present-day characteristics in defining the biosphere objects for the SE-SFL assessment.

Although natural landscape succession would result in lakes being infilled, there remains potential for people to maintain some lakes, e.g. for use as water reservoirs (Section 4.3 of the Biosphere Synthesis report). Increasing terrestrialisation, and the loss of lakes from the landscape in general, would provide an increased driver for maintaining at least some areas of surface water. This driver may be increased by a potentially warmer climate. Potential for artificial lakes is explicitly recognised in the context of the alternative discharge area evaluation case (Section 7.3.3 of the Biosphere Synthesis report).

Walke et al. (2016) also highlighted the sensitivity of doses to delineation of the biosphere objects at Forsmark. This has been confirmed the results of the sensitivity analyses undertaken in SE-SFL. For example, Section 12.2.7 of the Biosphere Synthesis report summarises that doses from drained mires decrease as the size of the object increases. This is because larger objects have typically have greater groundwater flows that result in greater dilution of all radionuclides. The thickness of the regolith was also important for radionuclides that sorb significantly (e.g. Mo-93 and Tc-99), with doses decreasing as the regoligth thickness, and extent of sorption increases. SKB note the sensitivity of results to assumptions regarding regolith thicknesses and state that sites with large and deep basins would, in theory, be preferable. However, they also highlight that uncertainty in projecting flow paths from repository depths to the biosphere make projections of discharge locations difficult to reliably quantify (Section 16.6 of the Biosphere Synthesis report). One might also add uncertainty in the predictive capability of landscape development modelling over periods of time extending beyond future glacial episodes.

Object 206 is a small, but relatively deep lake basin, with comparatively high specific discharge of groundwater from the bedrock (Section 12.2.7 of the Biosphere Synthesis report). Therefore, use of object 206 in the present-day evaluation case, and as a basis for many sensitivity cases, is likely to be cautious in the context of understanding whether the repository concept has the potential to fulfil the regulatory requirements for post-closure safety. However, it is notable that object 206 does have a thick layer of peat which prevents activity in the underlying glacial clay being exposed following draining and cultivation of a mire. The doses from radionuclides that sorb to the clay (e.g. Tc-99) would be higher if the peat was thinner, resulting in exposure of the clay and the associated sorbed radionuclides. Hence, although object 206 may be cautious in the present-day Laxemar context, it may not result in upper bound doses[2].

SKB's approach to delineating biosphere objects is conceptually sensible, and by defining the objects as areas with relatively homogeneous biotic properties and abiotic characteristics this greatly simplifies development of biosphere assessment models. For a future safety assessment, it will be important to build confidence in the delineation of biosphere objects by providing supporting evidence and arguments. In addition to geographical information on the spatial distribution of areas with relatively homogeneous properties, this would also include the relationship between the delineated area and the anticipated radionuclide discharge location in the basin (further discussed below); the size of the object and areas needed to support the potentially exposed groups; and the nature and size of downstream ecosystems. This information is important to build confidence that calculated doses will be dominated by occupancy and use of the biosphere object as a whole, and significant additional exposures could not arise from occupancy and use of either (i) a small region of a relatively large biosphere object, (ii) a discharge area outside the biosphere object, or (iii) areas downstream of the biosphere object.

In the documents studied as part of this review, we have not found a diagram that compares the groundwater discharge areas (from particle tracks) with the outline of the biosphere objects. In Figure 8, information from Figures 5-3 and 5-6 of the Biosphere Synthesis report are combined to provide an approximate comparison of the area of biosphere

[2] This is illustrated by Figure 12-4 of the Biosphere Synthesis report (reproduced as Figure 19 here), which shows higher potential doses from biosphere objects at Forsmark that develop on slopes without a lake and with thin layers of peat.

object 206 and the locations of radionuclide discharge to basin 206. Although manipulation of SKB's figures is likely to have some error, the results show that some of the discharge to basin 206 is likely to be outside the boundaries of biosphere object 206. The discharge would be to areas that are currently forest, so it is not likely to lead to any significant additional exposures compared with discharge to agricultural land. SKB's assumption that all the discharge is to the agricultural land is likely to be a little cautious, but not important compared with the more significant assumption that the entire radionuclide flux from the repository discharges to biosphere object under evaluation (e.g. Section 7.2.2 of the Biosphere Synthesis report), i.e. discharges to other basins / biosphere objects are cautiously neglected. This simplified approach is appropriate given the objectives of SE-SFL because it allows biosphere objects to be compared on a common basis. It also removes uncertainties associated with the distribution of particle tracks between different biosphere objects, and the exact discharge locations of the particle tracks with respect to individual biosphere objects.

The locations and areas that are assumed to be occupied by the potentially exposed groups and the area of biosphere object 206 are compared in Figure 9 (Hunter Gatherers, HG, are excluded from the figure as they occupy a larger area than shown in the figure). The figure shows that family farmers would occupy most of biosphere object 206 (6 ha of the 8 ha are occupied). It is conceivable that radionuclide concentrations might be higher in the downstream part of the object, where particle tracking indicates that deep groundwaters discharge, than in the upstream part of the object. However, unless there is a reason to assume the family farmers preferentially occupy one part of the biosphere object, the average dose would be given by the average radionuclide concentrations across the area of the object. This is consistent with SKB's modelling assumption that radionuclide concentrations are uniform across the area of the biosphere object.

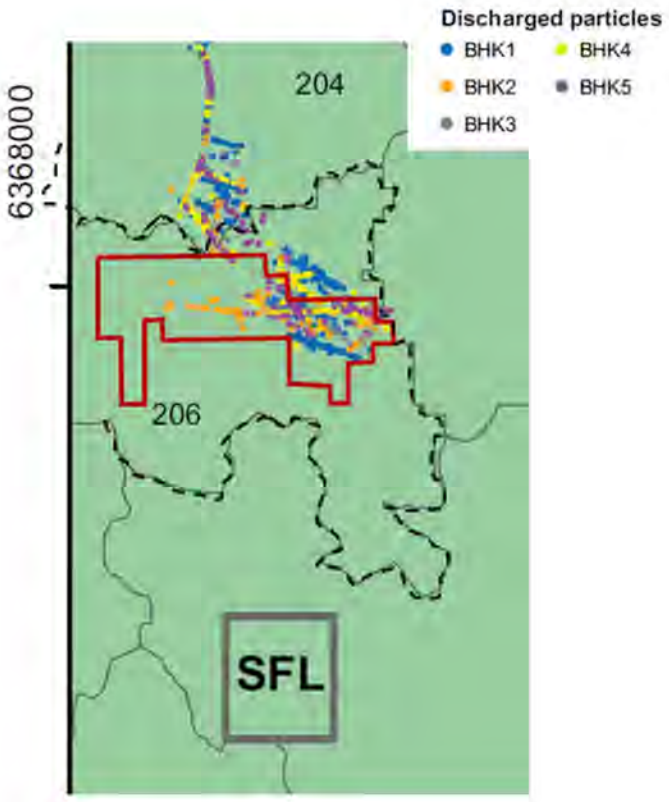

Figure 8: Particle tracks from five stochastic fracture network realisations for the assumed SFL repository location, from the BHK vault to Basin 206, and the area of object 206 (after Figure 5-3 and Figure 5-6 of the Biosphere Synthesis report)

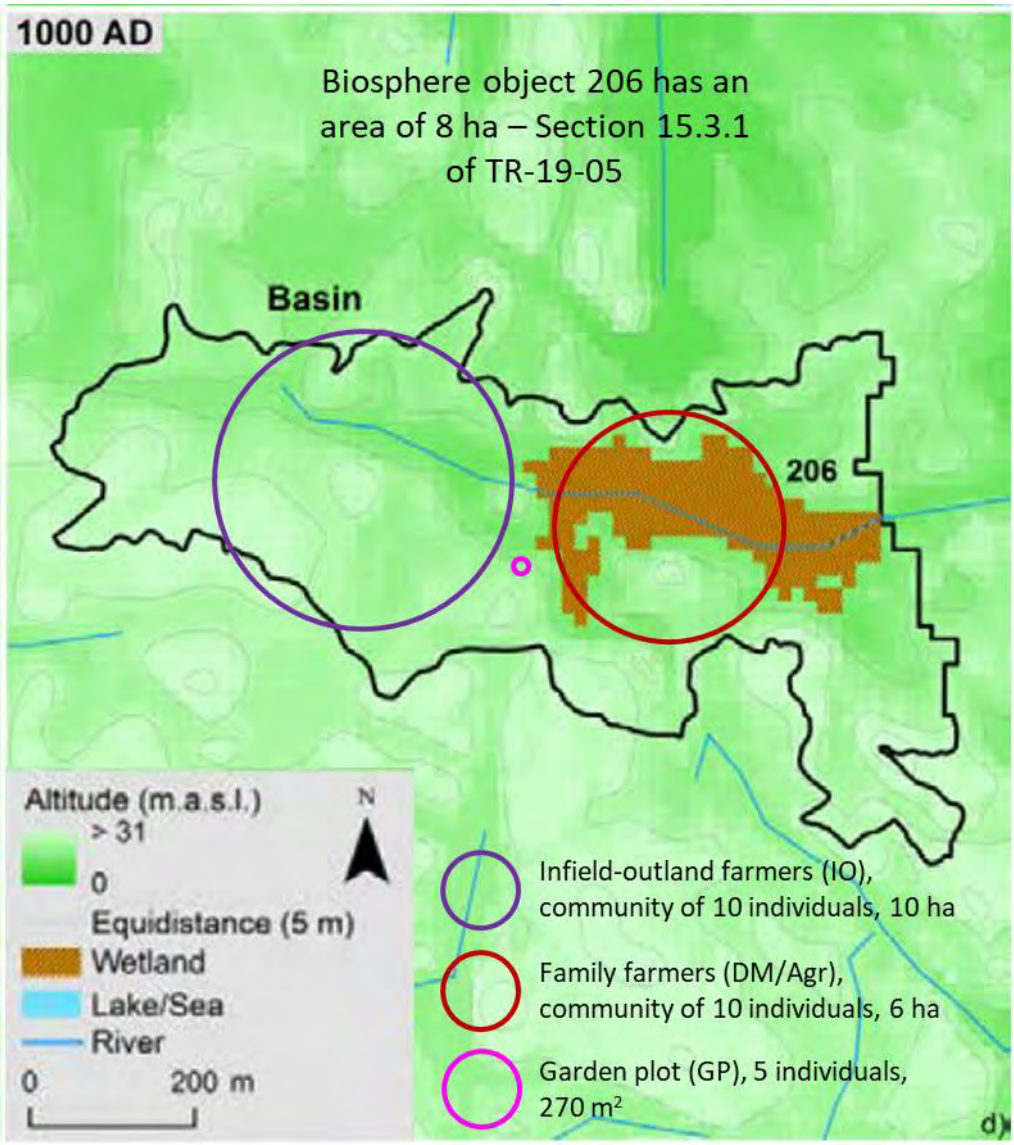

Figure 9: Comparison of biosphere object 206 and the locations and areas occupied by potentially exposed groups (after Figure 5-8 and Section 7.3.4 of the Biosphere Synthesis report)

If the biosphere object associated with this discharge area had been defined to be larger than object 206, then average radionuclide concentrations across the area of the biosphere object would be lower and the doses would be lower. This would be a realistic result for biosphere objects where the radionuclide flux into the object, and concentrations within the object, are uniform across the areas of the object. However, it is more likely that radionuclide fluxes into the object, and concentrations within the object will not be spatially uniform (see also the results of SKB's detailed COMSOL modelling in Section 3.2 and illustrated in Figure 16). Therefore, calculated doses will be sensitive to the part of the

biosphere object that is assumed to be occupied by the family farmers. This suggests that there is merit in considering sub-dividing biosphere objects that are significantly larger than the area used by family farmers, taking into consideration the spatial distribution of discharge and contamination within the object, but also any other factors that might affect occupancy within the object. If the biosphere object were smaller than the area needed by the family farmers, then it would be reasonable to reduce occupancy and use of resources to the levels that can be supported by the area of the object. Greater discussion relating the final delineation of biosphere objects to the spatial scales of relevance to the primary end points of interest (e.g. human communities) would be welcome in future.

The same arguments apply to potentially exposed groups located outside the object that make use of resources inside the object (i.e. inland-outland farmers and garden plot).

Finally, in SE-SFL, SKB do not explicitly model the potential for radionuclide transport and accumulation in downstream objects, based on the observation that potential exposures in the object receiving the groundwater discharges was "*generally higher*" in the SR-Site and SR-PSU assessments. This is supported by Table 10-1 in the SR-PSU Biosphere Synthesis report (TR-14-06). However, the SR-PSU assessment focused on radionuclide releases to biosphere object 157_2 that was somewhat unusual, in that it did not evolve through a lake stage. The atypical nature of biosphere object 157_2 is highlighted in analysis of the *alternative discharge area* evaluation case in SE-SFL, as a clear outlier in Figure 12-9 of the Biosphere Synthesis report. Additionally, the one radionuclide for which a downstream object gave a higher dose in Table 10-1[3] of the SR-PSU Biosphere Synthesis report was Mo-93, which is important in the context of the SFL and SFR wastes. These observations suggest that some consideration of potential exposures arising in downstream objects remains warranted in future assessments.

3.2. Hydrogeological interpretation

Groundwater discharge, surface hydrology and near-surface hydrogeology are important aspects of the SE-SFL study and are reviewed in the sub-sections below.

3.2.1. Approach to representing hydrogeology in biosphere models

SKB have developed hydrological models of the Laxemar and Forsmark areas using MIKE SHE software. The model for Laxemar represents the whole region, and consistent with this scale, represents the regolith more simply than the RDM. Two regolith layers (Rego1 and Rego2: Figure 10) were found to be sufficient to reach an acceptable agreement between measured and calculated levels of ground and surface water, and of stream discharge (Section 5.3 of R-19-18). Section 5.3 of R-19-18 explains that the upper layer in MIKE SHE (Rego1) typically corresponds to more recently deposited regolith layers, while the lower layer (Rego2) typically corresponds to older deposits (Table 3). This division into two regolith layers is conceptually sensible, noting that the laterally extensive, low permeability glacial clay at the top of the lower regolith layer will tend to hydraulically separate the underlying till from the overlying regolith layers.

[3] Table 10-1 of the SR-PSU Biosphere Synthesis report does not report the magnitude of the difference in the landscape dose factor (LDF) between the biosphere object receiving the radionuclide discharge in groundwater, and the higher LDF in the downstream object.

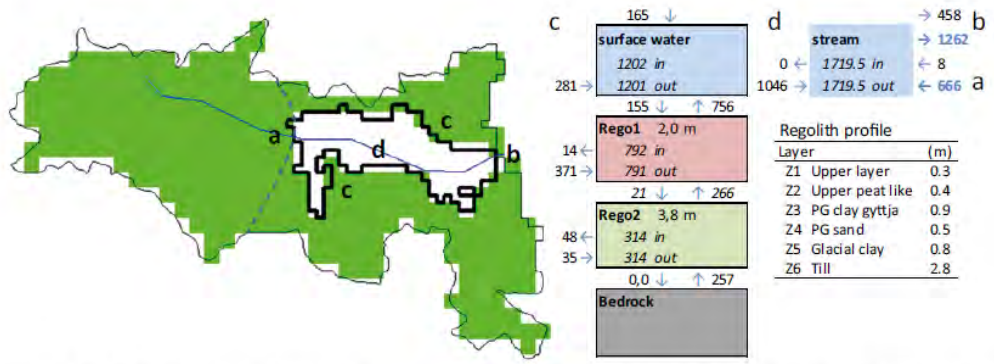

Figure 5-6. Water balances for present conditions of biosphere object 206 in Laxemar. Map of the biosphere object and its catchment. The thin black line outlines the borders of the basin. The green and the white areas represent the watershed and the object within the basin, respectively. The blue line represents a stream, and the dotted line approximately subdivides the basin into the catchments of the inlet and outlet of the stream, where the area to the right of the line corresponds to the sub-catchment. Right) Stacked boxes represent Mike SHE calculation layers within the object and arrows represent water fluxes across object or regolith layer boundaries. Numbers in the boxes show net in- and outflow of water. Blue numbers indicate streamflow (from Mike11). All units are in 10^{-3} m^3 m^{-2} $year^{-1}$ (normalised to the area of the object). Average regolith depth for the calculation layers are given in the boxes, and the average depth of geological layers are listed in the table. For details on the methodology see Section 5.3 in Grolander and Jaeschke (2019). Letters are used to link components in the left and right panels.

Figure 10: Water balance for biosphere object 206 from MIKE SHE for present conditions (Figure 5-6 of the Biosphere Synthesis report)

Table 3: Correlation between MIKE SHE, RDM layers and regolith compartments in the biosphere model (Section 5.3 and Figure 5-5 of R-19-18)

MIKE SHE	**RDM**	**Biosphere (BioTEx) model**	
		Agriculture	**Mire**
			RegoUp
Rego1	Z1 - Cultivated organic soils	RegoUp	RegoPeat
	Z2 – Peat	RegoSub	
	Z3 - Clay-gyttja	RegoPG	RegoPG
	Z4 - Post-glacial sand		
Rego2	Z5 - Glacial clay	RegoGL	RegoGL
	Z6 – Till	RegoLow	RegoLow

The MIKE SHE models were used to derive water balances for the biosphere objects, and parameters for the biosphere (BioTEx) assessment model were calculated from these (Section 8.4.2 of the Biosphere Synthesis report). Section 16.2.2 of the Biosphere Synthesis report notes that it would be preferable if all the individual regolith layers were represented in the MIKE SHE model, to provide more direct parameterisation of the biosphere model. SKB have undertaken some scoping work to understand the feasibility of doing this and have identified that this could be possible for future safety assessments. Splitting the Rego 2 layer into till, glacial clay and sand resulted in little change to the regional water balance and stream discharges and improved the model calibration. However, separation of the Rego 1 layer would have required recalibration of the MIKE SHE model, which is beyond SKB's requirements for SE-SFL.

The effect of discretisation on the water balance of biosphere objects 207 (lake) and 212 (agricultural, including an area that is currently forest) was explored. Changing the discretisation changed upwards flows in the lower half of the regolith by 25-30% (Section 16.2.2 of the Biosphere Synthesis report). The effects in the upper parts of the regolith profile were stronger. The effects are summarised in Section 16.2.2 of the Biosphere Synthesis report for objects 207 and 212, but they are not discussed here as the MIKE SHE model would need to be recalibrated to accurately understand the effects.

For Forsmark, MIKE SHE water balances were available for the three natural successional stages (sea, lake-mire and mire) for all six biosphere objects (Section 7.3.4 of the Biosphere Synthesis report) from SKB's SR-PSU safety assessment for SFR. However, water balances are only available for the present-day conditions of the Laxemar landscape. Therefore, for SE-SFL, SKB have developed stylised water balance models for Laxemar biosphere objects. These models include three natural successional stages: sea; lake and mire; and agricultural land, including unsaturated regolith layers and ditches (Figure 11). The stylised models reflect the compartmental structure of the biosphere models, and therefore provide flows that are used directly in the biosphere model (note that in the radionuclide transport models for SE-SFL, the RegoLow and RegoGL layers are further sub-divided into five compartments, but this is not shown in Figure 11). The flows have been calculated using empirically derived rules for percolation and object-specific boundary conditions (Section 8.4.2 of the Biosphere Synthesis report).

The simplified representation of the regolith in the MIKE SHE model for Laxemar, and the process SKB have used to derive stylised water balances for biosphere objects at Laxemar, mean that the associated biosphere models should capture the key features of the hydrogeology, but their parameterisation might change for future safety assessments. This approach is appropriate given SKB's objectives for SE-SFL. For future safety assessments, it would be preferable for all the regolith layers to be represented in the MIKE SHE model, and to use the MIKE SHE model to explore alternative conditions, so there is a simple and transparent process of exporting flows from the MIKE SHE model into the biosphere model, i.e. a one-to-one mapping of MIKE SHE layers and net flows across boundaries to biosphere model compartments and flows between compartments. However, an interpretive step may still be necessary, and the new simplified representation might appropriately provide that interpretive step. Furthermore, it might be argued that developing detailed MIKE SHE models for situations far in the future, following a future glaciation, would require disproportionate effort, especially given the uncertainties in far future regolith geology, climate and weather patterns. SKB's new simplified representation could be more appropriate for these situations.

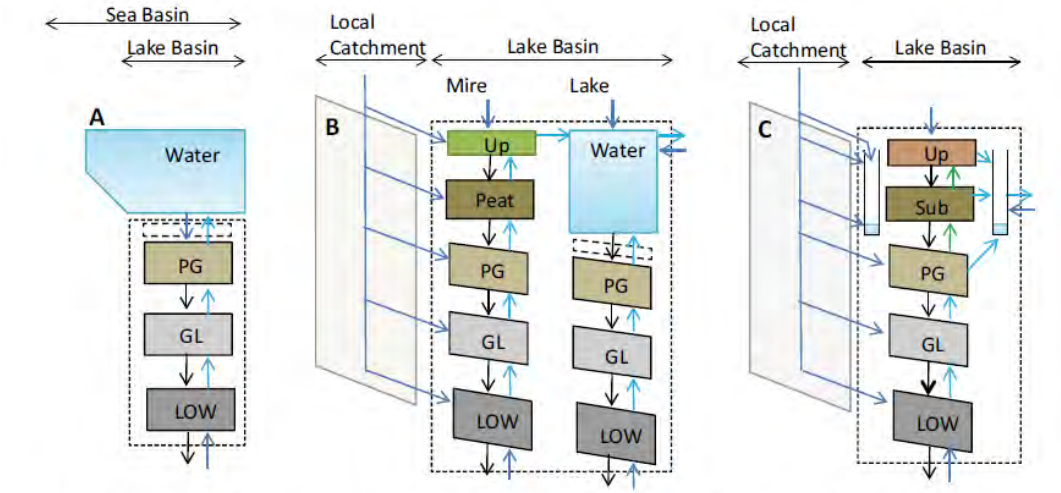

Figure 8-3. Stylised water balance models for biosphere objects in three successional stages: A) sea basin, B) lake-mire complex and C) continuously cultivated land. Boxes represent regolith layers or surface water, and arrows represent flows of water. Dark blue arrows indicate water discharged into the object across its boundary. Black arrows indicate percolating water. Light blue arrows represent discharging groundwater within the object. Green arrows represent groundwater uptake driven by plants. Arrows towards the right-hand side represent the stream inlet (dark blue) and outlet (light blue). Dashed compartment indicates that the upper part of aquatic sediments (RegoUp) is regarded as having little hydraulic resistance and the flows through this compartment are assumed to be the same as at the top of the consolidated sediments (RegoPG). When the biosphere object is cultivated (panel C), all discharge from the upper part of the local catchment (i.e. above the groundwater table), and from the stream inlet, is drained into the ditch surrounding the cultivated area. The local catchment (i.e. the area of the sub-catchment less the area of the biosphere object) is indicated in light grey.

Figure 11: Stylised water balance models used to parameterise the biosphere models for biosphere objects in Laxemar (Figure 8-3 of the Biosphere Synthesis report)

Figure 11 shows that the biosphere models represent each object as a 1D series of compartments, in which groundwater upflowing from depth mixes with surface recharge, and discharges to surface waters (sea, lake or ditch). This 1D structure is consistent with SKB's assumptions for defining biosphere objects, as areas with reasonably homogenous biotic properties and abiotic characteristics.

The 1D approach assumes that all the regolith layers are continuous across the biosphere object, and that all groundwater upflowing from depth flows through the glacial clay layer. A new development for SE-SFL has been to sub-divide the RegoLow and RegoGL biosphere model compartments each into five compartments. Use of a single compartment is expected to result in significant numerical dispersion in the biosphere model, and therefore the model is likely to overestimate dispersion of radionuclides during transport through these layers, especially radionuclides that sorb significantly.

Dividing each compartment into five compartments should result in an amount of numerical dispersion that is similar to the expected amount of physical dispersion (e.g. Quintessa, 2020a). Model comparisons presented in Sections 9.4 and 9.5 of the Biosphere Synthesis report do indeed confirm that in general increasing the discretisation of the RegoLow and RegoGL layers has the expected effect delaying migration of radionuclides through these layers. However, as summarised in Section 16.2.1 of the Biosphere Synthesis report, the precise effects depend on the object type and properties, as well as the radionuclide (i.e. sorption behaviour and half-life):

"…in an area with a high bedrock discharge, where the contribution of discharge from the local catchment to upward flow is limited, the increased discretisation had marginal or no effect on steady-state groundwater concentrations. On the other hand, in an area with a limited discharge from the bedrock, the release and accumulation of sorbing radionuclides in surface layers may be noticeably reduced with a more realistic representation of dispersion. In the presented examples, an increased discretisation resulted in a reduction of the release of Mo-93 to, and accumulation in, the upper regolith profile (where plant uptake occurs) by a factor of two, whereas the release of Ni-59 was reduced by an order of magnitude."

Increasing the discretisation of the till and glacial clay layers in the biosphere model thus improves the representation of radionuclide transport through the regolith, even though the benefit is limited in some situations. SKB plan to retain this level of refinement in future safety assessments (Section 17.3 of the Biosphere Status Report). However, an important and related question is whether the clay layer is likely to be sufficiently permeable to transmit all the upward flow, as assumed in SKB's 1D biosphere model.

Figure 10 shows that the calculated upward flow through the clay layer in biosphere object 206 is 0.266 m/y. Assuming there is unit hydraulic gradient across the clay layer (i.e. excluding artesian conditions), the clay layer would require a hydraulic conductivity of 0.266 m/y, i.e. 8×10^{-9} m/s, to support this flow. This is at the upper end of the range expected for a glacial clay, for example Fetter (1994) gives a hydraulic conductivity range of 1×10^{-11} to 1×10^{-8} m/s for clay. This suggests that some groundwater discharge could flow through the clay and the rest (potentially all) would flow around the clay, either around the edges of the clay, or through any areas where the clay is absent.

This is potentially important for radionuclide transport and calculation of doses. Some radionuclides (e.g. Mo-93 and Tc-99) sorb significantly onto the clays, thereby reducing the fluxes of these radionuclides to surface waters and the upper, cultivated, layers of regolith. The 1D representation in the biosphere model might overestimate sorption of these radionuclides onto clays, and therefore underestimate doses from these radionuclides. Conversely, if sorption onto the clay is overestimated, doses associated with exposure to the clay, e.g. during cultivation of a mire, will be overestimated. We also note, that if sorption onto the clay is lower than calculated using SKB's current biosphere model, then the calculated doses will tend to be less sensitive to the assumed thickness of peat overlying the clay, and whether the clay is exposed during cultivation of a mire. It is not desirable for safety assessment results to potentially be sensitive to small changes in the assumed thickness of regolith layers (i.e. peat), so a more realistic representation that reduces, or eliminates this sensitivity would be beneficial. This is especially true for scenarios involving future glacial cycles, because confidence in predicting the thickness of the regolith layers deposited at the end of the glacial cycle, and post-glaciation, to an accuracy of the order of ten or twenty centimetres is assumed to be quite low[4].

3.2.2. Spatial variability within the biosphere objects

Although the biosphere objects are defined as areas with relatively homogeneous biotic properties and abiotic characteristics, there is still spatial variability within biosphere objects, for example conditions immediately adjacent to a stream or ditch may be somewhat different to those further away.

[4] Note we have not reviewed SKB's RLDM, including its performance at predicting the present regolith thicknesses, as part of this review.

SKB have recognised the potential for regolith layers to be absent in part of a biosphere object, and for water to flow around, rather than through, the glacial clay. They are currently undertaking research to improve their understanding and develop a more realistic biosphere model. Progress with this research is described in Section 15 of the Biosphere Synthesis report.

SKB have used the COMSOL Multiphysics software to develop a detailed 3-D flow and transport model of basins 206 and 210. Particle tracks, calculated from regional groundwater flow model results, have been used to describe the spatially distributed flux of radionuclides into the base of the COMSOL model. Sorption of radionuclides has been modelled using a K_d approach. This model is described as the 'distributed K_d model'.

A second model has been developed using COMSOL coupled to PHREEQC. This model represents retention through several geochemical processes. It is more computationally demanding that the simple K_d approach, so only a sub-area of basin 206, where radionuclides discharge to the biosphere object, was modelled. This model is described as the 'distributed reactive model'.

Figure 12 and Figure 13 show the results of calculations in which upflowing groundwater flows around the edges of the glacial clay at the margin of the basin. There also seems to be some local flow through the clay, towards the centre of cross-section 206 xz, where the glacial clay is thin.

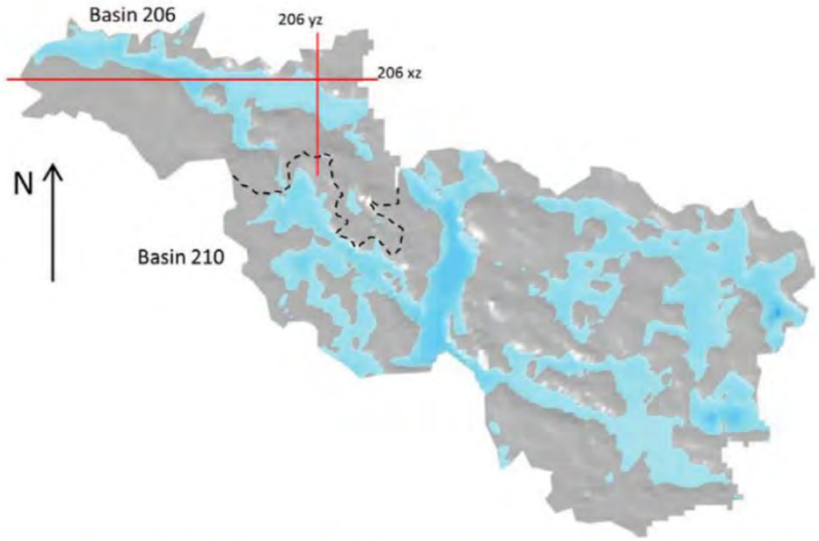

Figure 15-1. *Areas with water discharge at the ground surface of the regolith (light blue). The outside borders of the displayed domain correspond to the watershed boundaries that surround the adjoining basins 206 and 209. The dashed black line indicates the watershed divide that separates basin 206 from 210. The red lines indicate the location of the vertical 2D cross-sections (206xz and 206yz) for which more detailed graphical results are presented.*

Figure 12: Areas of surface water discharge (light blue) and flow cross-sections (Figure 15-1 of the Biosphere Synthesis report)

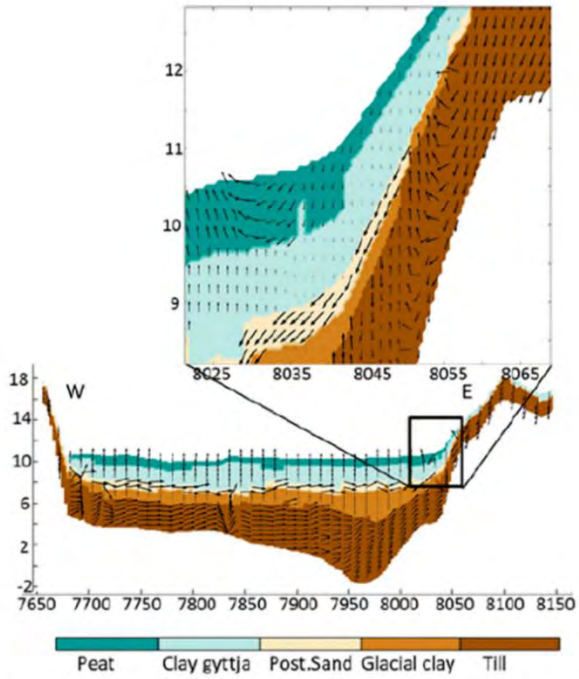

Figure 15-2. Detail of the cross-section 206 xz (see location on Figure 15-1) showing the groundwater velocity vectors. The size of the vector is proportional to the Darcy velocity magnitude. Colours illustrate the materials. The vertical axis is exaggerated 5 times. The coordinate system of the figure and all data presented is RT90 with local references as described in figure 15-3.

Figure 13: Regolith layers and groundwater flows in cross-section 206xz – see Figure 12 (Figure 15-2 of the Biosphere Synthesis report)

Figure 14 shows that dissolved concentrations of Ni-59 are highest in the till and glacial clay layers in the area where upflowing groundwater enters the basin. The concentrations of dissolved and sorbed Ni-59 are significantly lower above the clay layer. The lower concentrations above the glacial clay layer are due to significant dilution by infiltration, and water flowing laterally through the regolith layers: the latter is particularly important for the post-glacial sand. The highest concentration of sorbed Ni-59 occurs in the glacial clay. Section 15.2.1 of the Biosphere Synthesis report notes that the K_d for Ni is highest in the glacial clay and is forty times higher in the clay than the till. Accumulation of Ni-59 in the clay is due to diffusion.

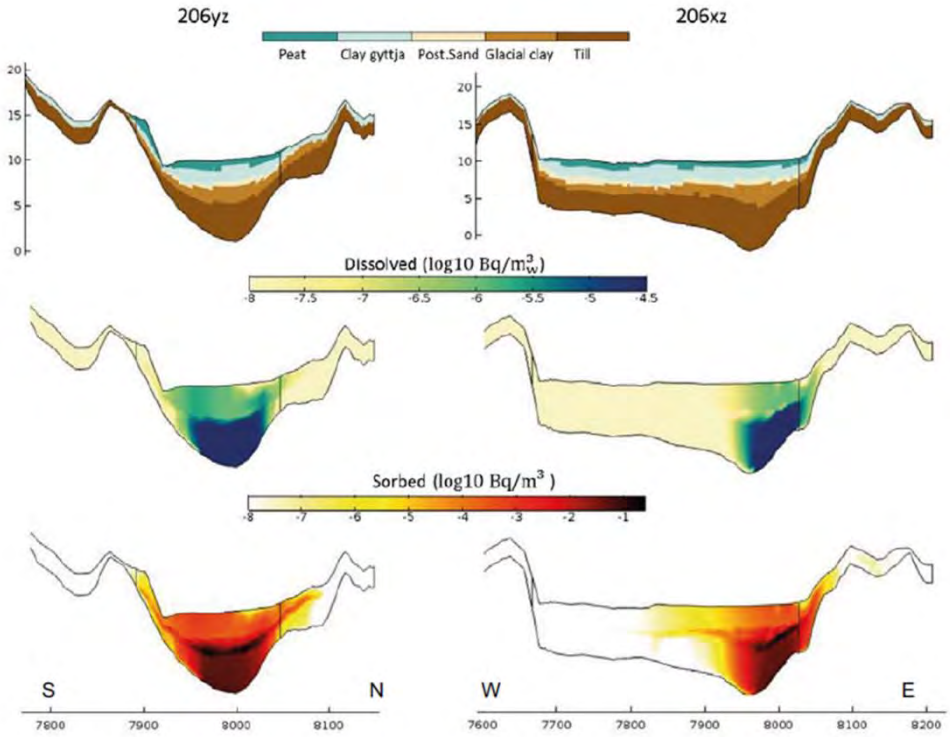

Figure 15-3. Nickel-59 activity concentration in pore water (log_{10} Bq m^{-3}water) and sorbed (log_{10} Bq m^{-3}) at 206 yz (left) and 206 xz (right) vertical profiles in basin 206 at 10 000 years. The location of the cross-section is shown in Figure 15-1. Regolith materials are shown in the topmost panel. The vertical axis is exaggerated 5 times. Note that the concentrations are displayed in a logarithmic scale. A local reference system is used with X = XRT90−X0 and Y = YRT90−Y0, where X0 = 1 539 000 m and Y0 = 6 360 000 m.

Figure 14: Ni-59 concentrations in cross-section 206xz – see Figure 12 (Figure 15-3 of the Biosphere Synthesis report)

Section 15.2.1 of the Biosphere Synthesis report states:
"Water discharge areas were located at topographic depressions, for example at the east of basin 206 and at the south-eastern part of basin 210 (Figure 15-1). Most of the water streamlines ended at the arable lands of basins 206 and 210 (i.e. the biosphere objects). Around 10 % of the water inflow into the domain occurred through the bottom surface (i.e. the regolith-bedrock interface) where radionuclides entered the domain (Table 15-2). The remaining 90 % of the water entered the domain through the ground surface, leading to a substantial dilution of the radionuclide-rich water in the regolith. The amount of water that exits the domain through the regolith-bedrock interface is twice as large as the amount of water entering through it. Thus, the bottom boundary acts as a net sink on the basin scale."

The fact that the bottom boundary acts as net sink on the basin scale is not conceptually reasonable. The 3D-flow model predicts that water exits the regolith-bedrock interface towards the margins of the basin (Figure 13), which are areas of groundwater recharge due to their topographic location (e.g. Figure 6-4 of the Main Report). The fate of this water needs further consideration. There are two possibilities:

- the water flows laterally into an adjacent basin before discharging to surface waters in that basin; or

- the water forms, or mixes with groundwater upflowing from depth, before re-entering the deeper part of the basin, and then ultimately discharging to surface waters in the basin.

If the latter situation is relevant, then the amount of water entering the deeper part of the basin could be underestimated, with implications for the calculated flows and transport of radionuclides. In particular, retention in the deeper regolith layers could be overestimated, and spread of radionuclides within the basin could be underestimated. The calculated distribution of radionuclides within the basin in the 3D COMSOL model is also affected by transport out of the bottom model boundary. For example, 57% of the geosphere release of Mo-93 is lost through the base of the model (Section 15.3.1 of the Biosphere Synthesis report).

This suggests there is potential for SKB to review and possibly improve the bottom boundary in the research-level 3D COMSOL modelling and associated boundary condition(s).

As part of their ongoing research, SKB have modified the structure and parameterisation (i.e. flows) of the compartment model for object 206 to try and better reflect the 3D structure of the regolith layers in object 206. This includes addition of compartments explicitly representing the layer of post-glacial sand, inclusion of 'bypass' flows calculated by the COMSOL model and use of different properties including K_d values. Biosphere models have been constructed at two scales: object 206, and the sub-area of object 206 where upflowing deep groundwater discharges to the basin (i.e. the release area). The structure of the modified compartment model for object 206 is shown in Figure 15.

It is interesting to note that, in general, the bypass flows are a relatively small proportion of the total flow, in both the object and release area scale models. The only exception is downwards flow from the clay gyttja to the till in the object scale model (Figure 15). The relatively small bypass flows suggest the results of the modified compartment model might not be very different from the results of the original (1D) compartment model for radionuclides that do not sorb significantly onto the bypassed layers. However, no such comparison is provided in the Biosphere Synthesis report.

The high downwards bypass flow in the COMSOL model, from the clay gyttja to the till, might be associated with flow out of the base of the model. However, there is no downwards flow out of the base of the compartment model, so this downwards flow must be balanced by flow upwards and laterally out of the till. Exclusion of downwards flow out of the base of the compartment model makes conceptual sense because, as noted above, groundwater recharge around the perimeter of the basin is likely to form groundwater discharge towards the middle of the basin.

On the one hand, the Biosphere Synthesis report notes that *slow, vertical transport seemed to be a primary driver for accumulation patterns of adsorbing radionuclides in the lower regolith layers*, reflecting the relatively small proportion of bypass flow. However, the COMSOL modelling demonstrates that the small bypass flow has potential to drive *a significant fraction of the transport* from the till directly to the clay gyttia (above the glacial clay), particularly in the context of Mo-93.

Lateral flows in and out of the regolith layers (light blue arrows on the right-hand side of in Figure 15) are not included in either the BioTEx assessment model or in the adapted

version calibrated against the research-level COMSOL modelling. The lateral outflows are small compared with the upward flows, so the majority of radionuclides will be transported upwards within the biosphere object, rather than laterally into the adjacent basin. This simplifying assumption was explored in the context of the SR-PSU review in Section 2.3 of Walke et al. (2017a); that review demonstrated that small sub-horizontal flows between adjacent biosphere objects can have a relatively limited effect on calculated exposures. However, it was also demonstrated that more significant preferential flow from the till towards an adjacent lake could be significant in the case of C-14.

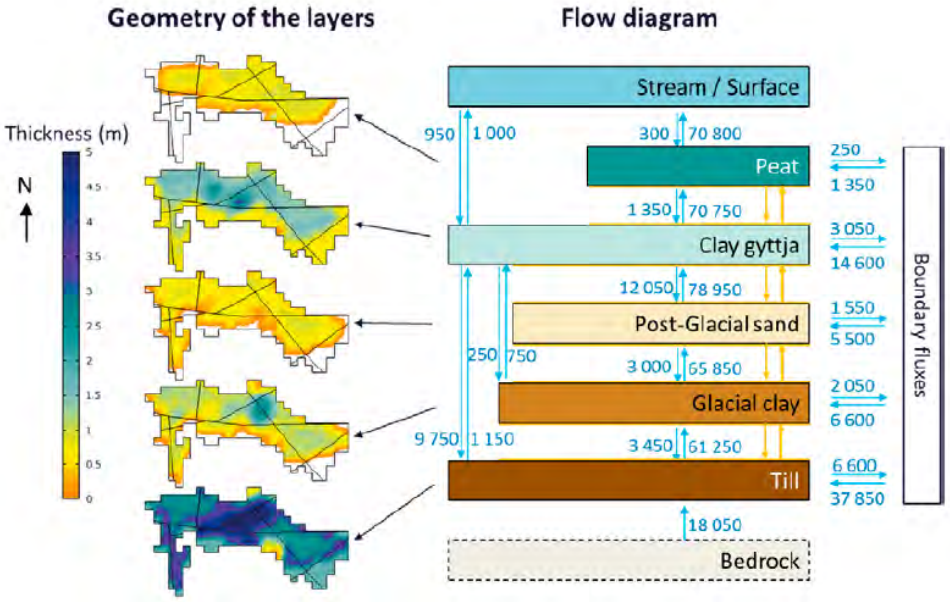

Figure 15-8. Thickness of the regolith layers in object 206 (left) and gross groundwater flow (m^3 $year^{-1}$) between the layers. The structure of the flow diagrams corresponds to that of the stylised compartment model. That is, each regolith layer was represented by one compartment, and advective transport between the layers was proportional to groundwater flow (vertical blue arrows). However, in the stylised model horizontal exchange of groundwater across the boundary (i.e. the horizontal blue lines) was excluded, and diffusion (yellow arrows) was limited to the major contact areas between adjacent regolith layers (yellow lines) only.

Figure 15: Modified biosphere model to represent the 3D regolith structure and flows for object 206 (Figure 15-8 of the Biosphere Synthesis report)

Section 15.3.1 of the Biosphere Synthesis report compares the distribution of Mo-93 activity between regolith layers calculated by the modified compartment model for object 206 with the distribution calculated using the COMSOL-based distributed Kd model (see Figure 15-10 of the Biosphere Synthesis report). The comparison is made assuming a constant input flux of 1 Bq/y for 10,000 years (note the distributed Kd model results have been corrected for transport out of the base of the model). SKB found that the modified compartment model broadly reproduced the distribution of activity calculated using the distributed Kd model. This included the overall pattern of increasing dilution towards the surface and of preferential accumulation in clay gyttja, and to a lesser degree also in glacial clay. The concentrations in the two uppermost regolith layers were similar in the two models. However, steady state conditions were approached more rapidly in the compartment model, due to greater (unrealistic) numerical dispersion, while the compartment model tends to yield higher porewater concentrations in the post-glacial sand, and higher accumulation in the clay gyttja.

The modified compartment model for the release area, considers the region within object 206 where upflowing groundwater discharges, as well as the adjacent area where upflowing groundwater discharge occurs outside the biosphere object (see previous discussion in relation to Figure 8). The resultant compartment model is about 70% of the original area of object 206 (Section 15.3.2 of the Biosphere Synthesis report). The results of the modified compartment model for Mo-93 were compared with the results of the distributed K_d model (again scaled to correct for transport out of the base of the model).

The Mo-93 concentrations calculated by both models were higher than the concentrations calculated by both object scale models. This is because the same flux was released into a smaller area. The differences between the COMSOL and compartment model results showed a similar pattern to the comparison of results for the object scale models, although the patterns were now a little more similar for the concentration of Mo-93 in the post-glacial sand, and the amount of Mo-93 that accumulates in the clay gyttja.

The Biosphere Synthesis report does not provide a comparison of the modified and original biosphere models for object 206. It would be interesting to make this comparison in the future, as it would show whether the modifications to the biosphere model make a significant difference to the calculated concentrations. If the modifications do not significantly affect the biosphere model results this would be beneficial because it may be challenging to confidently identify areas of the biosphere objects where regolith layers are currently absent; and very challenging to predict where regolith layers that will be deposited in the future could be absent in evolving biosphere objects. If the modifications to the biosphere model do make a significant difference, it will be important to understand where bypass flows are typically possible and ensure this is reflected in the RLDM.

The other factor that is not discussed in the Biosphere Synthesis report is the implication of more realistic representation of the spatial distribution of discharges for the estimation of doses. It would be interesting for future research to also compare the results of doses calculated using the original and modified biosphere models, and the distributed K_d model, taking into consideration the areas occupied by the potentially exposed groups. For example, the family farmers occupy almost the entire area of object 206 (6 ha of the 8 ha are assumed to be occupied, see Figure 9). Although radionuclides are preferentially retained close to the area where upflowing deep groundwater discharges, the family farmers' exposure is averaged across the entire biosphere object, so this is not likely to be important for doses. The average radionuclide concentrations over the area of the biosphere object, calculated by a 1D biosphere model, are likely to be representative of the average concentrations the family farmers are exposed to. However, if there is preferentially occupancy and use of the part of the biosphere object where radionuclide concentrations are highest, e.g. one family preferentially occupies and farms this sub-area, then a 1D biosphere model of the whole object would underestimate the doses. For example, if radionuclides are preferentially located in one half of the biosphere object, and there is preferential occupancy of that sub-area of the object, then doses could be up to a factor of two higher than calculated. This highlights the importance of correlating the object area, release area and occupied areas when parameterising the biosphere model.

Similarly, for potentially exposed groups living outside the biosphere object, but using resources from within it (i.e. inland-outland farmers and garden plot), it is relevant to consider whether all the resources could be drawn from the most contaminated part of the biosphere object, or if they would have to be drawn from a wider area within the biosphere object to provide the assumed quantities.

To ensure doses are appropriately calculated for all potentially exposed groups, the biosphere model might only represent the sub-area of the biosphere object where most of the contamination is expected to be present. If this area is too small to support the habits of the potentially exposed groups, then the assumed occupancies of the contaminated area, and amounts of foodstuffs and resources take from the area, can be reduced to the levels the contaminated area can support. Alternatively, the area of the biosphere model might be set to the area needed to support the PEGs (assuming this is smaller than the area of the biosphere object), with discharges and radionuclide concentrations averaged over the occupied area.

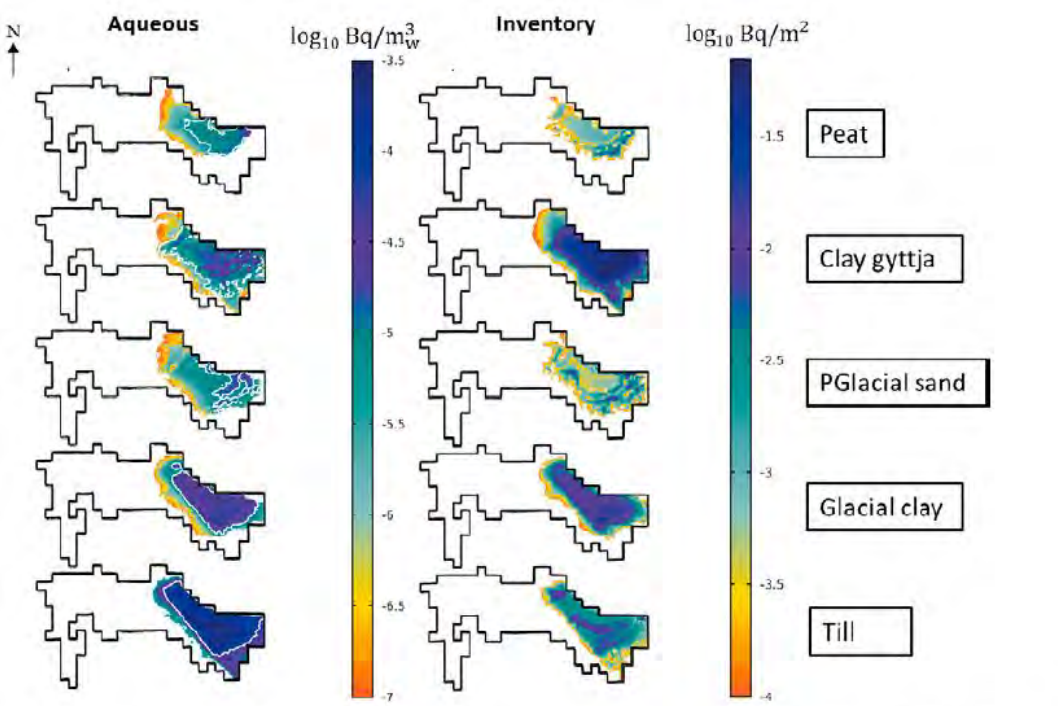

Figure 15-9. Spatial distribution of Mo-93 aqueous activity concentration (Bq m_w^{-3}) (left) and sorbed activity concentration per unit area (Bq m^{-2}) (right) in the regolith materials after 10 000 years in object 206. The aqueous concentration is the average concentration of the regolith layers. Note that aqueous values below 1×10^{-7} (Bq m^{-3}) and sorbed values below 1×10^{-4} (Bq m^{-2}) are not plotted in the figure. The white lines in aqueous Mo-93 show the average concentration of Mo. Note that concentrations are displayed on a logarithmic scale.

Figure 16: Spatial distribution of Mo-93 in the distributed K_d model for object 206 (Figure 15-9 of the Biosphere Synthesis report)

3.2.3. Effects of repository location and climate change on hydrology

SKB have explored how regional differences in climate (rainfall and temperature) could affect flows in the regolith, and therefore transport of radionuclides through the regolith (the 'alternative regional climate' evaluation case). SKB have considered three regions outside of Laxemar, that broadly cover the whole of Sweden. The evaluation case explores the implications for biosphere object 206, for continuously cultivated land and drained mire ecosystems. The climate conditions in the three alternative regions all resulted in an increase in hydrologically effective rainfall (HER), i.e. rainfall less evapotranspiration. Increased HER results in increases in groundwater discharge from the bedrock, and runoff from the surface catchments. This results in increased dilution in all regolith layers and reduced doses, which is a conceptually reasonable result.

The effects of warmer and colder climate conditions have also been explored in the 'increased greenhouse effect' and 'simplified glacial cycle' evaluation cases respectively. A warmer climate leads to reduced HER and therefore, reduced discharge from the bedrock and reduced runoff (Section 7.4.4 of the Biosphere Synthesis report). This has the expected effect of increasing the radionuclide transport time through the regolith, and reducing dilution, but the impact on doses is radionuclide specific (Section 12.4 of the Biosphere Synthesis report). For example, increased accumulation of Cl-36 in peat leads to increased doses if the mire is drained for agricultural use, whereas for Mo-93 increased accumulation is offset to an extent by increased decay. These results are conceptually reasonable and are consistent with the results of the alternative regional climate evaluation case.

In the simplified glacial cycle evaluation case, the discharge location changes as the surface conditions evolve: from release to a mire under temperate conditions; to release to a talik under periglacial conditions (because permafrost restricts direct discharge to soils); and to a sea basin under glacial conditions. Objects 206, 207 and 208 have been assumed to be representative of these conditions respectively. Post-glaciation, release of radionuclides is assumed to be to object 206. This is initially submerged, but as the land rebounds object 206 evolves into a bay, then a lake and then a mire. Section 7.7.4 of the Biosphere Synthesis report states that groundwater flows for each object and state were calculated using the conceptual water-balance models in combination with empirically derived rules for percolation and discharge from the surrounding local catchment, i.e. the approach used to calculate flows for Laxemar objects described earlier in this review report.

Figure 7-6 of the Biosphere Synthesis report explains how the object-specific discharge ($m^3\ y^{-1}$) was scaled by a flow factor (between 0 and 35) depending on the climate domain (temperate or periglacial), the position of the ice front (end of second periglacial period and glacial), or water depth (during the submerged domain). The changes shown in Figure 7-6 of the Biosphere Synthesis report are conceptually logical, but we have not reviewed the detailed work underpinning work that the scaling factors are derived from, or the chosen scaling factors.

Figures 12-16 and 12-17 of the Biosphere Synthesis report show that peak doses occur under present-day (temperate) climate conditions, associated with draining and cultivation of a mire (biosphere object 206). The potential doses from C-14 during the first periglacial period are notable (biosphere object 207, which is a lake, is assumed to be representative of a talik), but are still more than one order of magnitude lower than the doses

from a drained mire during temperate conditions. Therefore, more detailed review of the work underpinning the bedrock flow scaling factors is not a priority at this stage.

3.2.4. Discussion of hydrogeological interpretation

SKB have undertaken an impressive amount of work to try and bound the biosphere conditions that might be encountered at a future site for SFL and to calculate the associated potential doses. This should significantly contribute to achieving their objectives for SE-SFL.

The work presented in the Biosphere Synthesis report includes:

- Development of biosphere models for Laxemar, following the approach previously used by SKB to develop biosphere models for their SR-PSU safety assessment for SFR, and using the SR-PSU biosphere models as a basis for the SE-SFL biosphere models.
- Updates to the SR-PSU biosphere models for SE-SFL in response to regulatory peer review comments of SR-PSU and improvements in understanding since SR-PSU.
- 'Interim' approaches to develop water balances for the SE-SFL biosphere models from an existing MIKE SHE model for Laxemar (described here as 'interim' approaches because the approaches that would be used for a future safety assessment are not clear at present – see discussion below).
- Results from ongoing work to further develop the biosphere modelling approach, examining the detailed characteristics of flow and transport in the biosphere objects.

Much detailed and useful information is presented in the Biosphere Synthesis report. The report assumes the reader has good familiarity with SKB's SR-PSU assessment, and the associated biosphere models. This helps to keep the report focussed on the issues relevant to SE-SFL. A general comment is that the document could be improved by providing a stronger narrative, especially for readers who are not familiar with SKB's previous biosphere assessments. It would be particularly beneficial to provide a stronger narrative of the following.

- The updates that have been made to SKB's biosphere assessment approach and models and why. What the implications are for SE-SFL and whether SKB might to retain the updates for any future safety assessment?
- Why 'interim' approaches have been used, the potential implications for SE-SFL, and whether SKB might further develop the approaches for any future safety assessment or use a different approach?
- The implications of ongoing research for SE-SFL and how they might influence any future safety assessment.

In the context of the hydrogeological models, there is potentially significant complexity in using stylised water balance models to calculate flows for use in the biosphere models. While the stylised models reduce the demand on detailed MIKE SHE modelling, having a simple consistent process of exporting flows from the MIKE SHE models for use directly in the biosphere models is more transparent. It also reduces the potential for inconsistencies to be introduced or unrealistic assumptions to be made. However, an interpretive step may still be necessary and the new simplified representation might appropriately provide that interpretive step. Furthermore, it might be argued that developing detailed

MIKE SHE models for situations far in the future, following a future glaciation, would require disproportionate effort, especially given the uncertainties in far future regolith geology, climate and weather patterns. SKB's new simplified representation could be more appropriate for these situations.

The COMSOL models provide important insights to the distributions of radionuclides within a biosphere object, and these insights can be reflected in the compartmental biosphere assessment model. Although robust COMSOL models can be developed for the present-day biosphere objects, models for situations far in the future following a future glaciation will be inherently uncertain, e.g. due to uncertainties in the regolith geology, climate and weather patterns. Therefore, it may not be beneficial to develop COMSOL models for situation in the far future, but stylised understanding from COMSOL modelling of present-day biosphere objects might be applied to situations in the far future.

Both this sub-section and the preceding sub-section have highlighted the importance of correlating the object area, release area and occupied areas when parameterising the biosphere model. SKB's biosphere model results currently show that doses decrease as the size of the biosphere model increases. However, this is an artefact of averaging radionuclide concentrations over the whole area of the biosphere object without considering whether radionuclides may be dominantly present in a sub-area of the object, and how that sub-area correlates to the area that may be occupied and exploited by potentially exposed groups.

Future biosphere models for radionuclide transport and exposure could represent a sub-area of the biosphere object where most of the contamination is expected to be present. If this area is too small to support the habits of the potentially exposed groups, then the assumed occupancies of the contaminated area, and amounts of foodstuffs and resources take from the area, can be reduced to the levels the contaminated area can support. Alternatively, the area of the biosphere model might be set to the area needed to support the PEGs (assuming this is smaller than the area of the biosphere object), with discharges and radionuclide concentrations averaged over the occupied area.

Object 206 has been used as a 'base case' for SE-SFL. The area of this object (8 ha) is similar to the area assumed to be occupied by family farmers (6 ha). Since the highest doses are associated with draining and cultivating mires by family farmers, object 206 should appropriately represent the relationship between the radionuclide fluxes to the biosphere and the peak assessment doses. This is important for SKB's objective of evaluating the conditions in the waste, barriers and repository environments under which the repository concept has the potential to fulfil the regulatory requirements for post-closure safety.

3.3. Exposure assumptions

The potential exposure groups included in the SE-SFL evaluation remain the same as those considered in the SR-PSU assessment. They are designed to represent *credible bounding cases* and help ensure that potential exposure are not underestimated.

- Hunter-gatherers (HG): predominantly exposed via foraging in the landscape and drinking surface water; typically numbering 30 people and using an area of approximately 200 km^2.
- Infield-outland farmers (IO): self-sufficient agricultural group with livestock and growing crops on areas not subject to groundwater discharge, but where the soil

is fertilised through use of manure from animals fed on hay from the wetlands; typically numbering 10 people and using water from a dug well or surface water. A wetland area of 10 ha is needed to provide winter fodder.

- Drained-mire farmers (DM): self-sufficient agricultural group using drained mire for agriculture (crops and grazing/fodder) and drinking water from a dug well or from surface water; typically numbering 10 people and requiring an area of 6 ha.
- Garden-plot householder (GP): self-sufficient household with respect to vegetables and root crops from small-scale horticulture, using a dug well or surface water for drinking and irrigation; typically numbering 5 people and needing 140 m^2.

Previous observations concerning the representation of exposure groups remain valid (e.g. see discussion in Walke et al., 2017b). The four exposure groups demonstrate a reasonable range of different lifestyles, based on consideration of present-day and historical land use. Tracing assumptions through the model indicates a relatively small degree of local resource usage, which might be unexpected for groups designed to be credible bounding cases. The following observations were made in the context of the SR-PSU review.

- The GP group spend only 54 hours per year in the potentially contaminated region and obtain only 8% of their intake from the fruit and vegetables that they grow.
- The DM group spend only 54 hours per year in the biosphere object where they grow cereals, potatoes and animal fodder.
- The IO group spend 120 hours per year on arable land growing cereals and 100 hours per year harvesting hay from the wet meadows.
- The HG group obtained only 0.7% of their dietary carbon intake from biosphere object 157_2 (biosphere object 206 is smaller than 157_2).
- Explanation of the larger size of the HG group has not been found. Discussion in the biosphere FEP report for SR-PSU (Section 3.4.1 of R-14-02) relates the group to evidence of behaviours of Mesolithic and Neolithic communities.
- The larger HG is the only group considered to have potential to consume fish. It has previously been demonstrated that reducing the size of the group to ten individuals (consistent with the other groups) increases potential doses from ingestion of fish by a factor of three[5].

Future assessments would benefit from a clearer description of the exact extent of exposure to the biosphere objects and explanation of why they can be considered to be credible and bounding.

Section 6.3 of the Biosphere Synthesis report notes that three exposure pathways have been excluded in the biosphere assessment for SE-SFL (external exposure from outdoor vegetation, external exposure from aquatic sediments, and inadvertent ingestion of soil). These exposure pathways were found to be insignificant in SR-PSU. They were evaluated against the radionuclides of interest in the context of SE-SFL and excluded on the basis of significance (see Appendix B to the Biosphere Synthesis report). Exclusion of these exposure pathways is handled and explained well in SE-SFL, especially recognition that conclusions based on potential significance in the context of SFR should be reviewed for the radionuclides and inventory being considered for SFL. It provides a good example of how iterative assessments provide an opportunity for introducing simplifications, where justified.

[5] The inverse linear relationship results from model that links potential resource usage with the productivity of the biosphere objects. See Section 2.4.3 of Walke et al. (2017).

There is a notable change in the way the potential use of groundwater wells is explored in SE-SFL in comparison to SR-PSU. In the latter, the IO, DM and GP groups have potential to draw water from either a well dug into the till, or from a well drilled into the bedrock. However, in SE-SFL, potential use of water from a drilled well is separated from the central calculations and considered in a specific variant evaluation case. It appears that Table 6-2 of the Biosphere Synthesis report has been copied from the SR-PSU assessment without being updated, as it still lists potential for the three groups to draw water from "*a bedrock well*".

The change in the treatment of groundwater wells between assessments is interesting.

- The SR-Site assessment, similarly based on a groundwater pathway from a geological repository at a depth of 500 m, assumed that individuals obtain half their drinking water from surface water and half from a drilled well. The drilled well proved to be an important exposure pathway for most radionuclides (see Section 3.1 in Walke and Limer, 2014).
- In SR-PSU, the exposure groups above could draw water from surface water, a well dug into the till, or from a well drilled into the bedrock.
- In SE-SFL, potential use of water from a drilled well is solely considered in a variant calculation.

The treatment and justification for changing assumptions with regards to drilled wells merits further discussion by SKB in future assessments. Most of the fresh surface water in the area is strongly coloured due to high concentrations of humic substances, leading to very high concentrations of dissolved organic carbon. This provides a potential driver for seeking cleaner, more palatable water for human use. Section 3.7 of the Biosphere Synthesis report references Morosini and Hultgren (2003) as describing more than 200 private wells in the Laxemar area, with one third of them being drilled to considerable depth.

Figure 12-19 of the Biosphere Synthesis report demonstrates that the radionuclide concentration in water from a drilled well is calculated to be at least a factor of two higher than that in dug wells for almost all radionuclides, and in many cases it can be several orders of magnitude higher. Further review of the representation of drilled wells in SE-SFL is provided in Section 3.4.

3.4. Treatment of groundwater wells

SKB have included an evaluation case to assess the potential doses from abstraction and use of water from a well drilled into the bedrock that intersects fractures containing contaminated groundwater (Section 7.8 of the Biosphere Synthesis report). Potential locations where wells might intersect contaminated groundwater were identified from the results of pathlines analyses, and three factors that would affect the viability of a well:

- low areas in the landscape, such as wetlands and agricultural land, were avoided as surface water inflow to the well could affect drinking water quality;
- to avoid unnecessarily deep wells, locations in high areas in the landscape were avoided; and
- the well would need to intersect at least one fracture in the flowing fracture network to provide sufficient yield.

The particle tracking results from five realisations of the groundwater flow model were considered in the analysis (Section 7.8.2 or the Biosphere Synthesis report) and five potential well locations were identified. Note that the locations are not constrained to being within the biosphere objects. Indeed, as the biosphere objects are associated with topographic lows, they may not be suitable for a drilled well due to the risk of surface water inflow. However, the potential well locations are located close to biosphere objects. This is expected, as the wells intersect fractures containing contaminated groundwater at relatively shallow depth (60 m) and, therefore, cannot be located far from the discharge locations. The method used to identify the locations is sensible, and the locations identified are of interest in the context of their spatial relationships to the biosphere objects.

Only one realisation of the groundwater flow model was used to calculate the well capture fractions (Section 4.7.2 of R-19-02). For the assumed abstraction rate, only well 3 captured any particles (Section 4.7.3 of R-19-02). 3.1% of particle tracks from BHA were intercepted and 2.1% from BHK (Section 7.8.3 of the Biosphere Synthesis report). These are small fractions, and while conceptually reasonable, it would be interesting to understand under what conditions higher capture fractions might be possible, including for alternative realisations of the groundwater flow model..

The deformation zones are strongly associated with topographic lows, as evidenced by the correlation between the deformation zones and streams in Figure 17. Rhén and Hartley (2009) note that the deformation zones are around an order of magnitude more permeable than the surrounding rock. This suggests the deformation zones will be areas of preferential groundwater flow. It is not clear from SKB's figures whether the wells intersect the deformation zones at depth. It would be interesting to know whether the capture fraction for wells that intersect the deformation zones is greater or less than for wells that do not.. The capture fraction in the deformation zones could be higher or lower than outside due to two competing factors: more of the radionuclide flux may transported through the deformation zones; but the radius of influence of the well will generally be lower within the deformation zones than outside.

Although locations within the biosphere objects might present challenges for groundwater quality, it would be interesting to know whether these would make a well totally unviable, or only further reduce the probability of a drilled well. It would also be interesting to know what the capture fraction could be for a well that intercepts the fracture paths that connect to the localised discharge zone.

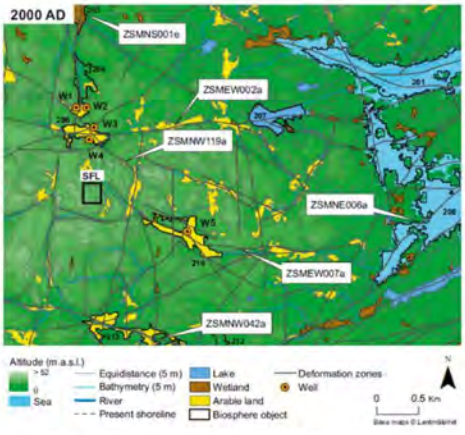

Figure 7-7. Potential well locations (orange, labelled W1 to W5) in the present Laxemar landscape. Biosphere objects are identified by numbers (e.g. 204, 206 and 210) and the names of deformation zones are given in white squares (ZSM). The spatial location and extent of deformation zones is for a depth of 20 m below sea level. The example location for the SFL repository is indicated with a square. Grey contour lines follow constant elevation, with a difference of 5 m between lines. Figure modified from Joyce et al. (2019).

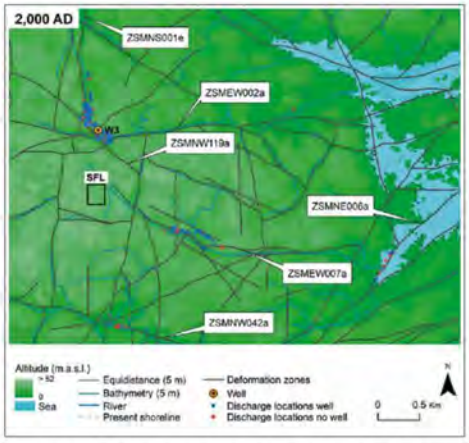

Figure 4-139. Particle discharge locations with pumping well W5 (blue) and with no well (red) at the ground surface for Case 1 of the facility focussed model at 2000 AD. The model surface is coloured by elevation (land in green, sea in blue). Rivers (blue), present shoreline (dashed grey), deformation zones at −20 m elevation (dark grey) and the SFL repository location (black) are added for context. Well location W3 is in orange.

Figure 17: Potential well locations (Figure 7-7 of the Biosphere Synthesis report), the location of well 3 (W3) relative to discharge locations for a single realisation of the groundwater flow model, and the impact of well 1 on the discharge locations for that realisation (Figure 4-159 of R-19-02).

4. Biosphere modelling

SKB's approach for modelling radionuclide transport and exposure is considered in Section 4.1. Independent calculations are presented and discussed in Section 4.2. The inclusion of a new approach for modelling long-term agriculture on drained mire areas is considered in Section 4.3. Some comments on the modelling of C-14 in the biosphere are then provided in Section 4.4.

4.1. Radionuclide transport and exposure modelling

SKB's approach to modelling radionuclide transport and exposure within biosphere objects is summarised in Section 4.1.1. Observations concerning the way in which the modelling approach was applied in SE-SFL are provided in Section 4.1.2.

4.1.1. Modelling approach for biosphere objects

The modelling of radionuclide transport and potential exposure pathways in SE-SFL builds on that used in the SR-PSU assessment and has been termed the BioTEx model by SKB. The approach is illustrated in Figure 18 and includes potential to explicitly model the transition from aquatic to terrestrial ecosystems, using a 1D vertical representation for each of these parts of the system.

The approach adopted in SE-SFL includes several refinements compared to SR-PSU, which are well summarised in Table 8-1 and discussed in Section 9 of the of the Biosphere Synthesis report. Some of the changes have been introduced by SKB as a result of internal review, and some have been introduced in response to review by SSM and its external experts (these are explicitly recognised in Table 8-1 of the Biosphere Synthesis report). The transparency with which SKB have described and explored model developments is welcome. Observations concerning some of the developments are provided below.

Extra discretisation introduced within the till and glacial clay helps to ensure that the time-dependency of radionuclide transport through these regolith layers is more appropriately represented. This addresses SSM feedback on SR-Site (Walke and Limer, 2014) and repeated in review of SR-PSU (Walke et al., 2016) biosphere modelling. SKB note that the additional discretisation reduces the level of numerical dispersion when modelling advection of radionuclides through these layers with groundwater flow. This means that more strongly sorbed radionuclides now take longer to migrate through the till and glacial clay layers. In reviewing the impact of the model refinements for a sub-set of radionuclides (C-14, Cl-36, Mo-93 and Ni-59), SKB note that the additional discretisation has a limited impact on those radionuclide with little retention or long half-lives (C-14 and Cl-36), but that there is a notable reduction of activity reaching the upper regolith layers for Mo-93 and Ni-59. These conclusions are valid, but it is also worth noting that improved representation of the transport time through the till and glacial clay will also result in an increase in the degree of in-growth within some decay chains, most notably for daughters of Ra-226 (Pb-210 and Po-210), which are of greater radiological significance compared to their parent radionuclide.

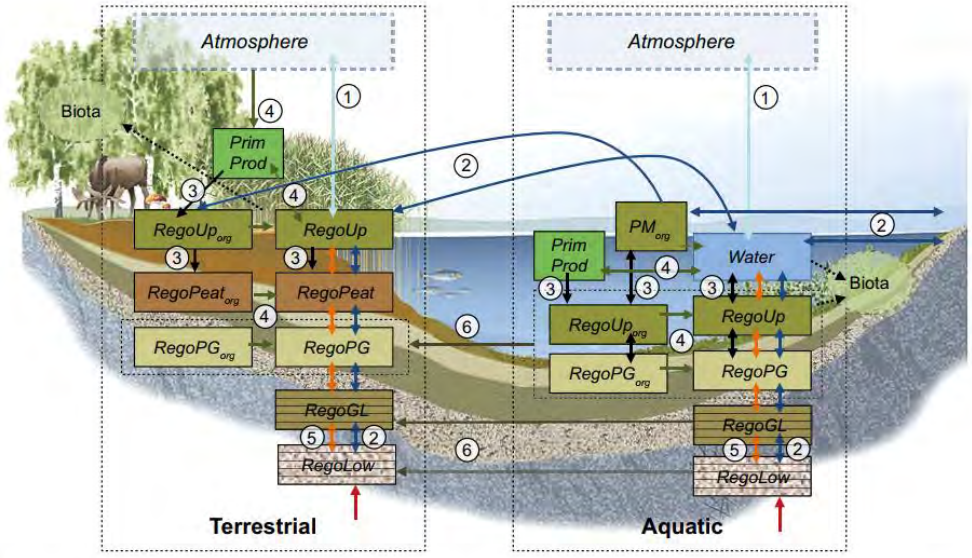

Figure 8-1. Conceptual model corresponding to the BioTEx model used to simulate transport and accumulation in a discharge area with two natural ecosystems (delimited by thin dotted black lines). Each box in the two ecosystems corresponds to a radionuclide inventory associated with a physical or biological compartment. Note that in SE-SFL the two lowermost regolith layers are represented by five compartments each. Arrows represent flows of radionuclide between compartments and flows into and out of the system. Radionuclide flows are linked to mass flows of gas (1, light blue), water (2, dark blue) and solid matter (3, black), to transitions between inorganic and organic forms of radionuclides (4, green), to diffusion in soil pore water (5, red), and to ingrowth of wetland vegetation (6). The red arrow indicates that the geosphere release enters the biosphere via groundwater discharge to the till. Dotted boxes (atmosphere and biota) are assumed to be in equilibrium with the corresponding environmental media, and the uptake of radionuclides into biota (dotted arrow) is not included in the mass balance of the BioTEx model.

Figure 18: Conceptual model for radionuclide behaviour within a biosphere object for SE-SFL (Figure 8-1 of the Biosphere Synthesis report)

The modelling of retention of radionuclides in plant material has been simplified, as it was shown to be unimportant. The enhanced BIOMASS methodology notes that long-term biosphere modelling should aim to be as simple as can be justified (Lindborg, 2018). SKB demonstrate good practice in drawing on previous modelling to justify simplifications, where appropriate.

4.1.2. Approach to evaluation cases included in SE-SFL

Based on particle tracking for the illustrative repository location and depth at Laxemar, SKB assess potential dose consequences arising from 100% of the modelled discharge to the biosphere being received by a single biosphere object. This is clearly a pessimistic approach (as also noted in Section 3.1.3), although Section 5.3 of the Biosphere Synthesis report notes that in excess of 60% of particles modelled and tracked from the repository may end up within or close to one of biosphere objects 204, 206 or 210, depending on the stochastic fracture network realisation, so it is not necessarily grossly pessimistic.

The SE-SFL assessment neglects explicit modelling of biosphere objects downstream from the object receiving the contaminated groundwater discharge. This is reasonable,

given the objectives of the assessment, but, as also noted in Section 3.1.3, merits on-going review, given that a down-stream object gave a higher landscape dose conversion factor for Mo-93 in the SR-PSU assessment, when a unit release was modelled.

Most of the radionuclide transport and exposure modelling for SE-SFL has been undertaken for objects without explicitly modelling the transition between the sea-lake-mire states. This simplifies the assessment and is broadly justified based on previous assessments, as well as independent modelling undertaken for Forsmark for biosphere objects without transition in Walke and Limer (2014). Modelling including biosphere transitions is included within a variant evaluation case, although that is based on the larger biosphere object 201, rather than object 206, which is the main focus for the base case. Results when ecosystem transition is explicitly included were found to be similar to those when modelled without transition. SKB conclude that using a time-independent representation of lake and mire ecosystems (as done in the base case) is a reasonable and sound simplification. This conclusion should however be reviewed in the context of each assessment. For example, Walke and Limer (2014) found that modelling Forsmark objects without transition had potential to underestimate dose consequence for some radionuclides by more than an order of magnitude (see Figure 7 in Walke and Limer, 2014). Those notably include Se-79 and I-129, which are of greater interest in the context of a disposal facility for spent nuclear fuel compared to the SFL concept.

SKB explore potential implications of radionuclide releases to biosphere objects with a comprehensive range of characteristics, based on consideration of both the Laxemar and Forsmark regions through the *alternative discharge area* evaluation case. The main results are reproduced from the Biosphere Synthesis report in Figure 19, with the reference biosphere object 206 highlighted in the middle. It is evident that, although the selected biosphere object is relatively pessimistic for the modelled releases from the BHK vault (lower part of the figure), results for some biosphere objects, notably 157_2 from Forsmark, could be higher in the case of releases from the BHA vault. This is attributed to relatively thin post-glacial sediments in biosphere object 157_2, which allows radionuclides bound within the glacial clay to be drawn into the agricultural soils. The sensitivity of results to the assumed thickness of the post-glacial sediments is notable, especially given the intrinsic uncertainties associated with landscape development modelling on such long timescales (Section 16.3.1 of the Biosphere Synthesis report).

The SE-SFL assessment includes a very comprehensive exploration of the biosphere modelling results and associated uncertainties. SKB have used a wide range of approaches for exploring and illustrating the results, which is commendable. Direct comparison of radionuclide fluxes to the biosphere with associated doses for the present-day evaluation case is a case in point (see Figure 20). The comparison highlights where processes within the biosphere, coupled with radiotoxicity of each radionuclide, play an important role in shaping the assessment results and motivates further exploration of the results by SKB. For example, the figure highlights that:

- C-14 dominates calculated radionuclide releases to the biosphere, but that it does not dominate the peak calculated doses; this is due to the way in which it is dispersed relatively rapidly upon reaching the surface; and
- the significant delay in Tc-99 from the BHA vault reaching the surface regolith layers, due to very high sorption within the glacial clay.

That SKB have shared the detailed analysis of results is welcome; however, some detail is difficult to follow and may merit relegation to appendices or even supporting reports in

assessments supporting a formal licence application. The synthesis of radionuclide property effects on dose is a case in point (Section 11.7 of the Biosphere Synthesis report).

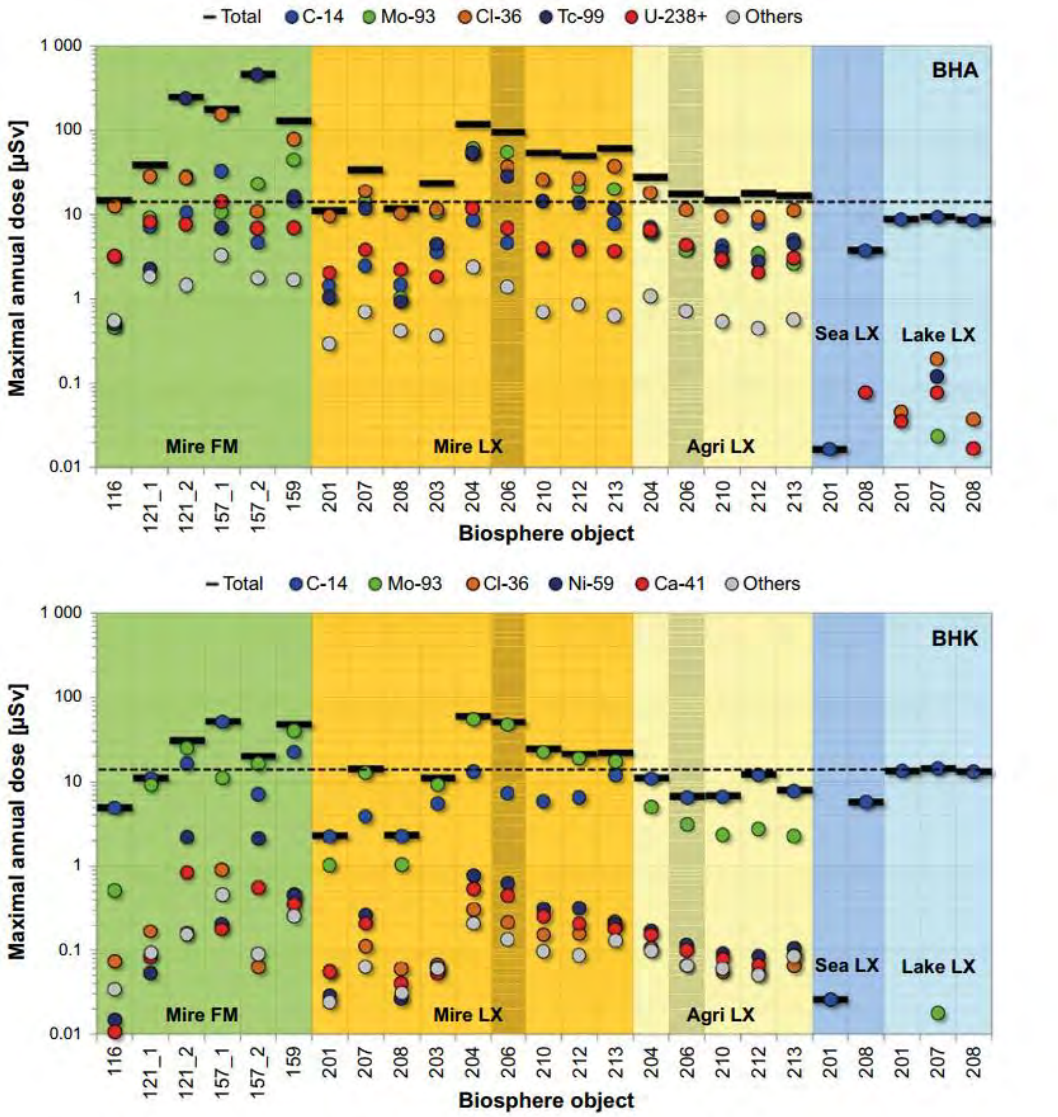

Figure 12-4. *Maximum annual doses from the most important radionuclides in Forsmark objects (green background) and Laxemar objects (all other background colours) from BHA (upper panel) and BHK (lower panel) radionuclide releases. The base case object 206 is indicated in darker shade. Time-independent mire objects in Forsmark (FM, green background) and Laxemar (LX, orange) are represented by drained mire doses including exposure from a dug well, time-independent agricultural objects (yellow) include exposure from a dug well and time-independent sea (blue) and lake (light blue) objects are represented by doses to hunters and gatherers. The dose corresponding to the regulatory risk criterion is shown with a dashed horizontal black line (14 μSv). Observe that the sum of the radionuclide-specific maximum doses can be larger than the maximum of the total dose, since the doses from individual radionuclides reach their maximum levels at different times.*

Figure 19: SKB's analysis of the alternative discharge area evaluation case (Figure 12-4 from the Biosphere Synthesis report)

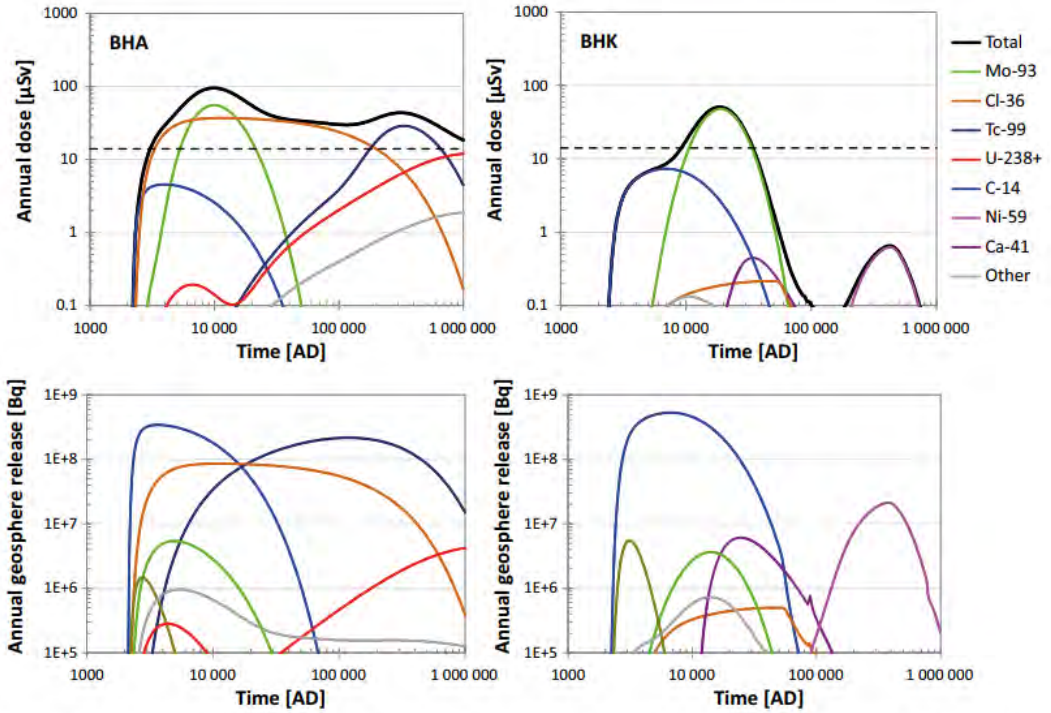

Figure 11-3. *Annual dose (upper panels) in the drained mire case from BHA (left panels) and BHK (right panels) respectively and annual geosphere releases (lower panels) for the radionuclides contributing most to total dose. For comparison, the annual dose (14 µSv) corresponding to the regulatory risk criterion is indicated by the black hatched horizontal line in the upper panels. Doses and releases of radionuclides in the U-238 decay chain (U-238+) are analysed in Section 11.2.5.*

Figure 20: Radionuclide fluxes to the biosphere (lower figures) and associated calculated doses to drained mire farmers (upper figures) for the present-day evaluation case[6] (Figure 11-3 from the Biosphere Synthesis report)

4.2. Independent modelling

In SSM's experts' reviews of biosphere aspects of the SR-PSU assessment (Walke et al., 2017a; b), independent modelling was undertaken to support review of the comprehensiveness of the documentation of the biosphere models and data and to verify SKB's calculations. SKB's biosphere model was implemented in the generic compartment modelling code AMBER (Quintessa, 2020a) and reasonable agreement with SKB's results was achieved (Figure 21). The model takes radionuclide fluxes from the geosphere to the biosphere (Bq per year) calculated by SKB as the input and calculates potential doses to different receptors for releases to different biosphere objects.

[6] The olive coloured radionuclide released to the biosphere at relatively early times is not identified in the key, but is not radiologically significant.

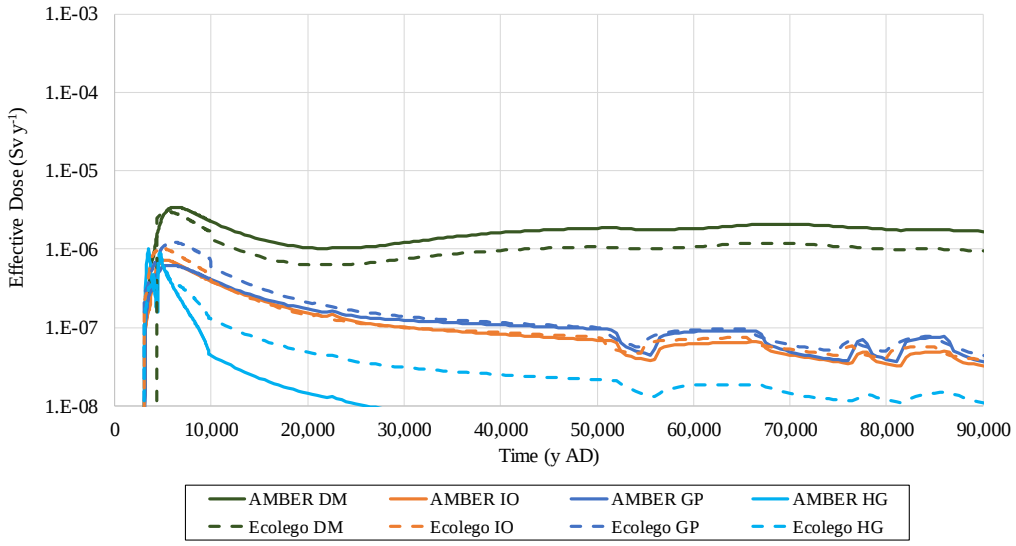

Figure 21: Total calculated effective doses to 90,000 AD for drained mire farmers (DM), infield-outland farmers (IO) and garden plot group (GP) based on biosphere object 157-2 and for hunter gatherers (GM). Comparison of SR-PSU biosphere model in Ecolego and re-implemented in AMBER. Reproduced from Figure 1 in Walke et al. (2017a).

SKB include some direct comparison between the SR-PSU and SE-SFL biosphere models in Section 9 of the Biosphere Synthesis report. However, those comparisons are limited to steady-state systems (typically unit fluxes into the biosphere). It is interesting to compare the quantitative differences between the SR-PSU and SE-SFL biosphere models when time-dependency in the source term to the biosphere is included and when the explicit evolution of the biosphere system is included in the SR-PSU modelling, to match the central assumptions used in that assessment.

To facilitate such a comparison, the radionuclide fluxes from the SE-SFL geosphere (for BHA and BHK) have been input to the SR-PSU biosphere AMBER model, and the resulting doses compared with the results from SE-SFL.

The SE-SFL geosphere fluxes are taken from Figure 11-3 in the Biosphere Synthesis report using the GraphGrabber tool (Quintessa, 2020b). This figure shows only those radionuclides that contribute to the highest doses in the drained mire case: Mo-93, Cl-36, Tc-99 and C-14 for BHA; Mo-93, Cl-36, C-14, Ni-59 and Ca-41 for BHK (see Figure 20). The U-238 chain is not included in the comparison since only the total geosphere fluxes for the chain are shown in the figure. There will be some uncertainty in the interpreted fluxes due to the imprecision in reading fluxes from the figure, and the fact that only fluxes within the ranges of the graph axes can be read. These fluxes have been imported directly into the AMBER implementation of the SR-PSU biosphere model.

In the comparison, the geosphere discharges from BHK and BHA are assumed to release separately into the SR-PSU biosphere object 157_2, consistent with the main SR-PSU assessment calculations and the way in which the SE-SFL results are presented. The two downstream objects (157_1 and 116) are also explicitly modelled in the independent AMBER implementation. As in the SE-SFL assessment, the main doses are to the drained

mire farmer, so these are the focus of the comparison. The drilled well interception fraction for BHA and BHK is set to zero since this is only included as a variant evaluation case in SE-SFL.

The comparisons between the SR-PSU biosphere AMBER doses and SE-SFL biosphere doses are shown in Figure 22 and Figure 23 for the BHA and BHK releases, respectively. The SE-SFL doses are taken from Figure 11-3 in the Biosphere Synthesis report using GraphGrabber. The SE-SFL assessment timeframe is 1,000,000 years but the SR-PSU results are only available for 90,000 years so this time period is the focus of the comparison. Ni-59 only contributes significantly to the BHK dose only after this time so is excluded from Figure 23. Doses are reported for the exposure groups in the release object (157_2); doses in the downstream objects are significantly lower. This finding provides some support to SKB's focus on the biosphere objects receiving the contaminated groundwater from depth and ignoring explicit representation of downstream objects in SE-SFL.

The SE-SFL doses for biosphere object 206 for Mo-93 and C-14 are higher than those calculated in theSR-PSU AMBER biosphere model for object 157_2 for both the BHA and BHK releases, though not dramatically so (within a factor of two).

For the BHK release, the comparison shows broadly similar results between the SE-SFL results for Ca-41 and the AMBER implementation of the SR-PSU model.

For Cl-36 and Tc-99, the results of the AMBER implementation of the SR-PSUPSU model for biosphere object 157_2 yields doses that are significantly higher than the SE-SFL results arising from object 206.

The higher results for Tc-99 (BHA only) are, to some extent, corroborated by SKB's alternative discharge area results, which show notably higher Tc-99 results for biosphere object 157_2 (see Figure 19). This suggests that the discrepancy is, to some extent, a reflection of the different characteristics of biosphere objects 157_2 and 206. As noted above, the result can be attributed to the thinner post-glacial deposits in biosphere object 157_2, which allows glacial clay to be drawn into the drained mire soils. The very high degree of modelled sorption for Tc-99 on glacial clay means that this has a significant effect on calculated doses.

The higher results for Cl-36 cannot be attributed to the different characteristics of the biosphere objects, because SKB's comparison, reproduced in Figure 19, shows a reduction in the Cl-36 dose between biosphere objects 206 and 157_2. This suggests that the higher results from the AMBER implementation of the SR-PSU model may be attributable to the changes in the modelling approach for Cl-36 between the two assessments and/or the explicit representation of ecosystem transition in the SR-PSU results. A potentially important difference may be the change to a specific activity model for plant uptake for Cl-36, as discussed in Section 5.3.

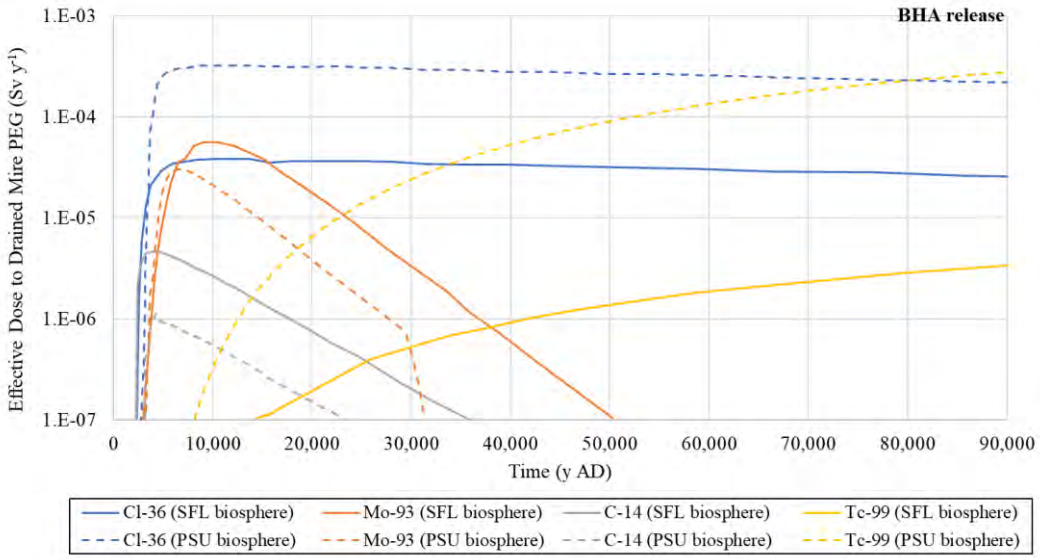

Figure 22: Annual dose in the drained mire case from BHA for the key radionuclides. Comparison of the SE-SFL biosphere model (reproduced from Figure 11-3 of the Biosphere Synthesis report) and SR-PSU biosphere model, re-implemented in AMBER.

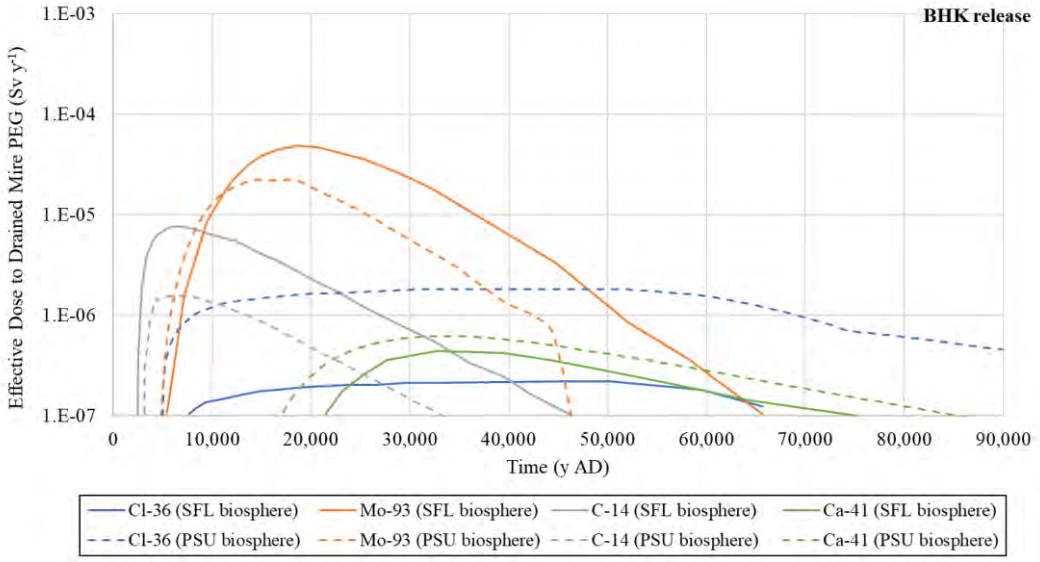

Figure 23: Annual dose in the drained mire case from BHK for the key radionuclides. Comparison of the SE-SFL biosphere model (reproduced from Figure 11-3 of the Biosphere Synthesis report) and SR-PSU biosphere model, re-implemented in AMBER.

4.3. New model for permanent agriculture

The Biosphere Synthesis report notes that farming in the Laxemar area is believed to date back about 500 years, with farming expanding until about 1900 AD and now in general decline. In the SR-Site and SR-PSU assessments, potential for long-term cultivation of drained mires was excluded on the basis that the significant organic matter content of drained mire soils would degrade relatively quickly and the structure of the soils would

subside to a point where further agricultural use becomes untenable. Evidence for longer-term agriculture in the Laxemar region means that this assumption has been revisited for the SE-SFL assessment.

The model for drained mire farming in SR-PSU includes initial contamination of the drained soils as a result of radionuclide accumulation in the mire peat, with subsequent losses through leaching, radioactive decay and degassing. Allowance is also made for potential further uptake of radionuclides with groundwater uptake from the saturated zone below the drained soil. An analytical solution is used to simulate the average concentration in the drained soil in the first 50 years after the mire is originally drained (see Section 7.2.1 of R-13-46).

The new SE-SFL model for continuous agriculture on drained mire soils is illustrated in Figure 24. The model allows long-term interaction between the drained soils and the regolith below to be explicitly modelled, although it is notable that, unlike the SR-PSU model for drained mire soils, it excludes initial contamination that would have been present in the peat prior to initial drainage. The configuration of the radionuclide transport and exposure model for SE-SFL explicitly includes both the original SR-PSU model for drained mire soils, as well as the new model for continuous agriculture (Agri).

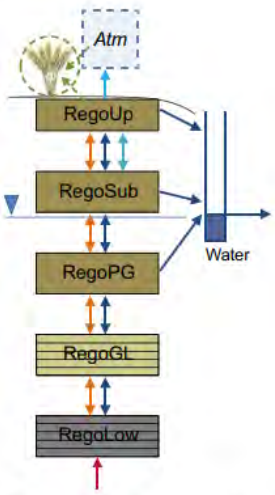

Figure 8-2. *Conceptual model corresponding to the radionuclide transport model (BioTEx) used for continuously cultivated agricultural ecosystems. Each large box corresponds to a radionuclide inventory associated with a regolith layer. Note that the two lowermost regolith compartments are represented by five sub-compartments each. Solid arrows represent radionuclide fluxes between compartments and fluxes out of the system. Radionuclide fluxes are linked to diffusion of gas (light blue) and solutes (orange), and to mass fluxes of water (dark blue). The water from the three uppermost compartments is drained to a ditch (marked 'Water' in the figure). The red arrow indicates that the geosphere release enters the biosphere via groundwater discharge to the till. The activity concentrations in the atmosphere and in the crops are calculated assuming equilibrium conditions.*

Figure 24: New model for continuous agriculture on drained mire soils used in SE-SFL (Figure 8-2 from the Biosphere Synthesis report)

Results for the full range of biosphere objects at Laxemar indicate that the original SR-PSU model for drained mire farming results in higher calculated concentrations compared to the model for continuous agriculture (see Figure 12-3 of the Biosphere Synthesis report). This is likely due to the importance of the initial contamination within the peat, which is excluded in the model for continuous agriculture. Nonetheless, consideration of

the potential for continuous agriculture is justified by the Laxemar context and could be carried through to assessments for other potential sites (including Forsmark) as well. That the two types of drained mire farming are treated differently can, to some extent, be considered to be an artefact of the way in which SKB has chosen to model initial draining of the mire for agriculture.

4.4. Representation of C-14 in the biosphere

SKB have included some refinements to the way in which C-14 in the biosphere is modelled; these are summarised in Table 8-1 on the Biosphere Synthesis report. The refinements explicitly represent some parameter interdependencies and address some potential inconsistencies identified in review of the SR-PSU assessment, which were of most relevance to probabilistic simulation. The approach to modelling C-14 is otherwise largely consistent with that used in the SR-PSU assessment, such that associated review findings remain valid.

The particular importance of carbon in the mire systems of interest is recognised in SKB's modelling approach, with explicit representation of organic carbon in surface regolith layers.

SKB adopt a novel approach to modelling C-14 transfers in the biosphere. It was noted during the SR-PSU review that SKB's assumed degassing rates from the upper regolith are much higher than those used in other assessments (Walke et al., 2017b). This, coupled with the 1D groundwater flow assumptions, which tends to drive contaminants straight to the upper regolith from where degassing becomes possible, results in a relatively short residence time for C-14 in biosphere object 206 of 15 years (Section 11.5 of the Biosphere Synthesis report). The previous review noted that there is no explicit consideration of the speciation of C-14 in the biosphere model beyond distinction between the organic and inorganic carbon pools. This means that distinction in behaviour of different forms if not explicitly modelled. SKB acknowledge that further revision of their assessment model should account for the relevant forms of carbon in the environment (Section 17.7 of the Biosphere Synthesis report).

Previous review also noted that the explicit modelling of C-14 uptake into primary producers in aquatic systems, and subsequent uptake by fish, results in an effective concentration ratio between the surface water and fish that is significantly lower than that used in other assessments (Walke et al., 2017b). In this context, the very high dissolved organic carbon content of surface water in the lake-mire system is noted, which may justify lower uptake by fish when compared to a standard concentration ratio approach. Nonetheless, further discussion and justification has not been found for SE-SFL; therefore, there remains potential for further confidence to be built in this part of the model through further discussion and consideration by SKB in future assessments.

5. Biosphere data

SKB's approach to managing parameter uncertainties in the SE-SFL study is discussed in Section 5.1. Traceability and transparency of the justifications for a selection of key parameters is then reviewed in Section 5.2. The new specific-activity approach for modelling plant uptake of certain elements is then reviewed in Section 5.3.

5.1. Approach to management of parameter uncertainty

The SR-PSU assessment adopted a probabilistic approach to accounting for parameter uncertainty in the central calculations. SE-SFL adopts a deterministic approach in most cases, with probabilistic simulations reserved for some of the sensitivity cases. This is reasonable for a proof-of-concept level study.

Comparison between landscape dose factors calculated in SR-PSU based on unit source-terms to the biosphere demonstrated that the arithmetic mean values from the probabilistic simulation were always equal to or higher than the corresponding values from a single simulation based on best estimate parameter values (Section 10.9.1 and Table A4-1 of TR-14-06). For C-14, Cl-36, Mo-93 and Tc-99, the arithmetic mean of the SR-PSU probabilistic results is between about a factor of two and five higher than the best estimate results. That distributions for many biosphere parameters are log-transformed means that arithmetic average results from probabilistic sampling typically reside above the peak of each distribution. This likely pessimistically skews the arithmetic mean taken as the 'expectation value' used as the basis for the comparison with the deterministic 'best estimate' approach.

SE-SFL explores some alternative parameter sets as part of sensitivity studies. These notably include a sensitivity case exploring potential implications of aged soils, and a case exploring potential results using generic values for K_d and soil-to-plant concentration ratios. In each case, the studies are limited by practical considerations:

- sorption values were varied in the aged soil analysis, but soil-to-plant uptake parameters (CR) were not; and
- limited applicability of the IAEA (2010) K_d and CR data (for typical agricultural soils) for the regolith layers and redox conditions applicable to the mire context, coupled with the need to draw on element analogues for much of the data.

The use of site-specific data is well founded for the SE-SFL context. In the absence of some data for Laxemar, then use of data for the Forsmark site is understandable, albeit SKB note that the geochemical conditions differ between the two sites.

Section 14 of the Biosphere Synthesis report summarises reviews of the behaviour of Cl, Mo and Ni in the biosphere, as these radionuclides are recognised as being of potential importance for SE-SFL. The assessment results indicate that a similar level of review would have been merited for C-14 and Tc-99 as well.

5.2. Review of key parameters for important radionuclides

The Biosphere Synthesis report presents an analysis of the key radionuclides and exposure pathways which contribute to the peak annual doses. Doses from the drained mire

farming (DM) exceed doses from the other land-use variants. Radionuclides which contribute most to the dose to the drained mire farmer are Mo-93, Cl-36 and C-14 for both BHA and BHK, as well as Tc-99 and the U-238 chain for BHA. The main pathway is ingestion of crops from the cultivated soil.

Table 11-1 of the Biosphere Synthesis report presents key properties of the radionuclides that contribute significantly to the dose from BHA:

- half-lives;
- sorption coefficients (K_d);
- concentration ratios (CR); and
- dose coefficients for ingestion (DC_{ing}).

Those parameters are the main focus of this review, for the key radionuclides: Cl-36, C-14, Mo-93, Tc-99 and the U-238 chain (U-238, U-234, Th-230, Ra-226, Pb-210, Po-210). The model for C-14 is discussed in Section 4.4.

The Biosphere Parameters report (R-19-18) gives more details of the values used in the SE-SFL biosphere model. Section 2 of the report presents the radionuclide-specific parameters including half-lives and dose coefficients, for which values are given in Appendix A.

Section 6 of the Biosphere Parameters report discusses the approach to selecting element-specific parameters including sorption coefficients and concentration ratios. The K_d and CR values are affected by local conditions (including pH, CEC, organic matter and clay content), so site-specific data are preferred. The data have all been taken from the SR-PSU report (Tröjbom et al., 2013) which presents K_d and CR values from Laxemar, Forsmark, and various literature sources. Laxemar data have been used where available. Where Laxemar data are not available, data from Forsmark has been used in preference to literature data since it is deemed to be a similar Swedish site even though the geochemical properties differ. When no data from either site is available for a particular radionuclide, element analogues are used. Finally, literature data are used to fill in the remaining gaps. The values in the SE-SFL Biosphere Parameters report are presented to three significant figures, compared to two significant figures in SR-PSU report (Tröjbom et al., 2013).

The key sorption coefficients identified in the Biosphere Synthesis report as affecting the main exposure pathway are for 6 different sediment types: lower regolith/till (kD_regoLow), glacial clay (kD_regoGL), postglacial sediments (kD_regoPG), terrestrial regolith/peat (kD_regoPeat), the upper oxic layer of terrestrial regolith/peat (kD_regoUp_ter) and cultivated soils in the drained mire (kD_regoUp_Drained mire). It should be noted that in Table 11-1 of the Biosphere Synthesis report, "regoUp (Agri)" refers to the cultivated soils in the drained mire ("kD_regoUp_Drained mire" in the Biosphere Parameters report) and "regoUp (Mire)" refers to the upper oxic layer of terrestrial regolith/peat ("kD_regoUp_ter" in the Biosphere Parameters report). The terminology is not entirely consistent between the two reports and could lead to confusion.

No data are available from Laxemar for any of the terrestrial soil types so all of these K_d values are taken from Forsmark and are therefore unchanged from the SR-PSU assessment. The SR-PSU report (Tröjbom et al., 2013) describes in detail how the data are derived and the overlap with literature data. Site data for Cl and Mo in particular are noted to be higher than literature data; for most other radionuclides, there is overlap between the site data and literature data such as IAEA (2010).

Bi is used as an element analogue for Po, although it is noted in Tröjbom et al. (2013) that site data for Bi are often higher than literature data for Po so this may result in an overestimate of some sorption coefficients. Zr(IV) and Re are used as analogues for Tc depending on whether the conditions are reducing (regoLow, regoGL, regoPG, regoPeat) or oxic (regoUp). These assumptions are discussed in SSM's review of the SR-PSU biosphere (Walke et al., 2017a) and further review (Walke et al., 2017b), which concluded that there is some justification for using these element analogues but there is a large amount of variability in the data for Tc and Mo could also be a suitable analogue. The selected K_d values for Tc in glacial clay and till are two orders of magnitude higher than Mo.

There is also no CR data from Laxemar for terrestrial vegetation, so again the data are unchanged from SR-PSU. A review of these values has been undertaken in Walke et al. (2017b). The largest doses in SE-SFL result from ingestion of cereals, with the next highest dose from ingestion of tubers (potatoes). Concentration ratios are not used to model uptake of Cl which instead uses a specific activity approach (discussed in Section 5.3).

For cereals, data from Forsmark have been used for all the key elements except Ra. Similar to the K_d data, Bi is used as an element analogue for Po and Re is used as an analogue for Tc. No data from Forsmark are available for Ra so data from IAEA (2010) are used instead; specifically, transfer factors for cereals (grain) in a temperate environment using the 'all soils' category. The other concentration ratios derived from Forsmark data generally fall within the range of literature data in IAEA (2010) except Mo and Tc which use slightly lower values and Po which uses a slightly higher value.

For tubers, literature data have been used from IAEA (2010); specifically, transfer factors for tubers in a temperate environment using the 'all soils' category. The exception is Mo for which the 'root crop' category is used instead of tubers in the absence of tuber data. The transfer factors in IAEA (2010) are in $kg_{dw\_plant}\ kg_{dw\_soil}^{-1}$, whereas the SFL documentation presents concentration ratios in $kg_{dw}\ kg_{C}^{-1}$, i.e. normalised by the carbon content of each biota sample (CC). This complicates the comparison, since the SFL documentation do not give values for CC used in the assessment. This data can only be found in Appendix F of the underlying SR-PSU biosphere data report (Tröjbom et al., 2013). Using this to normalise the IAEA (2010) values confirms that the selected values are consistent with the underlying reference.

5.3. Move to a specific activity approach for Cl, K and Ca

SKB have modified its approach to modelling the uptake of certain elements that can be regarded as macronutrients rather than trace contaminants. It has adopted a "specific activity" approach rather than the previously-used concentration ratio model, arguing that this provides a more appropriate basis for estimating the concentration in plants. The specific activity approach treats the concentration of macronutrients in plants as being regulated by the plant and therefore not dependent on the concentration of the element in the soil. For radioisotopes of these elements (and SKB consider macronutrients to include Cl, K and Ca) the concentration in the plant can be determined from the ratio of the stable element concentration in the plant and that in the soil pore water. For example, the concentration of Cl-36 in a plant ($C_{Cl-36,Plant}$, g kgC^{-1}) is calculated with:

$$C_{Cl-36,Plant} = C_{Cl\ stable,Plant} \frac{C_{Cl-36,SW}}{C_{Cl\ stable,SW}}$$

Where

$C_{Cl-36,SW}$ is the concentration of Cl-36 in the soil pore water (g m^{-3});
$C_{Cl\ stable,Plant}$ is the concentration of stable Cl in the plant (g kgC^{-1});
$C_{Cl\ stable,SW}$ is the concentration of stable Cl in the soil pore water (g m^{-3}).

IAEA (2010) also considers the specific activity approach as being valid for biologically-regulated essential elements that are mobile in the environment. Indeed, IAEA describes the application of a specific activity model for Cl-36 alongside that for H-3 and C-14. Although IAEA (2010) does not present such a model for Ca and K, these elements can both be regarded as comfortably fitting the criteria – i.e. they are essential nutrients present in significant concentrations in plant and soil, and they are environmentally mobile and thus capable of active regulation in the organism.

Of the radionuclides relevant to SE-SFL, Cl-36 is a significant contributor to the total dose from the disposal concept, being the second most important radionuclide for the BHA inventory (contributing around 30 µSv y^{-1} to the peak dose of 100 µSv y^{-1}) (SKB, 2019b). Ca-41 also gives rise to a notable contribution to the dose from the BHK, dominating in times after 100,000 y, with a peak dose of around 0.7 µSv y^{-1}.

The dose from Cl-36 is primarily due to ingestion of food. According to the specific activity model, concentrations in food depend on the pore water activity concentration in the cultivated soil. This, in turn, is derived primarily from the accumulated inventory of Cl-36 in the upper regolith layers before draining and the pore water concentration in the postglacial clay-gyttja through groundwater uptake. For Ca-41, SKB (2019b) note that the behaviour of the radionuclide is similar to that of Mo-93, which is the dominant radionuclide in terms of radiation dose. Mo-93 is, however, around 100 times more significant than Ca-41 due to its greater sorption in peat and higher radiotoxicity.

Calculation of the concentration of the relevant radioisotopes in plants using the form of equation above (determining the dose from this pathway) requires the following information:

- the concentration of Cl-36 in soil water, a time-dependent quantity calculated by SKB's radionuclide transport models;
- a reference concentration of stable concentration in relevant plant species; and
- a reference concentration of stable concentration in relevant soil types.

The reference concentration data for stable elements of Ca, Cl and K that is assumed by SKB is shown in Table 4 and Table 5. Data for Cl and Ca in vegetation was based on measurements at Forsmark; insufficient data were available from Laxemar. For Cl, there was no difference in concentrations in grains, stems and roots so a single value was applied for all plants. For Ca and K, the different parts of a cereal plants had different concentrations and the results were used as values for vegetables, fodder and tubers. Separate data were available for Ca and K in mushrooms. Grolander and Jaeschke (2019) note that the Ca concentration in cereals at Forsmark was a factor of two higher than found in spring wheat from elsewhere, but values were similar for K.

Table 4: Elemental concentrations in foodstuffs (g kgC^{-1}) assumed by SKB (Biosphere Parameters report)

Plant	Ca	Cl	K
Cereal	1.46	0.567	10.6
Fodder	4.31	0.567	11.5
Mushroom	0.47	0.567	86.6
Tuber	7.34	0.567	10.6
Vegetables	4.31	0.567	11.5

For Cl and K, there were insufficient data on concentrations in the relevant regolith types at Laxemar, so data for Forsmark were used. Limited data from Laxemar were also available for Ca, but noting that the porewater concentration can depend on $CaCO_3$ in the soil, these were used.

Table 5: Elemental concentrations in soil porewater (g m^{-3}) assumed by SKB (Biosphere Parameters report)

Soil Type	Ca	Cl	K
RegoUp_D (infield-outland)	46.4	5.28	1.66
RegoUp_D (garden plot)	46.4	5.28	1.66
Rego_gyttja_D (drained mire)	46.4	5.28	1.66
RegoUp_peat_D (drained mire)	46.4	2.53	0.728
RegoUp_ter_D	46.4	13.9	6.00

Parameter Value Assumptions

IAEA (2010) provides data on stable Cl concentrations in foodstuffs and soils, for use in specific activity calculations, which can be compared with the values assumed by SKB. These are shown in Table 6. The concentration of stable Cl in soil pore water used by SKB appears to be somewhat lower than suggested by IAEA in groundwater although similar to that in surface water. Concentrations in soil (by mass) in agricultural soil are given by IAEA as 0.2 g kg^{-1}, but elsewhere values for Sweden are reported to be typically lower, around 0.05 g kg^{-1}, although it is noted they can be 10 times greater in peaty soil (Svensson et al., 2021).

Noting that SKB express concentrations in terms of kgC^{-1}, and that carbon content of plants is typically around 0.4 and that dry matter content of 0.9 for cereals and 0.1 – 0.2 for vegetables, the reference values used by SKB are lower than the ranges given by IAEA for all vegetables, significantly so in vegetables with a high water content. Note that the data in IAEA (2010) are slightly ambiguous as to whether they are by fresh weight or dry weight, and the application of the dry matter content in converting the values could explain much of the difference.

Table 6: Stable chlorine concentrations in environmental media and foodstuffs (IAEA, 2010)

Medium	Concentration in medium	Plant	Concentration in Plant^ (g kgC^{-1})
Groundwater	16 g m^{-3}	Cereals (grains)	0.59 – 2.7
River water	7 g m^{-3}	Root vegetables	1.7 – 13
Rain water	11 g m^{-3}	Leafy vegetables	3.3 – 45
Soil	0.2 g kg^{-1} (dw)		

Note: ^Concentrations in plant are given by IAEA in terms of fresh weight of the plant. These have been converted to kgC^{-1} by dividing by the product of the dry matter content and the carbon content, using data from SKB.

Turning to Ca, White and Broadley (2003) indicate that around 5 g kg^{-1} of Ca is found in shoots of plants grown in soils with a concentration of 1 mM Ca (40 g m^{-3}) indicating the assumptions for Ca in plants and soils are reasonable.

For K in plants, data from Finland and Estonia, collated in a database (Vergutz et al., 2012) indicate an average concentration of 0.28 % [dw] (i.e. 2.8 g kg^{-1}), somewhat lower that the average for all data collected globally of 0.95 %. The overall average is similar to the values used for vegetation by SKB with the exception of mushrooms. Potassium content in soils in coastal regions of Sweden are typically around 150 mg kg^{-1} (26 g m^{-3}, if SKB's sorption coefficient for garden soil is applied) (Ballabio et al., 2019). Inland areas can be more deficient, at less than 100 mg kg^{-1} (17 g m^{-3}). The difference between these values and the lower concentrations used by SKB could, however, be related to the Kd value used. For comparison, K in untreated drinking water is reported to be in the range of <1 – 8 g m^{-3} with a mean value of 2.5 g m^{-3} (WHO, 2009) suggesting that the values adopted by SKB are reasonable.

Comparison with Concentration Ratios

In previous safety assessment studies, SKB have used concentration ratios for Ca and Cl (see Tröjbom et al. (2013)) and has not assessed the contribution of radioisotopes of K. Concentration ratios for Ca and K are also provided by IAEA (2010) which can give an additional point of comparison. These are presented in Table 7.

Table 7: Best-estimate soil-to-plant concentration ratios (kg kgC^{-1})

Plant type	Source	Ca	Cl	K
Cereals	SKB	0.23	7.3	-
Cereals	IAEA^	20	-	1.7
Fodder	SKB	0.93	390	-
Mushrooms	SKB	0.051	390	-
Tubers	SKB	0.39	34	-
Vegetables	SKB	2.0	69	-
Leafy Vegetables	IAEA^	42	-	-
Legumes	IAEA^	-	-	3.4

Note: ^IAEA values have been converted from kg^{-1} to kgC^{-1} by dividing by the concentration ratio by the carbon content (in kgC kg^{-1}).

The equation presented earlier can be used to determine effective "specific activity concentration ratios" for Ca, Cl and K which can be compared with the values presented in Table 7. However, these are in terms of g kg^{-1} in soil, whereas the specific activity method relates the concentration to soil pore-water (i.e. g m^{-3}). The former value can be calculated from the latter by application of the sorption coefficient (Kd, m^3 kg^{-1}):

$$C_{Cl-36,SM} = Kd_{Cl}\, C_{Cl-36,SW}$$

Where

$C_{Cl-36,SM}$ is the concentration of Cl-36 in the soil pore water (g m^{-3});
Kd_{Cl} is the sorption coefficient of Cl in the soil (m^3 kg^{-1}).

Using this relationship, the "specific activity concentration ratio" ($CR_{Cl-36,SA}$) implied by the specific activity approach can determined with:

$$CR_{Cl-36,SA} = \frac{C_{Cl\ Stable,Plant}}{Kd_{Cl}\, C_{Cl\ Stable,SW}}$$

The "specific activity concentration ratios" are presented in Table 8. Noting that (true) concentration ratios can often vary by more than an order of magnitude between plant species, the two can be compared to illustrate the effect on foodchain dose calculations of the change of approach. For Cl, the specific activity method results in a lower concentration in all foods except cereals. For some (e.g. mushrooms and fodder) the difference is considerable – a factor of 20. For Ca, the specific activity approach will lead to reasonably similar concentrations in foods to those that would be calculated using SKB's previously-used data. However, it is noted that data compiled by IAEA suggests higher concentration ratios (for cereals and leafy vegetables) than the specific activity approach.

Table 8: "Concentration ratios" calculated from the specific activity relationship for Ca, Cl and K

Plant type	**Ca**	**Cl**	**K**
Cereals	0.22	19	490
Fodder	0.66	19	530
Mushrooms	0.072	19	4000
Tubers	1.1	19	490
Vegetables	0.66	19	530

Relatively few data are available for K for the concentration ratio approach. However, when the values implied by the specific activity approach are compared with the information available from IAEA (2010) it appears that the method will result in very much greater concentrations in plants (more than 100 times that which would be calculated using a concentration ratio approach). A factor in this significant difference could be the low sorption of K.

Conclusions

The use of a specific activity approach for radioisotopes of Ca, Cl and K is considered to be appropriate, given the relative mobility in the environment of these elements, the significant stable isotope concentrations in soils and plants, and the role of these elements as macronutrients. Although this is not yet a typical approach for these elements in radiological assessments, it is noted that IAEA propose a specific activity approach for the

most significant radionuclide (Cl-36) and that Ca and K are less frequently considered in assessments.

The data used by SKB have been compared with some examples in the literature. Broadly, the values adopted for Ca and K appear to be in line with reported concentrations in soils and plants. Values for Cl in plants were significantly lower than reported by IAEA, although there is some uncertainty about this comparison as IAEA are unclear as to whether their data are in terms of fresh or dry weight. However, it is noted that for all elements, environmental concentrations can vary substantially:

- Ca concentrations can vary due to differing amounts of $CaCO_3$ in soil;
- Cl concentrations can vary with proximity to marine water bodies;
- K concentrations can vary with the extent to which soil fertilizer is applied.

All these factors could significantly change the concentration of these radioisotopes found in plants. Some commentary by SKB on the potential range of stable isotope concentrations, and factors that could influence them, would be helpful. This would help add confidence to the values selected by SKB for use in its specific activity models.

The effect in terms of calculated doses from the changed approach can be gauged by comparing an effective "specific activity concentration factor", derived using SKB's data, with concentration factors previously used and applied elsewhere. Concentration factors themselves are very variable, and can be uncertain, so differences can be expected. The comparison shows that the specific activity method results in a lower concentration of Cl in all foods except cereals, considerably lower (a factor of 20) in mushrooms and fodder. For Ca, the specific activity approach will lead to similar concentrations in foods to that which would be calculated using SKB's previously-used data. Concentrations in foods implied using the data for K are very much higher than (more than 100 times) would be calculated using a concentration ratio approach. It is possible that this could be connected with the low sorption of this element, as the stable element concentrations used by SKB appear to be comparable with those reported in the literature.

6. Discussion

The SE-SFL study draws on SKB's biosphere modelling approach that has been developed through application in SR-Site and SR-PSU, along with data gathered for the Laxemar site, to provide an illustrative assessment of potential dose consequences of disposal of long-lived and intermediate-level radioactive waste in concrete and bentonite disposal vaults at a depth of 500 m (termed the SFL facility). The aim of the assessment is to explore potential for the SFL concept to meet regulatory requirements. SE-SFL does not represent a formal licence application, but is instead aimed at informing SKB's concept development for SFL and site selection process.

Although essentially a proof-of-concept type study, SE-SFL includes some refinements to the way in which the biosphere is represented compared to the SR-PSU assessment and provides an indication of modelling approaches and development that could be included in future licence applications.

6.1. Overall comments

The SE-SFL assessment includes a comprehensive assessment of potential impacts. The study builds on the approach that SKB has developed through the SR-Site and SR-PSU assessments. As such, it represents a relatively complex assessment for a proof-of concept level study. However, this is considered appropriate because:

- it builds on approaches that have already been subject to regulatory scrutiny;
- the approach has been refined to address some of the previous regulatory feedback; and,
- in addition to assessing potential for the SFL concept to meet regulatory requirements, the study provides an opportunity to explore further developments in the way in which the biosphere is represented in SKB's long-term post-closure assessments.

In addition to presenting an initial evaluation of the performance of the SFL concept against regulatory criteria, the biosphere component of SE-SFL is supported by several newer strands of underlying research and analysis. As such, the biosphere components of the study represent a hybrid between a licence application and a research study, including some very detailed analyses. Some model changes in the way in which the biosphere is addressed in SE-SFL reflect the scoping nature of the study, some reflect developments that SKB may carry through to future licence applications, and some represent elements of research that may not be taken further. The motivation for particular approaches and modelling decisions can, as a result, be unclear at times.

The underlying methodology used by SKB is consistent with international best practice and developing international guidance. The structure of the documentation for SE-SFL, and for the biosphere component, in particular, is logical and few editorial issues were found. A wide range of cases are explored and the results are evaluated in detail, supported by a range of different approaches to help identify and illustrate important FEPs.

Although the overall approach is complex, SKB have taken the opportunity to introduce some simplifications, e.g. by discounting some exposure pathways that have previously been demonstrated to be insignificant in this context. These simplifications demonstrate

good practice. Iteration and refinement should not result in ever more complicated models. Given the extraordinary timescales being considered, and the associated uncertainties, these studies should seek to be no more complicated than is necessary.

In assessing the relevance of biosphere modelling results, and the supporting research studies, SKB have taken the broader context of the work into account, including the illustrative nature of the study (e.g. Section 12.2.6 of the Biosphere Synthesis report). Within Section 16 of the Biosphere Synthesis report, SKB also review the overall uncertainties in the broader context of the study within a framework that is consistent with international guidance.

Whilst the representation of individual biosphere objects in the BioTEx assessment model is essentially 1D in nature, SKB have begun to support that approach with reference to detailed 3D research-level modelling of individual objects in COMSOL. The level of detail in COMSOL means that it entails a high overhead and the level of complexity is fraught with its own uncertainties. Although impressive in spatial resolution, care is needed to avoid placing too great an emphasis on the level of precision and detail in the results. Nonetheless, the approach is valuable in helping to establish a more realistic conceptualisation of the configuration, features and processes within the individual biosphere objects in support of the necessarily more stylised approach used in the assessment-level modelling. The implications of calibrating the assessment-level groundwater flow understanding and compartment modelling to COMSOL for the headline assessment results are not fully explored.

6.2. Notable developments in assessment-level modelling

There are several notable developments in SKB's approach to representing the biosphere in SE-SFL compared to the preceding SR-PSU assessment.

SKB have introduced additional vertical discretisation in the representation of the lower regolith and glacial clay layers of the 1D model for biosphere objects. This helps to address previous feedback in regulatory reviews by improving the modelling of the time-dependency of radionuclide transfer. Implications are explored by SKB for radionuclides that are not part of decay chains, and the refinement is shown to reduce the calculated rate of transfer to the upper layers of the regolith. The implication for radionuclides in decay chains are not fully explored; the longer modelled transit time through the lower regolith would allow more time of in-growth of radioactive progeny. This can be important for decay chains where the progeny are more radiotoxic than the parent radionuclides, e.g. within the Ra-226 decay chain.

SKB have introduced a capability to model continuous agriculture within a drained mire context, in response to conditions and land uses that are evident in the Laxemar area. That the model for continuous agriculture needs to be distinct from that for initial drainage of a mire for agriculture is, to some extent, an artefact of the way in which drained mire farming is represented. Nonetheless, explicit potential to be able to model continuous agriculture makes SKB's biosphere modelling capability more generally applicable.

SKB have developed a new approach for interpreting and abstracting catchment-scale hydrogeological modelling to support representation of groundwater flows in the assess-

ment-level compartment models. It is anticipated that this element of the biosphere models will continue to be developed, especially given the refinements that were found to be needed in comparison with the detailed 3D COMSOL modelling of groundwater flows.

SKB have introduced a new specific activity modelling approach for representing plant uptake for radioisotopes of elements that are macronutrients. The basis for this approach is well founded. The change in approach results in notable reduction in modelled uptake of Cl-36, which is an important radionuclide in the context of this study. The approach would benefit from further confidence building in relation to the selection of key parameter values.

6.3. Potential areas for further consideration by SKB

Some specific aspects of the SE-SFL study that may merit further consideration or refinement in future SKB assessments are summarised below.

Although integration of the biosphere within the overall assessment is given emphasis by SKB, the behaviour of the near-field and geosphere were not modified for some of the evaluation cases affecting groundwater recharge rates, notably those exploring enhanced global warming and alternative regional climates. This introduces a degree of uncertainty in the interpretation of the results of these cases that would merit further discussion and/or greater integration in future assessment studies.

SKB acknowledge that a broader range of potential climates should be considered in future assessments, including alternative greenhouse gas emission scenarios. It is noted that there is potential to tie the representation of climate to explicit long-term global climate modelling that has been undertaken by SKB.

The way in which drilled wells are included in SKB's safety assessments continues to evolve. Within the SR-Site study, with disposal at 500 m depth, use of groundwater from drilled wells was included within the central calculations. Within the SR-PSU study, calculations allowed for potential use of either drilled or dug groundwater wells. In SE-SFL, central calculations only include use of dug wells, even though SKB notes that a third of the wells in the Laxemar area are drilled into the bedrock. In SE-SFL, drilled wells, which result in higher calculation concentrations in well water, are assessed separately, within their own evaluation case. The evolving way in which drilled wells are represented merits further explanation and justification in future assessments.

Detailed research-level modelling of contaminant transport within a biosphere object using COMSOL has demonstrated that contamination of biosphere objects will likely not be uniform, even within the smallest biosphere objects that are represented. The SE-SFL analyses include consideration of biosphere objects with a wide range of characteristics; this element of the study is considered robust. However, potential for only part of a biosphere object to be contaminated has particular implications for the relevance of modelling sub-catchments that are many times the size needed to support the drained mire farming group. It should be feasible to develop a relatively simple hierarchy of arguments considering discharge areas, homogeneity and spatial scales relevant to the endpoints of interest in defining biosphere objects. In the context of assessing doses to humans, the spatial scale of relevance is the area needed to support the potential exposure group. In the context of assessing doses to non-human biota, the spatial scale would be that relevant

to the biota populations, which relates to habitat areas. Some of the larger biosphere objects considered by SKB may, therefore, be justifiable when considering habitat-scale endpoints, but may be of less relevance to assessing potential doses to people.

SKB use a carbon balance approach to take the degree of productivity within individual biosphere objects into account when defining characteristics for the potentially exposed groups. Relating human habits to the potential productivity of the biosphere objects is a sound approach, however, previous reviews have noted that it comes at the cost of being able to clearly understand the extent of exposure that is being modelled. Future assessments would benefit from more explicit description and justification of the resulting habits, in terms of dietary intakes and occupancies.

In addition to further refinement in the interpolation of catchment-scale hydrological modelling (discussed in Section 6.2), the overall structure of the compartment models for individual biosphere objects and the 1D vertical routing of groundwater flows merits ongoing review. There is some ambiguity in SKB's interpretation of the potential importance of groundwater flows that bypass the glacial clay layer within the biosphere objects.

The assessment results are shown to be sensitive to assumptions concerning the thickness of post-glacial regolith layers. In particular, the relatively high degree of sorption of Tc-99 onto the glacial clay means that potential for glacial clay to be drawn into agricultural soils within biosphere objects with relatively thin post-glacial sediments has a significant implication for the assessed doses. This means that the magnitude of the results are sensitive to assumptions supporting the landscape development modelling, and it is notable that SKB acknowledge landscape modelling on such timescales as being intrinsically uncertain.

The BioTEx assessment model that forms the basis of the evaluation has been developed with a focus on modelling lake to mire transition within the context of the biosphere at Forsmark. Particle tracking for Laxemar indicates potential for radionuclide releases to riparian areas adjacent to streams in valleys that are subject to flooding and sediment deposition. There is a need to build further confidence that the configuration and processes for these streams, valleys and flooding contexts are adequately represented within the BioTEx structure.

Further refinement of the biosphere models for C-14 and Cl-36 would be beneficial, in particular, explicit consideration of relevant chemical forms in the biosphere. This specific topic is acknowledged by SKB. Building further confidence in the relatively novel approach to modelling the loss of C-14 to the atmosphere, in particular, would be welcomed.

6.4. Potential topics for further consideration by SSM

The new biosphere modelling approaches and the supporting research-level studies undertaken by SKB and reported in support of the SE-SFL assessment highlight some topics that may merit further consideration by SSM.

The detailed 3D COMSOL modelling for individual biosphere objects has proved to be interesting and will motivate refinements in the 1D way in which biosphere objects are represented by SKB at the assessment level. The BioTEx model represents a cornerstone

to the way in which SKB represent the biosphere in its post-closure assessments. There is potential for SSM to review the adequacy of the BioTEx structure with an investigative study into modelling one or a few biosphere objects with a greater degree of spatial discretisation coupled to supporting hydrogeological modelling. This would not involve development of COMSOL-scale highly discretised models, but could represent a potential intermediate position whereby the configuration of the regolith layers within a biosphere object is more explicitly represented.

There is potential for SSM to build understanding and confidence in SKB's modelling of C-14 in the biosphere through application of SKB's models and data to C-14 measurements at the Duke Swamp site in Canada. That case study has been reviewed within the international collaborative BIOPROTA forum, and represents a context of C-14 releases in groundwater to a wetland (see Thorne et al., 2018).

Finally, the behaviour of Mo and Tc in the mire systems is shown to be particularly important in the SE-SFL study. There is potential to build confidence in the representation of these elements within the assessment-level modelling through review of the parameterisation, especially relating to geochemical conditions, including redox status, and mobility.

7. References

Ballabio C., Lugato E., Fernández-Ugalde O., Orgiazzi A., Jones A., Borrelli P., Montanarella L. and Panagos P., 2019. Mapping LUCAS topsoil chemical properties at European scale using Gaussian process regression. Geoderma, 355: 113912, database at : https://esdac.jrc.ec.europa.eu/content/chemical-properties-european-scale-based-lucas-topsoil-data

Birkinshaw S.J., Thorne M.C. and Younger P.L. 2005. Reference Biospheres for Post-closure Performance Assessment: Inter-comparison of SHETRAN Simulations and BIOMASS results, J. Radiol. Prot., 25, 33-49

Bosson E., Sassner M., and Gustafsson L.-G. 2009. Numerical modelling of surface hydrology and near-surface hydrogeology at Laxemar-Simpevarp. Site descriptive modeling SDM-Site Laxemar. R-08-72.

Fetter C.W. 1994. Applied Hydrogeology. Third Edition. Prentice Hall.

Grolander S. 2013. Biosphere parameters used in radionuclide transport modelling and dose calculations in SR-PSU. SKB R-13-18, Svensk Kärnbränslehantering AB.

Grolander S. and Jaeschke B. 2019. Biosphere parameters used in radionuclide transort modelling and dose calculations in SE-SFL. SKB R-19-18, Svensk Kärnbränslehantering AB.

IAEA. 2010. Handbook of Parameter Values for the Prediction of Radionuclide Transfer in Terrestrial and Freshwater Environments, Technical Reports Series No. 472, International Atomic Energy Agency, Vienna.

IAEA. 2020. Development of a Common Framework for Addressing Climate and Environmental Change in Post-closure Radiological Assessment of Solid Radioactive Waste Disposal. Report of Working Group 6 of the IAEA MODARIA programme, IAEA-TECDOC-1904.

ICRP. 2012. Compendium of Dose Coefficients based on ICRP Publication 60. ICRP Publication 119.

Joyce S., Appleyard P., Hartley L., Tsitsopoulos V., Woolard H., Marsic N., Sidborn M. and Crawford J. 2019. Groundwter flow and reactive transport modelling of temperate conditions. SKB R-19-02, Svensk Kärnbränslehantering AB..

Lindborg T. (ed). 2018. BIOPROTA. BIOMASS 2020: Interim report. BIOPROTA report, produced in association with IAEA MODARIA II working group 6. Published as SKB R-18-02, Svensk Kärnbränslehantering AB.

Lord N.S, Ridgwell A., Thorne M.C. and Lunt D.J. 2015. The ‘long tail’ of anthropogenic CO_2 decline in the atmosphere and its consequences for post-closure performance assessments for disposal of radioactive wastes. Mineralogical Magazine 79, 1613–1623.

Lord N.S., Crucifix M., Lunt D.J., Thorne M.C., Bouncer N., Dowsett H., O'Brien C.L. and Ridgwell A. 2017. Emulation of long-term changes in global climate: Application to the mid-Pliocene and future. Climate of the Past 13, 1539–1571.

Lord N.S., Lunt D. and Thorne M.C. 2019a. Modelling Changes in Climate over the Next 1 Million Years. SKB TR-19-09, Svensk Kärnbränslehantering AB.

Lord N.S., Lunt D. and Thorne M.C. 2019b. Modelling Changes in Climate over the Next 1 Million Years. Posiva report 2019-04.

Morosini M. and Hultgren H. 2003. Inventering av privata brunnar i Simpevarpsområdet, 2001-2002. SKB report P-03-05, Svensk Kärnbränslehantering AB.

NEA. 2012. Methods for Safety Assessment of Geological Disposal Facilities for Radioactive Waste, Outcomes of the NEA MeSA initiative, Nuclear Energy Agency (NEA) report No. 6923, Paris (2012).

Quintessa. 2020a. AMBER 6.5 User Guide. QPUB-AMBER-2, Quintessa Limited.

Quintessa. 2020b. GraphGrabber 2.0.2 User Guide. QRS-4007AT7-1-UG, Version 2.0.2.

Rhén I. and Hartley L. 2009. Bedrock hydrology Laxemar. Site descriptive modelling SDM-Site Laxemar. SKB R-08-92, Svensk Kärnbränslehantering AB.

SKB. 2011. Long-term safety for the final repository for spent nuclear fuel at Forsmark: Main report of the SR-Site project. SKB report TR-11-01, Svensk Kärnbränslehantering AB.

SKB. 2015. Safety analysis for SFR Long-term safety. Main report for the safety assessment SR-PSU. Revised edition. SKB TR-14-01, Svensk Kärnbränslehantering AB

SKB. 2019a. Post-closure safety for a proposed repository concept for SFL. Main report for the safety evaluation SE-SFL. SKB TR-19-01, Svensk Kärnbränslehantering AB.

SKB. 2019b. Radionuclide transport and dose calculations for the safety evaluation SE-SFL. SKB TR-19-06, Svensk Kärnbränslehantering AB.

SKB. 2019c. Biosphere synthesis for the safety evaluation SE-SFL. SKB TR-19-05, Svensk Kärnbränslehantering AB.

SKB. 2019d. Climate and climate-related issues for the safety evaluation SE-SFL. SKB TR-19-04 Svensk Kärnbränslehantering AB.

SKB. 2020. Climate and climate-related issues, PSAR version. Post-closure safety for the final repository for spent nuclear fuel at Forsmark. SKB TR-20-12 Svensk Kärnbränslehantering AB..

SSM. 2008. The Swedish Radiation Safety Authority's regulations and general advice concerning the protection of human health and the environment in connection with the final management of spent nuclear fuel and nuclear waste. Swedish Radiation Safety Authority SSMFS 2008:37.

Svensson T., Kylin H., Montelius M., Sandén P. and Bastviken D. 2021. Chlorine cycling and the fate of Cl in terrestrial environments. Environmental Science and Pollution Research (2021) 28:7691–7709.

Thorne M.C., Smith K., Kovalets I., Avila R. and Walke R.C. 2018. C-14 in the Biosphere: Terrestrial Model-Data Comparisons and Review of Carbon Uptake by Fish. Bioprota report QRS-1769B-1, Version 1.0.

Tröjbom M., Grolander S., Rensfeldt V. and Nordén S. 2013. Kd and CR used for transport calculations in the biosphere in SR-PSU. SKB R-13-01, Svensk Kärnbränslehantering AB.

Walke R.C. and Limer L.M.C. 2014. Further Modelling Comparison of Simple Reference Biosphere Models with the LDF Modelling Approach: Main Review Phase. SSM report 2014:54.

Walke R.C., Limer L.M.C. and Shaw G.G. 2016. Review of dose assessment - biosphere models for specific radionuclides – SR-PSU. In: SSM's external experts' reviews of SKB's safety assessment SR-PSU – radionuclide transport, dose assessment, and safety analysis methodology - Initial review phase. SSM report 2016:09.

Walke R.C., Limer L.M.C. and Shaw G.G. 2017a. Review of specific topics relating to the biosphere dose assessment for key radionuclides. In: SSM's external experts' review of SKB's safety assessment SR-PSU – consequence analysis - Main review phase. SSM report 2017:30.

Walke R.C., Limer L.M.C. and Shaw G.G. 2017b. In-depth review of key issues regarding biosphere models for specific radionuclides in SR-PSU. In: SSM's external experts' review of SKB's safety assessment SR-PSU – dose assessment, Kd-values, and safety analysis methodology - Main review phase. SSM report 2017:33.

White P.J. and Broadley M.R. 2003. Calcium in Plants, Ann Bot. 2003 Oct; 92(4): 487–511.

WHO. 2009. Potassium in drinking-water. WHO/HSE/WSH/09.01/7

Vergutz L., Manzoni S., Porporato A., Novais R.F. and Jackson R.B. 2012. A Global Database of Carbon and Nutrient Concentrations of Green and Senesced Leaves. ORNL DAAC, Oak Ridge, Tennessee, USA. https://doi.org/10.3334/ORNLDAAC/1106

Appendix 1. Coverage of reviewed reports

SKB Report Number	Coverage
TR-19-01: SE-SFL Main Report	Overall description of assessment in the summary, executive summary, introduction and discussion reviewed in detail to understand context. Biosphere related aspects of sections on methodology, FEPs, initial state, reference evolution, safety evaluation for base and variant cases and discussion reviewed.
TR-19-05: SE SFL Biosphere Synthesis Report	Main body of report reviewed in detail, with the exception of Section 14. Appendices not reviewed in detail.
R-19-18: SE-SFL Biosphere Parameters	Sections and appendices on radionuclide- and element-specific parameters reviewed.
R-13-01: SR-PSU Biosphere Kd and CR	Sections on Kd and CR reviewed in support of parameter derivation review.

Appendix 2. Previous review findings

One of the objectives for the review of the biosphere dose assessment methodology employed by SKB in its SE-SFL assessment was to evaluate development of the methodology in SE-SFL by comparing it to the methodology used previously by SKB. As input to that component of the review, findings from reviews of the biosphere modelling undertaken in support of SSM's reviews of the SR-PSU and SR-Site assessments have been collated. The collated findings provided input, context and focus for the SE-SFL review documented in this report. The collated findings the review of biosphere modelling in SR-PSU are documented in Table A2-1, and SR-Site in Table A2-2.

Table A2-1: Collated Findings from Review of Biosphere Modelling in the SR-PSU Assessment

#	SSM Review Report	Short Description of Finding	Relevance to SE-SFL Review
1	2016:09 initial review of landscape modelling	Note that object with highest doses (157_2) is unusual in that it is not at topographic low, so no lake phase	Nature of biosphere object(s) receiving groundwater discharge of key interest
2	2016:09 initial review of landscape modelling	Praise general preference towards site-specific data, but significant criticism of (i) defining PDFs on the basis of only 3+ data points and stating as having 'good' confidence in the resulting distributions, and (ii) lack of clear justification for some chemical analogue assumptions	Review general approach to justification and use of site-specific data and claims on quality where the amount of data is lacking
3	2016:09 initial review	Criticism of approach of combining 100 geosphere release realisations with 1000 biosphere realisations	Approach to calculations of interest
4	2016:09 initial review of specific radionuclides	Note focus on release to a single object – losing defence in depth from SR-Site approach. Distributing release shown to result in higher dose factors	Approach to uncertainty in the nature of the biosphere object(s) that might receive a groundwater discharge is of interest
5	2016:09 initial review of specific radionuclides	SKB analysis of landscape modelling shows they can miss lakes that might remain	Presence or absence of lakes in biosphere objects receiving groundwater discharge is of interest
6	2016:09 initial review of specific radionuclides	SKB analysis shows the effect of uncertainty in delineation of biosphere objects and could increase doses by up to an order of magnitude for key radionuclides	Emphasises importance in treatment of uncertainty around the nature of biosphere objects
7	2016:09 initial review of specific radionuclides	Slightly improved discretisation of regolith, but still relatively coarse	Management of numerical dispersion is of interest
8	2016:09 initial review of specific radionuclides	No dynamic modelling of agricultural soil	Approach to representing potential use of mire soils for agriculture is of interest
9	2016:09 initial review of specific radionuclides	Lack of lake in 157_2 reduces potential doses from C-14. Also losses to down-stream object 157_1 are by 'diffuse overland flow' which may also be subject to degassing and further reduce potential for C-14 to reach the last in 157_1	C-14 was modelled as being rapidly lost from surface soils/sediments, so potential for pathways to surface water (where uptake to fish is an important exposure pathway) is of interest [Implication of a lake in 157_2 was explored by SKB in complementary information 1571087]
10	2016:09 initial review of specific radionuclides	Contamination of well water based on low plume interception fractions, which are based on rather arbitrary assumptions	Direct use of groundwater is of interest, especially justification for plume capture fractions

#	SSM Review Report	Short Description of Finding	Relevance to SE-SFL Review
11	2016:09 initial review of specific radionuclides	Comparison of dose factors between SR-Site and SR-PSU show significant changes and help to emphasise uncertainty in biosphere modelling, even for relatively well understood systems	Effect of modelling changes between SR-PSU and SE-SFL is of interest
12	2016:09 initial review of specific radionuclides	Highlights omission of potential gas pathway to surface	Query to near-field/geosphere regarding potential for direct gas pathway
13	2016:09 initial review of specific radionuclides	Uncertainty in the consideration and treatment of C-14 labelled methane in the biosphere	Review any further discussion/justification for approach to modelling C-14, especially with regards to form of C-14
14	2017:33 main review phase for landscape models	The dose assessment model is overly complicated and an optimisation is recommended	Review opportunities for simplification
15	2017:33 main review phase for landscape models	Landscape development modelling is detailed and results in overly prescriptive interpretation of future landscape development within the dose assessment modelling	Review level of detail in the context of the assessment and potential source-term to the biosphere
16	2017:33 main review phase for specific radionuclides	Some of the modelling complexity cannot be supported by data, e.g. (i) distinguishing aquatic primary producers, (ii) reducing radionuclides in manure without any data	Review justification for level of detail, especially where the detail is not supported by available data
17	2017:33 main review phase for specific radionuclides	Some key parameters are not varied, including timescales for land evolution, water flow rates and the very small well capture fractions, whereas effort is assigned to defining PDFs for parameters like the width of a barley leaf	Review consistency in handling parameter uncertainties
18	2017:33 main review phase for specific radionuclides	Abstraction of water flows is again noted, with potential non-conservative effect. E.g. lateral flows are ignored “for simplicity”, driving flows vertically (through clay layer) to surface, where C-14 can be lost rapidly	Review abstraction of groundwater flow modelling into assessment model
19	2017:33 main review phase for specific radionuclides	Analytical solution for agricultural soils is (i) not good for radionuclides with half-lives that are shorter than the 50-year averaging time, (ii) mixing deterministic and probabilistic assumptions (e.g. deterministic scaling factors for in-growth)	Review treatment of agricultural soils

#	SSM Review Report	Short Description of Finding	Relevance to SE-SFL Review
20	2017:33 main review phase for specific radionuclides	Inconsistencies in modelling of peat thickness, and litter production	Check to see if these inconsistencies have been addressed
21	2017:33 main review phase for specific radionuclides	Non-pessimistic exposure group assumptions, including (i) intake fractions for garden plot group are very low, (ii) low occupancies for agricultural groups, (iii) size of the hunter-gatherer group (30 individuals) dilutes degree of exposure	Review exposure group assumptions
22	2017:33 main review phase for specific radionuclides	No discussion of methane and oxidation in C-14 modelling	See #13
23	2017:33 main review phase for specific radionuclides	Model for C-14 degassing rates gives values that appear to be higher than found in field observations for organic soils	Check for further review/justification for degassing rates for C-14 [Degassing rates for C-14 was explored further in SKB complementary information 1610560]
24	2017:33 main review phase for specific radionuclides	Model for C-14 uptake to fish gives values significantly lower than IAEA concentration ratios	Check for further justification for approach to modelling of C-14 in surface water
25	2017:33 main review phase for specific radionuclides	Limited site-specific data for Kd and CR in many cases. Also, questionable use of GSD for all elements where data was lacking for some elements	Check for further discussion/justification for approach to use of site data
26	2019-16 further review for hydrogeological aspects	Well capture fractions did not consider drawing effect of pumping rates (estimated factor of two), nor potential effect of heterogeneity (estimated factor of three), meaning capture fractions could have been a factor of six higher. Risk scaling for wells also fails to take account of potential increase use of wells in future (e.g. with climate change and as lakes disappear)	If well capture is included, then check for treatment of well draw and increased potential for wells in future.

Table A2-2: Collated Findings from Review of Biosphere Modelling in the SR-Site Assessment

#	SSM Review Report	Short Description of Finding	Relevance to SE-SFL Review
a	2012:46 landscape modelling review	Seeking to be "as realistic as possible" drives detail which has the potential to obscure the identification and justification of necessary assumptions that are inevitably associated with extending landscape evolution projections over long timescales	Review justification of the level of detail given the context of the assessment (linked to #15)
b	2012:46 landscape modelling review	Weichselian is not a good basis for the current extended interglacial; greater emphasis on the global warming and even the extended global warming cases may be appropriate	Review treatment of climate change given context for the assessment and potential source-term to the biosphere
c	2012:46 landscape modelling review	SKB use a fixed rate of land rise and don't explicitly explore alternative rates, even though the transitional period is shown to be important	Review assumptions about landscape development
d	2012:46 landscape modelling review	Fixed 2 m above sea-level assumption for wetlands to be available for agriculture, without grazing on wetlands	See #c
e	2012:46 landscape modelling review	Potential for irrigation with well water not fully explored	Check to see if potential for use of well water is included (especially irrigation)
f	2012:46 landscape modelling review	Opaque nature of dietary assumptions when based on model of primary productivity	Review exposure group assumptions regarding dietary intakes (linked with #21)
g	2012:46 landscape modelling review	Need for abstraction of groundwater flow assumptions into the assessment model is a key area	See #18
h	2014:34 simple biosphere models	SKB assume radionuclides distributed across whole biosphere objects	Review assumptions regarding biosphere object areas and contamination.
i	2014:34 simple biosphere models	Simple models were developed as part of review to consider smaller family group	See #21
j	2014:34 simple biosphere models	SKB exclude consideration of agriculture over clayey silty till, which has better potential for long-term agriculture than mires	Check to see if assessment focuses on release to topographic lows, and potential for exposures to arise via other routes
k	2014:34 simple biosphere models	SKB well surveys show people using groundwater for irrigation, but excluded from central SKB calculations	This was taken further in SR-PSU and so is superseded
l	2014:34 simple biosphere models	Coarse discretisation of SKB biosphere objects means dynamics of accumulation are poorly represented	See #7

#	SSM Review Report	Short Description of Finding	Relevance to SE-SFL Review
m	2014:34 simple biosphere models	Abstraction of detailed modelling of groundwater flows a notable uncertainty, along with inappropriate use of net water exchanges	See #18
n	2014:34 simple biosphere models	Acknowledge pessimism in using highest LDF across all objects for each radionuclide	Review treatment of uncertainty about timescales of release and nature of objects receiving release
o	2014:35 alternative biosphere modelling	Abstraction of detailed modelling of groundwater flows and use of 'snapshots' make the hydrology a notable uncertainty	See #18
p	2014:35 alternative biosphere modelling	Difficult to track data through to Kd and CR recommendations	Approach to data was updated in SR-PSU, so this is superseded
q	2014:54 further use of simple biosphere model	Ingestion of well water dominates for 32 of 39 radionuclides and doesn't require biosphere modelling	Review importance and modelling for any well water pathways
r	2014:54 further use of simple biosphere model	SKB omitted to include a flux of Po-210 into the biosphere and omitted to add short-lived daughters to dose coefficients	Review consistency in explicit/implicit treatment of radionuclides
s	2014:54 further use of simple biosphere model	Coarse discretisation underestimates in-growth so underestimates dose factors for chains, including Ra-226	See #7
t	2015:22 further alternative biosphere modelling	Potential underestimate of dose factors for more strongly sorbing elements and for decay chains	See #7
u	2015:48 groundwater flow abstraction	Critical of the way in which flows were normalised, averaged and mapped across to the dose model	See #18
v	2019:22 review of additional SKB studies	Conceptual basis for including Rn-222 is not well described	Review treatment of Rn-222
w	2019:22 review of additional SKB studies	SKB need to adapt LDF model for new robustness calculations to keep results below the risk limit. This is done by changing to Kd and CR from SR-PSU and modelling time-dependent flux to the biosphere	Review consistency in treatment of different scenarios
x	2019:22 review of additional SKB studies	Timing of sudden widening of canister defects just after all lakes have gone from the landscape is convenient for C-14	Review timing of key changes in relation to source term, especially terrestrialisation in relation to C-14 release

The Swedish Radiation Safety Authority has a comprehensive responsibility to ensure that society is safe from the effects of radiation. The Authority works from the effects of radiation. The Authority works to achieve radiation safety in a number of areas: nuclear power, medical care as well as commercial products and services. The Authority also works to achieve protection from natural radiation an to increase the level of ratiation safety internationally.

The Swedish Radiation Safety Authority works proactively and presentively to protect people and the environment from the harmful effects of radiation, now and in the future.
The Authority issues regulations and supervises compliance, while also supporting research, providing training and information, and issuing advice. Often, activities involving radiation require licences issued by the Authority. The Swedish Radiation Safety Authority maintains emergency preparedness around the clock with the aim of limiting the aftermath of radiation accidents and the unintentional spreading of radioactive substances. The Authority participates in international co-operation in order to promote radiation safety and finances projects aiming to raise the level of radiation safety in certain Eastern European countries.

The Authority reports to the Ministry of the Environment and has around 300 employees with competencies in the fields of engineering, natural and behavioral sciences, law, economics and communications. We have recieved quality, environmental and working environment certification.

Publikationer utgivna av Strålsäkerhetsmyndigheten kan laddas ned via stralsäkerhetsmyndigheten.se eller beställas genom att skicka e-post till registrator@ssm.se om du vill ha broschyren i alternativt format, som punktskrift eller daisy.

Strålsäkerhetsmyndigheten
Swedish Radiation Safety Authority
SE-171 16 Stockholm
Phone: 08-799 40 00
Web: ssm.se
E-mail: registrator@ssm.se

E-print AB, 2021